Airway pathogens and immune responses in severe asthma

Dr Maisha Farzana Jabeen

Nuffield Department of Medicine

St Cross College

University of Oxford

Supervised by

Prof. Timothy SC Hinks

Prof. Paul Klenerman

Prof. Ian Pavord

Abstract

Asthma is a heterogenous, chronic inflammatory disease of the airways, and the world's most common chronic lung disease. Ten percent of patients have airways inflammation resistant to inhaled corticosteroid therapy. I explored several treatable traits amongst these patients. First, the airway microbiome is more likely to be altered and dominated by pathogenic bacteria in these patients, driving symptoms, asthma attack risk and steroid resistant neutrophilic airways inflammation. The nature of this problem had not been fully defined. However, the macrolide azithromycin, which has antimicrobial and anti-inflammatory properties is an effective targeted therapy but is associated with antimicrobial resistance and the dominant mechanism was unknown. A second group of patients with treatment resistant disease is characterised by severe type-2 inflammation and high levels of the biomarker fractional exhaled nitric oxide.

I performed a metagenomic study using Nanopore sequencing, which found a dominant pathogen in 20-30% of adults with severe asthma associated with neutrophilic inflammation. I undertook a mechanistic interventional bronchoscopy study of azithromycin in 10 patients meeting clinical criteria for treatment. Using single cell sequencing I identified both antibacterial and anti-inflammatory effects of azithromycin, making it effective in the presence or absence of infection. Azithromycin supports recovery and normal functioning of the airway epithelium and secretory cells, shapes innate immune responses by neutrophils and macrophages, dampening overzealous responses which could cause tissue damage, whilst inducing a quiescent state in airway T cells which upregulate mediators involved in tissue repair. I demonstrate the microbiome and cellular composition of the upper and lower airway are very distinct. I characterised T cells in a second, larger, single cell bronchoscopy study of 43 participants with severe asthma and health. This unique resource constitutes the largest single cell dataset in severe asthma to date, with which I will explore mechanisms driving corticosteroid resistant disease.

Statement of authorship

The majority of the work presented in this thesis has been completed by myself, Maisha Jabeen, under the supervision of Prof. Timothy Hinks, Prof. Paul Klenerman and Prof. Ian Pavord.

It should be noted that some figures and text in this thesis were previously published in either Jabeen *et al*., 2022 (10.1128/spectrum.02279-21) or Jabeen *et al*., 2024 (10.1111/all.16269), as has been indicated in the text. I was the first author and primarily involved in data generation and writing of these manuscripts.

Collaborative work has been included where data analysis and figure design or generation was performed jointly.

This thesis has not been submitted in part or as a whole for any other university degree at the University of Oxford or elsewhere.

Dr Maisha Jabeen

20/05/2025

Acknowledgements

I would like to thank my supervisors Prof. Timothy Hinks, Prof. Paul Klenerman and Prof. Ian Pavord for their dedicated supervision, support and guidance. I am particularly grateful to Prof. Hinks for his mentorship from the early days of my Academic Clinical Fellowship – for always encouraging me to explore new ideas and opportunities. I thank key collaborators Dr Teresa Street, for scientific input, and Dr Nicholas Sanderson and Dr Emanuele Marchi for bioinformatic support critical to the metagenomics studies presented in this thesis. I am grateful to Prof. Peter Howarth (University of Southampton) for entrusting us with the Wessex metagenomics samples.

I also thank Bianka Brassanyi, Wojciech Lason, Raghad Yamani and Mahdi Mahdi for their help in delivering the MORSE /AMASS studies. I am incredibly grateful to Dr Lucy Garner for her supervision of my bioinformatic analyses. I thank my wonderful colleagues in the Hinks and Klenerman lab groups for their warmth and friendship.

I am indebted to the Severe Asthma MDT for their support in delivering the bronchoscopy studies particularly as we navigated the challenges of the COVID-19 pandemic together, alongside the Oxford Airways Study patients for their time and openness to be involved in research.

I am grateful for my early mentors who inspired me to pursue academic medicine through their infectious enthusiasm for science – Prof. Ian Sabroe and Prof. Moira Whyte – alongside Prof. Sarah Walmsley for her ongoing guidance and wisdom.

None of this would have been possible without my family by my side – my husband George with his continued encouragement and positivity, our daughter Amalia who has brought endless joy since her arrival in the final year of this DPhil, my loving parents (Abbu, Ammu) who always look after us all and my brother Hisham with his heartfelt kindness and support. My wonderful in-laws (Ian, Sachiko and Emma) have cheered me along throughout this journey. I cannot thank them all enough.

Abbreviations

7AAD	7-amino-actinomycin D
ACQ	Asthma Control Questionnaire
ACT	Asthma Control Test
ADT	Antibody-derived tag
AMASS	Azithromycin Mechanisms in Asthma Study
AMR	Antimicrobial resistance
ARDS	Acute respiratory distress syndrome
ATS	American Thoracic Society
BAL	Bronchoalveolar lavage
BH	Benjamini-Hochberg
BHI	Brain heart infusion
BNA	Bayesian network analysis
BSA	Bovine serum albumin
BTS	British Thoracic Society
cAMP	cyclic Adenosine monophosphate
CCL	C-C chemokine ligand
CCR	Chemokine receptor
CD	Cluster of differentiation
cDNA	Complementary DNA
CF	Cystic fibrosis
CFU	Colony forming unit
CI	Confidence interval
CITE-seq	Cellular indexing of transcriptomes and epitopes by sequencing
CLRs	C-type lectin receptors
COPD	Chronic obstructive pulmonary disease
CRP	C-reactive protein
CS	Corticosteroids
CXC	CXC family
CXCR	CXC chemokine receptor
DAMPs	Damage-associated molecular patterns
DC	Dendritic cells
DHFR	Dihydrofolate reductase
DNA	Deoxyribonucleic acid
dsRNA	Double-stranded ribonucleic acid
DTT	Dithiothreitol
ECG	Electrocardiogram
EDTA	Ethylenediaminetetraacetic acid
ELISA	Enzyme-linked immunosorbent assay
ENT	Ear nose throat

ERS	European Respiratory Society
FASTA	FASTA format
FC	Fold change
FDR	False discovery rate
FeNO	Fractional exhaled nitric oxide
FEV1	Forced expiration volume in 1 second
FF	Fluticasone furoate
FMO	Fluorescence minus one
FP	Fluticasone propionate
FVC	Forced vital capacity
GEX	Gene expression
GINA	Global Initiative for Asthma
GO	Gene ontology
GSEA	Gene set enrichment analysis
GTPase	Guanosine triphosphatase
HC	Healthy control
HDM	House dust mite
HLA	Human leukocyte antigen
HRCT	High-resolution computed tomography
HRV	Human rhinovirus
HSP	Heat shock protein
ICAM-1	Intercellular adhesion molecule 1
ICS	Inhaled corticosteroids
IFN	Interferon
Ig	Immunoglobulin
IL	Interleukin
ILC	Innate lymphoid cells
INCA	INhaler Compliance Assessment
iNOS	Inducible nitric oxide synthase
IQR	Interquartile range
ISG	Interferon-stimulated gene
IU	International units
LABA	Long-acting beta-2 agonist
LPS	Lipopolysaccharide
LYZ	Lysozyme
MAIT	Mucosal-associated invariant T cell
MALDI-TOF	Matrix-assisted laser desorption/ionization time-of-flight
MAST	Model-based analysis of single-cell transcriptomics
MIF	Migration inhibitory factor
MIP	Macrophage inflammatory protein
MMP	Matrix metalloproteinase
MORSE	MultiOmics pRoject Study gEnomics
MPO	Myeloperoxidase

mRNA	Messenger ribonucleic acid
MSD	Meso Scale Discovery
mTOR	Mammalian target of rapamycin
NB	Nasal brush
NET	Neutrophil extracellular trap
NF-kB	Nuclear factor kappa B
NICE	National Institute for Health and Care Excellence
NK	Natural killer cells
NKT	Natural killer T cells
NLR	NOD-like receptor
NSAIDs	Non-steroidal anti-inflammatory drugs
NTHi	Nontypeable *Haemophilus influenzae*
NTM	Non-tuberculous mycobacteria
ONT	Oxford Nanopore Technologies
OTU	Operational taxonomic unit
PAMPs	Pathogen-associated molecular patterns
PBMC	Peripheral blood mononuclear cell
PBS	Phosphate buffered saline
PCD	Primary ciliary dyskinesia
PCR	Polymerase chain reaction
PERMANOVA	Permutational multivariate analysis of variance
PID	Patient ID
PM	Particulate matter
pMDI	Pressurised metered dose inhaler
PRR	Pattern recognition receptor
QC	Quality control
qPCR	Quantitative real-time PCR
RBC	Red blood cell
RLRs	RIG-I-like receptors
RNA	Ribonucleic acid
RPMI	Roswell Park Memorial Institute
rRNA	Ribosomal RNA
RSV	Respiratory syncytial virus
RT	Room temperature
RV	Rhinovirus
SA	Severe asthma
SARS-CoV	Severe acute respiratory syndrome Coronavirus
scRNAseq	Single-cell RNA sequencing
SD	Standard deviation
SEM	Standard error of mean
SPRI	Solid phase reversible immobilization
TCR	T cell receptor
TGF	Transforming growth factor

TIMP	Tissue inhibitor of metalloproteinases
TLR	Toll-like receptor
TNF	Tumour necrosis factor
Tris-HCl	Tris(hydroxymethyl)aminomethane hydrochloride
TRM	Tissue-resident memory
TSLP	Thymic stromal lymphopoietin
UMAP	Uniform manifold approximation and projection
VEGF	Vascular endothelial growth factor

Table of Contents

List of Figures **6**

List of Tables **9**

Chapter 1: Introduction ***10***

1.1 An overview of asthma **10**

1.1.1 Aetiology of asthma 10

1.1.2 Asthma pathogenesis 13

1.1.3 Heterogeneity of asthma and treatable traits 21

1.1.4 Inflammatory biomarkers in severe asthma 22

1.2 The Respiratory Microbiome **24**

1.2.1 Respiratory microbiome in health 26

1.2.2 Early life microbiome and asthma 28

1.2.3 The microbiome in adult asthma 32

1.2.4 Potentially pathogenic bacterial species in severe asthma 34

1.2.5 Haemophilus influenzae in airways disease 35

1.3 Azithromycin in Severe Asthma **39**

1.3.1 Immunomodulatory functions of macrolides 40

1.3.2 Azithromycin therapy in treatment refractory asthma 43

1.3.3 The lung resistome and anti-microbial resistance associated with macrolides 47

1.4 Key outstanding questions and objectives **48**

Chapter 2: Materials and Methods ***52***

2.1 Study populations **52**

2.1.1 Definition of moderate and severe asthma in study populations 52

2.1.2 Metagenomics of Severe Asthma 53

2.1.3 Longitudinal and cross-sectional bronchoscopy studies: AMASS and MORSE 54

2.2 Clinical measurements **58**

2.2.1 Spirometry and reversibility 58
2.2.2 Exhaled nitric oxide and suppression testing 58
2.2.3 Electrocardiogram (ECG) 59
2.2.4 Asthma control questionnaire 59

2.3 Clinical classification 61

2.4 Clinical sample handling 65

2.4.1 Phlebotomy and blood sample handling 65
2.4.2 Isolation of peripheral blood mononuclear cells 65
2.4.3 Nasal brushing 66
2.4.4 Nasal brush processing 66
2.4.5 Sputum induction 67
2.4.6 Sputum processing 68
2.4.7 Cytospin preparation 68
2.4.8 Definitions of sputum inflammatory phenotypes 69

2.5 Metagenomic sequencing of airway samples 69

2.5.1 Sputum culture 69
2.5.2 Bacterial spiking of sputum samples 70
2.5.3 Microbial DNA extraction from sputum and nasal lavage samples 70
2.5.4 Microbial DNA extraction with saponin based host DNA depletion 71
2.5.5 Metagenomic sequencing with Illumina MiSeq 72
2.5.6 Metagenomic sequencing with Oxford Nanopore Technologies (ONT) 72
2.5.7 Total 16S and pathogen specific qPCR assays 73
2.5.8 Measurement of inflammatory mediators 73
2.5.9 Bioinformatic and statistical analysis 74
2.5.10 Data availability 77

2.6 Bronchoscopy 78

2.6.1 Bronchoscopic technique 78
2.6.2 BAL processing 79
2.6.3 Endobronchial biopsy processing 80

2.7 Single cell RNA sequencing (scRNA-seq) 81

2.7.1 Single cell RNA-seq tissue processing 81

2.7.2 Library generation 84

2.7.3 Bioinformatic analysis 85

2.8 Flow cytometry 88

2.8.1 MR1/5-OP-RU tetramer 88

2.8.2 Sorting and data acquisition prior to single cell sequencing 88

2.9 Meso-Scale Discovery platform 90

2.10 Quantification of Neutrophil Extracellular Traps 91

Chapter 3: Metagenomics of Severe Asthma 93

3.1 Introduction 93

3.2 Hypothesis 95

3.3 Aims 95

3.4 Oxford Nanopore Technologies for airway metagenomic sequencing 96

3.4.1 Clinical characteristics of pilot cohort 96

3.4.2 Airway microbiome in severe asthma and definition of pathogen dominance in a pilot cohort 97

3.4.3 Comparison of Nanopore and Illumina sequencing 100

3.4.4 Co-existent airway pathogens in severe asthma 104

3.4.5 Bacterial spiking and limits of detection 105

3.4.6 Discussion 106

3.5 Integrated metagenomic and proteomic analysis of microbe-immune interactions in severe asthma 110

3.5.1 Clinical characteristics of Oxford and Wessex asthma cohorts 111

3.5.2 The metagenome of severe asthma and pathogen dominant microbiome 113

3.5.3 Microbiome differences by sputum inflammatory phenotype 119

3.5.4 Integration of cytokine and metagenomic analyses 121

3.5.5 Neutrophilic inflammation with pathogen dominance in severe asthma 123
3.5.6 Bayesian network analysis in severe asthma 123
3.5.7 Microbiome and cytokine milieus in the upper and lower airway 125
3.5.8 Discussion 127
3.6 Conclusions 134
Chapter 4: The Azithromycin Mechanisms in Asthma Study (AMASS) 135
4.1 Introduction 135
4.2 Hypothesis 137
4.3 Aims 138
4.4 Study population 138
4.5 Clinical response to azithromycin 140
4.6 Regulation of airway mediators and neutrophils by azithromycin 141
4.7 Single cell characterisation of treatment responses to azithromycin 145
4.7.1 scRNAseq of upper and lower airway samples in severe asthma 145
4.7.2 Characterisation of epithelial and immune cell populations in the asthmatic airway in the AMASS cohort 148
4.7.3 Transcriptomic changes in epithelial cells after azithromycin treatment 157
4.7.4 Transcriptomic changes in myeloid cells after azithromycin treatment 162
4.7.5 Transcriptomic changes in lymphoid cells after azithromycin treatment 165
4.7.6 Airway infection status and azithromycin activity 169
4.8 Discussion 180
4.9 Conclusions 184
Chapter 5: MultiOmics pRoject Study gEnomic (MORSE) 186
5.1 Introduction 186
5.2 Hypotheses 186

5.3 Aims 187

5.4 Study population 187

5.5 Generation of a reference lymphoid single cell dataset in health and asthma 190

5.5.1 scRNAseq of upper and lower airway samples from healthy controls and patients with severe asthma 190

5.5.2 Characterisation of lymphoid cell population in the MORSE cohort 191

5.6 Discussion 196

5.7 Conclusions 198

Chapter 6: Discussion 199

6.1 Neutrophilic asthma and *H. influenzae* 199

6.2 Azithromycin in severe asthma 203

6.3 Treatment refractory phenotypes of severe asthma 206

6.4 Future work 207

6.5 Conclusions 209

References 210

Appendix 1: Jabeen et al 2022 240

Appendix 2: Jabeen et al. 2024 245

Appendix 3: Supplemental results for Chapter 4 AMASS 277

List of Figures

Figure 1.1 Schematic concept diagram of asthma. 22

Figure 1.2 The role of NTHi in neutrophilic airway inflammation.....36

Figure 1.3 NTHi adheres to and invades primary bronchial epithelial cells. 36

Figure 2.1 GINA asthma treatment steps (Global Initiative for Asthma, 2024) 53

Figure 2.2 Flow diagram of bronchoscopy studies.....57

Figure 2.3 Clinical and inflammatory phenotyping criteria 62

Figure 2.4 Flow cytometry gating strategy for sorting cells prior to scRNA sequencing.....90

Figure 3.1 Sputum microbiome with Nanopore and Illumina sequencing; 102

Figure 3.2 H. influenzae genome coverage by Nanopore (ONT) and Illumina MiSeq; 103

Figure 3.3 Single nucleotide polymorphism (SNP) distance matrix;.....103

Figure 3.4 Recovery of spiked bacterial species using Nanopore and qPCR; 106

Figure 3.5 Metagenomic study design.....113

Figure 3.6 Relative abundance of species in sputum; 116

Figure 3.7 Taxonomic profiles in sputum in severe asthma;.....118

Figure 3.8 Integrated analyses of microbiome and inflammatory mediators in sputum;.....120

Figure 3.9 Heatmap displaying correlations between integrated sputum microbiome and cytokine data; 122

Figure 3.10 Integrated Bayesian Network Analysis;.....124

Figure 3.11 Upper and lower airway microbiome and cytokines;.....126

Figure 4.1 Lung function, symptom scores and type-2 biomarkers post-azithromycin therapy.....141

Figure 4.2 Airway chemokines pre- and post-azithromycin therapy. 143

Figure 4.3 Airway cytokines pre- and post-azithromycin therapy; 144

Figure 4.4 Modulatory cytokines pre- and post- azithromycin therapy; 145

Figure 4.5 BAL neutrophil frequency and quantification of airway NET load pre- and post- azithromycin;.....145

Figure 4.6 Upper and lower airway cells captured by scRNAseq. 147

Figure 4.7 Epithelial and stromal cell lineage. 149

Figure 4.8 Myeloid lineage. 151

Figure 4.9 Lymphoid lineage. 154

Figure 4.10 T cell tissue residency makers and phenotypic profiling. 155

Figure 4.11 CD4 expression and identification of cells. 156

Figure 4.12 Differences in pre- and post-azithromycin gene expression in all upper and lower airway epithelial cells. 160

Figure 4.13 Differences pre- and post- azithromycin treatment in sub-populations of epithelial cells. 161

Figure 4.14 GO term enrichment in nasal club cells. 162

Figure 4.15 Differences in pre- and post- azithromycin treatment in myeloid cell populations. 164

Figure 4.16 Differences pre- and post- azithromycin across all lower and upper airway T cells; 167

Figure 4.17 Differences pre- and post-azithromycin in lymphoid cell subsets. 168

Figure 4.18 Differences in gene expression in neutrophils seen post-azithromycin treatment between groups with or without detection of a pathogen on BAL culture; 171

Figure 4.19 Differences in gene expression in macrophages seen post-azithromycin treatment between groups with or without detection of a pathogen on BAL culture; 174

Figure 4.20 Differences in gene expression in CD8 T cells seen post-azithromycin treatment between groups with or without detection of a pathogen on BAL culture; 177

Figure 4.21 Differences in gene expression in multiciliated cells seen post-azithromycin treatment between groups with or without detection of a pathogen on BAL culture; 178

Figure 4.22 Differences in gene expression in goblet seen post-azithromycin treatment between groups with or without detection of a pathogen on BAL culture; 179

Figure 5.1 Clinical characteristics of patients with severe asthma at baseline bronchoscopy;.....189

Figure 5.2 FeNO suppression test results based on outcome; 189

Figure 5.3 Lymphoid lineage from MORSE dataset; 192

Figure 5.4 Upper and lower airway lymphoid cell captured by scRNAseq;.....193

Figure 5.5 cellular composition in the upper and lower airways in health and asthma; 195

Figure 5.6 Dot plot of additional transcription factors and cytokines used for classification of cells 195

List of Tables

Table 1.1 Summary of key clinical trials of azithromycin in asthma.....45

Table 2.1 Asthma Control Questionnaire.....61

Table 2.2 Bronchoscopy sample surface staining panel for flow cytometry.....83

Table 2.3 CITE-seq antibodies.....84

Table 2.5 MSD Panels.....91

Table 3.1 Clinical characteristics of participants in pilot cohort.....97

Table 3.2 Summary of sputum microbiology results and inflammatory phenotype .99

Table 3.3 Top 5 abundant species detected by Nanopore and Illumina MiSeq in HI+ samples.....101

Table 3.4 Clinical characteristics of Wessex and Oxford severe asthma cohorts ..112

Table 4.1 Clinical characteristics of participants in the AMASS study 139

Table 4.2 BAL culture results pre and post azithromycin therapy for the AMASS cohort.....139

Table 5.1 Clinical characteristics of MORSE study population.....188

Chapter 1: Introduction

1.1 An overview of asthma

Asthma is the commonest chronic lung disease in the world, affecting 350 million people and causing 400,000 deaths annually (Collaborators, 2017). In the UK it affects 1 in 12 adults (Mukherjee et al., 2016). Asthma is a heterogenous condition, and whilst most individuals with asthma respond to inhaled corticosteroid and bronchodilator therapy, 10% do not. This form of severe treatment refractory disease accounts for the majority of health service and societal cost of asthma (annually £1.1 billion in the UK), alongside disease associated mortality. Severe asthma thus remains a significant unmet clinical need for individuals affected by it and wider society.

1.1.1 Aetiology of asthma

Asthma is a complex inflammatory condition. Its aetiology is not fully understood, although a range of host factors are increasingly appreciated to attribute risk. Atopy remains the most important predisposing factor for asthma. It is characterised by excess immunoglobulin (Ig)-E responses mounted against common environmental allergens (Arshad, 2005). Prevalence of asthma increases with serum IgE. Atopy is strongly heritable, with hypersensitivity to aeroallergens being particularly common in children and young adults with asthma, affecting boys more than girls until the age of 10 years (Arshad, 2005). In contrast, severe asthma with high symptom burden in adults is more common in women (Postma, 2007). Sex differences in asthma are considerable and likely relate to a wide range of genetic and physiological factors (Jenkins et al., 2022).

Genetics plays a key role in the risk of asthma. Several gene loci have been linked to asthma susceptibility, likely interacting with one another and the environment to exert their

effect – these include ADAM33 (Blakey et al., 2005), HLA-DQ, IL33, SMAD3, IL2RB (Moffatt et al., 2010), IRAK-M/IRAK-3 (Balaci et al., 2007) and YKL-40 (Ober et al., 2008). Epigenetic modifications, which are heritable phenotypic changes influencing gene expression without altering the underlying DNA sequence, add a further dimension to individual risk (Stikker et al., 2023).

Maternal risk factors for atopy also plays a role. Several studies have demonstrated that maternal type-2 cytokines can influence the risk of childhood asthma. Increased maternal interleukin(IL)-5 in pregnancy (Soto-Ramirez et al., 2012) is associated with risk of asthma in the infant whereas a higher ratio of type-1 cytokine interferon (IFN)-ɣ to prototypic type 2 cytokines (IL-13, IL-4), (Rothers et al., 2018) are associated with lower rates of asthma. This relationship between IFNɣ:IL-4 also extends to risk of atopy (Kim et al., 2008).

The prevalence of atopy and autoimmune conditions have risen in the past few decades, particularly in Western countries – an observation referred to as the ‘hygiene hypothesis’, accounting for rising rates of allergic diseases due to lack of immune priming by microbes or microbial products. These exposures facilitate maturation of the immune system and are further discussed later in this chapter in relation to the microbiome (Schaub et al., 2006).

Dietary factors have also been associated with asthma, in particular vitamin D deficiency (O'Sullivan et al., 2021). This can act together with obesity and interact with environmental risks such as air pollution to increase the overall susceptibility to asthma (Bose et al., 2019). However, dietary supplementations have not shown much promise to date (Weiss and Litonjua, 2011).

Alongside predisposing host factors, environmental causal factors can impact the likelihood of developing asthma in susceptible individuals. In childhood, early inhaled allergen exposure and airways infection play an important role. The commonest source of indoor

allergen is house dust mite, followed by those derived from domestic pets and fungi. There is a correlation between long term allergen exposure and asthma, with symptoms often improving with removal of the offending allergen (Platts-Mills et al., 2000). The number of respiratory illnesses early in life is also associated with the risk of development in asthma and has been described later in this chapter in relation to the microbiome and development of mucosal immunity (Bonnelykke et al., 2015). In adults, occupational exposures and smoking are the commonest risk factor in susceptible individuals. Occupational agents can be broadly classified as high molecular weight compounds from plant and animal sources, which act via an IgE mediated mechanism or low molecular weight compounds such as isocyanates; less is known about the immunological mechanisms involved in this latter group (Vandenplas, 2011). Exposure to cigarette smoke pre- and postnatally can significantly affect lung health and development, alongside the risk of asthma (Gopal et al., 2016; Miyake et al., 2023). In adults, it can compound the effect of occupational exposures (Mapp et al., 2005) and significantly worsen symptoms whilst reducing the treatment effect of inhaled corticosteroids (Chaudhuri et al., 2003).

Other exposures linked to asthma are drugs and air pollution. Intolerance to aspirin and related non-steroidal anti-inflammatory drugs (NSAIDs) affects approximately 20% of patients with asthma, classically presenting with nasal polyposis. In susceptible individuals there is an enzymatic defect leading to the accumulation of pro-inflammatory cysteinyl leukotrienes (Babu and Salvi, 2000). There has been considerable interest in the role of air pollution on asthma. Pollutants such as ozone, nitrogen dioxide and particulate matter (<2.5 μm, PM2.5) can cause airways inflammation, while ozone and nitrogen dioxide can induce airway hyperresponsiveness. A large systematic review and metanalysis of 25 studies has recently reported that increased ambient exposure PM2.5 and nitrogen dioxide might present an additional risk factor in adult asthma, however there was heterogeneity amongst studies (Lee et al., 2024). In patients with asthma, short term exposures can

however increase the risk of exacerbations and mortality (Guarnieri and Balmes, 2014; Liu et al., 2019).

Therefore, there is a complex interplay between genetic factors and their influence on susceptibility to environmental exposures which determine whether there is development of clinical disease. These directly and indirectly shape immune responses from early on in life.

1.1.2 Asthma pathogenesis

Asthma is a heterogenous chronic inflammatory condition which affects the conducting airways (Huber and Koessler, 1922). There is recurrent episodic airflow obstruction, which can clinically present with breathlessness, wheeze, chest tightness and cough. Symptoms are driven by airways inflammation triggering bronchial hyperresponsiveness (BHR), mucus secretion and airway remodelling. Airway remodelling occurs and becomes most prominent in those with chronic and severe asthma (James and Wenzel, 2007). These structural changes include thickening of the basement membrane, mucus hypersecretion, hypertrophy and hyperplasia of airway smooth muscle with inflammatory infiltration (Brightling et al., 2002; Huber and Koessler, 1922; James et al., 2012). Remodelling and mucus plugging of the airways can lead to more persistent, rather than variable, airflow obstruction with high symptom burden (Dunican et al., 2018). Epithelial dysfunction is the central driver of asthma pathogenesis – it is the source of alarmins which drive complex inflammatory networks within the asthmatic airways and responsible for increased susceptibility to viral infections due to impairment of anti-viral responses (Holgate, 2007; Wark et al., 2005).

Asthma had historically been described as allergic and non-allergic. Allergic asthma is often seen in childhood and driven by T helper (Th)-2 cells, following early life encounters with

environmental allergens such as house dust mite (HDM) but can occur following new exposures later in life (Hammad and Lambrecht, 2021). Non-allergic asthma on the other hand is usually late onset, with higher prevalence in women and in obesity (Pakkasela et al., 2020). It is often a difficult to treat phenotype with high symptoms burden and was further classified as Th2 or non-Th2.

However, this dichotomous classification has evolved over time into the use of endotypes, better accounting for the heterogeneity. An endotype is a subtype of a condition defined by a distinct pathophysiological mechanism (Lotvall et al., 2011), thus serving greater utility in predicting treatment response to therapies such as inhaled corticosteroids and novel biologics. In asthma a type-2 high and type-2 low endotype are described. Type-2 high disease is driven by eosinophilic inflammation and prototypic cytokines IL-4, IL-5 and IL-13, (Hammad and Lambrecht, 2021) with well validated biomarkers (blood eosinophil count and fraction of exhaled nitric oxide [FeNO]). Type-2 low disease is defined by the absence of type-2 immunopathology, it lacks biomarkers and is difficult to treat (Hinks et al., 2021b).

Key cell types and mechanisms involved in asthma are summarised below.

1.1.2.1 The airway epithelium in asthma and early interaction with innate immunity

The airway epithelial cell barrier undergoes disruption with loss of tight junctions and increased permeability in asthma, this damage correlates with disease severity (Papi et al., 2018). As part of the first line of defence, lung epithelial cells express a range of pattern recognition receptors (PRRs) which recognise exogenous highly conserved molecular structures derived from pathogenic organisms (pathogen-associated molecular patterns [PAMPs]) and endogenous damage associated molecular patterns (DAMPs) released by damage to tissue, inflammation and necrosis (Li and Wu, 2021). The epithelial cell PRR repertoire includes cell surface toll-like receptors (TLRs), C-type lectin receptors (CLRs),

protease activated receptors (PAR) and cytosolic DNA receptors such as retinoic acid-inducible gene (RIG)-I-like receptors (RLRs), and nucleotide-binding oligomerization domain (NOD)-like receptors (NLRs). Ligation of these TLRs, CLRs and PARs by allergen and viruses can induce the release of epithelial alarmins. In the airway the key alarmins are IL-25, IL-33 and thymic stromal lymphopoietin (TSLP) (Whetstone et al., 2022). These drive Th2 responses in murine models of eosinophilic asthma (Lambrecht et al., 2019). In human asthma IL-33 production by epithelial cells is increased, levels are elevated in blood and correlate with disease severity (Li et al., 2018). IL1RL1 which encodes the IL-33 receptor ST2, together with IL33 are important susceptibility loci for asthma (Moffatt et al., 2010). IL-25 and TSLP expression in also associated with disease severity and TSLP levels in bronchoalveolar lavage correlate with neutrophilic inflammation (Li et al., 2018).

Epithelial derived cytokines activate key immune cells to drive type-2 inflammatory responses in the lung. These include eosinophils, Th2 cells, mast cells, basophils, innate lymphoid cells (ILCs) and dendritic cells (DCs).

1.1.2.2 Key innate immune cells in asthma

Eosinophils are the key player of type-2 high asthma. IL-5 is responsible for their maturation in the bone marrow and egress during allergic inflammation, driving activation, proliferation and survival once eosinophils are in tissue (Lambrecht et al., 2019). In the lungs, eosinophils release cytotoxic granule proteins, type 2 cytokines and pro-inflammatory cytokines and chemokines (tumour necrosis factor [TNF]-α, IL-1β, IL-8)_alongside lipid mediators. Eosinophil cytotoxic granules and fibrogenic growth factors (e.g. transforming growth factor [TGF]-β) can cause lung remodelling (Canas et al., 2018), whereas broader inflammatory products are associated with BHR and goblet cell metaplasia (Kanda et al., 2020).

Mast cell infiltration of airway smooth muscle is unique to asthma and their density correlates with BHR (Brightling et al., 2002). They are the principal mediator of type-I hypersensitivity, and degranulate following cross-linkage of immunoglobulin (Ig)-E by allergens alongside release of other potent mediators (e.g. histamine) and *de novo* generation of lipid mediators driving allergic inflammation and bronchoconstriction (Marone et al., 2005).

Basophils are the smallest circulating population of granulocytes and are potent producers of IL-4 and IL-13. Their frequency in sputum is increased in eosinophilic asthma and in bronchial biopsies. They express the high affinity IgE receptor and have increased capacity for histamine release in asthma (Marone et al., 2005).

Neutrophils have been linked to corticosteroid resistant severe asthma with inflammasome activation (Rossios et al., 2018). Airway neutrophilia is often seen in the presence of pathogenic airway bacteria in asthma (Taylor et al., 2018). Neutrophils are the most abundant circulating leukocyte, they navigate to sites of infection and inflammation in response to chemokines (prototypically IL-8/CXCL8) released in response to PAMPS/DAMPS (Summers et al., 2010). They are responsible for microbial killing through phagocytosis with cytolytic killing and degranulation, releasing reactive oxygen species and proteolytic enzymes such as elastase. They also extrude neutrophil extracellular traps (NETs) which are a web-like structure of chromatin, histones and granule proteins to trap bacteria, but also contribute to airway pathology, mucus hyperviscosity and support biofilm production (Keir et al., 2021). In asthma, neutrophils upregulate serine proteases, increase NET formation and demonstrate enhanced chemotaxis but impaired phagocytosis and innate defences (including IFN production) (Crisford et al., 2021). Neutrophil elastase causes mucus gland hyperplasia and airway smooth muscle hyperplasia (Baines et al., 2011). They are numerically associated with a faster decline in FEV1 and diminished airflow reversibility (Boulet et al., 2003).

Macrophages play a diverse role in the innate immune system, they are involved in phagocytic killing of invading microorganisms, antigen presentation, shaping inflammatory responses and tissue homeostasis. They have been shown to acquire a pro-inflammatory M1 phenotype in response to stimulation (e.g. bacterial lipopolysaccharide [LPS]) or have a more antiparasitic/tissue resolution phenotype (M2) in response to type -2 cytokines, but *in vivo* studies show that there is more likely a spectrum of activation (Murray et al., 2014). Corticosteroids can reduce macrophage IL-1β production but in severe asthma phenotypes alveolar macrophages acquire resistance to this effect (Bhavsar et al., 2008) and show evidence of impaired phagocytosis (Ackland et al., 2022).

DCs are key antigen presenting cells of the immune system. There are two main classes of conventional DCs – cDC1 and cDC2, cDC2 cells are implicated in asthma (Guilliams et al., 2014). In murine models of allergic asthma, which have informed understanding of the early dynamics of type-2 responses, DCs are essential for establishment of eosinophilic airways inflammation in an IL-13 and type I IFN dependent mechanism (Webb et al., 2017). Complementary to this, in human airways the frequency of DCs increases following allergen inhalation (Dua et al., 2010; El-Gammal et al., 2016).

1.1.2.3 Key adaptive immune cells in asthma

The lungs house predominantly memory CD4+ and CD8+ T cell populations which persist in the tissue as tissue-resident memory cells (TRM), similarly to other barrier sites. These cells are transcriptionally distinct from circulating memory T cells and express CD69 (early activation marker and blocks cell egress) and CD103 (mediating binding to epithelial E-cadherin). The vast majority have an effector-memory phenotype. These include populations generated by exposure to respiratory pathogens and vaccination, providing host defence. Lung CD4 TRM cells generated in response to allergen challenge promote allergic inflammation in asthma (Snyder and Farber, 2019).

T cells are the main source of type-2 cytokines which induce inflammatory changes classically associated with asthma including eosinophilia (IL-5), goblet cell metaplasia (IL-4, IL-13) and bronchial hyperresponsiveness (IL-13) (Lambrecht et al., 2019). In type-2 high asthma, conventional Th2 cells were first recognised to drive eosinophilic inflammation and found in high abundance within bronchoalveolar lavage (BAL) fluid of asthmatic patients with allergic eosinophilic asthma (Robinson et al., 1992) and isolated from blood in patients with asthma IL. Transcriptionally Th2 cells in human asthma and murine models of allergic eosinophilic asthma are similar (Tibbitt et al., 2019) – producing prototypic cytokines and expressing the peroxisome proliferator activated receptor-(PPAR)-γ receptor which can in turn promote the expression of the IL-33 receptor on Th2 cells (Chen et al., 2017).

Other sources of type-2 cytokines include CD8+ Tc2 cells, type-2 innate lymphoid cells (ILC2) and Th9, IL-9 expressing pathogenic Th2 cells seen in response to allergen challenge in mouse(Koch et al., 2017) and human (Alladina et al., 2023). While CD8+ T cells can be protective in allergic disease with secretion of type 1 cytokines such as IL-12 and IFNɣ, they have the capacity to undergo transcriptional reprogramming into Tc2 cells, producing IL-13 and IL-5, and are enriched in peripheral blood and lungs in eosinophilic and non-eosinophilic asthma (Hilvering et al., 2018). These cells play an important role as they are abundant and relatively corticosteroid insensitive (Hinks et al., 2019). ILC2s express the transcription factor GATA-3 and produce IL-5, IL-9 and IL-13. They respond to IL-33, IL-25 and TSLP through proliferation and activation. In asthma their frequency is increased in BAL and blood following allergen challenge (Winkler et al., 2019). In murine models tissue resident CD4+ memory cells are a potent source of type-2 cytokines upon repeated allergen challenge (Hondowicz et al., 2016), whilst a similar population of memory cells exists in the lungs it is yet to be determined if this observation translates to human disease (Vieira Braga et al., 2019).

B cells are involved through their preferential production of IgE under the influence of IL-4 and IL-13. In asthma IgG positive memory B cells class switch to IgE production, transitioning into plasma cells (Hoof et al., 2020). IgE binds to its high affinity receptor (FcεRI) expressed by basophils, mast cells, eosinophils, DCs, epithelium, smooth muscle and endothelium. Allergen induced cross-linkage of mast cells and basophils results in release of pre-formed mediator such as histamine and proteases (tryptase, chymase), production of lipid mediators (cysteinyl leukotrienes and prostaglandin D2) and type-2 cytokines. The downstream effects of this are bronchial hyperresponsiveness and increased expression of adhesion molecules promoting the transmigration of eosinophils and other inflammatory cells into the lung (Hammad and Lambrecht, 2021). IgE can also facilitate allergen presentation to memory Th2 cells perpetuating a cycle of allergen specific-IgE production by B cells (Hammad and Lambrecht, 2021).

1.1.2.4 T2 low asthma

In contrast to type-2 high disease, type-2 low asthma is defined by the absence of type-2 cytokines, and clinical biomarkers of eosinophilic inflammation. It has limited treatment options and carries significant morbidity (Hinks et al., 2021b). T2-low asthma encompasses neutrophilic and paucigranulocytic disease and is characteristically insensitive to corticosteroid. It tends to be more severe and associated with later onset, female sex, obesity and absence of atopy (Haldar and Pavord, 2007) alongside smoking and occupational exposures (Anees et al., 2002). Less is known about its mechanisms compared to type-2 high disease, but it is known to occur with airway neutrophilia and inflammasome activation (Rossios et al., 2018) and elevated airway IL-6 levels (Li et al., 2020) and oxidative stress (Singhania et al., 2018). Transcriptomics of airways samples in neutrophilic asthma show neutrophil chemoattractant (CXCL8), IL-17 inducible chemokines and mucins, accompanied by a gene signature suggestive of antibacterial response (CD14, TLR2) (Singhania et al., 2018). This and metagenomic studies in asthma demonstrating neutrophilia in presence of airway pathogens (Green et al., 2014; Taylor et al., 2018)

suggest a link to airway bacteria, which could in turn induce Th17 cells to produce IL-17 (Zhao et al., 2013). Tissue damage induced by insults such as oxidants and pathogens (bacteria, virus) can stimulate the release of alarmins from the epithelium, and may account for the benefit seen with anti-TSLP in non-eosinophilic asthma (Corren et al., 2017).

1.1.2.5 Use single cell transcriptomics in asthma research

Corticosteroid resistant phenotypes of asthma, such as T2 low asthma represents a significant unmet clinical need. Murine models have limitations in asthma, but have informed understanding of the dynamics of type-2 inflammation and aided translation to human studies. A similar perspective has not been available for type-2 low disease (Hammad and Lambrecht, 2021). Given the heterogeneity of asthma phenotypes, single cell sequencing can offer unique insights by capturing cellular heterogeneity and rare cell populations, particularly through the addition of cell surface protein and T cell receptor profiling. The potential to integrate with spatial technologies is a significant advantage when studying diseases affecting the airway and to better understand cell-cell interactions (Gomes et al., 2019). The publication of the Human Lung Cell Atlas as a critical reference (Sikkema et al., 2023; Vieira Braga et al., 2019) has been a positive step in the field. A recent study has applied this approach in a human model of allergen induced asthma to provide new insight into Th2 cells/mononuclear phagocytes/basal cells in driving inflammatory networks which could promote airway remodelling (Alladina et al., 2023). No similar studies have been performed in more severe non-allergic asthma phenotypes where our understanding of mechanisms is poor. This is a gap in the field and needs to be addressed with carefully phenotyped patient cohorts to best understand underlying mechanisms.

1.1.3 Heterogeneity of asthma and treatable traits

Asthma is clinically heterogenous. The concept of treatable traits was devised to provide more personalised care in airways disease, as a positive move forward from more restrictive step wise treatment guidelines. Patients are assessed for specific treatable traits which can be easily identified and treated with a targeted therapy (Pavord et al., 2018). These traits can be broadly classified into pulmonary, extrapulmonary and behavioural/lifestyle related. Treatable traits and broader principles use for clinical phenotyping are summarised in Figure 1.1 (McDonald et al., 2019). Blood eosinophilia is a pulmonary treatable trait which has been very successfully applied in clinical practice. It is predictive of asthma attacks, lung function decline and response to inhaled corticosteroids. It has also shown success in clinical trials as a predictor of response to anti-IL-5 (mepolizumab) and anti-IL5 receptor α (IL-5Rα) monoclonal antibody therapy. The licencing criteria are therefore based on blood eosinophil count. The approach has been a simple and effective one – identify the treatable trait (eosinophilia) and treat it with a targeted therapy (biologic). It has been extended to other novel biologics alongside fractional exhaled nitric oxide (FeNO) which is a measure of IL-4 and IL-13 mediated induction of inducible nitric oxide synthase (iNOS) in the airway epithelium, making it a highly specific non-invasive biomarker of type-2 inflammation, predicting treatment response to anti-IL-4RA/IL-13 (dupilumab) and anti-TSLP (tezepelumab). Overall the approach has introduced greater precision and can avoid potentially harmful use of oral corticosteroid in biomarker low patients (Melhorn et al., 2022).

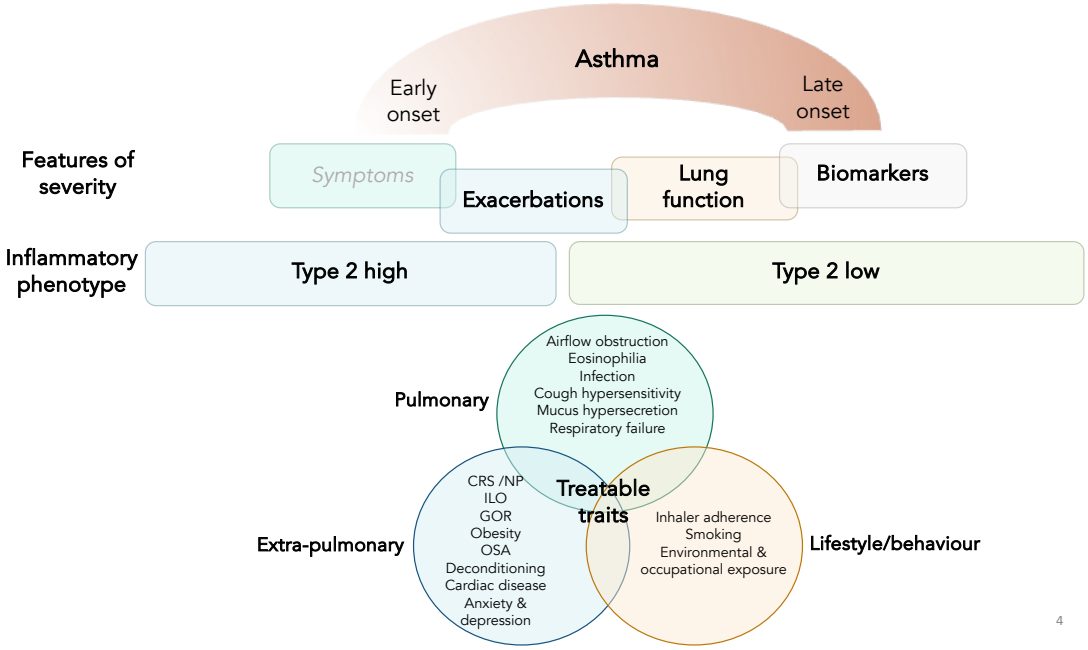


Figure 1.1 Schematic concept diagram of asthma.

Adapted from Wenzel 2012 (DOI: https://doi.org/10.1038/nm.2678). The clinical features, inflammatory phenotype and treatable traits together have been an informative and more personalised approach to delivering patient care

1.1.4 Inflammatory biomarkers in severe asthma

Sputum differential cell counts were first introduced as a biomarker of airways inflammation but lacked wider application due to the need for skilled interpretation – its use is largely restricted to research (Simpson et al., 2010). As described above, blood eosinophil count has proven highly accessible and successful for identification of patient at high risk of severe exacerbations. FeNO is also promising as a non-invasive biomarker, particularly given its utility as a measure of corticosteroid sensitivity by suppression in FeNO levels which helps to identity poor adherence and also a more resistant inflammatory type-2 high phenotype as described below (Heaney et al., 2018).

1.1.4.1 'Magnet and bomb' theory

The 'bomb' (blood eosinophil) and 'magnet' (FeNO) concept (Couillard et al., 2022b) was developed in our group following a number of observations from clinical trials and growing

recognition of how blood eosinophils and FeNO, both biomarkers of type-2 inflammation, identify different aspects of type-2 biology. Post-hoc analyses of the phase 2b DREAM study of mepolizumab (anti-IL-5) (Shrimanker et al., 2019), and phase 3 study Liberty Asthma QUEST of dupilumab (anti-IL-4Rα) (Busse et al., 2021) in moderate to severe asthma both found that high baseline FeNO in combination with an elevated blood eosinophil count was most strongly predictive of risk of severe asthma exacerbations. Extending on from this observation, a cross-sectional analysis was performed of serum and sputum type-2 inflammatory mediators which demonstrated a strong correlation between FeNO and sputum eosinophil count, IL-4, IL-5, IL-13, TSLP, eotaxin-3 and thymus activation–regulated cytokine (TARC), together with risk of asthma attacks in the preceding year. In contrast blood eosinophil count correlated with serum IL-5, but not airway mediators (Couillard et al., 2021).

FeNO suppression testing provides a convenient means of identifying treatment non-adherence and studying corticosteroid resistant disease. It looks for a reduction in FeNO following a period of monitored inhaled corticosteroid therapy to objectively demonstrate treatment adherence. Its wider use in clinical studies has identified that approximately a third of patients with severe eosinophilic asthma have a corticosteroid resistant elevation of FeNO despite proven adherence (Heaney et al., 2018). FeNO non-suppression is associated with elevated sputum eosinophils and IL-4, IL-33, TSLP, eotaxin-3, TARC and frequency of exacerbations. Blood eosinophil count in this group correlated positively with serum IL-5.

Thus, FeNO appears reflective of active type-2 inflammation and chemotactic pull to the airway (‘magnet’) and blood eosinophils correlate to the size of the circulating pool of cells and IL-5 (‘bomb’). Clinically these findings could offer greater personalisation of biologic therapies based on biomarker profile – considering biologics relevant to airway mucosal

targets such as anti-TSLP (tezepelumab) or anti-IL4Rα (dupilumab) in presence of high FeNO. Blood eosinophil count has already been used to target anti-IL-5 therapy in this way.

An important unanswered question is why the type-2 inflammatory signal remains switched on in this subset of patients. Understanding the underlying mechanisms would allow novel approaches to treatment to be considered and offer insights into other corticosteroid resistant phenotypes of asthma such as severe neutrophilic disease which is associated with low FeNO.

1.2 The Respiratory Microbiome

The lungs, once thought to be a sterile environment, are now known to house a community of microorganisms including bacteria, viruses, archaea and fungi. Their collective genomes make up the respiratory microbiome, which has been increasingly profiled over the last ~15 years with application of culture independent sequencing technologies. At mucosal barrier sites, including the airways, these microbes alongside their local microenvironment play a critical role in the development and regulation of the immune system. The total surface area of the airways is approximately 70m^2 making it the second largest barrier site after the gut mucosa in human (Man et al., 2017), however the lung microbiome is distinctly lower in biomass (Man et al., 2017) which can present challenges to the design and interpretation of metagenomic studies.

The majority of early studies utilised 16S rRNA sequencing, often supplemented with PCR to achieve species level discrimination where sequencing was restricted to genus level (Green et al., 2014; Simpson et al., 2016). The prokaryotic 16S rRNA gene is ~1500bp in length with nine hypervariable regions which are interspersed between conserved regions. The traditional workflow for 16S amplicon sequencing utilises primers to amplify the hypervariable regions prior to sequencing, clustering sequences based on similarity into

operational taxonomic units (OTUs) and mapping representative OTU sequences to publicly available taxonomic databases for phylogenetic classification (Johnson et al., 2019; Weisburg et al., 1991). However, OTU assignment relies on the assumption of sequence similarity above a threshold representing the same genus or species (typically 97%) (Johnson et al., 2019), Whilst it is an accessible and low-cost method, using a single marker gene to capture microbial diversity is limiting (Rossello-Mora and Amann, 2001), particularly given differences generated by use of distinct variable regions (Abellan-Schneyder et al., 2021). Recent studies have however shown that sequencing the entire 16S gene is superior for taxonomic resolution to species level (Johnson et al., 2019).

An alternative approach, which followed 16S sequencing, is shotgun metagenomic sequencing – an untargeted sequencing of all microbial genomes within a sample. This can allow simultaneous detection of bacterial, viral, archaea and fungal genetic material and thus functional inferences to be made about constituent organisms (Quince et al., 2017). The main drawbacks of this technique are cost, high levels of host DNA which can overwhelm the microbial signal particularly in low biomass samples, requiring appropriate experimental considerations, and need for more complex bioinformatic analysis pipelines (Dulanto Chiang and Dekker, 2020; Quince et al., 2017).

With the evolution of next generation sequencing technologies, alongside short-read sequencing (e.g. Illumina sequencing technologies), newer long read methods (e.g. Oxford Nanopore Sequencing, with read lengths) have emerged for metagenomic sequencing. A key benefit of long read sequencing in metagenomic profiling is the capture of longer continuous reads to aid taxonomic calling and functional inferences from the microbial genome (Chapman et al., 2023), and whilst relatively higher per base error rates had previously been considered a limiting factor in methods such as Nanopore (Zhang et al., 2023), there have been significant improvements with technological advancement (Sereika et al., 2022; Zhang et al., 2023).

16S based microbiome studies widely apply measures derived from ecology including alpha and beta diversity indices. The alpha diversity describes richness (number of species) or evenness (distribution of species) within a sample and is reported using several different metrics. The most common is the Shannon diversity index, accounting for both richness and evenness. Beta diversity compares the similarity of two or more communities using different statistical approaches, which can account for the contribution of rare species (Campbell et al., 2022). Given their origin, the assumptions applied by these metrics are not always directly applicable to microbiome data (Cassol et al., 2025), and there is potential for diversity to be overestimated with 16S amplicon sequencing in low biomass samples (Caruso et al., 2019). The term dysbiosis is often applied when there is a compositional shift from the constituents of the healthy microbiome. This can be associated with adverse immune responses, tissue remodelling and clinical features (Green et al., 2014; Simpson et al., 2016). In asthma, as discussed below, it is the identification of specific potentially pathogenic species dominating the microbiome have offered greater potential for clinical translation rather than compositional dynamics.

1.2.1 Respiratory microbiome in health

The composition of the microbiome is anatomically segregated in the upper (anterior nares, nasal passages, paranasal sinuses, pharynx, and supraglottic portion of the larynx) and lower (subglottic portion of the larynx, trachea and lungs) tracts with differing epithelial cell lining and exposure to environmental factors (Man et al., 2017). The upper tract has relatively higher biomass; in the nasopharynx the dominant taxa include skin colonizers *Staphylococcus*, *Propionibacterium* and *Corynebacterium* (Oh et al., 2014) alongside *Moraxella*, *Dolosigranulum*, *Haemophilus* and *Streptococcus* (Frank et al., 2010; Zhou et al., 2014) whereas the oropharynx is abundant in *Streptococcus*, *Neisseria*, *Rothia*, and

anaerobes, including *Veillonella*, *Prevotella* and *Leptotrichia* species (Charlson et al., 2010; de Steenhuijsen Piters et al., 2016; Segata et al., 2012; Stearns et al., 2015).

In the lower airway the most abundant phyla are *Bacteroidota (previously named Bacteroidetes)* and *Bacillota* (previously named *Firmicutes)*, with prominent genera including *Prevotella*, *Veillonella* and *Streptococcus* (Morris et al., 2013; Segal et al., 2013). The microbiota of the lung most closely resembles the oropharynx, with greatest overlap seen in the right upper lobe (Bassis et al., 2015; Venkataraman et al., 2015). Bronchoscopic sampling has shown relative uniformity across intrapulmonary sites in healthy individuals (Dickson et al., 2015) in contrast to those with advanced lung disease in whom microbiota can vary significantly within the lung suggesting that local conditions are more relevant in sustaining microbial growth in this setting (Erb-Downward et al., 2011; Goddard et al., 2012; Willner et al., 2012). In health, bacterial load and community membership of the lung microbiome is thought to be determined by a balance between immigration and elimination (Dickson et al., 2015; Dickson et al., 2014). Microbial elimination is a continuous process achieved through propulsion by the mucociliary escalator and coughing, and a range of local innate and adaptive immune mechanisms (Dickson et al., 2016). Combined metagenomic and metatranscriptomic studies detecting microbial DNA and RNA, respectively, have demonstrated metabolically viable oral commensals in the lower airway given RNA is rapidly degraded following cell lysis and thus its presence suggestive of survival after likely aspiration events (Sulaiman et al., 2021).

Subclinical microaspiration, which occurs commonly in health (Gleeson et al., 1997; Huxley et al., 1978), is the primary route of immigration although direct dispersion along mucosal surfaces and inhalation cannot be ruled out (Dickson et al., 2015). The community richness and biomass (Charlson et al., 2011) declines in the lung with increasing distance from the upper respiratory tract, the proposed source (Dickson et al., 2015).

Despite clearance of bacteria following microaspiration, murine models have demonstrated the potential for longer term immune modulation following exposure to oral commensals. In an aspiration model, oral commensals *Prevotella melaninogenica, Veillonella parvula* and *Streptococcus mitis* activated CD4+ and CD8+ T cells, recruited IL-17 producing T helper 17 (Th17) and γδT cells (in a MyD88 dependent manner) and increased the frequency of T regulatory (Treg) cells (Wu et al., 2021). In a healthy human study, BAL enrichment of *Prevotella, Rothia* and *Veillonella* was shown to correlate with Th17 cells, their associated cytokines (IL-1α, IL-1β, IL-6, fractalkine and IL-17) and neutrophil frequency. Epithelial cells were transcriptomically distinct and alveolar macrophages had relatively blunted *ex vivo* TLR4 responses compared to those without this pattern of commensal enrichment (Segal et al., 2016). *Prevotella spp*. are Gram-negative organisms but unlike pathogenic *Pseudomonadota* (previously named *Proteobacteria*) implicated in respiratory infection, their signalling via TLR2 induces limited neutrophilic inflammation and no lung pathology, likely due to differences in LPS structure (Larsen et al., 2015). Activation of pattern recognition receptors can stimulate microbiota shaping antimicrobial peptide release by Th17 cells (Kao et al., 2004), which themselves are induced by commensal species (Atarashi et al., 2015). Taken together these studies suggest that the microbiome can determine immune phenotype. Broadly, the respiratory microbiome has been implicated in shaping mucosal immunity early in life and participates in immune tolerance.

1.2.2 Early life microbiome and asthma

A multitude of host and environmental factors have been linked to the risk of wheeze and asthma in childhood. There is a complex interplay between genetic susceptibility, viral infections (mainly human rhinovirus [HRV] and respiratory syncytial virus [RSV]) and atopic sensitisation, alongside environmental exposures which by extension influence the lung and gut microbiome and early immune function (Pijnenburg et al., 2022). Exposures in the first few hours, including mode of delivery, and subsequent environment in the following 4-

5 months shape the respiratory microbiome (Arrieta et al., 2015; Biesbroek et al., 2014; Teo et al., 2015). Due to challenges of lower airway sampling with bronchoscopy in children most microbiome studies sample the upper airway, which is not entirely reflective of the lungs (Kloepfer et al., 2018). In paediatric healthy and chronic lung disease populations, *Streptococcus* is present in both the upper and lower airway, but *Corynebacterium, Staphylococcus, Alloiococcus, Haemophilus*, and *Moraxella* appear prevalent in the upper airway (Teo et al., 2015), compared to *Veillonella* and *Prevotella* in the lower airway (Marsh et al., 2016). Combined oropharyngeal and nasopharyngeal microbiomes show greater overlap with bronchoalveolar lavage sampling, than each compared independently (Marsh et al., 2016).

Microbiomes shape and are shaped by local and systemic immune function. Several birth cohort studies have demonstrated that airway (Teo et al., 2015) and gut microbiome (Durack et al., 2018b; Lee-Sarwar et al., 2023) disruption, with loss of diversity, in the earliest stages of life are characteristic in childhood atopy and asthma. In industrialised societies, phylogenetic differences in indoor dust microbiome (particularly *Lactococcus* enrichment) (Karvonen et al., 2019) and lower environmental endotoxin exposure (Lynch et al., 2014; Stein et al., 2016) are linked to asthma development, the latter shown to shape innate immune signalling.

The seminal study by Bisgaard *et al.* (Bisgaard et al., 2007) was one of the first prospectively linking airway colonisation with potentially pathogenic bacterial organisms and risk of recurrent wheeze and asthma in early life in the Copenhagen Prospective Studies on Asthma in Childhood (COPSAC) cohort. Hypopharyngeal sample culture from neonates with maternal asthma identified colonisation with *M. catarrhalis*, *H. influenzae, S. pneumonia* or a combination of these organisms, but not *S. aureus*, increased the risk of early persistent wheeze and asthma at 5 years of age. Moreover, this was associated with frequency of lower respiratory tract infections, bronchodilator responsiveness, elevated

blood eosinophil count and total IgE (Bisgaard et al., 2007). Within this cohort acute wheezy episodes were also linked to bacterial infections, separately to viral infections, suggesting that bacteria could independently contribute to the burden of childhood wheeze (Bisgaard et al., 2010). *M. catarrhalis* and *H. influenzae* colonisation had a stronger association with development of asthma and in keeping with this, examination of the airway mucosal lining fluid showed elevated Th1/Th17 (IL-1β, TNFα, MIP-1β, IL-17, IL-8) and Th2 cytokines (IL-5, IL-4, IL-13) versus non-colonised controls (Folsgaard et al., 2013). Follow-up at 18 years, and replication in a secondary cohort using culture and 16S sequencing, demonstrated neonatal airway colonisation produced a 4-fold increase in persistent wheeze or asthma up to the age of 7 years only, with an increase in exacerbation frequency. Interestingly there was no association with lung function, FeNO or allergic sensitisation up to 18 years of age (Sunde et al., 2024).

A subsequent study, characterising the developmental trajectories of the nasopharyngeal microbiome with 16S sequencing and PCR revealed dominance of *Staphylococcus* in the first 6 months was related to childhood asthma risk, alongside detection of rhinovirus and *Moraxella* abundance in the setting of acute wheezing illness (Tang et al., 2021). Nasal *S. aureus* colonisation is not associated with asthma outcomes in adults (Davis et al., 2015). High abundance of *Moraxella* and *Corynebacterium/Dolosigranulum* in the nasopharynx has been reported to be predictive of compositional stability, positively associated with breastfeeding in early life and lower rates of parent-reported respiratory infections, whilst less stable profiles have high abundance of *Haemophilus* or *Streptococcus* (Biesbroek et al., 2014). Interestingly, microbiome shift towards dominance of potentially pathogenic bacterial genera precedes detection of viral pathogens, accounting for >80% of infectious events, or symptoms. In sensitised children this sequence of events is associated with persistent wheeze and asthma, yet in non-sensitised children it causes transient wheeze resolving by 3 years of age (Teo et al., 2018).

This thesis focuses on the airway microbiome and whilst a full description of the gut microbiome and gut-lung-axis is beyond the scope, it is worth considering a few salient findings. The gut microbiome develops in utero (Stokholm et al., 2018) and grows in diversity over the first few years of life. Its composition is influenced by maternal microbiome (Mueller et al., 2015), mode of delivery (Shao et al., 2019), exposure to smoking and pets, siblings, breastfeeding and environment (Arrieta et al., 2015; de Steenhuijsen Piters et al., 2016). Preserving microbial diversity in the first year provides protection against allergic sensitisation (Bisgaard et al., 2011). The mechanism of communication in the gut-lung axis has not been fully elucidated but is partly mediated by bacterial metabolites exerting immune responses remotely (Roduit et al., 2019). Animal models have demonstrated bidirectional interactions (Liu et al., 2017; Looft and Allen, 2012; Madan et al., 2012). Furthermore, antibiotic administration altering the gut microbiome in early life is linked to asthma (Metsala et al., 2015; Patrick et al., 2020). Children at highest risk of developing asthma, with wheeze at 1 year of age, have reduced gut *Faecalibacterium, Lachnospira, Rothia,* and *Veillonella* by 3 months of age (Arrieta et al., 2015). This coincides with reduced small chain fatty acid production, which can act as substrate for host cells and as a signalling molecule. In a germ-free asthma model deficiency of these commensals has been shown to drive sustained type-I inflammatory responses (Arrieta et al., 2015). Moreover, the pattern of dysbiosis seen in childhood asthma and atopy can promote T2 immunity with depletion of Treg cells (Fujimura et al., 2016).

Taken together, these data suggest that potentially pathogenic organisms in the airway can influence the development of asthma in early life by skewing immune responses. Their presence in the upper airway is of particular relevance in a paediatric population given interaction with viral infections, whereby bacterial colonisation can promote acquisition of virus and conversely viral infection can favour a pathogen dominant microbiome. The lower airway microbiome cannot be directly extrapolated from the nasopharynx which is the

commonest site of sampling in paediatric populations. The gut-lung axis is further implicated in overall risk of asthma.

1.2.3 The microbiome in adult asthma

From the breadth of microbiome studies in asthma, profiling varied disease severity and clinical phenotypes, a few key findings have emerged. The first linking an altered microbiome in childhood to atopic asthma, as elaborated above. In adult asthma it has been the recognition of loss of microbial diversity in severe, treatment refractory asthma driven by a very limited repertoire of potentially pathogenic bacterial species, predictive of treatment response to macrolides and offering an opportunity to leverage metagenomics for targeted therapy instead of ecological descriptions alone. Common limitations of early studies were use of sequencing approaches unable to perform species level discrimination, variations in clinical phenotyping criteria and small sample size (Diver et al., 2020; Durack et al., 2017; Goleva et al., 2013; Simpson et al., 2016).

Hilty *et al.* were first to dispel the view of lung sterility with 16s rRNA sequencing and described the microbiome in asthma using endobronchial brushings (Hilty et al., 2010). This and subsequent studies, extended to BAL and sputum samples, reported *Pseudomonadota* enrichment particularly *Haemophilus, Moraxella* and *Neisseria spp.* (Green et al., 2014; Hilty et al., 2010; Huang et al., 2015), with relative depletion of airway commensals *Veillonella* and *Prevotella* in mild/moderate and severe asthma (Taylor et al., 2018). Sampling method influences community composition, the greatest similarity is seen between endobronchial brush and induced sputum, despite relative enrichment of oral bacteria in the latter (Durack et al., 2018a), it remains superior to nasal brush or oral wash for lower airway microbiome studies.

Clinical features including the extent of airflow obstruction (Denner et al., 2016), bronchial hyper-responsiveness (Huang et al., 2011) and presence of atopy (Durack et al., 2017) in mild-to-moderate disease have been linked to changes in the microbiome. The α-diversity correlates inversely with FEV1, corticosteroid use and BAL eosinophils (Denner 2016). Airway hyperresponsiveness (measured by methacholine PC20 concentration) also inversely correlates with α-diversity and is associated with *Pseudomonadota* (syn. *Proteobacterial*) enrichment on endobronchial brushing (Huang et al., 2011). Early studies had conflicting reports of reduced α-diversity in asthma compared to health (Huang et al., 2011) alongside reduced abundance of *Bacillota*, *Bacteroidota* and *Actinomycetota* (previously named *Actinobacteria*) in BAL (Denner et al., 2016).

In severe asthma, microbiome composition has been linked to symptom burden (ACQ) and sputum total leukocyte count (predominantly *Pseudomonadota*), alongside high body mass index (*Bacteroidota/Bacillota*) (Huang et al., 2015). Applying an unsupervised clustering approach on sputum microbiome, two distinct microbial clusters have been described. The more severe cluster demonstrated poor lung function, airway or sputum neutrophilia, and refractory disease requiring add-on therapy which was linked to decreased microbial richness and diversity. Specifically, there was reduction in *Veillonella*, *Prevotella*, *Rothia* and *Neisseria*, with concurrent increase in *H. influenza*, *M. cararrhalis* and *S. pseudopneumoniae*. The microbiome was found to be stable in all groups at 18 months follow-up (Abdel-Aziz et al., 2021). Sputum neutrophil count is the strongest predictor of microbiome composition in severe uncontrolled asthma (Moore et al., 2014). This often overlaps with longer disease duration and more severe airflow obstruction (Diver et al., 2022). When compared by sputum inflammatory phenotype, neutrophilic asthma has the most distinctively altered microbiome with low microbial diversity, higher frequency of *Haemophilus* and *Moraxella*, and reduced *Streptococcus*, *Gemella* and *Porphyromonas* taxa (Taylor et al., 2018). In contrast, *Streptococcus*, *Neisseria* and *Gemella* taxa positively correlated with eosinophil percentage, in addition *Pseudomonadota* was shown to

negatively correlate with biopsy eosinophil count (Huang et al., 2015). However, *Tropheryma whipplei* has been reported at higher frequency in eosinophilic asthma (Simpson et al., 2016). Overall, across disease severity, type-2 high eosinophilic inflammation has been linked to lower total bacterial load (Durack et al., 2020; Huang et al., 2015) and greater α-diversity (Sverrild et al., 2017; Taylor et al., 2018). Consistent with this, high FeNO has been associated with low *Pseudomonadota* abundance, and absence of *H. influenzae* (Diver et al., 2022).

There has been growing interest in how the microbiome may interact with resident viruses (virome) and fungi (mycobiome), both of which are compositionally altered in asthma (Choi et al., 2021; van Woerden et al., 2013). The virome in asthma is composed mainly of Herpes viruses and their abundance negatively correlates with symptom burden and airway obstruction (Choi et al., 2021). The mycobiome has been shown to vary by type-2 status – with lower fungal diversity present in type-2 high disease with dominant organisms including Aspergillus, Alternaria and Wallemia (van Woerden et al., 2013). ICS treatment can also increase fungal burden, including Aspergillus (Fraczek et al., 2018).

1.2.4 Potentially pathogenic bacterial species in severe asthma

An emergent, replicated and highly clinically relevant finding in metagenomic studies in adult asthma, particularly in presence of severe disease, is the dominance by specific airway pathogens, often reported as positive PCR findings. *H. influenzae* is by far the most frequently isolated pathogen in the lower airway (Diver et al., 2020; Jabeen et al., 2022; Simpson et al., 2016), followed by *S. pneumonia* and *M. catarrhalis*. This is linked to commensal depletion (namely, *Streptococcus, Gemella*, and *Porphyromonas* taxa) (Taylor et al., 2018), neutrophilic inflammation and poor asthma outcomes (Abdel-Aziz et al., 2021).

1.2.5 Haemophilus influenzae in airways disease

H. influenzae is a Gram-negative coccobacillus, classified into typeable (type a to f) or non-typeable strains based on the presence of a polysaccharide capsule. It commonly resides as a nasal commensal, particularly in children (Bogaert et al., 2011; Lemon et al., 2010) with 44% colonised by the age of 2 years (Faden et al., 1995). It is also a pathogen of the lower airway and implicated in invasive infection including meningitis and sepsis, at the extremes of age and in immunocompromised populations. Whilst there has been a dramatic and sustained decline in invasive disease caused by capsulate strains after introduction of the *H. influenzae* type b conjugate vaccine (Gessner and Adegbola, 2008; Singleton et al., 1994), the prevalence related to non-typeable strains (NTHi) has risen and is associated with a case fatality ratio of 12-22% (Van Eldere et al., 2014). NTHi remains the commonest bacterial cause of upper and lower respiratory tract infections in paediatric and adult populations, causing exacerbations of asthma and chronic obstructive pulmonary disease (COPD), chronic infection in cystic fibrosis (CF) lung disease, bacterial sinusitis, bronchitis and pneumonia (Van Eldere et al., 2014).

The acquisition of NTHi is facilitated by changes to the epithelium, and goblet cell hyperplasia as a consequence of mucin (MUC5AC) upregulation in the asthmatic airway (Man et al., 2017) causing bronchostasis and providing a favourable microenvironment for colonisation. Corticosteroid therapy, exposure to cigarette smoke and viral infections suppress airway mucosal defences in this context producing a permissive environment for colonisation (Brown et al., 2022; Hinks et al., 2016a). This is compounded by NTHi induced MUC5AC transcription via p38 mitogen activated protein kinase (MAPK) activation (Wang et al., 2002), NFκB dependent MUC2 mucin transcription and impairment of ciliary function (Bailey et al., 2012; Denny, 1974; Johnson and Inzana, 1986). The airway epithelium shows loss of integrity and barrier dysfunction (Kaufhold et al., 2017) with reduced expression of the tight junction protein E-cadherin *in vitro* (Kaufhold et al., 2017).

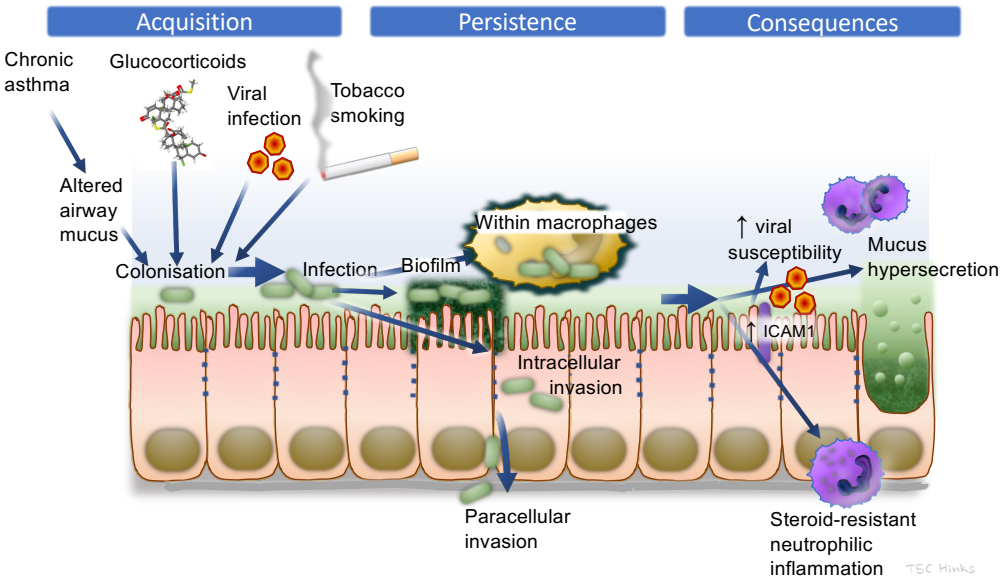


Figure 1.2 The role of NTHi in neutrophilic airway inflammation.

Reproduced with permission from TSC Hinks (doi: 10.1183/16000617.0008-2022) Viral infection and tobacco smoke lead to neutrophilic inflammation and impaired mucocilliary clearance. ICS delays neutrophil apoptosis and suppress anti-bacterial responses. NTHi can persist within macrophages, biofilms, airway epithelial cells or via paracellular invasion through the epithelium. Persistent infection leads to susceptibility to respiratory viruses, mucus hypersecretion and steroid-resistant neutrophilic inflammation. ICAM1, intracellular cell adhesion molecule 1; NTHi, non-typeable Haemophilus influenzae.

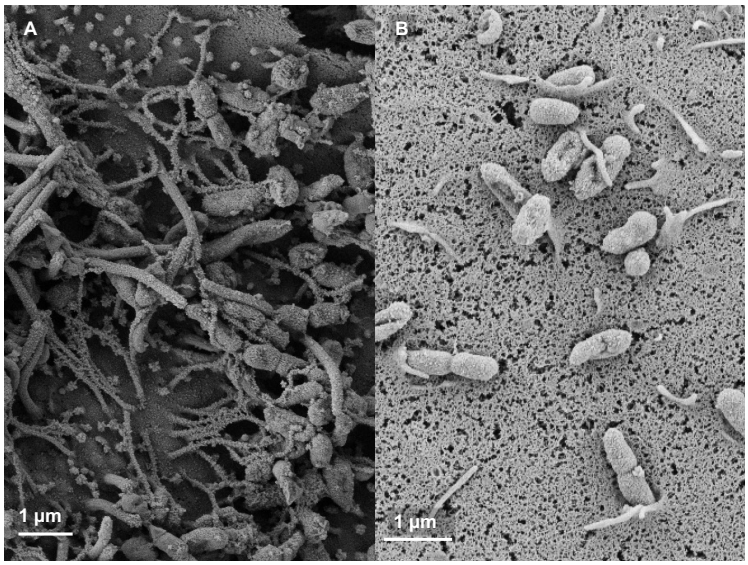


Figure 1.3 NTHi adheres to and invades primary bronchial epithelial cells.

Primary bronchial epithelial cells grown in air-liquid interface; (A) scanning electron micrograph 21,900 x magnification, multiplicity of infection (MOI) 200. NTHi being internalised by epithelial cells; (B)18,900 x magnification, MOI 20. Images: M Jabeen (produced during my NIHR ACF)

Once acquired, NTHi can utilise several mechanisms to persist within the airway including biofilm formation and facultative survival in host cells following internalisation, allowing evasion of humoral immunity and extracellular pathogen removal. Due to enormous strain and outer membrane protein variation, NTHi can gain entry through varied mechanisms (Clementi and Murphy, 2011) including receptor mediated endocytosis (Ahren et al., 2001), and requires microtubule assembly, lipid raft integrity and PI3K signalling in human epithelial cells where it has been located in a metabolically active, non-replicate state within an endosome like acidified subcellular compartment (Morey et al., 2011). It survives in macrophages (Ahren et al., 2001), undergoing transcriptomic reprogramming of metabolic pathways in response to availability of host substrates (Ackland et al., 2021; Baddal et al., 2015) and resists macrophage mediated killing (Craig et al., 2001). In longitudinal COPD patient cohorts, isolation of the same NTHi strain before and after prolonged periods of negative sputum culture have been proposed as potential evidence of persistence within an individual (Pettigrew et al., 2018), with persistent strains also reported to vary virulence functions over time (Murphy et al., 2004).

NTHi elicits a broad inflammatory response dominated by the IL-1 family of cytokines driven through inflammasome activation, specifically NLR family pyrin domain containing 3 (NLRP3) (Rotta Detto Loria et al., 2013). Inflammasomes are intracellular multiprotein complexes composed of a sensor protein, adaptor and pro-caspase-1, responding to PAMPs and DAMPs. The canonical inflammasomes (NLRP1, NLRC4 and absent in melanoma 2 (AIM2)) are a platform for pro-caspase-1 engagement, oligomerisation and proteolytic activation into active caspase-1, which processes IL-1β and IL-18 into their active forms (Li et al., 2021). IL-1β, CXCL2, CXCL8 and TNFα secretion are also stimulated through MAPK and NFκB signalling following TLR engagement, predominantly by macrophages and epithelial cells (Shuto et al., 2001). Repeated exposure to aerosolised NTHi lysate in a murine model has been shown to induce airways infiltration of macrophages, CD8 T cells and B cells and collagen deposition (Moghaddam et al., 2008).

The NLRP3 and AIM2 inflammasome complexes are activated in human alveolar macrophages (Brown et al., 2022), but in the presence of chronic airways inflammation, as in COPD, they show diminished cytokine responses (Berenson et al., 2006). In severe asthma there is evidence of NTHi persistence within pulmonary macrophages, type 17 inflammatory responses and airways neutrophilia (Ackland et al., 2022). These inflammatory signals drive neutrophil recruitment and NETs (Keir et al., 2021). In the airways, NTHi induced NETs have been proposed to amplify inflammatory response through IL-6 trans-signalling (IL-6TS) whereby cells interact with IL-6 bound to a soluble form of the receptor (sIL-6R) which engages with the cell membrane signal transducer gp130 leading to activation of Janus kinases and pro-inflammatory signalling (Keir and Chalmers, 2021). In COPD, high airway *Haemophilus* load has been reported in presence of high IL-6TS profiles in the sputum (sIL-6R, IL06, IL-1β, IL-8), with high matrix metalloproteinases and sputum neutrophilia (Winslow et al., 2021). In asthma, elevated serum IL-6 correlates with higher ICS dose, poor lung function, blood neutrophils and eosinophils (Ilmarinen et al., 2016).

Viruses are the major cause of exacerbations in airways diseases, with rhinovirus (RV) accounting for 60% of viral exacerbations (Kelly and Busse, 2008). There are bidirectional interactions between NTHi and respiratory viruses. *In vitro* exposure of primary bronchial epithelial cells to NTHi upregulate expression of ICAM-1, the receptor for major group RV, with subsequent increased viral replication and release of infectious particles (Gulraiz et al., 2015). Conversely, in a murine model, RV infection delayed clearance of secondary bacterial infection with NTHi, with suppression of chemokines (KC/CXCL1, MIP-2/CXCL2) and neutrophil recruitment, with similar attenuation of CXCL8 within *in vitro* epithelial cell models. The proposed mechanism underlying this is IRAK-1 (adapter protein in MyD88 signalling) degradation by RV (Unger et al., 2012). Experimental RV infection in patients with COPD has been shown to lead to secondary bacterial infection in 60%, with high airway neutrophil elastase and reduction in antimicrobial peptides SLPI and elafin (Johnston et al.,

2016). In keeping with this, an expansion of *Haemophilus* species in the airway microbiome has been reported following RV infection in COPD with 16S sequencing (Molyneaux et al., 2013).

NTHi is thus the key bacterial pathogen of the airway in asthma, with the capacity to drive inflammation and exacerbations in severe asthma. It is emerging as an important treatable trait, particularly in patients with treatment refractory neutrophilic airways inflammation in whom azithromycin has been demonstrated to be a highly effective targeted therapy. It is not known whether this effect is entirely antimicrobial in the presence of NTHi. There is also a lack of consensus regarding diagnostic testing in airways diseases – PCR appears to be most clinically applicable, with clinically relevant cut-offs (Bafadhel et al., 2015), but would require prospective validation.

1.3 Azithromycin in Severe Asthma

Azithromycin is a second-generation synthetic macrolide antibiotic with broad-spectrum of action against predominantly Gram-positive and some Gram-negative bacteria. Macrolides are used to treat respiratory, skin, soft tissue and urogenital infections, exerting their bacterostatic effect by competitively binding the 50S ribosomal subunit to inhibit protein synthesis (Zimmermann et al., 2018). In addition to anti-bacterial capacity, a range of immunomodulatory and antiviral properties have been reported. The concept of macrolide therapy primarily for immune modulation emerged through a seminal study of diffuse panbronchilitis, a rare, progressive inflammatory lung condition causing irreversible remodelling and respiratory failure (Poletti et al., 2006) in which the macrolide erythromycin dramatically improved survival independent of bacterial colonisation with *Pseudomonas* (Kudoh et al., 1987), with clinical benefit seen at serum concentrations below antibacterial levels (Altenburg et al., 2011). This has led to significant interest in the use of low-dose macrolides to modulate the immune response in chronic inflammatory diseases affecting

the lung. In the UK, national guidelines (Smith et al., 2020) recommend consideration of long term low dose macrolides in a broad range of inflammatory lung diseases including refractory asthma, alongside patients with cystic fibrosis (CF), bronchiectasis or COPD suffering frequent exacerbations, and to prevent bronchiolitis obliterans post lung-transplantation.

Azithromycin is unique in this class due to its rapid absorption after oral administration and large volume of distribution (Rapp, 1998), with long serum half-life of approximately 3 days and maintenance of subinhibitory concentration for up to 30 days (Serisier, 2013). Like other macrolides it can accumulate in host cells, particularly in phagocytes with further intracellular retention and concentration within lysosomes of 100- to 3000-fold before release upon cell death (Capitano et al., 2004; Lucchi et al., 2008; Wilms et al., 2006). Whilst therapeutically attractive, it presents significant risk of community antimicrobial resistance to macrolides and penicillin with widespread unsolicited use due to shared mobile genetic elements (Serisier, 2013). Azithromycin is the only macrolide antibiotic to have shown significant clinical response, with reduction in exacerbation frequency, in moderate to severe asthma. Whilst this effect may be due to bacterial clearance, its effectiveness eosinophilic and non-eosinophilic asthma is suggestive of additional immunomodulatory effects (Gibson et al., 2017).

1.3.1 Immunomodulatory functions of macrolides

Macrolides have been shown to modulate innate and adaptive immune defences. A broad range of effects are achieved by inhibiting TLR signalling pathways including NF-kB, p38, ERK and JNK, thereby preventing induction of inflammatory gene expression and cytokine/chemokine secretion. Macrolides can inhibit endosome acidification which impairs TLR-ligand dissociation and downstream signalling (Huang et al., 2016; Nujic et al., 2012). They reduce nuclear translocation of NFκB and inhibit phosphorylation of JNK and ERK

(Nujic et al., 2012). Alongside diminished NLRP3 inflammasome activation, macrolides can inhibit caspase 4 activation and thus NLRC4 inflammasome (Fan et al., 2017).

Azithromycin affects the processing of tight junction proteins *in vitro* in human airway epithelium, and enhances barrier function (Asgrimsson et al., 2006), protecting against *P. aeruginosa* infection independently of antibacterial effect through epithelial repair (Halldorsson et al., 2010) and inhibiting MUC5AC production (Imamura et al., 2004). It enhances CXCL8 release by epithelial cell *in vitro* in response to LPS challenge (Shinkai et al., 2006), but long-term therapy with macrolide roxithromycin in chronic rhinosinusitis suppresses local CXCL8 (Wallwork et al., 2006). Epithelial cells are transcriptionally altered with upregulation of lipid/cholesterol genes and downregulation of cell cycle and mitogenesis genes (Ribeiro et al., 2009). Erythromycin also inhibits release of integrin ICAM-1 from endothelial cells in vitro, thereby influencing transmigration of cells (Khair et al., 1995). Of relevance to asthma, azithromycin can reduce large airway contractility (Daenas et al., 2006) and smooth muscle proliferation (Stamatiou et al., 2009), thereby potentially limiting airway remodelling (Kang et al., 2016).

The bulk of innate immune regulatory mechanisms involve neutrophils and macrophages. Azithromycin can inhibit neutrophil migration via the extracellular signal-regulated kinase (ERK)-1/2 pathway (Tsai et al., 2004). Long term low dose azithromycin can reduce airway NETs (Keir et al., 2021). It acutely enhances neutrophil degranulation however with sustained exposure there is reduction in IL-6, myeloperoxidase (Culic et al., 2002) and the oxidative burst capacity (Nozoe et al., 2016), with enhanced apoptosis (Culic et al., 2002) *in vitro* and *in vivo* animal models (Fischer et al., 2011; Moges et al., 2018). Similarly in a murine model of LPS challenge pretreatment with azithromycin or clarithromycin suppressed neutrophil influx and MPO concentration, through likely inhibition of alveolar macrophage derived GM-CSF and IL-1β (Bosnar et al., 2011). In severe asthma oral clarithromycin similarly suppressed sputum CXCL8 levels alongside neutrophil elastase

and MMP-9 (Simpson et al., 2008) *in vivo*. There is enhanced efferocytosis, phagocytic clearance of dead cells, in presence of erythromycin (Yamaryo et al., 2003) and azithromycin (Polancec et al., 2012). Azithromycin has been shown to modify the macrophage J774 cell line phenotype with reduction in IL-12 and IL-6, and enhanced IL-10 levels following stimulation with IFNɣ, LPS or type 2 cytokines (IL-4 and IL-13) (Murphy et al., 2008), moreover there is stabilisation of the macrophage lysosome against oxidative damage (Persson et al., 2012). Overall macrophages assume an anti-inflammatory (M2-like) phenotype (Zhang et al., 2019). In monocytes, azithromycin can affect mRNA stability for key inflammasome component NALP3, resulting in reduced LPS mediated IL-1β production (Lendermon et al., 2017) whereas in dendritic cells it increases production of IL-10 and expression of co-stimulatory molecules (Iwamoto et al., 2011; Sugiyama et al., 2007), assuming a tolerogenic phenotype (Iwamoto et al., 2011).

Within the adaptive immune system, azithromycin can inhibit proliferation of CD4+ T cells and suppresses IL-17 production (Ratzinger et al., 2014). Macrolides can bind to macrophilin-12 to inhibit calcineurin (similarly to the immunosuppressant tacrolimus), thus preventing T cell activation and as a consequence, granulocyte populations involved in the type 2 immune response including eosinophils and basophils (Rolfe et al., 1997).

Further immune modulation by macrolides is provided through potential anti-viral effects across numerous species, including respiratory viruses such as human rhinovirus (RV), and influenza A. *In vitro* azithromycin reduces RV replication in primary bronchial epithelial cells derived from healthy donors (Gielen et al., 2010) and patients with cystic fibrosis (Schogler et al., 2015), increasing major and minor group RV induced interferons (type I and III, IFN-1β and IFN-λ1) and interferon-stimulated gene (ISG) mRNA and protein levels (Gielen et al., 2010). The oleandomycin derivative Mac5 has been shown to have a similar, more potent effect and its derivatives shown to possess anti-viral/anti-inflammatory properties without anti-bacterial effect, thus offering unique potential as an alternative therapy with

reduced risk of antimicrobial resistance (Porter et al., 2016). Clarithromycin has been shown, in addition, to reduce IL-1β, IL-6, IL-8 and induction of ICAM-1, used for viral attachment (Jang et al., 2006). The influenza A data is less compelling; a small open label study reported a more rapid decline in serum IL-6, CXCL8, IL-17, CXCL9, STNF, IL-18 and CRP with oseltamivir-azithromycin compared to oseltamivir alone but no difference in symptom resolution, with ex vivo confirmation of reduced induction of IL-6 and CXCL8 with azithromycin in peripheral blood mononuclear cells (Lee et al., 2017). However, combination therapy with azithromycin in a murine model of H1N1 infection showed no significant difference in survival, viral titres or cytokines (Fage et al., 2017). Azithromycin was not found to have a clinically significant effect in mild to moderate or severe SARS-CoV infection (Group, 2021; Hinks et al., 2021a).

Macrolides thus have a broad range of innate and adaptive immunomodulatory properties which likely contribute to their clinical efficacy, alongside antibacterial capacity, in chronic inflammatory lung diseases. In asthma the dominant mechanism remains to be determined and highly relevant for improved targeting of therapy and antimicrobial stewardship.

1.3.2 Azithromycin therapy in treatment refractory asthma

Azithromycin is the only macrolide to be recommended in international guidelines for the treatment of asthma (Global Initiative for Asthma, 2024). This change in practice has been driven by the results of the AMAZES clinical trial of the effects of azithromycin in asthma exacerbations and quality of life in persistent uncontrolled asthma (Gibson et al., 2017). Prior to this, several placebo-controlled, randomised clinical trials of macrolides had been conducted in asthma but were underpowered, shorter in duration and often recruited patients with a less severe phenotype. This was reflective in the latest inconclusive Cochrane review of macrolides as a class in chronic asthma – despite acknowledging that azithromycin may be beneficial in severe disease based on the evidence summarised

below – the overall low quality, heterogeneity of cohorts and reporting biases in previous macrolide trials had been limiting (Undela et al., 2021). Key clinical trials of long-term azithromycin in asthma are summarised in Table (1.1).

Table 1.1 Summary of key clinical trials of azithromycin in asthma;

RCT, randomised controlled trial; ACQ, asthma control questionnaire; ICS, inhaled corticosteroid; LABA, long acting β2 agonist; Azm, azithromycin; FEV1, forced expiratory volume in 1s; FP, fluticasone proprionate; OCS, oral corticosteroid; FeNO fractional exhaled nitric oxide; LRTI, lower respiratory tract infection; AQLQ, asthma quality life questionnaire; References: 1. Gibson PG et al., Lancet. 2017 Aug 12;390(10095):659-668, 2. Brusselle GG et al., Thorax. 2013 Apr;68(4):322-9, 3. Cameron EJ et al., Eur Respir J. 2013 Nov;42(5):1412-5, 4. Hahn D et al., J Am Board Fam Med. 2012 Jul-Aug;25(4):442-59

Study	Design	Key inclusion criteria	Intervention	Duration	N	Primary outcome	Main findings
Gibson 2017[1]	RCT Double blind Placebo controlled	Compatible history, proven variable airflow obstruction and bronchodilator response, symptomatic (ACQ6 ≥ 0.75) despite maintenenace ICS/LABA, no exacerbation or change in medication ≥ 4 weeks, non-smoker	Azithromycin 500mg 3 times weekly	48 weeks	420 (Azm=213)	Total number of exacerbations	Reduced asthma exacerbations (incidence rate ratio 0.59, p<0.0001) Improved asthma related quality of life (AQLQ) and symptoms (ACQ6) Improvement in FEV1 and reduction in sputum eosinophils Improvement in nasal symptoms, cough and sputum production
Brusselle 2013[2]	RCT Double blind Placebo controlled	Persistent asthma, GINA step 4/5, high dose ICS (≥1000mg FP eq) + LABA, ≥2 exacerbations requiring OCS/antibiotics in last 12 months, FeNO less than upper limit of normal	Azithromycin 250mg 5 days then 3 times weekly or placebo	26 weeks	109 (Azm = 55)	Severe asthma exacerbations and/or LRTI requiring antibiotics	No overall reduction in rate of severe exacerbations but rate reduction in non-eosinophilic subgroup (0.44 v 1.03, p = 0.013) Reduced symptom scores (AQLQ) Increased oropharyngeal macrolide resistant *Streptococci*
Cameron 2013[3]	RCT Double blind Placebo controlled	Current smoker (≥5 PY) Chronic asthma > 1 year duration No RTI ≥ 6 weeks	4 week run in ICS (400µg BDP eq ± LABA) Azithromycin 250mg daily or placebo	12 weeks	77 (Azm = 39)	PEF at 12 weeks	No change in primary outcome No improvement in symptoms scores or spirometry No change in measures of airway inflammation (FeNO/granulocytes)
Hahn 2012[4]	Community based RCT Double blind Placebo controlled	Physician diagnosed asthma and objective evidence of reversible airflow obstruction Diagnosis ≥6 months prior to enrollment	Azithromycin 600mg for 3 days, followed by 600mg weekly	11 weeks	78 (Azm=38)	Asthma symptoms	No statistically significant change in trial Azm offered open label to patients with severe persistent asthma declining randomisation, documented improvement in symptoms and QOL

Azithromycin has also been trialled in the setting of acute asthma attacks but did not show a significant difference in the primary outcome of symptom improvement at day 10 compared to placebo (Johnston et al., 2016).

In AMAZES, participants were randomised to placebo or azithromycin 500mg three times weekly for 48 weeks. There was a significant reduction in incidence of asthma exacerbations, including severe exacerbations requiring hospitalisation, with azithromycin (rate ratio 0.59, 95% CI 0.47-0.74, $p<0.0001$), in those with or without a pathogen detected by routine sputum culture, and in both eosinophilic and non-eosinophilic asthma. At the end of the treatment period sputum eosinophil, but not neutrophil, count was reduced (Gibson et al., 2017). There was an improvement in asthma-related quality of life and asthma symptoms control, with reduction in nasal symptoms, cough and sputum production. Diarrhoea was the most common adverse event, affecting 34% of patients taking azithromycin (Gibson et al., 2017). In further secondary analyses the authors reported a higher rate of clinical remission defined by the absence of exacerbations or oral corticosteroid use over 6 months (evaluated after 12 months), good symptom control and additional normal spirometric criteria (Thomas et al., 2024). An individual participant data meta-analysis of azithromycin, extracting data from Gibson et al., Brusselle et al. and Hahn et al. (summarised in Table 1.1, combined n = 604) reported a consistent reduction in exacerbations following azithromycin therapy in eosinophilic, non-eosinophilic and severe asthma (Hiles et al., 2019).

Azithromycin reduces *H. influenzae* load (but not total bacterial load), measured by PCR, compared to placebo (Taylor et al., 2019) and its abundance is predictive of treatment response (Taylor et al., 2020). Whilst this might suggest a direct antibacterial effect accounts for azithromycin's effectiveness, other factors may be at play given *H. influenzae* upregulates ICAM-1 and TLR3, receptors for RV and dsRNA, thus antibacterial effects may also contribute indirectly to reduce viral induced exacerbations (Sajjan et al., 2006)

alongside broader immune modulation to limit airways inflammation. It is important to consider however that treatment with azithromycin was linked to a significant increase in macrolide and tetracycline resistance genes in AMAZES (Taylor et al., 2019).

In a subgroup of the AMAZES cohort, sputum and serum TNF and TNF receptor (TNFR) 1 and 2 were measured – sputum (but not serum) TNFR1 and 2 levels were significantly increased in the neutrophilic phenotype, correlating with disease severity, poor lung function and disease control, and increasing age. Following azithromycin therapy, there was a significant reduction in sputum TNFR2 and TNF, and serum TNF, in non-eosinophilic asthma, both in baseline culture positive and negative individuals (Niessen et al., 2021).

Taken together, there is growing evidence to suggest that an antibacterial role is likely to be important in the efficacy of azithromycin in asthma, particularly given the link to *H. influenzae* load, however the treatment benefits seen in eosinophilic patients and in the absence of a positive sputum culture, when considered together with the broad immunomodulatory capabilities of azithromycin equally highlights the need to better understand alternative mechanisms which might be involved in the airway. In addition, other antimicrobials have not been shown to produce such a significant clinical benefit in numerous clinical trials. Understanding the mechanisms through which azithromycin exerts its effects is a particular priority given the lack of alternative therapies and the potential for use of non-antibacterial macrolide compounds to subvert concerns surrounding antimicrobial resistance.

1.3.3 The lung resistome and anti-microbial resistance associated with macrolides

Long term antimicrobial regimens exert a selective pressure, promoting antimicrobial resistance on a global scale (Serisier, 2013). Traditional anti-microbial susceptibility testing

is limited to the study of resistance patterns in single isolated pathogens (Somayaji et al., 2019), however next generation metagenomic sequencing technologies can be applied to evaluate antimicrobial resistance genes and mechanisms within a complex ecosystem rather than in the context of single organisms (Somayaji et al., 2019). Antimicrobial resistance (AMR) genes are transmitted through horizontal gene transfer using mobile genetic elements, such as plasmids and phages (Partridge et al., 2018), permitting exchange between the resident commensals and transient pathogens invading this space. The airways are a key reservoir for this exchange, referred to as the resistome (Chu et al., 2024). The AMR gene expression within this pool has been shown to vary between chronic lung diseases with bronchiectasis and COPD, having a greater breadth of AMRs than asthma (Mac Aogain et al., 2020). However overall, there is a “core” resistome driven primarily by macrolide, followed by β-lactam, fluoroquinolone and tetracycline resistance genes not found to correlate with antibiotic use or disease severity (Mac Aogain et al., 2020). In a study of recently intubated, critically unwell patients, detection of AMR increased with age (Chu et al., 2024).

This further highlights the importance of selective, targeted use of long-term macrolides to limit individual and community risk of resistance to macrolides and other antimicrobial classes cumulatively over time (Serisier, 2013).

1.4 Key outstanding questions and objectives

Whilst there have been huge leaps taken in the field of asthma in terms of wider acceptance of a targeted and personalised treatable traits approach with the development of novel biologic therapies for type-2 high severe asthma, patients with type 2 low disease remains a significant unmet clinical need. The corticosteroid resistant nature of this phenotype presents clinical challenges and is a feature shared by a group of patients with particularly

refractory type-2 high airways inflammation (FeNO non-suppressors). There is a paucity of validated biomarkers for type-2 low disease and specifically targeted therapies for those failing to respond to corticosteroid therapy and not meeting criteria for available biologic therapies. Pathogen dominance in the microbiome has emerged as a potential treatable trait in steroid insensitive neutrophilic asthma and azithromycin presents a promising therapeutic option. However, the mechanisms of its action are not fully known, and widespread use is associated with high risk of antimicrobial resistance. The prevalence of pathogen dominance in the airway was not known at the start of my DPhil

The key outstanding questions were:

- Do changes in the microbiome, specifically with airway dominance by pathogenic bacterial strains, present a treatable trait for in treatment refractory asthma? And what is the prevalence of this?
- What is the mechanism of action for azithromycin's efficacy in severe asthma? Is it a purely antimicrobial effect or are immunomodulatory mechanisms involved?
- What are the shared and unique mechanisms driving corticosteroid resistant airways inflammation in type-2 high and type-2 low patients?

Objectives

The objective of this DPhil was to define the prevalence and nature of a pathogen dominant microbiome in severe asthma, outline the mechanisms through which azithromycin exerts its effect in severe asthma in a human intervention study and elucidate mechanism of corticosteroid resistant disease in the on the background of type-2 and type-low inflammatory milieu by undertaking detailed transcriptomic analyses of highly phenotyped groups of patients. My aims were broadly divided into three areas of study

Aim 1: Metagenomics of severe asthma

- To optimise a method for metagenomic sequencing of low biomass induced sputum samples using Nanopore, comparing validity of results against sputum culture, qPCR and Illumina sequencing.
- To define the prevalence of pathogen-dominance within the microbiome, by inflammatory phenotype, in severe asthma using Nanopore sequencing.
- To discern inflammatory signals driving inflammation in the context of pathogen dominance through integrated metagenomic and proteomic analysis.
- To compare the upper and lower airway microbiome and proteome in severe asthma.

Aim 2: Mechanisms of azithromycin

- To measure clinical response to azithromycin therapy with lung function and ACQ-5
- To measure changes in lower airway cytokine and chemokine profiles following azithromycin treatment
- To characterise epithelial and immune compartments in the upper and lower airways in asthma using scRNAseq
- To characterise the effects of azithromycin therapy on the upper and lower airway as a whole and determine how the presence of pathogenic bacterial organisms can drive differential responses

Aim 3: Transcriptomics of corticosteroid resistant airways inflammation in severe asthma

- To devise a clinically relevant framework for phenotyping patients with type-2 high and corticosteroid resistant asthma to guide recruitment to a bronchoscopy study aiming to offer novel immunological insight through scRNAseq of airway tissue.

- To recruit patients with proven corticosteroid sensitive or resistant airways inflammation, and healthy controls to a mechanistic bronchoscopy study.
- To use scRNAseq approaches to characterise lymphoid populations in the upper and lower airways within these cohorts.
- To provide novel insight into mechanisms driving corticosteroid resistant inflammation.
- To provide insight into fundamental differences in T cells phenotype and T cell receptor repertoire by airway compartment to better understand the regulation of mucosal immunity at these barrier sites.

Chapter 2: Materials and Methods

2.1 Study populations

2.1.1 Definition of moderate and severe asthma in study populations

Moderate asthma

Patients with moderate asthma were established on Global Initiative for Asthma (GINA) step 4 treatment (Global Initiative for Asthma, 2024) (Figure 2.1) with confirmed adherence >80% of prescribed doses (McNicholl et al., 2012) and not meeting the criteria for severe asthma.

Severe asthma

Participants with severe asthma met the American Thoracic Society (ATS)/European Respiratory Society (ERS) definition of severe asthma (Chung et al., 2014b) and were established on Global Initiative for Asthma (GINA) step 4-5 treatment (Global Initiative for Asthma, 2024) (Figure 2.1) with confirmed adherence >80% of prescribed doses (McNicholl et al., 2012).

The ATS/ERS definition of severe asthma is as follows (Chung et al., 2014b):

- Asthma which requires treatment with guideline-suggested medications for GINA steps 4–5 asthma for the previous year or systemic corticosteroids (CS) for ≥50% of the previous year to prevent it from becoming “uncontrolled” or which remains “uncontrolled” despite this therapy

    Uncontrolled asthma defined as at least one of the following:

    1) Poor symptom control: Asthma Control Questionnaire (ACQ) consistently ≥1.5, Asthma Control Test (ACT) <20 (or “not well controlled” by GINA guidelines)

2) Frequent severe exacerbations: two or more bursts of systemic CS (≥3 days each) in the previous year

3) Serious exacerbations: at least one hospitalisation, ICU stay or mechanical ventilation in the previous year

4) Airflow limitation: after appropriate bronchodilator FEV_1 <80% predicted (in the face of reduced FEV_1/FVC defined as less than the lower limit of normal)

- Controlled asthma that worsens on tapering of these high doses of inhaled corticosteroids (ICS) or systemic CS (or additional biologics)

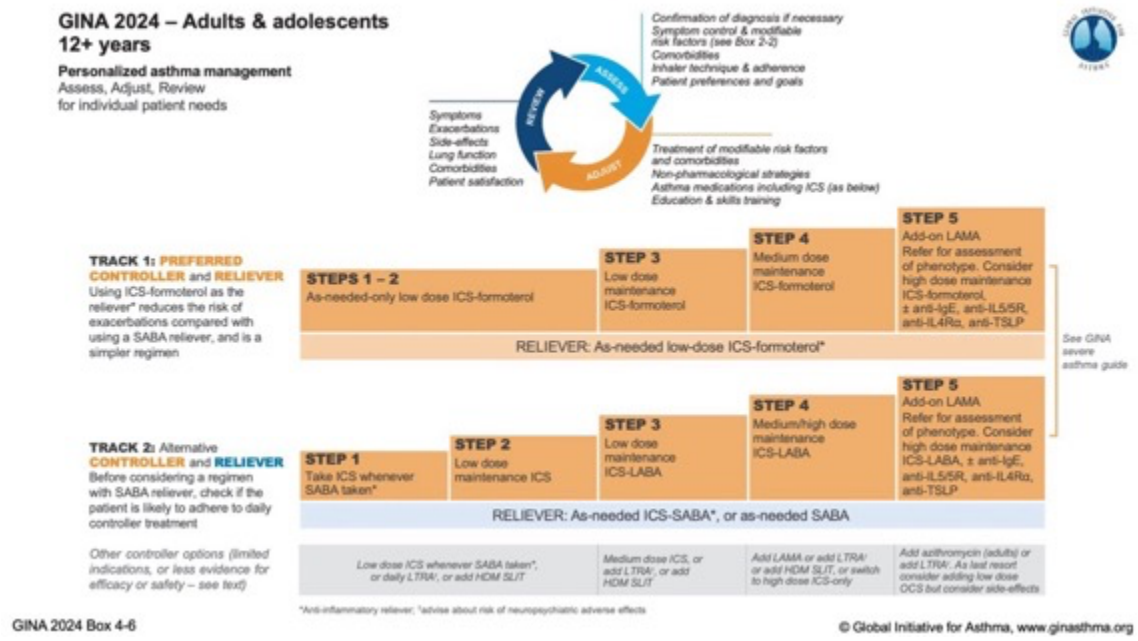


Figure 2.1 GINA asthma treatment steps (Global Initiative for Asthma, 2024)

2.1.2 Metagenomics of Severe Asthma

Oxford Severe Asthma Cohort

Participants with severe asthma were recruited to the Oxford Airways Study between December 2017 and February 2020 (John Radcliffe Hospital, Oxford, UK, NHS Research Ethics approval 08/H0406/189) from outpatient clinics. They comprised two distinct cohorts

– (1) pilot study cohort (n=23) and, (2) definitive cross-sectional cohort (n=30). Participants were recruited for sputum induction during a time of clinical stability, with no exacerbations requiring oral corticosteroids or antibiotics in the preceding 4-weeks.

Wessex Severe Asthma Cohort

Induced sputum and nasal lavage samples were provided by Prof. Peter Howarth (University of Southampton). Participants with severe asthma (n=51), mild/moderate asthma (n=10) and healthy controls (n=5) had been recruited from outpatient clinics (University Hospital Southampton and Queen Alexandra Hospital Portsmouth) between April 2009 and January 2014 (Hinks et al., 2015) in a study approved by Southampton and South-West Hampshire Research Ethics Committee A (09/H0502/37). The study protocol is published elsewhere (Hinks et al., 2015; Hinks et al., 2016b).

2.1.3 Longitudinal and cross-sectional bronchoscopy studies: AMASS and MORSE

Participants were recruited to the Oxford Airways Study (John Radcliffe Hospital, Oxford, UK, NHS Research Ethics approval 08/H0406/189) between December 2020 and October 2023. Subjects recruited were willing to undergo bronchoscopy and met the inclusion criteria, specific to each cohort. The Azithromycin Mechanisms ASthma Study (AMASS) cohort represents a subset of patients from the MultiOmics pRoject Study gEnomics (MORSE) study meeting clinical criteria for add-on azithromycin therapy (250mg, 3 times weekly for 6 months) and consenting to a second longitudinal bronchoscopy following 4-months of treatment.

Inclusion criteria for participants

- Ability to provide written informed consent
- Over 18 years of age

- Clinical diagnosis of asthma
- Meeting outlined criteria for moderate asthma or meeting ATS/ERS definition of severe asthma, on GINA step 4-5 treatment
- Assessment in specialist airways clinic with inhaled therapy optimised and proven adherence ≥80% of prescribed doses
- Baseline FEV_1 ≥ 40% of predicted
- Chest x-ray or high-resolution computed tomography (HRCT) in preceding 12 months prior to enrolment excluding any other clinically significant lung disease
- No acute illness or changes to treatment in the 4-weeks preceding bronchoscopy

Additional Azithromycin Mechanisms in ASthma Study (AMASS) inclusion criteria

- General inclusion criteria for met
- Willingness to undergo two longitudinal bronchoscopies
- Meeting British Thoracic Society (BTS) treatment criteria (Smith et al., 2020) for add-on therapy with azithromycin (ICS dose >800 mcg/day and at least one exacerbation requiring oral corticosteroids in the past year)

Inclusion criteria for healthy, non-asthmatic controls

- Ability to provide written informed consent
- Over 18 years of age
- No clinically significant medical disease
- FEV1 >80% predicted and FEV1/FVC ratio ≥70% with no bronchodilator reversibility
- Non-smoker
- Normal total IgE and no detectable specific IgE

Exclusion criteria

- Unable to provide written informed consent

- Clinically significant abnormality on screening laboratory tests which, in the opinion of the research team, could pose additional risk at time of bronchoscopy
- Current pregnancy or planned pregnancy during course of study
- Known malignancy or under evaluation for potential malignancy
- Significant medical history which, in the opinion of the research team, could pose additional risk at time of bronchoscopy
- On therapeutic anticoagulation or antiplatelet agents
- Known immunodeficiency or, use of systemic immunomodulatory or immunosuppressive therapy
- Suspected or known current pulmonary tuberculosis

Additional exclusion criteria for severe asthma

- Requiring maintenance oral corticosteroid therapy
- Lung disease other than asthma

AMASS additional exclusion criteria

- Previous isolate of non-tuberculous mycobacteria (NTM) on sputum culture
- Evidence of parenchymal lung disease on high resolution CT thorax
- Hearing impairment
- Prolonged QT_c interval on 12-lead ECG (>450 ms in men or >470 ms in women) and/or history of arrhythmic syncope

MultiOmics pRoject Study gEnomics (MORSE) additional exclusion criteria

- Use of licensed monoclonal antibody therapy for severe asthma
- Former smoker with ≥10 pack year smoking history or current smoker

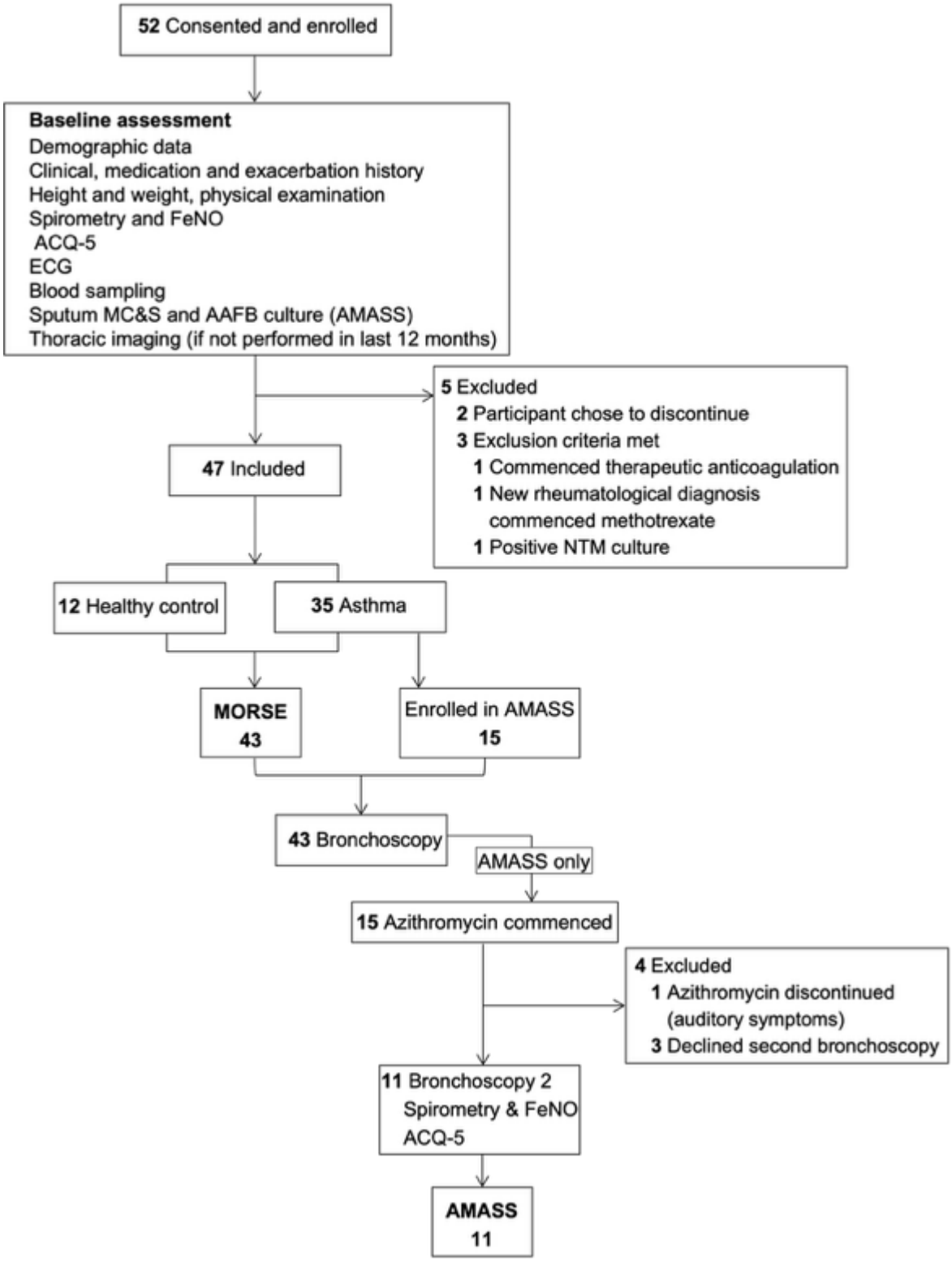


Figure 2.2 Flow diagram of bronchoscopy studies

2.2 Clinical measurements

2.2.1 Spirometry and reversibility

Spirometry was performed using the Vitalograph Alpha spirometer (Vitalograph, Maids Moreton, UK) and forced expiratory volume in 1 second (FEV_1), forced vital capacity (FVC), and forced expiratory ratio (FEV_1/FVC) calculated.

To assess bronchodilator reversibility, spirometry was performed before and 10-15 minutes after administration of salbutamol 400 mcg via pressurised metered dose inhaler (pMDI) with an AeroChamber Plus® device (Trudell Medical UK Ltd, Basingstoke, UK). A positive bronchodilator reversibility test was defined as an increase in FEV_1 of at least 12% and 200 ml post-bronchodilator (BTS/NICE/SIGN, 2024).

2.2.2 Exhaled nitric oxide and suppression testing

Fractional exhaled nitric oxide (FeNO) is a non-invasive surrogate marker of airway inflammation in asthma and correlates with type-2 inflammation of the airway mucosa and eosinophil chemotactic pull to the airways (Couillard et al., 2022b; Couillard et al., 2021). Its suppression following monitored therapy is a predictor of ICS response and can thus help identify nonadherence to therapy. FeNO was measured using the Niox VERO device (NIOX Group plc, Oxford, UK). Normal FeNO in adults was defined as <25 ppb (Jackson et al., 2021; Khatri et al., 2021).

Suppression testing was performed in participants with high FeNO (≥45 ppb), by switching maintenance ICS/LABA therapy to Relvar Ellipta 184/22 (fluticasone furoate [FF]/vilanterol trifenatate) one puff once daily administered via an inhaler device with monitoring sensor (Hailie® for Ellipta, Propeller Health, Didcot, UK) for 7 days. FeNO and spirometry was performed on day 0 and day 7 by the research team. Adherence data were reviewed via the ‘Hailie®’ mobile application and online portal. This was a pragmatic adaptation of earlier

protocols which added 1000 mcg fluticasone propionate (FP) via a monitored INhaler Compliance Assessment ('INCA') device to the patient's usual ICS/LABA inhaler for 7 days with daily at home FeNO measurements (Heaney et al., 2018). Relvar was selected as FF is a highly potent ICS with greater affinity for and longer retention in lung tissue (active 24 hours after administration) compared to FP, with a favourable safety profile, thus offering the benefit of once daily dosing to support longer term adherence (O'Byrne et al., 2014; Woodcock et al., 2017). Patients were offered a switch to Relvar Ellipta 184/22 at the end of suppression testing as their regular maintenance therapy. Niox VERO devices could not be issued for at home monitoring during the COVID-19 pandemic due to infection control concerns and limited resources. To reduce the frequency of monitoring visits FeNO was measured twice, at the start and end of the monitoring period.

A positive FeNO suppression test was defined as ≥42% fall in FeNO from baseline, as previously described (Heaney et al., 2018), and FeNO <45 ppb on day 7 of monitored therapy.

2.2.3 Electrocardiogram (ECG)

A 12-lead ECG was performed immediately prior to commencing azithromycin therapy. A corrected QTc of <450 ms for men and <470 ms for women was required to be considered for azithromycin therapy.

2.2.4 Asthma control questionnaire

The Asthma Control Questionnaire (ACQ) was developed and validated to quantify the adequacy of treatment as outlined in international asthma guidelines using 7 items, namely 5 symptom related scores, rescue short-acting bronchodilator use and FEV_1% of predicted normal. Each parameter is scored against a 7-point scale with an overall score calculated

as the mean of the responses. A cut off score of ≥1.5 was shown to confidently identify inadequately controlled asthma (positive predictive value 0.88) (Juniper et al., 2006).

The shortened ACQ-5 includes symptoms alone (night-time waking, symptoms on waking, activity limitation, shortness of breath and wheeze), and has a high degree of agreement with the original version in clinical trial data (interclass corelation coefficient 0.94) (Juniper et al., 2005). In this study ACQ-5 is used as international guidelines and clinical practice have moved towards wider use of ICS-formoterol maintenance and reliever therapy, over short-acting β2-agonists as rescue therapy, but the optimum method for incorporating ICS-formoterol use in the ACQ is not established.

The ACQ-5 questions are shown below (Table 2.1). Participants were asked to circle the most appropriate response to each question.

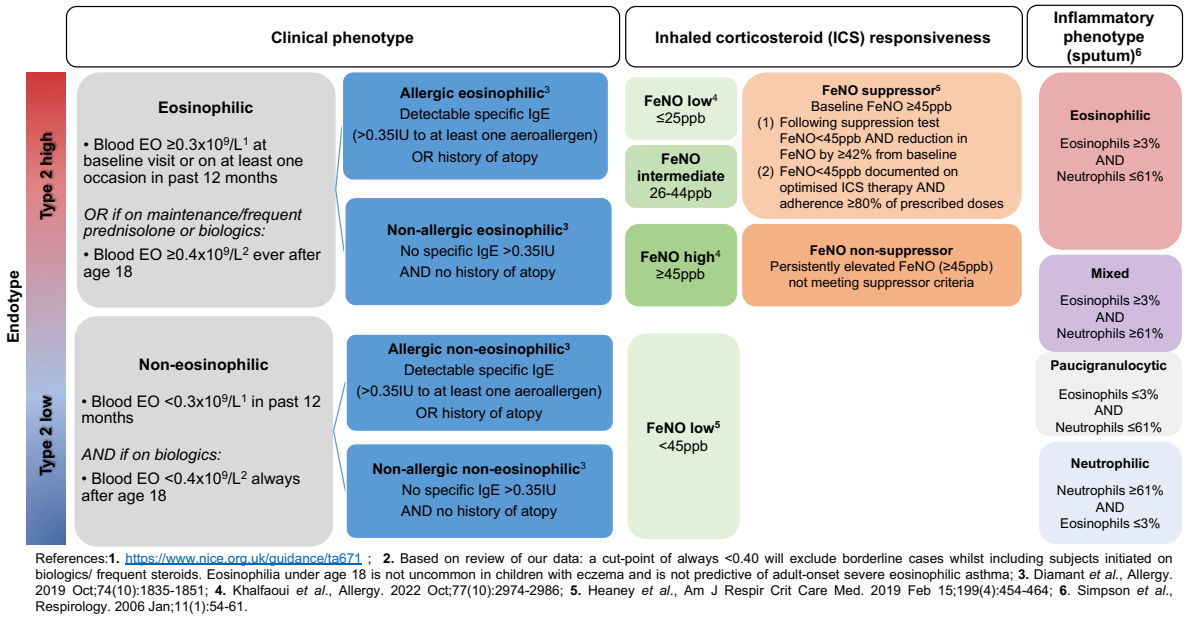
Table 2.1 Asthma Control Questionnaire

Asthma Control Questionnaire 5 (ACQ-5)	
On average, during the past week, how often were you woken by your asthma during the night?	0 = never 1 = hardly ever 2 = a few times 3 = several times 4 = many times 5 = a great many times 6 = unable to sleep because of asthma
On average, during the past week, how bad were your asthma symptoms when you woke up in the morning?	0 = no symptoms 1 = very mild symptoms 2 = mild symptoms 3 = moderate symptoms 4 = quite severe symptoms 5 = severe symptoms 6 = very severe symptoms
In general, during the past week, how limited were you in your activities because of your asthma?	0 = not limited at all 1 = very slightly limited 2 = slightly limited 3 = moderately limited 4 = very limited 5 = extremely limited 6 = totally limited
In general, during the past week, how much shortness of breath did you experience because of your asthma?	0 = none 1 = very little 2 = a little 3 = a moderate amount 4 = quite a lot 5 = a great deal 6 = a very great deal
In general, during the past week, how much of the time did you wheeze?	0 = not at all 1 = hardly any of the time 2 = a little of the time 3 = a moderate amount of time 4 = a lot of the time 5 = most of the time 6 = all of the time

2.3 Clinical classification

To offer novel immunological insight between different cohorts of severe asthma patients with treatment refractory, corticosteroid insensitive asthma I aimed to make clinically and biologically relevant comparisons by subclassifying patients using highly validated biomarkers (blood eosinophils, exhaled nitric oxide, IgE) (Diamant et al., 2019) and an objective measure of corticosteroid responsive airways inflammation (FeNO suppression

testing) (Heaney et al., 2018). When analysing immunological and genomic data (focusing on T cells in this thesis), this allowed shared and/or unique features to be considered through comparison of type-2 high or low, and corticosteroid responsive or resistant disease in addition to the presence or absence of atopy. The criteria used are defined below and shown in Figure 2.3.



References:**1.** https://www.nice.org.uk/guidance/ta671 ; **2.** Based on review of our data: a cut-point of always <0.40 will exclude borderline cases whilst including subjects initiated on biologics/ frequent steroids. Eosinophilia under age 18 is not uncommon in children with eczema and is not predictive of adult-onset severe eosinophilic asthma; **3.** Diamant *et al.*, Allergy. 2019 Oct;74(10):1835-1851; **4.** Khalfaoui *et al.*, Allergy. 2022 Oct;77(10):2974-2986; **5.** Heaney *et al.*, Am J Respir Crit Care Med. 2019 Feb 15;199(4):454-464; **6.** Simpson *et al.*, Respirology. 2006 Jan;11(1):54-61.

Figure 2.3 Clinical and inflammatory phenotyping criteria

A blood eosinophil value of ≥ 0.3x10^9/L defining the type-2 high group was based on the UK licensing criteria (NICE, 2021) for anti-IL-5 therapy and has previously been linked to higher risk of exacerbations in observational cohorts (Couillard et al., 2022a; Price et al., 2015) and clinical trials (Pavord et al., 2012). In addition, based on review of clinical data from the severe asthma clinic, any documented blood eosinophilia over 18 years of age ≥0.4x10^9/L classified an individual as type-2 high, as this captures those on frequent oral corticosteroids or commenced on biologic therapy with suppressed blood eosinophils. High FeNO is widely defined as ≥45ppb as it is predictive of frequent exacerbations and ICS response (Heaney et al., 2018; Khalfaoui et al., 2022) and has been used here. A low (normal) FeNO threshold of <25 ppb is based on classification of biomarker low patients in

a *post-hoc* analysis of the UK severe asthma registry data (Jackson et al., 2021). An intermediate group encompassed patients with FeNO ranging 25-44 ppb. Type-2 high patients with low-to-intermediate FeNO represented individuals with FeNO suppression on formal testing or a comparable historical pattern of reduction in FeNO following optimisation of inhaled therapy with confirmed adherence >80% of prescribed doses (McNicholl et al., 2012). The type-2 low group was defined by blood eosinophil count $<0.3x10^9$/L and FeNO <45 ppb. Patients with severe asthma and FeNO below 45 ppb have been shown by Heaney *et al.* to achieve only small reductions in FeNO with monitored optimised therapy and no reduction in peripheral blood eosinophils, ACQ-5 or lung function (Heaney et al., 2018). This may reflect greater adherence to ICS in this subset of patients and alternative mechanisms to type-2 immunopathology driving the persistent airways inflammation.

Where an individual could not be uniquely assigned to a single category within the above classification, they were assigned according to a nearest fit based on the consensus agreement of two expert clinicians.

As part of the AMASS study, bronchoalveolar lavage culture was performed at the time of bronchoscopy and the results used to subgroup culture positive patients with an isolated lower airway pathogen.

Severe asthma subclassification criteria:

- **Type-2 high (eosinophilic)**
    - Peripheral blood eosinophil count $\geq 0.3x10^9$/L at baseline visit or on at least one occasion in preceding 12 months OR if requiring maintenance or frequent prednisolone (≥3 short courses in the preceding 12 months), or biologics
    - Peripheral blood eosinophils ever exceeding $0.4x10^9$/L after the age of 18 years

- Atopic and non-atopic participants were included as defined below:
  - Allergic: Total IgE >120 kU/L based on Oxford University Hospitals clinical laboratory cut-off for total serum IgE and detectable specific IgE (>0.35 IU to at least one aeroallergen), or history of atopy
  - Non-allergic: No detectable specific IgE (<0.35 IU) or history of atopy
- Participants with varied inhaled corticosteroid responsiveness were included and subclassified as follows:
  - FeNO low (<25 ppb)
  - FeNO intermediate (25 – 44 ppb)
  - FeNO high (≥ 45 ppb). These individuals underwent further clinical assessment to determine inhaled corticosteroid response following formal suppression testing or optimisation of inhaled therapy:-

    - FeNO suppressor

      Following formal suppression test FeNO <45 ppb AND reduction of FeNO by ≥42% from baseline

      OR

      FeNO <45 ppb documented after optimising ICS therapy AND proven adherence assessed as ≥80% of prescribed inhaled doses

    - FeNO non-suppressor

      Persistently elevated FeNO (≥45n ppb) and not meeting suppressor criteria

- **Type-2 low (non-eosinophilic)**
  - General inclusion criteria met

- Peripheral blood eosinophil count <0.3x10^9/L at baseline visit and in the past 12 months
- Peripheral blood eosinophils < 0.4x10^9/L after the age of 18 years
- FeNO <45 ppb
- Atopic and non-atopic participants were included as defined as above

2.4 Clinical sample handling

2.4.1 Phlebotomy and blood sample handling

Venepuncture was performed for the collection of serum samples into serum tubes, full blood count into ethylenediaminetetraacetic acid (EDTA) tubes and isolation of blood cells into lithium heparin tube (Vacuette, 455084).

Full blood count samples were sent to the National Health Service laboratory (John Radcliffe Hospital, Oxford) for processing by automated cytometers.

The serum sample was allowed to clot for 30-60 min at room temperature (RT) prior to centrifugation (600 g for 10 min). The supernatant was then aspirated and stored in 400 µl aliquots at -80 °C until use in immunological assays.

2.4.2 Isolation of peripheral blood mononuclear cells

Blood for peripheral blood mononuclear cell (PBMC) isolation was collected into 9 ml lithium heparin tubes (VacuetteR, Grenier Bio-One, Stonehouse, UK) following venepuncture. Heparinised blood from two tubes (~18 ml) was diluted with Dulbecco's phosphate buffered saline (PBS) with no Mg^{2+} or Ca^{2+} (PBS; Sigma-Aldrich, D8537) to a final volume of 30 ml before mixing by gentle inversion. Diluted blood (30 ml) was overlayed on 15 ml Lymphoprep^{TM} (Stemcell Technologies, 18061) and centrifuged at 600 g for 25 min with the brake off. The buffy coat layer was collected and washed with 50 ml PBS, before pelleting

cells by centrifugation at 400 g for 5 min. Cells were resuspended in 1ml PBS and 10 µl of the cell suspension used for counting in trypan blue (Gibco, 15250061) with the Countess 3 automated cell counter as per manufacturer's protocol (Invitrogen, Thermo Fisher Scientific, Massachusetts, USA). Cells were resuspended at the required concentration in appropriate cell culture media, PBS or cell staining buffer based on the downstream application.

2.4.3 Nasal brushing

Cytology brushes (DRYSWAB^{TM} sampling brush, Medical Wire & Equipment Co Ltd., Corsham, UK) were introduced through each nostril under direct visualization, angled towards the middle turbinate avoiding direct contact with the nasal septum to reduce discomfort. Brushes were rotated gently 10 times before depositing cells into cells into 4 ml ice cold Roswell Park Memorial Institute (RPMI) 1640 media without phenol red (Gibco, 11835030), to minimise irrelevant fluorescence in subsequent flow cytometry, by gently agitating the brush before cutting both brushes into a single collection tube. Samples were transferred to the lab on wet ice.

2.4.4 Nasal brush processing

Residual nasal cells were flushed off the brush with 4 ml collection media, before discarding the brush. The cell suspension was then centrifuged at 500g for 5 min at 4 °C. The resulting supernatant was removed and retained for metagenomic studies as described below. The cell pellet was resuspended in 2ml Cell Staining Buffer (BioLegend, 420201) before aspirating through a 23G needle (BD Microlance 3, 300800) into a 2 ml Luer lock syringe (BD, 309628), then passed into a 5 ml test tube with 35 µm cell strainer snap cap (Thermo Fisher Scientific, 10585801) to disperse nasal cells. This cell suspension was used for flow cytometry or single cell RNA sequencing as detailed below.

The nasal cell-free supernatant was ultracentrifuged (12,000 g for 4 min at 4 °C) to precipitate bacteria. The resulting supernatant was discarded, the pellets resuspended in the residual media before pooling and combining in 400 µl of sterile 10% glycerol (Sigma-Aldrich, G7757) in PBS. This sample stored at -80 °C until required for microbial DNA extraction and metagenomic sequencing.

2.4.5 Sputum induction

Sputum induction was performed following a standardised published protocol during a period of clinical stability (Djukanovic et al., 2002; Hinks et al., 2015). Baseline heart rate, oxygen saturations and pre-bronchodilator spirometry was performed. If FEV_1 was below 1L and/or <50% predicted, the procedure was abandoned. Bronchodilatation was achieved with Salbutamol (4 puffs, 100 mcg/inhalation via AeroChamber Plus) or an equivalent dose of the participant's own prescribed short acting bronchodilator inhaler. Post-bronchodilator spirometry was performed after 20 min and baseline FEV_1 recorded. Hypertonic saline (3%) was administered via a nebuliser device at a delivery rate of 1 ml/min. FEV_1 was remeasured after 5 min, any sputum produced was collected and oral rinse with water performed to reduce squamous and oral cavity bacterial contamination of subsequent samples.

Nebulisation of 4% and then 5% hypertonic saline followed similarly, unless FEV_1 dropped by >20% of the post-bronchodilator recording or an adequate sample was collected. Following induction of sputum, participants were observed until FEV1 returned to 95% of pre-bronchodilator value. Sputum samples were stored at 4 °C until processing, within 1 h of collection.

2.4.6 Sputum processing

Sputum was processed as previously described (Hinks et al., 2016b). Briefly, for use in metagenomic studies, sputum plugs were isolated from induced samples using fine-tipped forceps and stored at -80 °C in sterile Brain Heart Infusion (BHI; Sigma-Aldrich, 53286) broth containing 10% glycerol until required. Samples were thawed on ice and diluted with four times volume (sputum weight) of 0.2% dithiothreitol (DTT, Sigma Aldrich G7757), a reducing agent used to dissociate disulphide bonds, reducing sputum viscosity. Samples were placed on a bench rocker on ice for 15 min to disperse cells, before filtering through a 50 µm nylon mesh filter and proceeding to culture or DNA extraction.

2.4.7 Cytospin preparation

Glass microscope slides (Epredia SuperFrost Plus, Epredia, J1800AMNZ) were labelled and placed in a cage with a cytofunnel and filtercard (5991022) in the Thermo Cytospin (CY94231404). Sputum or bronchoalveolar lavage cells were resuspended at a concentration of $1x10^{6}$ cells/ml in PBS and 75 µl per slide transferred to the cytofunnel and centrifuged for6 minutes at 450 rpm. Slides were allowed to dry for 15 minutes before staining with the Rapi Diff II Staining Kit (Atom Scientific, Rapi Solution B RRSP134-D/ Solution C RRSP135-D,) before allowing to dry for 24 h. Slides were immersed in methanol (Fisher Chemical M/4056/15) for 5 min, then allowed to air dry for 3 min (or appeared dry). Slides then stained with solution B and solution D as per manufacturer's instructions. Once dry, slides were mounted with DPX mountant reagent (Sigma Aldrich, 06522) and coverslip and 400 cells counted, recording eosinophils, neutrophils, monocytes/macrophages and epithelial cells. A count in excess of >20% squamous epithelial cells was considered suggestive of significant upper airway contamination. Cytospin preparation and cell counts were performed by my colleague Mahdi Mahdi.

2.4.8 Definitions of sputum inflammatory phenotypes

Sputum inflammatory phenotypes were defined using a widely accepted classification as follows – participants with >3% sputum eosinophils were classified as eosinophilic asthma and those with >61% sputum neutrophils and <3% eosinophils were classified as neutrophilic asthma. Participants with >61% sputum neutrophils and >3% eosinophils were classified as mixed granulocytic asthma, and those with <61% sputum neutrophils and <3% eosinophils were classified as paucigranulocytic asthma (Simpson et al., 2010; Simpson et al., 2006).

2.5 Metagenomic sequencing of airway samples

The methods described in the following section were used for preparation, sequencing and analysis of airway samples from three studies as indicated in the text – pilot method development (Jabeen et al. 2022), metagenomics of severe asthma (Jabeen et al. 2024) and the AMASS bronchoscopy study.

2.5.1 Sputum culture

Routine sputum culture was performed using homogenised sputum according to the Health Protection Agency (HPA) standard operating procedures. All cultured organisms were identified by matrix-assisted laser desorption/ionization time-of-flight (MALDI-TOF) mass spectrometry on a Microflex LT using Biotyper, version 3.1 (Bruker Daltonics, Ballerica, MA, USA). In addition, prospective *Haemophilus* species were also identified using X (hemin), V (nicotinamide adenine dinucleotide, NAD) and XV discs (hemin and NAD) (BD BBL Taxo differentiation discs for *Haemophilus* spp., Wokingham, UK) on nutrient agar (Oxoid Ltd, Basingstoke, UK). Clinical laboratory results from the John Radcliffe Hospital Microbiology Laboratory, Oxford, UK have been provided for three samples.

2.5.2 Bacterial spiking of sputum samples

Sputum plugs collected from five donors with no significant growth of potentially pathogenic respiratory organisms on culture (participant identifier (PID): 1052, 5, 1055, 315, 187) were homogenised with DTT as above and pooled together to generate a baseline sample for all spiking conditions. The pooled sample was then split for spiking simultaneously with *Haemophilus influenzae, Streptococcus pneumoniae, Staphylococcus aureus, Moraxella catarrhalis* and *Pseudomonas aeruginosa*. Bacteria were cultured overnight (37 °C with 5% CO_2, shaking at 180 rpm) in 10 ml culture broth as indicated by species (*H. influenzae* in BHI with 10 mcg/ml NAD and hemin [Sigma-Aldrich], *S. pneumoniae* in BHI and *S. aureus/M. catarrhalis/P. aeruginosa* in nutrient broth [E&O laboratories, BM4181]). Once optical density at 600 nm reached 0.5 (exponential phase) bacteria were pelleted and resuspended in BHI or nutrient broth containing 10% glycerol and stored at -80 °C until use. Serial dilutions (in PBS) and confirmatory colony forming unit (CFU) counts were performed to determine bacterial stock concentrations. The five cultured bacterial species were spiked simultaneously from stock solutions into the pooled homogenised sputum samples, producing three spiked samples containing 10^4, 10^6 or 10^8 CFU/ml of each bacterial species. Microbial DNA was extracted from the unspiked and spiked pooled samples.

2.5.3 Microbial DNA extraction from sputum and nasal lavage samples

In the pilot study two methods for extraction of high-quality microbial DNA and depletion of human cells/DNA, were tested. The first was differential centrifugation, whereby homogenised sputum was centrifuged (400 g, 5 min) to pellet human cells. The supernatant was collected, split into smaller volume aliquots (up to 1 ml) and centrifuged again (13,000 g, 5 min). This supernatant was discarded, bacterial pellets from multiple aliquots combined for DNA extraction using the QIAamp DNA Mini Kit (Qiagen, 51304) as per manufacturer's instructions. The second method utilised the NEBNext® Microbiome DNA Enrichment Kit (New England Biolabs, E2612S) as per manufacturer's instructions – this kit facilitates

enrichment of microbial DNA by selectively binding and removing CpG-methylated human DNA.

In the larger definitive cohort homogenised sputum or nasal lavage underwent differential centrifugation prior to DNA extraction using the QIAamp DNA Mini Kit (Qiagen, 51304) as per manufacturer's instructions. AMPure XP bead (Beckman-Coulter, A63881) clean up (1.8x) was performed by combining 108 µl of beads with 60 µl of DNA before thoroughly mixing and incubating at RT for 10 min. Samples were placed on to a magnetic stand for 3 min before removing the supernatant and washing twice with 80% ethanol, then air drying the pellet (maximum 10 min). The pellet was resuspended in 25 µl 1 x Tris-EDTA (Sigma-Aldrich, 93283), placed on a magnetic stand for 3 min before transferring the supernatant into DNA low-bind Eppendorf tube and then quantifying with a Qubit 2.0 fluorometer (Life Technologies, Paisley, UK).

2.5.4 Microbial DNA extraction with saponin based host DNA depletion

In light of a modified saponin based host DNA depletion method recently published following validation in a large respiratory metagenomics study, predominantly using BAL (Charalampous et al., 2024), an adapted extraction protocol was used for BAL and nasal brush samples collected in the AMASS bronchoscopy study in an effort to reduce contaminating host DNA and maximise bacterial reads on sequencing.

Samples were centrifuged (12000 g, 5 min) before carefully removing the supernatant, leaving approximately 50 µl with the pellet. Then 200 µl of PBS (Gibco) and 200 µl of HL-SAN buffer (5M of NaCl and 100 mM of $MgCl_2$ in molecular grade water) were added along with 40 µl of 1% saponin (Sigma-Aldrich, S7900) and 10 µl of HL-SAN DNase (ArcticZymes, 70910-202). Samples were incubated on a thermomixer at 37 °C shaking at 1000 rpm for 10 min to induce host cell lysis and digest of newly released host DNA, then washed with

800 µl PBS and centrifuged (12000 g, 3 min) to pellet microbial organisms. DNA extraction was then performed using the QIAamp DNA Mini Kit as previously described. After AMPure XP bead clean up, DNA was eluted in 12 µl 1 x Tris-EDTA.

Unfortunately, despite a pilot run of this protocol demonstrating no excessive reduction in DNA concentration, when applied to BAL and nasal brush derived samples in the AMASS study the DNA concentrations were found to be in the lower range (0.3 – 2.46 ng/ul) and sequencing with Nanopore yielded low to no usable reads.

2.5.5 Metagenomic sequencing with Illumina MiSeq

After quantification with a Qubit 2.0 fluorometer (Life Technologies, Paisley, UK), DNA extracts were sequenced on a MiSeq desktop sequencer (Illumina, San Diego, CA, USA). Libraries were prepared using a variation of the Illumina Nextera XT protocol (Votintseva et al., 2015). Briefly, 1 ng of DNA was prepared using the Nextera XT protocol modified with 15 cycles during the index PCR. DNA quantification with a Qubit 2.0 fluorometer was followed by determination of their average sizes on an Agilent 2200 TapeStation (Agilent Technologies, Santa Clara, CA, USA) before samples were manually normalized. Paired-end sequencing was performed using a 600-cycle MiSeq reagent kit (version 3, Illumina, MS-102-3003), and samples were sequenced in batches of 12 on a single flow cell.

2.5.6 Metagenomic sequencing with Oxford Nanopore Technologies (ONT)

Libraries were prepared for sequencing on an Oxford Nanopore GridION (Oxford Nanopore Technologies [ONT], Oxford, UK) using the Rapid Barcoding Sequencing (ONT, SQK-RBK004) kit where 333 ng template DNA was available per sample (in pilot study only), using the manufacturer's protocol. For the majority of samples (maximum 10 ng template DNA per sample) the Rapid PCR Barcoding kit (ONT, SQK-RPB004) with published modifications to the manufacturer's protocol was used (Charalampous et al., 2019). Post-

PCR, DNA samples were purified with AMPure XP SPRI beads and eluted in 10 mM Tris-HCl pH 8.0 with 50 mM NaCl. DNA was quantified with a Qubit 2.0 fluorometer. Between 95-99.6 fmol of combined library were loaded per flow cell. Samples were sequenced on ONT FLO-MIN106D (ONT v.R9.4.1) flow cells in batches of 6 samples per flow cell.

2.5.7 Total 16S and pathogen specific qPCR assays

Quantitative real-time PCR (qPCR) was performed to quantify relative abundance of *H. influenzae, S. pneumoniae, S. aureus, M. catarrhalis*, *P. aeruginosa* and total 16S (Eubacteria) within the total DNA extracts. Human Pathogen Detection Genesig kits and PrecisionPLUS 2x qPCR Mastermix by Primerdesign (Eastleigh, UK) were used as per manufacturer's instructions. Primers and probes were used for the following bacterial targets: outer membrane protein P6 (*H. influenzae*), alpha fucosidase (*S. pneumoniae*), FEMB (*S. aureus*), major outer membrane protein/copB (*M. catarrhalis*), toxin A synthesis regulating gene/RegA (*P. aeruginosa*) and 16S ribosomal gene (total 16S). Reactions were performed in 20 µl with 5 µl template DNA (10 ng). Positive control templates for each bacterial species of interest (containing $2x10^5$ copies/µl) were used to prepare a standard curve dilution series ranging from $2x10^5$ to 20 copies/µl. Negative controls using nuclease free water (ThermoFisher, Waltham, MA, USA) in place of DNA template were used. All assays were performed in duplicate and mean values utilised in analyses. The qPCR conditions were: enzyme activation 2 min at 95 °C followed by amplification for 50 cycles at 95°C for 10 s and 60 °C for 60 s. qPCR assays were performed on a Bio-RadCFX96 instrument (Bio-Rad, Watford, UK).

2.5.8 Measurement of inflammatory mediators

Existing dataset utilised from the multicentre cross-sectional study by Hinks *et al*. (Hinks et al., 2016b). Inflammatory mediators measured from sputum by enzyme linked immunosorbent assays (ELISA) were myeloperoxidase (MPO), elastase (Hycult),

eosinophil cationic protein (MBL International), interleukin (IL)-5 (Abnova), IL-6, ENA-78, Eotaxin, FGF, osteopontin, VEGF, YKL-40 (R&D Systems), tryptase and α2-macroglobulin (A Walls4), as per manufacturer's instructions. Fluoroenzyme immunoassay was used for total and specific IgE (ImmunoCAP, Phadia) and cytokine bead array (Luminex®) for matrix metalloproteases (MMPs), tissue inhibitor of matrix metalloproteinase 1 (TIMP-1), G-CSF, GM-CSF, Gro-α, IFN-γ, IL-1α, IL-1 β, IL-1RA, IL-2, IL-4, IL-8, IL6SR, IL-10, IL-13, IL-17, MCP-1, MIP-1 α, MIP-1 β and TNF-α.

In addition, sputum and nasal lavage samples were analysed by O-link (Uppsala, Sweden) using a 92-mediator in-house Proseek Multiplex Inflammation I panel (listed in Jabeen *et al.* 2024 Supplementary Methods).

2.5.9 Bioinformatic and statistical analysis

Statistical analyses were performed using Rstudio (Version 2022.12.0+353) and GraphPad Prism (Version 9). Data were logarithmically transformed if non-normal distribution. Parametric and nonparametric data are displayed as mean (SEM) and median (range), with comparisons between groups made using unpaired t-test or Mann–Whitney test, respectively. For all analyses, 2-tailed p <0.05 were considered significant. Where indicated, overall, 5% significance level was adjusted for multiple comparisons with Benjamini-Hochberg procedure. Correlations were tested with Pearson's or Spearman's r statistic, as described in the text.

Taxonomic analysis of raw data[1]; Illumina; Raw sequencing reads were adapter trimmed using BBDuk (https://sourceforge.net/projects/bbmap/) and the adapter sequence file provided within the BBMap package; the following parameters were used: minlength, 36; k,19; ktrim, r; hdist, 1; mink, 12. Taxonomic classification of trimmed reads was performed

[1] Performed by Dr N Sanderson

using Centrifuge (Kim et al., 2016) and a database constructed from complete genomes of bacteria, viruses, and fungi uploaded to NCBI refseq as of 2019-08-24. The human genome (GRCh38) was included for host DNA detection. *Haemophilus influenzae* classified reads were mapped to reference genome NC_000907.1 using BWA MEM (version 0.7.12-r1039) and SAMtools (version 1.9) (Li et al., 2009). **Oxford Nanopore**; Sequences were basecalled using Guppy (ONT, version 3.3.0+ef22818) and analysed using the CRuMPIT pipeline (Sanderson et al., 2018) with the same Centrifuge database used for Illumina sequence analysis. This pipeline used Minimap2 (version 2.17-r954-dirty) (Li, 2018) to align *Haemophilus influenzae* classified reads to reference genome NC_000907.1. A complete description of the bioinformatics used and secondary analyses are described GitLab repositories: https://gitlab.com/ModernisingMedicalMicrobiology/asthmas-methods-paper-analysis and https://gitlab.com/ModernisingMedicalMicrobiology/wessex_analysis. For comparison of *H. influenzae* genome between clinical samples and cultured strains consensus fasta sequences were generated using Minimap2 and CLAIR2 using the genericbugONTworflow previously optimised and described (Sanderson et al., 2020). (https://gitlab.com/ModernisingMedicalMicrobiology/genericbugontworkflow). A single nucleotide polymorphism (SNP) analysis was performed, and a distance matrix was generated using snp-dists.

Visualisation of metagenomic data; Kraken style reports were produced following taxonomic classification of trimmed reads. In the pilot study, heatmaps of relative abundances of bacterial species were displayed using z scores. In the larger cohort, raw species level reads (Wessex, n=66; Oxford, n=30) from sputum samples were combined into two datasets, 7644 and 3860 unique species were identified respectively. Low abundance species (<1000 reads across all samples) were removed prior to normalisation (DESeq2) thereby reducing unique species to 253 and 72, respectively. The two datasets were merged by common detected species (n=70) and z-scores derived for heatmaps. Principal component analysis (PCA) plots were produced to provide a low dimensional

representation of the 3 participant groups (healthy, moderate and severe asthma) in the Wessex cohort and the two severe asthma groups (Wessex and Oxford). Groups of samples were compared by permutational multivariate ANOVA (PERMANOVA) performed using the adonis function in the Vegan package. Wald test used to identify species uniquely abundant or depleted in HC, MA and SA, or by inflammatory phenotype (using DESeq2, log fold change [LFC] >1 or <1 respectively, adjusted P <0.05).

Sankey visualisations; Individual or combined Kraken style reports used to produce Sankey visualisations of taxonomic profiles using Pavian3. Where a dominant pathogen was identified on metagenomic sequencing in more than one individual, the relative abundance of these bacteria (*H. influenzae, M. catarrhalis, S. pneumonia*) was compared against the relative abundance of other detected species within each sample using Wilcoxon rank-sum test, using Benjamini-Hochberg [BH] correction FDR 0.05, to provide statistical support for the skewed metagenomic profiles shown.

Normalisation, integration and visualisation of cytokine and metagenomic data; Raw cytokine measurements were centralised by z-score, clustering was performed by cytokine and subjects, with clustering distances visualised in heatmap representing correlation distances. To integrate metagenomic and cytokine data within the combined Wessex dataset (HC, MA, SA), species level reads were normalised, and log transformed, while cytokines were centralised by z-score prior to computation of Spearman correlation between shared species (~253) and cytokines by matching across samples (adjusted for multiple comparisons with Benjamini–Hochberg procedure [FDR 0.05]). The 50 species with greatest variance in abundance across subjects were selected for clustering analysis by cytokines (columns) and species (rows).

Bayesian network analysis; Connections between cytokines associated to airways infection, clinical parameters, and differentially abundant bacterial species in severe asthma

was explored by Bayesian network analysis (Genie 2.0; Decision Systems Laboratory, University of Pittsburgh, Pittsburgh, Pa). Data from 51 severe asthmatics (60 variables) were discretised into 2 (binary variables) or 3 to 5 (continuous variables) bins (variables shown in Table S8). Using the 'clustering algorithm' (BayesFusion) 34/60 variables were retained in the model. The Bayesian network generated was re-plotted using shinyBN (Chen et al., 2019). In a subsequent separate analysis strengths of associations were further explored using Pearson (between species) or Spearman correlation (between cytokines). Positive linear correlations are highlighted with a green edge.

Integration of nasal lavage and sputum metagenomics and O-link data; Low abundance species (<200 reads across all individuals) were removed from nasal lavage and sputum samples (filtering to 94 and 349 species respectively) prior to scaling bacterial reads within samples. A combined dataset of shared nasal lavage and sputum species was produced (n=23) by selecting organism with highest variance in abundance across all samples ($P<0.05$). A PCA plot was produced using these samples and the two groups of samples compared by permutational multivariate ANOVA (PERMANOVA) performed using the adonis function in the Vegan package. Spearman correlation was performed using paired O-link proteomic data (92 protein panel) in sputum and nasal lavage and significantly correlated pairs of cytokines were filtered ($P<<0.001$) following adjustment for multiple corrections (n=38; sputum = 16, nasal=22).

2.5.10 Data availability

Raw FASTQ data is available on the European Nucleotide Archive with the project accession PRJEB47876 (Jabeen *et al.* 2022) and PRJEB62780 (Jabeen *et al.* 2024).

2.6 Bronchoscopy

2.6.1 Bronchoscopic technique

Bronchoscopies were performed in accordance with the British Thoracic Society (BTS) guideline for diagnostic flexible bronchoscopy (Du Rand et al., 2013) in adults and established research protocols (Hinks et al., 2016b), using a flexible fibreoptic bronchoscope (Pentax) in Day Case Theatre, John Radcliffe Hospital, Oxford. Participants were instructed to fast for 6 h prior to the procedure and underwent routine physical examination, measurement of vital signs, spirometry and FeNO measurement (if not performed in last 7 days). Venepuncture was performed and intravenous cannula was inserted. The procedure was conducted with light sedation using fentanyl 0-100 mcg and/or midazolam 0-5 mg. Continuous three lead cardiac monitoring and pulse oximetry was performed. Topical airway anaesthesia was achieved with 6-8 sprays (60-80 mg) of 10% lidocaine orally, 6 ml of 2% lidocaine to the vocal cords and up to 10 ml 1% lidocaine throughout the bronchial tree.

The order of sampling comprised: 10 endobronchial brushings, 10 endobronchial biopsies and 120 ml bronchoalveolar lavage. Brushings were taken first to reduce contamination with blood as these samples were used for epigenetic analyses as part of a separate DPhil project. Prior to sampling, up to 5 ml of sterile normal saline was injected through the bronchoscope sampling port, the first 1 ml was collected into a sterile Eppendorf and stored at -80C for future microbiological analysis (negative control, scope wash).

Endobronchial brushes were introduced under direct visualisation with 10 strokes performed per sample using sterile 2 mm disposable cytology brushes from 1st to 3rd order bronchi in the right and left lower lobes and middle lobe. The samples were gently agitated in 4 ml ice cold RPMI 1640 media without phenol red (Gibco, 11835030) before rinsing the cytology brushes in sterile saline (0.9%) prior to reintroduction for sampling.

Endobronchial biopsies were taken from 1st to 4th order carinae bilaterally using 2 mm oval, fenestrated swing jaw forceps. Biopsies were deposited into 4 ml ice cold RPMI 1640 media without phenol red.

Bronchoalveolar lavage (BAL) was performed in the right upper lobe, following anaesthesia, using 1 aliquot of 40 ml, and 4 subsequent aliquots of 20 ml warmed, sterile normal saline, injected and aspirated with 20 ml syringes. BAL fluid was transferred into sterile 50 ml Falcon tubes for transport.

Nasal brushings, as previously described, were performed after completion of bronchoscopic sampling. All samples were transferred to the laboratory on ice for immediate processing.

Participants were observed for at least one hour in the Theatre Admissions Unit, John Radcliffe Hospital and discharged after confirmation of satisfactory vital signs and swallowing assessment.

2.6.2 BAL processing

Bronchoalveolar lavage (BAL) was passed through a 100 µm sterile cell strainer and 2 x 1 ml aliquots of the filtrate (Raw BAL) were taken for storage at -80 °C. The remainder of the filtrate was centrifuged at 400 g for 5 min at 4 °C to sediment human cells. A 15 ml aliquot of cell-free supernatant was transferred into a fresh tube and the remainder discarded without disturbing the cell pellet. The cell-free supernatant was split into 10 x 1.1 ml aliquots and ultracentrifuged at 12,000 g for 5 min at 4 °C to precipitate bacteria, 1 ml supernatant was then transferred into new tubes (10 x cell free BAL supernatant) and stored at -80 °C until use in immunological assays. The pellets were resuspended in the residual volume

and the volume from 5 tubes combined to form 2 samples – the BAL raw pellet, and the BAL glycerol pellet (for metagenomic studies) to which 500 µl of 10% glycerol was added. Both samples were then stored at -80 °C. The BAL cell pellet was resuspended in the residual volume and if heavily blood stained, a red cell haemolysis was performed by adding 4.5 ml sterile water for 30 s followed by 500 µl 10x PBS (Invitrogen™, AM9624) before making up the volume to 50 ml with 1x PBS and centrifuging at 400 g for 5 min at 4 °C. The PBS wash was discarded, and cells resuspended in 1 ml fresh PBS. Viability count, with trypan blue (Gibco, 15250061), was performed using 10 µl and the concentration of the cell suspension adjusted to $1x10^6$ cells/ml prior to staining cells for flow cytometry and producing cytospins as previously described.

2.6.3 Endobronchial biopsy processing

2.6.3.1 Collagenase dispersal

Endobronchial biopsies were dispersed in 4 ml of type 1 collagenase from Clostridium histolyticum, (1 mg/ml C0130, Sigma-Aldrich, 9001-12-1) reconstituted in RPMI 1640 media without phenol red (Gibco, 11835030) for 1 h at 37 °C with magnetic stirring. The cell suspension was aspirated through a 23G needle into a 2 ml Luer lock syringe, then passed into a 5 ml test tube with 35 µm cell strainer snap cap (Thermo Fisher Scientific, 10585801) and centrifuged at 400 g for 5 min at 4°C. The supernatant was discarded, cells resuspended in the residual volume before haemolysing red cells by adding 2.7 ml sterile nuclease free water (DEPC treated, Invitrogen™, AM9915G) for 30 s followed by 300 µl sterile nuclease free 10x PBS (Invitrogen™, AM9624) and immediately centrifuging at 400 g for 5 min. Cells were then resuspended in 50 µl Cell Staining Buffer (BioLegend, 420201) for immediate flow cytometric staining and single cell RNA sequencing.

This method has been used by our group for dispersal of endobronchial biopsies given its favourable cell viability and yield, making it suitable in the present study in which single cell

genomic data was the key readout from this sample type (Hinks et al., 2015; Hinks et al., 2016b). However, enzymatic dispersal can sometimes cause cleavage of the CD4 co-receptor with diminished CD4 staining by flow cytometry (Hagman et al., 2012). This has been considered in the analysis of the flow cytometry and cell surface protein expression data.

2.7 Single cell RNA sequencing (scRNA-seq)

The following steps elaborate how dispersed nasal and endobronchial cells underwent flow cytometric and cell surface protein labelling for scRNA-seq (Cellular Indexing of Transcriptomes and Epitopes by sequencing, CITE-seq), flow cytometric sorting of viable cells, single cell capture using the 10x Genomics platform (10x Genomics, California, USA) and preparation of barcoded next-generation sequencing cDNA libraries for Illumina sequencing (Illumina, San Diego, CA, USA). In addition to isolating viable cells and thereby improving sample quality, flow cytometric sorting was used to equalise the proportion of CD45 positive:CD45 negative cells to ensure adequate capture of immune and non-immune populations respectively when generating single cell libraries. Without this step, given the higher proportion of CD45 negative cells in nasal brush and bronchial biopsy samples, immune cell populations would be inadequately captured for meaningful classification of cellular subsets in the analysis. This is a sorting approach that has been widely used in the Human Cell Atlas project, however meant that inferences could not be made about differences in absolute cell number across conditions or individuals over time in my analysis.

2.7.1 Single cell RNA-seq tissue processing

The aim was to co-stain for flow cytometric sorting and CITE-seq simultaneously to minimise sample handling and cell losses through repeated wash steps. As shown in Table 2.2 and Table 2.3, largely the same cell surface epitopes were targeted by both modalities for cross-validation of sequencing with flow cytometric data, ensuring no major cellular

subsets were disproportionately excluded in the single cell data through sample handling protocols or bioinformatic analysis. Where possible distinct clones were selected for each epitope target in the two panels to reduce the effect of steric hindrance limiting staining efficiency.

TotalSeq-C™ hashtag antibodies (Biolegend) were used to label nasal and bronchial cells from each donor and thus allow combination of two samples from these distinct anatomical sites when loading onto the 10x Chromium Controller (10x Genomics, Pleasonton, California, USA), with later bioinformatic separation of cells by site during analysis. Given the lower yield from bronchial biopsy compared to nasal brush, this allowed more cells to be loaded per channel to maximises the capture efficiency and avoided an intra-individual batch effect which would have been introduced by running the two samples in parallel channels. Total-Seq C™ antibody dilutions were prepared according to manufacturer's instructions.

Nasal or bronchial cells were resuspended in 50 µl of Cell Staining Buffer (BioLegend, 420201) and 5 µl of Human TruStain FcX™ Fc Blocking reagent (BioLegend, 422301) added before incubating for 10 min at 4 °C. A TotalSeq-C™ antibody pool was made (including IgG controls) and centrifuged at 14,000 g for 10 min at 4 °C as per manufacturer's recommendation. Cells were stained with TotalSeq-C™ antibodies, surface fluorochrome conjugated antibodies (shown in Table 2.2, excluding CRTH2), TotalSeq-C™ anti-human hashtag antibody (distinct for each sample type) and the final volume expanded to 100 µl with Cell Staining Buffer (BioLegend, 420201) before incubating for 15 min at 4 °C. Each sample was then split into two by volume and chemoattractant receptor-homologous molecule expressed on Th2 cells (CRTH2) antibody added to half, the other half of the sample acted as a fluorescence minus one (FMO) control. This has been shown to be a key control for identifying CRTH2 expressing, type-2 cytokine producing cells by our group (Hilvering et al., 2018). The sample was then incubated for a further 15 min at 4 °C. Cells

were washed with Cell Staining Buffer (BioLegend, 420201), centrifuged at 400 g for 5 min at 4 °C, then resuspended in 200 µl Cell Staining Buffer for flow cytometric sorting using the BD FACSAria III (BD Bioscience) by Dr Helen Ferry, as further elaborated in section 2.9.

Hashed nasal and endobronchial cells from each individual were combined, following flow cytometric equalisation of CD45+:CD45- ratio, and up to 50,000 cells loaded per individual participant on the 10x Chromium controller (10x Genomics) using 10x Genomics Chromium Next GEM Single Cell 5′ Reagent Kits v2 (Dual Index) as per manufacturer's instructions. The first 8 pilot samples were processed at the Oxford Centre for Genomics however following challenges with chip failure and low sequencing output, suspected due to transit time affecting cell viability, the remaining samples were processed in house and are included in the analysis.

Table 2.2 Bronchoscopy sample surface staining panel for flow cytometry

Target	Clone	Fluorophore	Company	Product code	Dilution (1/X)
CD161	DX12	BV786	BD Optibuild™	744096	10
CD25	SK1	BUV805	BD Horizon™	612889	50
CD19	SJ25C1	BV650	BioLegend	363026	15
CD45	HI30	BV605	BioLegend	304042	20
CD4	OKT4	BV570	BioLegend	317445	10
MAIT cell (MR1/5-OP-RU tetramer)	–	BV421-SA	NIH tetramer core, BioLegend	405225	30
CD16	B73.1	PerCP	BioLegend	360720	5
CD3	SK7	AF488	BioLegend	344810	20
CD294/CRTH2	BM16	PE-Cy7	BioLegend	350118	125
CD14	TuK4	PE-Texas Red	Invitrogen	MHCD1417	500
CD8	RPA-T8	AP-Cy7	BD Pharmingen™	GR3395607-1	40
CD127	HIL-7R-M21	APC-R700	BD Horizon™	565185	20
CCR3/CD193	61828	APC	R&D Systems	FAB155A-100	4

Table 2.3 CITE-seq antibodies

CITE-seq antibody	Clone	Barcode sequence	Company	Product code
TotalSeq™-C0048 CD45	2D1	TCCCTTGCGATTTAC	BioLegend	368545
TotalSeq™-C0083 CD16	3G8	AAGTTCACTCTTTGC	BioLegend	302065
TotalSeq™-C0050 CD19	HIB19	CTGGGCAATTACTCG	BioLegend	302265
TotalSeq™-C0081 CD14	M5E2	TCTCAGACCTCCGTA	BioLegend	301859
TotalSeq™-C0159 HLA-DR	L243	AATAGCGAGCAAGTA	BioLegend	307663
TotalSeq™-C0034 CD3	UCHT1	CTCATTGTAACTCCT	BioLegend	300479
TotalSeq™-C0046 CD8	SK1	GCGCAACTTGATGAT	BioLegend	344753
TotalSeq™-C0072 CD4	RPA-T4	TGTTCCCGCTCAACT	BioLegend	300567
TotalSeq™-C0581 TCR Vα7.2	3C10	TACGAGCAGTATTCA	BioLegend	351735
TotalSeq™-C0149 CD161	HP-3G10	GTACGCAGTCCTTCT	BioLegend	339947
TotalSeq™-C0584 TCR Vα24-Jα18	6B11	AACTTCTGTGGTAGC	BioLegend	342925
TotalSeq™-C0397 CD193 (CCR3)	5E8	ACCAATCCTTTCGTC	BioLegend	310733
TotalSeq™-C0124 CD31	WM59	ACCTTTATGCCACGG	BioLegend	303139
TotalSeq™-C0410 CD38	HB-7	CCTATTCCGATTCCG	BioLegend	356637
TotalSeq™-C0055 CD138	MI15	ACTCTTTCGTTTACG	BioLegend	356539
TotalSeq™-C0090 IgG1 Isotype control	MOPC-21	GCCGGACGACATTAA	BioLegend	400187
TotalSeq™-C0091 IgG2 Isotype control	MOPC-173	CTCCTACCTAAACTG	BioLegend	400293
TotalSeq™-C0251 Hashtag 1	LNH-94;2M2	GTCAACTCTTTAGCG	BioLegend	394661
TotalSeq™-C0252 Hashtag 2	LNH-94;2M2	GATGGCCTATTGGG	BioLegend	394663
TotalSeq™-C0254 Hashtag 4	LNH-94;2M2	AGTAAGTTCAGCGTA	BioLegend	394667
TotalSeq™-C0255 Hashtag 5	LNH-94;2M2	AAGTATCGTTTCGCA	BioLegend	394669
TotalSeq™-C0256 Hashtag 6	LNH-94;2M2	GGTTGCCAGATGTCA	BioLegend	394671
TotalSeq™-C0257 Hashtag 7	LNH-94;2M2	TGTCTTTCCTGCCAG	BioLegend	394673
TotalSeq™-C0258 Hashtag 8	LNH-94;2M2	CTCCTCTGCAATTAC	BioLegend	394675

2.7.2 Library generation

Sequencing libraries (5’ gene expression, cell surface protein and VDJ) were generated using the 10x Genomics Chromium Next GEM Single Cell 5′ Reagent Kits v2 (Dual Index) as per manufacturer’s instructions, at the advanced single cell omics facility (Wojciech Lason and Maria Greco, MRC Weatherall Institute of Molecular Medicine, University of Oxford) or in house by Bianka Brassanyi. Libraries were sequenced by Novogene (Cambridge, UK) using the NovoSeq X Plus platform (Illumina) with minimum target sequencing output of 120Gb, 24Gb and 12Gb for gene expression, cell surface protein and VDJ libraries, respectively.

2.7.3 Bioinformatic analysis

Raw data processing

FASTQ files were generated from BCL files using Illumina bcl2fastq. FASTQ files for gene expression, ADT and TCR data were processed using the 10x genomics Cell Ranger multi pipeline, using version 7.1.0 (with human reference genome GRCh38-2020-A) for the AMASS study samples and 9.0.0 (with human reference genome GRCh38-2024-A) for the MORSE study samples.

Quality control (QC) and filtering

The raw_feature_barcode_matrix from the Cell Ranger multi pipeline was imported into R using Seurat (v5.3.0) (Hao et al., 2021) for initial QC and filtering of individual samples.

DropletUtils (v1.20.0) (Griffiths et al., 2018; Lun et al., 2019) was used for identification and removal of empty droplets. Cells with low unique molecular identifiers (<150) and very high percentage mitochondrial reads (>20%) were removed, before using the consensus calling algorithm in cellhashR (v1.2.0) (Boggy et al., 2022) with the following methods: BFFcluster, BFFraw, GMM-Demux, MULTI-seq, Seurat HTODemux and DropletUtils hashedDrops, if ADT/HTO data was available. In these samples, cells called as consensus singlets were retained. Ambient RNA removal was performed using SoupX (v1.6.2) (Young and Behjati, 2020). Scrublet (v3.9.18) was used on the ambient corrected data for identification and filtering of cell doublets (Wolock et al., 2019) for all samples.

Samples were combined into a single data object for each study and a curated filtering approach based on cell lineage determined by mapping to the Human Lung Cell Atlas (Sikkema et al., 2023) was used. This was to ensure that neutrophils were not excluded, as often occurs in standardised workflows, due to their low RNA content (Wigerblad et al., 2022). Cells were filtered on minimum genes per droplet of 500, except for neutrophils (threshold 150), and less than 6-10% mitochondrial gene counts depending on cell lineage.

Normalization, integration, dimensionality reduction and clustering

In each study all samples were combined and normalised using SCTansform in Seurat. Cells from different donors were integrated using Harmony (v1.2.3) (Korsunsky et al., 2019) in Seurat. After integration, dimensionality reduction was performed using principal component analysis (PCA), and the elbow of a Scree plot was used to determine number of PCs for downstream UMAP generation and clustering. Clusters were identified using the Seurat graph-based clustering approach.

Cluster based annotation

Data was mapped against the Human Lung Cell Atlas (Sikkema et al., 2023), Human Tonsil Cell Atlas (Massoni-Badosa et al., 2024) and Human PBMC reference (Hao et al., 2021) using Azimuth (v0.5.0) (Hao et al., 2021). This approach was required as the human lung cell atlas lacked a granulocyte reference population, and neutrophils were typically assigned a label of CD14+ Monocyte. The Human Tonsil atlas contained reference populations of granulocytes and was helpful for identification of the myeloid lineage. Cluster markers were identified using Seurat FindAllMarkers using log-transformed normalised counts generated using the NormalizeData function in Seurat. These were defined as genes with significantly higher expression in a given cluster of interest relative to the average of all other clusters (log fold change >1, $p < 0.05$). Cluster annotations were refined manually using canonical markers defined by lineage.

Differential gene expression analysis

Differential gene expression analysis between different anatomical compartments or cell type before and after treatment with azithromycin was performed using MAST (Finak et al., 2015) with cellular detection rate and patient ID (PID) as covariates. In secondary analyses of the AMASS dataset, when samples were separated by presence or absence of infection, cellular detection rate was used as a covariate. The input data was log-transformed normalised counts. Genes with a fold change >0.25 and Benjamini-Hochberg adjusted p

values < 0.05 were defined as significantly expressed. Genes with identified as high ambient contaminants in at least 2 samples by SoupX were removed from differential gene expression analyses results. Two lists of genes were used based on cell lineage – one for epithelial cells and the second for myeloid and lymphoid cells. The second list removed the genes WFDC2, MUC5AC, SLPI, SCGB1A1, BPIFA1, BPIFB1, SCGB3A1, SERPINB3 and PIGR which were high ambient contaminants but expressed by airway epithelial cells and thus retained in the first list. The majority of remaining genes were long non-coding RNA, mitochondrial and immunoglobulin genes as would be expected.

List 1 (epithelial) – FP236383.3, MT-CO1, MALAT1, HBB, AC067930.1, MT-CO2, MT-CYB, SLC26A3, B2M, OOEP, LYPD2, MSMB, S100A6, AC010271.1, AC020922.3, AGR2, FP671120.4, FTH1, IGHV3-11, IGLV1-51, LINC00840, AC005387.1, AC008764.3, IGHV1-69D, IGLV1-40, IGLV3-10, LINC02637, MT-ND5

List 2 (myeloid and lymphoid) – FP236383.3, MT-CO1, MALAT1, WFDC2, MUC5AC, SLPI, HBB, AC067930.1, SCGB1A1, BPIFA1, BPIFB1, MT-CO2, SCGB3A1, SERPINB3, MT-CYB, SLC26A3, B2M, OOEP, LYPD2, MSMB, S100A6, AC010271.1, AC020922.3, AGR2, FP671120.4, FTH1, IGHV3-11, IGLV1-51, LINC00840, AC005387.1, AC008764.3, IGHV1-69D, IGLV1-40, IGLV3-10, LINC02637, MT-ND5, PIGR

Gene set enrichment analysis (GSEA) and over-representation analysis

Enriched gene sets were identified with GSEA using the FGSEA package (v1.32.4) (Sergushichev, 2016). Genes were ranked by the following score: avglog2FC x log10(p adj value + 10^-4) and assessed for enrichment against MSigDB's Hallmark gene set list collection. Over-representation analysis was performed using clusterProfiler (v4.14.6) (Yu et al., 2012) and ReactomePA (v1.50.0) (Yu and He, 2016) for gene ontology (GO) terms and Reactome pathways, respectively. The simplify function in clusterProfiler was used to

remove redundant terms. For conversion of gene symbols to Entrez IDs using the package org.Hs.eg.db (v3.20.0) was used.

Differential abundance testing with miloR

The Milo statistical framework in the miloR package (v2.2.0) was used to test for differences in cell abundance post-azithromycin therapy (Dann et al., 2022). A Milo object was constructed and a generalised linear model employed to account for PID as a covariate.

Plots

Plots were generated using the R package ggplot2 (v3.5.2) or GraphPad Prism (v10; GraphPad Software, LLC).

2.8 Flow cytometry

2.8.1 MR1/5-OP-RU tetramer

Biotinylated human MR1/5-OP-RU was supplied by the NIH Tetramer Core Facility. Tetramers were generated with Brilliant Violet 421 (BV421)-Streptavidin (BioLegend, 405225) following the NIH Tetramer Core Facility protocol. Tetramer staining was performed concurrently with cell surface staining.

2.8.2 Sorting and data acquisition prior to single cell sequencing

2.8.2.1 Single colour controls

To maximise nasal and bronchial cells for sorting, controls for flow cytometry were derived from heparinised blood collected following venepuncture on the day of bronchoscopy. Unstained, single colour and fully stained controls were generated from 100 µl unlysed whole blood per sample. Samples were stained for 30 min at RT. Red cell lysis was performed as per manufacturer's protocol with 10x RBC lysis buffer (BioLegend, 420301) or with BD FACS™ lysing solution 10x (BD, 10141013) to produce fixed dead cells for viability stain, both diluted 10-fold in sterile deionised water. Cells were washed with 2 ml

Cell Staining buffer (BioLegend, 420201), centrifuged at 400 g for 5 min at 4 °C before resuspending in 200 µl Cell staining buffer.

2.8.2.2 Staining BAL cells

BAL cells were isolated as described in section 2.7.2. Up to $5x10^5$ cells were stained using the panel shown in Table 2.2 in 200 µl Cell Staining Buffer (Biolegend, 420201) for 30 min at 4 °C, with an FMO control as previously described for CRTH2.

2.8.2.3 Cell sorting and data acquisition

Flow cytometric sorting of nasal and bronchial cells, and acquisition of data from blood and BAL cells was performed on the BD FACSAria III (BD Bioscience, Wokingham, UK) using a 100 µm nozzle. Samples were acquired and sorted using FACS DivaTM software (BD). Nasal and bronchial samples were prepared as described in section 2.7. Cells were stained with 5 µl 7-amino-actinomycin D (7AAD, BioLegend, 420403) as per manufacturer's instructions, 5 min prior to running.

Sorted cells were collected into 10% nuclease free BSA (Invitrogen™, AM2616) in PBS. All CD45 positive cells (capped at 15,000 cells) were sorted and a proportionate number of CD45 negative cells added, with a maximum of 30,000 cells collected from each sample to limit sorting time and avoid delays in single cell sequencing.

2.8.2.4 Gating strategy for immune cell populations in bronchoscopy study

The gating strategy used for sorting of CD45+/CD45- cells for downstream single cell analysis is shown below and is exemplified using a nasal brush sample. Cell numbers from endobronchial biopsy were typically lower. Additional immune cell populations are shown. This data helped to verify early on what populations of cells were likely to be captured in the single cell dataset.

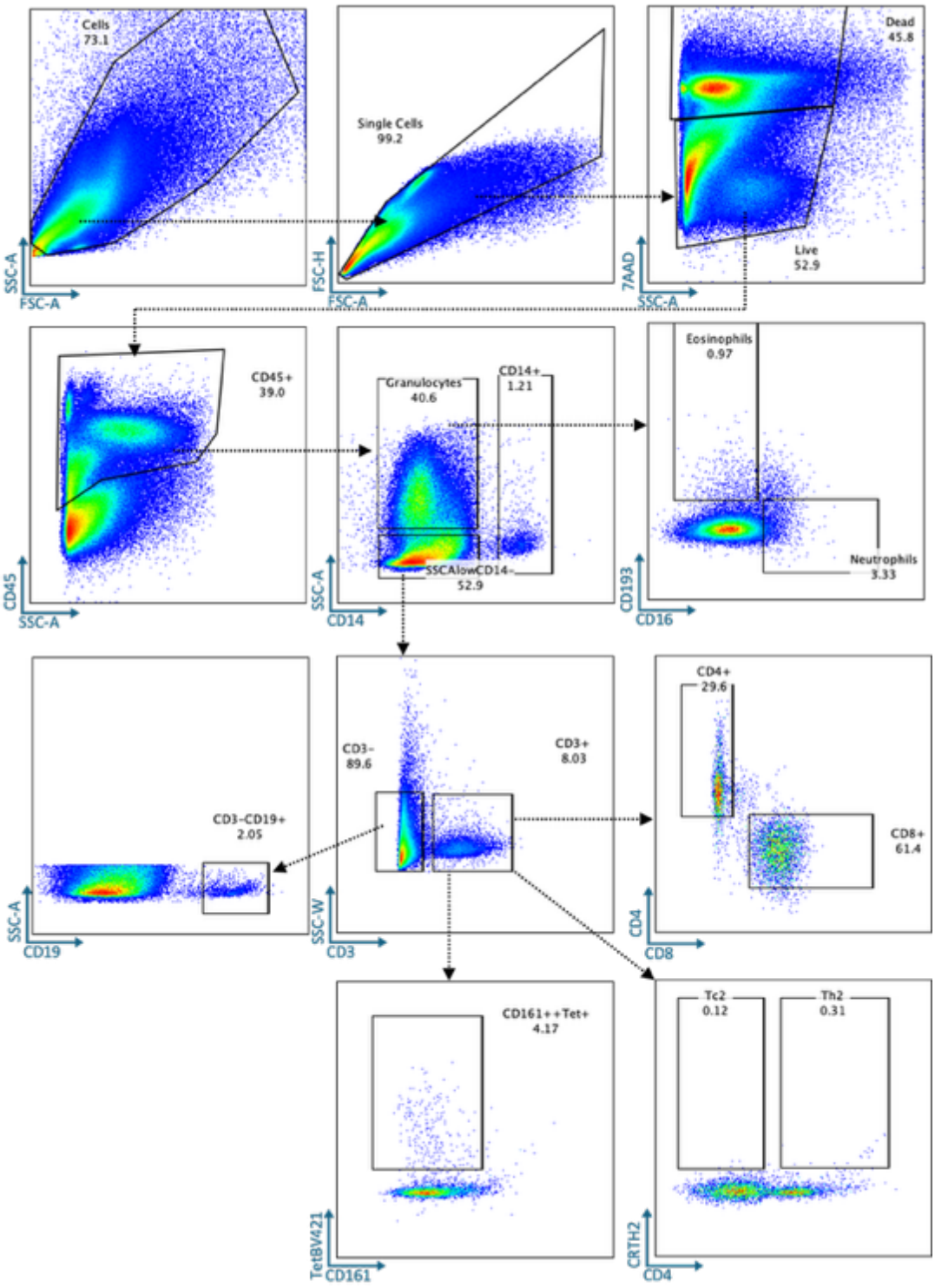


Figure 2.4 Flow cytometry gating strategy for sorting cells prior to scRNA sequencing

2.9 Meso-Scale Discovery platform

The Meso Scale Discovery (MSD, Maryland, USA) platform was selected for quantification of BAL chemokines and cytokines for its high sensitivity and multiplex functionality from a

small sample volume. The electrochemilumonescence technology it employs offers higher sensitivity than enzyme-linked immunosorbent assay (ELISA) and thus MSD was also used for a select number of single detection assays.

BAL supernatant samples were analysed using customised human V-PLEX assays restricted to biomarkers of interest as shown in Table 2.4, following the standard protocol with modifications after discussion with the manufacturer (personal communications with Chris Walker, Vice President Scientific Support). A minimum 2-fold dilution of samples is generally recommended with the provided diluent which contains components designed to reduce non-specific binding, however in the case of BAL which was deemed to have a very simple matrix by the manufacturer this dilution step was excluded and samples loaded neat on to the assay plate to increase sensitivity, alongside lengthening incubation time of the plate from 2 h to overnight at 4 °C. Plates were analysed on the MESO QuickPlex SQ 120MM (MSD, Maryland, USA).

Table 2.4 MSD Panels

Panel	Biomarkers
Proinflammatory Panel 1	IFN-γ, IL-1β, IL-2, IL-4, IL-6, IL-10, IL-12p70, IL-13, TNF-α
Cytokine Panel 1	GM-CSF, IL-5, IL-17A
Chemokine Panel 1	Eotaxin, MIP-1β, Eotaxin-3, TARC, IP-10, MIP-1α, IL-8, MCP-1, MDC
Angiogenesis Panel 1	bFGF
TH17 Panel 1	IL-22
Cytokine Panel 2	IL-1RA

2.10 Quantification of Neutrophil Extracellular Traps

Abundance of neutrophil extracellular traps (NETs) was measured using a protocol kindly shared by Prof. Sarah Walmsley (University of Edinburgh). This combined human neutrophil elastase/ELA2 (R&D Systems Inc., DY9167-05) and cell death detection (Roche, 11544675001) kits to measure DNA-elastase complexes in BAL. In sputum DNA-elastase has been shown to correlate with individual measures of NET constituents including cell-

free DNA, myeloperoxidase (MPO) and neutrophil elastase (Dicker et al., 2018). Early time-course studies have also shown correlation between NET-associated elastase and DNA with immunofluorescence imaging techniques (Fuchs et al., 2007). Imaging is often considered the gold standard of NET quantification as it objectively distinguishes cell death mechanism. A 96-well microplate was coated with the neutrophil elastase capture antibody (100 µl/well) at working concentration in PBS and incubated overnight at RT. The plate was washed 3 times with 300 µl/well of wash buffer (0.05% Tween 20 in PBS) before adding 150 µl/well of blocking buffer (2% BSA in PBS) and incubating for 1 h at RT with shaking (500 rpm). The plate was washed as before, 50 µl of BAL supernatant loaded per well in duplicate and incubated for 2 h at RT with shaking. Using the cell death detection kit reagents, the plate was washed 3 times with 300 µl/well of wash buffer, 5 0µl/well of anti-DNA-POD conjugation solution was then added before incubating for 2 h at RT with shaking. The plate was washed as before wash buffer and 100 µl/well of substrate solution added. The plate was read at 5-minute intervals up to 20 min at OD 405 nm and OD 490 nm on the SPECTROstar Nano (BMG Labtech).

Chapter 3: Metagenomics of Severe Asthma[2]

3.1 Introduction

Culture independent techniques of microbial detection have been pivotal in dispelling the theory of lung sterility, instead, they have revealed the niche specificity of the airway microbiota by anatomical location and compositional changes accompanying inflammatory responses in chronic airways diseases (Hilty et al., 2010). In asthma, the field of airway metagenomics first expanded with wider application of bacterial 16S rRNA sequencing (Diver et al., 2020; Durack et al., 2017; Goleva et al., 2013; Simpson et al., 2016) and more recently shotgun metagenomic sequencing approaches.

Early studies were restricted by sequencing approaches unable to assign taxonomic identification at species level, limited clinical phenotyping, and were often further limited by small sample size. These reported diminished bacterial α-diversity, *Pseudomonadota* enrichment particularly *Haemophilus, Moraxella* and *Neisseria spp.* (Green et al., 2014; Hilty et al., 2010; Huang et al., 2015), with depletion of airway commensals in severe asthma (Taylor et al., 2018). Clinical features including the extent of airflow obstruction (Denner et al., 2016), bronchial hyper-responsiveness (Huang 2011) and presence of atopy (Durack et al., 2017) in mild-to-moderate disease have been linked to changes in the microbiome, alongside corticosteroid responsiveness in asthma (Durack et al., 2020; Huang et al., 2015). Across a spectrum of disease severity, type-2 high eosinophilic inflammation has been linked to lower total bacterial load (Durack 2020, Huang 2015) and greater α-diversity (Sverrild et al., 2017; Taylor et al., 2018) compared to type-2 low asthma.

[2] Where indicated text and data included in this chapter have been published previously in Jabeen *et al.*, Microbiology Spectrum, 2022 (DOI: 10.1128/spectrum.02279-21) or Jabeen *et al.*, Allergy, 2024 (DOI: 10.1111/all.16269)

The composition of the upper airway (nasal) microbiome is also altered in asthma compared to health (Chen et al., 2022).

A widely replicated and highly clinically relevant finding was the emergent pattern of dominance by specific airway pathogens, most often *H. influenzae* in the lower airway of patients with severe asthma, detected using pathogen specific PCR assay or metagenomic sequencing (Diver et al., 2020; Jabeen et al., 2022; Simpson et al., 2016); this was linked to commensal depletion (namely, *Streptococcus, Gemella*, and *Porphyromonas* taxa) (Taylor et al., 2018), neutrophilic inflammation and poor asthma outcomes (Abdel-Aziz et al., 2021). The AMAZES clinical trial (Gibson et al., 2017) demonstrated that long term low dose azithromycin could be a highly effective targeted therapy within this group, particularly in the presence of high *H. influenzae* load (Taylor et al., 2020).

At the time of conception of this study, the prevalence of airway dominance with *H. influenzae* or other airway pathogens had not been reported using a metagenomic approaches resolved to species level in a highly phenotyped cohort, I hypothesised that it was a common treatable trait in severe asthma accompanying neutrophilic airways inflammation, driven by type-1 cytokine responses. In the following chapter I outline how I tested this hypothesis using metagenomic sequencing with Oxford Nanopore Technologies. These sequencing devices use flow cells containing an array of protein nanopores embedded in an electro-resistant membrane through which a voltage is applied in an electrolytic solution to generate an ionic current which drives DNA or RNA molecules through the nanopore. Translocation produces changes in the ionic current, corresponding to the nucleotide sequence and can be decoded real-time computationally. Nanopore offers rapid long-read sequencing, with improved species level taxonomic classification and assembly quality compared to short-read Illumina platforms (Greenman et al., 2024). In addition, its unique capacity for real-time analysis of direct clinical samples provides greater ease of application and earlier results than routine culture when translated to clinical

workflows. I developed a method for metagenomic sequencing of induced sputum samples using Nanopore in a pilot cohort of severe asthma patients, comparing the method with sputum culture as the gold standard for microbiological diagnostics, semi-quantitative qPCR and widely used short-read Illumina sequencing. I then expanded this sequencing approach to a larger population of severe asthma patients from the Wessex and Oxford cohorts, performing an integrated metagenomic and proteomic analysis of the upper and lower airways.

3.2 Hypothesis

- Metagenomic sequencing using Nanopore achieves reliable species-level taxonomy when applied to induced sputum samples collected during clinical stability from patients with severe asthma.

- A pathogen-dominant airway microbiome is common in severe asthma, confined to the lower airways, associated with type-1 inflammatory responses and airways neutrophilia.

3.3 Aims

- To optimise a method for metagenomic sequencing of low biomass induced sputum samples using Nanopore, comparing validity of results against sputum culture, qPCR and Illumina sequencing.
- To define the prevalence of pathogen-dominance within the microbiome, by inflammatory phenotype, in severe asthma using Nanopore sequencing.
- To discern inflammatory signals driving inflammation in the context of pathogen dominance through integrated metagenomic and proteomic analysis.

- To compare the upper and lower airway microbiome and proteome in severe asthma.

3.4 Oxford Nanopore Technologies for airway metagenomic sequencing[3]

3.4.1 Clinical characteristics of pilot cohort

Induced sputum was collected from 23 adult participants with severe asthma during a period of clinical stability, and one healthy participant. Baseline characteristics are summarised in

***Table* 3.1** and the healthy participant's demographic data shown in Table S1 of Appendix 1 (Jabeen *et al.* 2022). In this small cohort, all severe asthma patients received high dose inhaled corticosteroids with 39% requiring maintenance oral corticosteroids. None had commenced biologic therapy. There was a history of smoking in 52%, with mean 12 pack years smoked.

[3] Text and figures in this section are largely derived from Jabeen *et al.*, Microbiology Spectrum, 2022 (DOI: 10.1128/spectrum.02279-21). Experimental work was undertaken during my NIHR Academic Clinical Fellowship (2017–2018). Data analysis and manuscript publication was completed during this DPhil.

Table 3.1 Clinical characteristics of participants in pilot cohort

Characteristic	Severe Asthma (n=23)		*H. influenzae* negative (n=15)		*H. influenzae* positive (n=8)		P Value
Male sex, n (%)	13	(57)	9	(69)	4	(31)	0.66
Age (years), Mean (SD)	67	(10)	69	(9)	62	(10)	0.07
BMI (kg/m^2), Mean (SD)	28.4	(6.10)	28.2	(6.20)	28.8	(28.2)	0.83
Ex-smoker, n (%)	12	(52)	7	(58)	5	(42)	0.49
Pack years, Mean (SD)	12	(10)	11	(6)	14	(15)	0.62
Baseline inhaled corticosteroid use (BDP eq., mcg/d), Median (Range)	2000	(1700)	2000	(1700)	2000	(1200)	0.97$^{\#}$
Maintenance oral corticosteroid, n (%)	9	(39)	8	(89)	1	(11)	0.06
Unscheduled GP/ hospital visits in 12 months, Median (Range)	4	(7)	4	(5)	5	(6)	0.79$^{\#}$
Corticosteroid courses in 12 months, Median (Range)	3	(10)	2	(10)	3	(9)	0.84$^{\#}$
Antibiotic courses in 12 months, Median (Range)	0	(7)	0	(7)	2	(6)	0.40$^{\#}$
Presence of atopy, n (%)	11	(48)	6	(55)	5	(46)	0.33
Presence of nasal polyps, n (%)	7	(30)	4	(57)	3	(43)	0.61
FEV1 (%predicted), Mean (SD)	69.6	(16.8)	69.9	(15.1)	68.9	(20.8)	0.58$^{\#}$
FEV1/FVC, Mean (SD)	0.58	(0.10)	0.56	(0.10)	0.62	(0.10)	0.21
FeNO (ppb), Mean (SD)	62	(68)	75	(74)	40	(53)	0.26
Blood eosinophils (x10^9/L), Mean (SD)	0.50	(0.44)	0.53	(0.35)	0.45	(0.58)	0.56$^{\#}$
Sputum eosinophils (%), Median (Range)	0.50	(23)	1	(23)	0.10	(2)	**0.01$^{\#}$**
Sputum neutrophils (%), Median (Range)	72	(79)	54	(65)	93	(37)	**<0.01$^{\#}$**
Sputum Inflammatory phenotype[1], n (%)							
Total with valid data	21		13		8		
Eosinophilic	5	(24)	5	(38)	0	(0)	
Neutrophilic	13	(62)	5	(38)	8	(0)	
Mixed granulocytic	0	(0)	0	(0)	0	(0)	
Paucigranulocytic	3	(14)	3	(23)	0	(0)	

BMI, body mass index; GP, general practitioner; FEV1, forced expiratory volume in 1s; FVC, forced vital capacity; FeNO, exhaled nitric oxide; 1. Percentages given are provided from subjects with valid data; Inflammatory phenotyes: eosinophilic ≥3% sputum eosinophils, neutrophilic ≥61% sputum neutrophils and <3% eosinophils, mixed granulocytic >61% sputum neutrophils and >3% eosinophils, paucigranulocytic <61% sputum neutrophils and <3% eosinophils; Comparisons between groups made using unpaired t test or $^{\#}$Mann-Whitney test. P values < 0.05 are highlighted in bold.

3.4.2 Airway microbiome in severe asthma and definition of pathogen dominance in a pilot cohort

H. influenzae emerged as the most frequently detected, potentially pathogenic organism in sputum using both routine culture and molecular techniques. Pathogen dominance was defined by a clinically significant qPCR result of ≥1x10^6 copies/ml, a threshold demonstrated to have 98% concordance with routine culture and longitudinally reproducible for detection of neutrophilic bacterial exacerbations in COPD (Bafadhel et al., 2015), and highest abundance (%reads/total bacterial reads) on metagenomic sequencing (Nanopore and Illumina), with or without a positive culture result. Full microbiological results are shown in **Table 3.2**. Using these criteria, **Table 3.1** further summarises participants by the absence (HI-) or presence (HI+) of a *H. influenzae* dominant microbiome. HI+ participants had sputum neutrophilia, with a significantly lower sputum eosinophil:neutrophil ratio (p = 0.03,

Mann-Whitney test), and relatively lower mean FeNO (HI- 75 ppb vs. HI+ 40 ppb). There were no statistically significant differences in blood eosinophil count or smoking history.

Table 3.2 Summary of sputum microbiology results and inflammatory phenotype

PID	Age (yrs)	Sex	Smoking status (pack yrs)	*H. inf* culture	*H. inf* reads (%bacterial reads)	*H. inf* qPCR	*S. pneu* qPCR	*M. cat* qPCR	*P. aeru* qPCR	*S. aur* qPCR	Total 16S	Sputum neutrophils (%)	Sputum eosinophils (%)	FeNO (ppb)
						(x10^6 copies/ml)								
1054	53	M	Ex (10)	+	93.5	**983.80**	**1.89**	−	−	−	8510	**93.2**	0.5	nd
278	50	M	Ex (40)	+	86.5	**435.40**	−	0.79	−	−	2832	**84.7**	0	11
133	60	F	Never	+	66.6	**91.70**	**1.99**	−	−	−	1643	**98.2**	0	29
297	76	F	Never	+	66.6	**40.00**	**1.72**	−	−	−	1042	**75**	0	21
288	67	M	Ex (9)	+	58.0	**31.00**	−	−	−	0.02	572	**96.7**	0.2	**169**
29	76	F	Ex (10)	+	47.1	**16.50**	0.17	−	−	−	633	**62.7**	0.5	9
214	54	M	Ex (<1)	+	17.1	**12.50**	−	−	−	−	338	**99.5**	0	20
1049	57	F	Never	−	51.3	**12.40**	−	−	−	−	297	**91.7**	2	20
235	57	M	Never	−	3.3	0.70	−	−	−	−	335	20.5	0.5	37
306	69	F	Never	−	0.03	0.30	−	−	−	−	1006	**82.2**	1	**85**
187	66	M	Ex (12)	−	0.05	0.03	−	−	−	−	1822	25.2	**7.5**	**300**
1052	79	M	Never	−	0.1	0.02	−	**35.63**	−	−	695	**65.2**	1.2	**125**
294	62	F	Never	−	0.05	0.02	−	−	−	−	43	nd	0.5	28
1055	70	F	Ex (15)	−	0.6	0.01	−	−	−	−	91	58.2	**15.5**	**138**
1053	59	M	Ex (10)	−	0.5	0.01	−	−	−	−	1754	**85.7**	0.7	**64**
1041	73	F	Ex (8)	−	1.0	0.01	−	−	−	−	286	43.2	0.5	8
5	67	M	Never	−	0.07	−	−	−	−	−	661	53.7	11	8
275	76	F	Never	−	2.8	−	**5.95**	−	−	−	696	**83.7**	0.7	20
315	61	M	Never	−	0.05	−	−	−	−	−	115	22.2	0.2	**78**
1060	86	M	Ex (8)	−	0.0	−	−	−	−	−	58	32.7	**22.9**	16
279	60	F	Never	−	0.05	−	−	−	−	−	216	nd	nd	48
295	81	M	Ex (20)	−	0.4	−	−	−	−	−	191	**72**	0	**78**
1058	72	M	Ex (3)	−	1.0	−	−	−	−	−	95	41.5	**15.1**	**89**

Threshold values; qPCR: *H.inf/ S.pneumoniae/ M.catarrhalis/ P.aeruginosa/ S.aureus* >1X10^6 copies/ml, sputum neutrophilia ≥61%, sputum eosinophilia ≥3%, high FeNO ≥45 ppb. Values above indicated threshold levels are shown in bold. Participants are ranked according to detection of *H.influenzae* by quantitative PCR. +, denotes organism detected and −, denotes organism not detected by routine culture and MALDI-TOF

3.4.3 Comparison of Nanopore and Illumina sequencing

A limited comparison (n=2) was made between two methods of host DNA depletion in sputum, namely differential centrifugation and the NEBNext Microbiome DNA enrichment kit, prior to DNA extraction using the QIAamp DNA minikit. Differential centrifugation relies on a two-step centrifugation process first removing large host cells, then precipitating bacteria through ultracentrifugation, whereas the NEBNext kit enriches microbial DNA by selectively binding and removing CpG-methylated host DNA. Differential centrifugation produced 2.6 to 2.7-fold increase in total bacterial reads, whereas the NEBNext Microbiome kit achieved 2.9 to 3.1-fold increase when compared to matched samples with no host DNA depletion. This corresponded to up to 8.2% and 13.5% reduction in the proportion of unfiltered human reads, respectively. Differential centrifugation was selected for use with Nanopore sequencing given the benefits of less sample handling (lower risk of introducing metagenomic contaminants), and lower per sample cost.

Metagenomic sequencing of total DNA transcripts with Nanopore was compared with Illumina MiSeq and gold standard sputum culture. This sequencing approach was selected over 16s rRNA gene amplicon sequencing as the aim was to ensure resolution of dominant organisms to a species level over higher taxonomic ranks. Total bacterial load (16S) was measured by qPCR. All organisms isolated by sputum culture are shown in Table S2 of Appendix 1 (Jabeen et al. 2022). Close concordance was seen between molecular methods and sputum culture in HI+ participants; only 1/8 participants had a negative culture in presence of a positive qPCR result (**Table 3.2**). A direct comparison was made of Nanopore and Illumina MiSeq. As expected, longer read lengths were achieved with Nanopore (median of average read length/sample: Nanopore 2,013 bp vs. Illumina MiSeq 172 bp) but Illumina MiSeq had a higher quality score (median [IQR] Q20: Nanopore 50% [41%] vs. Illumina MiSeq 76% [20%]). Full raw read statistics generated using SeqKit are shown in

Appendix 1 (Jabeen et al. 2022, Supplementary file). There was near complete taxonomic agreement between the two technologies, with similar composition observed at species level, demonstrated using paired HI+ samples in **Table 3.3**, and heatmaps shown in Figure 3.1 of relative abundance of species from all samples.

Table 3.3 Top 5 abundant species detected by Nanopore and Illumina MiSeq in HI+ samples

PID	Nanopore	%Bacterial reads	Ilumina MiSeq	%Bacterial reads
1054	*Haemophilus influenzae*	93.5	*Haemophilus influenzae*	90.9
	Streptococcus pneumoniae	0.8	*Streptococcus pneumoniae*	1.3
	Escherichia coli	0.3	*Neisseria meningitidis*	0.4
	Neisseria meningitidis	0.3	*Tropheryma whipplei*	0.3
	Haemophilus haemolyticus	0.2	*Haemophilus haemolyticus*	0.1
278	*Haemophilus influenzae*	86.5	*Haemophilus influenzae*	82.6
	Escherichia coli	1.3	*Moraxella catarrhalis*	0.1
	Salmonella enterica	0.3	*Haemophilus parainfluenzae*	0.1
	Shigella flexneri	0.2	*Haemophilus haemolyticus*	0.1
	Helicobacter pylori	0.2	*Streptococcus pseudopneumoniae*	0.1
133	*Haemophilus influenzae*	66.6	*Haemophilus influenzae*	72.9
	Streptococcus pneumoniae	7.3	*Streptococcus pneumoniae*	8.8
	Escherichia coli	2.7	*Haemophilus haemolyticus*	0.6
	Salmonella enterica	0.6	*Prevotella melaninogenica*	0.2
	Shigella boydii	0.5	*Haemophilus parainfluenzae*	0.2
297	*Haemophilus influenzae*	66.6	*Haemophilus influenzae*	67.6
	Streptococcus pneumoniae	12.8	*Streptococcus pneumoniae*	14.4
	Escherichia coli	3.2	*Haemophilus parainfluenzae*	0.1
	Shigella boydii	0.4	*Haemophilus haemolyticus*	0.1
	Salmonella enterica	0.3	*Streptococcus mitis*	0.1
288	*Haemophilus influenzae*	58.0	*Haemophilus influenzae*	79.8
	Escherichia coli	3.7	*Neisseria subflava*	0.9
	Shigella flexneri	1.0	*Haemophilus aegyptius*	0.5
	Salmonella enterica	0.9	*Haemophilus parainfluenzae*	0.5
	Shigella boydii	0.7	*[Haemophilus] ducreyi*	0.4
29	*Haemophilus influenzae*	47.1	*Haemophilus influenzae*	69.4
	Escherichia coli	4.6	*Streptococcus pneumoniae*	4.6
	Streptococcus pneumoniae	1.8	*Rothia dentocariosa*	1.0
	Shigella boydii	0.9	*Rothia mucilaginosa*	1.0
	Salmonella enterica	0.9	*Veillonella dispar*	0.8
214	*Haemophilus influenzae*	17.1	*Haemophilus influenzae*	80.7
	Escherichia coli	15.4	*Haemophilus haemolyticus*	0.3
	Helicobacter pylori	3.6	*Prevotella oris*	0.3
	Salmonella enterica	1.9	*Veillonella dispar*	0.2
	Shigella flexneri	1.3	*Haemophilus parainfluenzae*	0.2
1049	*Haemophilus influenzae*	51.3	*Haemophilus influenzae*	53.7
	Tropheryma whipplei	10.9	*Tropheryma whipplei*	29.9
	Escherichia coli	5.2	*Veillonella parvula*	0.6
	Shigella boydii	0.8	*Haemophilus haemolyticus*	0.3
	Shigella flexneri	0.6	*Streptococcus pseudopneumoniae*	0.2

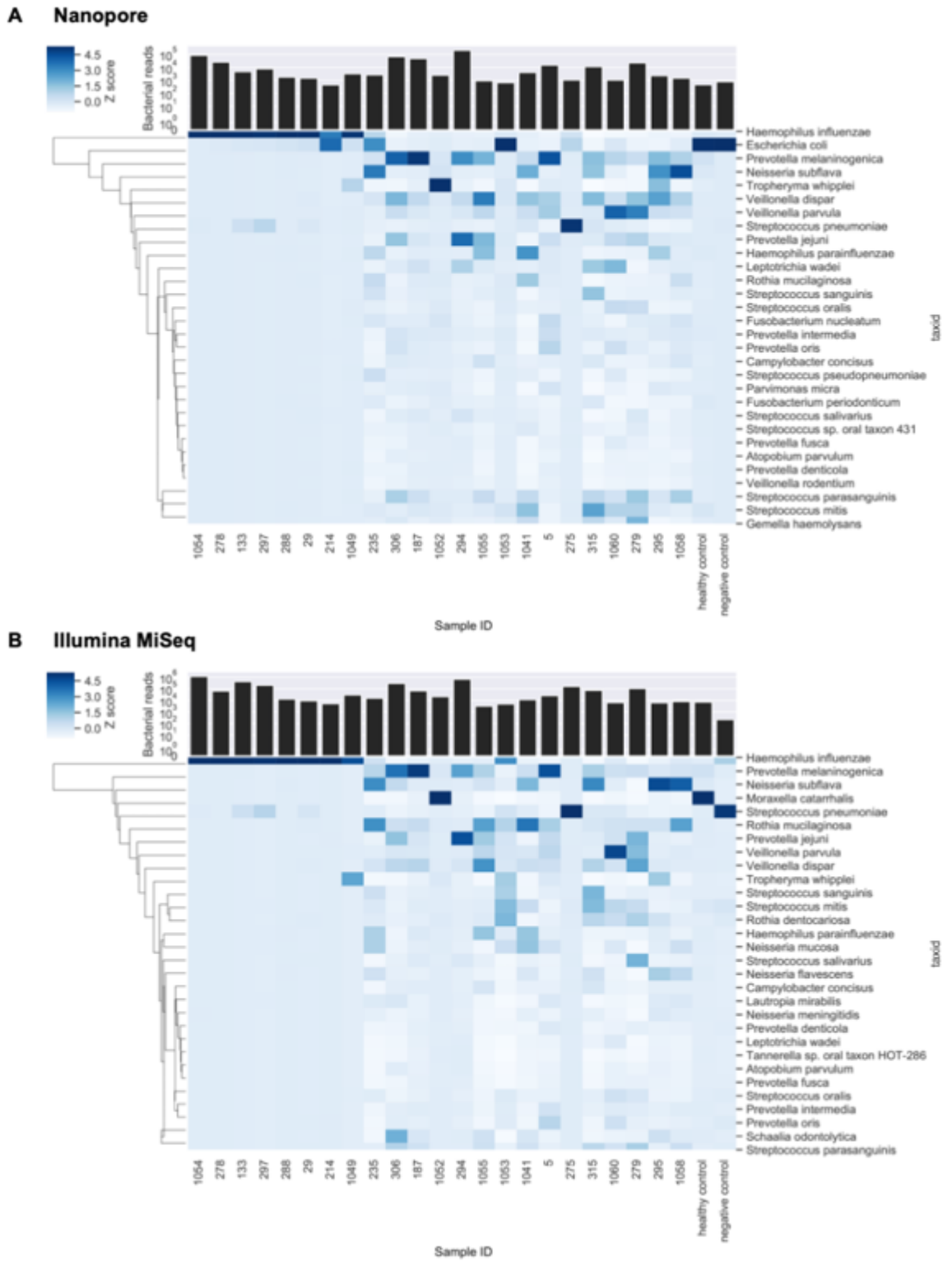


***Figure 3.1 Sputum microbiome with Nanopore and Illumina sequencing**;*

Heatmap of relative abundances of bacterial species on metagenomic sequencing using (A) Nanopore or (B) Illumina MiSeq, Z-scores, denoted by shade, represent the number of standard deviations above the mean number of bases per taxon for each sample. Total bacterial reads detected per sample are also shown in stacked bar charts[4].

[4] Heatmap produced by Dr ND Sanderson

In addition, Nanopore provided greater *H. influenzae* genome coverage at any given depth of sequencing compared with Illumina MiSeq, in all sequenced samples (**Figure 3.2**). Four isolated clinical strains were cultured and sequenced by Nanopore (PID 278, 133, 29 and 288). Consensus *H. influenzae* genomes were constructed from sequences derived from the cultured and corresponding clinical samples. Using this approach, reconstructed genomes from two clinical samples (PID 278 and 133) achieved adequate coverage (91.4% and 53.8% respectively) for reliable comparison with sequences from the cultured strains. In **Figure 3.3**, the single nucleotide polymorphism (SNP) distance matrix shows very few SNPs (high degree of similarity) between *H. influenzae* genomes reconstructed from the clinical samples and their corresponding cultured clinical strains.

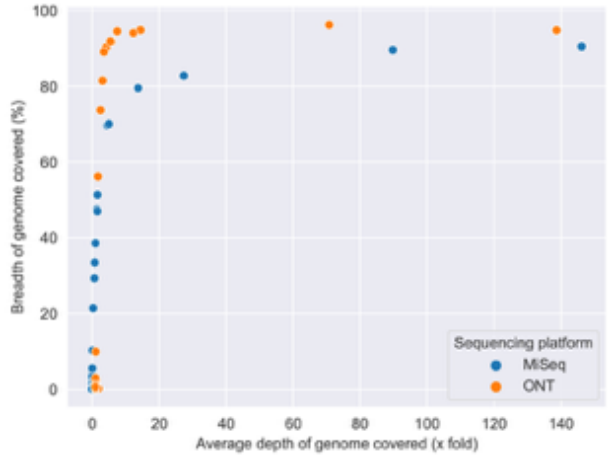


Figure 3.2 H. influenzae genome coverage by Nanopore (ONT) and Illumina MiSeq; *breadth of reference genome coverage against average depth of coverage by sequencing technology*[5].

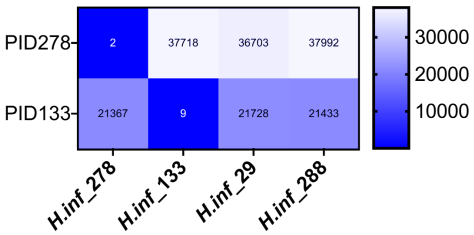


Figure 3.3 Single nucleotide polymorphism (SNP) distance matrix; *pairwise comparisons (n=4) of SNPs amongst metagenomic sequences from direct clinical samples and cultured clinical H. influenzae isolates with Nanopore sequencing.*

[5] Figure produced by Dr ND Sanderson

M. catarrhalis was detected by Illumina MiSeq but not Nanopore in the healthy control and a single clinical sample (PID1052), in the absence of positive culture results (**Figure 3.1** B). Both samples had a clinically significant PCR result ($1.8x10^6$ and $35.6x10^6$ copies/ml, respectively). The healthy control sample had low total reads on sequencing; with Illumina MiSeq 58.9% of total bacterial reads were assigned to *M. catarrhalis* yet with Nanopore *E. coli* had highest abundance (12.5%) followed by *M. catarrhalis* (10.2%). In PID1052, *M. catarrhalis* was the most abundant species detected with Illumina MiSeq (74.5% of total bacterial reads) but not Nanopore (<1% of total bacterial reads).

The negative control sample yielded low total reads following sequencing with Nanopore or Illumina MiSeq, however the composition was noted to differ by modality (**Figure 3.1**). *Escherichia coli* was detected with Nanopore and is thought to represent either low level contamination or metagenomic misclassification, thereby also accounting for its relative abundance in samples with lower total reads (PID: 214, 235, 1053, 275 and healthy control). *S. pneumoniae* was found to be the most abundant organism using Illumina MiSeq (12% total bacterial reads), but fell below the limit of detection of the S*. pneumoniae* qPCR assay and was not considered a significant contaminating signal as it did not appear as a dominant organism in other samples with a negative qPCR result.

3.4.4 Co-existent airway pathogens in severe asthma

In addition to H. influenzae, qPCR was also performed for other common respiratory pathogens in airways disease including Streptococcus pneumoniae, Staphylococcus aureus, Moraxella catarrhalis and Pseudomonas aeruginosa with the same clinically significant threshold of $>1x10^6$ copies/ml. A positive result for S. pneumoniae by qPCR (

Table 3.2) was found in 38% of HI+ participants (n= 3/8), in whom it was also detected as the second most abundant species on sequencing and present on sputum culture. In this pilot cohort, sputum neutrophilia and a positive PCR result for *S. pneumoniae* (PID 275) or *M. catarrhalis* (PID 1052) alone was detected in one participant each with concordance seen by culture and Nanopore sequencing for *S. pneumonia,* but not *M. catarrhalis.*

3.4.5 Bacterial spiking and limits of detection

I attempted to evaluate the limit of detection for *H. influenzae, S. pneumoniae, S. aureus, M. catarrhalis*, and *P. aeruginosa* in clinical samples using Nanopore sequencing, comparing against single pathogen qPCR assays. A pooled airway sample was generated from 5 individuals with no single dominant pathogen, to capture a variation in lung microbiota within a cohort of patients with severe asthma during a period of clinical stability and allow the same baseline sample to be tested across the spiking conditions. Three pooled and spiked samples were produced containing 10^4, 10^6 or 10^8 CFU/ml of each bacterial organism. An increase was seen in total bacterial reads with increasing concentrations of bacterial spike, corresponding with a rise in 16S PCR load from a background level of $4.8x10^8$ copies/ml (unspiked pool) to $1.5x10^{10}$ copies/ml with 10^8 CFU/ml spike. Reads classified as *H. influenzae, S. pneumoniae, S. aureus, M. catarrhalis* and *P. aeruginosa* were observed in the pooled un-spiked and spiked samples. The greatest proportional rise in total bacterial reads upon spiking was achieved by *H. influenzae* and *S. pneumoniae* (**Figure 3.4**), with near complete genome coverage achieved at 10^6 CFU/ml. A modest increase was observed in bacterial reads upon spiking with *P. aeruginosa*, with >1% bacterial reads and 50% genome coverage at 10^6 CFU/ml. Recovery of *S. aureus*, and more so, *M. catarrhalis* were poor with both Nanopore (<1% of total bacterial reads) and PCR. A high abundance of *H. influenzae* and *P. aeruginosa* (>$1x10^6$ copies/ml) was present in the pooled sample, crossing the threshold of clinical significance. This threshold

was surpassed by *S. pneumoniae* at 10^4 CFU/ml and *S. aureus* at 10^8 CFU/ml but not by *M. catarrhalis*.

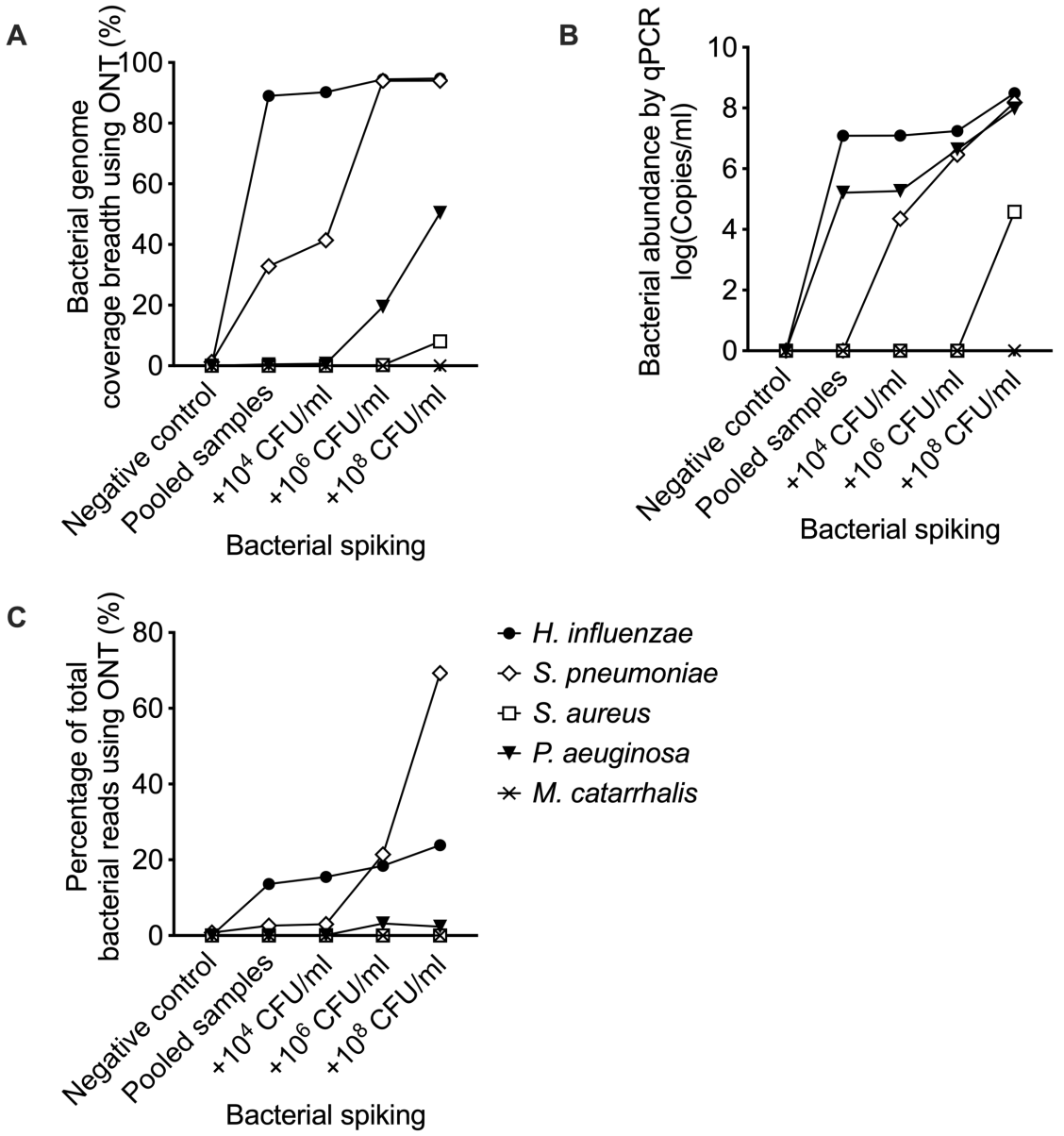


Figure 3.4 Recovery of spiked bacterial species using Nanopore and qPCR;

recovery of spiked organisms (H. influenzae, S. pneumoniae, S. aureus, P. aeruginosa or M. catarrhalis) recovered on Nanopore sequencing expressed as (A) coverage breadth of reference genome and (C) proportion of total bacterial reads, or (B) pathogen specific qPCR

3.4.6 Discussion

This study was the first to report a method for direct from sample metagenomic sequencing using Nanopore in asthma. Within this pilot cohort, a pathogen dominant microbiome was

detected in ~35% (n=8/23), with *H. influenzae* as the prevalent organism. The results were validated using Illumina MiSeq, qPCR and the gold standard of clinical diagnostics, sputum culture.

Concordance between Nanopore and Illumina as demonstrated here in sputum, has also been reported in nasal microbiome (Heikema et al., 2020). At the time of publication, Nanopore had been used for the diagnosis of bacterial lower respiratory tract infection using respiratory samples of higher biomass than sputum plugs (Charalampous et al., 2019). Despite this, near complete genome coverage was achieved in the majority of HI+ samples in this study. Moreover, compared to Illumina MiSeq, Nanopore achieved superior breadth of genome coverage at any sequencing depth within the HI+ group. The breadth of reconstructed consensus genomes using Nanopore also allowed similarities between *H. influenzae* strains to be appreciated. A high level of agreement was observed between Illumina MiSeq and Nanopore sequencing, most notably in samples with a positive pathogen qPCR result or culture. An exception to this was the detection of *M. catarrhalis* by Illumina MiSeq but not Nanopore in the presence of a positive PCR result. This was hypothesised to be an artefact of Nanopore library preparation rather than a systematic sequencing technology error as Nanopore successfully identified pathogen dominance by *M. catarrhalis* in the presence of concordant positive PCR results in the larger definitive cohort of severe asthma patients (Jabeen et al., 2024). Detection of *M. catarrhalis* in the healthy control – with normal lung function, sputum neutrophil count and no history of acute respiratory illness – could represent capture of asymptomatic respiratory carriage given *M. catarrhalis* has been reported in the nasopharynx of 3.4% of healthy adults <60 years of age (Morris et al., 2022).

A multiplex approach with 6 samples per flow cell was used with Nanopore sequencing. Multiplexing achieved adequate sequencing depth and breadth for species level taxonomic identification, but higher sequencing yields could be achieved by reducing the number of

samples per flow cell, although this would have significant implications on cost per sample. The increased depth of sequencing this affords could counteract high host DNA content and may be beneficial when making inferences from reconstructed consensus genomes, such as the approach shown here comparing SNPs in *H. influenzae* genomes between clinical and cultured samples.

This pilot study had several limitations. Firstly, a small sample size was available for method development. A limited number of methods of host DNA depletion was thus trialled and differential centrifugation selected (achieving up to 2.7-fold increase in bacterial reads). For insight into whether species specific differences arise in metagenomic sequences following host-depletion, comparison of host-DNA depleted and non-depleted samples by Nanopore and Illumina sequencing could have been used but was not performed due to small sample volume and low DNA yields which would result from splitting a sample for such analyses. After completion of this study more extensive comparisons of human/extracellular DNA depletion methods from sputum samples were published (Charalampous et al., 2019; Nelson et al., 2019; Oriano et al., 2019). Nelson *et al.* reported hypotonic lysis of host cells followed by a modified endonuclease (benzonase) digestion of extracellular DNA could reduce human reads by 37% and increase microbial reads by 14-fold on average in sputum samples from patients with cystic fibrosis (CF) using Illumina platforms (n=4). This translated to increased sequencing depth. *P. aeruginosa* abundance was reduced; as a common biofilm producing pathogen in CF, their finding was thought to result from reduced extracellular bacterial DNA (Nelson et al., 2019). However, this nuclease-based method can decrease overall DNA yield by several logs thus necessitating larger input samples compared to standard methods. Charalampous *et al.* reported a saponin based method for host DNA depletion with Nanopore sequencing for the diagnosis of lower respiratory tract infections from sputum, BAL and endotracheal aspirate which achieved median 600-fold depletion of human DNA. However, this method led to 5.7-fold loss of *S. pneumoniae* in host-depleted samples (Charalampous et al., 2019). I elected to use sputum plugs isolated

from induced sputum over spontaneously expectorated sputum to better capture the lower airway microbiome and reduce oropharyngeal/salivary contamination of the sample. These were lower volume and biomass samples, distinct from those collected in studies of bronchiectasis or acute respiratory tract infection, thus the above methods would require adaptation to further conserve bacterial genomes. Whilst differential centrifugation yielded a modest reduction in host DNA, there was consistent species level discrimination with robust bacterial genome coverage in this study. The same method of sputum sequencing was applied to a larger cohort of patients with severe asthma.

A novel enrichment method unique to Nanopore is adaptive sampling, using a target FASTA sequence this allows enrichment or depletion using a software driven enrichment strategy. Individual pores are controlled as they sequence DNA molecules, this is compared in real-time against the target reference to determine if further sequencing should continue after the first few hundred bases are examined, or if the molecule should be ejected (by reversing the current across the pore). This frees the pore to capture a new molecule, thus increasing the capacity for molecules of interest (Loose et al., 2016). This technology has been leveraged for depletion of host DNA from respiratory samples in the context of pulmonary infection, both in isolation (Cheng et al., 2022) or with enzyme-based host depletion (Gan et al., 2021), resulting in increased microbial sequence yield. This approach could be used to improve sequencing yield for induced sputum plug samples but would require further consideration when preparing the sequencing libraries to maximise pore occupancy and data output (OxfordNanoporeTechnologies, 2024), alongside adequate computational power and appropriate bioinformatic pipelines.

The high background bacterial level in the unspiked pooled sputum samples presented a further limitation of this study as it restricted comparisons of limit of detection between PCR and Nanopore. Limit of detection has now been shown to vary by species and level of background commensal abundance in sputum samples sequenced using Nanopore

(Charalampous et al., 2019). In the spiking experiment, *M. catarrhalis* had poorest recovery by qPCR and Nanopore, up to a concentration of 10^8 CFU/ml, and it is hypothesised that the overall bacterial load in the pooled spiked samples disproportionately affected its DNA extraction efficiency compared to other species. Therefore, limit of detection using Nanopore metrics (such as proportion of bacterial reads/bases and genome coverage) could have been better assessed by including a baseline sample with lower bacterial abundance within the spiking experiment. In the absence of this approach pathogen specific qPCR provided additional value in confirmation of Nanopore and culture results in this study.

In summary, a method for direct metagenomic sequencing of sputum plug samples using Nanopore was developed showing a high degree of concordance with Illumina MiSeq, alongside routine culture and qPCR. Long read sequencing had historically been criticised for lower base calling accuracy (Nanopore ~95% vs Illumina MiSeq 99.9%) (Zhang et al., 2023), however with advancements in Nanopore flow cells and reagents the accuracy has been substantially enhanced to approximately 99% (Sereika et al., 2022; Zhang et al., 2023). This together with the operational advantages offered by Nanopore, including lower per sample cost, real-time data acquisition, longer contiguous reads for accurate microbial genome reconstruction and functional inferences (including antimicrobial resistance patterns), make it a promising technology for clinical respiratory diagnostic workflows (Chapman et al., 2023).

3.5 Integrated metagenomic and proteomic analysis of microbe-immune interactions in severe asthma[6]

[6] Text and figures in this section are largely derived from Jabeen *et al.*, Allergy, 2024 (DOI: 10.1111/all.16269).

Metagenomic sequencing with Nanopore was applied to upper (nasal lavage) and lower (sputum) airway samples collected from patients with severe asthma from two separate cohorts. Species level metagenomic data was integrated with inflammatory mediators to characterise the prevalence of a pathogen dominant microbiome and host immune responses in this context.

3.5.1 Clinical characteristics of Oxford and Wessex asthma cohorts

Baseline participant characteristics are summarised in **Table 3.4**, and shown by cohort in Tables E1 and E2 within Appendix 2 (Jabeen *et al.* 2024). Wessex and Oxford severe asthma cohorts geographically and temporally separated, but had comparable demographic features, baseline ICS use and lung function within the severe group. The Wessex cohort encompassed health, mild and severe asthma. As it dated from a pre-biologic era, there was greater maintenance oral corticosteroid use in severe disease with a higher proportion of neutrophilic (25.5 *vs*. 20%) and paucigranulocytic (39 *vs*. 13.3%) sputum phenotypes. In addition, it included more current smokers (33 *vs*. 3.3%), but mean pack years smoked was less than 10. The Oxford cohort included severe asthma alone, with a higher baseline blood eosinophil count (mean $0.4x10^9$/L *vs*. $0.2x10^9$/L) and eosinophilic sputum phenotype (36.7 *vs*. 25.5%). Three patients were on biologic therapy with mepolizumab (median duration 5 months). Overall, severe asthma patients had high (mean >1.5) asthma control questionnaire scores (ACQ-5 in Oxford and ACQ-7 in Wessex cohort), indicative of uncontrolled disease (Juniper et al., 2005).

Table 3.4 Clinical characteristics of Wessex and Oxford severe asthma cohorts

Characteristic	Wessex						Oxford	
	Healthy (n=5)		Mild Asthma (n=10)		Severe Asthma (n=51)		Severe asthma (n=30)	
Male sex, n (%)	3	(60)	5	(50)	22	(43)	14	(46.7)
Age (years), Mean (SD)	28.5	(12.3)	44.1	(15.9)	49.1	(14.7)	59.5	(15.0)
BMI (kg/m^2), Mean (SD)	24.9	(4.4)	27.5	(6.0)	32.2	(8.1)	29.2	(6.2)
Presence of atopy, n (%)	0	(0)	5	(50)	35	(69)	6	(20.0)
Presence of nasal polyps, n (%)	0	(0)	0	(0)	6	(12)	10	(33.3)
Smoking status, n (%)								
Never	4	(80)	5	(50)	27	(53)	22	(73.3)
Current	0	(0)	1	(10)	17	(33)	1	(3.3)
Ex-smoker	1	(20)	4	(40)	7	(14)	7	(23.4)
Pack years, Mean (SD)	7.5	–	1	(1.2)	8.4	(13.0)	12	(10)
Baseline inhaled corticosteroid use (BDP eq., mcg/d), Median (Q1,Q3)	na	na	300	(0, 400)	2080	(1800, 3575)	2000	(1600, 2000)
Maintenance oral corticosteroid, n (%)	na	na	0	(0)	19	(37)	4	(13.3)
Biologic therapy, n (%) (mepolizumab)	0	(0)	0	(0)	0	(0)	3	(10)
Unscheduled GP/ hospital visits in 12 months, Median (Q1,Q3)	na	na	0	(0, 0)	3	(0, 7)	2	(0,6)
FEV1 (%predicted), Mean (SD)	96.2	(9.8)	107	(12.8)	73.6	(24.5)	73.8	(20.6)
FEV1/FVC, Mean (SD)	1	(0.2)	0.8	(0.2)	0.6	(0.1)	0.6	(0.1)
FeNO (ppb), Median (Q1,Q3)	11	(8, 11)	31	(16, 45)	10	(7, 17)	38	(18, 64)
Blood eosinophils (x10^9/L), Median (Q1,Q2)	nd	nd	0.4	(0.2, 0.4)	0.2	(0.1, 0.3)	0.4	(0.2, 0.7)
Sputum eosinophils (%), Median (Q1,Q3)	1.1	(0.9, 3.3)	2.2	(1.2, 3.1)	1	(0.3, 7.7)	4.5	(1.0, 42.2)
Sputum neutrophils (%), Median (Q1,Q3)	31.3	(20.2, 37.3)	23.9	(16.7, 31.7)	51.8	(28.5, 76.1)	38.1	(17.0, 86.0)
Sputum Inflammatory phenotype, n (%)								
Eosinophilic	1	(20)	1	(10)	13	(25.5)	11	(36.7)
Neutrophilic	0	(0)	0	(0)	13	(25.5)	6	(20.0)
Mixed granulocytic	0	(0)	0	(0)	3	(6)	1	(3.3)
Paucigranulocytic	2	(40)	7	(70)	20	(39)	4	(13.3)
No data	2	(40)	2	(20)	2	(4)	8	(26.7)

BMI, body mass index; FEV1, Forced expiratory volume in 1s; FVC, Forced vital capacity; FeNO, exhaled nitric oxide; Inflammatory phenotyes: eosinophilic ≥3% sputum eosinophils, neutrophilic ≥61% sputum neutrophils and <3% eosinophils, mixed granulocytic ≥61% sputum neutrophils and ≥3% eosinophils, paucigranulocytic <61% sputum neutrophils and <3% eosinophils; SD, standard deviation; Q1, quartile 1; Q3, quartile3; na, not applicable; nd, no data

Nanopore sequencing was performed on 96 sputum and 17 nasal lavage samples. Sequencing statistics are provided in Appendix 2 (Jabeen *et al.* 2024). Median read length ranged from 1,684 to 5,490 bp (overall 2685 bp) with median 8,099 bacterial reads in sputum samples. In nasal lavage samples median read length ranged from 2,051 to 3,904 bp (overall 2935 bp) with median 4,010 bacterial reads per sample. An additional integrated analysis of clinical and cytokine data was performed in the Wessex cohort (n=66). The study design is summarised below (**Figure 3.5**).

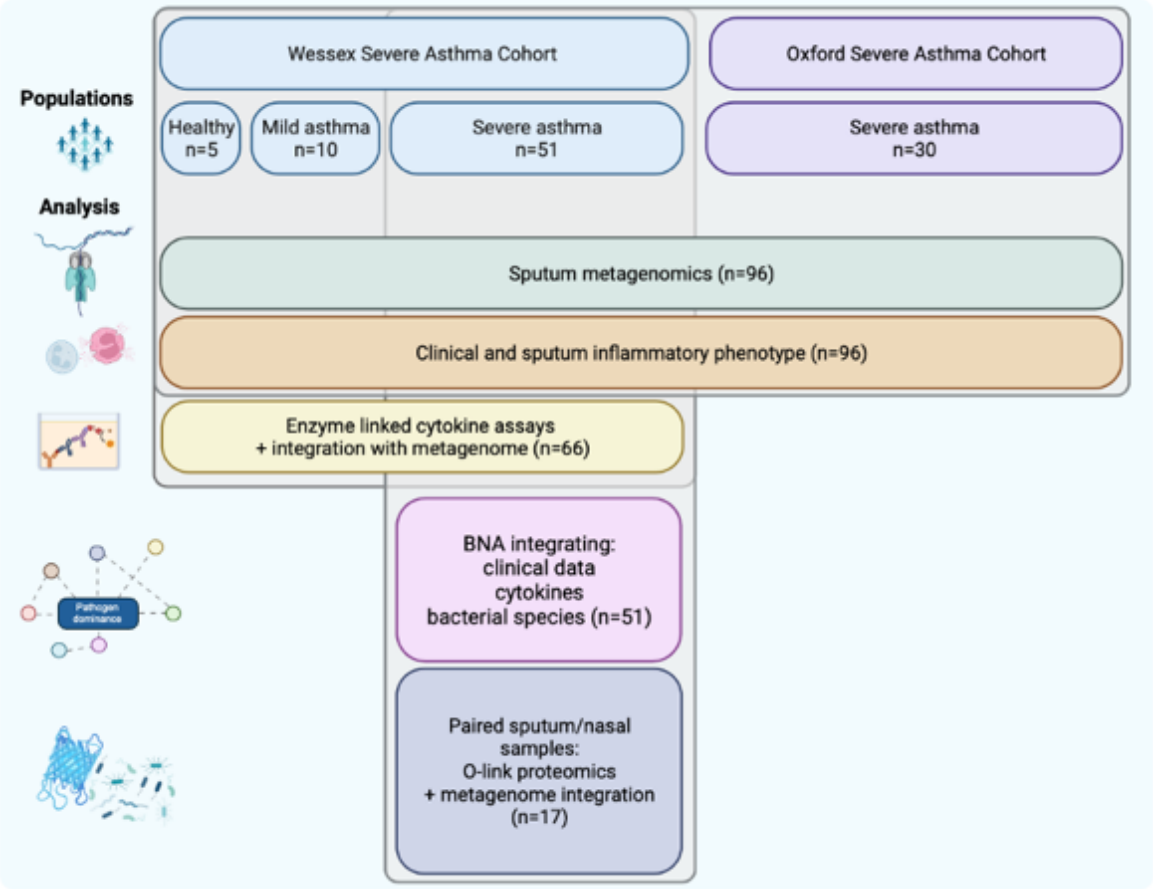


Figure 3.5 Metagenomic study design

3.5.2 The metagenome of severe asthma and pathogen dominant microbiome

The Z-scores of bacterial species that had greatest variability in abundance across health (HC), mild (MA) and severe asthma (SA) are shown in **Figure 3.6**, combining Oxford and

Wessex cohorts. This is shown separately by cohort in Figure E2 of Appendix 2 (Jabeen *et al.* 2024).

Using hierarchical clustering a cluster of 19/96 participants emerged, its members had severe asthma and skewed airway microbiome dominated by a single respiratory pathogen, namely *H. influenzae*, *M. catarrhalis* or *S. pneumoniae*. The remainder of the cohort displayed greater microbial diversity comprising commensal organisms of variable abundance, predominantly phyla *Actinomycetota*, *Bacteroidota* and *Bacillota*. Principal component analysis (PCA) of severe asthma metagenomes from the Oxford and Wessex cohorts showed no significant difference between the two groups (PERMANOVA = 0.19) as displayed in Figure E3 in Appendix 2 (Jabeen *et al.* 2024).

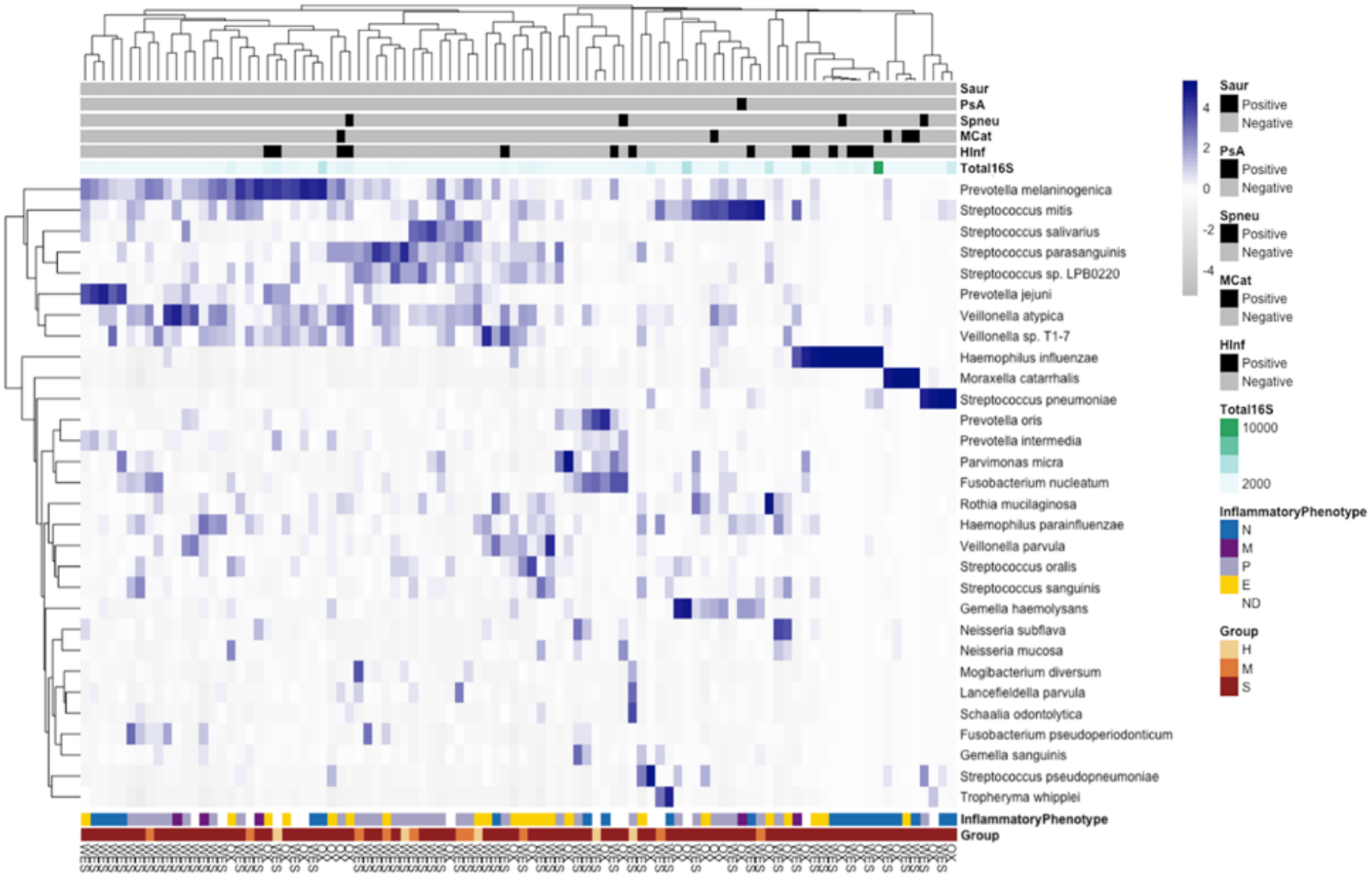

Saur
PsA
Spneu
MCat
HInf
Total16S
Prevotella melaninogenica
Streptococcus mitis
Streptococcus salivarius
Streptococcus parasanguinis
Streptococcus sp. LPB0220
Prevotella jejuni
Veillonella atypica
Veillonella sp. T1-7
Haemophilus influenzae
Moraxella catarrhalis
Streptococcus pneumoniae
Prevotella oris
Prevotella intermedia
Parvimonas micra
Fusobacterium nucleatum
Rothia mucilaginosa
Haemophilus parainfluenzae
Veillonella parvula
Streptococcus oralis
Streptococcus sanguinis
Gemella haemolysans
Neisseria subflava
Neisseria mucosa
Mogibacterium diversum
Lancefieldella parvula
Schaalia odontolytica
Fusobacterium pseudoperiodonticum
Gemella sanguinis
Streptococcus pseudopneumoniae
Tropheryma whipplei
InflammatoryPhenotype
Group
4
2
0
-2
-4
Saur
Positive
Negative
PsA
Positive
Negative
Spneu
Positive
Negative
MCat
Positive
Negative
HInf
Positive
Negative
Total16S
10000
2000
InflammatoryPhenotype
N
M
P
E
ND
Group
H
M
S

Figure 3.6 Relative abundance of species in sputum[7];

Heatmap of relative species abundance from induced sputum samples sequenced with Nanopore; Z-scores, denoted by shade, represent relative abundance by taxon within each individual patient (columns). Cohorts include Wessex (WES; Healthy [H]: n = 5, Mild [M]: n = 10 and Severe asthma [S]: n = 51) and Oxford (OX; Severe asthma [S]: n = 30). Clustering by species (rows) and individuals (columns) using Euclidian distance performed independently on samples and most differentially abundant bacterial species. Sputum inflammatory phenotypes are eosinophilic (E), neutrophilic (N), mixed granulocytic (M) and paucigranulocytic (P). Positive pathogen specific PCR results (>1 × 10^6 copies/mL) are indicated in black: S. aureus (Saur), P. aeruginosa (PsA), S. pneumoniae (Spneu), M. catarrhalis (Mcat) and H. influenzae (Hinf). Total eubacteria (16S) PCR load is denoted by shade (×10^6 copies/mL).

The Wessex cohort comprised HC (n=5), MA (n=10) and SA (n=51) participants, allowing differential abundance of species to be tested in these distinct groups. In HC sputum (HC vs MA/SA, log fold change [LFC] >1, adjusted P<0.05) the most conserved species included *Streptococcus viridans, Streptococcus* sp A12, *Streptococcus australis* and *Schaalia odontolytica* (see Table E3, Appendix 2, Jabeen et al. 2024). In MA sputum (MA *vs* HC/SA) 29 species, predominantly of phylum *Bacillota*, were identified similarly, out of which *Filifactor alocis, Mogibacterium diversum* and *Streptococcus* sp. A12 were significantly enriched (see Table E4, Appendix 2, Jabeen et al. 2024). SA (SA *vs* HC/MA) sputum showed marked compositional shift with greater abundance of species including *Rothia mucilaginosa, Rothia dentocariosa, H. influenzae* and *M. catarrhalis* (see Table E5, Appendix 2, Jabeen et al. 2024), and a relative depletion of oropharyngeal commensals.

Metagenomic dominance by a single airway pathogen, or pathogen dominance, was again observed in a subset of participants and defined as a known respiratory pathogen (*H. influenzae, M. catarrhalis, S. pneumoniae* or *P. aeruginosa*, in this dataset) appearing as the most abundant (%reads/total bacterial reads) species, with the proportion of detected reads (shown in Table E6, Appendix 2, Jabeen *et al.* 2024) being ≥2-fold of the second-most abundant species in the sample. Across the two cohorts, a pathogen dominant microbiome

[7] Heatmap plotted by Dr E Marchi

was observed in 23% of severe asthmatics (n=19/81) during a period of clinical stability. *H. influenzae* (n=10) was the most prevalent, followed by *M. catarrhalis* (n=4) and *S. pneumoniae* (n=4). In the majority of samples (n=18/19), sequencing breadth was at least 1/5th of the reference genome, providing high confidence species-level classification. *P. aeruginosa* was detected with a high proportion of total reads (73%) in one participant but low genome coverage (5.1%).

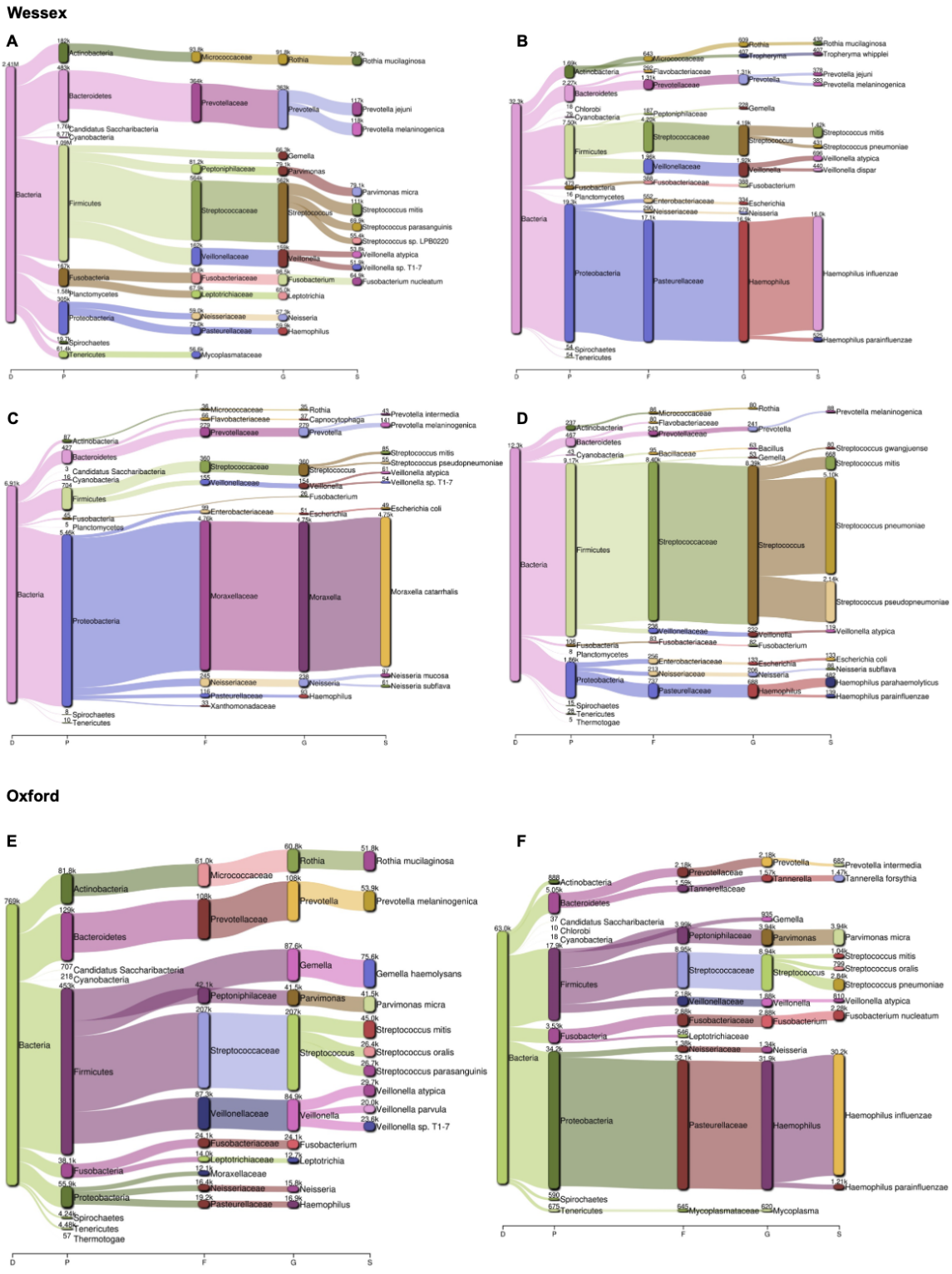


***Figure 3.7 Taxonomic profiles in sputum in severe asthma**;*

Sankey visualisation of taxonomic profiles in severe asthma in the absence or presence of a single dominant pathogen using Pavian; Kraken reports combined from patients with no single dominant organism on metagenomic sequencing from (A) Wessex (n=40) and (E) Oxford (n=22) cohorts for visualisation. Skewed taxonomic profiles in the presence of a single dominant pathogen (Wilcoxon rank-sum test, BH correction FDR 0.05; P≤0.01), one of (B)+(F) H. influenzae ([B] Wessex, n= 6; [F] Oxford, n=4), (C) M. catarrhalis (Wessex, n=3) or S. pneumoniae (Wessex, n=2) have been generated using the same method

Within pathogen dominant microbiomes the relative abundance of each pathogenic species was significantly greater than all other detected species, as shown in Sankey visualisations (**Figure 3.7**) (Wilcoxon rank-sum test, BH correction FDR 0.05; Figure 3.7(B) Wessex, *H. influenzae* p = $6.3x10^{-5}$; Figure 3.7(C) Wessex, *M. catarrhalis* p = $8.7x10^{-4}$; Figure 3.7(B) Wessex, *S. pneumoniae* p = 0.01; Figure 3.7(F) Oxford, *H. influenzae* p = $3.8x10^{-3}$; Figure E4(G) Oxford, *S. pneumoniae* P = 0.01). Pathogen-specific qPCR results are shown in **Figure 3.6** and Table E6 in Appendix 2 (Jabeen *et al.* 2024). As in the pilot study, a clinically significant positive result was identified as ≥$1x10_6$ copies/ml. Using this definition a positive qPCR result was identified in all Oxford samples meeting sequencing criteria of pathogen dominance, and 8/11 Wessex samples. Total bacterial load was quantified using 16S qPCR (**Figure 3.6**) and was higher in Oxford (median $364x10^6$, IQR $823x10^6$ copies/ml) than Wessex sputum samples (median $23x10^6$, IQR $83x10^6$ copies/ml).

3.5.3 Microbiome differences by sputum inflammatory phenotype

Pathogen dominant microbiomes in severe asthma (**Figure 3.7**) were associated with higher Pseudomonadota:Bacillota (syn. Proteobacteria:Firmicutes) ratio (p <0.001, see Figure E6 in Appendix 2, Jabeen *et al.* 2024), consistent with previous reports (Diver et al., 2022; Diver et al., 2020), but no significant differences were observed between SA and HC or MA, or across inflammatory phenotypes. This is consistent with *Pseudomonadota* species *H. influenzae* and *M. catarrhalis* having the greatest prevalence in severe disease, as recently reported in the large U-BIOPRED cohort (Versi et al., 2024; Versi et al., 2023). Pathogen dominance of the microbiome was not observed in health or mild asthma. Airways neutrophilia was associated with a *H. influenzae, M. catarrhalis, S. pneumoniae* or *P. aeruginosa* dominant microbiome in severe asthma sputum, with higher overall sputum neutrophil count (**Figure 3.8**(B), P<0.05) and higher prevalence of neutrophilic asthma (p <0.05, see Table E2, Appendix 2, Jabeen *et al.* 2024).

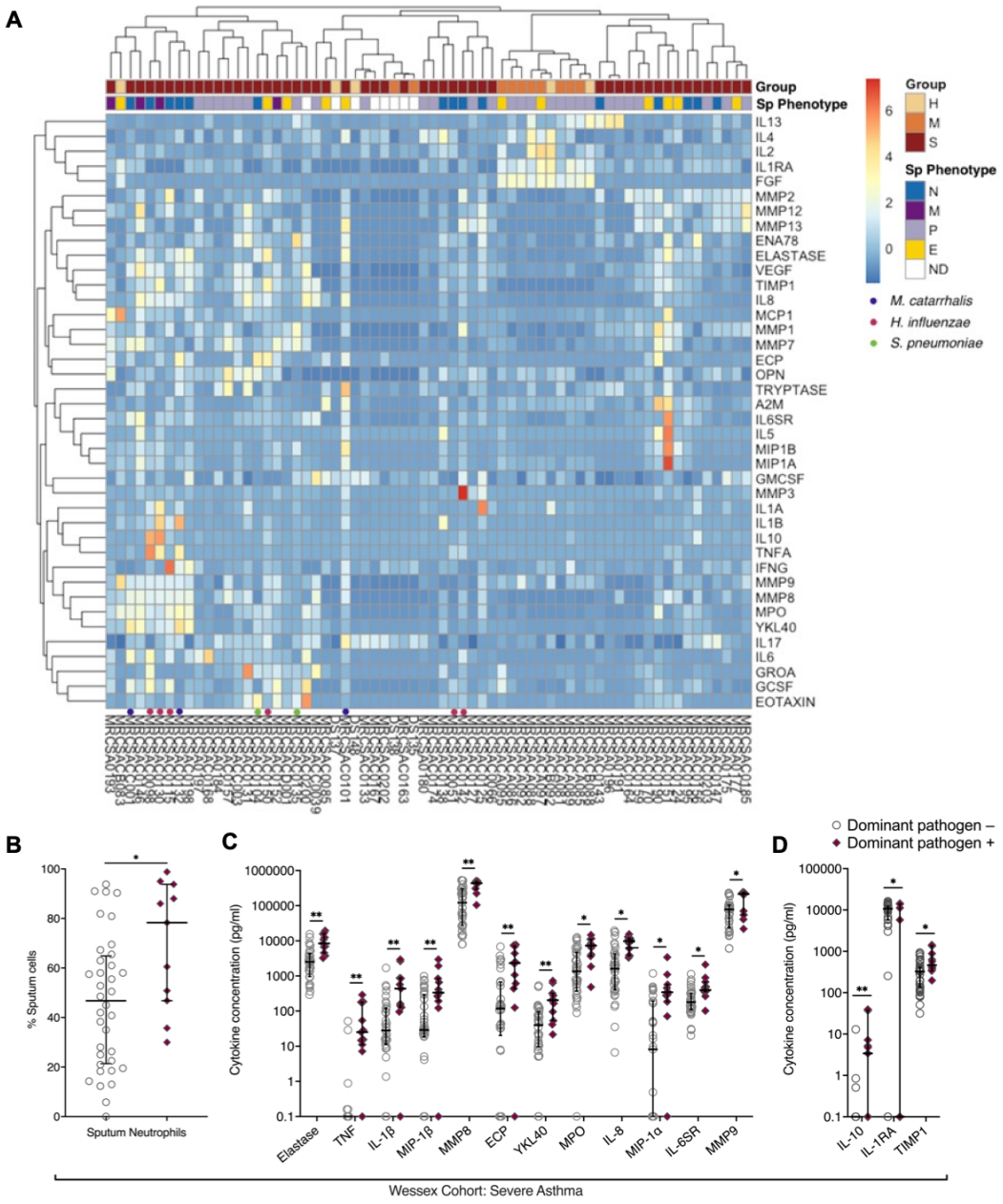


Figure 3.8 Integrated analyses of microbiome and inflammatory mediators in sputum;

*Integrated cytokine analysis (A) Heatmap of scaled and centralised sputum cytokines in health, mild and severe asthma[8]. Z-score centralised cytokine measurements denoted by shade. Independent clustering performed by subject (columns) and cytokine (rows). Clustering distances shown are representative of correlation distances. In severe asthma, presence of a dominant pathogenic organism on metagenomic sequencing is indicated as HI (H. inf), MC (M. cat) and SP (S. pneu); the pathogen-dominant microbiome in severe asthma (data only shown for participants with severe asthma) is associated with (B) sputum neutrophilia, (C) elevated type-1 cytokines and (D) anti-inflammatory mediators in sputum supernatant. Median/IQR shown −/+ Pathogen dominance ([C] Mann-Whitney test, [D]/[E] unpaired t-test, adjusted for multiple comparisons with BH procedure [FDR 0.05]. *p≤0.05, **p≤0.01).*

[8] Heatmap plotted by Dr E Marchi

Defining bacterial species associated with sputum inflammatory phenotypes in severe asthma were sought (LFC>1, adjusted P<0.05). Consistent with the above findings, H*. influenzae, M. catarrhalis, T. whipplei* and *S. pneumoniae* were strongly associated with neutrophilic asthma, but commensal *Streptococcus spp.* (Table E7, Appendix 2, Jabeen *et al.* 2024) including *S. salivarius, S. intermedius*, and *S. oralis* were relatively depleted (LFC< -1, adjusted P<0.05). In paucigranulocytic disease, *M. catarrhalis, H. influenzae* and *T. whipplei* abundance was lower (see Table E7, Appendix 2, Jabeen *et al.* 2024). In eosinophilic asthma there was higher relative abundance of *M. catarrhalis, S. intermedius* and *V. parvula* with less *H. influenzae, S. pneumoniae* and *Actinomyces pacaensis*, a relatively newly isolated Gram-positive organism in the human respiratory microbiome (Fonkou et al., 2018) (see Table E7, Appendix 2, Jabeen *et al.* 2024). No organisms uniquely defined the mixed inflammatory phenotype.

3.5.4 Integration of cytokine and metagenomic analyses

Sputum metagenomes from the Wessex cohort (n=66) were integrated with existing cytokine data measured using immunoassays (n=40) (Hinks et al., 2016b)(**Figure 3.8**(A)). Unsupervised clustering by cytokines identified HC and MA had higher expression of FGF, IL-1RA, IL-2 and IL-4 relative to SA clusters. In SA two clusters were seen. One was associated with predominantly proinflammatory and type 1 cytokines (left) including IL-1α, IL-1β, TNF, IFN-γ, MMP8, MMP9, MPO, YKL40, IL-17, IL-6, elastase, ECP, IL-8, GROα, G-CSF, eotaxin and TIMP-1. A pathogen-dominant microbiome was typically present with this. The second cluster (right) was composed of a mixture of sputum inflammatory phenotypes, without pathogen dominance, but with high expression of MMPs.

To dissect mucosal immune responses to individual species further this data was integrated, clustering (hierarchical) by species and by cytokine (**Figure 3.9**), selecting the 50 species showing highest variance in abundance across participants.

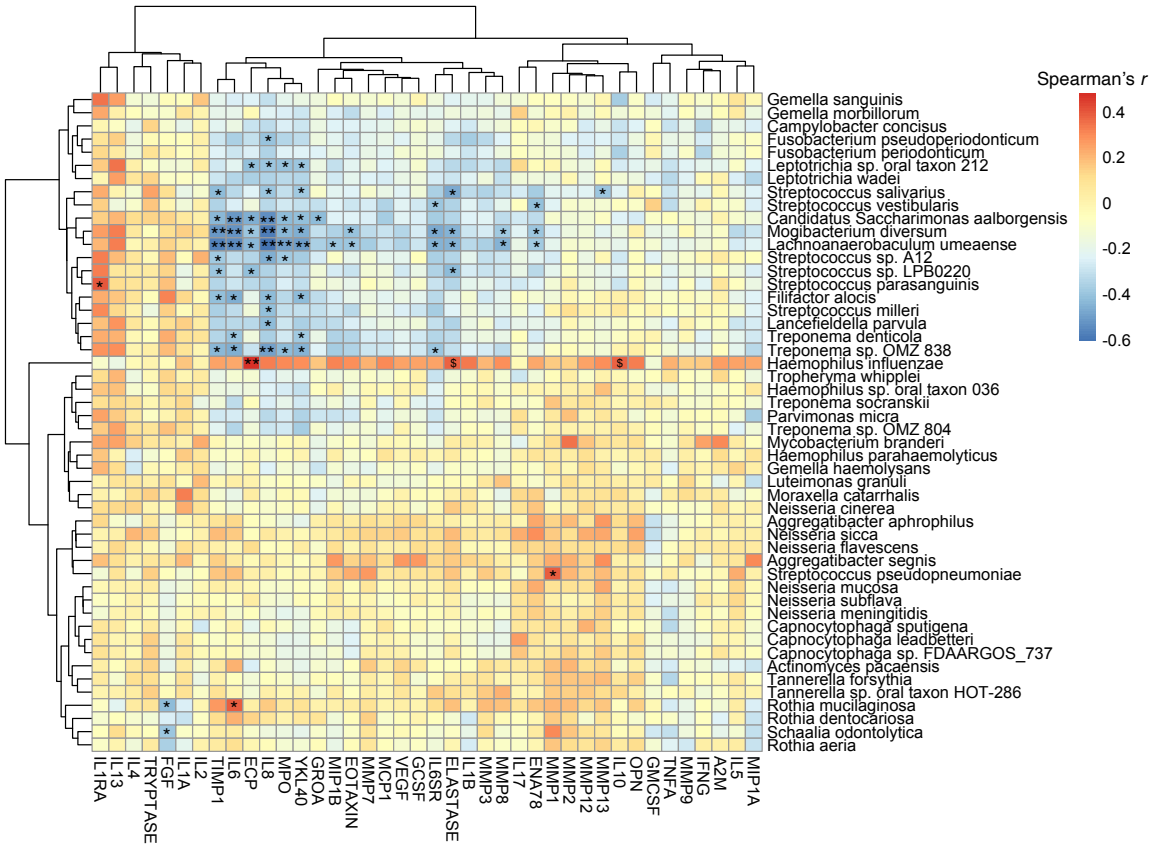


Figure 3.9 Heatmap displaying correlations between integrated sputum microbiome and cytokine data[9];

*The 50 most variable bacterial species across all subjects were selected. Spearman correlation coefficients between species and cytokines denoted by shade. Independent clustering performed by cytokine (columns) and species (rows). Statistically significant correlations have been annotated as $p = .05, *p < .05 and **p < .01. Adjustment for multiple comparisons was made using BH-procedure (FDR 0.05).*

The strongest positive correlations were between *H. influenzae* and Eosinophil Cationic Protein (ECP) (r=0.5, $p \leq 0.007$), IL-10 (r=0.4, $p = 0.05$) and elastase (r=0.4, $p = 0.05$); between *Rothia mucilaginosa* and IL-6 (r=0.4, $p < 0.05$); between *Streptococcus pseudopneumoniae* and MMP1 (r=0.4, $p < 0.05$); and between *Streptococcus parasanguinis* and IL-1RA (r=0.4, $p < 0.05$). Negative correlations were identified between predominantly Gram-positive oropharyngeal/respiratory commensals (top middle species cluster **Figure 3.9**) and pro-inflammatory cytokines, for example prototypic markers of neutrophilic inflammation – IL-8, IL-6, YKL40 and MPO, which correlated negatively (r<-0.4, $p < 0.05$) with anaerobic Gram-

[9] Heatmap plotted by Dr E Marchi

positive organisms *Mogibacterium diversum*, *Lachnoanaerobaculum umeaense* and the uncultured bacteria *Candidatus Saccharimonas aalborgensis*. TIMP-1 and MMP8 correlated negatively Gram-positive and negative commensals. Conversely *R. mucilaginosa*, which had highest overall detected reads in severe asthma (see Table E5, Appendix 2, Jabeen *et al.* 2024), was linked to low FGF levels (r=-0.4, p <0.05).

3.5.5 Neutrophilic inflammation with pathogen dominance in severe asthma

Using the pragmatic metagenomic sequencing derived definition of pathogen dominance, patients with severe asthma were dichotomised by presence or absence of this trait. In addition to sputum neutrophilia (**Figure 3.8**(B), p <0.05), a pathogen-dominant microbiome was associated with significantly elevated type-1 cytokines and airway proteases, namely: elastase, TNF, IL-1βα, MIP-1β, MMP8, ECP, YKL40, MPO, MIP-1α, IL-6SR and MMP9 (refer to **Figure 3.8**(C), p < 0.05 and Table E8, Appendix 2, Jabeen *et al.* 2024). Of the immunomodulatory mediators IL-1RA was deficient, whereas TIMP-1 and IL-10 levels were higher in presence of pathogen dominance (see **Figure 3.8**(D), p <0.05 and Table E8, Appendix 2, Jabeen *et al.* 2024).

3.5.6 Bayesian network analysis in severe asthma

Next I sought to investigate in an unbiased manner how different clinical, immunological and microbiological parameters related to each other within the dataset. A Bayesian network is an acyclic directed graph in which nodes represent variables, and connecting arcs show direct probabilistic dependencies between these (Puga et al., 2015). It is, in essence, an unbiased probabilistic method allowing exploration of how different parameters relate to each other, as the network structure models interactions among the variable in the model. BNA was applied to data from Wessex severe asthma participants (n=51), integrating sputum cytokines significantly elevated in presence of a pathogen-dominant microbiome (n=15), clinical

parameters (n=20), and bacterial species with significant differential abundance (either increased or decreased) in severe asthma (n=25) (**Figure 3.10**).



***Figure 3.10 Integrated Bayesian Network Analysis**;*

Bayesian network showing strongest interactions between most differentially abundant bacterial species, inflammatory mediators, and clinical features in severe asthma (WES, n=51). Nodes are coloured by class: bacterial species (blue), infection status (red), inflammatory mediators (green) and clinical features (orange). Nodes without strong interactions have been excluded. Line thickness represents strength of interaction (Euclidean distance) as shown in the scale. Interactions with a positive linear correlation are shown with a green edge

The 'clustering algorithm' was used (BayesFusion; Lauritzen SL, 1988), this retained 34/60 parameters within the model (Table E9, Appendix 2, Jabeen *et al.* 2024). To further explore pair-wise interactions retained in this network, in a separate secondary analysis, Spearman (between cytokine) or Pearson (between bacterial species) were performed (see Figures E7 and E9 in Appendix 2, Jabeen *et al.* 2024). Positive linear correlations are shown as green edges in the Bayesian network. No negative correlations were found. This analysis explored the interactions between key microbial and immune variables specific to severe asthma, thus supplementing the earlier integrated analyses applied to the full Wessex cohort.

Connectivity was observed between the *H. influenzae*/*M. catarrhalis* abundance nodes and 'pathogen dominance', alongside cytokines linked to pathogen dominance in earlier analyses. A non-linear relationship was seen between *M. catarrhalis* and FeNO or IL-1β. In addition,

connectivity appeared between phylogenetically related bacterial species, with positive correlations most notably in members of *Bacillota*, and *Neisseria* spp (see Figure E9, Appendix 2, Jabeen *et al.* 2024).

This approach highlighted associations between *H. influenzae* abundance and IL-10 in sputum (Figure E7a, r=0.32, p <0.05, Appendix 2, Jabeen *et al.* 2024), and IL-10 and TNF-α (Figure E7b, r=0.62, p <0.0001 , Appendix 2, Jabeen *et al.* 2024). Macrophage chemoattractant, MIP1α, was a highly connected node within **Figure 3.10** (and Supplementary Figure E7 in Appendix 2, Jabeen *et al.* 2024) specifically to complementary chemokine MIP1β (r=0.88, p <0.0001), alongside IL-6SR (r=0.65, p <0.0001), TIMP-1 (r=0.65, p <0.0001) and IL-8 (r=0.73, p <0.0001). Sputum YKL40 was strongly linked to MPO (r=0.92, p <0.0001), IL-6SR (r=0.75, p <0.0001) and IL-1β (r=0.63, p <0.0001). Neutrophilic markers MPO and IL-8 were strongly correlated (r=0.85, p <0.0001).

3.5.7 Microbiome and cytokine milieus in the upper and lower airway

Paired nasal lavage and sputum samples were available in a subset of Wessex severe asthma participants (n=17). Nasal lavage was considered representative of the upper airway microbiome whereas sputum samples were more representative of the lower airways, despite an inevitable component of oropharyngeal contamination. The relative abundances of shared bacterial species between the upper and lower airway compartments are shown in **Figure 3.11**. The metagenomic profiles clustered distinctly by anatomical location rather than by individuals the paired samples originated from (PCA plot shown in Supplementary Figure E11, PERMANOVA = 0.001, Appendix 2, Jabeen *et al.* 2024). In severe asthma, nasal lavage was enriched in *S. epidermidis* and *S. aureus*, with higher abundance of *D. pigrum*, *M. catarrhalis* and *E. coli* compared to sputum. Sputum was enriched for *Bacillota* (predominantly *Streptococcal* spp.) with higher relative abundance of *H. influenzae* and *H. parainfluenzae*.

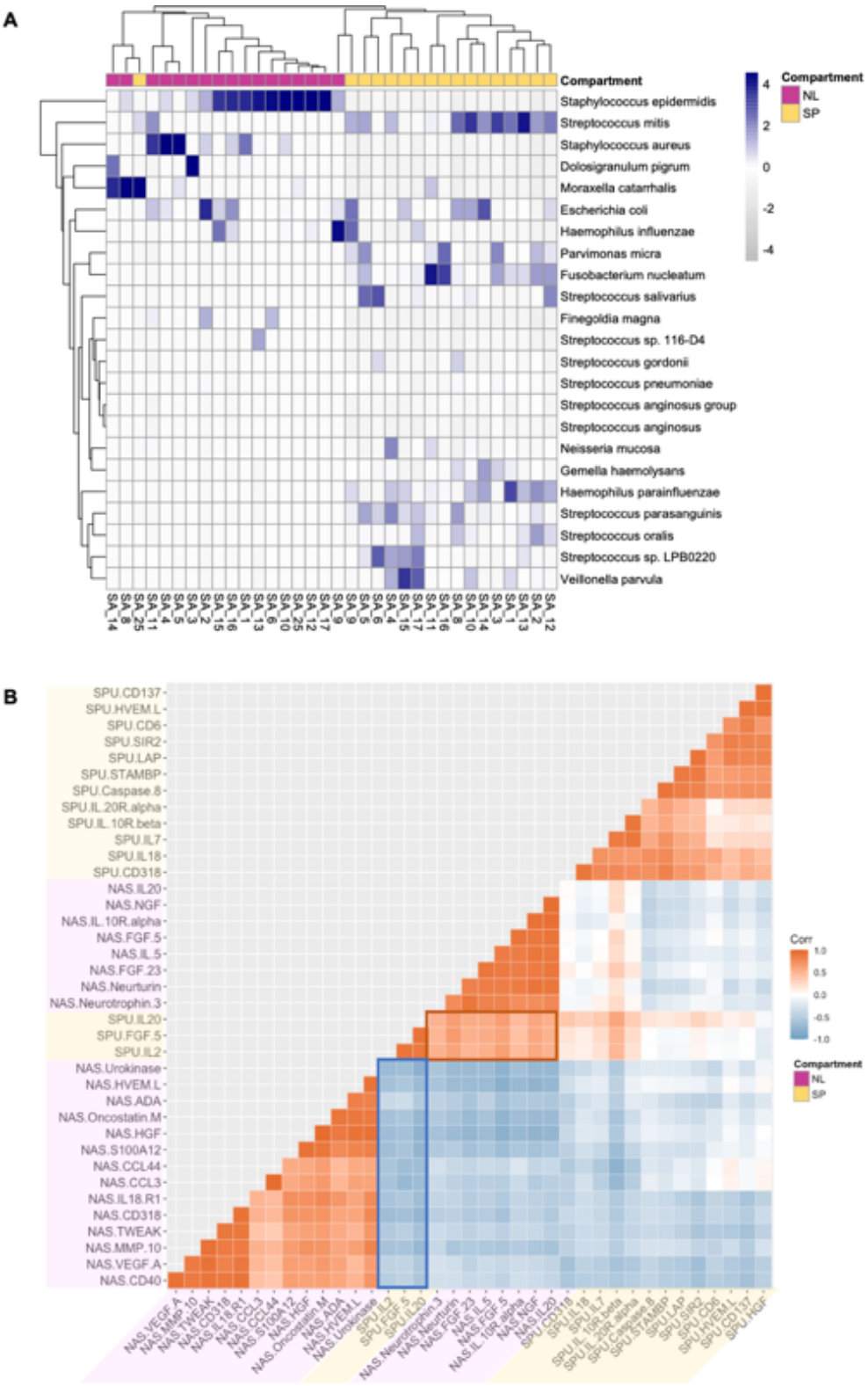


Figure 3.11 Upper and lower airway microbiome and cytokines;

(A) Heatmap of relative abundances of bacterial species on metagenomic sequencing of paired nasal lavage (NL) and sputum (SP) samples from severe asthmatics (n = 17). Z-score denoted by shade. Independent clustering by samples (columns) and 23 most variable species (rows) using Euclidian distance. (B) Correlation matrix of the most significantly correlated (p < .001) proteins in paired nasal lavage (NAS) and sputum (SPU) cytokines (O-link). Significantly correlated pairs displayed (p < .001, adjusted for multiple comparisons with Benjamini–Hochberg procedure [FDR 0.05]).

The cytokine milieu of the upper and lower airways was compared using paired O-link proteomics of nasal lavage and sputum, proteins with most statistically significant correlations (P<0.001) are shown in **Figure 3.11**(B). Proteins were generally seen to correlate most strongly with others from the same sample type, producing a separation by compartment. The exceptions to this were two clusters showing positive or negative correlations between sputum IL-20, FGF5 and IL-2, and a broad range of nasal lavage proteins.

3.5.8 Discussion

This was the first large-scale study to use long-read Nanopore sequencing for species-level description of the airway microbiome in severe asthma. A pathogen-dominant microbiome was identified, with dominance of a single pathogenic bacterial species, and associated mucosal inflammation, in 20-30% of participants with severe asthma during stable disease. A limited repertoire of species drove the pathogen dominant microbiome; *H. influenzae* being the most prevalent, followed by *M. catarrhalis* and *S. pneumoniae*. Although metagenomic measures do not imply bacterial tissue invasion, strong correlations between pathogen dominance and airway neutrophilia with associated mucosal inflammation as shown in this chapter is beyond that expected by simple commensal colonisation. Novel supervised and unsupervised approaches used to integrate species-level metagenomics with cytokine and protein datasets showed consistent evidence of type-1 inflammatory responses accompanied by neutrophilia in presence of a pathogen-dominant microbiome. This coincided with commensal depletion (largely *Bacillota*), which has been linked to worse asthma outcomes (Abdel-Aziz et al., 2021). Commensal organisms detected in induced sputum showed an expected overlap with oropharyngeal flora (Durack et al., 2018a). These results were consistent with, and built upon, findings of previous studies (Abdel-Aziz et al., 2021; Diver et al., 2020; Taylor et al., 2018) and recent findings from the large European U-BIOPRED cohort (Versi et al., 2024; Versi et al., 2023). Finally, the lower airway microbiome was shown to be distinct from the upper airways in severe asthma, with concurrent anatomical compartmentalisation of the cytokine milieu.

In severe asthma, three species dominated the airway microbiome, and their presence in both neutrophilic and non-neutrophilic disease might explain the striking clinical efficacy of long-term, low dose azithromycin therapy in both of these phenotypes (Gibson et al., 2017), but particularly with high *H. influenzae* abundance, measured by qPCR (Taylor et al., 2020). The symptom score (ACQ-7) was not linked to presence of a dominant pathogen in the BNA, likely due to insensitivity of ACQ to sputum volume or purulence. Indeed, azithromycin achieved a very small improvement in symptom score (0.1 points on ACQ-6) amongst participants with severe asthma in the AMAZES trial (Gibson et al., 2017). Whilst azithromycin is mechanistically primarily antibacterial, additional anti-viral (Oliver and Hinks, 2021) and anti-inflammatory (Niessen et al., 2021) effects have been reported. However, antimicrobial resistance with widespread azithromycin therapy is a significant concern (Serisier, 2013), and if the antibacterial effect is dominant, this could be addressed through targeting therapy to those with pathogen dominance identified through molecular techniques.

In my pilot study Nanopore was shown to identify clinically relevant airway pathogens, as verified with complementary sputum culture and semi-quantitative pathogen specific qPCR results (Jabeen et al., 2022). In this larger cohort similar consistency was observed between Nanopore sequencing defined pathogen dominance of the airway microbiome and positive pathogen specific qPCR results for *H. influenzae*, *S. pneumoniae*, *M. catarrhalis* and *P. aeruginosa* in samples from the Oxford cohort. The lower, 73% concordance between sequencing and qPCR results in the Wessex cohort (n=8/11) could be attributable to age-related sample degradation in this historical cohort, as total 16S load was >15-fold lower in Wessex than Oxford samples. A stringent qPCR cut-off of $1x10^6$ copies/ml was set for a positive result based on its use to identify bacteria associated neutrophilic inflammation in COPD upon longitudinal sampling (Bafadhel et al., 2015) and agreement with sputum culture results. It is worth noting that prevalence of potentially pathogenic microorganisms in COPD is relatively high (Wang et al., 2021) and sputum culture has limited sensitivity (Bafadhel et

al., 2015). If a lower threshold of $0.5x10^6$ copies/ml was used, there would have been no discrepancy. Overall, Nanopore sequencing gave a detailed species level description of the microbiome but, for operational reasons, qPCR on a selected panel of respiratory pathogens may offer the most accessible, cost-effective and accurate means of identifying pathogen-dominance for targeted therapy in routine clinical practice. However, significant progress has been made in the implementation of Nanopore sequencing in clinical practice. A pilot study has demonstrated the clinical utility of respiratory metagenomics as a diagnostic test for lower respiratory tract infections in routine clinical settings, achieving 93% sensitivity and 81% specificity for clinically relevant pathogens compared to routine testing, with a median turnaround time <7 hours from sample receipt (Charalampous 2024). This has important clinical implications as continuing developments in sequencing workflows, sample multiplexing capacity and bioinformatic pipelines for screening antimicrobial resistance genes, could guide increasingly cost-effective personalised antimicrobial therapy in patients with severe asthma and other airways diseases.

Nanopore sequencing provided further insights into microbiome by distinct sputum inflammatory phenotype. In addition to *H. influenzae, M. catarrhalis* and *S. pneumoniae*, *T. whipplei* was also strongly linked to neutrophilic asthma. This predominantly intracellular bacterium causes chronic multi-system inflammation in Whipple's disease and may be involved in airways disease. *T. whipplei* has been reported in up to 40% of severe asthma patients, linked to both eosinophilic disease (Simpson et al., 2016), particularly in smokers (Versi et al., 2023), and corticosteroid resistant inflammation (Goleva et al., 2013) albeit in a smaller cohort. Its ability to grow within acidic vacuoles, induce M2 macrophage polarisation and apoptosis, are virulence traits capable of sustaining chronic infection (Gorvel et al., 2010). The asthmatic airway is susceptible to persistent infection with intracellular bacteria, most often non-typeable strains of *H. influenzae* (Hinks et al., 2021b) (NTHi) which facultatively enter macrophages and airway epithelial cells. High dose ICS exposure could also render mucosa susceptible to intracellular pathogens such as *T. whipplei* and further research is

needed to determine if specific innate immune deficiencies could promote intracellular infection. The microbiome in eosinophilic asthma varies with disease severity and in severe disease displays high relative abundance of *Bacillota* (syn. Firmicutes) (Diver et al., 2022). Interestingly, *M. catarrhalis* showed increased abundance in eosinophilic asthma in this study, alongside *Bacillota S. intermedius* and *V. parvula*, although this comparison was underpowered and warrants replication. In contrast, in the U-BIOPRED studies *M. catarrhalis* and *Prevotella spp.* negatively correlated with sputum eosinophils, whereas *T. whipplei* was positively correlated (Versi et al., 2023). The U-BIOPRED cohort had a larger proportion of eosinophilic asthmatics (43% vs 30%), the study used short-read sequencing and a different analytical approach (correlating abundance of top 16 species with clinical and inflammatory features) which might account for these differences. BNA linked the abundance of *M. catarrhalis* to FeNO level. FeNO has been reported to negatively correlate with *Pseudomonadota* abundance (Diver et al., 2022), consistent with this, *H. influenzae* abundance was observed to have a mutually exclusive relationship with elevated FeNO level (see Supplementary Figure E8, Appendix 2, Jabeen *et al.* 2024) suggesting that this species could interfere with FeNO production in the airway mucosa.

In SA, notably in the absence of a dominant pathogen, there was greater abundance of *Rothia* spp., previously detected in mild non-eosinophilic asthma (Sverrild et al., 2017) and bronchiectasis, where its abundance in sputum negatively correlated with IL-8, IL-1β, MMP-1, MMP-8 and MMP-9 (Rigauts et al., 2022). Of these species, *R. mucilaginosa* is most often detected in chronic lung diseases, including severe asthma and COPD (Mac Aogain et al., 2020). It inhibits NF-κB activation in lung epithelium *in vitro*, probably at the level of IKK activation, and can reduce lung pathology *in vivo* (Rigauts et al., 2022). Whilst it is not known why *Rothia* are more abundant in SA, it is likely that as facultative anaerobes they can colonise airway niches with reduced oxygen tension secondary to mucus plugging. In this dataset an association was seen between IL-6 and *R. mucilaginosa* but a concurrent negative correlation was present with FGF, which itself positively correlated with oropharyngeal commensals.

FGFs form a diverse group of growth factors exerting pleiotropic effects via tyrosine kinase receptors. FGF-2 promotes bronchial smooth muscle hyperplasia, with higher expression in asthma, and alongside FGF-1 stimulates MAPK-dependent VEGF production, inhibited by azithromycin and dexamethasone (Willems-Widyastuti et al., 2013). Thus, microbial composition could influence airway remodelling processes and be further manipulated by corticosteroids and macrolides.

Integration of metagenome and inflammatory mediators, together with BNA offered additional novel insights. Overall, a pattern emerges linking a pathogen-dominant microbiome and type-1 inflammation (IL-1β, TNF) with neutrophilic infiltration (IL-8, YKL40), release of neutrophil granule proteins and proteases (MMP8, MMP9, MPO and elastase), counter regulatory mechanisms (TIMP-1, IL-10), and macrophage recruitment (MIP1α and MIP1β) which could be facilitated through IL-6 signalling (IL-6SR). This is highly consistent with a post-hoc analysis of metagenomic data from the U-BIOPRED cohort, published after the present study, linking *H. influenzae* abundance with NET-osis, IL-6 transignalling and neutrophil activation using sputum transcriptomics (Versi et al., 2024). *H. influenzae* was also found to strongly correlate with the anti-inflammatory cytokine IL-10, consistent with data in COPD (Barker et al., 2015) and *in vitro* findings (Hosoki et al., 2013). Co-production of IL-10/TNF, induced via MyD88-dependent TLR activation following NTHi infection, may offer a regulatory response, and *H. influenzae* could harness excess IL-10 secretion as a virulence strategy. This could be explored further in murine studies.

H. influenzae also correlated strongly with sputum ECP, a cationic granule protein released by activated eosinophils. ECP release can be induced by Gram-negative organisms (Svensson and Wenneras, 2005) including NTHi (Ahren et al., 2003), it has antibacterial properties but is also associated with airways remodelling, inflammation and mucus hypersecretion (Granger et al., 2022). Thus, the strong association observed is more likely a consequence of airways infection, rather than eosinophilic inflammation predisposing to acquisition of *H. influenzae*. In

the Oxford cohort only 3/30 participants received biologic therapy with mepolizumab, thus unlikely to have impacted the results and underpowered to determine differences with non-biologic treated patients. Commencing mepolizumab has not been previously shown to alter microbial composition or increase *Pseudomonadota* load (Diver et al., 2022). In the large MEX study, 36% of clinically stable patients on mepolizumab had bacteria detected over a clinically significant PCR threshold, a higher proportion than this cohort (McDowell et al., 2021). Benralizumab therapy, which produces a more rapid and near complete depletion of eosinophils alongside wider effects on other IL-5R expressing cells, significantly increases the incidence of respiratory infections by threefold. However, the composition of the sputum microbiome is not significantly altered (Haldar et al., 2025). Whilst this could suggest an antibacterial role for eosinophils, alternate immune dysfunction related to benralizumab may be responsible (Poznanski et al., 2021).

IL-1RA and TIMP-1 were differentially regulated in a pathogen-dominant microbiome. IL-1RA, an antagonist to IL-1β and its receptor, was reduced, consistent with reduced IL-1RA:IL-1β ratio in neutrophilic asthma (Gao et al., 2015), potentially representing IL-1β quenching. IL-1RA is upregulated in steroid-naïve atopic asthma (Sousa et al., 1996), with IL-1RA polymorphisms increasing asthma risk. ICS dampens IL-1RA production (Arzt et al., 1994), as supported by relatively higher concentrations in healthy/mild asthmatic sputum (**Figure 3.8**(A)). TIMP-1, also elevated in presence of pathogen-dominance, possesses antiprotease activity. MMP-9:TIMP-1 ratio is reduced in asthma and chronic bronchitis (Vignola et al., 1998), correlating inversely with airflow obstruction, with TIMP-1 polymorphisms also associated with female asthma (Johnson, 2005). Thus, whilst TIMP-1 blocks proteolytic activity, in excess it might reduce extracellular matrix turnover resulting in remodelling. Thereby, IL-10, IL-1RA and TIMP-1 are likely integral to complex regulatory networks with differing roles dependant on the wider inflammatory landscape. This could be better characterised through dedicated transcriptomic and proteomic studies in well phenotyped severe asthmatics.

Paired metagenomic sequencing of nasal lavage and sputum samples has shown that the 'one airway, one disease' concept does not apply to the airway microbiome in severe asthma where distinct microbial niches appeared in the nasopharynx and lower airway. This is consistent with mild atopic asthma and health (Durack et al., 2018a; Hilty et al., 2010). The nasal microbiome can be informative, having been shown to predict exacerbation risk in paediatric asthma when dominated by *Moraxella* species, but present data and previous studies in mild asthma suggests nasopharyngeal samples should not replace lower airway sampling in stable state or exacerbation in adult asthma (Zhou et al., 2019). This distinction between paediatric and adult asthma remains unexplained. The cytokines IL-20 (Gong et al., 2014) and IL-2 (Hondowicz et al., 2016) in sputum, which have been linked to airway remodelling and allergic inflammation in asthma respectively, were found to correlate with nasal proteins involved in diverse cellular responses. The importance of cross-signalling between these compartments is not known but of interest given the burden of comorbid sinonasal disease in severe asthma.

This study had some limitations. Samples from the Wessex cohort, collected between 2009 and 2014, are from a pre-biologic era with widespread maintenance oral corticosteroid use which could confound detection of sputum inflammatory mediators. Sample collection and storage protocols can affect quality of metagenomic data, particularly in low biomass samples; some storage-related DNA degradation is suspected in Wessex samples as DNA was extracted after <11.5 years of storage. This study had limited power given the sample size, particularly low numbers of healthy controls and patients with mild asthma, which limits detection of smaller significant differences in microbial composition within the cohort. Future studies could be strengthened by including a larger cohort of mild and moderate asthma, and longitudinal data spanning exacerbations. Due to the nature of human respiratory samples with high host DNA content (Charalampous et al., 2019; Jabeen et al., 2022), sequencing depth directly from clinical samples can be inherently limited and variable, despite efforts to deplete host DNA. This may account for the limited number of reads assigned to commensal

organisms within individuals who have a pathogen dominant microbiome as species with greater abundance and thereby higher concentration of microbial DNA will be overrepresented within the sequencing results, and rare species better detected if sequencing is performed to a greater depth. In addition, previous work by Sanderson *et al*. has shown that ~20x coverage is required for consensus whole genome sequences allowing confident identification of antimicrobial resistance determinants, and SNPs, or similarly strain inferences. Consistent high depth sequences of this order are typically derived from sequencing bacterial isolates; clinical samples show far greater variation. The sequencing depth in this study was therefore inadequate for such functional analyses in the full dataset. Approaches to overcome these limitations could include achieving greater depth by multiplexing fewer samples per flow cell or using probe-based enrichment of pathogen specific DNA enabling deeper sequencing.

3.6 Conclusions

In conclusion, Nanopore sequencing offers species level profiling of the airway microbiome in asthma and could facilitate the integration of respiratory microbiome in clinical diagnostic workflows to tailor personalised antimicrobial therapies. Using Nanopore technology a pathogen-dominant microbiome was found to be a common treatable trait in severe asthma, present in 20-30% of patients, most often with *H. influenzae*. This was accompanied by neutrophilic inflammation, elevated airway proteases and disruption of counterregulatory immune responses which could facilitate pathogen persistence and airway remodelling.

Chapter 4: The Azithromycin Mechanisms in Asthma Study (AMASS)

4.1 Introduction

Azithromycin is a second-generation, synthetic macrolide antibiotic with a broad spectrum of activity against Gram-postive and some Gram-negative bacteria. Like other macrolides it is bacteriostatic, competitively binding the 50S ribosomal subunit to inhibit protein synthesis (Zimmermann et al., 2018), but uniquely undergoes rapid absorption following oral administration, and maintains a prolonged serum half-life of approximately 3 days with subinhibitory concentrations maintained for up to 30 days, with further intracellular retention and concentration, particularly in phagocytes (100- to 3000- fold within lysosomes) (Capitano et al., 2004; Lucchi et al., 2008; Wilms et al., 2006). Macrolides have also been shown to modulate the innate and adaptive immune system.

Long-term, low dose azithromycin add-on therapy has been shown to reduce exacerbation frequency, improving asthma related quality of life and symptom control in patients with moderate to severe asthma in the large randomised placebo-controlled AMAZES trial (Gibson et al., 2017). Following treatment there is a reduction in sputum *H. influenzae* load (but not total bacterial load), as measured by PCR, compared to placebo (Taylor et al., 2019), with its abundance predicting treatment response (Taylor et al., 2020). Airway dominance with pathogenic *Pseudomonadota* species, particularly *H. influenzae* is associated with airways neutrophilia (Jabeen et al., 2022; Jabeen et al., 2024; Simpson et al., 2016; Taylor et al., 2018). However, both non-eosinophilic and eosinophilic patients benefited from an improvement in exacerbation frequency in the AMAZES cohort, including those with a negative sputum culture result (Gibson et al., 2017). Although this suggests pharmacokinetic properties and

antibacterial effects might account for azithromycin's efficacy, there have been numerous negative randomised placebo-controlled clinical trials of macrolide (Undela et al., 2021) and non-macrolide antibiotics (Allinson et al., 2023) in airways diseases, implying that other mechanisms are likely involved. Azithromycin has been shown to exert a wide range of immune modulatory and anti-viral effects *in vitro* and *in vivo* which provides potential for alternative mechanisms to account for its efficacy.

Antimicrobial resistance is a significant concern with widespread azithromycin use (Serisier, 2013). The data presented in Chapter 3 supports the hypothesis that airway dominance with *H. influenzae* is a common 'treatable trait' in severe asthma given that the AMAZES trial suggests that azithromycin is a highly effective targeted therapy within this cohort of patients. However, azithromycin appears to be exerting an effect in patients outside of this phenotype and clinical guidelines recommend its use in refractory disease regardless of microbiological results.

Determining the dominant mechanisms of action in asthma with a human interventional study was hypothesised to improve targeting of azithromycin and could help determine whether non-antibacterial macrolides (Porter et al., 2016) should be further explored as an alternative therapy within specific patient cohorts. This would help to address the risks of individual and cumulative community antimicrobial resistance burden to macrolides and other classes of antibiotics developing through transfer of shared genetic elements (Serisier, 2013). One previous bronchoscopy study had aimed to determine the effect of azithromycin on the airway epithelial barrier in 10 patients with moderate to severe asthma after receiving 250mg of azithromycin for 6 weeks. This study reported enhanced barrier integrity, increased thickness, suppressed mucin production and endopeptidase MMP-9 release in primary human bronchial epithelial cell culture *in vitro*, but found no change in epithelial barrier thickness or mucin production *ex vivo* in human endobronchial biopsy samples. However, the duration of therapy

was short and there was no exploration of immune effects using bronchoscopic samples (Slater et al., 2016).

In the AMASS study, patients with moderate to severe asthma, assessed in a specialist airways clinic, with optimised inhaled therapy (GINA step 4-5) and proven adherence ≥80%, meeting the BTS criteria for add-on azithromycin therapy in persistent symptomatic asthma, were recruited. To meet inclusion criteria patients were required to have had no changes to maintenance therapy or acute illness in the 4 weeks prior to bronchoscopy. Patients underwent bronchoscopy before and 4 months after receiving azithromycin 250mg three times weekly. Endobronchial biopsies, nasal brushings and BAL samples collected before and after azithromycin therapy were used for microbiological (BAL culture), immunological (BAL cell counts, chemokine and cytokine quantification with MSD) and transcriptomic readouts (10x Genomics Chromium droplet based single cell RNA sequencing, scRNAseq).

4.2 Hypothesis

- Azithromycin has additional immunomodulatory effects, beyond clearance of potentially pathogenic airway bacteria
- Azithromycin suppresses inflammatory signalling in epithelial cells and promotes normal functioning of ciliated and secretory cells
- Azithromycin exerts its wider effects through innate and adaptive immune mechanisms both in the presence or absence of an airway pathogen
- Azithromycin specifically reduces neutrophilic airways inflammation
- The upper airway represents a unique compartment which is immunologically and transcriptionally distinct from the lower airway and through comparison of samples from these sites the shared and unique effects that azithromycin exerts in the respiratory tract can be appreciated

4.3 Aims

- To measure clinical response to azithromycin therapy with lung function and ACQ-5
- To measure changes in lower airway cytokine and chemokine profiles following azithromycin treatment
- To characterise epithelial and immune compartments in the upper and lower airways in asthma using scRNAseq
- To characterise the effects of azithromycin therapy on the upper and lower airway as a whole and determine how the presence of pathogenic bacterial organisms can drive differential responses

4.4 Study population

Between April 2021 and May 2023, 15 patients were enrolled to the AMASS study (Flowchart shown in Chapter 2, Figure 2.2), 4 patients were excluded and did not undergo a second bronchoscopy after azithromycin was discontinued due to auditory symptoms (n=1) or the patient declined a further procedure (n=3). Due to poor sample quality and failure of sequencing libraries, samples from one further patient were excluded. Baseline patient characteristics are summarised in Table 4.1, and includes 10 patients who completed the study and contributed samples for scRNAseq. Patients had moderate to severe asthma and were all on medium to high dose ICS/LABA inhaled therapy. Two patients were established on anti-IL-5 biologic therapy prior to commencing azithromycin (Mepolizumab, n=1; Benralizumab, n=1). Overall patients had high symptoms scores (mean ACQ-5 2.7, SD 0.9) with low FeNO (mean 26ppb, SD 13ppb) and blood eosinophil count (mean 0.21 × 10^9/L, SD 0.15 x10^9/L) at baseline. However, 60% (n=6) of patients had at least one historical blood eosinophil count > 0.30 × 10^9/L, in keeping with an eosinophilic phenotype (data not shown). Similarly to the AMAZES study, ex-smokers were included (maximum smoking history of 13 pack years), with proven asthma and no evidence of emphysema on imaging.

Following the first bronchoscopy, BAL clinical culture results (Table 4.2) identified patients with significant growth of a potentially pathogenic bacterial organism (clinical laboratory cut off > 10^4 CFU/ml).

Table 4.1 Clinical characteristics of participants in the AMASS study

Characteristic	Study cohort (n=10)	Positive BAL culture (n=5)	Negative BAL culture (n=5)	
Age (years), Mean (SD)	55 (19)	64 (9)	45	(22)
Sex				
Male (%)	5 (50)	2 (40)	3	(60)
Female (%)	5 (50)	3 (60)	2	(40)
BMI (kg/m^2), Mean (SD)	28 (6)	30 (7)	26	(4)
Ex-smoker, n (%)	3 (30)	2 (40)	1	(20)
Pack years, Mean (SD)	3 (5)	4 (5)	13	–
Presence of atopy, n (%)	4 (40)	2 (40)	2	(40)
Presence of nasal polyps, n (%)	2 (20)	2 (40)	0	(0)
Medications				
Baseline inhaled corticosteroid use (BDP eq., mcg/d), Median (Range)	1300 (1500)	2000 (1000)	1000	(1500)
Long-acting beta agonist, n (%)	10 (100)	5 (100)	5	(100)
Long-acting anti-muscarinic, n (%)	3 (30)	2 (40)	1	(20)
Leukotriene modifier, n (%)	2 (20)	1 (20)	1	(20)
Maintenance oral corticosteroid, n (%)	0 (0)	0 (0)	0	(0)
Biologic therapy, n (%)	2 (20)	2 (40)	0	(0)
Asthma history				
ACQ5 score, Mean (SD)	2.7 (0.9)	2.3 (0.9)	3	(1)
Unscheduled GP/ hospital visits in 12 months, Median (Range)	2 (12)	4 (12)	0	(7)
Corticosteroid courses in 12 months, Median (Range)	1 (14)	1 (6)	2	(14)
Antibiotic courses in 12 months, Median (Range)	2 (14)	4 (12)	0	(14)
Spirometry				
FEV1 (%), Mean (SD)	81 (18)	89 (17)	73	(17)
FVC (%), Mean (SD)	99 (13)	103 (17)	96	(6.8)
FEV1/FVC, Mean (SD)	0.66 (0.15)	0.70 (0.13)	0.63	(0.17)
FeNO (ppb), Mean (SD)	26 (13)	69 (62)	22	(12)
Blood eosinophils (x10^9/L), Mean (SD)	0.21 (0.15)	0.23 (0.2)	0.18	(0.11)
Positive BAL culture, n (%)	5 (50)	5 (100)	0	(0)
H. influenzae, n (%)		4 (80)		
S. viridans sp., n (%)		1 (20)		

BMI, body mass index; BDP, beclomethasone diproprionate; ACQ5, Asthma Control Questionnaire 5; GP, general practitioner; FEV1, forced expiratory volume in 1s; FVC, forced vital capacity; FeNO, exhaled nitric oxide; BAL, bronchoalveolar lavage

Table 4.2 BAL culture results pre and post azithromycin therapy for the AMASS cohort

	BAL Culture Result (CFU/ml)	
PID	Bronchoscopy 1	Bronchoscopy 2
OAS1269*	*H. influenzae, S. viridans* (1x10^4-10^5)	*H. influenzae* (<1x10^4)
OAS1384*	*S. viridans* (>1x10^5), *Neisseria sp.* (>1x105)	*Neisseria sp*. (1x10^4-10^5)
OAS1513	*H. influenzae* (1x10^4-10^5)	*Haemophilus sp.* (<1x10^4)
OAS1522	*H. influenzae* (1x10^4-10^5)	*H. influenzae* (<1x10^4)
OAS1571	*H. influenzae* (>1x10^5)	*S. viridans* (<1x10^4)
OAS1336	*S. viridans* (<1x10^4)	*None*
OAS1367	*Enterococci* (<1x10^4)	*Enterococci* (<1x10^4)
OAS1439	*Streptococci* (<1x10^4)	*S. viridans, Neisseria sp.* (<1x10^4)
OAS1532	*Coliforms* (<1x10^4)	*S. viridans, Neisseria sp.* (<1x10^4)
OAS1543	*S. viridans* (<1x10^4)	*No data*

Positive results highlighted, *Patient on biologic therapy; OAS1269, Mepolizumab; OAS1384, Benralizumab

H. influenzae was the most common organism isolated. Both patients receiving biologic therapy had a positive BAL culture. In addition, those with a positive culture had higher frequency of unscheduled GP/hospital visits and antibiotic courses in the preceding 12 months (4 *vs.* 0), alongside higher mean baseline FeNO (69 *vs.* 22ppb) and marginally higher blood eosinophil count (0.23 *vs.* 0.18 × 10^9/L). Culture yield (CFU/ml) reduced at 4 months into azithromycin therapy. Patients were continued on treatment for at least 6 months in keeping with BTS guidelines (Smith et al., 2020).

4.5 Clinical response to azithromycin

Clinical response to azithromycin was assessed by measuring lung function and symptom score with ACQ-5 at 4 months post-azithromycin therapy. FeNO and blood eosinophil count were repeated to investigate whether azithromycin influenced type-2 biomarkers, as predictors of corticosteroid responsiveness (**Figure 4.1**).

After 4 months of azithromycin add-on therapy there was a significant increase in FEV1 and FVC, accompanied by a marked reduction in ACQ-5 symptom score ($p < 0.05$). This was consistent with the findings of the AMAZES trial, reporting an improvement in FEV1 and ACQ-6 (Gibson et al., 2017). No significant changes were seen in type-2 biomarkers overall.

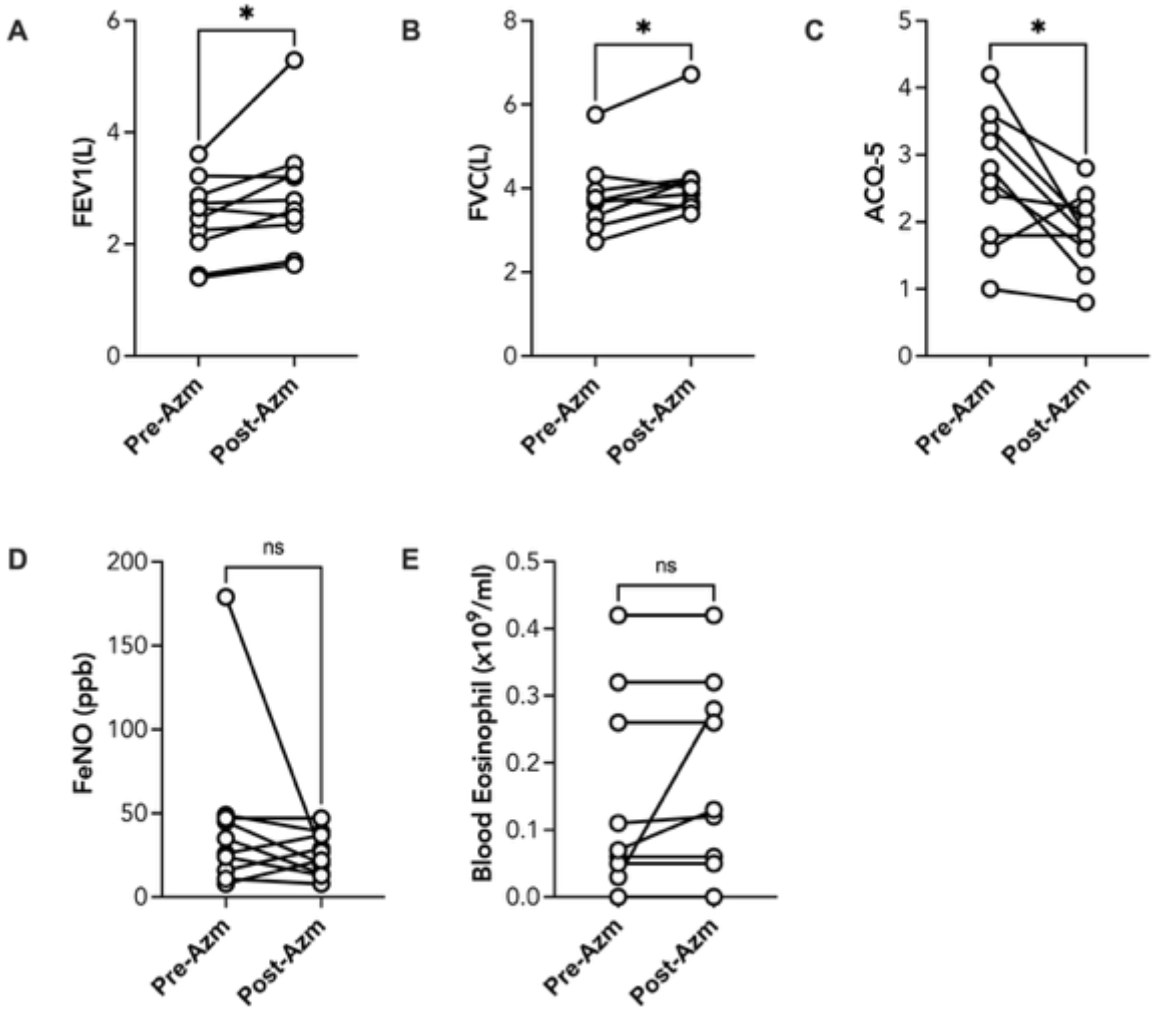


Figure 4.1 Lung function, symptom scores and type-2 biomarkers post-azithromycin therapy.

*Paired data shown pre- and 4 months post-azithromycin therapy (n=10), (A) Forced expiratory volume in 1s (FEV1), (B) Forced vital capacity, (C) Asthma control score 5 (ACQ-5), (D) Fraction of exhaled nitric oxide (FeNO), (E) Blood eosinophil count (paired t-test *p<0.05)*

4.6 Regulation of airway mediators and neutrophils by azithromycin

Chemokines (eotaxin, eotaxin 3, MDC, TARC, CXCL8, MCP-1, CCL3/MIP-1α, CCL4/MIP-1β, IP-10), inflammatory cytokines (IL-1β, IFNγ, TNFα, GM-CSF, IL-12p70, IL-17A, IL-2) type-2 cytokines (IL-4, IL-5, IL-13) and modulatory/tissue homeostasis related cytokines (IL-10, IL-1RA, bFGF) were measured in BAL pre- and post-azithromycin therapy using MSD electrochemiluminescent assays due its higher sensitivity than standard ELISAs and its

capability to multiplex mediators of interest. There was an overall reduction in markers of neutrophilic airways inflammation and a significant reduction in BAL neutrophil count after azithromycin treatment. Neutrophil NET load reduced numerically but did not reach statistical significance in this small cohort. Cytokines and chemokines measured were not significantly altered following multiple correction testing (FDR < 0.05), however there was a reduction in CXCL8, IL-1β, TNF, IP-10, IL-2 and IL-4.

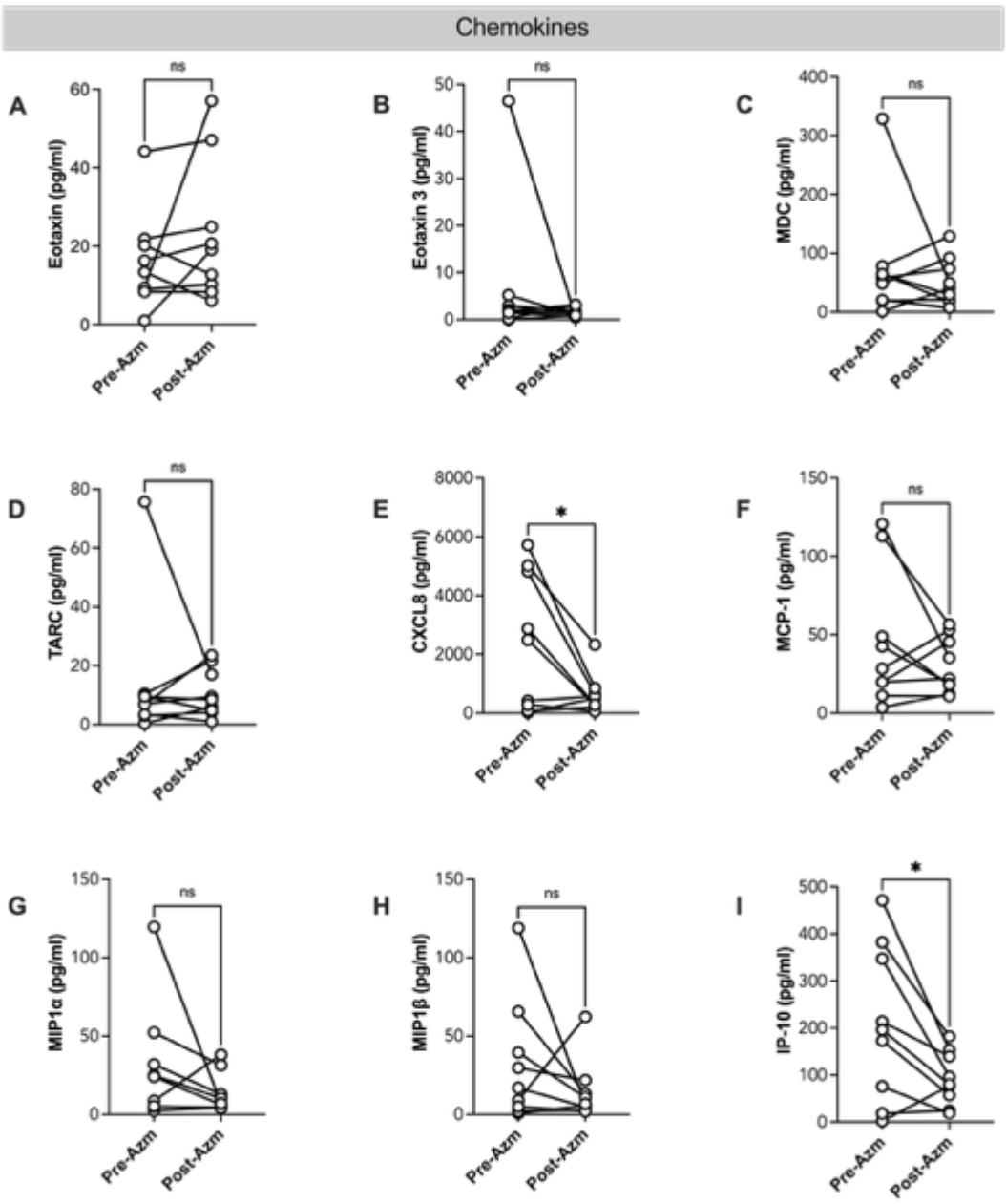


Figure 4.2 Airway chemokines pre- and post-azithromycin therapy.

*Chemokines were quantified in available paired BAL supernatants using MSD (n=9). (A) Eotaxin, (B) Eotaxin-3, (C) MDC, (D) TARC, (E) CXCL8, (F) MCP-1, (G) MIP-1α, (H) MIP-1β, (I) IP-10 (paired t-test *p<0.05, however NS on multiple correction testing with FDR<0.05)*

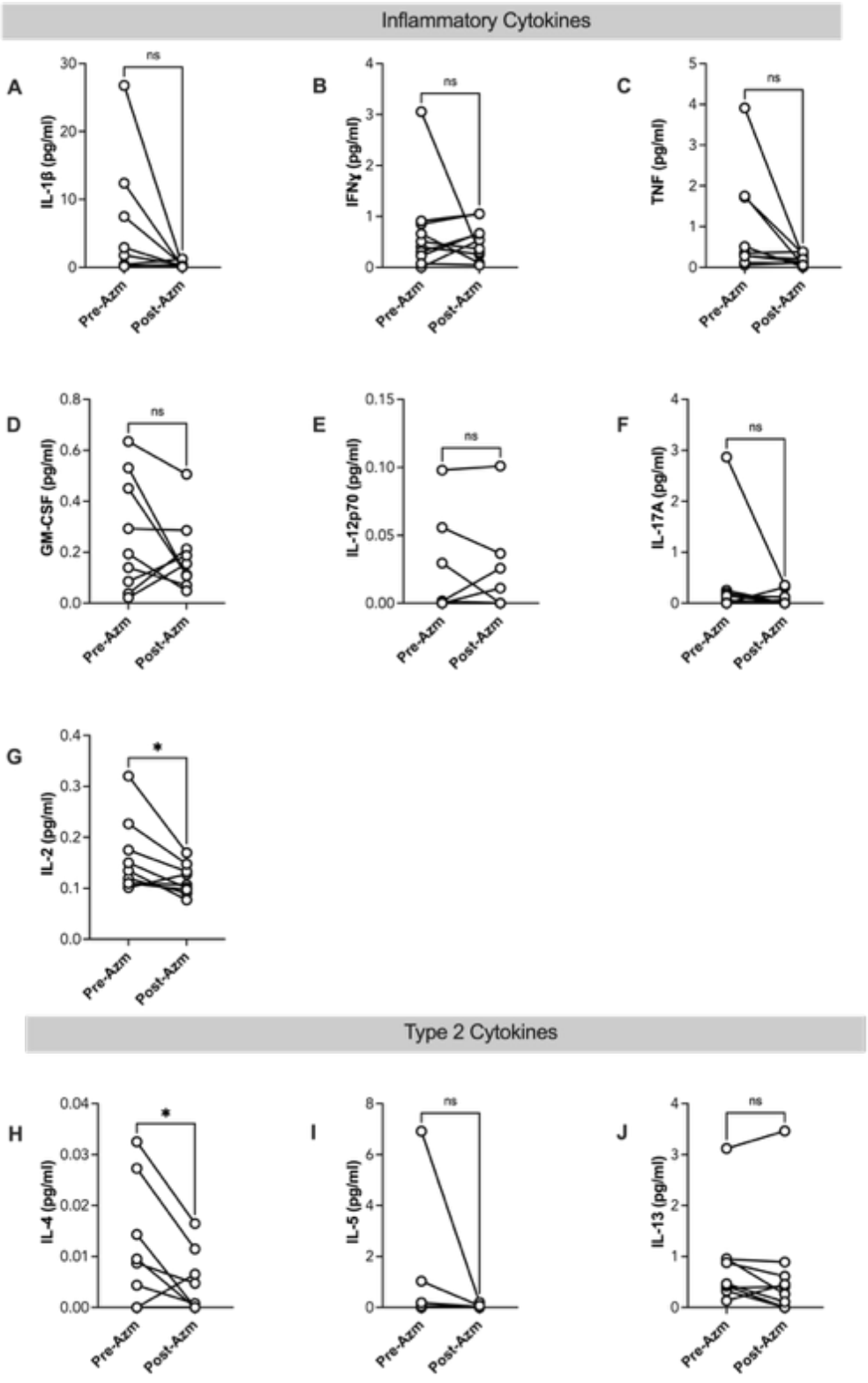


Figure 4.3 Airway cytokines pre- and post-azithromycin therapy*;*

*Inflammatory/Type-1 and Type-2 cytokines were quantified in available paired BAL supernatants using MSD (n=9). (A) IL-1β, (B) IFN$_\gamma$, (C) TNF, (D) GM-CSF, (E) IL-12p70, (F) IL-17A, (G)IL-2, (H) IL-4, (I) IL-5, (J) IL-13 (paired t-test *p<0.05, however NS on multiple correction testing with FDR<0.05)*

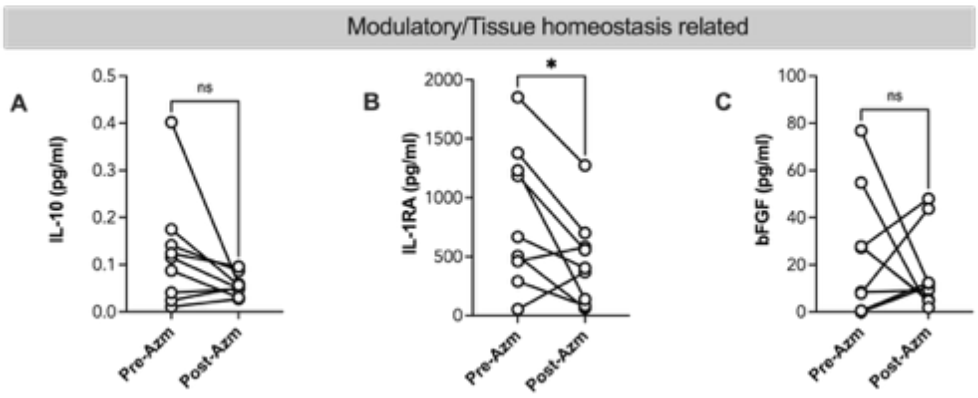


Figure 4.4 Modulatory cytokines pre- and post- azithromycin therapy;

*Cytokines were quantified in available paired BAL supernatants using MSD (n=9). (A) IL-10, (B) IL-1RA, (C) bFGF (paired t-test *p<0.05, however NS on multiple correction testing with FDR<0.05)*

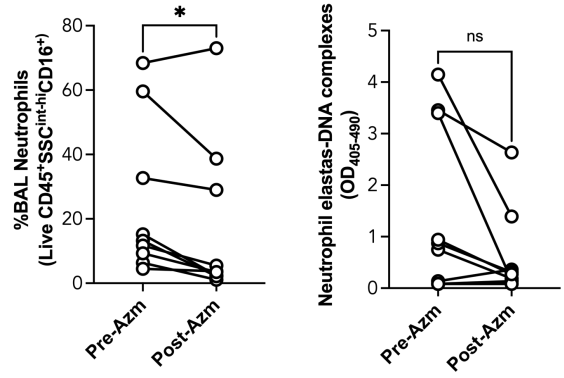


Figure 4.5 BAL neutrophil frequency and quantification of airway NET load pre- and post-azithromycin*;*

*(A) BAL neutrophils identified as proportion of CD45+ SSCint-hiCD16+ cells by flow cytometry; (B) NETs quantified by measurement of neutrophil elastase-DNA complexes using ELISA, mean OD405-490 reported (paired t-test *p<0.05)*

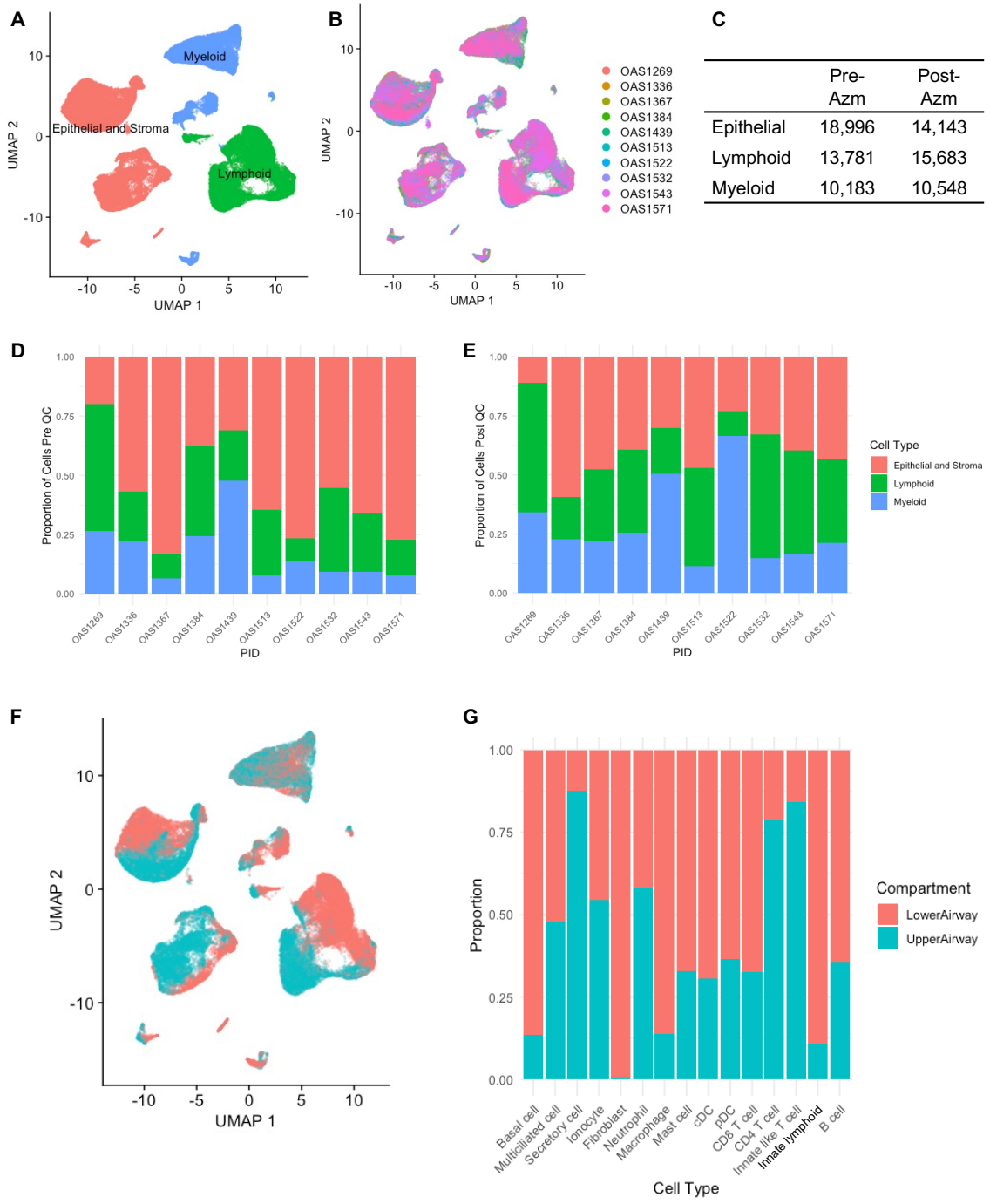
4.7 Single cell characterisation of treatment responses to azithromycin

4.7.1 scRNAseq of upper and lower airway samples in severe asthma

Paired endobronchial biopsies and nasal brushing were collected from 10 patients enrolled to the AMASS study before and after treatment with azithromycin for 4 months. There were 224,937 cells prior to quality control and 83,337 cells following filtering. Subclustering and

annotation using the Human Lung Cell Atlas (Sikkema et al., 2023) was performed to broadly classify cells into 3 compartments: (1) epithelial and stromal, (2) lymphoid and (3) myeloid for quality control. A curated approach was taken to ensure neutrophils were not excluded, as often occurs in standardised workflows, due to their low RNA content (Wigerblad et al., 2022). Cells were filtered based on minimum genes per droplet of 500, except for neutrophils (threshold 150), and less than 6-10% mitochondrial gene counts depending on the cellular compartment. Further mapping against the reference Human Lung Cell Atlas (lacking granulocytes), Human Tonsil Atlas (including granulocytes) and Human PBMC Atlas (for lymphocyte subsets) was initially run with refinement of all final annotations performed manually. This approach identified 33,139 epithelial and 29,467 lymphoid and 20,731 myeloid cells of high quality which are shown in the combined UMAP and used to identify cluster markers (**Figure 4.6**). The greatest loss in proportion of cells was seen in the epithelial compartment and thought to be related to large cell size and fragility contributing to poorer survival through microfluidic systems (**Figure 4.6** D-E). Upper and lower airway samples from the same patient on the day of bronchoscopy were barcoded using hashtag oligos and combined before running on a single 10x channel to reduce batch effects and allow later bioinformatic separation into upper and lower airway cells. However, due to poor ADT library quality in a limited number of samples (n=4/20, affecting 3 patients in total), it was possible to confidently separate 29,793 nasal brush cells and 32,738 bronchial biopsy cells. The proportion of pre- and post- treatment cells by compartment are shown in **Figure 4.6** C and were included in all differential gene expression analyses.

Differential gene expression results tables have been provided in Appendix 3.



	Pre-Azm	Post-Azm
Epithelial	18,996	14,143
Lymphoid	13,781	15,683
Myeloid	10,183	10,548

Figure 4.6 Upper and lower airway cells captured by scRNAseq.

(A) Uniform manifold approximation and projection (UMAP) visualisation shows the epithelial, myeloid and lymphoid lineages included in the study; (B) UMAP visualisation of sample integration by PID using Harmony; (C) Numbers of cells included by lineage pre- and post-azithromycin therapy in downstream analyses; (D) Proportion of cells types within dataset prior to bioinformatic QC and filtering; (E) Proportion of cells types within dataset after bioinformatic QC and filtering; (F) UMAP coloured by compartment (upper or lower airway) to demonstrate separation of cells by anatomical location; (G) Bar plot showing proportion of cell type by airway compartment

4.7.2 Characterisation of epithelial and immune cell populations in the asthmatic airway in the AMASS cohort

As shown in **Figure 4.6** F-G, there was a distinct separation of upper and lower airway cells in epithelial and immune cell compartments on the UMAP, indicating discrete populations based upon their site of origin in the airway. A higher proportion of cells annotated as ionocytes, fibroblasts, macrophages and NKT cells originated from the lower airway. Whereas a higher proportion of secretory cells, innate like T cells and CD4 T cells were captured from the upper airway.

4.7.2.1 Epithelial and stromal lineage

Within the epithelial and stromal cell lineages, seven cell types were identified. Cluster markers are summarised in **Figure 4.7** C. This included a large multiciliated population of epithelial cells (*EPCAM, FOXJI, SNTN, C5orf49*) separated by airway compartment, secretary cells including goblet (*MUC5AC, PI3, LCN2*) and club cells (*CEACAM6, KRT7, PGR, ELF3 and MUC5AC* negative), basal cells (*KRT5, S100A2, SFN*), ionocytes (*FOXI1, CFTR, ASCL3, ATP6V1A*) and fibroblasts (*PDGFRA, DCN, MGP*). In addition, a population of cells with overlapping club and goblet cell markers and high expression of Runt-related transcription factor 2 (*RUNX2*) was identified. *RUNX2* can acts as a regulator for goblet cell differentiation and is reported to have greater expression in primary bronchial epithelial cells *in vitro* during IL-13 induced differentiation and mucus production (Shi et al., 2017). It can also bind to the promoter of high mobility group box 1 (*HMGB1*), an alarmin promoting eosinophil survival, with elevated levels detected in induced sputum from patients with asthma (Wu et al., 2022). These cells have thus been labelled RUNX2 high transitional cells, with a larger population captured from nasal brushings.

There was some variation in the proportions of each cell type (shown in **Figure 4.7** D-E as mean and SD in each cluster) pre- and post-azithromycin therapy, most notably with a relative increase in lower airway basal cells after treatment.

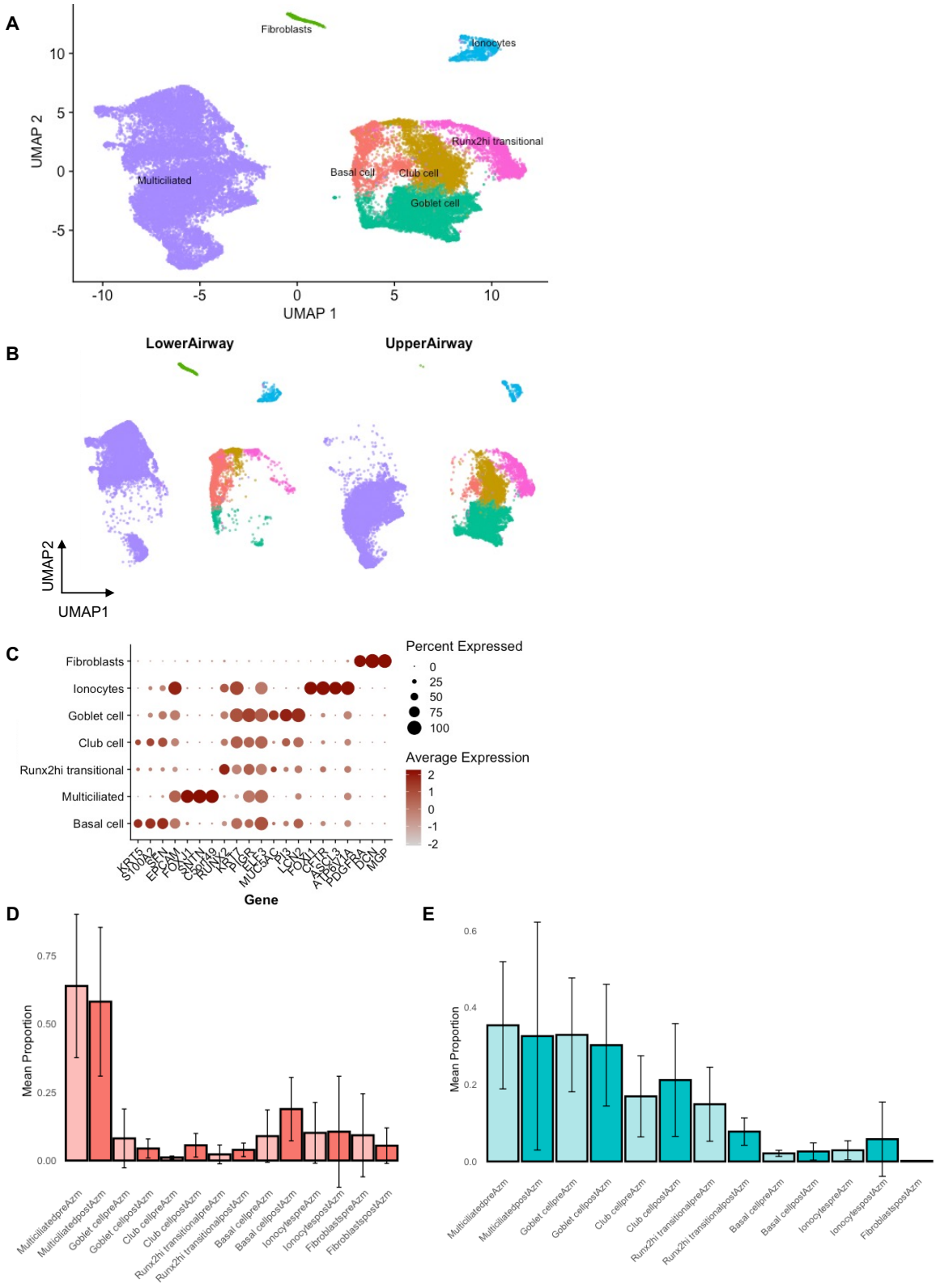


Figure 4.7 Epithelial and stromal cell lineage.

(A) UMAP showing sub-populations identified; (B)UMAP showing split of cells by compartment; (C) Dotplot showing expression of defining cluster markers; (D) Mean proportion and SD across donors of cell types in the lower airway pre- and post- azithromycin treatment; (E) Mean proportion and SD across donors of cell types in the upper airway pre- and post- azithromycin treatment from each donor

4.7.2.2 Myeloid lineage

In the myeloid lineage broadly five populations of cells were identified: neutrophils, macrophages, conventional dendritic cell expressing CD1C (cDC2), plasmacytoid dendritic cell (pDC), and mast cells. Lineage specific cluster markers are shown in **Figure 4.8**. Neutrophils expressed prototypic markers including *S100A8, S100A9, FCGR3B*, and *CXCL8*, alongside *IFITM2*, a marker of tissue infiltration. Higher resolution clustering revealed subpopulations of neutrophils. The largest population likely represents classical neutrophils with high *S100A8, S100A9* and *CXCL8* expression. However over 50% of cells upregulated myeloid nuclear differentiation antigen (*MNDA*) which is cleaved by caspases and accumulates in the cytoplasm facilitating constitutive apoptosis. Failure of this process is reported to lead to parallel accumulation of myeloid cell leukemia-1 (*MCL-1*) and delayed apoptosis in sepsis (Fotouhi-Ardakani et al., 2010). Other clusters were defined by high expression of prokineticin-2 (*PROK2*), a marker upregulated in tumour infiltrating neutrophils (Sasaki et al., 2018), the neutrophil chemokine *CXCL1*, *CCL4L2* which has been linked to ICS non-response when measured in peripheral blood and tissue (Tsai et al., 2023), and the anti-inflammatory peptidase inhibitor – elafin (*PI3*) (Allaeys et al., 2021). A further small cluster of neutrophils expressed an interferon stimulated gene signature (ISGhi) with high levels of *IFIT2, IFIT3* and *ISG15*, previously reported in inflammatory bowel disease single cell data (Garrido-Trigo et al., 2023) and associated with impaired chemotaxis and antibacterial killing in acute respiratory distress syndrome (ARDS) (Malcolm et al., 2011). Macrophages (*CD14, VCAN, HLA-DRA*) could be subclustered into populations of cells expressing high levels of ficolin 1 (*FCN1*), a soluble pattern recognition molecule previously reported to promote LPS driven IL-1β production via *NLRP3* in tissue infiltrating macrophages (Chen et al., 2023), cathepsin L (*CTSL*) a lysosomal cysteine protease upregulated by LPS in alveolar macrophages (Ishii et al., 2014) also implicated in pulmonary extracellular matrix degradation, and heat shock protein high (*HSPA1A/HSPA1B/HSP90AA1* high) – these

proteins have been shown to reduce IL-1β secretion in macrophages (Brykczynska et al., 2020). Overall macrophages upregulated transcription factor *NFKB* (**Figure 4.8** D).

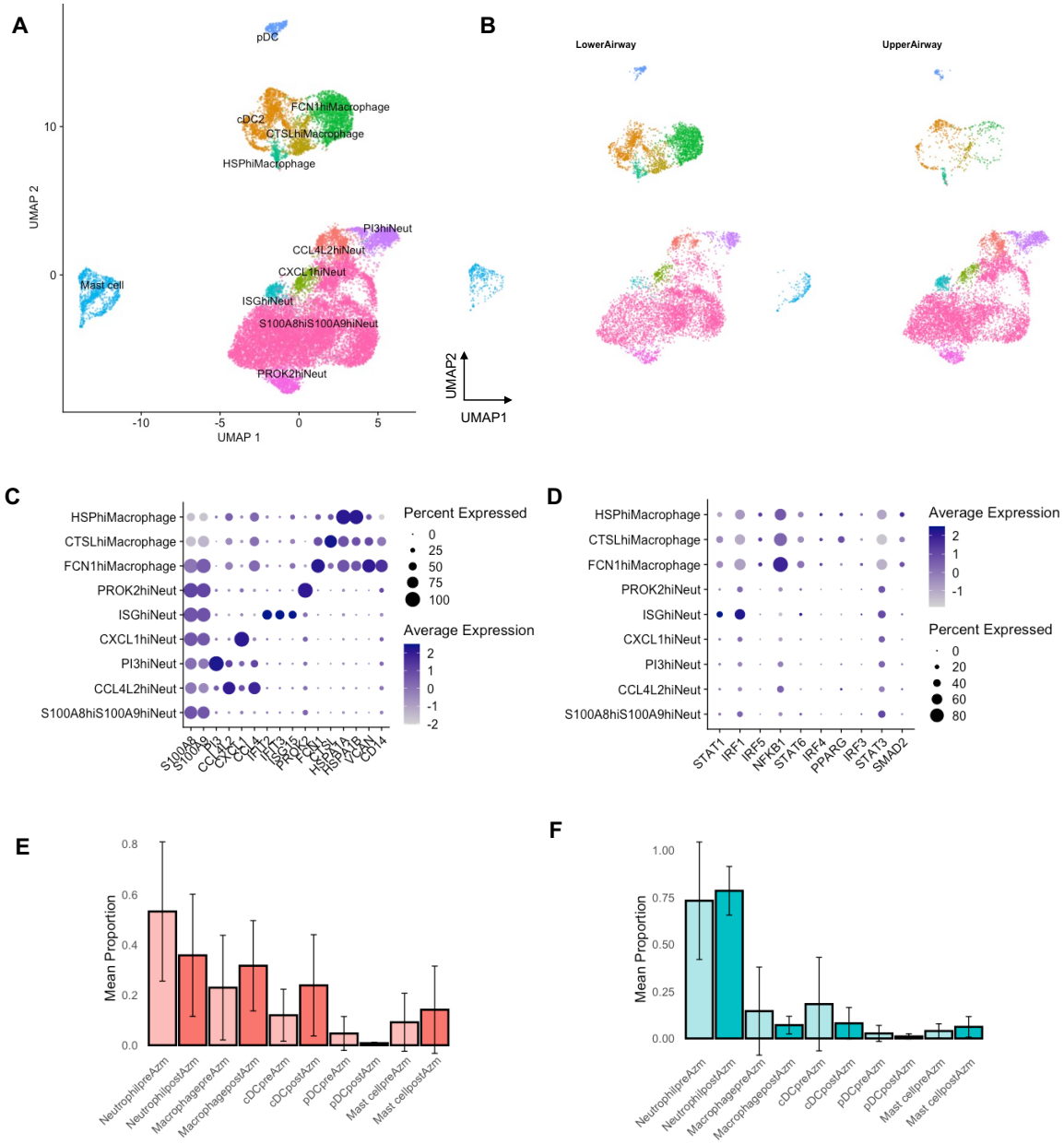


Figure 4.8 Myeloid lineage.

(A) UMAP showing sub-populations identified; (B) UMAP showing split of cells by compartment; (C) Dotplot showing expression of defining cluster markers; (D) Dotplot of key myeloid transcription factors expressed across macrophage and neutrophil sub-populations; (E) Mean proportion and SD across donors of cells types in the lower airway pre- and post- azithromycin treatment; (E) Mean proportion and SD across donors of cells types in the upper airway pre- and post- azithromycin treatment from each donor

In the lung there appeared to be a relative reduction in neutrophils captured and increase in macrophage populations overall following azithromycin therapy (**Figure 4.8** E). In the upper airway neutrophils were the largest population of myeloid cells (**Figure 4.8** F).

4.7.2.3 Lymphoid lineage

In the lymphoid lineage (**Figure 4.9**), 17 different populations were identified. There was a separation by compartment. Within the upper and lower airway, a large population of nasal and bronchial CD8-expressing tissue-resident memory (TRM) cells were present. These were identified as granzyme positive (*A, B, H*) cells expressing markers of tissue residency (*ITGAE, CD69, CXCR6*). They lacked expression of homing receptors *CCR7, CD62L* and *CX3CR1* (Behr et al., 2018). Cluster markers are shown in **Figure 4.9** F and expression of tissue residency markers and further phenotypic evaluation in **Figure 4.10**. There was no significant difference in proportions of T cell subsets before and after treatment with azithromycin in the upper or lower airways.

Three distinct TRM populations were identified with high early growth response gene-1 (*EGR1*) expression, granzyme K or amphiregulin (*AREG* (Delacher et al., 2024)) expression. EGR1 is a transcription factor activated by the protein kinase A (PKA) and MAPK pathways, and is induced early following ligation of the T cell receptor (TCR) (Singh et al., 2004), promoting activation and IL-2 production (Collins et al., 2006). In the airways, EGR1 has been shown to regulate transforming growth factor (TGF)-α mediated pulmonary remodelling and airway hyperresponsiveness in an *in vivo* transgenic TGF-α/EGR1 knockout mouse model (Kramer et al., 2009). CD8+ granzyme K expressing memory like T cells have recently been reported to cause complement activation in nasal polyp tissue and correlate with disease severity and risk of recurrence. *In vivo,* granzyme K promoted airways inflammation and goblet cell hyperplasia in an ovalbumin induced model of asthma (Lan et al., 2025). AREG is a ligand of the epidermal growth factor receptor (EGF), involved in regeneration and remodelling. Activated ($PD1^{+}TIGIT^{+}$) and effector T cell derived AREG has been shown to

promote healing in *in vitro* wound healing assays (Delacher et al., 2024) but it is also implicated in driving type-2 and rhinovirus induced inflammatory responses in asthma (Deacon and Knox, 2015).

A cluster of activated CD8 T cells was identified with high expression of chemokines XCL1/XCL2 with *IRF4* expression (Boutet et al., 2021), and an activated effector cluster defined by high *CCL4* chemokine expression alongside *TNFα* and IFN_{γ} (Szabo et al., 2019).

There were three innate lymphoid cell populations mainly localised to the lung. These comprised $CD16^{+}CD56^{dim}$ and $CD16^{-}CD56^{dim}$ cells which have been labelled as NK/NKT cells due to some expression of *CD3* within each cluster. A small population of lineage negative, but *NCAM1, AREG, KIT, IL7R* and *KLRB* expressing cells have been labelled as NK/ILC cells (Sikkema et al., 2023). Innate like T cells were predominantly captured from the upper airway and included γδ T cells (*TRDV1/TRGV9* expressing, *TRG-AS1, GNLY* high) and MAIT cells (*KLRB1, SLC4A10, RORC* high).

A single distinct CD4+ population was identified with high *CD161, RORC, IL23R* and *CCR6* expression (Sikkema et al., 2023). These cells are identified as Th17 cells. I sought to identify any additional CD4 T cells by selecting cells with high CD4 cell surface protein expression, and low CD8 cell surface protein expression (as shown in **Figure 4.11**). This was not successful in identifying additional CD4 cells as subclustering demonstrated mixed T/NK/B cell markers. As shown in **Figure 4.11** B, CD4 protein expression was seen in Treg, naïve CM and Th17 cells – it is likely that using a more stringent cut-off for protein expression in my approach would simply subset these cells.

Other populations included naïve central memory T cells (*KLF2, CCR7, LEF1, SELL*), regulatory T cells (*FOXP3, CTLA4*), proliferating CD8 T cells (*NKG7, SLC7A5, PIK3R1*) and

B cells (*CD19, CD79A, CD79B, MS4A1*) (Sikkema et al., 2023). Cluster markers are highlighted in **Figure 4.9** (F).

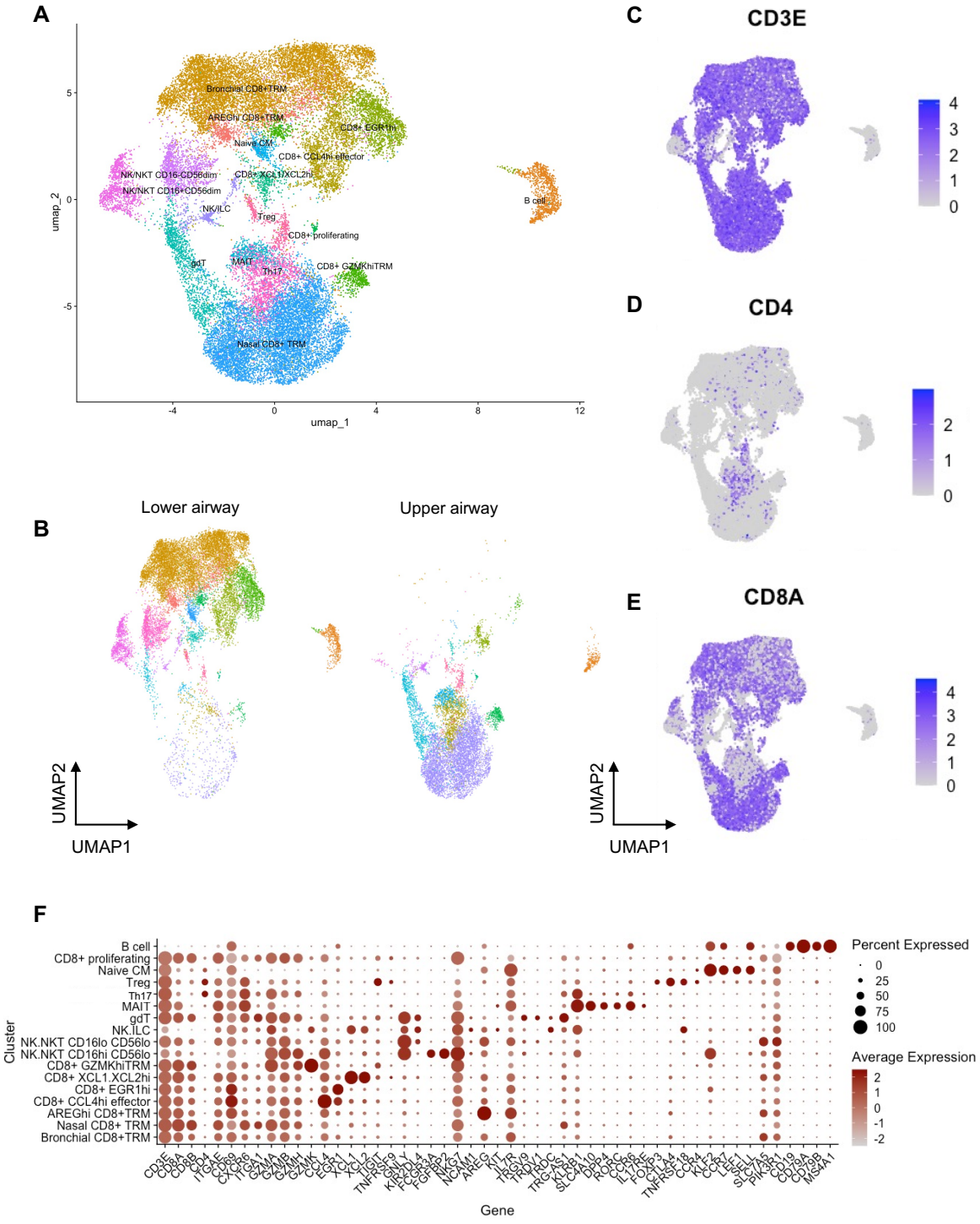


Figure 4.9 Lymphoid lineage.

(A) UMAP showing sub-populations identified; (B) UMAP showing split of cells across compartments; UMAPS coloured by expression of (C) CD3E, (D) CD4, (E) CD8 genes; (F) Dotplot showing expression of defining cluster markers

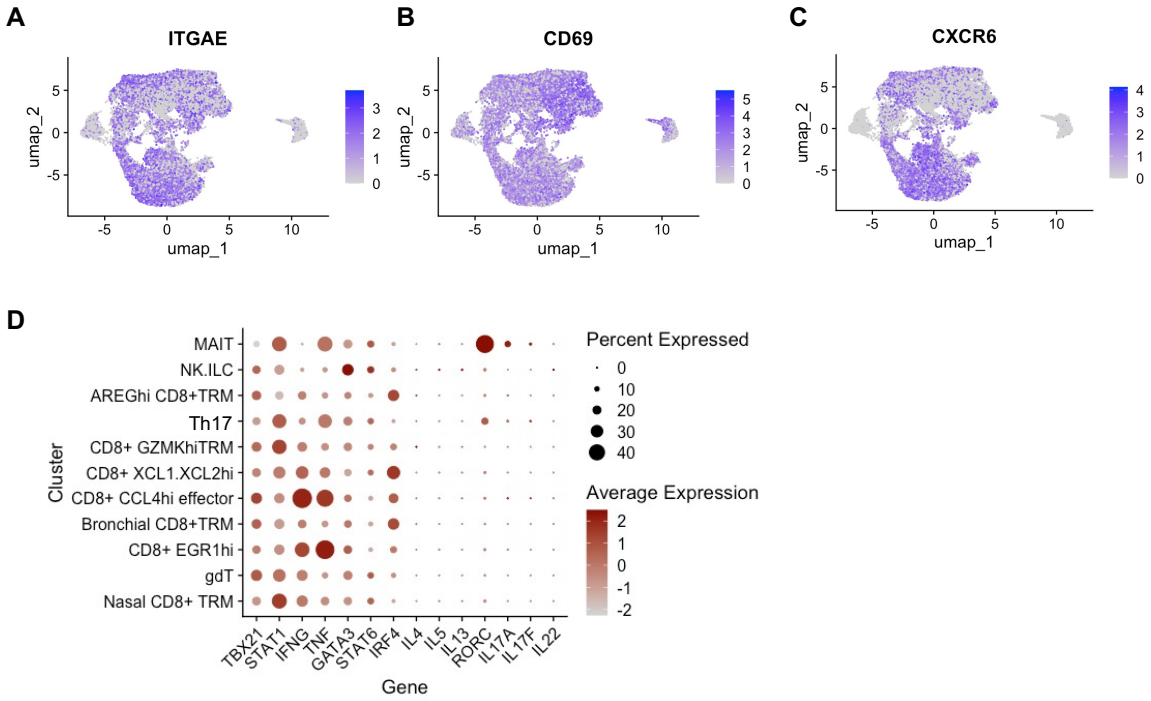
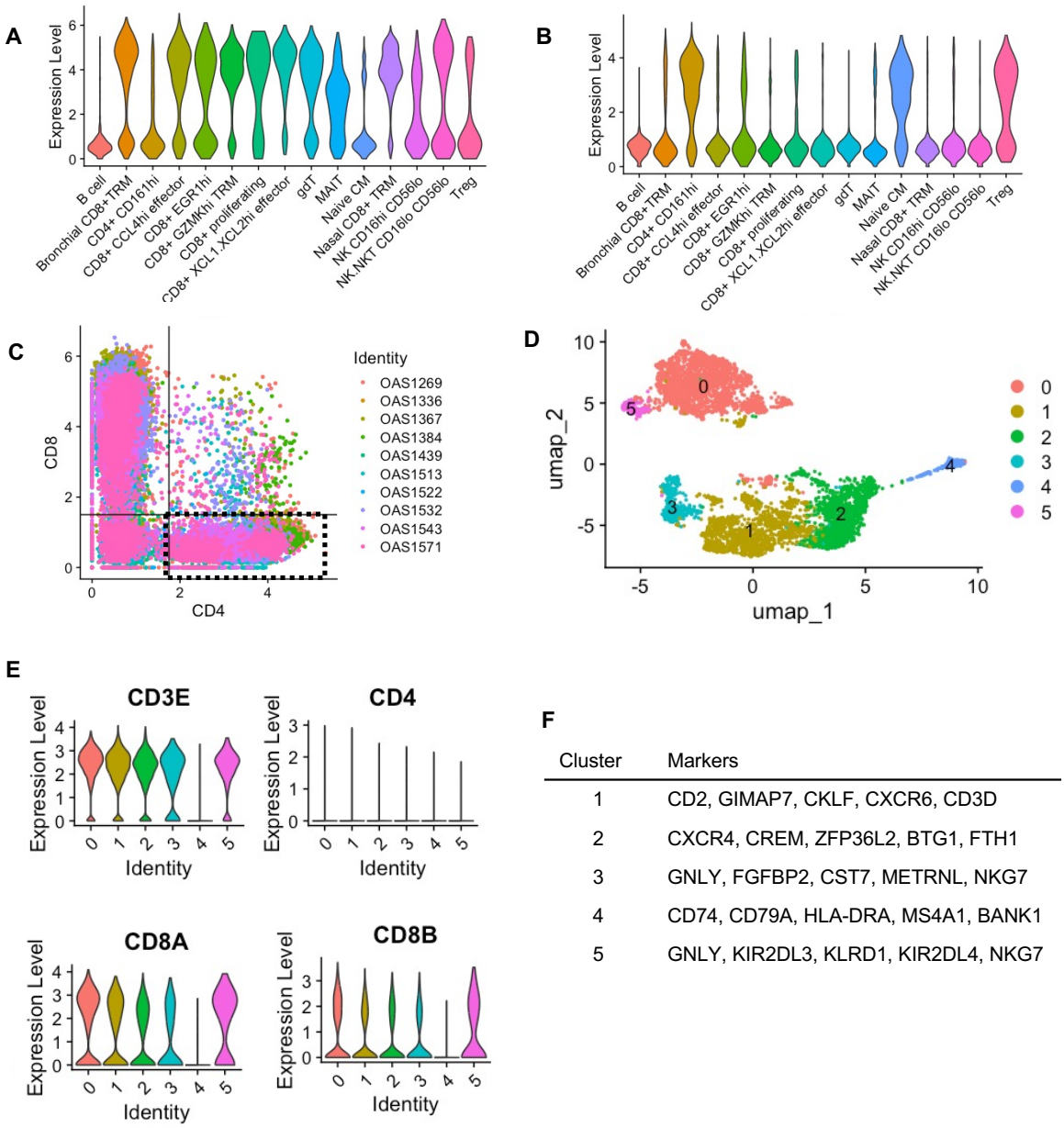


Figure 4.10 T cell tissue residency makers and phenotypic profiling.

UMAPS coloured by expression of (A) ITGAE, (B) CD69, (C) CXCR6 gene expression; (D) Dot plot of key transcription factors and cytokines used for phenotypic classification of cells



F

Cluster	Markers
1	CD2, GIMAP7, CKLF, CXCR6, CD3D
2	CXCR4, CREM, ZFP36L2, BTG1, FTH1
3	GNLY, FGFBP2, CST7, METRNL, NKG7
4	CD74, CD79A, HLA-DRA, MS4A1, BANK1
5	GNLY, KIR2DL3, KLRD1, KIR2DL4, NKG7

Figure 4.11 CD4 expression and identification of cells.

(A) Violin plot of CD8 gene expression across clusters; (B) Violin plot of CD4 gene expression across clusters; (C) Scatter plot of CD4 against CD8 protein expression in T cell population with subset of cells with CD4+CD8- protein expression selected for subclustering; (D) UMAP of cells identified in panel (C), coloured by cluster number; (E) Violin plot showing CD3, CD4, CD8A, CD8B gene expression by clusters shown on UMAP in panel (D); (F) Top ranked cluster associated genes identified using FindAllMarkers in Seurat

4.7.3 Transcriptomic changes in epithelial cells after azithromycin treatment

The epithelial and stromal compartment showed the greatest number of differentially regulated genes in this study. All significantly upregulated genes are defined as average log2fold change >0.25 and adjusted p value <0.05 and all significantly downregulated genes are defined as average log2fold change <−0.25, and adjusted p value <0.05. In endobronchial biopsy samples 1718 genes were significantly upregulated and 1876 genes downregulated following azithromycin treatment, whereas in the nasal brush samples 411 genes were upregulated and 240 genes downregulated. The predominant gene ontology (GO) pathways enriched in the upregulated and downregulated gene sets from the upper airway are shown in **Figure 4.12**. Upregulated pathways were driven by genes including *FOXQ1* (transcription factor involved in epithelial mesenchymal transition and type 2 signalling) (Ovsiy et al., 2017), the transmembrane glycoprotein *CD44* (promotes leukocyte recruitment) (Katoh, 2021), *TP63* (basal cell transcription factor), *IER3* (regulation of apoptosis), *VEGFA* (induced by tissue hypoxia) and *NOTCH1* (involved in lung homeostasis, dysregulated in asthma promoting type 2 inflammation) (Zong et al., 2016). Genes related to cilial development were downregulated as reflected in the GO analysis. In the upper airway expression of genes such as *IFITM1, STAT1, IRAK1, MYD88, LGALS9* (Galectin-9), *ISGO20* and *ISG15*, alongside expression of *HLA-E, HLA-F, HLA-DQB1* reflected upregulated viral response and immune pathways.

Differential gene expression analysis was performed by cell type in the upper and lower airway as summarised in **Figure 4.13**. In both compartments the multiciliated and goblet cells showed the highest number of differentially regulated genes. Multiciliated cells of the upper and lower airway most significantly upregulated genes related to cilial movement (*CFAP73, CCDC74A, TCTEX1D4*) and the antimicrobial secreted protein *WFDC6* (Bingle et al., 2006). In the upper airway there was upregulation of *HLA-DR5* and notably *DTT*, a structural and functional homolog of *MIF*, which has been shown to promote growth of epithelial cells *in vitro* (Song et al., 2021). Mitochondrial genes were amongst those most upregulated in nasal epithelium. The down regulated genes in both compartments were involved in cell growth and

DNA synthesis (*DHFR, STEAP1B*) and intracellular signalling/regulation, namely *PDE3A* (a phosphodiesterase acting via cAMP), shown to promote inflammation and impaired barrier function within *in vivo* models of allergic asthma (Beute et al., 2018). Downregulated genes in the lower airway included interferon stimulated genes (ISGs) including *IFITM1* and *IFI6,* and the transcription factor *ZBTB16*. In the upper airway there was downregulation of macrophage migration inhibitory factor (*MIF*) and acute phase proteins serum amyloid A1/A2 (*SAA1/A2*), alongside dual oxidases which can drive oxidative stress in common inflammatory conditions.

Goblet cells of the upper and lower airway showed distinct changes after azithromycin treatment, mainly in the upper airway, with upregulation of HLA-genes and mucin *MUC1*and downregulation of ribosomal proteins. Trefoil factor family 3 (*TFF3*) which is secreted with mucin (Weste et al., 2022), was the only marginally upregulated goblet cell gene in the lung. Downregulated genes included *GALANT11* which is involved in mucin type-O glycosylation (Bennett et al., 2012). Shared down regulated genes included *PI3* (elafin) and *DHFR*.

Differential abundance testing was performed on the *k*-nearest neighbourhood graph using miloR (Dann et al., 2022), accounting for treatment status and paired design within the generalised linear model (**Figure 4.13**). This demonstrated that 37% of neighbourhoods containing basal cells had greater abundance following azithromycin treatment (mean log FC 4.2) in the lower airway. By comparison 12% of multiciliated cell neighbourhoods changed in abundance. Lung basal cells upregulated *BTG1, ID2, JUN, GADD45B* and *IER2* – which are mainly involved in regulation of the cell cycle. The most significantly downregulated protein coding genes included *DHFR, STEAP1B, RBFOX2A, ARMC9* and the serine protease inhibitor, *SERPINB2*. *RUNX2* high and lung club cells also downregulated DHFR.

A population shift in basal cells or other cell types was not seen in the upper airway, nor were there any significantly differentially expressed genes. Nasal club cells did however undergo transcriptional changes (49 genes up, 79 genes down). MUC1, PSCA, HLA-B, HLA-E and

TSPAN1 were most upregulated and RBFOX2, STEAP1B and numerous ribosomal proteins downregulated. In keeping with this, the most enriched GO terms related to upregulated pathways of antigen presentation and T cell activation, and downregulated cytoplasmic translation (**Figure 4.14**).

Thus, epithelial cells show reduced cilial generation but potential for increased motility, with greater HLA expression in the lower airway. Interestingly there was no significant change in mucin secretion in the lower airway.

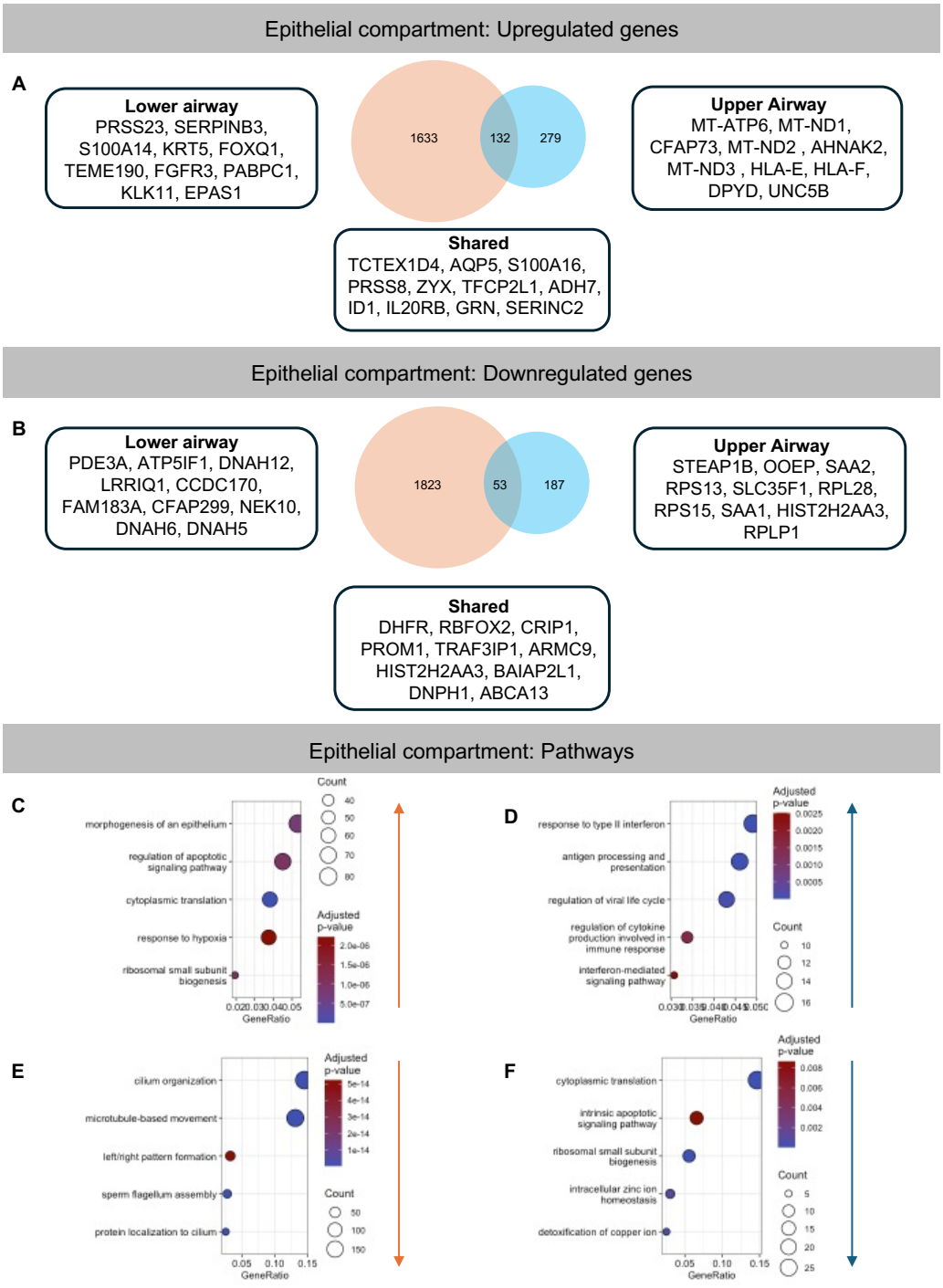


Figure 4.12 Differences in pre- and post-azithromycin gene expression in all upper and lower airway epithelial cells.

In the following figures the top ranked differentially regulated genes are shown – (A) Venn diagram and summary of shared and uniquely differentially upregulated genes in the lower (orange) and upper (blue) airways. Protein coding genes most differentially expressed and highly ranked by composite measure of average log2 fold change change, p value and proportion of cells are shown (by Seurat FindMarkers with MAST, using PID and cellular detection rate as latent variables); (B) Venn diagram and summary of shared and uniquely differentially downregulated genes in the lower (orange) and upper (blue) airways. Selected as described in (A); (C) Gene ontology (GO) term enrichment with upregulated genes from the lower airway; (D) GO term enrichment in upregulated genes from the upper airway; (E) GO term enrichment with downregulated genes from the lower airway; (F) GO term enrichment in downregulated genes from the upper airway

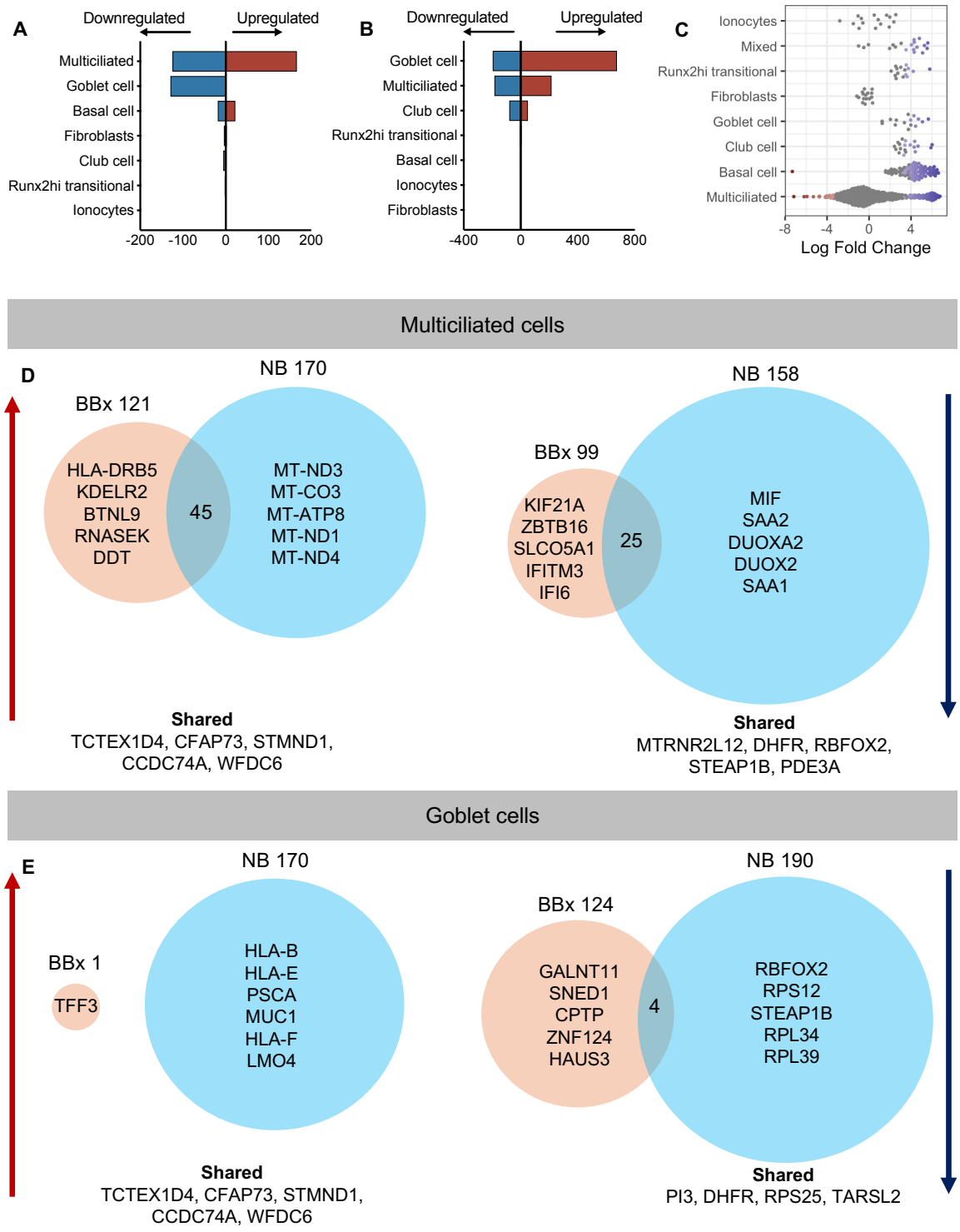


Figure 4.13 Differences pre- and post- azithromycin treatment in sub-populations of epithelial cells.

(A) Number of up- and downregulated genes by cell type in the lower airway; (B) Number of up- and downregulated genes by cell type in the upper airway; (C) Bee swarm plot of the distribution of log fold change pre- and post-azithromycin therapy in neighbourhoods containing cells from identified cell types. Each dot represents a neighbourhood and those with differential abundance at 10% FDR are coloured. Mixed neighbourhoods span clusters or cell type; In the following figures the top ranked

differentially regulated genes are shown – (D)Venn diagram and summary of shared and uniquely differentially upregulated genes in the lower – BBx (orange) and upper - NB (blue) airway multiciliated cells. Protein coding genes most differentially expressed and highly ranked by composite measure of average log2 fold change, p value and proportion of cells are shown (by Seurat FindMarkers with MAST, using PID and cellular detection rate as latent variables); (E) Venn diagram and summary of shared and uniquely differentially upregulated genes in the lower – BBx (orange) and upper - NB (blue) airway goblet cells. Genes included have been identified and selected as in (D)

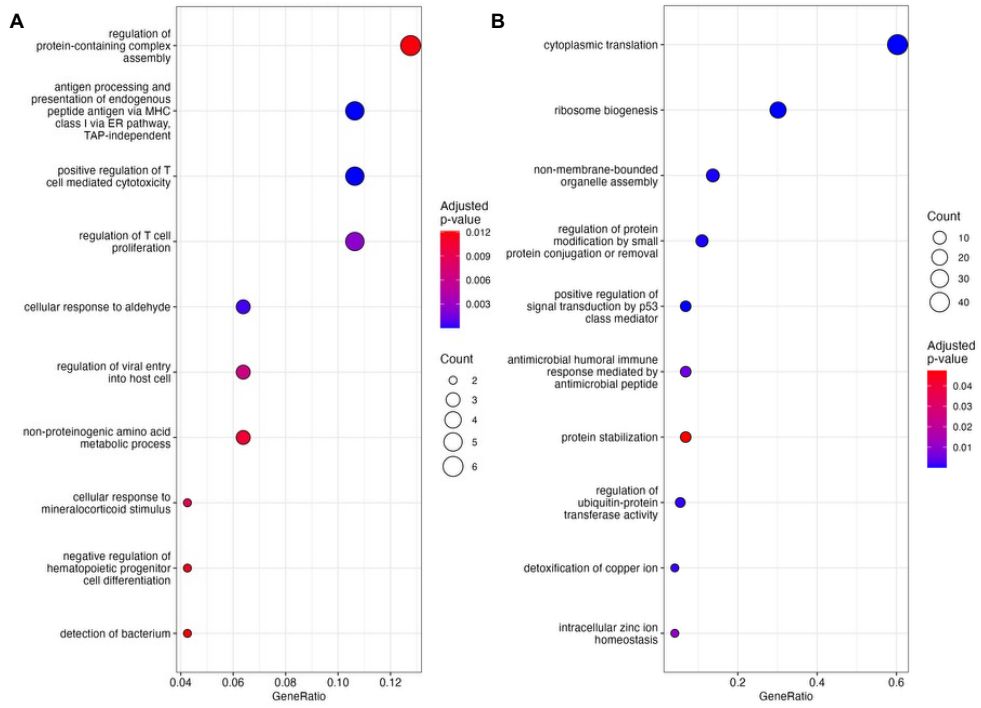


Figure 4.14 GO term enrichment in nasal club cells.

(A) with significantly upregulated genes; (B) with significantly downregulated genes

4.7.4 Transcriptomic changes in myeloid cells after azithromycin treatment

Within the myeloid lineage lower airway macrophages had the highest frequency of differentially regulated genes (120 up, 102 down), greater than cDC2 (12 up, 13 down) or pDC (1 down) cells, and neutrophils (1 up, 4 down), summarised in **Figure 4.15**. As shown in the volcano plot in **Figure 4.15** D, macrophages upregulated genes related to antigen presentation (*HLA-DRB5, HLA-DRB1, IFI30, CD74*). Galectin-3, involved in macrophage phagocytosis (Sano et al., 2003), was upregulated. Macrophages differentially regulated cathepsins (*CTS*), lysosomal proteases involved in intracellular protein degradation and immune response including inflammasome activation, with upregulation of *CTSB, CTSZ* and

CTSL and downregulation of *CTSS* (Yadati et al., 2020). Fatty acid binding protein 5 (*FABP5*) was upregulated. *FABP5* is involved in fatty acid uptake and its deficiency has been reported regulate macrophage phenotype and drive inflammation in murine allergic airways inflammation (Hou et al., 2022). Myeloid associated inflammatory proteins implicated in asthma, *S100A8, S100A9* and *S100A12* (Kang et al., 2015), were downregulated as was lysozyme (*LYZ*) and versican (*VCAN*) (Wight et al., 2020) – all markers of macrophage activation. The type I interferon stimulated *ISG15* was also downregulated. This is consistent with enrichment of GO terms of chemotaxis, cell adhesion, antigen processing and presentation, with reduced activation and anti-bacterial responsiveness. Differential abundance testing with miloR showed an expansion in macrophage neighbourhood size.

Similarly to macrophages, cDC2 cells upregulated *HLA-DRB5* and *IFI30*, but downregulated *HLA-DQB1*. Annexin A2 (*ANXA2*) which plays a role in phagocytosis/endocytosis (Gerke and Moss, 2002) was also upregulated.

In the upper airway there were limited differential gene expression findings, both in terms of numbers of genes and magnitude of change.

Taken together, within the myeloid lineage, azithromycin appeared to have the greatest effect on lower airway macrophages with a gene expression profile suggesting a less inflammatory phenotype. Whilst neutrophils were numerically reduced in the airway, as shown in BAL, they did not demonstrate significant detectable transcriptional change in this analysis. However, given the importance of myeloid cells in defence against bacterial pathogens and impaired neutrophil and macrophage function in the presence of NTHi, a further analysis was performed comparing patients with or without airways infection.

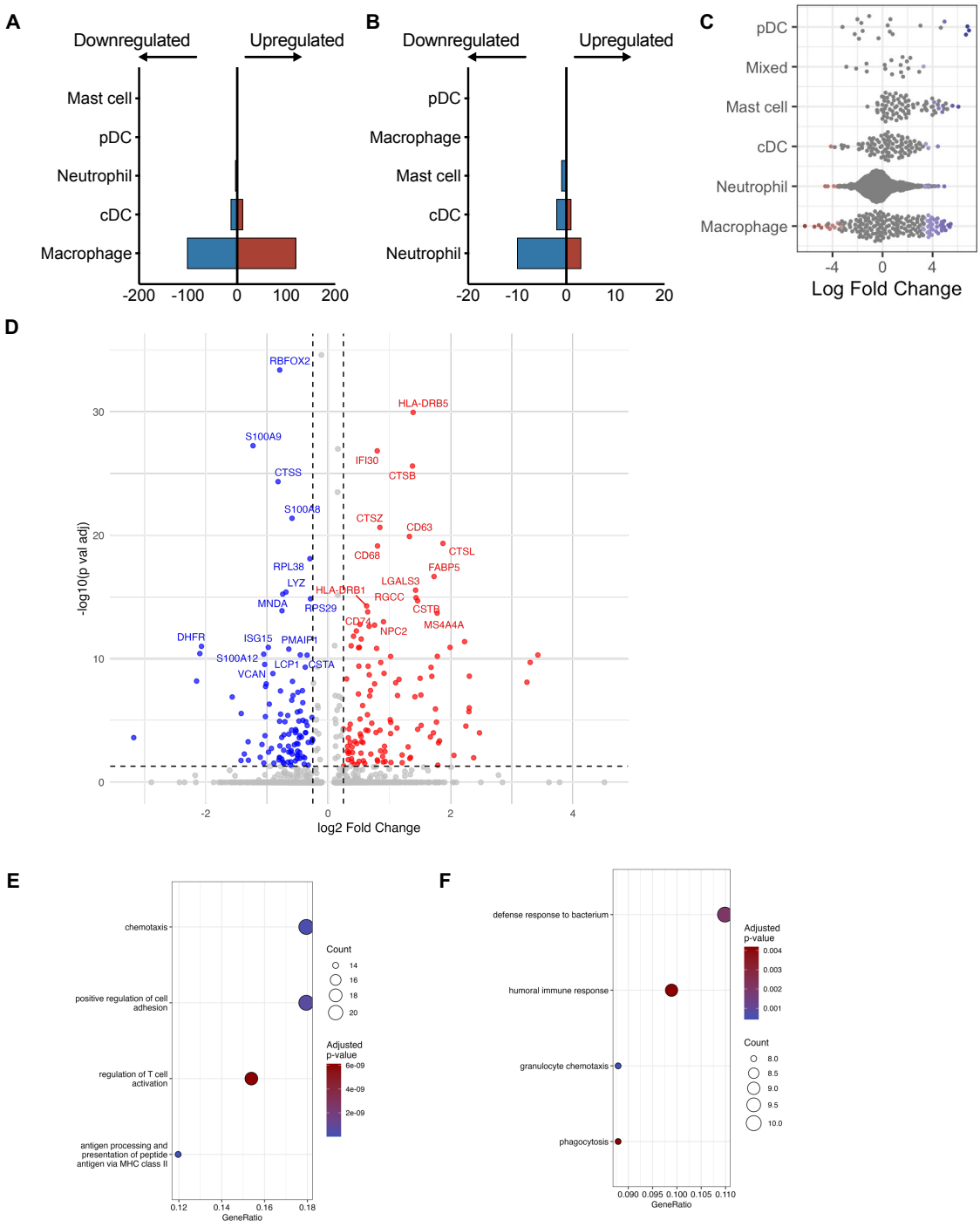


Figure 4.15 Differences in pre- and post- azithromycin treatment in myeloid cell populations.

(A) Number of up- and downregulated genes by cell type in the lower airway; (B) Number of up- and downregulated genes by cell type in the upper airway; (C) Bee swarm plot of the distribution of log fold change pre- and post-azithromycin therapy in neighbourhoods containing cells from identified cell types. Each dot represents a neighbourhood and those with differential abundance at 10% FDR are coloured. Mixed neighbourhoods span clusters or cell type; (D)Volcano plot depicting differentially expressed genes in macrophages post azithromycin treatment. Protein coding genes most differentially expressed and ranked by composite measure of avglog2fold change, p value and proportion of cells (by Seurat FindMarkers with MAST, using PID and cellular detection rate as latent variables) have been labelled; GO term enrichment performed with (E) significantly upregulated genes and (F) with significantly downregulated genes

4.7.5 Transcriptomic changes in lymphoid cells after azithromycin treatment

In the lymphoid lineage there were more differentially regulated genes in in the lower airway (237 up, 233 down), than in the upper airway (124 up, 68 down). Gene set enrichment analysis (GSEA) in the combined T cell population showed a significant enrichment in oxidative phosphorylation and hypoxia signalling pathways in the lower airway as shown in **Figure 4.16** A-B. Leading edge genes are summarised in **Figure 4.16** C. No significant gene set enrichment was found in the upper airway. GO over representation analysis is shown in **Figure 4.16** D-G. Consistent with the GSEA results, pathways enriched in upregulated genes in the lung were related to metabolism and regulation of T cell activation, whilst intracellular signalling pathways were enriched in downregulated genes. Upper airway over-representation analysis showed a similar pattern of broad T cell regulation.

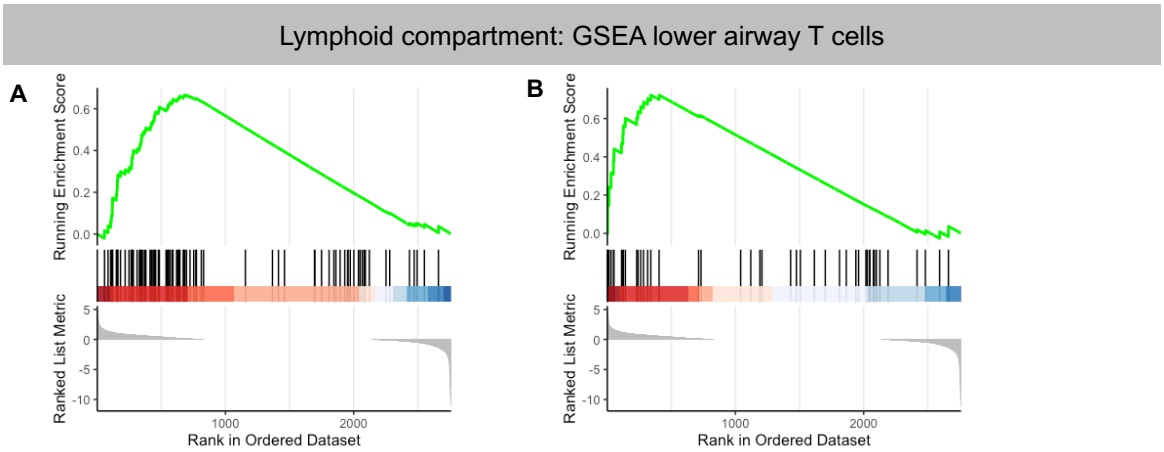
In both airway compartments CD8 TRM cells were most transcriptionally altered (lower airway 128 genes up/78 genes down, upper airway 55 genes up/53 genes down) (**Figure 4.17** A-B). In lower airway CD8 TRM cells, the differential gene expression pattern appeared suggestive of a metabolic shift and cellular quiescence with upregulation of BTG1, involved in mRNA deadenylation and decay (Hwang et al., 2020), and DNA-damage-inducible transcript 4 (*DDIT4*), a mammalian target of rapamycin (*mTORC*) inhibitor (Zhang et al., 2018). In inflammatory settings phosphoinositide 3-kinase (*PI3K*)-Akt-mTOR signalling is activated by cytokines, enhances glycolysis, and mTOR drivenTh17 differentiation (Shi et al., 2025). *TSC22D4*, which was upregulated in both the upper and lower airway can also interact with Akt to regulate glycolysis (Demir et al., 2022). Consistent with this ribosomal gene and *LDHA* expression was downregulated, alongside dihydrofolate reductase (*DHFR*). The GTP-ase *RAC1* was a further shared upregulated gene and is involved in early development of T cells (Dumont et al., 2009). Lung CD8 T cells increased *ISG20* expression whereas nasal CD8 T

cells increased expression of *TNF*, the integrin *ITGB2* and T cell inhibitor cytokine-inducible SH2-containing protein (*CISH2*) (Jin et al., 2023).

Other TRM cells expressed a differential gene expression profile very similar to described above but together with CCL4hi cells increased expression of *AREG*. CCL4hi cells additionally upregulated *CXCR4*. The *EGR1* high population had increased expression of the activation protein (AP)-1 complex transcription factors *JUN* and *FOS*, involved in effector differentiation (Schnoegl et al., 2023). The overlap between downregulated genes in the prominent CD8 T cell subsets is shown in **Figure 4.17**. There was reduction in ribosomal gene expression across all cell types. EGR1hi cells down regulated the chemokine *CCL5/RANTES*. Other cell types of the lower airway showed minimal differential gene expression changes, mostly related to downregulation of ribosomal genes and *DHFR*.

In the upper airway both Th17 cells and MAIT cells upregulated expression of *FOS*, *FOSB*, *JUN* and *JUNB*, all part of the AP-1 family (Schnoegl et al., 2023).

Taken together, this analysis suggested that T cells undergo metabolic changes consistent with reduced activation and perhaps a shift towards quiescent state.



C

	Pathway	NES	P value adj	Leading edge genes
A	Hallmark Oxidative Phosphorylation	1.74	0.002	TCIRG1, SLC25A6, TOMM22, UQCRFS1, MDH2, POR, MRPL34, GPX4, PHB2, CYC1, IDH3B, NDUFV2, NDUFS7, ATP6V0B, ATP6V1F
B	Hallmark Hypoxia	1.64	0.020	SAP30, DDIT4, ISG20, BTG1, ZFP36, PRDX5, KLF6, CXCR4, PFKFB3, ANXA2, TNFAIP3, PNRC1, TPI1, UGP2, RBPJ

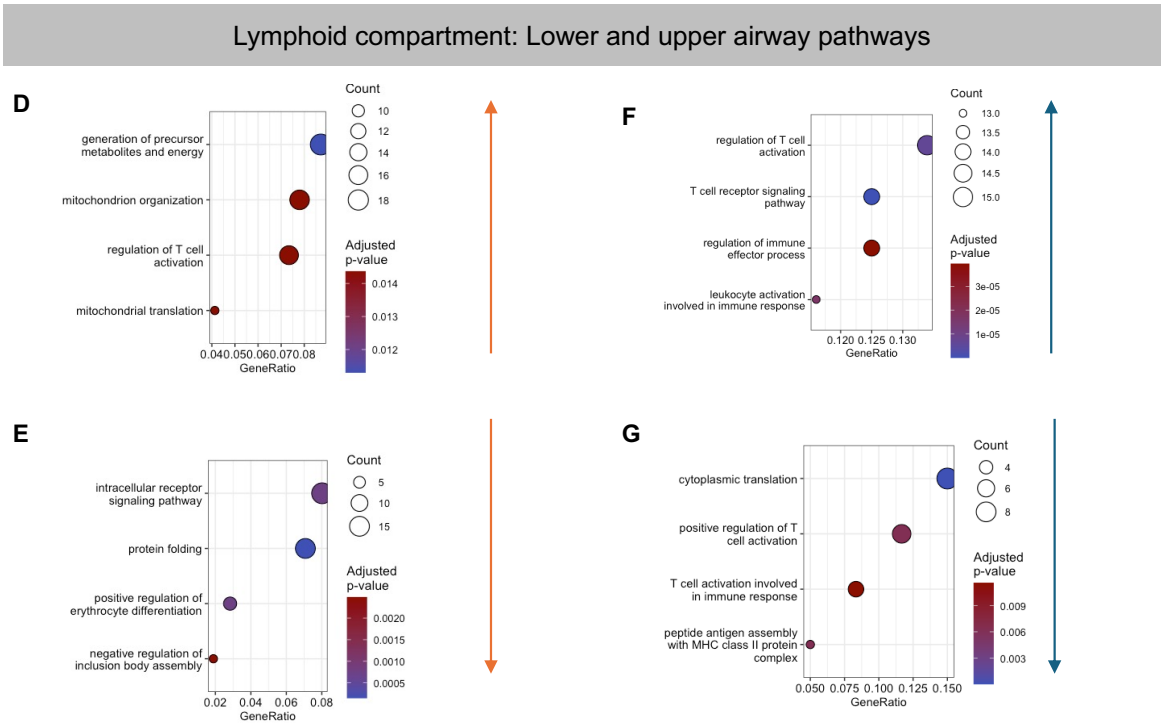


Figure 4.16 Differences pre- and post- azithromycin across all lower and upper airway T cells;

Gene set enrichment analysis performed for all T cells after azithromycin treatment using the MSigDB hallmark collection, avglog2FC-log10(adj p value) served as the rank statistic, Enrichment plots shown for (A)Oxidative phosphorylation and (B) Hypoxia; (C) Summary table of significantly enriched pathways, showing NES, adjusted p value (FDR < 0.05) and top leading edge genes; (D) GO term enrichment with upregulated genes from the lower airway; (E) GO term enrichment with downregulated genes from the lower airway; (F) GO term enrichment with upregulated genes from the upper airway; (G) GO term enrichment with downregulated genes from the upper airway*

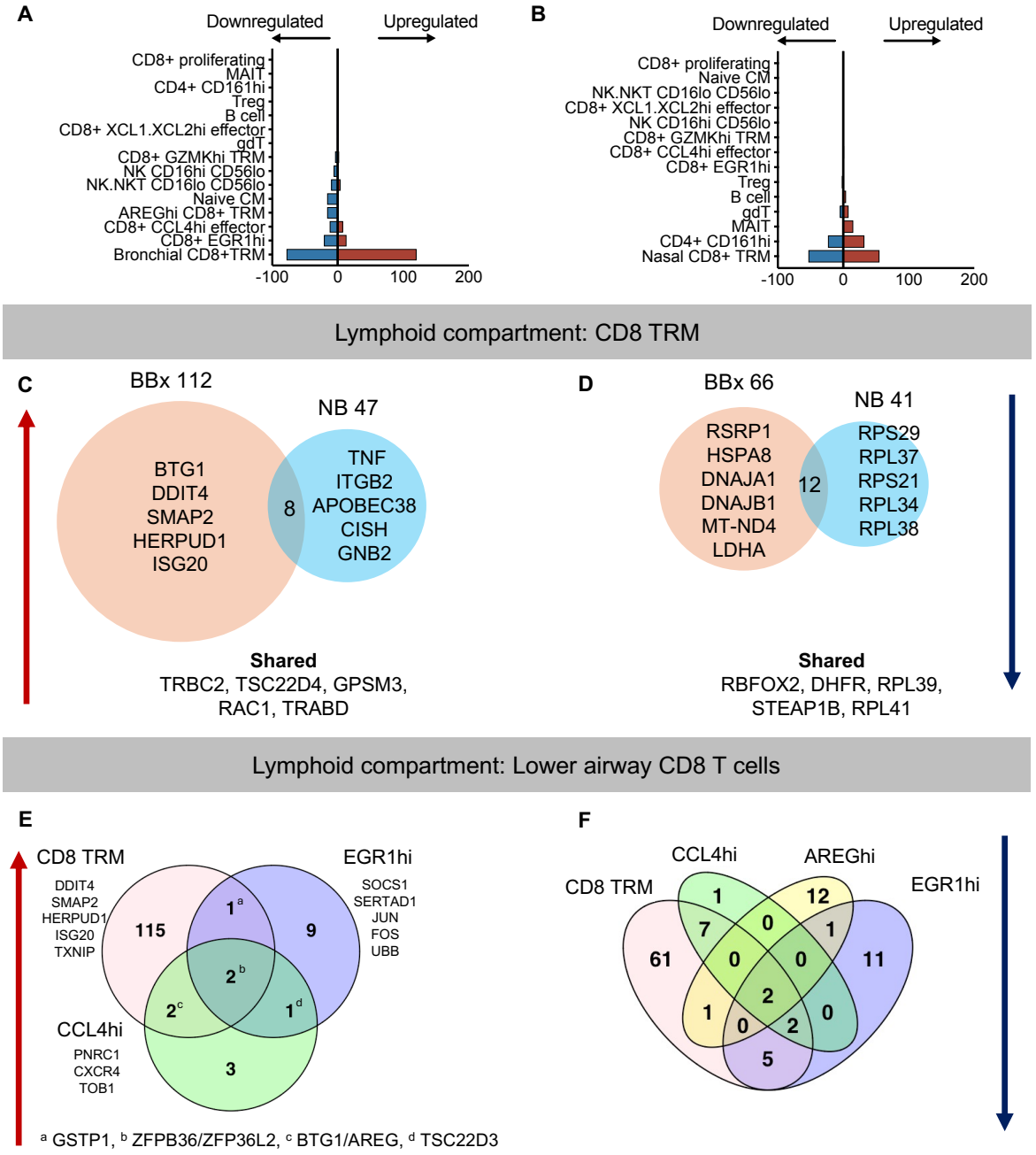


Figure 4.17 Differences pre- and post-azithromycin in lymphoid cell subsets.

(A) Number of up- and downregulated genes by cell type in the lower airway; (B) Number of up- and downregulated genes by cell type in the upper airway; In the following figure the top ranked differentially expressed genes are shown – (C) Venn diagram and summary of shared and uniquely differentially upregulated genes in the lower – BBx (orange) and upper - NB (blue) airway CD8 TRM cells. Protein coding genes most differentially expressed and highly ranked by composite measure of avglog2fold change, p value and proportion of cells are shown (by Seurat FindMarkers with MAST, using PID and cellular detection rate as latent variables); (E) Venn diagram and summary of shared and uniquely differentially upregulated genes in the lower airway CD8 TRM/EGR1hi/CCL4hi cells; (F) Venn diagram and summary of shared and uniquely differentially downregulated genes in the lower airway CD8 TRM/EGR1hi/CCL4hi/AREGhi cells

4.7.6 Airway infection status and azithromycin activity

Within the AMASS cohort 50% of patients had a positive BAL culture at baseline. *H. influenzae* was isolated in the majority of these individuals (n=4/5). Azithromycin is known to reduce *H. influenzae* airway load and neutrophil NETs but is also beneficial in the absence of a positive culture or airway neutrophilia. The non-antimicrobial, immune mechanisms underlying the clinical benefit have not been previously reported from an interventional treatment study. To decipher shared and unique transcriptomic changes, the cohort was stratified by BAL culture result (infected or uninfected) and differential gene expression analysis performed in the most biologically relevant lower airway cells following azithromycin therapy. This analysis was thus performed on lung multiciliated cells, goblet cells, macrophages, neutrophils and combined lung CD8+ T cells. Broader cell classifications were used to increase power for detection of differentially expressed genes. The results of differential gene expression analyses have been combined to show shared genes across these two groups, to allude to the broader effects of azithromycin therapy independent of infection status. Results discuss the top ranked genes (results ranked in Seurat FindMarkers with MAST, ranked on composite measure of average log2 fold change, adjusted p value and number of cells expressing the gene in the cell of interest after treatment [pct1]). Tables of DGE results are provided in Appendix 3.

4.7.6.1 Neutrophils

Taking this approach neutrophils (**Figure 4.18**) were found to differentially regulate a broad range of inflammatory genes and those with potential for immune modulation after azithromycin treatment. Shared upregulated genes included *IFI30* (involved in antigen presentation), 5-lipoxygenase-activating protein (*ALOXAP*), *CEBPD* (transcription factor of terminal granulocyte differentiation) (Lekstrom-Himes, 2001), chemokine receptor *CXCR4*, the pattern recognition receptor *TLR2* and chemokines *CLEC4E, CCL4L2* and *CXCL16*. The high affinity IgE receptor (*FCER1G*) was upregulated. Its expression on neutrophils has been shown in atopic asthma and delays neutrophil apoptosis *in vitro* culture (Saffar et al., 2007).

IRAK3 (Freihat et al., 2019) which negatively regulates TLR signalling, and glucocorticoid inducible regulator of MAPK, dual specificity phosphatase-1 (*DUSP1*) both showed increased expression (Hoppstadter and Ammit, 2019). The glucocorticoid-induced leucine zipper (GILZ) (*TSC22D3*) was upregulated, this corticosteroid inducible gene can repress downstream NFκB signalling and its induction is suppressed in severe asthma (Uehara et al., 2025) and can arise concurrently with TLR2 expression in response to budesonide (Mostafa et al., 2019). The peptidase inhibitor PI3 and anti-protease TIMP1 were also upregulated. Interestingly the circadian clock gene PER1 (Mostafa et al., 2019) had a high fold-change in both groups. Downregulated genes included the Rac GTP-ase activating protein *ARHGAP15* (negative regulator of neutrophils) (Costa et al., 2011), inflammatory protein *S100A12* and Cox-2 (*PTGS2*). In the absence of infection upregulated genes included the interferon stimulated gene *IFITM3* alongside formyl peptide receptor 1 (*FPR-1*) involved in chemotaxis (Leslie et al., 2020) and triggering receptor expressed on myeloid cells-1 (*TREM-1*) (Carrasco et al., 2019) and *HLA-C*. In the presence of a positive culture pre-azithromycin, expression of the NFκB inhibitors *NFKBIA* (Castro-Alcaraz et al., 2002) and *TNFAIP3* (Ma and Malynn, 2012) were increased, alongside the chemokine *CXCL8*, transcription factor *KLF6* required for maturation (Khoyratty et al., 2021), complement factor D and anti-oxidant superoxide dismutase-2 (*SOD2*) (Kapellos et al., 2023). Although CXCL8 levels are still elevated suggesting ongoing neutrophil recruitment, in BAL there was a reduction in neutrophils and there appear to be multiple counterbalancing effects at play. Furthermore, CXCL8 levels may reduce at a later time point. Azithromycin therapy was associated with reduced expression of pro-inflammatory neutrophil genes in absence of infection (I*L1B, NFKIBZ, NFKBIA, BCL2A1*) (Kapellos et al., 2023; Vier et al., 2016), and in presence of infection (*S100A8, S100A9, S100A12, FCGR3B, MNDA*).

These results suggest shared mechanisms of immune modulation in airways neutrophils in asthma following azithromycin therapy independent of presence of an airway pathogen, with differential retention of pro-inflammatory functionality.

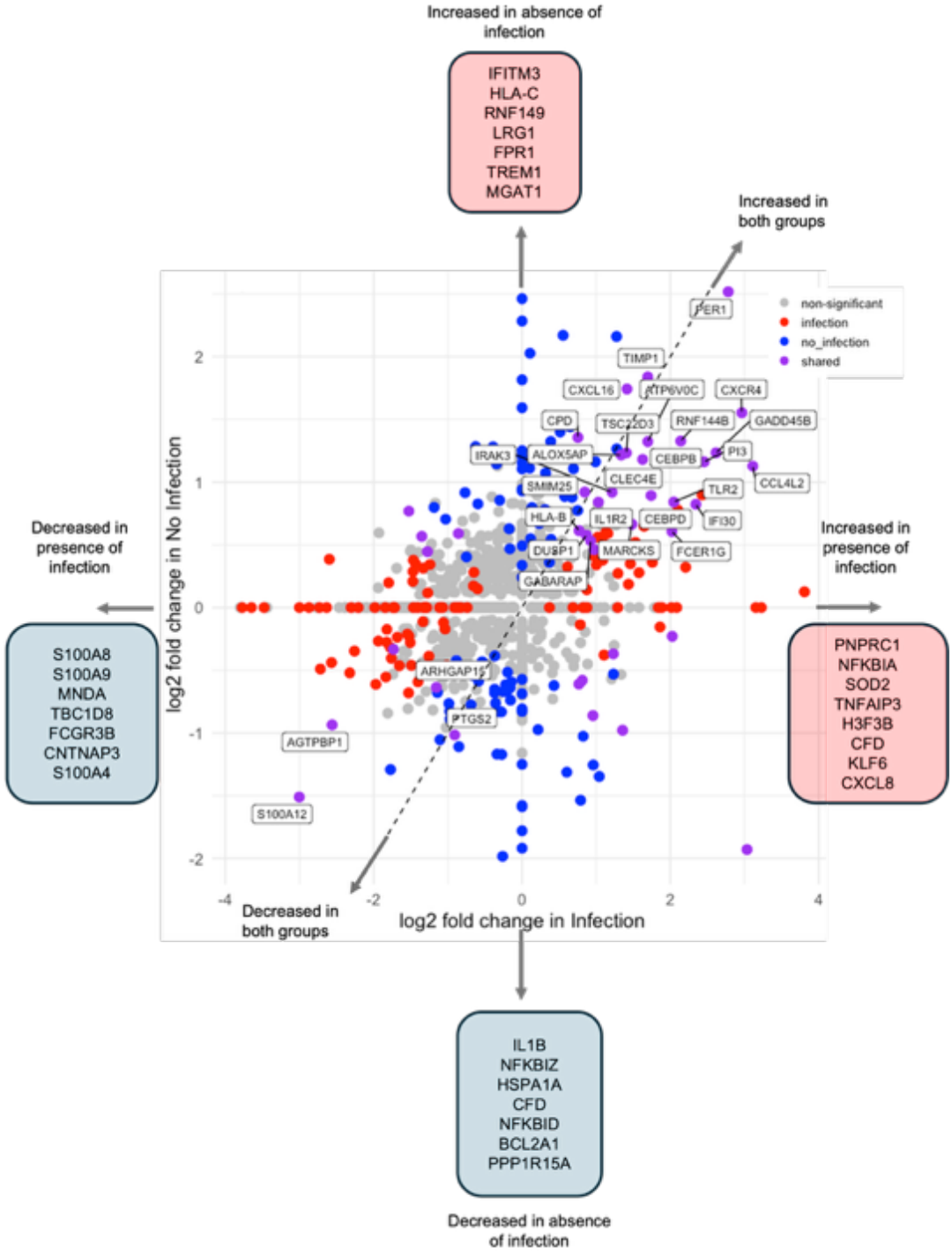


Figure 4.18 Differences in gene expression in neutrophils seen post-azithromycin treatment between groups with or without detection of a pathogen on BAL culture;

Differential expression comparing pre- and post- azithromycin treatment effects in groups with or without airways infection, using MAST. Log 2 fold change values are plotted and coloured by significance and presence infection group (red), non-infection group (blue) or shared (purple). Figure is also annotated with uniquely up/downregulated genes by group. Annotated genes were top ranked by composite measure of avglog2fold change, p value and proportion of cells expressing the gene

4.7.6.2 Macrophages

Within macrophages (**Figure 4.19**), shared upregulated genes independent of culture result included genes found to be differentially regulated in the earlier macrophage analyses, namely *CD63, CD74, CTSB, CTSL, LGALS3, MS4A4A* and *NPC2*. In addition, an increase in expression was seen in serine dehydratase (*SDS*) which is involved in gluconeogenesis, *IL7R, CTSz, CD59* (immunomodulatory, providing protection from membrane attack complex) (Couves et al., 2023), *MMP-19* which can be involved in homeostatic tissue remodelling and anti-protease *TIMP1*. In this analysis shared downregulated genes included *S100A9, S100A12, MNDA, DHFR, LCP1* and *VCAN*, identified earlier in the combined macrophage differential expression analysis. In addition, expression of the pore forming protein macrophage-expressed gene 1 (*MPEG1*) which is induced by *LPS* and *TNFα* (Bayly-Jones et al., 2020) was reduced, as was P21-activated kinases 1 (*PAK1*) (involved in pro-inflammatory polarisation) (Chang et al., 2020), transketolase/*TKT* (involved in pentose phosphate pathway) and *BRAF* (involved in MAPK signalling).

In absence of an airway pathogen macrophages upregulated *AREG*, expression of which was also upregulated within a population of CD8 T cells. Mesenchymal stem cells have been shown to induce macrophage *AREG* production and macrophage derived *AREG* to expand Tregs and sustain epithelial stem cells *in vitro* suggesting a role for it in tissue regeneration (Ko et al., 2020). The expression of sialic acid-binding immunoglobulin-like lectins (Siglec)-10, encoding an inhibitory receptor in macrophages was upregulated(Kukan et al., 2024), as was V-set immunoglobulin-domain-containing 4 (*VSIG4*) which limits macrophage effector functions by activating the PI3K/Akt–STAT3 pathway (Li et al., 2017). Other relevant upregulated genes included TNIP3, a negative regulator of NFκB signalling (Wullaert et al., 2007), and *BATF*, an *AP-1* transcription factor. *BATF* levels have been reported to be elevated in PBMCs from children with steroid naive asthma (Ubel et al., 2014) and in adult neutrophilic asthma (Liu et al., 2025). In the presence of a positive culture, genes identified in the earlier

analyses related to antigen presentation (*HLA-DRB5, IFI30, HLA-DRB1*) were upregulated with *CSTB* and *CD68* (involved in phagocytosis). Down regulated genes included pro-inflammatory mediators – in presence of infection these were *LYZ, S100A4* and *S100A8* and in the absence of infection this included *CXCL8, TNF*, *IL1B* and *PTGS2/COX-2.*

Thus, macrophages appear transcriptionally altered following azithromycin treatment both in the presence or absence of an airway pathogen, notably with a reduction also seen in prototypic inflammatory cytokines in absence of positive culture. Broadly other potentially immunomodulatory mechanisms were shared.

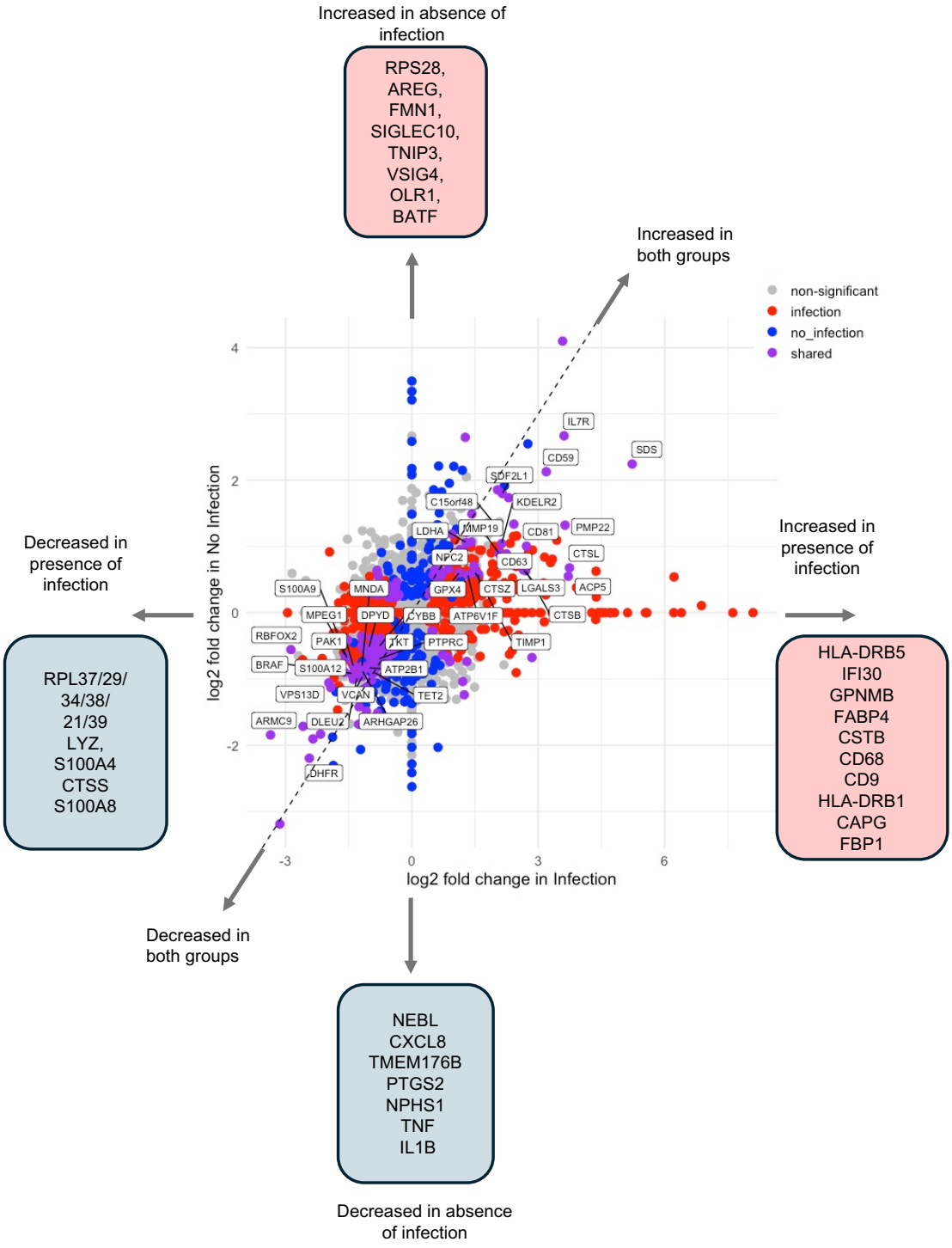


Figure 4.19 Differences in gene expression in macrophages seen post-azithromycin treatment between groups with or without detection of a pathogen on BAL culture;

Differential expression comparing pre- and post- azithromycin treatment effects in groups with or without airways infection, using MAST. Log 2 fold change values are plotted and coloured by significance and presence infection group (red), non-infection group (blue) or shared (purple). Figure is also annotated with uniquely up/downregulated genes by group. Annotated genes were protein coding, top ranked by composite measure of avglog2fold change, p value and proportion of cells expressing the gene

4.7.6.3 CD8 T cells

The comparative analysis of CD8 T cells (**Figure 4.20**) between culture positive and negative individuals was reflective of earlier T cell analyses, with increased expression of genes such as *AREG,* and *DDIT4* in both groups alongside the transcription factor *CEBPD*. *DHFR* expression was also seen to reduce alongside HSPs. In the absence of airways infection upregulated genes were linked the cell cycle (*ID2,* cyclin *D/CCND3*) and antioxidant/redox state (*TXNIP, MT2A, MT1E*), with downregulation of predominantly ribosomal genes. In the presence of infection there appeared to be regulations of genes more directly involved in immune activation (*IFNGR1, NFKB1A*) and modulation (*IL7R, FOS*).

4.7.6.4 Epithelial and goblet cells

In multiciliated epithelial cells (**Figure 4.21**), shared upregulated genes could be broadly considered as those related to a number of key functions including immune interaction with increased expression of *HLA-DR5, CTXN1* and *BTNL9*, involved in T cell co-stimulation (Melandri et al., 2018), and cellular signalling (*PTPMT1, TCTEX1D4, KDELR2*, *CABCOCO1*). Shared downregulated genes included those linked to cell cycling and signalling (*PDE3A, RRPML, DHFR*), transcriptional regulation (*RBFOX2, NFE2L3, GLI3*) and mitochondrial function. In presence of infection there was upregulation of *HLA-DQB1* with downregulation of ribosomal genes and mucin related *TFF3*. In the absence of differentially regulated genes appeared to have broad general functions in translation and metabolism. A number of sex related genes (RPS4Y1, DDX3Y, EIF1AY, USP9Y) have not been included in Figure 4.21, as these are largely non-functional and most likely represent an imbalance in cell numbers across sex in this analysis rather than a biologically relevant process.

Interestingly goblet cells (**Figure 4.22**) had the greatest frequency of downregulated genes in the absence of infection. These were not specific to mucus secretion and in fact the mucus

associated peptides *TFF3* and *WFCD2* (Bingle et al., 2006), which may have a role in innate host defence, showed increased expression after treatment in this group.

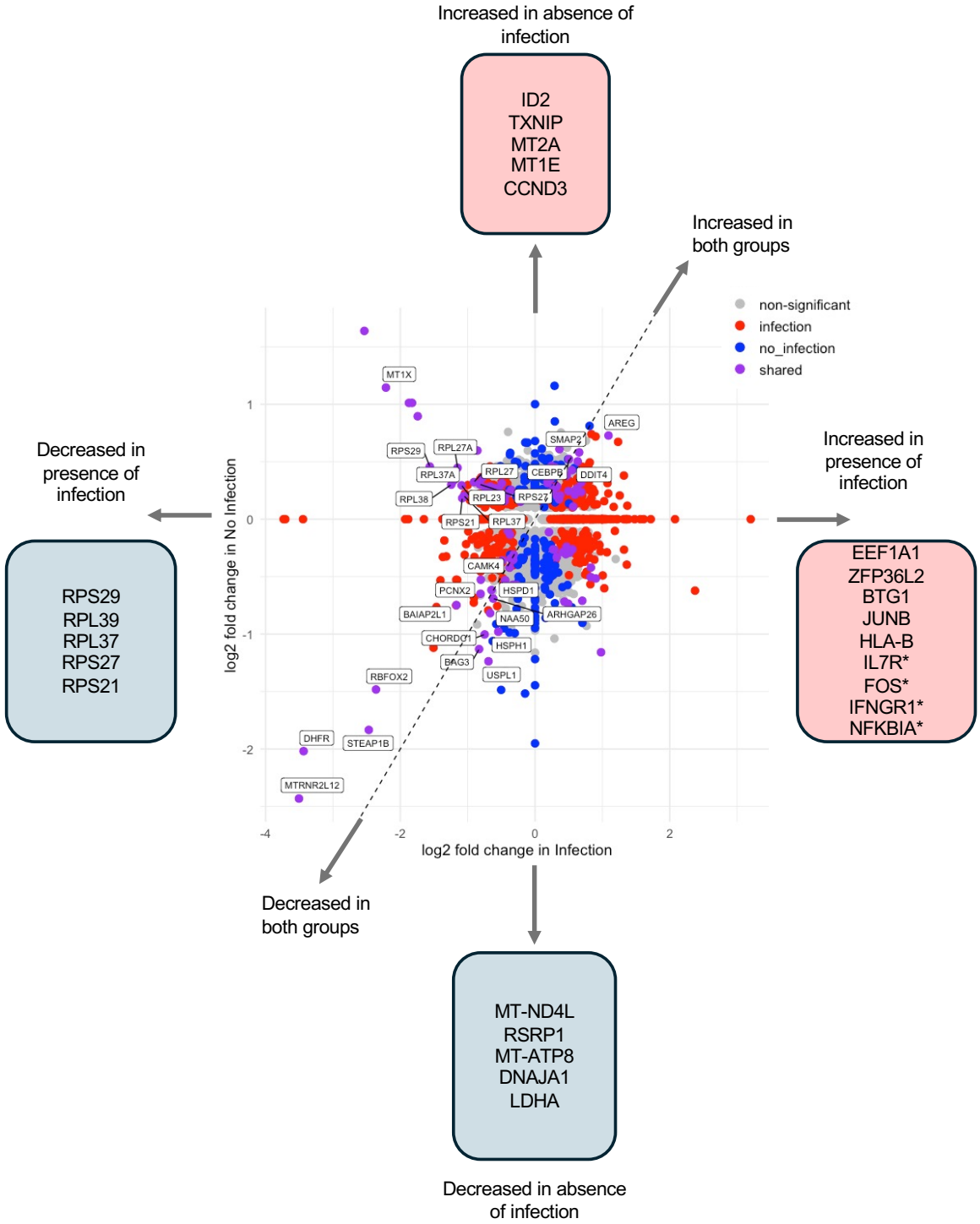


Figure 4.20 Differences in gene expression in CD8 T cells seen post-azithromycin treatment between groups with or without detection of a pathogen on BAL culture;

Differential expression comparing pre- and post- azithromycin treatment effects in groups with or without airways infection, using MAST. Log 2 fold change values are plotted and coloured by significance and presence infection group (red), non-infection group (blue) or shared (purple). Figure is also annotated with uniquely up/downregulated genes by group. Annotated genes were protein coding, top ranked by composite measure of avglog2fold change, p value and proportion of cells expressing the gene, (*) indicate lower ranked but still significant genes that are biologically relevant in context of infection

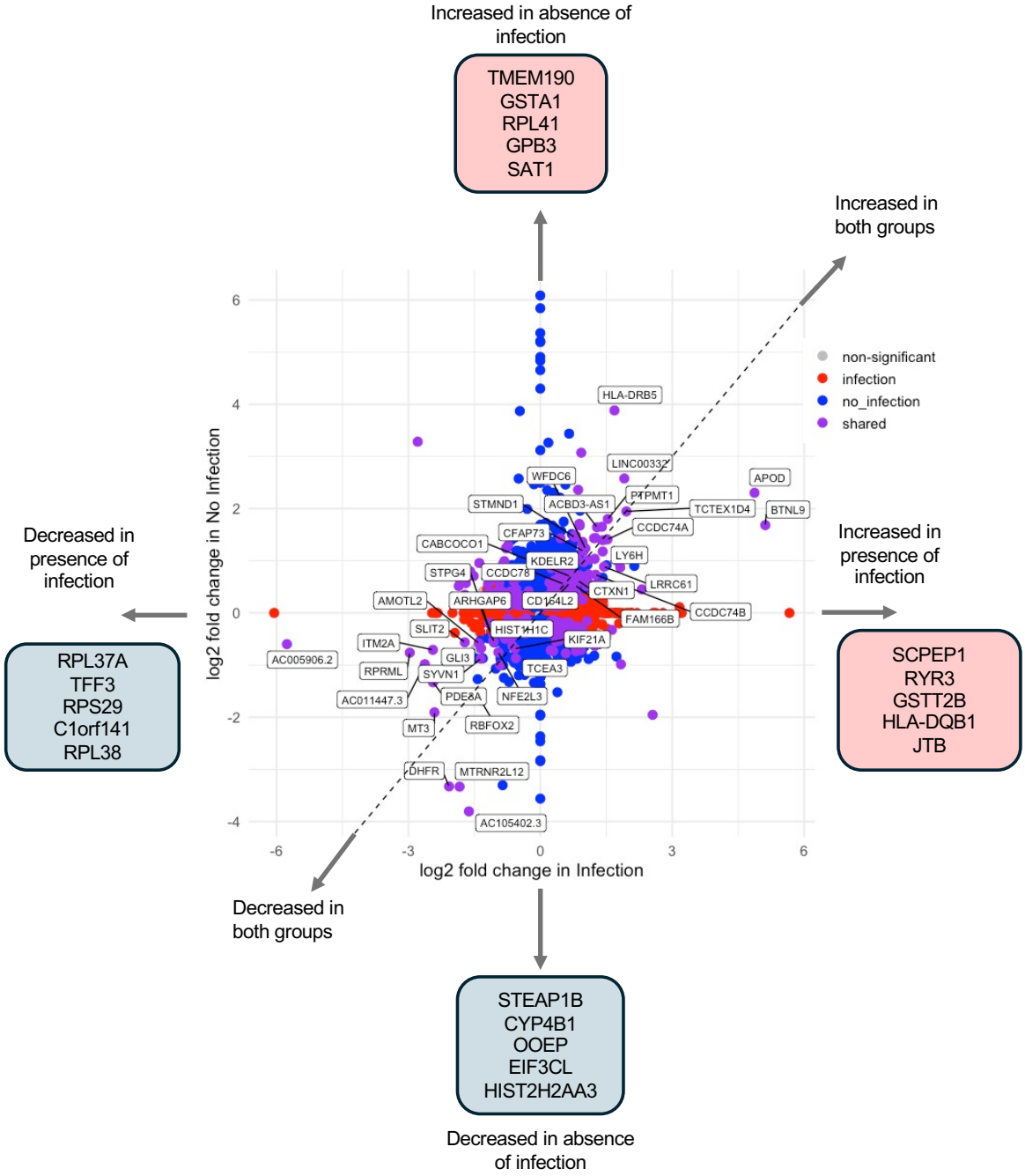


Figure 4.21 Differences in gene expression in multiciliated cells seen post-azithromycin treatment between groups with or without detection of a pathogen on BAL culture;

Differential expression comparing pre- and post- azithromycin treatment effects in groups with or without airways infection, using MAST. Log 2 fold change values are plotted and coloured by significance and presence infection group (red), non-infection group (blue) or shared (purple). Figure is also annotated with uniquely up/downregulated genes by group. Annotated genes were protein coding, top ranked by composite measure of avglog2fold change, p value and proportion of cells expressing the gene

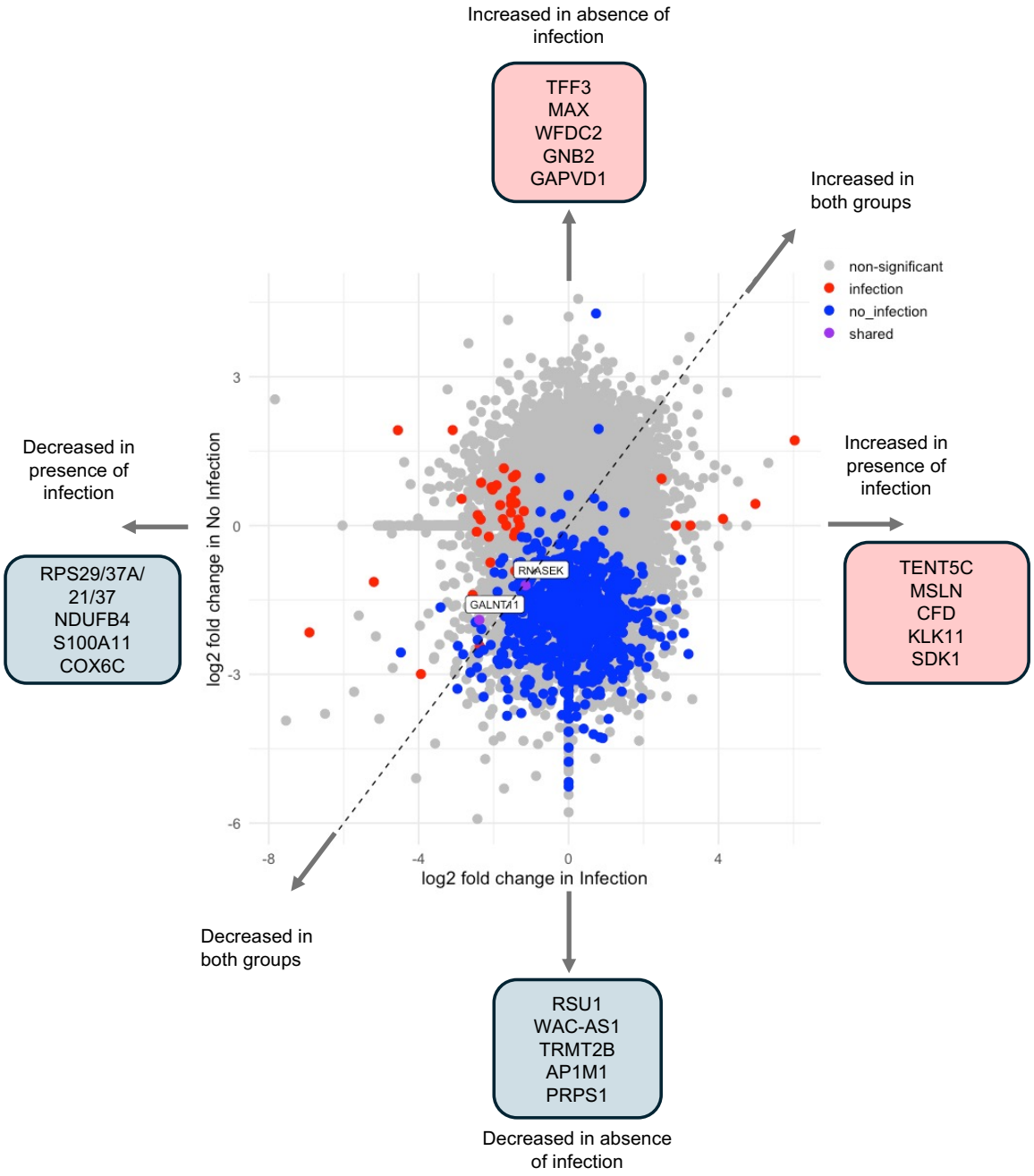


Figure 4.22 Differences in gene expression in goblet seen post-azithromycin treatment between groups with or without detection of a pathogen on BAL culture;

Differential expression comparing pre- and post- azithromycin treatment effects in groups with or without airways infection, using MAST. Log 2 fold change values are plotted and coloured by significance and presence infection group (red), non-infection group (blue) or shared (purple). Figure is also annotated with uniquely up/downregulated genes by group. Annotated genes were protein coding, top ranked by composite measure of avglog2fold change, p value and proportion of cells expressing the gene

4.8 Discussion

In the AMASS study 10 patients with treatment refractory moderate to severe asthma underwent upper and lower airway sampling before and 4 months after long term, low dose azithromycin therapy. A single cell sequencing approach was selected as knowledge of differential response to therapy by cell type have implications for mechanistic understanding and potential future therapeutic design. The aim was to characterise azithromycin mechanisms in a human interventional study rather than clinical response, but even in this small cohort of patients an improvement in lung function (FEV1 and FVC) and ACQ-5 symptom score could be appreciated, and was consistent with the AMAZES clinical trial (Gibson et al., 2017). Azithromycin has greatest efficacy in patients with a high airway load of *H. influenzae* when measured by PCR (Taylor et al., 2019). Whilst a positive culture was not a selection criterion for this study, at the time of the first bronchoscopy 50% of patients were found to have a positive BAL culture. *H. influenzae* was isolated in most of these cases (n=4/5). This prevalence is higher than seen in cross-sectional metagenomic studies reported in this thesis (~20-30%) but is likely a reflection of a higher incidence of neutrophilic asthma and carriage of potentially pathogenic organisms in those participants with treatment refractory disease despite observed adherence to therapy exceeding 80%. After 4 months of azithromycin treatment, patients either had no organisms detected on BAL culture or a marked reduction in CFU load which fell below the threshold of clinical significance (10^4 CFU/ml) demonstrating a known antibacterial effect.

Azithromycin reduces airway neutrophilia, CXCL8 levels and NET load in chronic respiratory diseases (Brown et al., 2022; Keir et al., 2021). In the AMASS cohort a significant reduction in BAL neutrophil count was observed after azithromycin treatment with a trend towards reduction in BAL NETs, CXCL8 and IL-1β level, with lack of significance likely due to limited statistical power in this relatively small cohort.

To characterise the effect of azithromycin on immune and non-immune cell populations in the lung a single cell sequencing approach was taken. The microbiome of the nasopharynx and lung are distinct, thus providing different cues to shape mucosal immunity at these sites. Moreover, NTHi is a commensal of the upper airway and an opportunistic pathogen in the lower airway. It was thus hypothesised that the upper and lower airway immune compartments would show unique features and likely respond to azithromycin differently. Using a paired sampling approach from each patient before and after treatment allowed this comparison to be made. Epithelial, myeloid and lymphoid populations were found to cluster distinctly by site of origin. These were compositionally broadly similar, however some differences were identified which could be explained by expected anatomical differences (low frequency of macrophages in the nose) or represent variable capture due to sampling differences (greater proportion of secretory cells captured with nasal brush *vs.* endobronchial biopsy). Epithelial and myeloid sub-populations were more comparable across compartments.

In the lymphoid lineage a segregation by site was seen with a greater frequency of CD8 effector phenotypes and innate lymphoid populations captured from the lung. In contrast the majority of innate like T cells (MAIT and γδT cells) and Th17 cells arose from nasal brushing. A high frequency of CD8+ TRM cells (Hinks et al., 2019; Snyder and Farber, 2019) were identified within lung and nasal tissue. These cells had a cytotoxic T (Tc1) phenotype, with IFNγ and TNF expression and no type 2 transcription factor or cytokine expression. In asthma, these CD8+ cell have been shown to be relatively insensitive to corticosteroids compared to CD4+ T cells (Chung et al., 2014a; Li et al., 2007). Despite the context of lower airways infection within this cohort, type-17 cells were not identified in the lung, with only a small population of Th17 (*RORC, IL23R, CCR6* expressing) cells identified in the upper airway. Following azithromycin treatment, the greatest transcriptional changes were seen in CD8 TRM cells, with some differential gene regulation within discrete populations displaying a more activated phenotype (*CCL4hi, EGR1hi*). A population of CD8+ TRM cells were found to express high levels of *AREG* alongside a small NK/ILC population. Furthermore, CCL4hi and

CD8 TRMs broadly appeared to increase expression of *AREG* post azithromycin. *AREG* is a ligand for the epidermal growth factor receptor, involved in tissue repair, remodelling and inflammation. Its levels are elevated in sputum with increased expression in airway epithelium, dendritic cells, ILCs, mast cells, neutrophils and basophils, with further induction in the epithelium by rhinovirus infection which can result in airway remodelling (Manzo et al., 2012). *AREG* can also promote smooth muscle hyperplasia via a bradykinin induced *COX-2* dependent process (Deacon and Knox, 2015). *AREG* expressing CD8 T cells have been shown *in vitro* to support tissue repair (Delacher et al., 2024). It has a protective role in helminth expulsion and tissue recovery (Zaiss et al., 2006), tissue repair following *in vivo* influenzae lung infections (Monticelli et al., 2011) and viral (influenza) and bacterial co-infection within murine models (Jamieson et al., 2013). The *AREG* signature seen in this dataset could thus represent higher baseline expression in asthma, with further induction following changes in the microenvironment, such as clearance of bacterial organisms and wider azithromycin effects given its expression was increased in macrophages as well.

Azithromycin had been reported to have wide ranging effects on the epithelium and secretory cells. Whilst there was no clear evidence of enhanced tight junction expression in this dataset, as reported *in vitro*, epithelial cell expression of genes involved in cilia turnover was suppressed with greater expression of genes involved in motility. The basal cell population appeared to expand following azithromycin treatment. Cilial dysfunction occurs in type 2 high severe eosinophilic asthma, particularly in those with low FEV1 (Devilliers et al., 2024). NTHi can cause cilia injury and reduce cilia beat frequency, through activation of protein kinase C in epithelial cells *in vitro* (Bailey et al., 2012) and it is known to be a common pathogen in primary ciliary dyskinesia (PCD) with susceptibility driven by impaired cilia function (Walker et al., 2017). Azithromycin has been shown to promote proliferation of nasal basal cells and multiciliated cells in PCD and dampened *in vitro* LPS induced production of cytokines including IL-6, CXCL8, IL-2, TNFα and TGFα (Varenyiova et al., 2023). Thus, azithromycin could account for the changes in multiciliated cell differential gene expression seen in this cohort

and have wider effects on epithelial-immune interaction given increased expression of *HLA-DR5, CTXN1* and *BTNL9* in both presence and absence of an airway pathogen. This interaction could be involved in tissue regeneration given *AREG* expression and increase in basal cell population. *MUC5AC* gene expression was not found to be significantly altered in this dataset as has been previously reported (Imamura et al., 2004), however expression of *MUC1* was suppressed with suppression of genes involved in mucus glycosylation after azithromycin treatment which could influence mucus viscosity. The nasal epithelial compartment showed broad enhancement of interferon responses. HRV is detected more often in the lower airway in asthma compared to health and in asthma is more likely to present with clinical features (Wos et al., 2008). Bronchial epithelial cells from patients with asthma show profound impairment of virus induced IFNβ expression (Wark et al., 2005). Thus, enhanced upper airway interferon responses could offer a protective mechanism preventing the dissemination of viruses to the lower airway, protecting against exacerbations.

Consistent with existing literature, in this study neutrophils and macrophages showed the greatest functional transcriptomic changes. Macrophages upregulated genes related to antigen presentation, adhesion and chemotaxis but suppressed genes related to inflammation (*S100A9, S100A12* both in presence and absence of infection) and proteolysis (*LYZ, VCAN*). There was specific suppression of *IL1B* and *NFKB* pathway related genes in the absence of infection supporting an immunomodulatory role for azithromycin. Similarly, neutrophils regulated genes involved in the suppression of TLR mediated and NFKB signalling. Upregulation of the steroid inducible anti-inflammatory gene *TSC22D3* could suggest a greater response to inhaled corticosteroids after treatment with azithromycin (Mostafa et al., 2019). Interesting in both presence or absence of asthma the circadian clock gene PER1 was upregulated, its expression has been shown to be increased in patients with nocturnal symptoms (Chen et al., 2021)however it is also induced by short acting beta agonists (Krakowiak and Durrington, 2018) and could thus represent a treatment effect pre-bronchoscopy, given patient ACQ-5 score was reduced.

This study had a number of limitations. The sample size was restricted by patients declining second bronchoscopy and some challenges with sequencing libraries which reduced the number of total cells which could be included in the analysis. Recruitment started in April 2021 was thus affected by the COVID-19 pandemic leading to reluctance of subjects to participate. In addition, BAL samples and nasal brush supernatants collected for planned metagenomic studies had exceedingly low DNA yield (as described in Methods) and failed to generate adequate metagenomic sequencing data upon Nanopore sequencing. Based on this experience, protected sterile brushing may be a preferable technique. In this study the lower airway was sampled by endobronchial biopsy rather than endobronchial brushings which were prioritised for a separate study of airway epigenetics in severe asthma underway in the lab. Brushings were selected for epigenetic studies as airway epithelial cells are hypothesised to undergo greatest epigenetic regulation in asthma and are captured in greater numbers using this technique. This difference in sampling of the upper (brushing) and lower airway (biopsy) is a caveat to this study and may account for differences in proportion of epithelial cells in the single cell dataset by compartment.

4.9 Conclusions

In conclusion, the clinical findings in the AMASS study were consistent with the results of the AMAZES trial. The airway load of *H. influenzae* fell in every case. Lower airway epithelial cells and basal cells upregulated genes involved in regeneration and cilial function whereas in the upper airway there was an enrichment of type II interferon. Goblet cells globally reduced their gene expression which could be reflected in reduced mucus secretion. The strongest effect is seen in the myeloid compartment with evidence of suppressed NFκB signalling and proinflammatory genes (S100A8/9/12). T cells did not show dramatic changes in gene expression. They appeared more quiescent (reduced DHFR expression), less inflammatory (immunometabolic shift to oxidative phosphorylation) and suppressed intracellular signalling pathways. CD8 TRM populations expressed AREG which may be involved in tissue repair and

regeneration, supporting return to homeostasis following pathogen clearance or modulation of innate immune pathways by azithromycin in absence of infection. The data presented in this chapter support both antibacterial and broader immunomodulatory effects for azithromycin. It is not possible to determine which is the predominant effect from this data but azithromycin is clinically much more effective than other antibiotics in airways disease, such as doxycycline (Allinson et al., 2023). This could be related to greater intracellular killing capacity, but more is likely due to immune modulation given the range of anti-inflammatory effects azithromycin possesses.

Chapter 5: MultiOmics pRoject Study gEnomic (MORSE)

5.1 Introduction

Severe asthma is a heterogenous condition. Whilst significant developments have been made in the treatment of type-2 high severe eosinophilic asthma using biomarker directed biologic therapies, less is known about the molecular pathways underlying severe asthma that is not type-2 cytokine (IL-5, IL-4, IL-13) or biomarker (blood eosinophil, FeNO) driven and is refractory to corticosteroid therapy. Type-2 high severe asthma is, by definition, relatively resistant to inhaled corticosteroids (Khalfaoui et al., 2022). This is particularly apparent in up to 35% of patients with type-2 disease who have persistently raised type-2 biomarkers despite electronically monitored high-dose inhaled corticosteroid (ICS) therapy (Heaney et al., 2018), referred to as FeNO non-suppressor.

Thus, there are type-2 high and type-2 low phenotypes of severe asthma which are treatment refractory, associated with significant individual morbidity and remain a significant unmet clinical need in the absence of specific targeted therapies.

5.2 Hypotheses

- In severe asthma, in the context of alterations in microbiome, chronic inflammation, and corticosteroid therapy, upper and lower airway tissue resident T cells acquire distinct transcriptomic features compared to health.

- Airway T cell populations derived from patients with corticosteroid resistant asthma will have unique transcriptomic features dependant on whether there is a background of type-2 high inflammation or non-type-2 high (typically neutrophilic) inflammation.
- There are shared and unique drivers of corticosteroid resistance within severe asthma populations.
- Upper and lower airway T cells are transcriptionally unique both in health and asthma. These differences are likely reflected in unique T cell receptor repertoires and functional distinctions.

5.3 Aims

- To devise a clinically relevant framework for phenotyping patients with type-2 high and corticosteroid resistant asthma to guide recruitment to a bronchoscopy study aiming to offer novel immunological insight through scRNAseq of airway tissue.
- To recruit patients with proven corticosteroid sensitive or resistant airways inflammation, and healthy controls to a mechanistic bronchoscopy study.
- To use scRNAseq approaches to characterise lymphoid populations in the upper and lower airways within these cohorts.
- To provide novel insight into mechanisms driving corticosteroid resistant inflammation.
- To provide insight into fundamental differences in T cells phenotype and T cell receptor repertoire by airway compartment to better understand the regulation of mucosal immunity at these barrier sites.

5.4 Study population

Between April 2021 and October 2024, 43 patients were enrolled to the MORSE study (Flow chart shown in Chapter 2, Figure 2.2). Baseline study characteristics are summarised in **Table 5.1** and includes the 43 participants who contributed samples towards the scRNAseq dataset.

The study recruited 12 non-atopic healthy control participants and 31 patients with severe asthma. Patients with severe asthma who were identified to have an elevated FeNO (≥ 45 ppb) (**Figure 5.1**) at baseline either underwent formal FeNO suppression testing or were found to meet FeNO suppression criteria (>42% reduction in FeNO and FeNO < 45 ppb on day 7 of assessment) after optimisation of inhaled corticosteroid therapy with proven adherence > 80%. Based on the outcome of this assessment patients have been subclassified as FeNO low (n = 14), FeNO suppressor (n = 8) and FeNO non-suppressor (n = 9). Change in FeNO within these groups is shown in **Figure 5.2**. Within the severe asthma population all patients were established on high dose ICS/LABA inhaled therapy. Patients receiving biologic therapy were excluded from this study. Blood eosinophil count was low in the FeNO low group (mean 0.19 $x10^9$/L, SD 0.11$x10^9$/L), in keeping with the type-2 low classification of these patients (**Figure 5.1** D). Blood eosinophil count was elevated in the FeNO suppressor (mean 0.55 x 10^9/L, SD 0.39 x 10^9/L) and non-suppressor (mean 0.51 x 10^9/L, SD 0.32 x 10^9/L) groups (**Figure 5.1** A). Overall, in severe asthma patients had high symptom scores, with mean ACQ-5 of 2.3 (SD 1.3). The FeNO low group had marginally higher ACQ-5 (mean ACQ-5 2.6, SD 1.3). Lung function was comparable between groups. Ex-smokers have been included and had minimal pack year smoking history and no evidence of emphysema on imaging.

Table 5.1 Clinical characteristics of MORSE study population

Characteristic	Healthy (n=12)	Severe Asthma (n=31)	FeNO low (n=14)	FeNO suppressor (n=8)	FeNO non-suppressor (n=9)
Age (years), Mean (SD)	37 (10)	53 (18)	56 (18)	51 (19)	51 (19)
Sex					
Male (%)	6 (50)	15 (48)	7 (50)	2 (25)	6 (66)
Female (%)	6 (50)	16 (52)	7 (50)	8 (75)	3 (34)
BMI (kg/m^2), Mean (SD)	26 (5)	29 (7)	31 (8)	28 (7)	26 (6)
Ex-smoker, n (%)	2 (16)	9 (29)	4 (28)	2 (40)	2 (22)
Pack years, Mean (SD)	1 (1)	1 (3)	2 (3)	2 (25)	0.5 (1)
Presence of atopy, n (%)	0 (0)	18 (58)	10 (71)	3 (37)	5 (55)
Presence of nasal polyps, n (%)	0 (0)	5 (16)	2 (14)	0 (0)	3 (33)
Baseline inhaled corticosteroid use (BDP eq., mcg/d), Median (Range)	NA NA	1600 (500)	1490 (540)	1825 (650)	1520 (580)
ACQ5 score, Mean (SD)	NA NA	2.3 (1.3)	2.6 (1.3)	1.9 (1.1)	2.4 (1.4)
Spirometry					
FEV1 (%), Mean (SD)	99 (10)	87 (22)	91 (19)	99 (23)	86 (21)
FVC (%), Mean (SD)	105 (11)	100 (19)	94 (15)	115 (17)	98 (20)
FEV1/FVC, Mean (SD)	0.80 (0.09)	0.70 (0.11)	0.69 (0.13)	0.70 (0.13)	0.72 (0.10)
FeNO (ppb), Mean (SD)	17 (6)	62 (63)	22 (18)	100 (42)	121 (77)
Blood eosinophils ($x10^9$/L), Mean (SD)	0.13 (0.07)	0.30 (0.25)	0.19 (0.11)	0.55 (0.39)	0.51 (0.32)

BMI, body mass index; BDP, beclomethasone diproprionate; ACQ5, Asthma Control Questionnaire 5; FEV1, forced expiratory volume in 1s; FVC, forced vital capacity; FeNO, exhaled nitric oxide

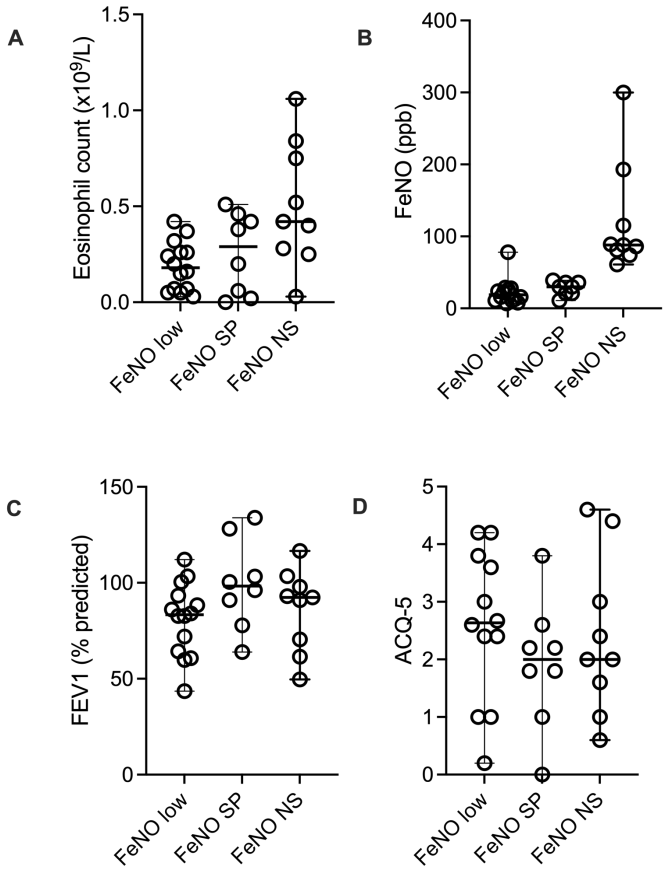


Figure 5.1 Clinical characteristics of patients with severe asthma at baseline bronchoscopy;

(A) Blood eosinophil count; (B) FeNO; (C) Percentage of predicted FEV1; (D) ACQ-5 symptom scores. Patients are grouped by baseline FeNO and subsequent result of FeNO-suppression testing. As described previously, FeNO suppressors saw a >42% fall in FeNO and had a FeNO<45 ppb following the test

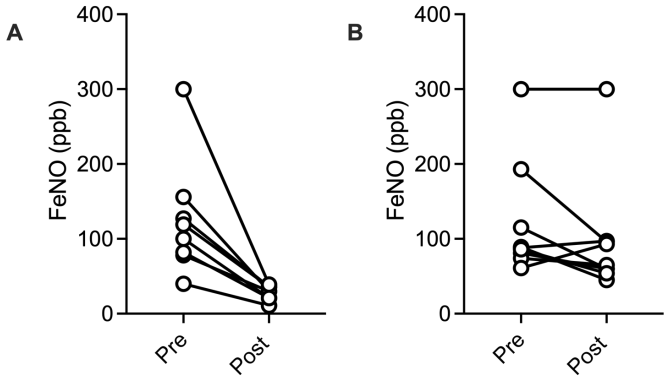


Figure 5.2 FeNO suppression test results based on outcome;

(A) Pre- and post- FeNO suppression test FeNO measurement in suppressors; (B) Pre- and post-FeNO suppression test FeNO measurement in non-suppressors

5.5 Generation of a reference lymphoid single cell dataset in health and asthma

5.5.1 scRNAseq of upper and lower airway samples from healthy controls and patients with severe asthma

Paired endobronchial biopsies and nasal brushings were included from 43 participants (healthy, n=12 and asthma, n=31). This was a large collaborative study encompassing multiple projects. I recruited, phenotyped and performed the bronchoscopies, and (assisted by Bianka Brassanyi, Raghad Yamani, Wojciech Lason), processed samples for scRNAseq analysis. I performed the data analysis described below. My focus was to extract the lymphoid lineage to generate a unique dataset which could be used to study fundamental differences in upper and lower airway T cell biology and offer novel insight into corticosteroid resistant severe asthma. To expedite the analysis, the myeloid and epithelial compartments are being analysed by others in the group with plans to integrate for publication. From the combined dataset of 277,461 cells, a subset of 70,709 (lower airway = 45,026, upper airway = 25,683) high quality lymphoid cells were included after QC. Cells were filtered based on minimum genes per droplet of 500, and less than 10% mitochondrial gene counts. Annotations were performed manually and compared against the Human Tonsil Atlas (Massoni-Badosa et al., 2024) and PBMC reference (Hao et al., 2021). Upper and lower airway cells were separated using hashtag oligos as previously described.

A combined UMAP projection of lymphoid cells split by disease status and compartment and are shown in **Figure 5.3** and **Figure 5.4**, respectively. These UMAPs demonstrate the cellular composition within the lymphoid lineage captured in this study and the previously demonstrated compartmental split of cells by the anatomical location of origin. This split by site of sampling was consistent between cells from healthy and asthma participants.

5.5.2 Characterisation of lymphoid cell population in the MORSE cohort

Within the lymphoid lineage 20 different populations were identified. There was a separation of cells by compartment. With greater variety and frequency of TRMs and activated T cells in the lung. UMAP projections are shown in **Figure 5.3** and **Figure 5.5**. In **Figure 5.4** the split of cell type in each airway compartment between healthy donors and patients with asthma is shown. However, there were fewer healthy participants in the cohort and their contribution to the total cell numbers was approximately half of the number contributed from patients with asthma. Therefore, differences in proportion shown in these plots cannot be directly assumed to represent a difference in phenotype. Defining cluster markers are shown in **Figure 5.3**.

As seen in the AMASS dataset, there was a large population of CD8+ TRM cells, these were *CD3/CD8* positive, granzyme expressing (GZM*A, GZMB, GZMH*) cells with upregulated tissue residency markers (*ITGAE, CD69, CXCR6*). However, unlike in the AMASS dataset where there were 2 discrete populations of TRMs distinguished mainly by their site of origin (thus annotated as nasal and bronchial CD8 TRMs), in this dataset both populations of CD8 TRMs (named CD8+ TRM1 and CD8+ TRM2) were well represented in the lower airway, with only one population seen in the upper airway (CD8+ TRM1). Whilst phenotypically similar, a distinguishing feature of the CD8+ TRM2 population was high expression of *CXCR4*. Additional markers and transcription factors are shown in **Figure 5.6**. These cells were clustered closely to other more activated T cell populations whereas the CD8+ TRM1 population was adjacent to Th17, Treg and GZMB expressing CD8+ cells. CD8+ TRM2 cells had not upregulated markers of exhaustion (*PDCD1, HAVCR2, LAG3, CTLA4, TIGIT*).

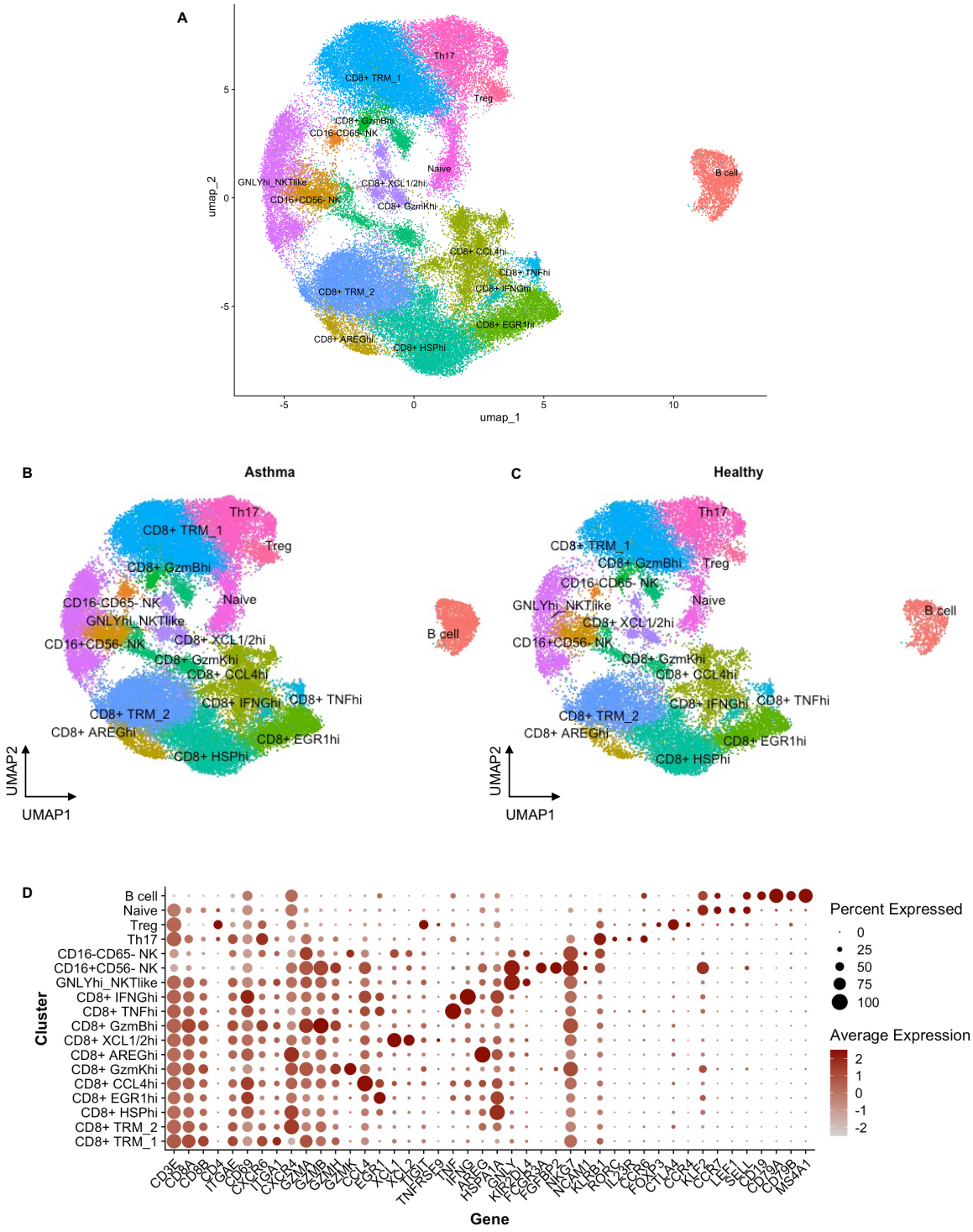


Figure 5.3 Lymphoid lineage from MORSE dataset;

(A) UMAP of all lymphoid cells in the MORSE dataset (B) UMAP visualisation of cells derived from asthmatic participants; (C) UMAP visualisation of cells derived from healthy control subject; (D) Dotplot showing expression of defining cluster markers.

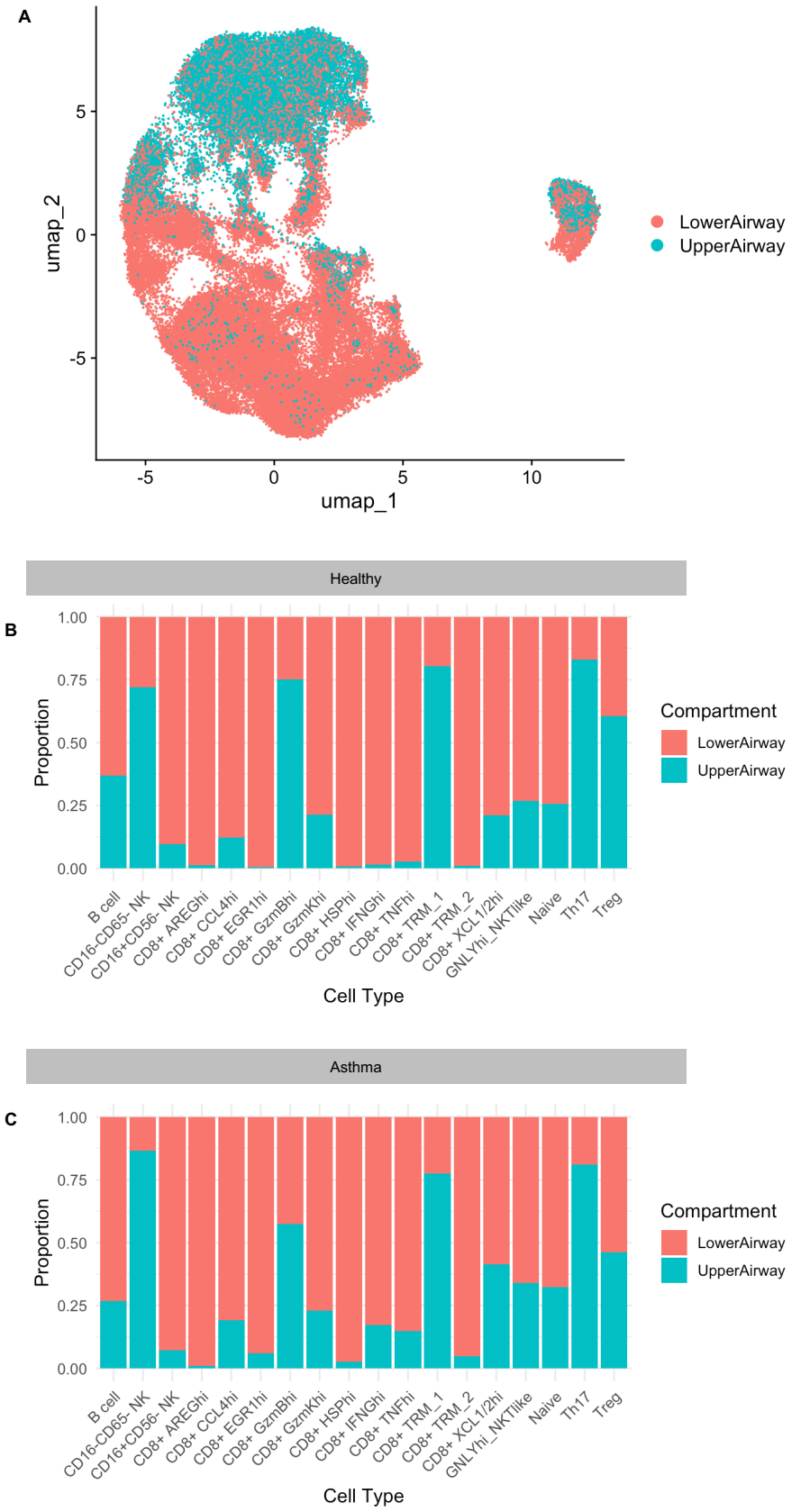


Figure 5.4 Upper and lower airway lymphoid cell captured by scRNAseq;

(A) UMAP visualisation showing lymphoid cells in the dataset, coloured by compartment (upper and lower airway) to demonstrate separation of cells by anatomical location; Bar plots showing proportion of cell type by airway compartment I (B) Health and (C) Asthma.

CXCR4 is a chemokine receptor for CXCL12 (stem cell derived factor-1α), expressed on most T cell subsets. Signalling via this receptor has broad ranging effects including adhesion, chemotaxis and transcriptional regulation of cell cycle and apoptosis (Kumar et al., 2006). It is highly expressed in Th2 cells and its inhibition in a mouse model of allergic asthma has been shown to attenuate type-2 eosinophilic responses in the airway and reduced airway hyperresponsiveness (Gonzalo et al., 2000; Lukacs et al., 2002). Thus, these cells may represent a disease specific subset of the lower airway in asthma. Several activated/effector T cell subsets were identified and defined by expression of cytokines *IFNG* and *TNF,* and upregulation of *EGR1, CCL4, XCL1/2*, heat shock proteins (HSPhi), and *GZMK*. Defining markers are summarised in **Figure 5.3**. A population of *AREG* enriched cells were again identified. Amongst innate T cells populations, similarly to the AMASS dataset, there were CD16+CD56- and CD16-CD56- subsets of NK cells. In addition, in this dataset an NKT-like population was identified, with CD3 expression alongside NK cell receptors (*KLRC1, KIR2DL4, KLRC2*) which was very highly enriched with *GNLY*.

A Th17 population was found with high expression of *RORC* and *CCR6*, with a greater proportion derived from nasal brushing (**Figure 5.6** and **Figure 5.5**). As in the AMASS dataset similar populations of Treg (*FOXP3, CTLA4, CCR4*), naïve T cells (*KLF2, CCR7, LEF1, SELL*) and B cells (*CD19, CD79A, MS4A1*) were identified, and key markers are summarised in **Figure 5.3**. Tregs expressed GATA3 as reported previously at mucosal barrier sites (Wang et al., 2011).

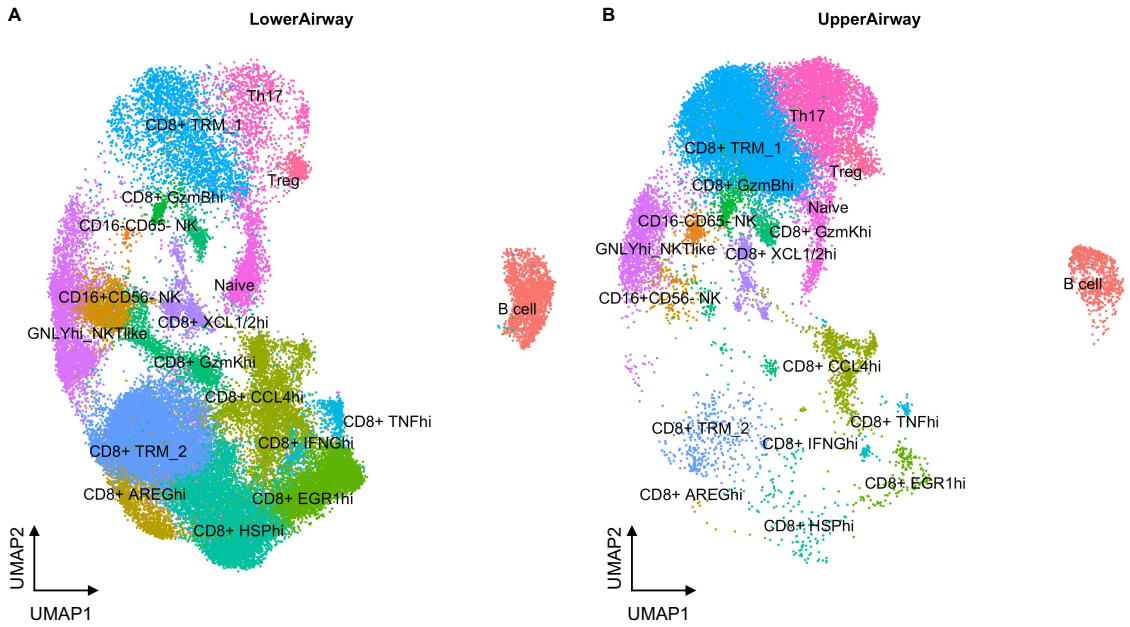


Figure 5.5 cellular composition in the upper and lower airways in health and asthma;

(A) UMAP projection of cells from the lower airway as captured from endobronchial biopsy; (B) UMAP projection of cells from the upper airway as captured by nasal brushing

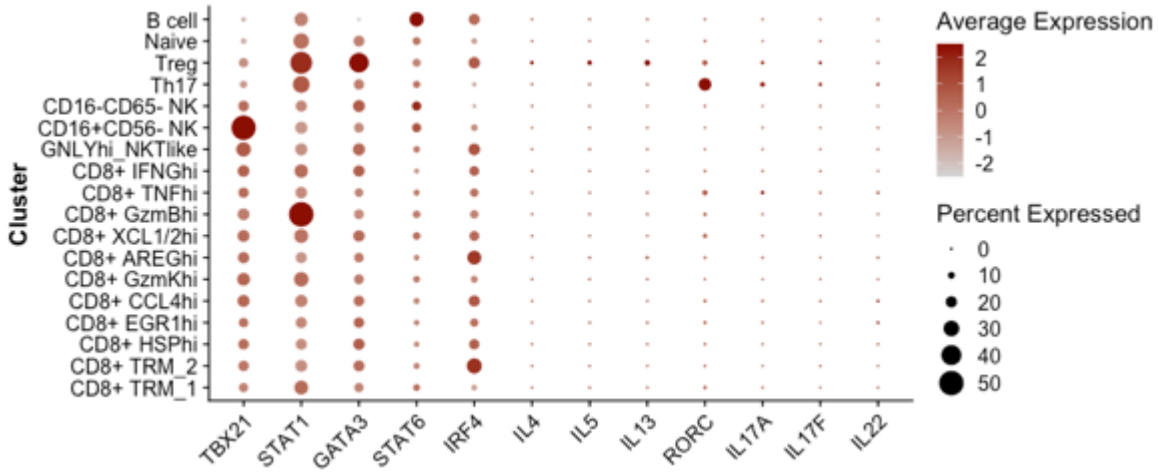


Figure 5.6 Dot plot of additional transcription factors and cytokines used for classification of cells

5.6 Discussion

The MORSE study is a large, collaborative multi-omics project devised to discover novel mechanisms in severe asthma. Within this study my aims included developing the framework for recruitment and stratification of patients to allow clinically meaningful comparisons to guide immunological comparisons within discrete groups of patients with corticosteroid resistant asthma on the background of either type-2 high or type-2 low inflammation. FeNO was central to this as a non-invasive biomarker offering an objective measure of ongoing airway inflammation driven by type-2 cytokines and epithelial alarmins. In individuals with corticosteroid sensitive disease, its suppression is a useful means of assessing adherence to therapy – whereas when persistently elevated despite monitored administration of inhaled corticosteroids it provides strong evidence of true corticosteroid resistant disease. FeNO originates from the epithelium, its basal production is physiological, however when produced in excess it is a reflection of inducible nitric oxide synthase (iNOS) induction by IL-4 and IL-13 acting on the epithelium. In excess FeNO acts as an oxidising agent causing cellular damage and contributing to the pathophysiology of asthma. As shown in this chapter FeNO was used to stratify patients with type-2 low disease and further classify those with type-2 high biomarkers into corticosteroid responsive suppressors or resistant non-suppressors.

Using scRNAseq I have identified and annotated the upper and lower airway lymphoid populations in health and within severe asthma phenotypes. As seen in the AMASS study and reported by others (Alladina et al., 2023), the largest population of cells within this compartment were CD8+ T cells. Several overlapping cell types were observed which have been described in the AMASS dataset including EGR1 high, Granzyme K high, AREG high and CCL4 high cells. In this dataset HSP high, Granzyme B high, IFN or TNF high clusters were identified. An NKT-like population was also found with high granulysin expression (*NCAM1* dim). These cells appear to be effector memory in phenotype, and more prevalent in

the lung. By comparison, the upper airway showed a Th17/Treg bias. These differences could be shaped by regional differences in microbiome or could be disease specific features.

Due to time limitations, it has not been possible for me to perform further downstream analyses of this dataset for my thesis but there is huge potential, and I will continue analyses as part of my ongoing future work. Differential expression analyses will be performed comparing health and the three groups of severe asthma patients described. This will allow differences between patients with eosinophilic/type-2 high disease but variable responses to corticosteroids to be made. A further important comparison, to address a key aim of this study, will be that of the FeNO low *vs.* FeNO non-suppressor groups, and the interaction with atopy. These phenotypes are dichotomous in terms of type-2 biomarkers but share the clinical feature of corticosteroid resistance. It is unlikely that the presence of an airway pathogen is the shared feature here given that we and others have shown that pathogen dominance tends to be associated with low FeNO (Diver et al., 2022; Jabeen et al., 2024).

Using existing published gene sets I will calculate enrichment scores for relevant cytokine signalling pathways including IL-4 and IL-13 (Giovannini-Chami et al., 2012), IL-17 (Singhania et al., 2017) and compare this across cell type and group. Over representation and gene set enrichment analyses will help to guide investigation of relevant pathways. I will perform differential abundance analyses to identify compositional differences across T cell subsets in health and across severe asthma phenotypes. I will integrate single cell TCR data to further refine annotations and perform clonotype analyses.

To better understand the differences seen across the upper and lower airway populations within individuals and across disease groups I will compare upper and lower airway T cell transcriptomes in health and asthma and integrate this with single cell TCR data. I hypothesise that these differences will be significant based on my metagenomic, proteomic and earlier transcriptomic analyses.

It will also be possible to investigate interactions with the myeloid and stromal compartments by cell-cell interaction analyses. I have stored BAL supernatants and paraffin embedded biopsies which could be used to validate any finding through traditional staining techniques or novel spatial techniques (proteomics, lipidomic, transcriptomics), in which our group has expertise. This would allow a greater number of targets to be interrogated from small biopsy samples.

5.7 Conclusions

The MORSE study has generated an exciting and unique dataset in severe asthma. To our knowledge, it is the largest single cell dataset of corticosteroid resistant asthma. I have generated an annotated lymphoid dataset and outlined my plans for the next stages of analyses.

Chapter 6: Discussion

In its broadest terms this thesis aimed to investigate drivers of corticosteroid resistant airways inflammation in severe asthma. Within this phenotype, the intent was to determine how widely dominant airway pathogens and neutrophilia could account for refractory disease, the mechanisms by which azithromycin exerts it action as a targeted therapy and to provide novel insights into broader mechanisms of corticosteroid resistance in severe asthma. I have undertaken metagenomic sequencing, conducted a bronchoscopy based human intervention study of azithromycin mechanisms in asthma and a further cross-sectional bronchoscopy study of immune mechanisms in asthma. I have used scRNAseq to offer novel insights within these patient groups.

6.1 Neutrophilic asthma and *H. influenzae*

The airways form the second largest barrier site in the human body after the gut. It interacts closely with the microbiome to shape local immune responses from birth. There is a critical window of opportunity for establishment of a favourable microbiome to support immune tolerance and determine the lifetime risk of atopy and asthma. In asthma it is known that early acquisition of airway pathogens *H. influenzae, M. catarrhalis* and *S. pneumoniae* increases risk of early wheeze and lifetime risk of asthma (Bisgaard et al., 2007). Once established asthma is associated with a loss of microbial diversity and a higher frequency of potentially pathogenic organisms. However, the field had been limited by lack of sequencing technologies to allow species level taxonomic identification of bacterial species, variation in clinical phenotyping which is particularly impactful given the heterogeneity in asthma and small sample size in early studies. With growing evidence that specific bacterial species (most often *H. influenzae*) likely drive immunopathology in severe asthma, particularly neutrophilic disease (Green et al., 2014; Simpson et al., 2016; Taylor et al., 2018), and with emergence of

azithromycin as a promising therapy for this trait, determining its prevalence with an appropriate sequencing approach became an important research question.

I sought to do this with Nanopore sequencing in my DPhil, leveraging the benefits of long read sequencing to describe the severe asthma microbiome at species level. I developed a method for long read metagenomic sequencing from induced sputum samples collected during periods of clinical stability. Applying nanopore sequencing to two highly phenotyped cohorts of severe asthma patient I found that a pathogen dominant microbiome was a feature of severe refractory asthma in up to 30% of patients, and was driven mainly by *H. influenzae,* but also *M. catarrhalis* and *S. pneumoniae*. In the absence of a pathogen dominant microbiome, *Rothia* spp. were found to have greater abundance in severe asthma. As facultative anaerobes it is speculated that these species may preferentially dominate airway niches with low oxygen tension secondary to mucus plugging, prevalent in severe disease. I also demonstrated that the microbiome and proteome of the upper and lower airways are distinct. During the course of my DPhil a few large cohort studies detected *H. influenzae* and *M. catarrhalis* as predominant pathogens in asthma, further strengthening these findings (Diver et al., 2020; Versi et al., 2024; Versi et al., 2023).

Presence of *H. influenzae* is associated with airways neutrophilia and treatment response to azithromycin (Taylor et al., 2020). It has long been speculated that neutrophilic asthma is driven by airway bacteria (Singhania et al., 2018). In this thesis I have shown that treatment with azithromycin in patients who have a positive culture for *H. influenzae* leads to a reduction in bacterial load and neutrophil frequency in BAL, alongside a clinical response (improvement in FEV1 and ACQ-5). This finding is consistent with the AMAZES clinical trial (Gibson et al., 2017) and supports the hypothesis of bacteria driving airways neutrophilia in severe asthma. Integration of metagenomic and cytokine data revealed the presence of type-1 inflammation (IL-1β, TNF) with markers of neutrophilic infiltration (IL-8, YKL40), release of neutrophil granule proteins and proteases (MMP8, MMP9, MPO and elastase), potential counter

regulatory mechanisms (TIMP-1, IL-10), and macrophage recruitment (MIP1α and MIP1β) which could be facilitated through IL-6 signalling (IL-6SR) in presence of an airway pathogen. In the UBIOPRED cohort, sputum transcriptomic data has linked *H. influenzae* with NETosis and IL-6 trans-signalling. In the AMASS study, neutrophils underwent transcriptomic changes reflective of immune modulation after azithromycin treatment irrespective of a positive BAL culture prior to treatment. There was increased expression of chemokine receptor CXCR4, chemokines (CLEC4E, CCL4L2, CXCL16) alongside IRAK3 and DUSP1 (negative regulators of pro-inflammatory signalling) and peptidase/protease inhibitors (PI3, TIMP1). Elevated TIMP1 was seen in presence of a pathogen dominant microbiome in my earlier studies and speculated to contribute to airway remodelling if produced chronically and preventing epithelial/stromal cell turnover. In the context of pathogen and NET clearance as occurs with azithromycin, it could represent a physiological response. The steroid inducible gene TSC22D3 (negative regulator of NFκB) was upregulated. A reduction in IL-1Ra was seen in BAL after azithromycin therapy. This could reflect a quenching of IL-1β, but given corticosteroids can suppress IL-1Ra (Arzt et al., 1994), taken together with TSC22DC upregulation this finding could imply enhanced ICS sensitivity following azithromycin therapy. Both in the presence (S100A8, S100A9, MNDA) and absence (IL1B, NFKBIZ) of a positive culture at baseline, there was a reduction in expression of inflammatory neutrophil mediators S100A8/A9 which are capable of activating the NLRP3 inflammasome and driving IL-1β production (Simard et al., 2013). NLPR3 and IL-1β expression are elevated in sputum in obese patients with severe asthma (Wood et al., 2019), and within murine models of neutrophilic airways inflammation induced by *Chlamydia* and *Haemophilus* infection (Kim et al., 2017). The suppression of genes encoding IL1B and neutrophil S100A8/A9 could be the consequence of clearance of infection or NETs by azithromycin (Keir et al., 2021) or a direct azithromycin effect (given IL1B is suppressed in absence of infection as well). Together these mechanisms could modify the inflammatory microenvironment to enhance corticosteroid sensitivity.

By taking a curated approach to single cell data filtering and QC, it was possible to retain a large population of neutrophils, which are often lost in single cell datasets due to their low RNA content and assumption that this is representative of poor quality/viability cells in standard bioinformatic workflows. An alternative approach to enhance capture and recovery of cells with low mRNA content is the microwell-based BD Rhapsody single cell sequencing platform (Scheiber et al., 2024). A head-to-head comparison of BD Rhapsody and 10x droplet-based sequencing has not been performed using lung tissue, however in other complex tissue 10x has been shown to have a higher overall cell capture rate and genes detected per cell, whereas BD Rhapsody detects more mRNA molecules per cell with greater capture of low mRNA cells but inferior capture of larger epithelial cells. In addition, higher mitochondrial transcripts and differences in transcript-specific mRNA capture efficiency (which can affect downstream marker-based cell annotation) has been observed with BD Rhapsody (Salcher et al., 2024). These distinct characteristics of sequencing technologies need to thus be considered in experimental design. In this study, using 10x, 6 populations of neutrophils were described and included CCL4L2 high neutrophils and PI3 high neutrophils. Differential abundance testing with miloR did not show any significant change in these population after treatment, however it may be that this analysis was underpowered, given the variability in cluster size. It would be intriguing to study these subpopulations further given CCL4L expression in the context of neutrophilic inflammation has been linked to ICS-nonresponse (Tsai et al., 2023) and PI3 is a peptidase inhibitor and may represent a more anti-inflammatory phenotype. My future plans include performing trajectory analysis on the neutrophil population as this could provide further insight into the dynamics of these sub-populations in the airway.

In conclusion, my findings of neutrophilic airways inflammation in the presence of a lower airway pathogen, typically *H. influenzae*, are in keeping with the existing literature. I show the inflammatory networks driving inflammation and improvement in neutrophilic inflammation with azithromycin. I have extended existing knowledge by demonstrating the treatment effect of azithromycin in the absence/presence of airways infection is conferred both by anti-bacterial

and potential anti-inflammatory mechanisms as elaborated further below. The unanswered question remains why a subset of patients are susceptible to these profound microbiome shifts – is it an accumulation of broader asthma susceptibility factors and chronic inflammation in the airways creating a permissive environment (e.g. with NET formation)? Or is there a fundamental defect in mucosal immunity in these individuals? are these differences related to early life microbial colonisation or sequential exposure to viral and bacterial insults against an asthmatic epithelium with impaired innate immune defences?

6.2 Azithromycin in severe asthma

Mechanistic studies of azithromycin have mainly been conducted *in vitro* or using *in vivo* mouse models. A single bronchoscopy study had been performed to study azithromycin mechanisms however, the duration of treatment was only 6 weeks, and no difference was found in their primary outcome of interest – epithelial barrier thickness and mucin production in endobronchial biopsy samples. No immune correlates were studied.

The AMASS study was therefore unique in its design, by applying scRNAseq technology to airway samples collected from the upper and lower airways, before and 4 months after administering low dose azithromycin therapy (250 mg, 3 times weekly) in patients qualifying for add-on therapy. The AMAZES clinical trial has proven the efficacy of azithromycin in severe asthma, but not fully elucidated its mechanism of action, although antibacterial effects had been suggested (Gibson et al., 2017; Taylor et al., 2019). The need for better mechanistic understanding is driven by significant concerns surrounding antimicrobial resistance associated with unrestricted use of macrolide antibiotics. Non-antimicrobial macrolides could offer a therapeutic alternative if immunomodulatory properties were proven to be sufficient.

In this thesis I have presented the transcriptional changes seen with azithromycin therapy in epithelial and immune cell populations. Key findings in the epithelium included upregulation of

genes involved in cilial motility, with downregulation of genes associated with cell turnover. Taken together with the relative expansion of basal cell, this builds a picture of regeneration within the epithelium. Lung goblet cells had overall reduced gene expression, suggestive of suppressed activity. The nasal epithelial compartment showed broad enhancement of type-I interferon responses. HRV is detected more often in the lower airway in asthma compared to health and in asthma is more likely to present with clinical features (Wos et al., 2008). Bronchial epithelial cells from patients with asthma infected with RV-16 show profound impairment of virus induced IFNβ expression with increased virus replication and cell lysis (Wark et al., 2005). Thus, enhanced upper airway interferon responses could offer a protective mechanism preventing the dissemination of viruses to the lower airway, and conferring protection against exacerbations.

In keeping with existing literature, the strongest signal was seen in the myeloid compartment where macrophages and neutrophils suppressed NFκB signalling (upregulation of its inhibitors e.g. NFKB1A, IRAK3), pro-inflammatory cytokines, chemokines and proteases. In addition, I report that azithromycin therapy reduced the expression of pro-inflammatory neutrophil genes in the absence of infection (IL1B, NFKIBZ, NFKBIA, BCL2A1), this finding supports an immunomodulation. Macrophages were found to upregulate genes involved in phagocytosis and downregulate myeloid inflammatory proteins implicated in asthma after azithromycin therapy in individuals with or without a positive BAL culture at baseline. NTHi can persist within macrophages and impair phagocytic killing, macrolide compounds have been shown to restore this function *in vitro* (Hodge et al., 2006; Hodge et al., 2008). It is possible to speculate that a similar process is seen here *in vivo*. In the absence of an airway pathogen, macrophages upregulated the expression of AREG, also expressed by CD8 T cells, which may play a role in tissue regeneration (Ko et al., 2020). Macrophages can play an important role in tissue homeostasis and azithromycin treatment could promote this phenotype by regulating inflammatory signalling and suppressing mucus hypersecretion and NET load.

T cells did not undergo profound changes in their transcriptomes reflective of direct anti-inflammatory effects but instead appeared more quiescent with upregulation of oxidative phosphorylation pathways, associated with anti-inflammatory, immunometabolic change with complementary downregulation of DHFR (Shi et al., 2025). AREG expression was upregulated by CD8 TRM populations and it is speculated that could be involved in supporting tissue repair following pathogen clearance with azithromycin. This is a novel finding. Interestingly a similar AREG expressing population was seen within the MORSE cohort – and is a cell type which will be further investigated in my future analyses.

Transcriptomic expression does not always correlate with changes in protein expression. Whilst the cytokine results presented in the AMASS failed to reach statistical significance, likely on account of the sample size, the pattern of reduction in IL-1β, CXCL8 and neutrophil NET load is consistent with the transcriptomic results and moreover, existing literature (Keir et al., 2021; Simpson et al., 2008; Taylor et al., 2019). The lack of microbiome data is a limitation in this study which I hope to overcome by performing pathogen specific PCR assays for common respiratory pathogens using stored samples which would not be adequate for the purposes of sequencing. Integration of this data should still provide valuable insight given that reduction in *H. influenzae* airway load has been shown to be predictive of treatment response with azithromycin in the AMAZES trial (Taylor et al., 2020).

The novelty of this data set has been the ability to study azithromycin effects *in vivo* within the clinically relevant phenotype of asthma. It has been possible to compare the effect of treatment depending on whether a dominant airway pathogen was present. This has offered new mechanistic insight however, it is not possible to determine from this data whether the antibacterial or immunomodulatory effect is predominant in presence of a positive culture. However, given the limited clinical efficacy of other classes of long-term antimicrobials in asthma, and azithromycin's broad anti-inflammatory effects, modulation of the immune

response is speculated to be significant. A biomarker guided (e.g. *H. influenzae* PCR) trial of azithromycin and non-antimicrobial macrolides could provide a more definitive picture.

This dataset allowed fundamental differences in epithelial and immune cell phenotype across the upper and lower airway to be appreciated in the context of asthma. It will be fascinating to compare this with compartmental differences seen in health, both in terms of cellular phenotype but also more specific differences in clonality across T cell populations given the differences in microbiome.

6.3 Treatment refractory phenotypes of severe asthma

A key aim of this study was to generate a single cell dataset derived from patients with corticosteroid resistant phenotypes of asthma and healthy participants to reveal novel mechanistic insights into treatment refractory disease. I developed a framework for classification of patients to allow objective assessment of treatment response with FeNO suppression testing which guided recruitment to a mechanistic bronchoscopy study. This, to our knowledge, is the largest dataset of its kind. scRNAseq offers the opportunity to capture cellular diversity and rare cell populations within small tissue samples. I hypothesise that careful phenotyping of patients will maximise the opportunity for discovery of biological differences conferring these phenotypes.

In MORSE, 43 participants were included in a scRNA seq analysis. I have produced an annotated T cell dataset and described the main lymphoid populations captured within it. Due to time restrictions, it has not been possible to include further results in this thesis, but analysis will continue as part of my future work as described below.

Work in our group has shown that FeNO non-suppression is linked to persistence of type-2 high inflammation within the airways, specifically elevated IL-4, IL-33, TSLP, eotaxin and TARC, accompanied by sputum eosinophilia (Couillard et al., 2021). It is not known why this signal remains 'switched on' within FeNO non-suppressors compared to patients who demonstrate a suppression in FeNO. The benefit of the MORSE dataset is that FeNO suppression was performed, and treatment adherence has been proven and thus eliminated as a confounding factor. FeNO low/type-2 low disease has been an unmet clinical need for decades (Hinks et al., 2021b) and I aim to offer novel mechanistic insight into its underlying drivers in my analysis. I have already shown in a predominantly type-2 low cohort that neutrophilic airways inflammation in relation to an airway pathogen can be cleared with azithromycin and is accompanied by a reduction in airway neutrophil load and significant regulation of pro-inflammatory pathways. In the absence of infection other mechanisms drive refractory inflammation and I aim to characterise these by comparing FeNO low patients against FeNO non-suppressors.

I have demonstrated that the upper and lower airway are distinct in their microbiome, proteome (Jabeen et al., 2024), cellular composition and transcriptome in asthma. I can now explore the similarities and differences in these findings by comparing with healthy individuals in the MORSE cohort. This will further our fundamental understanding of mucosal immunity at airway barrier sites, separated anatomically and by their distinct microenvironment and microbiome.

6.4 Future work

Future work and research questions are summarised by research study.

Using the AMASS dataset I will investigate the following:

- How does the airway load of potentially pathogenic bacterial species change after azithromycin treatment? Is it only an *H. influenzae* effect?

This will be achieved by undertaking pathogen specific PCR assays for *H. influenzae, S. pneumoniae, S. aureus, M. catarrhalis* and *P. aeruginosa* will be performed using raw BAL samples. The DNA yield form these samples are not adequate to proceed to sequencing therefore a PCR based approach which has been previously validated has been selected

- Given the differences seen in the microbiome and cell populations in the upper and lower airway, how does TCR repertoire differ within an individual across mucosal barrier sites?

  Single cell TCR sequencing data will be integrated with the existing scRNAseq data for clonotype analyses. Annotations will be reviewed in the context of this data.
- Are the neutrophil sub-populations observed distinct phenotypes, or do they represent different states of neutrophil activation?

  To answer this question, I will perform trajectory analysis to further characterise this populations. Within the MORSE dataset I can interrogate neutrophils captured from the healthy controls to compare differences in population structure as well.

Using the MORSE dataset I will investigate the following questions. These are likely to evolve and be informed by the data.

- How do nasal and pulmonary T cell populations vary:
  - Within individual cohorts (health and asthma).
  - Between health and severe asthma.
  - Between type-2 high disease phenotypes (FeNO suppressors and non-suppressors).
  - Between corticosteroid resistant phenotypes (FeNO non-suppressors and FeNO low).

  The aims of the above comparisons are to improve fundamental understanding of mucosal T cell populations at pulmonary barrier sites and understand the common and unique mechanisms driving disease across these asthma cohorts.

- What is the effect of atopy on population and transcriptomic differences?
- How does TCR diversity vary in the upper and lower airway?
- How do cells across the lymphoid, myeloid and epithelial compartments interact with one another?

The details of the analysis plan have been discussed in Chapter 5.

6.5 Conclusions

In this thesis I have demonstrated that a pathogen dominant microbiome is a common treatable trait in severe asthma, affecting 20-30% of patients and associated with neutrophilic inflammation. I went on to show that azithromycin is an effective targeted therapy and acts via both antimicrobial and anti-inflammatory mechanisms in asthma. I have generated a valuable asthma single cell reference dataset of corticosteroid resistant phenotypes and in my future work will investigate underlying drivers of disease in this cohort.

References

Abdel-Aziz, M.I., P. Brinkman, S.J.H. Vijverberg, A.H. Neerincx, J.H. Riley, S. Bates, S. Hashimoto, N.Z. Kermani, K.F. Chung, R. Djukanovic, S.E. Dahlen, I.M. Adcock, P.H. Howarth, P.J. Sterk, A.D. Kraneveld, A.H. Maitland-van der Zee, and U.B.S. Group. 2021. Sputum microbiome profiles identify severe asthma phenotypes of relative stability at 12 to 18 months. *J Allergy Clin Immunol*. 147:123-134.

Abellan-Schneyder, I., M.S. Matchado, S. Reitmeier, A. Sommer, Z. Sewald, J. Baumbach, M. List, and K. Neuhaus. 2021. Primer, Pipelines, Parameters: Issues in 16S rRNA Gene Sequencing. *mSphere*. 6.

Ackland, J., C. Barber, A. Heinson, A. Azim, D.W. Cleary, M. Christodoulides, R.J. Kurukulaaratchy, P. Howarth, T.M.A. Wilkinson, K.J. Staples, and W.s. investigators. 2022. Nontypeable Haemophilus influenzae infection of pulmonary macrophages drives neutrophilic inflammation in severe asthma. *Allergy*. 77:2961-2973.

Ackland, J., A.I. Heinson, D.W. Cleary, M. Christodoulides, T.M.A. Wilkinson, and K.J. Staples. 2021. Dual RNASeq Reveals NTHi-Macrophage Transcriptomic Changes During Intracellular Persistence. *Front Cell Infect Microbiol*. 11:723481.

Ahren, I.L., E. Eriksson, A. Egesten, and K. Riesbeck. 2003. Nontypeable Haemophilus influenzae activates human eosinophils through beta-glucan receptors. *Am J Respir Cell Mol Biol*. 29:598-605.

Ahren, I.L., D.L. Williams, P.J. Rice, A. Forsgren, and K. Riesbeck. 2001. The importance of a beta-glucan receptor in the nonopsonic entry of nontypeable Haemophilus influenzae into human monocytic and epithelial cells. *J Infect Dis*. 184:150-158.

Alladina, J., N.P. Smith, T. Kooistra, K. Slowikowski, I.J. Kernin, J. Deguine, H.L. Keen, K. Manakongtreecheep, J. Tantivit, R.A. Rahimi, S.L. Sheng, N.D. Nguyen, A.M. Haring, F.L. Giacona, L.P. Hariri, R.J. Xavier, A.D. Luster, A.C. Villani, J.L. Cho, and B.D. Medoff. 2023. A human model of asthma exacerbation reveals transcriptional programs and cell circuits specific to allergic asthma. *Sci Immunol*. 8:eabq6352.

Allaeys, I., F. Ribeiro de Vargas, S.G. Bourgoin, and P.E. Poubelle. 2021. Human Inflammatory Neutrophils Express Genes Encoding Peptidase Inhibitors: Production of Elafin Mediated by NF-kappaB and CCAAT/Enhancer-Binding Protein beta. *J Immunol*. 206:1943-1956.

Allinson, J.P., B.H. Vlies, S.E. Brill, M. Law, G. Burnside, L.J. Finney, L. Alves-Moreira, G.C. Donaldson, P.M.A. Calverley, P.P. Walker, and J.A. Wedzicha. 2023. A Double-Blind, Randomized, Placebo-controlled Trial of Long-Term Doxycycline Therapy on Exacerbation Rate in Patients with Stable Chronic Obstructive Pulmonary Disease. *Am J Respir Crit Care Med*. 208:549-558.

Altenburg, J., C.S. de Graaff, T.S. van der Werf, and W.G. Boersma. 2011. Immunomodulatory effects of macrolide antibiotics - part 2: advantages and disadvantages of long-term, low-dose macrolide therapy. *Respiration*. 81:75-87.

Anees, W., V. Huggins, I.D. Pavord, A.S. Robertson, and P.S. Burge. 2002. Occupational asthma due to low molecular weight agents: eosinophilic and non-eosinophilic variants. *Thorax*. 57:231-236.

Arrieta, M.C., L.T. Stiemsma, P.A. Dimitriu, L. Thorson, S. Russell, S. Yurist-Doutsch, B. Kuzeljevic, M.J. Gold, H.M. Britton, D.L. Lefebvre, P. Subbarao, P. Mandhane, A. Becker, K.M. McNagny, M.R. Sears, T. Kollmann, C.S. Investigators, W.W. Mohn, S.E. Turvey, and B.B. Finlay. 2015. Early infancy microbial and metabolic alterations affect risk of childhood asthma. *Sci Transl Med*. 7:307ra152.

Arshad, S.H. 2005. Primary prevention of asthma and allergy. *J Allergy Clin Immunol*. 116:3-14; quiz 15.

Arzt, E., J. Sauer, T. Pollmacher, M. Labeur, F. Holsboer, J.M. Reul, and G.K. Stalla. 1994. Glucocorticoids suppress interleukin-1 receptor antagonist synthesis following induction by endotoxin. *Endocrinology*. 134:672-677.

Asgrimsson, V., T. Gudjonsson, G.H. Gudmundsson, and O. Baldursson. 2006. Novel effects of azithromycin on tight junction proteins in human airway epithelia. *Antimicrob Agents Chemother*. 50:1805-1812.

Atarashi, K., T. Tanoue, M. Ando, N. Kamada, Y. Nagano, S. Narushima, W. Suda, A. Imaoka, H. Setoyama, T. Nagamori, E. Ishikawa, T. Shima, T. Hara, S. Kado, T. Jinnohara, H. Ohno, T. Kondo, K. Toyooka, E. Watanabe, S. Yokoyama, S. Tokoro, H. Mori, Y. Noguchi, H. Morita, Ivanov, II, T. Sugiyama, G. Nunez, J.G. Camp, M. Hattori, Y. Umesaki, and K. Honda. 2015. Th17 Cell Induction by Adhesion of Microbes to Intestinal Epithelial Cells. *Cell*. 163:367-380.

Babu, K.S., and S.S. Salvi. 2000. Aspirin and asthma. *Chest*. 118:1470-1476.

Baddal, B., A. Muzzi, S. Censini, R.A. Calogero, G. Torricelli, S. Guidotti, A.R. Taddei, A. Covacci, M. Pizza, R. Rappuoli, M. Soriani, and A. Pezzicoli. 2015. Dual RNA-seq of Nontypeable Haemophilus influenzae and Host Cell Transcriptomes Reveals Novel Insights into Host-Pathogen Cross Talk. *MBio*. 6:e01765-01715.

Bafadhel, M., K. Haldar, B. Barker, H. Patel, V. Mistry, M.R. Barer, I.D. Pavord, and C.E. Brightling. 2015. Airway bacteria measured by quantitative polymerase chain reaction and culture in patients with stable COPD: relationship with neutrophilic airway inflammation, exacerbation frequency, and lung function. *Int J Chron Obstruct Pulmon Dis*. 10:1075-1083.

Bailey, K.L., T.D. LeVan, D.A. Yanov, J.A. Pavlik, J.M. DeVasure, J.H. Sisson, and T.A. Wyatt. 2012. Non-typeable Haemophilus influenzae decreases cilia beating via protein kinase Cepsilon. *Respir Res*. 13:49.

Baines, K.J., J.L. Simpson, L.G. Wood, R.J. Scott, and P.G. Gibson. 2011. Systemic upregulation of neutrophil alpha-defensins and serine proteases in neutrophilic asthma. *Thorax*. 66:942-947.

Balaci, L., M.C. Spada, N. Olla, G. Sole, L. Loddo, F. Anedda, S. Naitza, M.A. Zuncheddu, A. Maschio, D. Altea, M. Uda, S. Pilia, S. Sanna, M. Masala, L. Crisponi, M. Fattori, M. Devoto, S. Doratiotto, S. Rassu, S. Mereu, E. Giua, N.G. Cadeddu, R. Atzeni, U. Pelosi, A. Corrias, R. Perra, P.L. Torrazza, P. Pirina, F. Ginesu, S. Marcias, M.G. Schintu, G.S. Del Giacco, P.E. Manconi, G. Malerba, A. Bisognin, E. Trabetti, A. Boner, L. Pescollderungg, P.F. Pignatti, D. Schlessinger, A. Cao, and G. Pilia. 2007. IRAK-M is involved in the pathogenesis of early-onset persistent asthma. *Am J Hum Genet*. 80:1103-1114.

Barker, B.L., K. Haldar, H. Patel, I.D. Pavord, M.R. Barer, C.E. Brightling, and M. Bafadhel. 2015. Association between pathogens detected using quantitative polymerase chain reaction with airway inflammation in COPD at stable state and exacerbations. *Chest*. 147:46-55.

Bassis, C.M., J.R. Erb-Downward, R.P. Dickson, C.M. Freeman, T.M. Schmidt, V.B. Young, J.M. Beck, J.L. Curtis, and G.B. Huffnagle. 2015. Analysis of the upper respiratory tract microbiotas as the source of the lung and gastric microbiotas in healthy individuals. *mBio*. 6:e00037.

BayesFusion. GeNIe Clustering algorithm.

Bayly-Jones, C., S.S. Pang, B.A. Spicer, J.C. Whisstock, and M.A. Dunstone. 2020. Ancient but Not Forgotten: New Insights Into MPEG1, a Macrophage Perforin-Like Immune Effector. *Front Immunol*. 11:581906.

Behr, F.M., A. Chuwonpad, R. Stark, and K. van Gisbergen. 2018. Armed and Ready: Transcriptional Regulation of Tissue-Resident Memory CD8 T Cells. *Front Immunol*. 9:1770.

Bennett, E.P., U. Mandel, H. Clausen, T.A. Gerken, T.A. Fritz, and L.A. Tabak. 2012. Control of mucin-type O-glycosylation: a classification of the polypeptide GalNAc-transferase gene family. *Glycobiology*. 22:736-756.

Berenson, C.S., C.T. Wrona, L.J. Grove, J. Maloney, M.A. Garlipp, P.K. Wallace, C.C. Stewart, and S. Sethi. 2006. Impaired alveolar macrophage response to Haemophilus antigens in chronic obstructive lung disease. *Am J Respir Crit Care Med*. 174:31-40.

Beute, J., M. Lukkes, E.P. Koekoek, H. Nastiti, K. Ganesh, M.J. de Bruijn, S. Hockman, M. van Nimwegen, G.J. Braunstahl, L. Boon, B.N. Lambrecht, V.C. Manganiello, R.W. Hendriks, and A. KleinJan. 2018. A pathophysiological role of PDE3 in allergic airway inflammation. *JCI Insight*. 3.

Bhavsar, P., M. Hew, N. Khorasani, A. Torrego, P.J. Barnes, I. Adcock, and K.F. Chung. 2008. Relative corticosteroid insensitivity of alveolar macrophages in severe asthma compared with non-severe asthma. *Thorax*. 63:784-790.

Biesbroek, G., E. Tsivtsivadze, E.A. Sanders, R. Montijn, R.H. Veenhoven, B.J. Keijser, and D. Bogaert. 2014. Early respiratory microbiota composition determines bacterial succession patterns and respiratory health in children. *Am J Respir Crit Care Med*. 190:1283-1292.

Bingle, L., S.S. Cross, A.S. High, W.A. Wallace, D. Rassl, G. Yuan, I. Hellstrom, M.A. Campos, and C.D. Bingle. 2006. WFDC2 (HE4): a potential role in the innate immunity of the oral cavity and respiratory tract and the development of adenocarcinomas of the lung. *Respir Res*. 7:61.

Bisgaard, H., M.N. Hermansen, K. Bonnelykke, J. Stokholm, F. Baty, N.L. Skytt, J. Aniscenko, T. Kebadze, and S.L. Johnston. 2010. Association of bacteria and viruses with wheezy episodes in young children: prospective birth cohort study. *BMJ*. 341:c4978.

Bisgaard, H., M.N. Hermansen, F. Buchvald, L. Loland, L.B. Halkjaer, K. Bonnelykke, M. Brasholt, A. Heltberg, N.H. Vissing, S.V. Thorsen, M. Stage, and C.B. Pipper. 2007. Childhood asthma after bacterial colonization of the airway in neonates. *N Engl J Med*. 357:1487-1495.

Bisgaard, H., N. Li, K. Bonnelykke, B.L. Chawes, T. Skov, G. Paludan-Muller, J. Stokholm, B. Smith, and K.A. Krogfelt. 2011. Reduced diversity of the intestinal microbiota during infancy is associated with increased risk of allergic disease at school age. *J Allergy Clin Immunol*. 128:646-652 e641-645.

Blakey, J., E. Halapi, U.S. Bjornsdottir, A. Wheatley, S. Kristinsson, R. Upmanyu, K. Stefansson, H. Hakonarson, and I.P. Hall. 2005. Contribution of ADAM33 polymorphisms to the population risk of asthma. *Thorax*. 60:274-276.

Bogaert, D., B. Keijser, S. Huse, J. Rossen, R. Veenhoven, E. van Gils, J. Bruin, R. Montijn, M. Bonten, and E. Sanders. 2011. Variability and diversity of nasopharyngeal microbiota in children: a metagenomic analysis. *PLoS One*. 6:e17035.

Boggy, G.J., G.W. McElfresh, E. Mahyari, A.B. Ventura, S.G. Hansen, L.J. Picker, and B.N. Bimber. 2022. BFF and cellhashR: analysis tools for accurate demultiplexing of cell hashing data. *Bioinformatics*. 38:2791-2801.

Bonnelykke, K., N.H. Vissing, A. Sevelsted, S.L. Johnston, and H. Bisgaard. 2015. Association between respiratory infections in early life and later asthma is independent of virus type. *J Allergy Clin Immunol*. 136:81-86 e84.

Bose, S., G.B. Diette, H. Woo, K. Koehler, K. Romero, A.M. Rule, B. Detrick, E. Brigham, M.C. McCormack, and N.N. Hansel. 2019. Vitamin D Status Modifies the Response to Indoor Particulate Matter in Obese Urban Children with Asthma. *J Allergy Clin Immunol Pract*. 7:1815-1822 e1812.

Bosnar, M., S. Cuzic, B. Bosnjak, K. Nujic, G. Ergovic, N. Marjanovic, I. Pasalic, B. Hrvacic, D. Polancec, I. Glojnaric, and V. Erakovic Haber. 2011. Azithromycin inhibits macrophage interleukin-1beta production through inhibition of activator protein-1 in lipopolysaccharide-induced murine pulmonary neutrophilia. *Int Immunopharmacol*. 11:424-434.

Boulet, L.P., H. Turcotte, O. Turcot, and J. Chakir. 2003. Airway inflammation in asthma with incomplete reversibility of airflow obstruction. *Respir Med*. 97:739-744.

Boutet, M., Z. Benet, E. Guillen, C. Koch, S. M'Homa Soudja, F. Delahaye, D. Fooksman, and G. Lauvau. 2021. Memory CD8(+) T cells mediate early pathogen-specific protection

via localized delivery of chemokines and IFNgamma to clusters of monocytes. *Sci Adv*. 7:eabf9975.

Brightling, C.E., P. Bradding, F.A. Symon, S.T. Holgate, A.J. Wardlaw, and I.D. Pavord. 2002. Mast-cell infiltration of airway smooth muscle in asthma. *N Engl J Med*. 346:1699-1705.

Brown, M.A., M. Jabeen, G. Bharj, and T.S.C. Hinks. 2022. Non-typeable Haemophilus influenzae airways infection: the next treatable trait in asthma? *Eur Respir Rev*. 31.

Brykczynska, U., M. Geigges, S.J. Wiedemann, E. Dror, M. Boni-Schnetzler, C. Hess, M.Y. Donath, and R. Paro. 2020. Distinct Transcriptional Responses across Tissue-Resident Macrophages to Short-Term and Long-Term Metabolic Challenge. *Cell Rep*. 30:1627-1643 e1627.

BTS/NICE/SIGN. 2024. Joint Guideline for the Diagnosis, Monitoring and Management of Chronic Asthma.

Busse, W.W., S.E. Wenzel, T.B. Casale, J.M. FitzGerald, M.S. Rice, N. Daizadeh, Y. Deniz, N. Patel, S. Harel, P.J. Rowe, N.M.H. Graham, T. O'Riordan, and I.D. Pavord. 2021. Baseline FeNO as a prognostic biomarker for subsequent severe asthma exacerbations in patients with uncontrolled, moderate-to-severe asthma receiving placebo in the LIBERTY ASTHMA QUEST study: a post-hoc analysis. *Lancet Respir Med*. 9:1165-1173.

Campbell, C.D., C. Barnett, and I. Sulaiman. 2022. A clinicians' review of the respiratory microbiome. *Breathe (Sheff)*. 18:210161.

Canas, J.A., B. Sastre, J.M. Rodrigo-Munoz, M. Fernandez-Nieto, P. Barranco, S. Quirce, J. Sastre, and V. Del Pozo. 2018. Eosinophil-derived exosomes contribute to asthma remodelling by activating structural lung cells. *Clin Exp Allergy*. 48:1173-1185.

Capitano, B., H.M. Mattoes, E. Shore, A. O'Brien, S. Braman, C. Sutherland, and D.P. Nicolau. 2004. Steady-state intrapulmonary concentrations of moxifloxacin, levofloxacin, and azithromycin in older adults. *Chest*. 125:965-973.

Carrasco, K., A. Boufenzer, L. Jolly, H. Le Cordier, G. Wang, A.J. Heck, A. Cerwenka, E. Vinolo, A. Nazabal, A. Kriznik, P. Launay, S. Gibot, and M. Derive. 2019. TREM-1 multimerization is essential for its activation on monocytes and neutrophils. *Cell Mol Immunol*. 16:460-472.

Caruso, V., X. Song, M. Asquith, and L. Karstens. 2019. Performance of Microbiome Sequence Inference Methods in Environments with Varying Biomass. *mSystems*. 4.

Cassol, I., M. Ibanez, and J.P. Bustamante. 2025. Key features and guidelines for the application of microbial alpha diversity metrics. *Sci Rep*. 15:622.

Castro-Alcaraz, S., V. Miskolci, B. Kalasapudi, D. Davidson, and I. Vancurova. 2002. NF-kappa B regulation in human neutrophils by nuclear I kappa B alpha: correlation to apoptosis. *J Immunol*. 169:3947-3953.

Chang, H., K.Y. He, C. Li, Y.Y. Ni, M.N. Li, L. Chen, M. Hou, Z. Zhou, Z.P. Xu, and M.J. Ji. 2020. P21 activated kinase-1 (PAK1) in macrophages is required for promotion of Th17 cell response during helminth infection. *J Cell Mol Med*. 24:14325-14338.

Chapman, R., L. Jones, A. D'Angelo, A. Suliman, M. Anwar, and S. Bagby. 2023. Nanopore-Based Metagenomic Sequencing in Respiratory Tract Infection: A Developing Diagnostic Platform. *Lung*. 201:171-179.

Charalampous, T., A. Alcolea-Medina, L.B. Snell, C. Alder, M. Tan, T.G.S. Williams, N. Al-Yaakoubi, G. Humayun, C.I.S. Meadows, D.L.A. Wyncoll, R. Paul, C.J. Hemsley, D. Jeyaratnam, W. Newsholme, S. Goldenberg, A. Patel, F. Tucker, G. Nebbia, M. Wilks, M. Chand, P.R. Cliff, R. Batra, J. O'Grady, N.A. Barrett, and J.D. Edgeworth. 2024. Routine Metagenomics Service for ICU Patients with Respiratory Infection. *Am J Respir Crit Care Med*. 209:164-174.

Charalampous, T., G.L. Kay, H. Richardson, A. Aydin, R. Baldan, C. Jeanes, D. Rae, S. Grundy, D.J. Turner, J. Wain, R.M. Leggett, D.M. Livermore, and J. O'Grady. 2019. Nanopore metagenomics enables rapid clinical diagnosis of bacterial lower respiratory infection. *Nat Biotechnol*. 37:783-792.

Charlson, E.S., K. Bittinger, A.R. Haas, A.S. Fitzgerald, I. Frank, A. Yadav, F.D. Bushman, and R.G. Collman. 2011. Topographical continuity of bacterial populations in the healthy human respiratory tract. *Am J Respir Crit Care Med*. 184:957-963.

Charlson, E.S., J. Chen, R. Custers-Allen, K. Bittinger, H. Li, R. Sinha, J. Hwang, F.D. Bushman, and R.G. Collman. 2010. Disordered microbial communities in the upper respiratory tract of cigarette smokers. *PLoS One*. 5:e15216.

Chaudhuri, R., E. Livingston, A.D. McMahon, L. Thomson, W. Borland, and N.C. Thomson. 2003. Cigarette smoking impairs the therapeutic response to oral corticosteroids in chronic asthma. *Am J Respir Crit Care Med*. 168:1308-1311.

Chen, H.C., Y.C. Chen, T.N. Wang, W.F. Fang, Y.C. Chang, Y.M. Chen, I.Y. Chen, M.C. Lin, and M.Y. Yang. 2021. Disrupted Expression of Circadian Clock Genes in Patients with Bronchial Asthma. *J Asthma Allergy*. 14:371-380.

Chen, J., R. Zhang, X. Dong, L. Lin, Y. Zhu, J. He, D.C. Christiani, Y. Wei, and F. Chen. 2019. shinyBN: an online application for interactive Bayesian network inference and visualization. *BMC Bioinformatics*. 20:711.

Chen, M., S. He, P. Miles, C. Li, Y. Ge, X. Yu, L. Wang, W. Huang, X. Kong, S. Ma, Y. Li, Q. Jiang, W. Zhang, and C. Cao. 2022. Nasal Bacterial Microbiome Differs Between Healthy Controls and Those With Asthma and Allergic Rhinitis. *Front Cell Infect Microbiol*. 12:841995.

Chen, T., C.A. Tibbitt, X. Feng, J.M. Stark, L. Rohrbeck, L. Rausch, S.K. Sedimbi, M.C.I. Karlsson, B.N. Lambrecht, G.B. Karlsson Hedestam, R.W. Hendriks, B.J. Chambers, S. Nylen, and J.M. Coquet. 2017. PPAR-gamma promotes type 2 immune responses in allergy and nematode infection. *Sci Immunol*. 2.

Chen, X., Y. Gao, J. Xie, H. Hua, C. Pan, J. Huang, M. Jing, X. Chen, C. Xu, Y. Gao, and P. Li. 2023. Identification of FCN1 as a novel macrophage infiltration-associated biomarker for diagnosis of pediatric inflammatory bowel diseases. *J Transl Med*. 21:203.

Cheng, H., Y. Sun, Q. Yang, M. Deng, Z. Yu, G. Zhu, J. Qu, L. Liu, L. Yang, and Y. Xia. 2022. A rapid bacterial pathogen and antimicrobial resistance diagnosis workflow using Oxford nanopore adaptive sequencing method. *Brief Bioinform*. 23.

Choi, S., K.H. Sohn, J.W. Jung, M.G. Kang, M.S. Yang, S. Kim, J.H. Choi, S.H. Cho, H.R. Kang, and H. Yi. 2021. Lung virome: New potential biomarkers for asthma severity and exacerbation. *J Allergy Clin Immunol*. 148:1007-1015 e1009.

Chu, V.T., A. Tsitsiklis, E. Mick, L. Ambroggio, K.L. Kalantar, A. Glascock, C.M. Osborne, B.D. Wagner, M.A. Matthay, J.L. DeRisi, C.S. Calfee, P.M. Mourani, and C.R. Langelier. 2024. The antibiotic resistance reservoir of the lung microbiome expands with age in a population of critically ill patients. *Nat Commun*. 15:92.

Chung, E.H., Y. Jia, H. Ohnishi, K. Takeda, D.Y. Leung, E.R. Sutherland, A. Dakhama, R.J. Martin, and E.W. Gelfand. 2014a. Leukotriene B4 receptor 1 is differentially expressed on peripheral T cells of steroid-sensitive and -resistant asthmatics. *Ann Allergy Asthma Immunol*. 112:211-216 e211.

Chung, K.F., S.E. Wenzel, J.L. Brozek, A. Bush, M. Castro, P.J. Sterk, I.M. Adcock, E.D. Bateman, E.H. Bel, E.R. Bleecker, L.P. Boulet, C. Brightling, P. Chanez, S.E. Dahlen, R. Djukanovic, U. Frey, M. Gaga, P. Gibson, Q. Hamid, N.N. Jajour, T. Mauad, R.L. Sorkness, and W.G. Teague. 2014b. International ERS/ATS guidelines on definition, evaluation and treatment of severe asthma. *Eur Respir J*. 43:343-373.

Clementi, C.F., and T.F. Murphy. 2011. Non-typeable Haemophilus influenzae invasion and persistence in the human respiratory tract. *Front Cell Infect Microbiol*. 1:1.

Collaborators, G.B.D.C.R.D. 2017. Global, regional, and national deaths, prevalence, disability-adjusted life years, and years lived with disability for chronic obstructive pulmonary disease and asthma, 1990-2015: a systematic analysis for the Global Burden of Disease Study 2015. *Lancet Respir Med*. 5:691-706.

Collins, S., L.A. Wolfraim, C.G. Drake, M.R. Horton, and J.D. Powell. 2006. Cutting Edge: TCR-induced NAB2 enhances T cell function by coactivating IL-2 transcription. *J Immunol*. 177:8301-8305.

Corren, J., J.R. Parnes, L. Wang, M. Mo, S.L. Roseti, J.M. Griffiths, and R. van der Merwe. 2017. Tezepelumab in Adults with Uncontrolled Asthma. *N Engl J Med*. 377:936-946.

Costa, C., G. Germena, E.L. Martin-Conte, I. Molineris, E. Bosco, S. Marengo, O. Azzolino, F. Altruda, V.M. Ranieri, and E. Hirsch. 2011. The RacGAP ArhGAP15 is a master negative regulator of neutrophil functions. *Blood*. 118:1099-1108.

Couillard, S., W.I.H. Do, R. Beasley, T.S.C. Hinks, and I.D. Pavord. 2022a. Predicting the benefits of type-2 targeted anti-inflammatory treatment with the prototype Oxford Asthma Attack Risk Scale (ORACLE). *ERJ Open Res*. 8.

Couillard, S., I.D. Pavord, L.G. Heaney, N. Petousi, and T.S.C. Hinks. 2022b. Sub-stratification of type-2 high airway disease for therapeutic decision-making: A 'bomb' (blood eosinophils) meets 'magnet' (FeNO) framework. *Respirology*. 27:573-577.

Couillard, S., R. Shrimanker, R. Chaudhuri, A.H. Mansur, L.P. McGarvey, L.G. Heaney, S.J. Fowler, P. Bradding, I.D. Pavord, and T.S.C. Hinks. 2021. Fractional Exhaled Nitric Oxide Nonsuppression Identifies Corticosteroid-Resistant Type 2 Signaling in Severe Asthma. *Am J Respir Crit Care Med*. 204:731-734.

Couves, E.C., S. Gardner, T.B. Voisin, J.K. Bickel, P.J. Stansfeld, E.W. Tate, and D. Bubeck. 2023. Structural basis for membrane attack complex inhibition by CD59. *Nat Commun*. 14:890.

Craig, J.E., A. Cliffe, K. Garnett, and N.J. High. 2001. Survival of nontypeable Haemophilus influenzae in macrophages. *FEMS Microbiol Lett*. 203:55-61.

Crisford, H., E. Sapey, G.B. Rogers, S. Taylor, P. Nagakumar, R. Lokwani, and J.L. Simpson. 2021. Neutrophils in asthma: the good, the bad and the bacteria. *Thorax*. 76:835-844.

Culic, O., V. Erakovic, I. Cepelak, K. Barisic, K. Brajsa, Z. Ferencic, R. Galovic, I. Glojnaric, Z. Manojlovic, V. Munic, R. Novak-Mircetic, V. Pavicic-Beljak, M. Sucic, M. Veljaca, T. Zanic-Grubisic, and M.J. Parnham. 2002. Azithromycin modulates neutrophil function and circulating inflammatory mediators in healthy human subjects. *Eur J Pharmacol*. 450:277-289.

Daenas, C., A.A. Hatziefthimiou, K.I. Gourgoulianis, and P.A. Molyvdas. 2006. Azithromycin has a direct relaxant effect on precontracted airway smooth muscle. *Eur J Pharmacol*. 553:280-287.

Dann, E., N.C. Henderson, S.A. Teichmann, M.D. Morgan, and J.C. Marioni. 2022. Differential abundance testing on single-cell data using k-nearest neighbor graphs. *Nat Biotechnol*. 40:245-253.

Davis, M.F., R.D. Peng, M.C. McCormack, and E.C. Matsui. 2015. Staphylococcus aureus colonization is associated with wheeze and asthma among US children and young adults. *J Allergy Clin Immunol*. 135:811-813 e815.

de Steenhuijsen Piters, W.A., E.G. Huijskens, A.L. Wyllie, G. Biesbroek, M.R. van den Bergh, R.H. Veenhoven, X. Wang, K. Trzcinski, M.J. Bonten, J.W. Rossen, E.A. Sanders, and D. Bogaert. 2016. Dysbiosis of upper respiratory tract microbiota in elderly pneumonia patients. *ISME J*. 10:97-108.

Deacon, K., and A.J. Knox. 2015. Human airway smooth muscle cells secrete amphiregulin via bradykinin/COX-2/PGE2, inducing COX-2, CXCL8, and VEGF expression in airway epithelial cells. *Am J Physiol Lung Cell Mol Physiol*. 309:L237-249.

Delacher, M., L. Schmidleithner, M. Simon, P. Stuve, L. Sanderink, A. Hotz-Wagenblatt, M. Wuttke, K. Schambeck, B. Ruhland, V. Hofmann, S. Bittner, U. Ritter, A. Pant, S.S. Helbich, M. Voss, N.A. Lemmermann, L. Bessiri-Schake, T. Bohn, A. Eigenberger, A.N. Menevse, C. Gebhard, N. Strieder, H. Abken, M. Rehli, J. Huehn, P. Beckhove, T. Hehlgans, H. Junger, E.K. Geissler, L. Prantl, J.M. Werner, C. Schmidl, B. Brors, C.D. Imbusch, and M. Feuerer. 2024. The effector program of human CD8 T cells supports tissue remodeling. *J Exp Med*. 221.

Demir, S., G. Wolff, A. Wieder, A. Maida, L. Buhler, M. Brune, O. Hautzinger, A. Feuchtinger, T. Poth, J. Szendroedi, S. Herzig, and B. Ekim Ustunel. 2022. TSC22D4 interacts with Akt1 to regulate glucose metabolism. *Sci Adv*. 8:eabo5555.

Denner, D.R., N. Sangwan, J.B. Becker, D.K. Hogarth, J. Oldham, J. Castillo, A.I. Sperling, J. Solway, E.T. Naureckas, J.A. Gilbert, and S.R. White. 2016. Corticosteroid therapy and

airflow obstruction influence the bronchial microbiome, which is distinct from that of bronchoalveolar lavage in asthmatic airways. *J Allergy Clin Immunol*. 137:1398-1405 e1393.

Denny, F.W. 1974. Effect of a toxin produced by Haemophilus influenzae on ciliated respiratory epithelium. *J Infect Dis*. 129:93-100.

Devilliers, M.A., A. Brisebarre, L.M.G. Petit, M. Polette, G. Deslee, R. Djukanovic, V. Dormoy, J.M. Perotin, and U.B. consortium. 2024. Airway epithelial cell cilia transcriptomic dysregulation is associated with the inflammatory phenotype in asthma. *Allergy*. 79:1982-1988.

Diamant, Z., S. Vijverberg, K. Alving, A. Bakirtas, L. Bjermer, A. Custovic, S.E. Dahlen, M. Gaga, R. Gerth van Wijk, S.D. Giacco, E. Hamelmann, L.G. Heaney, E. Heffler, O. Kalayci, K. Kostikas, R. Lutter, A.C. Olin, S. Sergejeva, A. Simpson, P.J. Sterk, E. Tufvesson, I. Agache, and S.F. Seys. 2019. Toward clinically applicable biomarkers for asthma: An EAACI position paper. *Allergy*. 74:1835-1851.

Dicker, A.J., M.L. Crichton, E.G. Pumphrey, A.J. Cassidy, G. Suarez-Cuartin, O. Sibila, E. Furrie, C.J. Fong, W. Ibrahim, G. Brady, G.G. Einarsson, J.S. Elborn, S. Schembri, S.E. Marshall, C.N.A. Palmer, and J.D. Chalmers. 2018. Neutrophil extracellular traps are associated with disease severity and microbiota diversity in patients with chronic obstructive pulmonary disease. *J Allergy Clin Immunol*. 141:117-127.

Dickson, R.P., J.R. Erb-Downward, C.M. Freeman, L. McCloskey, J.M. Beck, G.B. Huffnagle, and J.L. Curtis. 2015. Spatial Variation in the Healthy Human Lung Microbiome and the Adapted Island Model of Lung Biogeography. *Ann Am Thorac Soc*. 12:821-830.

Dickson, R.P., J.R. Erb-Downward, and G.B. Huffnagle. 2014. Towards an ecology of the lung: new conceptual models of pulmonary microbiology and pneumonia pathogenesis. *Lancet Respir Med*. 2:238-246.

Dickson, R.P., J.R. Erb-Downward, F.J. Martinez, and G.B. Huffnagle. 2016. The Microbiome and the Respiratory Tract. *Annu Rev Physiol*. 78:481-504.

Diver, S., K. Haldar, P.J. McDowell, J. Busby, V. Mistry, C. Micieli, V. Brown, C. Cox, F. Yang, C. Borg, R. Shrimanker, M.Y. Ramsheh, T. Hardman, J. Arron, P. Bradding, D. Cowan, A.H. Mansur, S.J. Fowler, J. Lordan, A. Menzies-Gow, D. Robinson, J. Matthews, I.D. Pavord, R. Chaudhuri, L.G. Heaney, M.R. Barer, C. Brightling, and P. Medical Research Council: Refractory Asthma Stratification. 2022. Relationship between inflammatory status and microbial composition in severe asthma and during exacerbation. *Allergy*. 77:3362-3376.

Diver, S., M. Richardson, K. Haldar, M.A. Ghebre, M.Y. Ramsheh, M. Bafadhel, D. Desai, E.S. Cohen, P. Newbold, L. Rapley, P. Rugman, I.D. Pavord, R.D. May, M. Barer, and C.E. Brightling. 2020. Sputum microbiomic clustering in asthma and chronic obstructive pulmonary disease reveals a Haemophilus-predominant subgroup. *Allergy*. 75:808-817.

Djukanovic, R., P.J. Sterk, J.V. Fahy, and F.E. Hargreave. 2002. Standardised methodology of sputum induction and processing. *Eur Respir J Suppl*. 37:1s-2s.

Du Rand, I.A., J. Blaikley, R. Booton, N. Chaudhuri, V. Gupta, S. Khalid, S. Mandal, J. Martin, J. Mills, N. Navani, N.M. Rahman, J.M. Wrightson, M. Munavvar, and G. British Thoracic Society Bronchoscopy Guideline. 2013. British Thoracic Society guideline for diagnostic flexible bronchoscopy in adults: accredited by NICE. *Thorax*. 68 Suppl 1:i1-i44.

Dua, B., R.M. Watson, G.M. Gauvreau, and P.M. O'Byrne. 2010. Myeloid and plasmacytoid dendritic cells in induced sputum after allergen inhalation in subjects with asthma. *J Allergy Clin Immunol*. 126:133-139.

Dulanto Chiang, A., and J.P. Dekker. 2020. From the Pipeline to the Bedside: Advances and Challenges in Clinical Metagenomics. *J Infect Dis*. 221:S331-S340.

Dumont, C., A. Corsoni-Tadrzak, S. Ruf, J. de Boer, A. Williams, M. Turner, D. Kioussis, and V.L. Tybulewicz. 2009. Rac GTPases play critical roles in early T-cell development. *Blood*. 113:3990-3998.

Dunican, E.M., B.M. Elicker, D.S. Gierada, S.K. Nagle, M.L. Schiebler, J.D. Newell, W.W. Raymond, M.E. Lachowicz-Scroggins, S. Di Maio, E.A. Hoffman, M. Castro, S.B. Fain, N.N. Jarjour, E. Israel, B.D. Levy, S.C. Erzurum, S.E. Wenzel, D.A. Meyers, E.R. Bleecker, B.R. Phillips, D.T. Mauger, E.D. Gordon, P.G. Woodruff, M.C. Peters, J.V. Fahy, L. National Heart, and P. Blood Institute Severe Asthma Research. 2018. Mucus plugs in patients with asthma linked to eosinophilia and airflow obstruction. *J Clin Invest*. 128:997-1009.

Durack, J., L.S. Christian, S. Nariya, J. Gonzalez, N.R. Bhakta, K.M. Ansel, A. Beigelman, M. Castro, A.M. Dyer, E. Israel, M. Kraft, R.J. Martin, D.T. Mauger, S.P. Peters, S.R. Rosenberg, C.A. Sorkness, M.E. Wechsler, S.E. Wenzel, S.R. White, S.V. Lynch, H.A. Boushey, Y.J. Huang, L. National Heart, and A. Blood Institute's. 2020. Distinct associations of sputum and oral microbiota with atopic, immunologic, and clinical features in mild asthma. *J Allergy Clin Immunol*. 146:1016-1026.

Durack, J., Y.J. Huang, S. Nariya, L.S. Christian, K.M. Ansel, A. Beigelman, M. Castro, A.M. Dyer, E. Israel, M. Kraft, R.J. Martin, D.T. Mauger, S.R. Rosenberg, T.S. King, S.R. White, L.C. Denlinger, F. Holguin, S.C. Lazarus, N. Lugogo, S.P. Peters, L.J. Smith, M.E. Wechsler, S.V. Lynch, H.A. Boushey, L. National Heart, and A. Blood Institute's. 2018a. Bacterial biogeography of adult airways in atopic asthma. *Microbiome*. 6:104.

Durack, J., N.E. Kimes, D.L. Lin, M. Rauch, M. McKean, K. McCauley, A.R. Panzer, J.S. Mar, M.D. Cabana, and S.V. Lynch. 2018b. Delayed gut microbiota development in high-risk for asthma infants is temporarily modifiable by Lactobacillus supplementation. *Nat Commun*. 9:707.

Durack, J., S.V. Lynch, S. Nariya, N.R. Bhakta, A. Beigelman, M. Castro, A.M. Dyer, E. Israel, M. Kraft, R.J. Martin, D.T. Mauger, S.R. Rosenberg, T. Sharp-King, S.R. White, P.G. Woodruff, P.C. Avila, L.C. Denlinger, F. Holguin, S.C. Lazarus, N. Lugogo, W.C. Moore, S.P. Peters, L. Que, L.J. Smith, C.A. Sorkness, M.E. Wechsler, S.E. Wenzel, H.A. Boushey, Y.J. Huang, L. National Heart, and A. Blood Institute's. 2017. Features of the bronchial bacterial microbiome associated with atopy, asthma, and responsiveness to inhaled corticosteroid treatment. *J Allergy Clin Immunol*. 140:63-75.

El-Gammal, A., J.P. Oliveria, K. Howie, R. Watson, P. Mitchell, R. Chen, A. Baatjes, S. Smith, D. Al-Sajee, T.J. Hawke, K.J. Killian, G.M. Gauvreau, and P.M. O'Byrne. 2016. Allergen-induced Changes in Bone Marrow and Airway Dendritic Cells in Subjects with Asthma. *Am J Respir Crit Care Med*. 194:169-177.

Erb-Downward, J.R., D.L. Thompson, M.K. Han, C.M. Freeman, L. McCloskey, L.A. Schmidt, V.B. Young, G.B. Toews, J.L. Curtis, B. Sundaram, F.J. Martinez, and G.B. Huffnagle. 2011. Analysis of the lung microbiome in the "healthy" smoker and in COPD. *PLoS One*. 6:e16384.

Faden, H., L. Duffy, A. Williams, D.A. Krystofik, and J. Wolf. 1995. Epidemiology of nasopharyngeal colonization with nontypeable Haemophilus influenzae in the first 2 years of life. *J Infect Dis*. 172:132-135.

Fage, C., A. Pizzorno, C. Rheaume, Y. Abed, and G. Boivin. 2017. The combination of oseltamivir with azithromycin does not show additional benefits over oseltamivir monotherapy in mice infected with influenza A(H1N1)pdm2009 virus. *J Med Virol*. 89:2239-2243.

Fan, L.C., J.L. Lin, J.W. Yang, B. Mao, H.W. Lu, B.X. Ge, A.M.K. Choi, and J.F. Xu. 2017. Macrolides protect against Pseudomonas aeruginosa infection via inhibition of inflammasomes. *Am J Physiol Lung Cell Mol Physiol*. 313:L677-L686.

Finak, G., A. McDavid, M. Yajima, J. Deng, V. Gersuk, A.K. Shalek, C.K. Slichter, H.W. Miller, M.J. McElrath, M. Prlic, P.S. Linsley, and R. Gottardo. 2015. MAST: a flexible statistical framework for assessing transcriptional changes and characterizing heterogeneity in single-cell RNA sequencing data. *Genome Biol*. 16:278.

Fischer, C.D., J.K. Beatty, C.G. Zvaigzne, D.W. Morck, M.J. Lucas, and A.G. Buret. 2011. Anti-Inflammatory benefits of antibiotic-induced neutrophil apoptosis: tulathromycin induces caspase-3-dependent neutrophil programmed cell death and inhibits NF-kappaB signaling and CXCL8 transcription. *Antimicrob Agents Chemother*. 55:338-348.

Folsgaard, N.V., S. Schjorring, B.L. Chawes, M.A. Rasmussen, K.A. Krogfelt, S. Brix, and H. Bisgaard. 2013. Pathogenic bacteria colonizing the airways in asymptomatic neonates stimulates topical inflammatory mediator release. *Am J Respir Crit Care Med*. 187:589-595.

Fonkou, M.D.M., M. Bilen, F. Cadoret, P.E. Fournier, G. Dubourg, and D. Raoult. 2018. 'Enterococcus timonensis' sp. nov., 'Actinomyces marseillensis' sp. nov., 'Leptotrichia massiliensis' sp. nov., 'Actinomyces pacaensis' sp. nov., 'Actinomyces oralis' sp. nov., 'Actinomyces culturomici' sp. nov. and 'Gemella massiliensis' sp. nov., new bacterial species isolated from the human respiratory microbiome. *New Microbes New Infect*. 22:37-43.

Fotouhi-Ardakani, N., D.E. Kebir, N. Pierre-Charles, L. Wang, S.P. Ahern, J.G. Filep, and E. Milot. 2010. Role for myeloid nuclear differentiation antigen in the regulation of neutrophil apoptosis during sepsis. *Am J Respir Crit Care Med*. 182:341-350.

Fraczek, M.G., L. Chishimba, R.M. Niven, M. Bromley, A. Simpson, L. Smyth, D.W. Denning, and P. Bowyer. 2018. Corticosteroid treatment is associated with increased filamentous fungal burden in allergic fungal disease. *J Allergy Clin Immunol*. 142:407-414.

Frank, D.N., L.M. Feazel, M.T. Bessesen, C.S. Price, E.N. Janoff, and N.R. Pace. 2010. The human nasal microbiota and Staphylococcus aureus carriage. *PLoS One*. 5:e10598.

Freihat, L.A., J.I. Wheeler, A. Wong, I. Turek, D.T. Manallack, and H.R. Irving. 2019. IRAK3 modulates downstream innate immune signalling through its guanylate cyclase activity. *Sci Rep*. 9:15468.

Fuchs, T.A., U. Abed, C. Goosmann, R. Hurwitz, I. Schulze, V. Wahn, Y. Weinrauch, V. Brinkmann, and A. Zychlinsky. 2007. Novel cell death program leads to neutrophil extracellular traps. *J Cell Biol*. 176:231-241.

Fujimura, K.E., A.R. Sitarik, S. Havstad, D.L. Lin, S. Levan, D. Fadrosh, A.R. Panzer, B. LaMere, E. Rackaityte, N.W. Lukacs, G. Wegienka, H.A. Boushey, D.R. Ownby, E.M. Zoratti, A.M. Levin, C.C. Johnson, and S.V. Lynch. 2016. Neonatal gut microbiota associates with childhood multisensitized atopy and T cell differentiation. *Nat Med*. 22:1187-1191.

Gan, M., B. Wu, G. Yan, G. Li, L. Sun, G. Lu, and W. Zhou. 2021. Combined nanopore adaptive sequencing and enzyme-based host depletion efficiently enriched microbial sequences and identified missing respiratory pathogens. *BMC Genomics*. 22:732.

Gao, P., P.G. Gibson, K.J. Baines, I.A. Yang, J.W. Upham, P.N. Reynolds, S. Hodge, A.L. James, C. Jenkins, M.J. Peters, J. Zhang, and J.L. Simpson. 2015. Anti-inflammatory deficiencies in neutrophilic asthma: reduced galectin-3 and IL-1RA/IL-1beta. *Respir Res*. 16:5.

Garrido-Trigo, A., A.M. Corraliza, M. Veny, I. Dotti, E. Melon-Ardanaz, A. Rill, H.L. Crowell, A. Corbi, V. Gudino, M. Esteller, I. Alvarez-Teubel, D. Aguilar, M.C. Masamunt, E. Killingbeck, Y. Kim, M. Leon, S. Visvanathan, D. Marchese, G. Caratu, A. Martin-Cardona, M. Esteve, I. Ordas, J. Panes, E. Ricart, E. Mereu, H. Heyn, and A. Salas. 2023. Macrophage and neutrophil heterogeneity at single-cell spatial resolution in human inflammatory bowel disease. *Nat Commun*. 14:4506.

Gerke, V., and S.E. Moss. 2002. Annexins: from structure to function. *Physiol Rev*. 82:331-371.

Gessner, B.D., and R.A. Adegbola. 2008. The impact of vaccines on pneumonia: key lessons from Haemophilus influenzae type b conjugate vaccines. *Vaccine*. 26 Suppl 2:B3-8.

Gibson, P.G., I.A. Yang, J.W. Upham, P.N. Reynolds, S. Hodge, A.L. James, C. Jenkins, M.J. Peters, G.B. Marks, M. Baraket, H. Powell, S.L. Taylor, L.E.X. Leong, G.B. Rogers, and J.L. Simpson. 2017. Effect of azithromycin on asthma exacerbations and quality of life in adults with persistent uncontrolled asthma (AMAZES): a randomised, double-blind, placebo-controlled trial. *The Lancet*.

Gielen, V., S.L. Johnston, and M.R. Edwards. 2010. Azithromycin induces anti-viral responses in bronchial epithelial cells. *Eur Respir J*. 36:646-654.

Giovannini-Chami, L., B. Marcet, C. Moreilhon, B. Chevalier, M.I. Illie, K. Lebrigand, K. Robbe-Sermesant, T. Bourrier, J.F. Michiels, B. Mari, D. Crenesse, P. Hofman, J. de Blic, L. Castillo, M. Albertini, and P. Barbry. 2012. Distinct epithelial gene expression phenotypes in childhood respiratory allergy. *Eur Respir J*. 39:1197-1205.

Gleeson, K., D.F. Eggli, and S.L. Maxwell. 1997. Quantitative aspiration during sleep in normal subjects. *Chest*. 111:1266-1272.

Global Initiative for Asthma. 2024. Global Strategy for Asthma Management and Prevention.

Goddard, A.F., B.J. Staudinger, S.E. Dowd, A. Joshi-Datar, R.D. Wolcott, M.L. Aitken, C.L. Fligner, and P.K. Singh. 2012. Direct sampling of cystic fibrosis lungs indicates that DNA-based analyses of upper-airway specimens can misrepresent lung microbiota. *Proc Natl Acad Sci U S A*. 109:13769-13774.

Goleva, E., L.P. Jackson, J.K. Harris, C.E. Robertson, E.R. Sutherland, C.F. Hall, J.T. Good, Jr., E.W. Gelfand, R.J. Martin, and D.Y. Leung. 2013. The effects of airway microbiome on corticosteroid responsiveness in asthma. *Am J Respir Crit Care Med*. 188:1193-1201.

Gomes, T., S.A. Teichmann, and C. Talavera-Lopez. 2019. Immunology Driven by Large-Scale Single-Cell Sequencing. *Trends Immunol*. 40:1011-1021.

Gong, W., X. Wang, Y. Zhang, J. Hao, C. Xing, Q. Chu, G. Wang, J. Zhao, J. Wang, Q. Dong, T. Liu, Y. Zhang, and L. Dong. 2014. Interleukin-20 promotes airway remodeling in asthma. *Inflammation*. 37:2099-2105.

Gonzalo, J.A., C.M. Lloyd, A. Peled, T. Delaney, A.J. Coyle, and J.C. Gutierrez-Ramos. 2000. Critical involvement of the chemotactic axis CXCR4/stromal cell-derived factor-1 alpha in the inflammatory component of allergic airway disease. *J Immunol*. 165:499-508.

Gopal, S.H., S. Mukherjee, and S.K. Das. 2016. Direct and Second Hand Cigarette Smoke Exposure and Development of Childhood Asthma. *J Environ Health Sci*. 2.

Gorvel, L., K. Al Moussawi, E. Ghigo, C. Capo, J.L. Mege, and B. Desnues. 2010. Tropheryma whipplei, the Whipple's disease bacillus, induces macrophage apoptosis through the extrinsic pathway. *Cell Death Dis*. 1:e34.

Granger, V., F. Zerimech, J. Arab, V. Siroux, P. de Nadai, A. Tsicopoulos, R. Matran, Z. Akiki, and R. Nadif. 2022. Blood eosinophil cationic protein and eosinophil-derived neurotoxin are associated with different asthma expression and evolution in adults. *Thorax*. 77:552-562.

Green, B.J., S. Wiriyachaiporn, C. Grainge, G.B. Rogers, V. Kehagia, L. Lau, M.P. Carroll, K.D. Bruce, and P.H. Howarth. 2014. Potentially pathogenic airway bacteria and neutrophilic inflammation in treatment resistant severe asthma. *PLoS One*. 9:e100645.

Greenman, N., S.A. Hassouneh, L.S. Abdelli, C. Johnston, and T. Azarian. 2024. Improving Bacterial Metagenomic Research through Long-Read Sequencing. *Microorganisms*. 12.

Griffiths, J.A., A.C. Richard, K. Bach, A.T.L. Lun, and J.C. Marioni. 2018. Detection and removal of barcode swapping in single-cell RNA-seq data. *Nat Commun*. 9:2667.

Group, R.C. 2021. Azithromycin in patients admitted to hospital with COVID-19 (RECOVERY): a randomised, controlled, open-label, platform trial. *Lancet*. 397:605-612.

Guarnieri, M., and J.R. Balmes. 2014. Outdoor air pollution and asthma. *Lancet*. 383:1581-1592.

Guilliams, M., F. Ginhoux, C. Jakubzick, S.H. Naik, N. Onai, B.U. Schraml, E. Segura, R. Tussiwand, and S. Yona. 2014. Dendritic cells, monocytes and macrophages: a unified nomenclature based on ontogeny. *Nat Rev Immunol*. 14:571-578.

Gulraiz, F., C. Bellinghausen, C.A. Bruggeman, and F.R. Stassen. 2015. Haemophilus influenzae increases the susceptibility and inflammatory response of airway epithelial cells to viral infections. *FASEB J*. 29:849-858.

Hagman, D.K., J.N. Kuzma, I. Larson, K.E. Foster-Schubert, L.Y. Kuan, A. Cignarella, E. Geamanu, K.W. Makar, J.R. Gottlieb, and M. Kratz. 2012. Characterizing and quantifying leukocyte populations in human adipose tissue: impact of enzymatic tissue processing. *J Immunol Methods*. 386:50-59.

Haldar, K., V. Mistry, M. Richardson, C. Hamblet, M. Jison, M.R. Barer, C. McCrae, and C.E. Brightling. 2025. Effect of benralizumab treatment on the airway microbiome in COPD. *ERJ Open Res*. 11.

Haldar, P., and I.D. Pavord. 2007. Noneosinophilic asthma: a distinct clinical and pathologic phenotype. *J Allergy Clin Immunol*. 119:1043-1052; quiz 1053-1044.

Halldorsson, S., T. Gudjonsson, M. Gottfredsson, P.K. Singh, G.H. Gudmundsson, and O. Baldursson. 2010. Azithromycin maintains airway epithelial integrity during Pseudomonas aeruginosa infection. *Am J Respir Cell Mol Biol*. 42:62-68.

Hammad, H., and B.N. Lambrecht. 2021. The basic immunology of asthma. *Cell*. 184:1469-1485.

Hao, Y., S. Hao, E. Andersen-Nissen, W.M. Mauck, 3rd, S. Zheng, A. Butler, M.J. Lee, A.J. Wilk, C. Darby, M. Zager, P. Hoffman, M. Stoeckius, E. Papalexi, E.P. Mimitou, J. Jain, A. Srivastava, T. Stuart, L.M. Fleming, B. Yeung, A.J. Rogers, J.M. McElrath, C.A. Blish, R. Gottardo, P. Smibert, and R. Satija. 2021. Integrated analysis of multimodal single-cell data. *Cell*. 184:3573-3587 e3529.

Heaney, L.G., J. Busby, P. Bradding, R. Chaudhuri, A.H. Mansur, R. Niven, I.D. Pavord, J.T. Lindsay, R.W. Costello, and U.K.R.A.S.P. Medical Research Council. 2018. Remotely Monitored Therapy and Nitric Oxide Suppression Identifies Non-Adherence in Severe Asthma. *Am J Respir Crit Care Med*.

Heikema, A.P., D. Horst-Kreft, S.A. Boers, R. Jansen, S.D. Hiltemann, W. de Koning, R. Kraaij, M.A.J. de Ridder, C.B. van Houten, L.J. Bont, A.P. Stubbs, and J.P. Hays. 2020. Comparison of Illumina versus Nanopore 16S rRNA Gene Sequencing of the Human Nasal Microbiota. *Genes (Basel)*. 11.

Hiles, S.A., V.M. McDonald, M. Guilhermino, G.G. Brusselle, and P.G. Gibson. 2019. Does maintenance azithromycin reduce asthma exacerbations? An individual participant data meta-analysis. *Eur Respir J*. 54.

Hilty, M., C. Burke, H. Pedro, P. Cardenas, A. Bush, C. Bossley, J. Davies, A. Ervine, L. Poulter, L. Pachter, M.F. Moffatt, and W.O. Cookson. 2010. Disordered microbial communities in asthmatic airways. *PLoS One*. 5:e8578.

Hilvering, B., T.S.C. Hinks, L. Stoger, E. Marchi, M. Salimi, R. Shrimanker, W. Liu, W. Chen, J. Luo, S. Go, T. Powell, J. Cane, S. Thulborn, A. Kurioka, T. Leng, J. Matthews, C. Connolly, C. Borg, M. Bafadhel, C.B. Willberg, A. Ramasamy, R. Djukanovic, G. Ogg, I.D. Pavord, P. Klenerman, and L. Xue. 2018. Synergistic activation of pro-inflammatory type-2 CD8(+) T lymphocytes by lipid mediators in severe eosinophilic asthma. *Mucosal Immunol*. 11:1408-1419.

Hinks, T.S., J.C. Wallington, A.P. Williams, R. Djukanovic, K.J. Staples, and T.M. Wilkinson. 2016a. Steroid-induced Deficiency of Mucosal-associated Invariant T Cells in the Chronic Obstructive Pulmonary Disease Lung. Implications for Nontypeable Haemophilus influenzae Infection. *Am J Respir Crit Care Med*. 194:1208-1218.

Hinks, T.S., X. Zhou, K.J. Staples, B.D. Dimitrov, A. Manta, T. Petrossian, P.Y. Lum, C.G. Smith, J.A. Ward, P.H. Howarth, A.F. Walls, S.D. Gadola, and R. Djukanovic. 2015. Innate and adaptive T cells in asthmatic patients: Relationship to severity and disease mechanisms. *J Allergy Clin Immunol*. 136:323-333.

Hinks, T.S.C., T. Brown, L.C.K. Lau, H. Rupani, C. Barber, S. Elliott, J.A. Ward, J. Ono, S. Ohta, K. Izuhara, R. Djukanovic, R.J. Kurukulaaratchy, A. Chauhan, and P.H. Howarth. 2016b. Multidimensional endotyping in patients with severe asthma reveals inflammatory heterogeneity in matrix metalloproteinases and chitinase 3-like protein 1. *J Allergy Clin Immunol*. 138:61-75.

Hinks, T.S.C., L. Cureton, R. Knight, A. Wang, J.L. Cane, V.S. Barber, J. Black, S.J. Dutton, J. Melhorn, M. Jabeen, P. Moss, R. Garlapati, T. Baron, G. Johnson, F. Cantle, D. Clarke, S. Elkhodair, J. Underwood, D. Lasserson, I.D. Pavord, S. Morgan, and D. Richards. 2021a. Azithromycin versus standard care in patients with mild-to-moderate COVID-19 (ATOMIC2): an open-label, randomised trial. *Lancet Respir Med*. 9:1130-1140.

Hinks, T.S.C., R.D. Hoyle, and E.W. Gelfand. 2019. CD8(+) Tc2 cells: underappreciated contributors to severe asthma. *Eur Respir Rev*. 28.

Hinks, T.S.C., S.J. Levine, and G.G. Brusselle. 2021b. Treatment options in type-2 low asthma. *Eur Respir J*. 57.

Hodge, S., G. Hodge, S. Brozyna, H. Jersmann, M. Holmes, and P.N. Reynolds. 2006. Azithromycin increases phagocytosis of apoptotic bronchial epithelial cells by alveolar macrophages. *Eur Respir J*. 28:486-495.

Hodge, S., G. Hodge, H. Jersmann, G. Matthews, J. Ahern, M. Holmes, and P.N. Reynolds. 2008. Azithromycin improves macrophage phagocytic function and expression of mannose receptor in chronic obstructive pulmonary disease. *Am J Respir Crit Care Med*. 178:139-148.

Holgate, S.T. 2007. Epithelium dysfunction in asthma. *J Allergy Clin Immunol*. 120:1233-1244; quiz 1245-1236.

Hondowicz, B.D., D. An, J.M. Schenkel, K.S. Kim, H.R. Steach, A.T. Krishnamurty, G.J. Keitany, E.N. Garza, K.A. Fraser, J.J. Moon, W.A. Altemeier, D. Masopust, and M. Pepper. 2016. Interleukin-2-Dependent Allergen-Specific Tissue-Resident Memory Cells Drive Asthma. *Immunity*. 44:155-166.

Hoof, I., V. Schulten, J.A. Layhadi, T. Stranzl, L.H. Christensen, S. Herrera de la Mata, G. Seumois, P. Vijayanand, C. Lundegaard, K. Niss, A. Lund, J. Ahrenfeldt, J. Holm, E. Steveling, H. Sharif, S.R. Durham, B. Peters, M.H. Shamji, and P.S. Andersen. 2020. Allergen-specific IgG(+) memory B cells are temporally linked to IgE memory responses. *J Allergy Clin Immunol*. 146:180-191.

Hoppstadter, J., and A.J. Ammit. 2019. Role of Dual-Specificity Phosphatase 1 in Glucocorticoid-Driven Anti-inflammatory Responses. *Front Immunol*. 10:1446.

Hosoki, K., A. Nakamura, K. Kainuma, M. Sugimoto, M. Nagao, Y. Hiraguchi, H. Tanida, R. Tokuda, H. Wada, T. Nobori, S. Suga, and T. Fujisawa. 2013. Differential activation of eosinophils by bacteria associated with asthma. *Int Arch Allergy Immunol*. 161 Suppl 2:16-22.

Hou, Y., D. Wei, Z. Zhang, H. Guo, S. Li, J. Zhang, P. Zhang, L. Zhang, and Y. Zhao. 2022. FABP5 controls macrophage alternative activation and allergic asthma by selectively programming long-chain unsaturated fatty acid metabolism. *Cell Rep*. 41:111668.

Huang, S.W., Y.J. Chen, S.T. Wang, L.W. Ho, J.K. Kao, M. Narita, M. Takahashi, C.Y. Wu, H.Y. Cheng, and J.J. Shieh. 2016. Azithromycin impairs TLR7 signaling in dendritic cells and improves the severity of imiquimod-induced psoriasis-like skin inflammation in mice. *J Dermatol Sci*. 84:59-70.

Huang, Y.J., S. Nariya, J.M. Harris, S.V. Lynch, D.F. Choy, J.R. Arron, and H. Boushey. 2015. The airway microbiome in patients with severe asthma: Associations with disease features and severity. *J Allergy Clin Immunol*. 136:874-884.

Huang, Y.J., C.E. Nelson, E.L. Brodie, T.Z. Desantis, M.S. Baek, J. Liu, T. Woyke, M. Allgaier, J. Bristow, J.P. Wiener-Kronish, E.R. Sutherland, T.S. King, N. Icitovic, R.J. Martin, W.J. Calhoun, M. Castro, L.C. Denlinger, E. Dimango, M. Kraft, S.P. Peters, S.I. Wasserman, M.E. Wechsler, H.A. Boushey, S.V. Lynch, L. National Heart, and N. Blood Institute's Asthma Clinical Research. 2011. Airway microbiota and bronchial hyperresponsiveness in patients with suboptimally controlled asthma. *J Allergy Clin Immunol*. 127:372-381 e371-373.

Huber, H.L., and K.K. Koessler. 1922. The pathology of bronchial asthma. *Archives of Internal Medicine*. 30:689-760.

Huxley, E.J., J. Viroslav, W.R. Gray, and A.K. Pierce. 1978. Pharyngeal aspiration in normal adults and patients with depressed consciousness. *Am J Med*. 64:564-568.

Hwang, S.S., J. Lim, Z. Yu, P. Kong, E. Sefik, H. Xu, C.C.D. Harman, L.K. Kim, G.R. Lee, H.B. Li, and R.A. Flavell. 2020. mRNA destabilization by BTG1 and BTG2 maintains T cell quiescence. *Science*. 367:1255-1260.

Ilmarinen, P., L.E. Tuomisto, O. Niemela, J. Danielsson, J. Haanpaa, T. Kankaanranta, and H. Kankaanranta. 2016. Comorbidities and elevated IL-6 associate with negative outcome in adult-onset asthma. *Eur Respir J*. 48:1052-1062.

Imamura, Y., K. Yanagihara, Y. Mizuta, M. Seki, H. Ohno, Y. Higashiyama, Y. Miyazaki, K. Tsukamoto, Y. Hirakata, K. Tomono, J. Kadota, and S. Kohno. 2004. Azithromycin

inhibits MUC5AC production induced by the Pseudomonas aeruginosa autoinducer N-(3-Oxododecanoyl) homoserine lactone in NCI-H292 Cells. *Antimicrob Agents Chemother*. 48:3457-3461.

Ishii, T., R.T. Abboud, A.M. Wallace, J.C. English, H.O. Coxson, R.J. Finley, K. Shumansky, P.D. Pare, and A.J. Sandford. 2014. Alveolar macrophage proteinase/antiproteinase expression in lung function and emphysema. *Eur Respir J*. 43:82-91.

Iwamoto, S., T. Kumamoto, E. Azuma, M. Hirayama, M. Ito, K. Amano, M. Ido, and Y. Komada. 2011. The effect of azithromycin on the maturation and function of murine bone marrow-derived dendritic cells. *Clin Exp Immunol*. 166:385-392.

Jabeen, M.F., N.D. Sanderson, D. Foster, D.W. Crook, J.L. Cane, C. Borg, C. Connolly, S. Thulborn, I.D. Pavord, P. Klenerman, T.L. Street, and T.S.C. Hinks. 2022. Identifying Bacterial Airways Infection in Stable Severe Asthma Using Oxford Nanopore Sequencing Technologies. *Microbiol Spectr*. 10:e0227921.

Jabeen, M.F., N.D. Sanderson, M. Tine, G. Donachie, C. Barber, A. Azim, L.C.K. Lau, T. Brown, I.D. Pavord, A. Chauhan, P. Klenerman, T.L. Street, E. Marchi, P.H. Howarth, and T.S.C. Hinks. 2024. Species-level, metagenomic and proteomic analysis of microbe-immune interactions in severe asthma. *Allergy*. 79:2966-2980.

Jackson, D.J., J. Busby, P.E. Pfeffer, A. Menzies-Gow, T. Brown, R. Gore, M. Doherty, A.H. Mansur, S. Message, R. Niven, M. Patel, L.G. Heaney, and U.K.S.A. Registry. 2021. Characterisation of patients with severe asthma in the UK Severe Asthma Registry in the biologic era. *Thorax*. 76:220-227.

James, A.L., J.G. Elliot, R.L. Jones, M.L. Carroll, T. Mauad, T.R. Bai, M.J. Abramson, K.O. McKay, and F.H. Green. 2012. Airway smooth muscle hypertrophy and hyperplasia in asthma. *Am J Respir Crit Care Med*. 185:1058-1064.

James, A.L., and S. Wenzel. 2007. Clinical relevance of airway remodelling in airway diseases. *Eur Respir J*. 30:134-155.

Jamieson, A.M., L. Pasman, S. Yu, P. Gamradt, R.J. Homer, T. Decker, and R. Medzhitov. 2013. Role of tissue protection in lethal respiratory viral-bacterial coinfection. *Science*. 340:1230-1234.

Jang, Y.J., H.J. Kwon, and B.J. Lee. 2006. Effect of clarithromycin on rhinovirus-16 infection in A549 cells. *Eur Respir J*. 27:12-19.

Jenkins, C.R., L.P. Boulet, K.L. Lavoie, C. Raherison-Semjen, and D. Singh. 2022. Personalized Treatment of Asthma: The Importance of Sex and Gender Differences. *J Allergy Clin Immunol Pract*. 10:963-971 e963.

Jin, J., Y. Mu, H. Zhang, I. Sturmlechner, C. Wang, R.R. Jadhav, Q. Xia, C.M. Weyand, and J.J. Goronzy. 2023. CISH impairs lysosomal function in activated T cells resulting in mitochondrial DNA release and inflammaging. *Nat Aging*. 3:600-616.

Johnson, A.P., and T.J. Inzana. 1986. Loss of ciliary activity in organ cultures of rat trachea treated with lipo-oligosaccharide from Haemophilus influenzae. *J Med Microbiol*. 22:265-268.

Johnson, J.S., D.J. Spakowicz, B.Y. Hong, L.M. Petersen, P. Demkowicz, L. Chen, S.R. Leopold, B.M. Hanson, H.O. Agresta, M. Gerstein, E. Sodergren, and G.M. Weinstock. 2019. Evaluation of 16S rRNA gene sequencing for species and strain-level microbiome analysis. *Nat Commun*. 10:5029.

Johnson, S.R. 2005. TIMP-1 in asthma: guilty by association. *Thorax*. 60:617-618.

Johnston, S.L., M. Szigeti, M. Cross, C. Brightling, R. Chaudhuri, T. Harrison, A. Mansur, L. Robison, Z. Sattar, D. Jackson, P. Mallia, E. Wong, C. Corrigan, B. Higgins, P. Ind, D. Singh, N.C. Thomson, D. Ashby, A. Chauhan, and A.T. Team. 2016. Azithromycin for Acute Exacerbations of Asthma : The AZALEA Randomized Clinical Trial. *JAMA Intern Med*. 176:1630-1637.

Juniper, E.F., J. Bousquet, L. Abetz, E.D. Bateman, and G. Committee. 2006. Identifying 'well-controlled' and 'not well-controlled' asthma using the Asthma Control Questionnaire. *Respir Med*. 100:616-621.

Juniper, E.F., K. Svensson, A.C. Mork, and E. Stahl. 2005. Measurement properties and interpretation of three shortened versions of the asthma control questionnaire. *Respir Med*. 99:553-558.

Kanda, A., Y. Yasutaka, D. Van Bui, K. Suzuki, S. Sawada, Y. Kobayashi, M. Asako, and H. Iwai. 2020. Multiple Biological Aspects of Eosinophils in Host Defense, Eosinophil-Associated Diseases, Immunoregulation, and Homeostasis: Is Their Role Beneficial, Detrimental, Regulator, or Bystander? *Biol Pharm Bull*. 43:20-30.

Kang, J.H., S.M. Hwang, and I.Y. Chung. 2015. S100A8, S100A9 and S100A12 activate airway epithelial cells to produce MUC5AC via extracellular signal-regulated kinase and nuclear factor-kappaB pathways. *Immunology*. 144:79-90.

Kang, J.Y., M.R. Jo, H.H. Kang, S.K. Kim, M.S. Kim, Y.H. Kim, S.C. Kim, S.S. Kwon, S.Y. Lee, and J.W. Kim. 2016. Long-term azithromycin ameliorates not only airway inflammation but also remodeling in a murine model of chronic asthma. *Pulm Pharmacol Ther*. 36:37-45.

Kao, C.Y., Y. Chen, P. Thai, S. Wachi, F. Huang, C. Kim, R.W. Harper, and R. Wu. 2004. IL-17 markedly up-regulates beta-defensin-2 expression in human airway epithelium via JAK and NF-kappaB signaling pathways. *J Immunol*. 173:3482-3491.

Kapellos, T.S., K. Bassler, W. Fujii, C. Nalkurthi, A.C. Schaar, L. Bonaguro, T. Pecht, I. Galvao, S. Agrawal, A. Saglam, E. Dudkin, A. Frishberg, E. de Domenico, A. Horne, C. Donovan, R.Y. Kim, D. Gallego-Ortega, T.E. Gillett, M. Ansari, J. Schulte-Schrepping, N. Offermann, I. Antignano, B. Sivri, W. Lu, M.S. Eapen, M. van Uelft, C. Osei-Sarpong, M. van den Berge, H.C. Donker, H.J.M. Groen, S.S. Sohal, J. Klein, T. Schreiber, A. Feisst, A.O. Yildirim, H.B. Schiller, M.C. Nawijn, M. Becker, K. Handler, M. Beyer, M. Capasso, T. Ulas, J. Hasenauer, C. Pizarro, F.J. Theis, P.M. Hansbro, D. Skowasch, and J.L. Schultze. 2023. Systemic alterations in neutrophils and their precursors in early-stage chronic obstructive pulmonary disease. *Cell Rep*. 42:112525.

Karvonen, A.M., P.V. Kirjavainen, M. Taubel, B. Jayaprakash, R.I. Adams, J.E. Sordillo, D.R. Gold, A. Hyvarinen, S. Remes, E. von Mutius, and J. Pekkanen. 2019. Indoor bacterial microbiota and development of asthma by 10.5 years of age. *J Allergy Clin Immunol*. 144:1402-1410.

Katoh, S. 2021. Critical Involvement of CD44 in T Helper Type 2 Cell-Mediated Eosinophilic Airway Inflammation in a Mouse Model of Acute Asthma. *Front Immunol*. 12:811600.

Kaufhold, I., S. Osbahr, K. Shima, S. Marwitz, K. Rohmann, D. Dromann, T. Goldmann, K. Dalhoff, and J. Rupp. 2017. Nontypeable Haemophilus influenzae (NTHi) directly interfere with the regulation of E-cadherin in lung epithelial cells. *Microbes Infect*. 19:560-566.

Keir, H.R., and J.D. Chalmers. 2021. IL-6 trans-signalling: how Haemophilus surfs the NET to amplify inflammation in COPD. *Eur Respir J*. 58.

Keir, H.R., A. Shoemark, A.J. Dicker, L. Perea, J. Pollock, Y.H. Giam, G. Suarez-Cuartin, M.L. Crichton, M. Lonergan, M. Oriano, E. Cant, G.G. Einarsson, E. Furrie, J.S. Elborn, C.J. Fong, S. Finch, G.B. Rogers, F. Blasi, O. Sibila, S. Aliberti, J.L. Simpson, J.T.J. Huang, and J.D. Chalmers. 2021. Neutrophil extracellular traps, disease severity, and antibiotic response in bronchiectasis: an international, observational, multicohort study. *Lancet Respir Med*. 9:873-884.

Kelly, J.T., and W.W. Busse. 2008. Host immune responses to rhinovirus: mechanisms in asthma. *J Allergy Clin Immunol*. 122:671-682.

Khair, O.A., J.L. Devalia, M.M. Abdelaziz, R.J. Sapsford, and R.J. Davies. 1995. Effect of erythromycin on Haemophilus influenzae endotoxin-induced release of IL-6, IL-8 and sICAM-1 by cultured human bronchial epithelial cells. *Eur Respir J*. 8:1451-1457.

Khalfaoui, L., F.A. Symon, S. Couillard, B. Hargadon, R. Chaudhuri, S. Bicknell, A.H. Mansur, R. Shrimanker, T.S.C. Hinks, I.D. Pavord, S.J. Fowler, V. Brown, L.P. McGarvey, L.G. Heaney, C.D. Austin, P.H. Howarth, J.R. Arron, D.F. Choy, and P. Bradding. 2022. Airway remodelling rather than cellular infiltration characterizes both type2 cytokine biomarker-high and -low severe asthma. *Allergy*. 77:2974-2986.

Khatri, S.B., J.M. Iaccarino, A. Barochia, I. Soghier, P. Akuthota, A. Brady, R.A. Covar, J.S. Debley, Z. Diamant, A.M. Fitzpatrick, D.A. Kaminsky, N.J. Kenyon, S. Khurana, B.J. Lipworth, K. McCarthy, M. Peters, L.G. Que, K.R. Ross, E.K. Schneider-Futschik, C.A. Sorkness, T.S. Hallstrand, I. American Thoracic Society Assembly on Allergy, and Inflammation. 2021. Use of Fractional Exhaled Nitric Oxide to Guide the Treatment of Asthma: An Official American Thoracic Society Clinical Practice Guideline. *Am J Respir Crit Care Med*. 204:e97-e109.

Khoyratty, T.E., Z. Ai, I. Ballesteros, H.L. Eames, S. Mathie, S. Martin-Salamanca, L. Wang, A. Hemmings, N. Willemsen, V. von Werz, A. Zehrer, B. Walzog, E. van Grinsven, A. Hidalgo, and I.A. Udalova. 2021. Distinct transcription factor networks control neutrophil-driven inflammation. *Nat Immunol*. 22:1093-1106.

Kim, D., L. Song, F.P. Breitwieser, and S.L. Salzberg. 2016. Centrifuge: rapid and sensitive classification of metagenomic sequences. *Genome Res*. 26:1721-1729.

Kim, J.H., K.H. Kim, H.Y. Woo, and J.Y. Shim. 2008. Maternal cytokine production during pregnancy and the development of childhood wheezing and allergic disease in offspring three years of age. *J Asthma*. 45:948-952.

Kim, R.Y., J.W. Pinkerton, A.T. Essilfie, A.A.B. Robertson, K.J. Baines, A.C. Brown, J.R. Mayall, M.K. Ali, M.R. Starkey, N.G. Hansbro, J.A. Hirota, L.G. Wood, J.L. Simpson, D.A. Knight, P.A. Wark, P.G. Gibson, L.A.J. O'Neill, M.A. Cooper, J.C. Horvat, and P.M. Hansbro. 2017. Role for NLRP3 Inflammasome-mediated, IL-1beta-Dependent Responses in Severe, Steroid-Resistant Asthma. *Am J Respir Crit Care Med*. 196:283-297.

Kloepfer, K.M., A.R. Deschamp, S.E. Ross, S.L. Peterson-Carmichael, C.M. Hemmerich, D.B. Rusch, and S.D. Davis. 2018. In children, the microbiota of the nasopharynx and bronchoalveolar lavage fluid are both similar and different. *Pediatr Pulmonol*. 53:475-482.

Ko, J.H., H.J. Kim, H.J. Jeong, H.J. Lee, and J.Y. Oh. 2020. Mesenchymal Stem and Stromal Cells Harness Macrophage-Derived Amphiregulin to Maintain Tissue Homeostasis. *Cell Rep*. 30:3806-3820 e3806.

Koch, S., N. Sopel, and S. Finotto. 2017. Th9 and other IL-9-producing cells in allergic asthma. *Semin Immunopathol*. 39:55-68.

Korsunsky, I., N. Millard, J. Fan, K. Slowikowski, F. Zhang, K. Wei, Y. Baglaenko, M. Brenner, P.R. Loh, and S. Raychaudhuri. 2019. Fast, sensitive and accurate integration of single-cell data with Harmony. *Nat Methods*. 16:1289-1296.

Krakowiak, K., and H.J. Durrington. 2018. The Role of the Body Clock in Asthma and COPD: Implication for Treatment. *Pulm Ther*. 4:29-43.

Kramer, E.L., E.M. Mushaben, P.A. Pastura, T.H. Acciani, G.H. Deutsch, G.K. Khurana Hershey, T.R. Korfhagen, W.D. Hardie, J.A. Whitsett, and T.D. Le Cras. 2009. Early growth response-1 suppresses epidermal growth factor receptor-mediated airway hyperresponsiveness and lung remodeling in mice. *Am J Respir Cell Mol Biol*. 41:415-425.

Kudoh, S., T. Uetake, K. Hagiwara, M. Hirayama, L.H. Hus, H. Kimura, and Y. Sugiyama. 1987. [Clinical effects of low-dose long-term erythromycin chemotherapy on diffuse panbronchiolitis]. *Nihon Kyobu Shikkan Gakkai Zasshi*. 25:632-642.

Kukan, E.N., G.L. Fabiano, and B.A. Cobb. 2024. Siglecs as modulators of macrophage phenotype and function. *Semin Immunol*. 73:101887.

Kumar, A., T.D. Humphreys, K.N. Kremer, P.S. Bramati, L. Bradfield, C.E. Edgar, and K.E. Hedin. 2006. CXCR4 physically associates with the T cell receptor to signal in T cells. *Immunity*. 25:213-224.

Lambrecht, B.N., H. Hammad, and J.V. Fahy. 2019. The Cytokines of Asthma. *Immunity*. 50:975-991.

Lan, F., J. Li, W. Miao, F. Sun, S. Duan, Y. Song, J. Yao, X. Wang, C. Wang, X. Liu, J. Wang, L. Zhang, and H. Qi. 2025. GZMK-expressing CD8(+) T cells promote recurrent airway inflammatory diseases. *Nature*. 638:490-498.

Larsen, J.M., H.S. Musavian, T.M. Butt, C. Ingvorsen, A.H. Thysen, and S. Brix. 2015. Chronic obstructive pulmonary disease and asthma-associated Proteobacteria, but not commensal Prevotella spp., promote Toll-like receptor 2-independent lung inflammation and pathology. *Immunology*. 144:333-342.

Lauritzen SL, S.D. 1988. Local Computations with Probabilities on Graphical Structures and Their Application to Expert Systems. *Journal of the Royal Statistical Society: Series B (Methodological)*. 50:157-194.

Lee, N., C.K. Wong, M.C.W. Chan, E.S.L. Yeung, W.W.S. Tam, O.T.Y. Tsang, K.W. Choi, P.K.S. Chan, A. Kwok, G.C.Y. Lui, W.S. Leung, I.M.H. Yung, R.Y.K. Wong, C.S.K. Cheung, and D.S.C. Hui. 2017. Anti-inflammatory effects of adjunctive macrolide treatment in adults hospitalized with influenza: A randomized controlled trial. *Antiviral Res*. 144:48-56.

Lee, S., D. Tian, R. He, J.J. Cragg, C. Carlsten, A. Giang, P.K. Gill, K.M. Johnson, and E. Brigham. 2024. Ambient air pollution exposure and adult asthma incidence: a systematic review and meta-analysis. *Lancet Planet Health*. 8:e1065-e1078.

Lee-Sarwar, K.A., Y.C. Chen, Y.Y. Chen, A.L. Kozyrskyj, P.J. Mandhane, S.E. Turvey, P. Subbarao, H. Bisgaard, J. Stokholm, B. Chawes, S.J. Sorensen, R.S. Kelly, J. Lasky-Su, R.S. Zeiger, G.T. O'Connor, M.T. Sandel, L.B. Bacharier, A. Beigelman, V.J. Carey, B.J. Harshfield, N. Laranjo, D.R. Gold, S.T. Weiss, and A.A. Litonjua. 2023. The maternal prenatal and offspring early-life gut microbiome of childhood asthma phenotypes. *Allergy*. 78:418-428.

Lekstrom-Himes, J.A. 2001. The role of C/EBP(epsilon) in the terminal stages of granulocyte differentiation. *Stem Cells*. 19:125-133.

Lemon, K.P., V. Klepac-Ceraj, H.K. Schiffer, E.L. Brodie, S.V. Lynch, and R. Kolter. 2010. Comparative analyses of the bacterial microbiota of the human nostril and oropharynx. *mBio*. 1.

Lendermon, E.A., T.A. Coon, J.S. Bednash, N.M. Weathington, J.F. McDyer, and R.K. Mallampalli. 2017. Azithromycin decreases NALP3 mRNA stability in monocytes to limit inflammasome-dependent inflammation. *Respir Res*. 18:131.

Leslie, J., B.J. Millar, A. Del Carpio Pons, R.A. Burgoyne, J.D. Frost, B.S. Barksby, S. Luli, J. Scott, A.J. Simpson, J. Gauldie, L.A. Murray, D.K. Finch, A.M. Carruthers, J. Ferguson, M.A. Sleeman, D. Rider, R. Howarth, C. Fox, F. Oakley, A.J. Fisher, D.A. Mann, and L.A. Borthwick. 2020. FPR-1 is an important regulator of neutrophil recruitment and a tissue-specific driver of pulmonary fibrosis. *JCI Insight*. 5.

Li, D., and M. Wu. 2021. Pattern recognition receptors in health and diseases. *Signal Transduct Target Ther*. 6:291.

Li, H. 2018. Minimap2: pairwise alignment for nucleotide sequences. *Bioinformatics*. 34:3094-3100.

Li, H., B. Handsaker, A. Wysoker, T. Fennell, J. Ruan, N. Homer, G. Marth, G. Abecasis, R. Durbin, and S. Genome Project Data Processing. 2009. The Sequence Alignment/Map format and SAMtools. *Bioinformatics*. 25:2078-2079.

Li, J., B. Diao, S. Guo, X. Huang, C. Yang, Z. Feng, W. Yan, Q. Ning, L. Zheng, Y. Chen, and Y. Wu. 2017. VSIG4 inhibits proinflammatory macrophage activation by reprogramming mitochondrial pyruvate metabolism. *Nat Commun*. 8:1322.

Li, L.B., D.Y. Leung, M.J. Strand, and E. Goleva. 2007. ATF2 impairs glucocorticoid receptor-mediated transactivation in human CD8+ T cells. *Blood*. 110:1570-1577.

Li, X., A.T. Hastie, M.C. Peters, G.A. Hawkins, W. Phipatanakul, H. Li, W.C. Moore, W.W. Busse, M. Castro, S.C. Erzurum, B. Gaston, E. Israel, N.N. Jarjour, B.D. Levy, S.E. Wenzel, D.A. Meyers, J.V. Fahy, E.R. Bleecker, L. National Heart, and N. Blood Institute's Severe Asthma Research Program. 2020. Investigation of the relationship between IL-6 and type 2 biomarkers in patients with severe asthma. *J Allergy Clin Immunol*. 145:430-433.

Li, Y., H. Huang, B. Liu, Y. Zhang, X. Pan, X.Y. Yu, Z. Shen, and Y.H. Song. 2021. Inflammasomes as therapeutic targets in human diseases. *Signal Transduct Target Ther*. 6:247.

Li, Y., W. Wang, Z. Lv, Y. Li, Y. Chen, K. Huang, C.J. Corrigan, and S. Ying. 2018. Elevated Expression of IL-33 and TSLP in the Airways of Human Asthmatics In Vivo: A Potential Biomarker of Severe Refractory Disease. *J Immunol*. 200:2253-2262.

Liu, C., X. Yang, Y. Tan, Y. Wang, J. Lan, P. Yang, and D. Zhao. 2025. BATF participates in airway inflammation of neutrophilic asthma via regulating Th17 cells activation. *Mol Immunol*. 181:40-52.

Liu, T., Z. Yang, X. Zhang, N. Han, J. Yuan, and Y. Cheng. 2017. 16S rDNA analysis of the effect of fecal microbiota transplantation on pulmonary and intestinal flora. *3 Biotech*. 7:370.

Liu, Y., J. Pan, H. Zhang, C. Shi, G. Li, Z. Peng, J. Ma, Y. Zhou, and L. Zhang. 2019. Short-Term Exposure to Ambient Air Pollution and Asthma Mortality. *Am J Respir Crit Care Med*. 200:24-32.

Looft, T., and H.K. Allen. 2012. Collateral effects of antibiotics on mammalian gut microbiomes. *Gut Microbes*. 3:463-467.

Loose, M., S. Malla, and M. Stout. 2016. Real-time selective sequencing using nanopore technology. *Nat Methods*. 13:751-754.

Lotvall, J., C.A. Akdis, L.B. Bacharier, L. Bjermer, T.B. Casale, A. Custovic, R.F. Lemanske, Jr., A.J. Wardlaw, S.E. Wenzel, and P.A. Greenberger. 2011. Asthma endotypes: a new approach to classification of disease entities within the asthma syndrome. *J Allergy Clin Immunol*. 127:355-360.

Lucchi, M., B. Damle, A. Fang, P.J. de Caprariis, A. Mussi, S.P. Sanchez, G. Pasqualetti, and M. Del Tacca. 2008. Pharmacokinetics of azithromycin in serum, bronchial washings, alveolar macrophages and lung tissue following a single oral dose of extended or immediate release formulations of azithromycin. *J Antimicrob Chemother*. 61:884-891.

Lukacs, N.W., A. Berlin, D. Schols, R.T. Skerlj, and G.J. Bridger. 2002. AMD3100, a CxCR4 antagonist, attenuates allergic lung inflammation and airway hyperreactivity. *Am J Pathol*. 160:1353-1360.

Lun, A.T.L., S. Riesenfeld, T. Andrews, T.P. Dao, T. Gomes, J. participants in the 1st Human Cell Atlas, and J.C. Marioni. 2019. EmptyDrops: distinguishing cells from empty droplets in droplet-based single-cell RNA sequencing data. *Genome Biol*. 20:63.

Lynch, S.V., R.A. Wood, H. Boushey, L.B. Bacharier, G.R. Bloomberg, M. Kattan, G.T. O'Connor, M.T. Sandel, A. Calatroni, E. Matsui, C.C. Johnson, H. Lynn, C.M. Visness, K.F. Jaffee, P.J. Gergen, D.R. Gold, R.J. Wright, K. Fujimura, M. Rauch, W.W. Busse, and J.E. Gern. 2014. Effects of early-life exposure to allergens and bacteria on recurrent wheeze and atopy in urban children. *J Allergy Clin Immunol*. 134:593-601 e512.

Ma, A., and B.A. Malynn. 2012. A20: linking a complex regulator of ubiquitylation to immunity and human disease. *Nat Rev Immunol*. 12:774-785.

Mac Aogain, M., K.J.X. Lau, Z. Cai, J. Kumar Narayana, R.W. Purbojati, D.I. Drautz-Moses, N.E. Gaultier, T.K. Jaggi, P.Y. Tiew, T.H. Ong, M. Siyue Koh, A. Lim Yick Hou, J.A. Abisheganaden, K. Tsaneva-Atanasova, S.C. Schuster, and S.H. Chotirmall. 2020. Metagenomics Reveals a Core Macrolide Resistome Related to Microbiota in Chronic Respiratory Disease. *Am J Respir Crit Care Med*. 202:433-447.

Madan, J.C., D.C. Koestler, B.A. Stanton, L. Davidson, L.A. Moulton, M.L. Housman, J.H. Moore, M.F. Guill, H.G. Morrison, M.L. Sogin, T.H. Hampton, M.R. Karagas, P.E. Palumbo, J.A. Foster, P.L. Hibberd, and G.A. O'Toole. 2012. Serial analysis of the gut and respiratory microbiome in cystic fibrosis in infancy: interaction between intestinal and respiratory tracts and impact of nutritional exposures. *mBio*. 3.

Malcolm, K.C., J.E. Kret, R.L. Young, K.R. Poch, S.M. Caceres, I.S. Douglas, C.D. Coldren, E.L. Burnham, M. Moss, and J.A. Nick. 2011. Bacteria-specific neutrophil dysfunction associated with interferon-stimulated gene expression in the acute respiratory distress syndrome. *PLoS One*. 6:e21958.

Man, W.H., W.A. de Steenhuijsen Piters, and D. Bogaert. 2017. The microbiota of the respiratory tract: gatekeeper to respiratory health. *Nat Rev Microbiol*. 15:259-270.

Manzo, N.D., W.M. Foster, and B.R. Stripp. 2012. Amphiregulin-dependent mucous cell metaplasia in a model of nonallergic lung injury. *Am J Respir Cell Mol Biol*. 47:349-357.

Mapp, C.E., P. Boschetto, P. Maestrelli, and L.M. Fabbri. 2005. Occupational asthma. *Am J Respir Crit Care Med*. 172:280-305.

Marone, G., M. Triggiani, and A. de Paulis. 2005. Mast cells and basophils: friends as well as foes in bronchial asthma? *Trends Immunol*. 26:25-31.

Marsh, R.L., M. Kaestli, A.B. Chang, M.J. Binks, C.E. Pope, L.R. Hoffman, and H.C. Smith-Vaughan. 2016. The microbiota in bronchoalveolar lavage from young children with chronic lung disease includes taxa present in both the oropharynx and nasopharynx. *Microbiome*. 4:37.

Massoni-Badosa, R., S. Aguilar-Fernandez, J.C. Nieto, P. Soler-Vila, M. Elosua-Bayes, D. Marchese, M. Kulis, A. Vilas-Zornoza, M.M. Buhler, S. Rashmi, C. Alsinet, G. Caratu, C. Moutinho, S. Ruiz, P. Lorden, G. Lunazzi, D. Colomer, G. Frigola, W. Blevins, L. Romero-Rivero, V. Jimenez-Martinez, A. Vidal, J. Mateos-Jaimez, A. Maiques-Diaz, S. Ovejero, J. Moreaux, S. Palomino, D. Gomez-Cabrero, X. Agirre, M.A. Weniger, H.W. King, L.C. Garner, F. Marini, F.J. Cervera-Paz, P.M. Baptista, I. Vilaseca, C. Rosales, S. Ruiz-Gaspa, B. Talks, K. Sidhpura, A. Pascual-Reguant, A.E. Hauser, M. Haniffa, F. Prosper, R. Kuppers, I.G. Gut, E. Campo, J.I. Martin-Subero, and H. Heyn. 2024. An atlas of cells in the human tonsil. *Immunity*. 57:379-399 e318.

McDonald, V.M., J. Fingleton, A. Agusti, S.A. Hiles, V.L. Clark, A.E. Holland, G.B. Marks, P.P. Bardin, R. Beasley, I.D. Pavord, P.A.B. Wark, P.G. Gibson, W. participants of the Treatable Traits Down Under International, and p. Treatable Traits Down Under International Workshop. 2019. Treatable traits: a new paradigm for 21st century management of chronic airway diseases: Treatable Traits Down Under International Workshop report. *Eur Respir J*. 53.

McDowell, P.J., S. Diver, F. Yang, C. Borg, J. Busby, V. Brown, R. Shrimanker, C. Cox, C.E. Brightling, R. Chaudhuri, I.D. Pavord, L.G. Heaney, and P. Medical Research Council: Refractory Asthma Stratification. 2021. The inflammatory profile of exacerbations in patients with severe refractory eosinophilic asthma receiving mepolizumab (the MEX study): a prospective observational study. *Lancet Respir Med*. 9:1174-1184.

McNicholl, D.M., M. Stevenson, L.P. McGarvey, and L.G. Heaney. 2012. The utility of fractional exhaled nitric oxide suppression in the identification of nonadherence in difficult asthma. *Am J Respir Crit Care Med*. 186:1102-1108.

Melandri, D., I. Zlatareva, R.A.G. Chaleil, R.J. Dart, A. Chancellor, O. Nussbaumer, O. Polyakova, N.A. Roberts, D. Wesch, D. Kabelitz, P.M. Irving, S. John, S. Mansour, P.A. Bates, P. Vantourout, and A.C. Hayday. 2018. The gammadeltaTCR combines innate immunity with adaptive immunity by utilizing spatially distinct regions for agonist selection and antigen responsiveness. *Nat Immunol*. 19:1352-1365.

Melhorn, J., I. Howell, and I.D. Pavord. 2022. Should we apply a treatable traits approach to asthma care? *Ann Allergy Asthma Immunol*. 128:390-397.

Metsala, J., A. Lundqvist, L.J. Virta, M. Kaila, M. Gissler, and S.M. Virtanen. 2015. Prenatal and post-natal exposure to antibiotics and risk of asthma in childhood. *Clin Exp Allergy*. 45:137-145.

Miyake, K., M. Kushima, R. Shinohara, S. Horiuchi, S. Otawa, Y. Akiyama, T. Ooka, R. Kojima, H. Yokomichi, Z. Yamagata, E. Japan, and G. Children's Study. 2023. Maternal smoking status before and during pregnancy and bronchial asthma at 3 years of age: a prospective cohort study. *Sci Rep*. 13:3234.

Moffatt, M.F., I.G. Gut, F. Demenais, D.P. Strachan, E. Bouzigon, S. Heath, E. von Mutius, M. Farrall, M. Lathrop, W. Cookson, and G. Consortium. 2010. A large-scale, consortium-based genomewide association study of asthma. *N Engl J Med*. 363:1211-1221.

Moges, R., D.D. De Lamache, S. Sajedy, B.S. Renaux, M.D. Hollenberg, G. Muench, E.M. Abbott, and A.G. Buret. 2018. Anti-Inflammatory Benefits of Antibiotics: Tylvalosin Induces Apoptosis of Porcine Neutrophils and Macrophages, Promotes Efferocytosis, and Inhibits Pro-Inflammatory CXCL-8, IL1alpha, and LTB(4) Production, While

Inducing the Release of Pro-Resolving Lipoxin A(4) and Resolvin D1. *Front Vet Sci*. 5:57.

Moghaddam, S.J., C.G. Clement, M.M. De la Garza, X. Zou, E.L. Travis, H.W. Young, C.M. Evans, M.J. Tuvim, and B.F. Dickey. 2008. Haemophilus influenzae lysate induces aspects of the chronic obstructive pulmonary disease phenotype. *Am J Respir Cell Mol Biol*. 38:629-638.

Molyneaux, P.L., P. Mallia, M.J. Cox, J. Footitt, S.A. Willis-Owen, D. Homola, M.B. Trujillo-Torralbo, S. Elkin, O.M. Kon, W.O. Cookson, M.F. Moffatt, and S.L. Johnston. 2013. Outgrowth of the bacterial airway microbiome after rhinovirus exacerbation of chronic obstructive pulmonary disease. *Am J Respir Crit Care Med*. 188:1224-1231.

Monticelli, L.A., G.F. Sonnenberg, M.C. Abt, T. Alenghat, C.G. Ziegler, T.A. Doering, J.M. Angelosanto, B.J. Laidlaw, C.Y. Yang, T. Sathaliyawala, M. Kubota, D. Turner, J.M. Diamond, A.W. Goldrath, D.L. Farber, R.G. Collman, E.J. Wherry, and D. Artis. 2011. Innate lymphoid cells promote lung-tissue homeostasis after infection with influenza virus. *Nat Immunol*. 12:1045-1054.

Moore, W.C., A.T. Hastie, X. Li, H. Li, W.W. Busse, N.N. Jarjour, S.E. Wenzel, S.P. Peters, D.A. Meyers, E.R. Bleecker, L. National Heart, and P. Blood Institute's Severe Asthma Research. 2014. Sputum neutrophil counts are associated with more severe asthma phenotypes using cluster analysis. *J Allergy Clin Immunol*. 133:1557-1563 e1555.

Morey, P., V. Cano, P. Marti-Lliteras, A. Lopez-Gomez, V. Regueiro, C. Saus, J.A. Bengoechea, and J. Garmendia. 2011. Evidence for a non-replicative intracellular stage of nontypable Haemophilus influenzae in epithelial cells. *Microbiology (Reading)*. 157:234-250.

Morris, A., J.M. Beck, P.D. Schloss, T.B. Campbell, K. Crothers, J.L. Curtis, S.C. Flores, A.P. Fontenot, E. Ghedin, L. Huang, K. Jablonski, E. Kleerup, S.V. Lynch, E. Sodergren, H. Twigg, V.B. Young, C.M. Bassis, A. Venkataraman, T.M. Schmidt, G.M. Weinstock, and H.I.V.M.P. Lung. 2013. Comparison of the respiratory microbiome in healthy nonsmokers and smokers. *Am J Respir Crit Care Med*. 187:1067-1075.

Morris, D.E., K.L. Osman, D.W. Cleary, and S.C. Clarke. 2022. The characterization of Moraxella catarrhalis carried in the general population. *Microb Genom*. 8.

Mostafa, M.M., C.F. Rider, S. Shah, S.L. Traves, P.M.K. Gordon, A. Miller-Larsson, R. Leigh, and R. Newton. 2019. Glucocorticoid-driven transcriptomes in human airway epithelial cells: commonalities, differences and functional insight from cell lines and primary cells. *BMC Med Genomics*. 12:29.

Mueller, N.T., E. Bakacs, J. Combellick, Z. Grigoryan, and M.G. Dominguez-Bello. 2015. The infant microbiome development: mom matters. *Trends Mol Med*. 21:109-117.

Mukherjee, M., A. Stoddart, R.P. Gupta, B.I. Nwaru, A. Farr, M. Heaven, D. Fitzsimmons, A. Bandyopadhyay, C. Aftab, C.R. Simpson, R.A. Lyons, C. Fischbacher, C. Dibben, M.D. Shields, C.J. Phillips, D.P. Strachan, G.A. Davies, B. McKinstry, and A. Sheikh. 2016. The epidemiology, healthcare and societal burden and costs of asthma in the UK and its member nations: analyses of standalone and linked national databases. *BMC Med*. 14:113.

Murphy, B.S., V. Sundareshan, T.J. Cory, D. Hayes, Jr., M.I. Anstead, and D.J. Feola. 2008. Azithromycin alters macrophage phenotype. *J Antimicrob Chemother*. 61:554-560.

Murphy, T.F., A.L. Brauer, A.T. Schiffmacher, and S. Sethi. 2004. Persistent colonization by Haemophilus influenzae in chronic obstructive pulmonary disease. *Am J Respir Crit Care Med*. 170:266-272.

Murray, P.J., J.E. Allen, S.K. Biswas, E.A. Fisher, D.W. Gilroy, S. Goerdt, S. Gordon, J.A. Hamilton, L.B. Ivashkiv, T. Lawrence, M. Locati, A. Mantovani, F.O. Martinez, J.L. Mege, D.M. Mosser, G. Natoli, J.P. Saeij, J.L. Schultze, K.A. Shirey, A. Sica, J. Suttles, I. Udalova, J.A. van Ginderachter, S.N. Vogel, and T.A. Wynn. 2014. Macrophage activation and polarization: nomenclature and experimental guidelines. *Immunity*. 41:14-20.

Nelson, M.T., C.E. Pope, R.L. Marsh, D.J. Wolter, E.J. Weiss, K.R. Hager, A.T. Vo, M.J. Brittnacher, M.C. Radey, H.S. Hayden, A. Eng, S.I. Miller, E. Borenstein, and L.R.

Hoffman. 2019. Human and Extracellular DNA Depletion for Metagenomic Analysis of Complex Clinical Infection Samples Yields Optimized Viable Microbiome Profiles. *Cell Rep*. 26:2227-2240 e2225.

NICE. 2021. Mepolizumab for treating severe eosinophilic asthma.

Niessen, N.M., P.G. Gibson, K.J. Baines, D. Barker, I.A. Yang, J.W. Upham, P.N. Reynolds, S. Hodge, A.L. James, C. Jenkins, M.J. Peters, G.B. Marks, M. Baraket, J.L. Simpson, and M. Fricker. 2021. Sputum TNF markers are increased in neutrophilic and severe asthma and are reduced by azithromycin treatment. *Allergy*. 76:2090-2101.

Nozoe, K., Y. Aida, T. Fukuda, T. Sanui, and F. Nishimura. 2016. Mechanisms of the Macrolide-Induced Inhibition of Superoxide Generation by Neutrophils. *Inflammation*. 39:1039-1048.

Nujic, K., M. Banjanac, V. Munic, D. Polancec, and V. Erakovic Haber. 2012. Impairment of lysosomal functions by azithromycin and chloroquine contributes to anti-inflammatory phenotype. *Cell Immunol*. 279:78-86.

O'Byrne, P.M., E.R. Bleecker, E.D. Bateman, W.W. Busse, A. Woodcock, R. Forth, W.T. Toler, L. Jacques, and J. Lotvall. 2014. Once-daily fluticasone furoate alone or combined with vilanterol in persistent asthma. *Eur Respir J*. 43:773-782.

O'Sullivan, B.P., L. James, J.M. Majure, S. Bickel, L.T. Phan, M. Serrano Gonzalez, H. Staples, J. Tam-Williams, J. Lang, J. Snowden, and I.D.S.P.C.T. Network. 2021. Obesity-related asthma in children: A role for vitamin D. *Pediatr Pulmonol*. 56:354-361.

Ober, C., Z. Tan, Y. Sun, J.D. Possick, L. Pan, R. Nicolae, S. Radford, R.R. Parry, A. Heinzmann, K.A. Deichmann, L.A. Lester, J.E. Gern, R.F. Lemanske, Jr., D.L. Nicolae, J.A. Elias, and G.L. Chupp. 2008. Effect of variation in CHI3L1 on serum YKL-40 level, risk of asthma, and lung function. *N Engl J Med*. 358:1682-1691.

Oh, J., A.L. Byrd, C. Deming, S. Conlan, N.C.S. Program, H.H. Kong, and J.A. Segre. 2014. Biogeography and individuality shape function in the human skin metagenome. *Nature*. 514:59-64.

Oliver, M.E., and T.S.C. Hinks. 2021. Azithromycin in viral infections. *Rev Med Virol*. 31:e2163.

Oriano, M., L. Terranova, A. Teri, S. Sottotetti, L. Ruggiero, C. Tafuro, P. Marchisio, A. Gramegna, F. Amati, F. Nava, E. Franceschi, L. Cariani, F. Blasi, and S. Aliberti. 2019. Comparison of different conditions for DNA extraction in sputum - a pilot study. *Multidiscip Respir Med*. 14:6.

Ovsiy, I., V. Riabov, I. Manousaridis, J. Michel, K. Moganti, S. Yin, T. Liu, C. Sticht, E. Kremmer, M.C. Harmsen, S. Goerdt, A. Gratchev, and J. Kzhyshkowska. 2017. IL-4 driven transcription factor FoxQ1 is expressed by monocytes in atopic dermatitis and stimulates monocyte migration. *Sci Rep*. 7:16847.

OxfordNanoporeTechnologies. 2024. Adaptive Sampling. Vol. 2024.

Pakkasela, J., P. Ilmarinen, J. Honkamaki, L.E. Tuomisto, H. Andersen, P. Piirila, H. Hisinger-Molkanen, A. Sovijarvi, H. Backman, B. Lundback, E. Ronmark, H. Kankaanranta, and L. Lehtimaki. 2020. Age-specific incidence of allergic and non-allergic asthma. *BMC Pulm Med*. 20:9.

Papi, A., C. Brightling, S.E. Pedersen, and H.K. Reddel. 2018. Asthma. *Lancet*. 391:783-800.

Partridge, S.R., S.M. Kwong, N. Firth, and S.O. Jensen. 2018. Mobile Genetic Elements Associated with Antimicrobial Resistance. *Clin Microbiol Rev*. 31.

Patrick, D.M., H. Sbihi, D.L.Y. Dai, A. Al Mamun, D. Rasali, C. Rose, F. Marra, R.C.T. Boutin, C. Petersen, L.T. Stiemsma, G.L. Winsor, F.S.L. Brinkman, A.L. Kozyrskyj, M.B. Azad, A.B. Becker, P.J. Mandhane, T.J. Moraes, M.R. Sears, P. Subbarao, B.B. Finlay, and S.E. Turvey. 2020. Decreasing antibiotic use, the gut microbiota, and asthma incidence in children: evidence from population-based and prospective cohort studies. *Lancet Respir Med*. 8:1094-1105.

Pavord, I.D., R. Beasley, A. Agusti, G.P. Anderson, E. Bel, G. Brusselle, P. Cullinan, A. Custovic, F.M. Ducharme, J.V. Fahy, U. Frey, P. Gibson, L.G. Heaney, P.G. Holt, M. Humbert, C.M. Lloyd, G. Marks, F.D. Martinez, P.D. Sly, E. von Mutius, S. Wenzel, H.J. Zar, and A. Bush. 2018. After asthma: redefining airways diseases. *Lancet*. 391:350-400.

Pavord, I.D., S. Korn, P. Howarth, E.R. Bleecker, R. Buhl, O.N. Keene, H. Ortega, and P. Chanez. 2012. Mepolizumab for severe eosinophilic asthma (DREAM): a multicentre, double-blind, placebo-controlled trial. *Lancet*. 380:651-659.

Persson, H.L., L.K. Vainikka, M. Sege, U. Wennerstrom, S. Dam-Larsen, and J. Persson. 2012. Leaky lysosomes in lung transplant macrophages: azithromycin prevents oxidative damage. *Respir Res*. 13:83.

Pettigrew, M.M., C.P. Ahearn, J.F. Gent, Y. Kong, M.C. Gallo, J.B. Munro, A. D'Mello, S. Sethi, H. Tettelin, and T.F. Murphy. 2018. Haemophilus influenzae genome evolution during persistence in the human airways in chronic obstructive pulmonary disease. *Proc Natl Acad Sci U S A*. 115:E3256-E3265.

Pijnenburg, M.W., U. Frey, J.C. De Jongste, and S. Saglani. 2022. Childhood asthma: pathogenesis and phenotypes. *Eur Respir J*. 59.

Platts-Mills, T.A., G. Rakes, and P.W. Heymann. 2000. The relevance of allergen exposure to the development of asthma in childhood. *J Allergy Clin Immunol*. 105:S503-508.

Polancec, D.S., V. Munic Kos, M. Banjanac, M. Vrancic, S. Cuzic, D. Belamaric, M.J. Parnham, D. Polancec, and V. Erakovic Haber. 2012. Azithromycin drives in vitro GM-CSF/IL-4-induced differentiation of human blood monocytes toward dendritic-like cells with regulatory properties. *J Leukoc Biol*. 91:229-243.

Poletti, V., G. Casoni, M. Chilosi, and M. Zompatori. 2006. Diffuse panbronchiolitis. *Eur Respir J*. 28:862-871.

Porter, J.D., J. Watson, L.R. Roberts, S.K. Gill, H. Groves, J. Dhariwal, M.H. Almond, E. Wong, R.P. Walton, L.H. Jones, J. Tregoning, I. Kilty, S.L. Johnston, and M.R. Edwards. 2016. Identification of novel macrolides with antibacterial, anti-inflammatory and type I and III IFN-augmenting activity in airway epithelium. *J Antimicrob Chemother*. 71:2767-2781.

Postma, D.S. 2007. Gender differences in asthma development and progression. *Gend Med*. 4 Suppl B:S133-146.

Poznanski, S.M., M. Mukherjee, N. Zhao, C. Huang, K. Radford, A.A. Ashkar, and P. Nair. 2021. Asthma exacerbations on benralizumab are largely non-eosinophilic. *Allergy*. 76:375-379.

Price, D.B., A. Rigazio, J.D. Campbell, E.R. Bleecker, C.J. Corrigan, M. Thomas, S.E. Wenzel, A.M. Wilson, M.B. Small, G. Gopalan, V.L. Ashton, A. Burden, E.V. Hillyer, M. Kerkhof, and I.D. Pavord. 2015. Blood eosinophil count and prospective annual asthma disease burden: a UK cohort study. *Lancet Respir Med*. 3:849-858.

Puga, J.L., M. Krzywinski, and N. Altman. 2015. Bayesian networks. *Nature Methods*. 12:799-800.

Quince, C., A.W. Walker, J.T. Simpson, N.J. Loman, and N. Segata. 2017. Shotgun metagenomics, from sampling to analysis. *Nat Biotechnol*. 35:833-844.

Rapp, R.P. 1998. Pharmacokinetics and pharmacodynamics of intravenous and oral azithromycin: enhanced tissue activity and minimal drug interactions. *Ann Pharmacother*. 32:785-793.

Ratzinger, F., H. Haslacher, W. Poeppl, G. Hoermann, J.J. Kovarik, S. Jutz, P. Steinberger, H. Burgmann, W.F. Pickl, and K.G. Schmetterer. 2014. Azithromycin suppresses CD4(+) T-cell activation by direct modulation of mTOR activity. *Sci Rep*. 4:7438.

Ribeiro, C.M., H. Hurd, Y. Wu, M.E. Martino, L. Jones, B. Brighton, R.C. Boucher, and W.K. O'Neal. 2009. Azithromycin treatment alters gene expression in inflammatory, lipid metabolism, and cell cycle pathways in well-differentiated human airway epithelia. *PLoS One*. 4:e5806.

Rigauts, C., J. Aizawa, S.L. Taylor, G.B. Rogers, M. Govaerts, P. Cos, L. Ostyn, S. Sims, E. Vandeplassche, M. Sze, Y. Dondelinger, L. Vereecke, H. Van Acker, J.L. Simpson, L. Burr, A. Willems, M.M. Tunney, C. Cigana, A. Bragonzi, T. Coenye, and A. Crabbe. 2022. R othia mucilaginosa is an anti-inflammatory bacterium in the respiratory tract of patients with chronic lung disease. *Eur Respir J*. 59.

Robinson, D.S., Q. Hamid, S. Ying, A. Tsicopoulos, J. Barkans, A.M. Bentley, C. Corrigan, S.R. Durham, and A.B. Kay. 1992. Predominant TH2-like bronchoalveolar T-lymphocyte population in atopic asthma. *N Engl J Med*. 326:298-304.

Roduit, C., R. Frei, R. Ferstl, S. Loeliger, P. Westermann, C. Rhyner, E. Schiavi, W. Barcik, N. Rodriguez-Perez, M. Wawrzyniak, C. Chassard, C. Lacroix, E. Schmausser-Hechfellner, M. Depner, E. von Mutius, C. Braun-Fahrlander, A.M. Karvonen, P.V. Kirjavainen, J. Pekkanen, J.C. Dalphin, J. Riedler, C. Akdis, R. Lauener, L. O'Mahony, and P.E.s. group. 2019. High levels of butyrate and propionate in early life are associated with protection against atopy. *Allergy*. 74:799-809.

Rolfe, F.G., J.E. Valentine, and W.A. Sewell. 1997. Cyclosporin A and FK506 reduce interleukin-5 mRNA abundance by inhibiting gene transcription. *Am J Respir Cell Mol Biol*. 17:243-250.

Rossello-Mora, R., and R. Amann. 2001. The species concept for prokaryotes. *FEMS Microbiol Rev*. 25:39-67.

Rossios, C., S. Pavlidis, U. Hoda, C.H. Kuo, C. Wiegman, K. Russell, K. Sun, M.J. Loza, F. Baribaud, A.L. Durham, O. Ojo, R. Lutter, A. Rowe, A. Bansal, C. Auffray, A. Sousa, J. Corfield, R. Djukanovic, Y. Guo, P.J. Sterk, K.F. Chung, I.M. Adcock, and T. Unbiased Biomarkers for the Prediction of Respiratory Diseases Outcomes Consortia Project. 2018. Sputum transcriptomics reveal upregulation of IL-1 receptor family members in patients with severe asthma. *J Allergy Clin Immunol*. 141:560-570.

Rothers, J., D.A. Stern, I.C. Lohman, A. Spangenberg, A.L. Wright, A. DeVries, D. Vercelli, and M. Halonen. 2018. Maternal Cytokine Profiles during Pregnancy Predict Asthma in Children of Mothers without Asthma. *Am J Respir Cell Mol Biol*. 59:592-600.

Rotta Detto Loria, J., K. Rohmann, D. Droemann, P. Kujath, J. Rupp, T. Goldmann, and K. Dalhoff. 2013. Nontypeable Haemophilus Influenzae Infection Upregulates the NLRP3 Inflammasome and Leads to Caspase-1-Dependent Secretion of Interleukin-1beta - A Possible Pathway of Exacerbations in COPD. *PLoS One*. 8:e66818.

Saffar, A.S., M.P. Alphonse, L. Shan, K.T. Hayglass, F.E. Simons, and A.S. Gounni. 2007. IgE modulates neutrophil survival in asthma: role of mitochondrial pathway. *J Immunol*. 178:2535-2541.

Sajjan, U.S., Y. Jia, D.C. Newcomb, J.K. Bentley, N.W. Lukacs, J.J. LiPuma, and M.B. Hershenson. 2006. H. influenzae potentiates airway epithelial cell responses to rhinovirus by increasing ICAM-1 and TLR3 expression. *FASEB J*. 20:2121-2123.

Salcher, S., I. Heidegger, G. Untergasser, G. Fotakis, A. Scheiber, A. Martowicz, A. Noureen, A. Krogsdam, C. Schatz, G. Schafer, Z. Trajanoski, D. Wolf, S. Sopper, and A. Pircher. 2024. Comparative analysis of 10X Chromium vs. BD Rhapsody whole transcriptome single-cell sequencing technologies in complex human tissues. *Heliyon*. 10:e28358.

Sanderson, N.D., T.L. Street, D. Foster, J. Swann, B.L. Atkins, A.J. Brent, M.A. McNally, S. Oakley, A. Taylor, T.E.A. Peto, D.W. Crook, and D.W. Eyre. 2018. Real-time analysis of nanopore-based metagenomic sequencing from infected orthopaedic devices. *BMC Genomics*. 19:714.

Sanderson, N.D., J. Swann, L. Barker, J. Kavanagh, S. Hoosdally, D. Crook, G. GonFast Investigators, T.L. Street, and D.W. Eyre. 2020. High precision Neisseria gonorrhoeae variant and antimicrobial resistance calling from metagenomic Nanopore sequencing. *Genome Res*. 30:1354-1363.

Sano, H., D.K. Hsu, J.R. Apgar, L. Yu, B.B. Sharma, I. Kuwabara, S. Izui, and F.T. Liu. 2003. Critical role of galectin-3 in phagocytosis by macrophages. *J Clin Invest*. 112:389-397.

Sasaki, S., T. Baba, H. Muranaka, Y. Tanabe, C. Takahashi, S. Matsugo, and N. Mukaida. 2018. Involvement of Prokineticin 2-expressing Neutrophil Infiltration in 5-Fluorouracil-induced Aggravation of Breast Cancer Metastasis to Lung. *Mol Cancer Ther*. 17:1515-1525.

Schaub, B., R. Lauener, and E. von Mutius. 2006. The many faces of the hygiene hypothesis. *J Allergy Clin Immunol*. 117:969-977; quiz 978.

Scheiber, A., M. Trebo, A. Pittl, I. Heidegger, T. Hautz, R. Oberhuber, Z. Trajanoski, F. Augustin, S. Sopper, D. Wolf, A. Pircher, and S. Salcher. 2024. Profiling low-mRNA content cells

in complex human tissues using BD Rhapsody single-cell analysis. *STAR Protoc*. 5:103475.

Schnoegl, D., A. Hiesinger, N.D. Huntington, and D. Gotthardt. 2023. AP-1 transcription factors in cytotoxic lymphocyte development and antitumor immunity. *Curr Opin Immunol*. 85:102397.

Schogler, A., B.S. Kopf, M.R. Edwards, S.L. Johnston, C. Casaulta, E. Kieninger, A. Jung, A. Moeller, T. Geiser, N. Regamey, and M.P. Alves. 2015. Novel antiviral properties of azithromycin in cystic fibrosis airway epithelial cells. *Eur Respir J*. 45:428-439.

Segal, L.N., A.V. Alekseyenko, J.C. Clemente, R. Kulkarni, B. Wu, Z. Gao, H. Chen, K.I. Berger, R.M. Goldring, W.N. Rom, M.J. Blaser, and M.D. Weiden. 2013. Enrichment of lung microbiome with supraglottic taxa is associated with increased pulmonary inflammation. *Microbiome*. 1:19.

Segal, L.N., J.C. Clemente, J.C. Tsay, S.B. Koralov, B.C. Keller, B.G. Wu, Y. Li, N. Shen, E. Ghedin, A. Morris, P. Diaz, L. Huang, W.R. Wikoff, C. Ubeda, A. Artacho, W.N. Rom, D.H. Sterman, R.G. Collman, M.J. Blaser, and M.D. Weiden. 2016. Enrichment of the lung microbiome with oral taxa is associated with lung inflammation of a Th17 phenotype. *Nat Microbiol*. 1:16031.

Segata, N., S.K. Haake, P. Mannon, K.P. Lemon, L. Waldron, D. Gevers, C. Huttenhower, and J. Izard. 2012. Composition of the adult digestive tract bacterial microbiome based on seven mouth surfaces, tonsils, throat and stool samples. *Genome Biol*. 13:R42.

Sereika, M., R.H. Kirkegaard, S.M. Karst, T.Y. Michaelsen, E.A. Sorensen, R.D. Wollenberg, and M. Albertsen. 2022. Oxford Nanopore R10.4 long-read sequencing enables the generation of near-finished bacterial genomes from pure cultures and metagenomes without short-read or reference polishing. *Nat Methods*. 19:823-826.

Sergushichev, A. 2016. An algorithm for fast preranked gene set enrichment analysis using cumulative statistic calculation.

Serisier, D.J. 2013. Risks of population antimicrobial resistance associated with chronic macrolide use for inflammatory airway diseases. *Lancet Respir Med*. 1:262-274.

Shao, Y., S.C. Forster, E. Tsaliki, K. Vervier, A. Strang, N. Simpson, N. Kumar, M.D. Stares, A. Rodger, P. Brocklehurst, N. Field, and T.D. Lawley. 2019. Stunted microbiota and opportunistic pathogen colonization in caesarean-section birth. *Nature*. 574:117-121.

Shi, N., J. Zhang, and S.Y. Chen. 2017. Runx2, a novel regulator for goblet cell differentiation and asthma development. *FASEB J*. 31:412-420.

Shi, Y., H. Zhang, and C. Miao. 2025. Metabolic reprogram and T cell differentiation in inflammation: current evidence and future perspectives. *Cell Death Discov*. 11:123.

Shinkai, M., G.H. Foster, and B.K. Rubin. 2006. Macrolide antibiotics modulate ERK phosphorylation and IL-8 and GM-CSF production by human bronchial epithelial cells. *Am J Physiol Lung Cell Mol Physiol*. 290:L75-85.

Shrimanker, R., O. Keene, G. Hynes, S. Wenzel, S. Yancey, and I.D. Pavord. 2019. Prognostic and Predictive Value of Blood Eosinophil Count, Fractional Exhaled Nitric Oxide, and Their Combination in Severe Asthma: A Post Hoc Analysis. *Am J Respir Crit Care Med*. 200:1308-1312.

Shuto, T., H. Xu, B. Wang, J. Han, H. Kai, X.X. Gu, T.F. Murphy, D.J. Lim, and J.D. Li. 2001. Activation of NF-kappa B by nontypeable Hemophilus influenzae is mediated by toll-like receptor 2-TAK1-dependent NIK-IKK alpha /beta-I kappa B alpha and MKK3/6-p38 MAP kinase signaling pathways in epithelial cells. *Proc Natl Acad Sci U S A*. 98:8774-8779.

Sikkema, L., C. Ramirez-Suastegui, D.C. Strobl, T.E. Gillett, L. Zappia, E. Madissoon, N.S. Markov, L.E. Zaragosi, Y. Ji, M. Ansari, M.J. Arguel, L. Apperloo, M. Banchero, C. Becavin, M. Berg, E. Chichelnitskiy, M.I. Chung, A. Collin, A.C.A. Gay, J. Gote-Schniering, B. Hooshiar Kashani, K. Inecik, M. Jain, T.S. Kapellos, T.M. Kole, S. Leroy, C.H. Mayr, A.J. Oliver, M. von Papen, L. Peter, C.J. Taylor, T. Walzthoeni, C. Xu, L.T. Bui, C. De Donno, L. Dony, A. Faiz, M. Guo, A.J. Gutierrez, L. Heumos, N. Huang, I.L. Ibarra, N.D. Jackson, P. Kadur Lakshminarasimha Murthy, M. Lotfollahi, T. Tabib, C. Talavera-Lopez, K.J. Travaglini, A. Wilbrey-Clark, K.B. Worlock, M. Yoshida, C. Lung

Biological Network, M. van den Berge, Y. Bosse, T.J. Desai, O. Eickelberg, N. Kaminski, M.A. Krasnow, R. Lafyatis, M.Z. Nikolic, J.E. Powell, J. Rajagopal, M. Rojas, O. Rozenblatt-Rosen, M.A. Seibold, D. Sheppard, D.P. Shepherd, D.D. Sin, W. Timens, A.M. Tsankov, J. Whitsett, Y. Xu, N.E. Banovich, P. Barbry, T.E. Duong, C.S. Falk, K.B. Meyer, J.A. Kropski, D. Pe'er, H.B. Schiller, P.R. Tata, J.L. Schultze, S.A. Teichmann, A.V. Misharin, M.C. Nawijn, M.D. Luecken, and F.J. Theis. 2023. An integrated cell atlas of the lung in health and disease. *Nat Med*. 29:1563-1577.

Simard, J.C., A. Cesaro, J. Chapeton-Montes, M. Tardif, F. Antoine, D. Girard, and P.A. Tessier. 2013. S100A8 and S100A9 induce cytokine expression and regulate the NLRP3 inflammasome via ROS-dependent activation of NF-kappaB(1.). *PLoS One*. 8:e72138.

Simpson, J.L., J. Daly, K.J. Baines, I.A. Yang, J.W. Upham, P.N. Reynolds, S. Hodge, A.L. James, P. Hugenholtz, D. Willner, and P.G. Gibson. 2016. Airway dysbiosis: Haemophilus influenzae and Tropheryma in poorly controlled asthma. *Eur Respir J*. 47:792-800.

Simpson, J.L., P. McElduff, and P.G. Gibson. 2010. Assessment and reproducibility of non-eosinophilic asthma using induced sputum. *Respiration*. 79:147-151.

Simpson, J.L., H. Powell, M.J. Boyle, R.J. Scott, and P.G. Gibson. 2008. Clarithromycin targets neutrophilic airway inflammation in refractory asthma. *Am J Respir Crit Care Med*. 177:148-155.

Simpson, J.L., R. Scott, M.J. Boyle, and P.G. Gibson. 2006. Inflammatory subtypes in asthma: assessment and identification using induced sputum. *Respirology*. 11:54-61.

Singh, A., J. Svaren, J. Grayson, and M. Suresh. 2004. CD8 T cell responses to lymphocytic choriomeningitis virus in early growth response gene 1-deficient mice. *J Immunol*. 173:3855-3862.

Singhania, A., H. Rupani, N. Jayasekera, S. Lumb, P. Hales, N. Gozzard, D.E. Davies, C.H. Woelk, and P.H. Howarth. 2017. Altered Epithelial Gene Expression in Peripheral Airways of Severe Asthma. *PLoS One*. 12:e0168680.

Singhania, A., J.C. Wallington, C.G. Smith, D. Horowitz, K.J. Staples, P.H. Howarth, S.D. Gadola, R. Djukanovic, C.H. Woelk, and T.S.C. Hinks. 2018. Multitissue Transcriptomics Delineates the Diversity of Airway T Cell Functions in Asthma. *Am J Respir Cell Mol Biol*. 58:261-270.

Singleton, R.J., N.M. Davidson, I.J. Desmet, J.E. Berner, R.B. Wainwright, L.R. Bulkow, C.M. Lilly, and G.R. Siber. 1994. Decline of Haemophilus influenzae type b disease in a region of high risk: impact of passive and active immunization. *Pediatr Infect Dis J*. 13:362-367.

Slater, M., E. Torr, T. Harrison, D. Forrester, A. Knox, D. Shaw, and I. Sayers. 2016. The differential effects of azithromycin on the airway epithelium in vitro and in vivo. *Physiol Rep*. 4.

Smith, D., I. Du Rand, C.L. Addy, T. Collyns, S.P. Hart, P.J. Mitchelmore, N.M. Rahman, and R. Saggu. 2020. British Thoracic Society guideline for the use of long-term macrolides in adults with respiratory disease. *Thorax*. 75:370-404.

Snyder, M.E., and D.L. Farber. 2019. Human lung tissue resident memory T cells in health and disease. *Curr Opin Immunol*. 59:101-108.

Somayaji, R., M.D. Parkins, A. Shah, S.L. Martiniano, M.M. Tunney, J.S. Kahle, V.J. Waters, J.S. Elborn, S.C. Bell, P.A. Flume, D.R. VanDevanter, and G. Antimicrobial Resistance in Cystic Fibrosis InternationalWorking. 2019. Antimicrobial susceptibility testing (AST) and associated clinical outcomes in individuals with cystic fibrosis: A systematic review. *J Cyst Fibros*. 18:236-243.

Song, S., B. Liu, H. Habibie, J. van den Bor, M.J. Smit, R. Gosens, X. Wu, C.A. Brandsma, R.H. Cool, H.J. Haisma, G.J. Poelarends, and B.N. Melgert. 2021. D-dopachrome tautomerase contributes to lung epithelial repair via atypical chemokine receptor 3-dependent Akt signaling. *EBioMedicine*. 68:103412.

Soto-Ramirez, N., W. Karmaus, M. Yousefi, H. Zhang, J. Liu, and V. Gangur. 2012. Maternal immune markers in serum during gestation and in breast milk and the risk of asthma-

like symptoms at ages 6 and 12 months: a longitudinal study. *Allergy Asthma Clin Immunol*. 8:11.

Sousa, A.R., S.J. Lane, J.A. Nakhosteen, T.H. Lee, and R.N. Poston. 1996. Expression of interleukin-1 beta (IL-1beta) and interleukin-1 receptor antagonist (IL-1ra) on asthmatic bronchial epithelium. *Am J Respir Crit Care Med*. 154:1061-1066.

Stamatiou, R., E. Paraskeva, K. Boukas, K.I. Gourgoulianis, P.A. Molyvdas, and A.A. Hatziefthimiou. 2009. Azithromycin has an antiproliferative and autophagic effect on airway smooth muscle cells. *Eur Respir J*. 34:721-730.

Stearns, J.C., C.J. Davidson, S. McKeon, F.J. Whelan, M.E. Fontes, A.B. Schryvers, D.M. Bowdish, J.D. Kellner, and M.G. Surette. 2015. Culture and molecular-based profiles show shifts in bacterial communities of the upper respiratory tract that occur with age. *ISME J*. 9:1246-1259.

Stein, M.M., C.L. Hrusch, J. Gozdz, C. Igartua, V. Pivniouk, S.E. Murray, J.G. Ledford, M. Marques Dos Santos, R.L. Anderson, N. Metwali, J.W. Neilson, R.M. Maier, J.A. Gilbert, M. Holbreich, P.S. Thorne, F.D. Martinez, E. von Mutius, D. Vercelli, C. Ober, and A.I. Sperling. 2016. Innate Immunity and Asthma Risk in Amish and Hutterite Farm Children. *N Engl J Med*. 375:411-421.

Stikker, B.S., R.W. Hendriks, and R. Stadhouders. 2023. Decoding the genetic and epigenetic basis of asthma. *Allergy*. 78:940-956.

Stokholm, J., M.J. Blaser, J. Thorsen, M.A. Rasmussen, J. Waage, R.K. Vinding, A.M. Schoos, A. Kunoe, N.R. Fink, B.L. Chawes, K. Bonnelykke, A.D. Brejnrod, M.S. Mortensen, W.A. Al-Soud, S.J. Sorensen, and H. Bisgaard. 2018. Maturation of the gut microbiome and risk of asthma in childhood. *Nat Commun*. 9:141.

Sugiyama, K., R. Shirai, H. Mukae, H. Ishimoto, T. Nagata, N. Sakamoto, H. Ishii, S. Nakayama, K. Yanagihara, Y. Mizuta, and S. Kohno. 2007. Differing effects of clarithromycin and azithromycin on cytokine production by murine dendritic cells. *Clin Exp Immunol*. 147:540-546.

Sulaiman, I., B.G. Wu, Y. Li, J.C. Tsay, M. Sauthoff, A.S. Scott, K. Ji, S.B. Koralov, M. Weiden, J.C. Clemente, D. Jones, Y.J. Huang, K.A. Stringer, L. Zhang, A. Geber, S. Banakis, L. Tipton, E. Ghedin, and L.N. Segal. 2021. Functional lower airways genomic profiling of the microbiome to capture active microbial metabolism. *Eur Respir J*. 58.

Summers, C., S.M. Rankin, A.M. Condliffe, N. Singh, A.M. Peters, and E.R. Chilvers. 2010. Neutrophil kinetics in health and disease. *Trends Immunol*. 31:318-324.

Sunde, R.B., J. Thorsen, M. Kim, A.M. Schoos, J. Stokholm, K. Bonnelykke, H. Bisgaard, and B. Chawes. 2024. Bacterial colonisation of the airway in neonates and risk of asthma and allergy until age 18 years. *Eur Respir J*. 63.

Svensson, L., and C. Wenneras. 2005. Human eosinophils selectively recognize and become activated by bacteria belonging to different taxonomic groups. *Microbes Infect*. 7:720-728.

Sverrild, A., P. Kiilerich, A. Brejnrod, R. Pedersen, C. Porsbjerg, A. Bergqvist, J.S. Erjefalt, K. Kristiansen, and V. Backer. 2017. Eosinophilic airway inflammation in asthmatic patients is associated with an altered airway microbiome. *J Allergy Clin Immunol*. 140:407-417 e411.

Szabo, P.A., H.M. Levitin, M. Miron, M.E. Snyder, T. Senda, J. Yuan, Y.L. Cheng, E.C. Bush, P. Dogra, P. Thapa, D.L. Farber, and P.A. Sims. 2019. Single-cell transcriptomics of human T cells reveals tissue and activation signatures in health and disease. *Nat Commun*. 10:4706.

Tang, H.H.F., A. Lang, S.M. Teo, L.M. Judd, R. Gangnon, M.D. Evans, K.E. Lee, R. Vrtis, P.G. Holt, R.F. Lemanske, Jr., D.J. Jackson, K.E. Holt, M. Inouye, and J.E. Gern. 2021. Developmental patterns in the nasopharyngeal microbiome during infancy are associated with asthma risk. *J Allergy Clin Immunol*. 147:1683-1691.

Taylor, S.L., K.L. Ivey, P.G. Gibson, J.L. Simpson, G.B. Rogers, and A.S.R. Group. 2020. Airway abundance of Haemophilus influenzae predicts response to azithromycin in adults with persistent uncontrolled asthma. *Eur Respir J*. 56.

Taylor, S.L., L.E.X. Leong, J.M. Choo, S. Wesselingh, I.A. Yang, J.W. Upham, P.N. Reynolds, S. Hodge, A.L. James, C. Jenkins, M.J. Peters, M. Baraket, G.B. Marks, P.G. Gibson, J.L. Simpson, and G.B. Rogers. 2018. Inflammatory phenotypes in patients with severe asthma are associated with distinct airway microbiology. *J Allergy Clin Immunol*. 141:94-103 e115.

Taylor, S.L., L.E.X. Leong, F.M. Mobegi, J.M. Choo, S. Wesselingh, I.A. Yang, J.W. Upham, P.N. Reynolds, S. Hodge, A.L. James, C. Jenkins, M.J. Peters, M. Baraket, G.B. Marks, P.G. Gibson, G.B. Rogers, and J.L. Simpson. 2019. Long-Term Azithromycin Reduces Haemophilus influenzae and Increases Antibiotic Resistance in Severe Asthma. *Am J Respir Crit Care Med*. 200:309-317.

Teo, S.M., D. Mok, K. Pham, M. Kusel, M. Serralha, N. Troy, B.J. Holt, B.J. Hales, M.L. Walker, E. Hollams, Y.A. Bochkov, K. Grindle, S.L. Johnston, J.E. Gern, P.D. Sly, P.G. Holt, K.E. Holt, and M. Inouye. 2015. The infant nasopharyngeal microbiome impacts severity of lower respiratory infection and risk of asthma development. *Cell Host Microbe*. 17:704-715.

Teo, S.M., H.H.F. Tang, D. Mok, L.M. Judd, S.C. Watts, K. Pham, B.J. Holt, M. Kusel, M. Serralha, N. Troy, Y.A. Bochkov, K. Grindle, R.F. Lemanske, Jr., S.L. Johnston, J.E. Gern, P.D. Sly, P.G. Holt, K.E. Holt, and M. Inouye. 2018. Airway Microbiota Dynamics Uncover a Critical Window for Interplay of Pathogenic Bacteria and Allergy in Childhood Respiratory Disease. *Cell Host Microbe*. 24:341-352 e345.

Thomas, D., V.M. McDonald, S. Stevens, M. Baraket, S. Hodge, A. James, C. Jenkins, G.B. Marks, M. Peters, P.N. Reynolds, J.W. Upham, I.A. Yang, and P.G. Gibson. 2024. Effect of Azithromycin on Asthma Remission in Adults With Persistent Uncontrolled Asthma: A Secondary Analysis of a Randomized, Double-Anonymized, Placebo-Controlled Trial. *Chest*. 166:262-270.

Tibbitt, C.A., J.M. Stark, L. Martens, J. Ma, J.E. Mold, K. Deswarte, G. Oliynyk, X. Feng, B.N. Lambrecht, P. De Bleser, S. Nylen, H. Hammad, M. Arsenian Henriksson, Y. Saeys, and J.M. Coquet. 2019. Single-Cell RNA Sequencing of the T Helper Cell Response to House Dust Mites Defines a Distinct Gene Expression Signature in Airway Th2 Cells. *Immunity*. 51:169-184 e165.

Tsai, C.H., A.C. Lai, Y.C. Lin, P.Y. Chi, Y.C. Chen, Y.H. Yang, C.H. Chen, S.Y. Shen, T.L. Hwang, M.W. Su, I.L. Hsu, Y.C. Huang, A.H. Maitland-van der Zee, M.J. McGeachie, K.G. Tantisira, Y.J. Chang, and Y.L. Lee. 2023. Neutrophil extracellular trap production and CCL4L2 expression influence corticosteroid response in asthma. *Sci Transl Med*. 15:eadf3843.

Tsai, W.C., M.L. Rodriguez, K.S. Young, J.C. Deng, V.J. Thannickal, K. Tateda, M.B. Hershenson, and T.J. Standiford. 2004. Azithromycin blocks neutrophil recruitment in Pseudomonas endobronchial infection. *Am J Respir Crit Care Med*. 170:1331-1339.

Ubel, C., N. Sopel, A. Graser, K. Hildner, C. Reinhardt, T. Zimmermann, R.J. Rieker, A. Maier, M.F. Neurath, K.M. Murphy, and S. Finotto. 2014. The activating protein 1 transcription factor basic leucine zipper transcription factor, ATF-like (BATF), regulates lymphocyte- and mast cell-driven immune responses in the setting of allergic asthma. *J Allergy Clin Immunol*. 133:198-206 e191-199.

Uehara, S., K. Hirai, T. Shirai, T. Akamatsu, and K. Itoh. 2025. PI3K pathway activation in severe asthma is linked to steroid insensitivity and adverse outcomes. *J Allergy Clin Immunol Glob*. 4:100439.

Undela, K., L. Goldsmith, K.M. Kew, and G. Ferrara. 2021. Macrolides versus placebo for chronic asthma. *Cochrane Database Syst Rev*. 11:CD002997.

Unger, B.L., A.N. Faris, S. Ganesan, A.T. Comstock, M.B. Hershenson, and U.S. Sajjan. 2012. Rhinovirus attenuates non-typeable Hemophilus influenzae-stimulated IL-8 responses via TLR2-dependent degradation of IRAK-1. *PLoS Pathog*. 8:e1002969.

Van Eldere, J., M.P. Slack, S. Ladhani, and A.W. Cripps. 2014. Non-typeable Haemophilus influenzae, an under-recognised pathogen. *Lancet Infect Dis*. 14:1281-1292.

van Woerden, H.C., C. Gregory, R. Brown, J.R. Marchesi, B. Hoogendoorn, and I.P. Matthews. 2013. Differences in fungi present in induced sputum samples from asthma patients and non-atopic controls: a community based case control study. *BMC Infect Dis*. 13:69.

Vandenplas, O. 2011. Occupational asthma: etiologies and risk factors. *Allergy Asthma Immunol Res*. 3:157-167.

Varenyiova, Z., L.S. Rojas-Hernandez, J. Spano, V. Capek, Y. Rosenberg-Hasson, T. Holmes, and C. Milla. 2023. Azithromycin promotes proliferation, and inhibits inflammation in nasal epithelial cells in primary ciliary dyskinesia. *Sci Rep*. 13:14453.

Venkataraman, A., C.M. Bassis, J.M. Beck, V.B. Young, J.L. Curtis, G.B. Huffnagle, and T.M. Schmidt. 2015. Application of a neutral community model to assess structuring of the human lung microbiome. *mBio*. 6.

Versi, A., A. Azim, F.X. Ivan, M.I. Abdel-Aziz, S. Bates, J. Riley, M. Uddin, N. Zounemat Kermani, A.H. Maitland-Van Der Zee, S.E. Dahlen, R. Djukanovic, S.H. Chotirmall, P. Howarth, I.M. Adcock, K.F. Chung, and U.B.s. group. 2024. A severe asthma phenotype of excessive airway Haemophilus influenzae relative abundance associated with sputum neutrophilia. *Clin Transl Med*. 14:e70007.

Versi, A., F.X. Ivan, M.I. Abdel-Aziz, S. Bates, J. Riley, F. Baribaud, N.Z. Kermani, P. Montuschi, S.E. Dahlen, R. Djukanovic, P. Sterk, A.H. Maitland-Van Der Zee, S.H. Chotirmall, P. Howarth, I.M. Adcock, K.F. Chung, and U.B. consortium. 2023. Haemophilus influenzae and Moraxella catarrhalis in sputum of severe asthma with inflammasome and neutrophil activation. *Allergy*. 78:2906-2920.

Vieira Braga, F.A., G. Kar, M. Berg, O.A. Carpaij, K. Polanski, L.M. Simon, S. Brouwer, T. Gomes, L. Hesse, J. Jiang, E.S. Fasouli, M. Efremova, R. Vento-Tormo, C. Talavera-Lopez, M.R. Jonker, K. Affleck, S. Palit, P.M. Strzelecka, H.V. Firth, K.T. Mahbubani, A. Cvejic, K.B. Meyer, K. Saeb-Parsy, M. Luinge, C.A. Brandsma, W. Timens, I. Angelidis, M. Strunz, G.H. Koppelman, A.J. van Oosterhout, H.B. Schiller, F.J. Theis, M. van den Berge, M.C. Nawijn, and S.A. Teichmann. 2019. A cellular census of human lungs identifies novel cell states in health and in asthma. *Nat Med*. 25:1153-1163.

Vier, J., M. Groth, M. Sochalska, and S. Kirschnek. 2016. The anti-apoptotic Bcl-2 family protein A1/Bfl-1 regulates neutrophil survival and homeostasis and is controlled via PI3K and JAK/STAT signaling. *Cell Death Dis*. 7:e2103.

Vignola, A.M., L. Riccobono, A. Mirabella, M. Profita, P. Chanez, V. Bellia, G. Mautino, P. D'Accardi, J. Bousquet, and G. Bonsignore. 1998. Sputum metalloproteinase-9/tissue inhibitor of metalloproteinase-1 ratio correlates with airflow obstruction in asthma and chronic bronchitis. *Am J Respir Crit Care Med*. 158:1945-1950.

Votintseva, A.A., L.J. Pankhurst, L.W. Anson, M.R. Morgan, D. Gascoyne-Binzi, T.M. Walker, T.P. Quan, D.H. Wyllie, C. Del Ojo Elias, M. Wilcox, A.S. Walker, T.E. Peto, and D.W. Crook. 2015. Mycobacterial DNA extraction for whole-genome sequencing from early positive liquid (MGIT) cultures. *J Clin Microbiol*. 53:1137-1143.

Walker, W.T., C.L. Jackson, R.N. Allan, S.A. Collins, M.J. Kelso, A. Rineh, N.R. Yepuri, B. Nicholas, L. Lau, D. Johnston, P. Lackie, S.N. Faust, J.S.A. Lucas, and L. Hall-Stoodley. 2017. Primary ciliary dyskinesia ciliated airway cells show increased susceptibility to Haemophilus influenzae biofilm formation. *Eur Respir J*. 50.

Wallwork, B., W. Coman, A. Mackay-Sim, L. Greiff, and A. Cervin. 2006. A double-blind, randomized, placebo-controlled trial of macrolide in the treatment of chronic rhinosinusitis. *Laryngoscope*. 116:189-193.

Wang, B., D.J. Lim, J. Han, Y.S. Kim, C.B. Basbaum, and J.D. Li. 2002. Novel cytoplasmic proteins of nontypeable Haemophilus influenzae up-regulate human MUC5AC mucin transcription via a positive p38 mitogen-activated protein kinase pathway and a negative phosphoinositide 3-kinase-Akt pathway. *J Biol Chem*. 277:949-957.

Wang, Y., M.A. Su, and Y.Y. Wan. 2011. An essential role of the transcription factor GATA-3 for the function of regulatory T cells. *Immunity*. 35:337-348.

Wang, Z., N. Locantore, K. Haldar, M.Y. Ramsheh, A.S. Beech, W. Ma, J.R. Brown, R. Tal-Singer, M.R. Barer, M. Bafadhel, G.C. Donaldson, J.A. Wedzicha, D. Singh, T.M.A. Wilkinson, B.E. Miller, and C.E. Brightling. 2021. Inflammatory Endotype-associated

Airway Microbiome in Chronic Obstructive Pulmonary Disease Clinical Stability and Exacerbations: A Multicohort Longitudinal Analysis. *Am J Respir Crit Care Med*. 203:1488-1502.

Wark, P.A., S.L. Johnston, F. Bucchieri, R. Powell, S. Puddicombe, V. Laza-Stanca, S.T. Holgate, and D.E. Davies. 2005. Asthmatic bronchial epithelial cells have a deficient innate immune response to infection with rhinovirus. *J Exp Med*. 201:937-947.

Webb, L.M., R.J. Lundie, J.G. Borger, S.L. Brown, L.M. Connor, A.N. Cartwright, A.M. Dougall, R.H. Wilbers, P.C. Cook, L.H. Jackson-Jones, A.T. Phythian-Adams, C. Johansson, D.M. Davis, B.G. Dewals, F. Ronchese, and A.S. MacDonald. 2017. Type I interferon is required for T helper (Th) 2 induction by dendritic cells. *EMBO J*. 36:2404-2418.

Weisburg, W.G., S.M. Barns, D.A. Pelletier, and D.J. Lane. 1991. 16S ribosomal DNA amplification for phylogenetic study. *J Bacteriol*. 173:697-703.

Weiss, S.T., and A.A. Litonjua. 2011. Vitamin D in asthma and allergy: what next? *Eur Respir J*. 38:1255-1257.

Weste, J., T. Houben, S. Harder, H. Schluter, E. Lucke, J. Schreiber, and W. Hoffmann. 2022. Different Molecular Forms of TFF3 in the Human Respiratory Tract: Heterodimerization with IgG Fc Binding Protein (FCGBP) and Proteolytic Cleavage in Bronchial Secretions. *Int J Mol Sci*. 23.

Whetstone, C.E., M. Ranjbar, H. Omer, R.P. Cusack, and G.M. Gauvreau. 2022. The Role of Airway Epithelial Cell Alarmins in Asthma. *Cells*. 11.

Wigerblad, G., Q. Cao, S. Brooks, F. Naz, M. Gadkari, K. Jiang, S. Gupta, L. O'Neil, S. Dell'Orso, M.J. Kaplan, and L.M. Franco. 2022. Single-Cell Analysis Reveals the Range of Transcriptional States of Circulating Human Neutrophils. *J Immunol*. 209:772-782.

Wight, T.N., I. Kang, S.P. Evanko, I.A. Harten, M.Y. Chang, O.M.T. Pearce, C.E. Allen, and C.W. Frevert. 2020. Versican-A Critical Extracellular Matrix Regulator of Immunity and Inflammation. *Front Immunol*. 11:512.

Willems-Widyastuti, A., B.M. Vanaudenaerde, R. Vos, E. Dilisen, S.E. Verleden, S.I. De Vleeschauwer, A. Vaneylen, W.J. Mooi, W.I. de Boer, H.S. Sharma, and G.M. Verleden. 2013. Azithromycin attenuates fibroblast growth factors induced vascular endothelial growth factor via p38(MAPK) signaling in human airway smooth muscle cells. *Cell Biochem Biophys*. 67:331-339.

Willner, D., M.R. Haynes, M. Furlan, R. Schmieder, Y.W. Lim, P.B. Rainey, F. Rohwer, and D. Conrad. 2012. Spatial distribution of microbial communities in the cystic fibrosis lung. *ISME J*. 6:471-474.

Wilms, E.B., D.J. Touw, and H.G. Heijerman. 2006. Pharmacokinetics of azithromycin in plasma, blood, polymorphonuclear neutrophils and sputum during long-term therapy in patients with cystic fibrosis. *Ther Drug Monit*. 28:219-225.

Winkler, C., T. Hochdorfer, E. Israelsson, A. Hasselberg, A. Cavallin, K. Thorn, D. Muthas, S. Shojaee, K. Luer, M. Muller, J. Mjosberg, O. Vaarala, J. Hohlfeld, and K. Pardali. 2019. Activation of group 2 innate lymphoid cells after allergen challenge in asthmatic patients. *J Allergy Clin Immunol*. 144:61-69 e67.

Winslow, S., L. Odqvist, S. Diver, R. Riise, S. Abdillahi, C. Wingren, H. Lindmark, A. Wellner, S. Lundin, L. Yrlid, E. Ax, R. Djukanovic, S. Sridhar, A. Higham, D. Singh, T. Southworth, C.E. Brightling, H.K. Olsson, and Z. Jevnikar. 2021. Multi-omics links IL-6 trans-signalling with neutrophil extracellular trap formation and Haemophilus infection in COPD. *Eur Respir J*. 58.

Wolock, S.L., R. Lopez, and A.M. Klein. 2019. Scrublet: Computational Identification of Cell Doublets in Single-Cell Transcriptomic Data. *Cell Syst*. 8:281-291 e289.

Wood, L.G., Q. Li, H.A. Scott, S. Rutting, B.S. Berthon, P.G. Gibson, P.M. Hansbro, E. Williams, J. Horvat, J.L. Simpson, P. Young, B.G. Oliver, and K.J. Baines. 2019. Saturated fatty acids, obesity, and the nucleotide oligomerization domain-like receptor protein 3 (NLRP3) inflammasome in asthmatic patients. *J Allergy Clin Immunol*. 143:305-315.

Woodcock, A., J. Vestbo, N.D. Bakerly, J. New, J.M. Gibson, S. McCorkindale, R. Jones, S. Collier, J. Lay-Flurrie, L. Frith, L. Jacques, J.L. Fletcher, C. Harvey, H. Svedsater, D. Leather, and I. Salford Lung Study. 2017. Effectiveness of fluticasone furoate plus vilanterol on asthma control in clinical practice: an open-label, parallel group, randomised controlled trial. *Lancet*. 390:2247-2255.

Wos, M., M. Sanak, J. Soja, H. Olechnowicz, W.W. Busse, and A. Szczeklik. 2008. The presence of rhinovirus in lower airways of patients with bronchial asthma. *Am J Respir Crit Care Med*. 177:1082-1089.

Wu, B.G., I. Sulaiman, J.J. Tsay, L. Perez, B. Franca, Y. Li, J. Wang, A.N. Gonzalez, M. El-Ashmawy, J. Carpenito, E. Olsen, M. Sauthoff, K. Yie, X. Liu, N. Shen, J.C. Clemente, B. Kapoor, T. Zangari, V. Mezzano, C. Loomis, M.D. Weiden, S.B. Koralov, J. D'Armiento, S.K. Ahuja, X.R. Wu, J.N. Weiser, and L.N. Segal. 2021. Episodic Aspiration with Oral Commensals Induces a MyD88-dependent, Pulmonary T-Helper Cell Type 17 Response that Mitigates Susceptibility to Streptococcus pneumoniae. *Am J Respir Crit Care Med*. 203:1099-1111.

Wu, W., J. Gao, D. Chen, G. Chen, Y. Feng, C. Chang, S. Chen, L. Yi, and G. Zhen. 2022. Epithelial microRNA-30a-3p targets RUNX2/HMGB1 axis to suppress airway eosinophilic inflammation in asthma. *Respir Res*. 23:17.

Wullaert, A., L. Verstrepen, S. Van Huffel, M. Adib-Conquy, S. Cornelis, M. Kreike, M. Haegman, K. El Bakkouri, M. Sanders, K. Verhelst, I. Carpentier, J.M. Cavaillon, K. Heyninck, and R. Beyaert. 2007. LIND/ABIN-3 is a novel lipopolysaccharide-inducible inhibitor of NF-kappaB activation. *J Biol Chem*. 282:81-90.

Yadati, T., T. Houben, A. Bitorina, and R. Shiri-Sverdlov. 2020. The Ins and Outs of Cathepsins: Physiological Function and Role in Disease Management. *Cells*. 9.

Yamaryo, T., K. Oishi, H. Yoshimine, Y. Tsuchihashi, K. Matsushima, and T. Nagatake. 2003. Fourteen-member macrolides promote the phosphatidylserine receptor-dependent phagocytosis of apoptotic neutrophils by alveolar macrophages. *Antimicrob Agents Chemother*. 47:48-53.

Young, M.D., and S. Behjati. 2020. SoupX removes ambient RNA contamination from droplet-based single-cell RNA sequencing data. *Gigascience*. 9.

Yu, G., and Q.Y. He. 2016. ReactomePA: an R/Bioconductor package for reactome pathway analysis and visualization. *Mol Biosyst*. 12:477-479.

Yu, G., L.G. Wang, Y. Han, and Q.Y. He. 2012. clusterProfiler: an R package for comparing biological themes among gene clusters. *OMICS*. 16:284-287.

Zaiss, D.M., L. Yang, P.R. Shah, J.J. Kobie, J.F. Urban, and T.R. Mosmann. 2006. Amphiregulin, a TH2 cytokine enhancing resistance to nematodes. *Science*. 314:1746.

Zhang, B., T.J. Kopper, X. Liu, Z. Cui, S.G. Van Lanen, and J.C. Gensel. 2019. Macrolide derivatives reduce proinflammatory macrophage activation and macrophage-mediated neurotoxicity. *CNS Neurosci Ther*. 25:591-600.

Zhang, F., G. Liu, D. Li, C. Wei, and J. Hao. 2018. DDIT4 and Associated lncDDIT4 Modulate Th17 Differentiation through the DDIT4/TSC/mTOR Pathway. *J Immunol*. 200:1618-1626.

Zhang, T., H. Li, S. Ma, J. Cao, H. Liao, Q. Huang, and W. Chen. 2023. The newest Oxford Nanopore R10.4.1 full-length 16S rRNA sequencing enables the accurate resolution of species-level microbial community profiling. *Appl Environ Microbiol*. 89:e0060523.

Zhao, J., C.M. Lloyd, and A. Noble. 2013. Th17 responses in chronic allergic airway inflammation abrogate regulatory T-cell-mediated tolerance and contribute to airway remodeling. *Mucosal Immunol*. 6:335-346.

Zhou, Y., D. Jackson, L.B. Bacharier, D. Mauger, H. Boushey, M. Castro, J. Durack, Y. Huang, R.F. Lemanske, Jr., G.A. Storch, G.M. Weinstock, K. Wylie, R. Covar, A.M. Fitzpatrick, W. Phipatanakul, R.G. Robison, and A. Beigelman. 2019. The upper-airway microbiota and loss of asthma control among asthmatic children. *Nat Commun*. 10:5714.

Zhou, Y., K.A. Mihindukulasuriya, H. Gao, P.S. La Rosa, K.M. Wylie, J.C. Martin, K. Kota, W.D. Shannon, M. Mitreva, E. Sodergren, and G.M. Weinstock. 2014. Exploration of bacterial community classes in major human habitats. *Genome Biol*. 15:R66.

Zimmermann, P., V.C. Ziesenitz, N. Curtis, and N. Ritz. 2018. The Immunomodulatory Effects of Macrolides-A Systematic Review of the Underlying Mechanisms. *Front Immunol*. 9:302.

Zong, D., R. Ouyang, J. Li, Y. Chen, and P. Chen. 2016. Notch signaling in lung diseases: focus on Notch1 and Notch3. *Ther Adv Respir Dis*. 10:468-484.

Appendix 1: Jabeen *et al* 2022

Identifying Bacterial Airways Infection in Stable Severe Asthma Using Oxford Nanopore Sequencing Technologies: Supplementary Material

Table S1: Clinical characteristics and airway inflammatory cell parameters of healthy control

Characteristic	Healthy control
Sex	Female
Age (years)	28
BMI (kg/m^2)	20.7
Presence of atopy	Nil
Smoking history	Ex-smoker
Pack years	10
FEV1 (L)	2.36
FVC (L)	2.78
FEV1/FVC	0.83
FeNO (ppb)	23
Blood eosinophils (x10^9/L)	0.16
Sputum eosinophils (%)	0
Sputum neutrophils (%)	53.2

Table S2: Sputum culture results; gold standard culture of induced sputum plug samples and speciation with MALDI-TOF

PID	Bacterial species identified on culture
1054	*Haemophilus influenzae, Streptococcus pneumoniae, Streptococcus parasanguinis, 2 unclassified species**
278	*Haemophilus influenzae, Streptococcus mitis, Streptococcus vestibularis*
133	*Haemophilus influenzae, Streptococcus pneumoniae, Streptococcus parasanguinis*
297	*Haemophilus influenzae, Streptococcus pneumoniae, Streptococcus vestibularis, 2 unclassified species**
288	*Haemophilus influenzae, Rothia mucilaginosa*
29	*Haemophilus influenzae, Streptococcus pneumoniae, Streptococcus salivarius, Rothia mucilaginosa*
214	*Haemophilus influenzae (clinical laboratory result)*
1049	*Streptococcus pneumoniae, Streptococcus agalactiae, Neisseria macacae, Streptococcus vestibularis, Streptococcus salivarius, Streptococcus oralis*
235	*Mixed upper respiratory tract flora (clinical laboratory result)*
306	*Streptococcus salivarius, Streptococcus parasanguinis, Rothia dentocarinosa, 2 unclassified species**
187	*Mixed upper respiratory tract flora (clinical laboratory result)*
1052	*Rothia mucilaginosa, Streptococcus parasangunis*
294	*Streptococcus vestibularis, Rothia mucilaginosa, Neisseria subflava, Streptococcus salivarius, Streptococcus parasanguinis, Neisseria flavescens*
1055	*Rothia mucilaginosa, Neisseria perflava, Streptococcus vestibularis, Streptococcus parasanguinis, Streptococcus salivarius*
1053	*Streptococcus mitis, Streptococcus sangunis, Streptococcus infantis*
1041	*Streptococcus pneumoniae, Streptococcus vestibularis, Rothia mucilaginosa, Streptococcus oralis*
5	*Rothia mucilaginosa, Streptococcus parasangunis, Streptococcus salivarius, Neisseria flavescens*
275	*Streptococcus pneumoniae, Streptococcus mitis, Streptococcus anginosus, 4 unclassified species**
315	*Streptococcus mitis, Streptococcus vestibularis, Neisseria flavescens, 3 unclassified species**
1060	*Streptococcus salivarius, Streptococcus parasanguinis, Streptococcus mitis*
279	*Streptococcus mitis, Streptococcus parasanguinis, Rothia dentocarinosa, Streptococcus vestibularis, Streptococcus salivarius, Streptococcus anginosus*
295	*Streptococcus salivarius, Rothia mucilaginosa, Streptococcus mitis, Streptococcus vestibularis*
1058	*Neisseria subflava, Neisseria flavescens, Streptococcus salivarius, Rothia dentocarinosa*

**Unclassified result on MALDI-TOF (including following formic acid treatment)*

Figure S1: Comparison of methods for depletion of human DNA with differential centrifugation and NEBNext microbiome DNA enrichment kit (n=2); (a) Percentage of total unfiltered reads by parameter detected using each DNA extraction method (mean, SD), (b) Total bacterial load measured by bacterial 16S RT-qPCR (mean, SD)

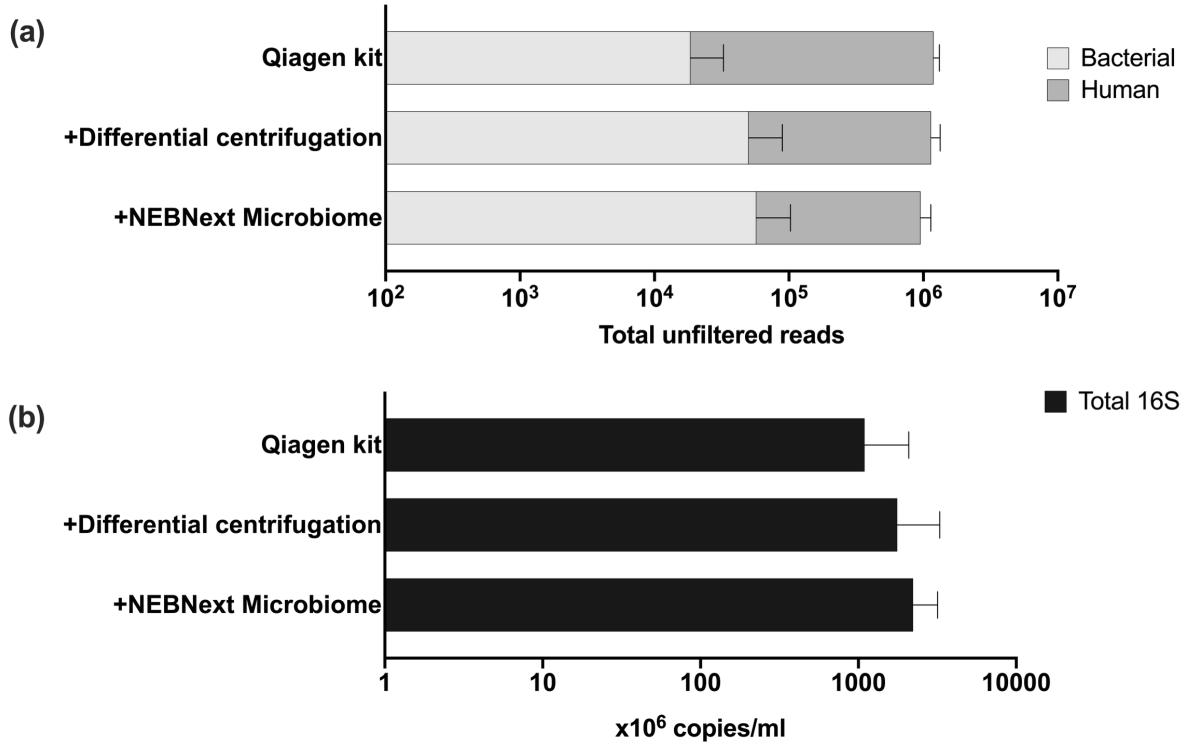


Figure S2: Total number of bacterial and human reads with (a) ONT and (b) Illumina MiSeq upon mapping all metagenomic sequencing reads. Total human reads are a sum of human reads removed following mapping to the human genome and residual reads subsequently detected by Centrifuge. This is plotted with the number human reads removed after mapping to the human genome in (c) and (d).

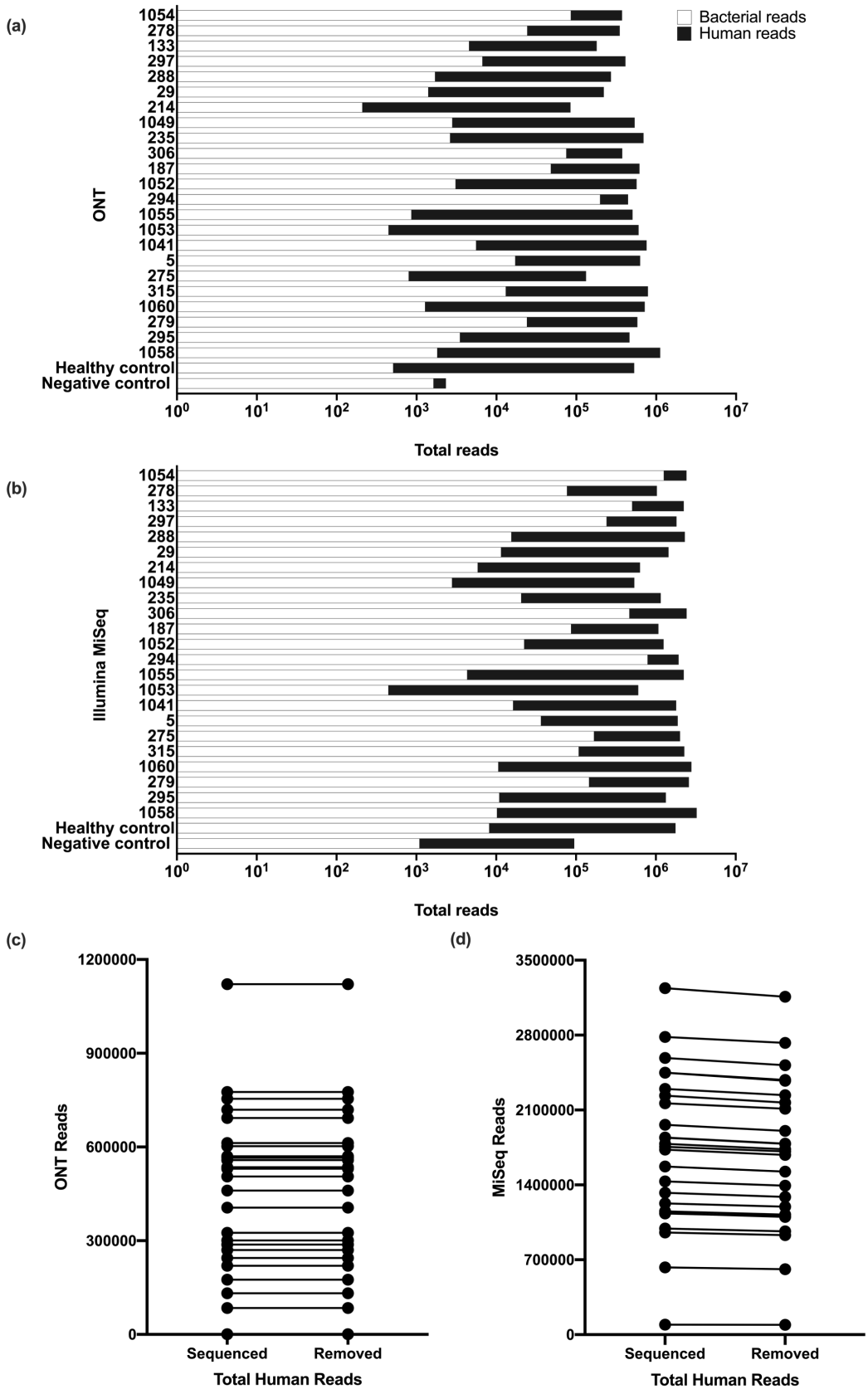


Table S3: Mapping coverage statistics of consensus fasta sequences; 4 clinical samples positive for H. influenzae (PID: 278, 133, 29, 288) and each corresponding bacterial isolate (*H.inf*_278, *H.inf*_133, *H.inf*_29, *H.inf*_288) are shown

Sample	As	Cs	Gs	Ns	Ts	Bases covered	% Covered	Length (bp)
PID 278	521515	317255	314865	157459	519044	1672679	91.4	1830138
H. inf_278	521365	321867	318231	149113	519562	1681025	91.9	1830138
PID 133	308467	184702	184786	846122	306061	984016	53.8	1830138
H. inf_133	521055	321265	318636	149903	519279	1680235	91.8	1830138
PID29	741	532	471	1827537	857	2601	0.1	1830138
H. inf_29	528329	325443	322892	126355	527119	1703783	93.1	1830138
PID 288	7581	4800	4415	1805539	7803	24599	1.3	1830138
H. inf_288	524167	323136	319242	141942	521651	1688196	92.2	1830138

Appendix 2: Jabeen *et al.* 2024

Supplementary and Results: Species-level, metagenomic and proteomic analysis of microbe-immune interactions in severe asthma

Supplementary Methods

1. Microbial DNA extraction with human DNA depletion

Established methods were used for microbial DNA extraction[1]. Briefly, homogenised sputum or nasal lavage underwent differential centrifugation prior to DNA extraction using the QIAamp DNA Mini Kit (Qiagen, Manchester, UK) as per manufacturer's instructions with previously described modification[1].

2. Oxford Nanopore Technologies (ONT) sequencing

Libraries were prepared for sequencing on an Oxford Nanopore GridION (Oxford Nanopore Technologies (ONT), Oxford, UK) using the Rapid PCR Barcoding kit (SQK-RPB004) with modifications to the manufacturer's protocol as previously reported [1]. Samples were sequenced on ONT FLOMIN106D (ONT v.R9.4.1) flow cells in batches of 6 samples per flow cell.

3. Pathogen specific PCR analysis

Quantitative real-time PCR (qPCR) was performed to quantify relative abundance of *H. influenzae*, *S. pneumoniae*, *S. aureus*, *M. catarrhalis* and *P. aeruginosa* using methods and reactions conditions previously described[1].

4. Measurement of inflammatory mediators

Existing dataset utilised from Hinks *et al*.[2]. Inflammatory mediators measured from sputum by enzymelinked immunosorbent assays (ELISA) were myeloperoxidase (MPO), elastase (Hycult), eosinophil cationic protein (MBL International), interleukin (IL)-5 (Abnova), IL-6, ENA-78, Eotaxin, FGF, osteopontin, VEGF, YKL-40 (R&D Systems), tryptase and α2-macroglobulin (A Walls4), as per manufacturer's instructions. Fluoroenzyme immunoassay was used for total and specific IgE (ImmunoCAP, Phadia) and cytokine bead array (Luminex®) for matrix metalloproteases (MMPs), tissue inhibitor of matrix metalloproteinase 1 (TIMP-1), G-CSF, GM-CSF, Gro-α, IFN-γ, IL-1 α, IL-1 β, IL-1RA, IL-2, IL-4, IL-8, IL6SR, IL-10, IL-13, IL-17, MCP-1, MIP-1 α, MIP-1 β and TNF-α.

In addition, sputum and nasal lavage samples were analysed by O-link (Uppsala, Sweden) using a 92 mediator in-house Proseek Multiplex Inflammation I panel including: 4E-BP1, Adenosine deaminase, Artemin, Axin-1, Beta-nerve growth factor, Caspase-8, C-C motif chemokine 11, C-C motif chemokine 13, C-C motif chemokine 19, C-C motif chemokine 2, C-C motif chemokine 20, C-C motif chemokine 23, C-C motif chemokine 25, C-C motif chemokine 28, C-C motif chemokine 3, C-C motif chemokine 4, C-C motif chemokine 7, C-C motif chemokine 8, CD antigen: CD, CD antigen: CD137, CD antigen: CD150, CD antigen: CD318, CD antigen: CD40, CD antigen: CD6, CD antigen: CD8a, CSF-1, C-X-C motif chemokine 1, C-X-C motif chemokine 10, C-X-C motif chemokine 11, C-X-C motif chemokine 5, C-X-C motif chemokine 6, C-X-C motif chemokine 9, Cystatin-D, Delta and Notch-like epidermal growth factor-related receptor, FGF-19, FGF-21, FGF-23, FGF-5, Flt3 ligand, Fractalkine, Hepatocyte growth factor, hGDNF, HVEM-L, IL-10R subunit alpha, IL-10R subunit beta, IL-12B, IL-15R-alpha, IL-20Ralpha, IL-22R-alpha-1, IL-2R subunit beta, Interferon

gamma, Interleukin-1 alpha, Interleukin-10, Interleukin-13, Interleukin-17A, Interleukin-17C, Interleukin-18, Interleukin-18 receptor 1, Interleukin-2,
Interleukin-20, Interleukin-24, Interleukin-33, Interleukin-4, Interleukin-5, Interleukin-6, Interleukin-7,
Interleukin-8, Kit ligand, LAP, LIF, LIF-R, Lymphotoxin-alpha, MMP-1, MMP-10, NAIL, Neurotrophin-3, Neurturin, Oncostatin-M, Osteoprotegerin, PD-L1, Protein S100-A12, RANKL soluble, SIR2-like protein 2, STAM-binding protein, Sulfotransferase 1A1, TGF-alpha, Thymic stromal lymphopoietin, TRAIL,
Tumor necrosis factor, TWEAK, U-plasminogen activator, VEGF-A, 4E-BP1, Adenosine deaminase, Artemin, Axin-1, Beta-nerve growth factor, Caspase-8, C-C motif chemokine 11, C-C motif chemokine 13, C-C motif chemokine 19, C-C motif chemokine 2, C-C motif chemokine 20, C-C motif chemokine 23, C-C motif chemokine 25, C-C motif chemokine 28, C-C motif chemokine 3, C-C motif chemokine 4, C-C motif chemokine 7 and C-C motif chemokine 8.

5. Bioinformatic analysis

Sequences were basecalled using Guppy (ONT, version 3.3.0+ef22818), analysed using the CRuMPIT pipeline, and taxonomic classification of trimmed reads performed using Centrifuge as previously described[1]. Kraken style reports, produced following taxonomic classification of trimmed reads, were used for downstream analysis. A description of bioinformatics and secondary analysis is provided in the GitLab repository: https://gitlab.com/ModernisingMedicalMicrobiology/wessex_analysis

Metagenomic and integrated cytokine analysis;

5.1 Visualisation of metagenomic data; Kraken style reports were produced following taxonomic classification of trimmed reads. Raw species level reads (Wessex, n=66; Oxford,

n=30) from sputum samples were combined into two datasets, 7644 and 3860 unique species were identified respectively. Low abundance species (<1000 reads across all samples) were removed prior to normalisation (DESeq2) thereby reducing unique species to 253 and 72, respectively. The two datasets were merged by common detected species (n=70) and z-scores derived for heatmaps. Principal component analysis (PCA) plots were produced to provide a low dimensional representation of the 3 participant groups (healthy, moderate and severe asthma) in the Wessex cohort and the two severe asthma groups (Wessex and Oxford). Groups of samples were compared by permutational multivariate ANOVA (PERMANOVA) performed using the adonis function in the Vegan package. Wald test used to identify species uniquely abundant or depleted in HC, MA and SA, or by inflammatory phenotype (using

DESeq2, log fold change [LFC] > 1 or <1 respectively, adjusted $P < 0.05$).

5.2 Sankey visualisations*;* Individual or combined Kraken style reports used to produce Sankey visualisations of taxonomic profiles using Pavian[3]. Where a dominant pathogen was identified on metagenomic sequencing in more than one individual, the relative abundance of these bacteria (*H. influenzae, M. catarrhalis, S. pneumonia*) was compared against the relative abundance of other detected species within each sample using Wilcoxon rank-sum test, using Benjamini-Hochberg [BH] correction FDR 0.05, in order to provide statistical support for the skewed metagenomic profiles shown.

5.3 Normalisation, integration and visualisation of cytokine and metagenomic data*;* Raw cytokine measurements were centralised by z-score, clustering was performed by cytokine and subjects, with clustering distances visualised in heatmap representing correlation distances. To integrate metagenomic and cytokine data within the combined Wessex dataset (HC, MA, SA), species level reads were normalised, and log transformed, while cytokines were centralised by z-score prior to computation of Spearman correlation between shared

species (~253) and cytokines by matching across samples (adjusted for multiple comparisons with Benjamini–Hochberg procedure [FDR 0.05]). The 50 species with greatest variance in abundance across subjects were selected for clustering analysis by cytokines (columns) and species (rows).

5.4 Bayesian network analysis*;* Connections between cytokines associated to airways infection, clinical parameters, and differentially abundant bacterial species in severe asthma was explored by Bayesian network analysis (Genie 2.0; Decision Systems Laboratory, University of Pittsburgh, Pittsburgh, Pa). Data from 51 severe asthmatics (60 variables) were discretised into 2 (binary variables) or 3 to 5 (continuous variables) bins (variables shown in Table S8). Using the 'clustering algorithm'[4] 34/60 variables were retained in the model. The Bayesian network generated was re-plotted using shinyBN[5]. In a subsequent separate analysis strengths of associations were further explored using Pearson (between species) or Spearman correlation (between cytokines). Positive linear correlations are highlighted with a green edge.

5.5 Integration of nasal lavage and sputum metagenomics and O-link data*;* Low abundance species (<200 reads across all individuals) were removed from nasal lavage and sputum samples (filtering to 94 and 349 species respectively) prior to scaling bacterial reads within samples. A combined dataset of shared nasal lavage and sputum species was produced (n=23) by selecting organism with highest variance in abundance across all samples (P<0.05). A PCA plot was produced using these samples and the two groups of samples compared by permutational multivariate ANOVA (PERMANOVA) performed using the adonis function in the Vegan package. Spearman correlation was performed using paired O-link proteomic data (92 protein panel) in sputum and nasal lavage and significantly correlated pairs of cytokines were filtered (P<<0.001) following adjustment for multiple corrections (n=38; sputum = 16, nasal=22).

References

Jabeen, M.F.*, et al.* Identifying Bacterial Airways Infection in Stable Severe Asthma Using Oxford Nanopore Sequencing Technologies. *Microbiol Spectr* 10, e0227921 (2022).

Hinks, T.S.C.*, et al.* Multidimensional endotyping in patients with severe asthma reveals inflammatory heterogeneity in matrix metalloproteinases and chitinase 3-like protein 1. *J Allergy Clin Immunol* 138, 61-75 (2016).

Breitwieser, F.P. & Salzberg, S.L. Pavian: interactive analysis of metagenomics data for microbiome studies and pathogen identification. *Bioinformatics* 36, 1303-1304 (2020).

BayesFusion. GeNIe Clustering algorithm. https://support.bayesfusion.com/docs/GeNIe/algorithms_clustering.html (accessed 202311-27.

Chen, J.*, et al.* shinyBN: an online application for interactive Bayesian network inference and visualization. *BMC Bioinformatics* 20, 711 (2019).

Supplementary Results

Data sharing

Raw FASTQ data are available on the European Nucleotide Archive with the project accession PRJEB62780. Remaining data analysed and presented in this study are available from the corresponding author on reasonable request, providing the request meets local ethical and research governance criteria after publication. Patient-level data will be anonymised.

Table E1 Clinical characteristics of severe asthma in Wessex Severe Asthma Cohort

Clinical characteristics of participants with severe asthma from the Wessex Severe Asthma Cohort without or with airways infection; BMI=body mass index; FEV1=Forced expiratory volume in 1s; FVC=Forced vital capacity; FeNO=exhaled nitric oxide; Inflammatory phenotypes: eosinophilic ≥3% sputum eosinophils, neutrophilic ≥61% sputum neutrophils and <3% eosinophils, mixed granulocytic ≥61% sputum neutrophils and ≥3% eosinophils, paucigranulocytic <61% sputum neutrophils and <3% eosinophils; SD= standard deviation, Q1=quartile 1, Q3=quartile3. †Student's t test, ‡Mann-Whitney U test, §Fisher exact test

Characteristic	**Airways infection absent** (n=41)	**Airways infection present** (n=11)	**P value**
Male gender, n (%)	16 (39.0)	6 (54.5)	0.49§
Age (years), Mean (SD)	49.0 (14.3)	51.0 (10.2)	0.63†
BMI (kg/m^2), Mean (SD)	32.9 (8.0)	29.1 (8.4)	0.20†
Presence of atopy, n (%)	25 (54.5)	7 (63.6)	>0.99§
Presence of nasal polyps, n (%)	6 (14.6)	1 (9.0)	>0.99§
Smoking status, n (%)			
Never	22 (53.6)	5 (45.5)	0.74§
Current	4 (9.8)	2 (18.2)	0.60§
Ex-smoker	15 (36.6)	4 (36.3)	>0.99§
Pack years, Mean (SD)	8.0 (12.8)	9.5 (14.2)	0.73†
Baseline inhaled corticosteroid use (BDP eq., mcg/d), Median (Q1,Q3)	2080 (1680, 3500)	2000 (1500,2600)	0.44‡
Maintenance oral corticosteroid, n (%)	16 (39.0)	3 (27.3)	0.47§

Unscheduled GP/ hospital visits in 12 months, Median (Q1,Q3)	1 (0,4)	1 (0,3)	0.98‡
FEV1 (%predicted), Mean (SD)	65.5 (25.0)	61.4 (27.8)	0.61†
FEV1/FVC, Mean (SD)	0.6 (0.1)	0.6 (0.2)	0.17†
FeNO (ppb), Mean (SD)	26.0 (29)	29.0 (26)	0.60†
Blood eosinophils (x10^9/L), Median (Q1,Q2)	0.2 (0.1,0.3)	0.2 (0.1, 0.6)	0.67‡
Sputum eosinophils (%), Median (Q1,Q3)	1.0 (0.3, 5.5)	1.5 (0.9,10.5)	0.21‡
Sputum neutrophils (%), Median (Q1,Q3)	46.8 (19.9, 62.5)	78 (48.8,87.5)	**0.01‡**
Sputum inflammatory phenotype, n (%)			
Eosinophilic	9 (22.0)	4 (36.0)	0.44§
Neutrophilic	8 (19.0)	5 (45.0)	0.07§
Mixed granulocytic	2 (5.0)	1 (9.5)	>0.99§
Paucigranulocytic	20 (49.0)	1 (9.5)	0.11§
No data	2 (5.0)	0 (0.0)	

Table E2 Clinical characteristics of severe asthma in Oxford Severe Asthma Cohort

Clinical characteristics of participants with severe asthma from the Oxford Severe Asthma Cohort without or with airways infection; BMI=body mass index; FEV1=Forced expiratory volume in 1s; FVC=Forced vital capacity; FeNO=exhaled nitric oxide; Inflammatory phenotypes: eosinophilic ≥3% sputum eosinophils, neutrophilic ≥61% sputum neutrophils and <3% eosinophils, mixed granulocytic ≥61% sputum neutrophils and ≥3% eosinophils, paucigranulocytic <61% sputum neutrophils and <3% eosinophils; SD= standard deviation, Q1=quartile 1, Q3=quartile3. *Student's t test, ‡Mann-Whitney U test, §Fisher exact test

Characteristic	**Airways infection absent** (n=22)	**Airways infection present** (n=8)	**P value**
Male gender, n (%)	11 (50)	3 (37.5)	0.69§
Age (years), Mean (SD)	58.0 (13.7)	66.0 (12.1)	0.15†
BMI (kg/m^2), Mean (SD)	29.0 (6.0)	30.0 (6.6)	0.72†
Presence of atopy, n (%)	5 (22.7)	1 (4.5)	>0.99§
Presence of nasal polyps, n (%)	7 (31.8)	1 (4.5)	0.39§
Smoking status, n (%)			
Never	16 (72.7)	6 (75.0)	>0.99§
Current	0 (0.0)	1 (4.5)	0.27§
Ex-smoker	6 (27.3)	1 (4.5)	0.63§
Pack years, Mean (SD)	7.1 (3.6)	25.5 (9.2)	0.01†
Baseline inhaled corticosteroid use (BDP eq., mcg/d), Median (Q1,Q3)	2000 (1600, 2000)	2000 (1700, 2000)	0.86‡
Maintenance oral corticosteroid, n (%)	3 (13.6)	1 (4.5)	0.94§
Unscheduled GP/ hospital visits in 12 months, Median (Q1,Q3)	2 (0, 7)	2 (0, 12)	0.98‡

FEV1 (%predicted), Mean (SD)	75.0 (21.5)	61.8 (30.0)	0.19†
FEV1/FVC, Mean (SD)	0.6 (0.1)	0.7 (0.1)	0.81†
FeNO (ppb), Mean (SD)	73.0 (73.2)	29.0 (16.1)	0.11†
Blood eosinophils (x10^9/L), Median (Q1,Q2)	0.4 (0.2, 0.9)	0.3 (0.1, 0.5)	0.53‡
Sputum eosinophils (%), Median (Q1,Q3)	12.0 (1.3, 51.5)	1.0 (0.1, 1.6)	**0.02‡**
Sputum neutrophils (%), Median (Q1,Q3)	31.0 (12.8, 56.4)	90.5 (51.5, 98.6)	**0.03‡**
Sputum inflammatory phenotype, n (%)			
Eosinophilic	11 (50.0)	0 (0.0)	**0.01§**
Neutrophilic	2 (9.0)	4 (50.0)	**0.03§**
Mixed granulocytic	1 (4.5)	0 (0.0)	>0.99§
Paucigranulocytic	3 (13.6)	1 (4.5)	>0.99§
No data	5 (22.7)	3 (37.5)	

Figure E1 Study design

(Created with BioRender.com)

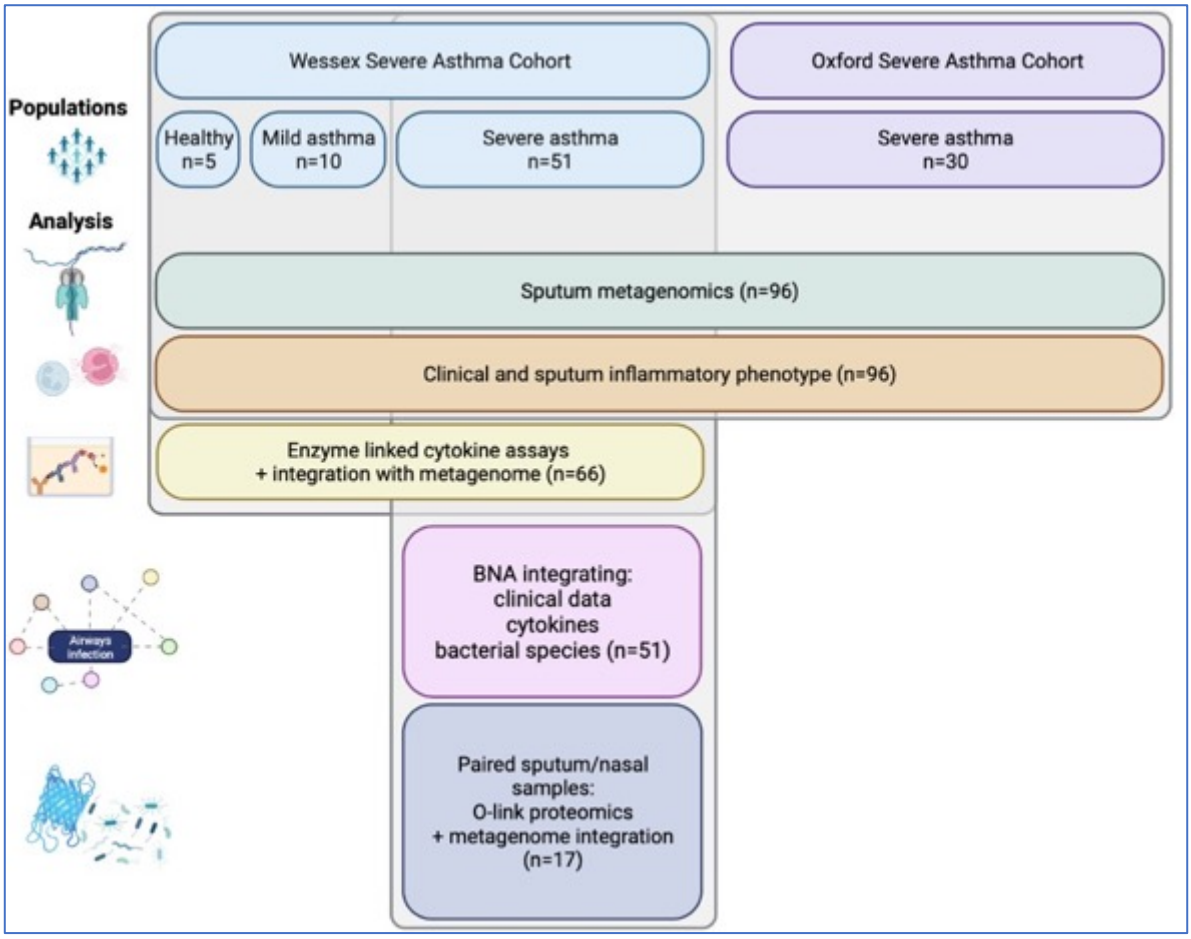
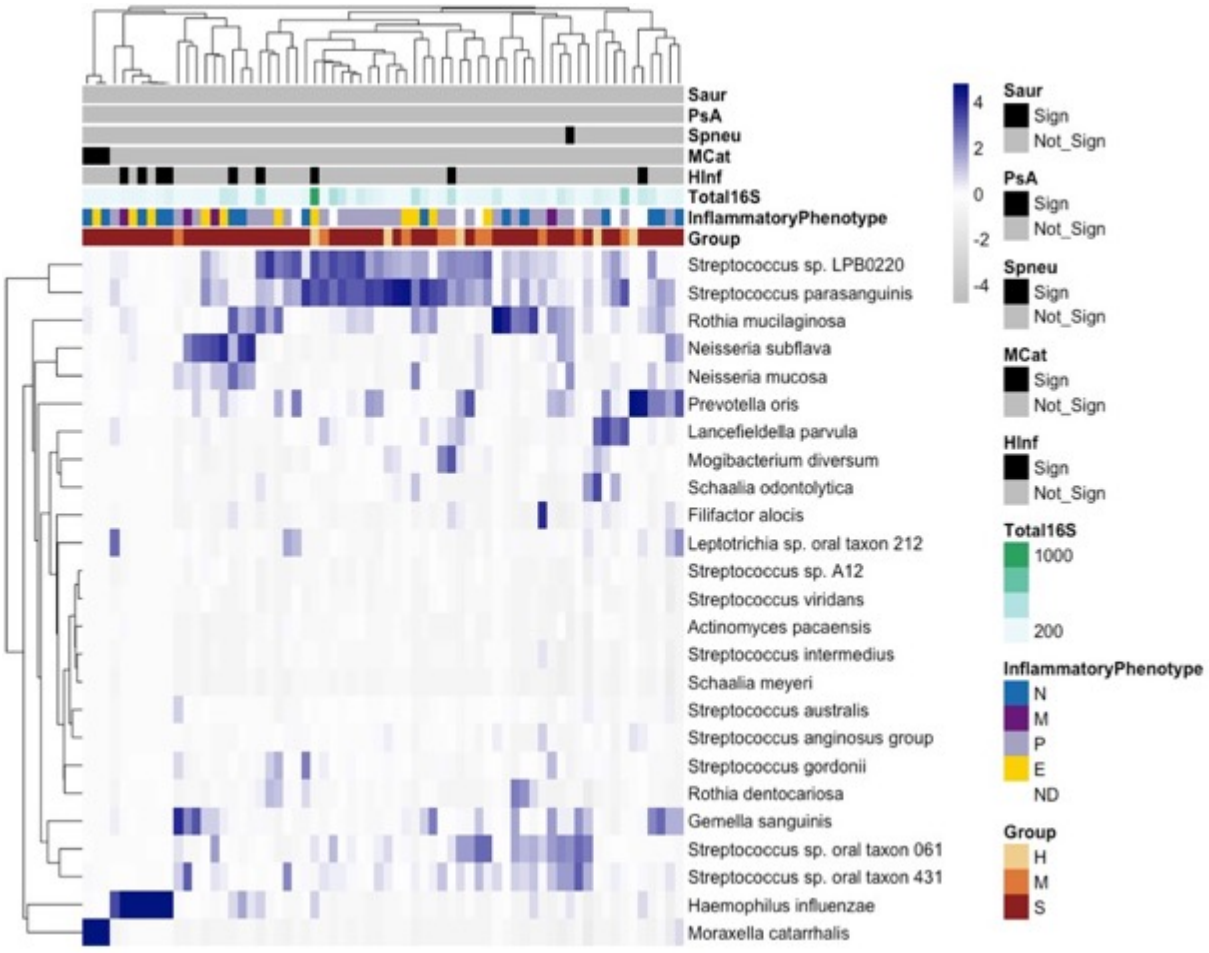


Figure E2 Heatmap of relative abundance of species

Heatmap of relative abundance of species from induced sputum sequenced samples using ONT; Zscores, denoted by shade, represent the number of standard deviations above the mean number of reads per taxon for each sample. Cohorts include (a) Wessex and (b) Oxford. Clustering performed independently on samples and most differentially abundant bacterial species. Sputum inflammatory phenotypes are eosinophilic (E), neutrophilic (N), mixed granulocytic (M) and paucigranulocytic (P). Positive pathogen specific PCR result (>1x10^{6}copies/ml) is indicated in black: S. aureus (Saur), P. aeruginosa (PsA), S. pneumoniae (Spneu), M. catarrhalis (Mcat) and H. influenzae (Hinf). Total eubacteria (16S) PCR load is denoted by shade (x10^{6}copies/ml).

(a)



(b)

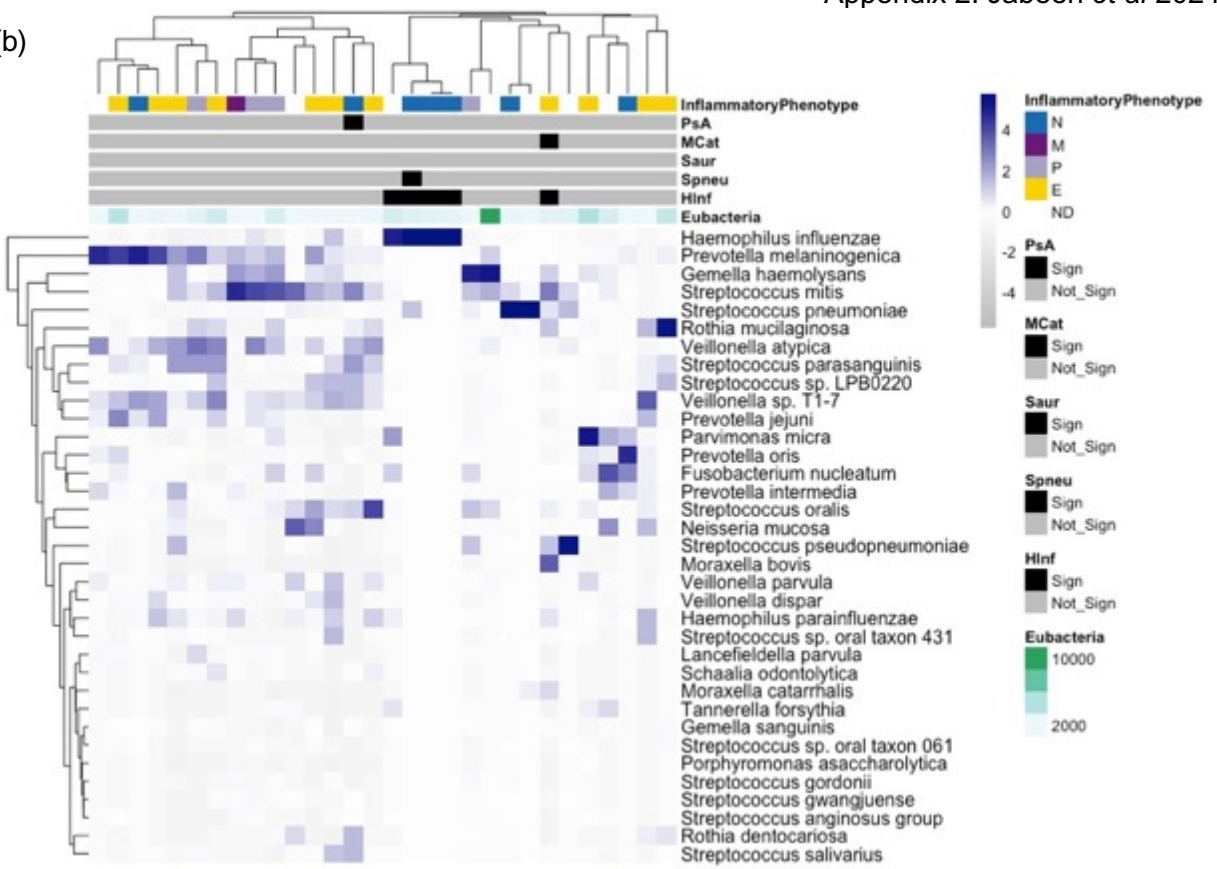
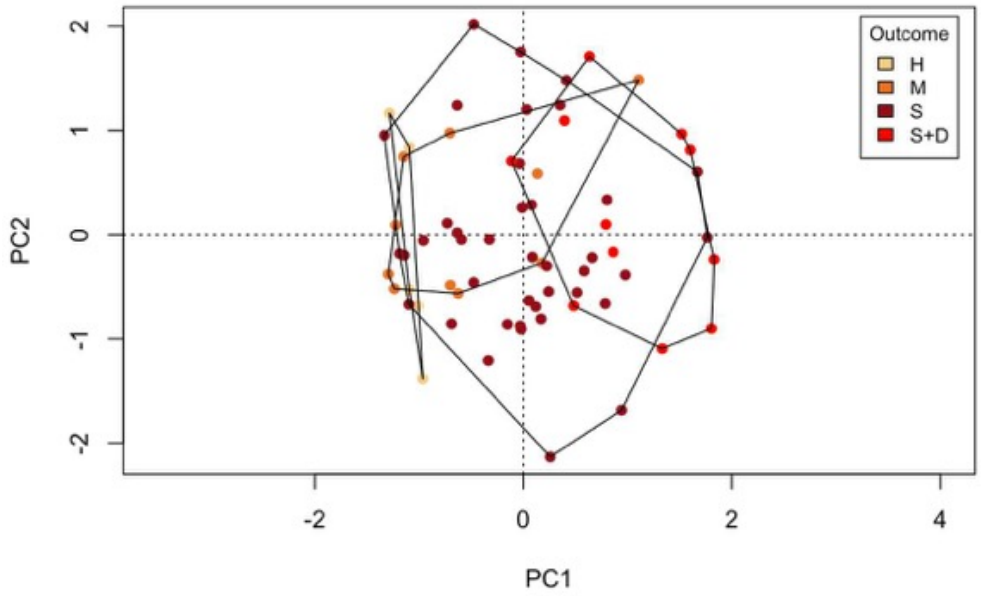

InflammatoryPhenotype
PsA
MCat
Saur
Spneu
HInf
Eubacteria
Haemophilus influenzae
Prevotella melaninogenica
Gemella haemolysans
Streptococcus mitis
Streptococcus pneumoniae
Rothia mucilaginosa
Veillonella atypica
Streptococcus parasanguinis
Streptococcus sp. LPB0220
Veillonella sp. T1-7
Prevotella jejuni
Parvimonas micra
Prevotella oris
Fusobacterium nucleatum
Prevotella intermedia
Streptococcus oralis
Neisseria mucosa
Streptococcus pseudopneumoniae
Moraxella bovis
Veillonella parvula
Veillonella dispar
Haemophilus parainfluenzae
Streptococcus sp. oral taxon 431
Lancefieldella parvula
Schaalia odontolytica
Moraxella catarrhalis
Tannerella forsythia
Gemella sanguinis
Streptococcus sp. oral taxon 061
Porphyromonas asaccharolytica
Streptococcus gordonii
Streptococcus gwangjuense
Streptococcus anginosus group
Rothia dentocariosa
Streptococcus salivarius
4
2
0
-2
-4
InflammatoryPhenotype
N
M
P
E
ND
PsA
Sign
Not_Sign
MCat
Sign
Not_Sign
Saur
Sign
Not_Sign
Spneu
Sign
Not_Sign
HInf
Sign
Not_Sign
Eubacteria
10000
2000

Figure E3 PCA of metagenomic profiles

Principal component analysis (PCA) based on metagenomic profiles with convex hulls plotted for (a) Wessex severe asthma cohort, representing healthy (H), moderate asthma (M), severe asthma (S) and severe asthma with presence of dominant pathogen (S+D), (PERMANOVA = 0.001); and (b) severe asthmatics from the Oxford (OX) and Wessex (WES) cohorts (PERMANOVA = 0.19). First two principal components are shown.

A)



B)

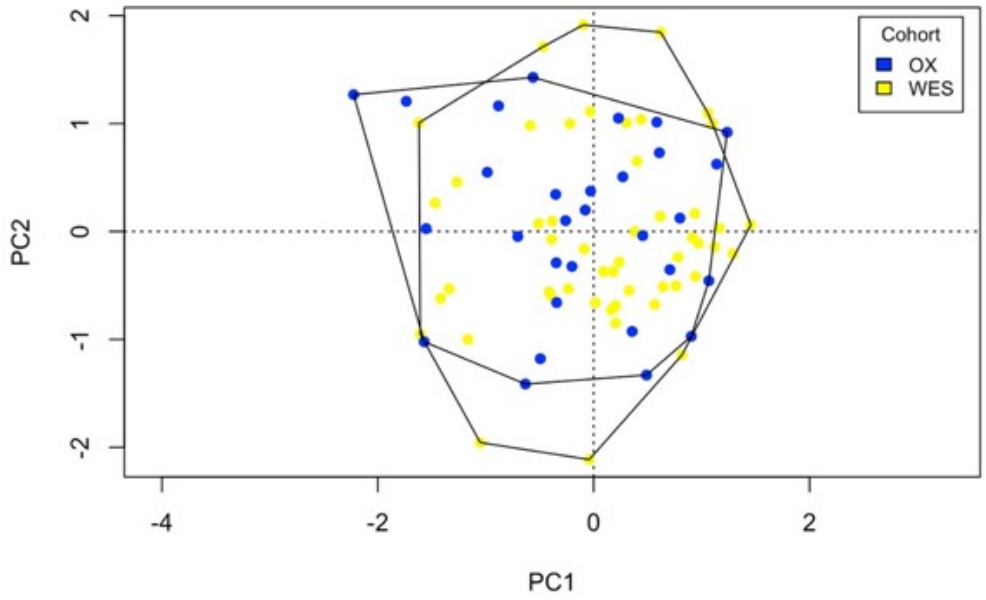
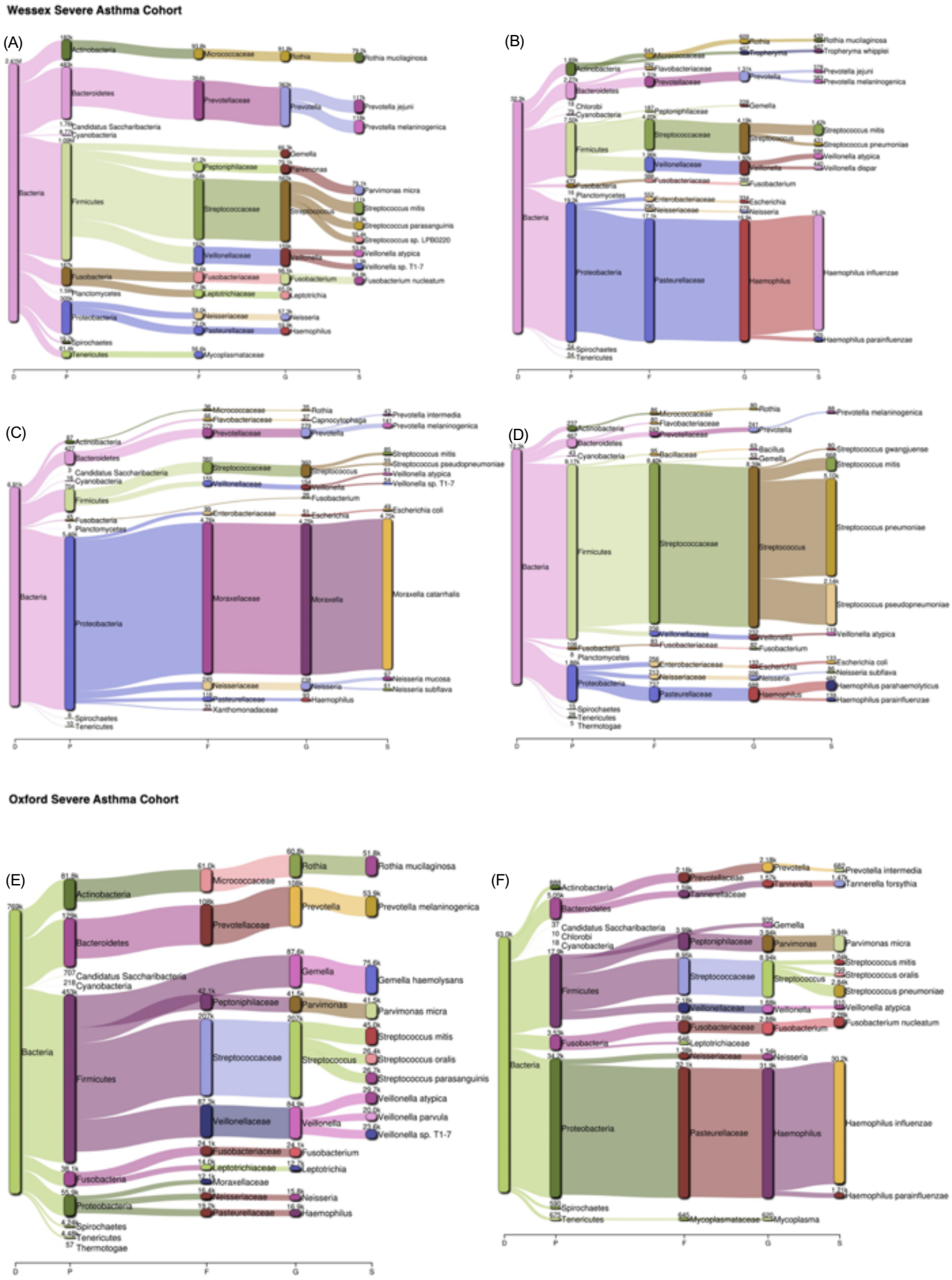
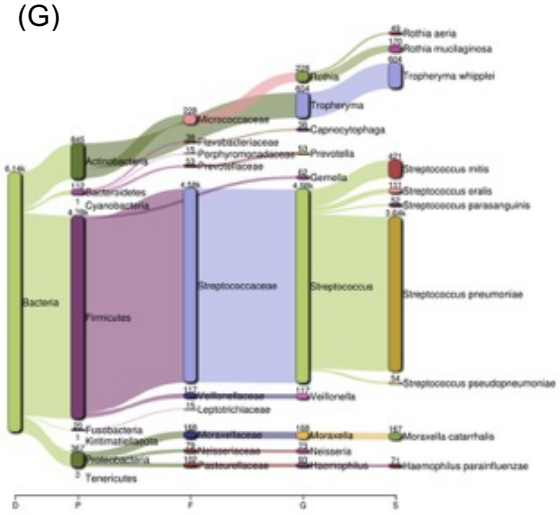


Figure E4 Taxonomic profiles in sputum in severe asthma



(G)


Rothia aeria
Rothia mucilaginosa
Tropheryma whipplei
Rothia
Tropheryma
Micrococcaceae
Capnocytophaga
Flavobacteriaceae
Porphyromonadaceae
Prevotellaceae
Prevotella
Actinobacteria
Bacteroidetes
Cyanobacteria
Gemella
Streptococcus mitis
Streptococcus oralis
Streptococcus parasanguinis
Streptococcaceae
Streptococcus
Streptococcus pneumoniae
Bacteria
Firmicutes
Streptococcus pseudopneumoniae
Veillonellaceae
Leptotrichiaceae
Veillonella
Fusobacteria
Kiritimatiellaeota
Moraxellaceae
Neisseriaceae
Pasteurellaceae
Moraxella
Neisseria
Haemophilus
Moraxella catarrhalis
Haemophilus parainfluenzae
Proteobacteria
Tenericutes
D
P
F
G
S

(H)

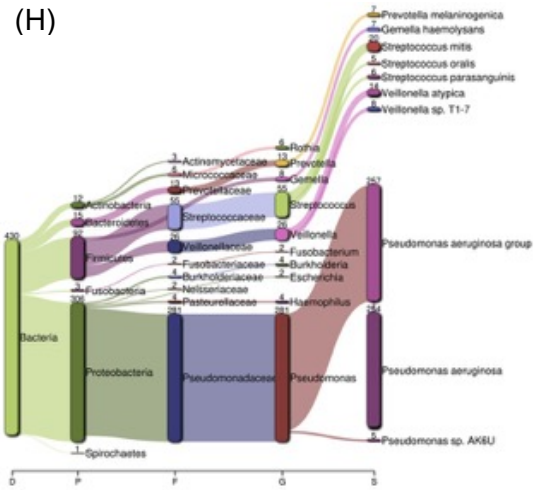

Prevotella melaninogenica
Gemella haemolysans
Streptococcus mitis
Streptococcus oralis
Streptococcus parasanguinis
Veillonella atypica
Veillonella sp. T1-7
Actinomycetaceae
Micrococcaceae
Prevotellaceae
Rothia
Prevotella
Gemella
Actinobacteria
Bacteroidetes
Streptococcaceae
Streptococcus
Veillonella
Fusobacterium
Burkholderia
Escherichia
Haemophilus
Pseudomonas aeruginosa group
Firmicutes
Veillonellaceae
Fusobacteriaceae
Burkholderiaceae
Neisseriaceae
Pasteurellaceae
Fusobacteria
Bacteria
Proteobacteria
Pseudomonadaceae
Pseudomonas
Pseudomonas aeruginosa
Spirochaetes
Pseudomonas sp. AK6U
D
P
F
G
S

Table E3 Top species in health

Top species in Healthy controls (n=5) vs Mild and severe asthmatics (n=61); Wald test used to identify uniquely abundant species using DESeq2, log fold change > 1 and adjusted P value < 0.05 following adjustment for multiple comparisons using Benjamini–Hochberg procedure (FDR 0.05). LFC, log fold change; SE, standard error.

Species	Base Mean	LFC	LFC (SE)	Wald statistic	P value	Adjusted P value
Streptococcus viridans	163.47	6.28	0.83	7.61	2.67E-14	6.77E-12
Streptococcus sp. A12	184.19	6.09	0.83	7.30	2.80E-13	3.54E-11
Streptococcus australis	208.41	5.04	0.75	6.74	1.59E-11	1.34E-09
Schaalia odontolytica	997.00	8.51	1.28	6.64	3.11E-11	1.97E-09
Schaalia meyeri	44.38	7.67	1.19	6.43	1.26E-10	6.38E-09
Lancefieldella parvula	886.86	6.79	1.07	6.37	1.86E-10	7.83E-09
Actinomyces pacaensis	146.66	6.29	1.02	6.14	8.00E-10	2.25E-08
Streptococcus intermedius	52.51	4.41	0.79	5.61	2.08E-08	4.79E-07
Mogibacterium diversum	535.90	5.97	1.14	5.24	1.61E-07	3.39E-06
Streptococcus gordonii	168.13	4.04	0.79	5.12	3.05E-07	5.52E-06
Streptococcus anginosus group	116.19	3.47	0.79	4.42	9.99E-06	1.10E-04
Gemella sanguinis	216.90	3.16	0.89	3.56	3.66E-04	2.11E-03
Streptococcus parasanguinis	580.65	2.91	0.88	3.32	9.03E-04	4.20E-03
Prevotella oris	200.84	2.48	0.75	3.31	9.21E-04	4.20E-03
Leptotrichia sp. oral taxon 212	104.88	3.03	0.92	3.31	9.18E-04	4.20E-03
Streptococcus sp. LPB0220	450.84	2.72	0.85	3.19	1.44E-03	5.93E-03
Streptococcus sp. oral taxon 431	209.08	2.25	0.75	3.00	2.68E-03	9.95E-03
Streptococcus sp. oral taxon 061	198.59	2.29	0.77	2.97	3.01E-03	1.09E-02
Streptococcus anginosus	50.74	2.49	0.88	2.83	4.72E-03	1.55E-02
Gemella morbillorum	64.14	2.38	0.88	2.69	7.22E-03	2.17E-02
Leptotrichia wadei	182.75	2.30	0.97	2.37	1.79E-02	4.38E-02

Table E4 Top species in mild asthma

Top species in Mild asthma (n=10) vs. Healthy controls and Severe asthma (n=56); Wald test used to identify uniquely abundant species using DESeq2, log fold change > 1 and adjusted P value < 0.05 following adjustment for multiple comparisons using Benjamini–Hochberg procedure (FDR 0.05). LFC, log fold change; SE, standard error.

Species	Base Mean	LFC	LFC (SE)	Wald statistic	P value	Adjusted P value
Filifactor alocis	46.16	2.64	0.78	3.37	7.38E-04	9.83E-03
Mogibacterium diversum	535.90	2.53	0.79	3.21	1.32E-03	1.52E-02
Streptococcus sp. A12	184.19	1.69	0.59	2.84	4.47E-03	4.04E-02
Streptococcus sp. oral taxon 061	198.59	1.45	0.55	2.64	8.41E-03	6.88E-02
Streptococcus salivarius	268.76	1.82	0.70	2.62	8.87E-03	7.01E-02
Streptococcus viridans	163.47	1.53	0.59	2.58	9.93E-03	7.62E-02
Streptococcus intermedius	52.51	1.15	0.58	1.98	4.72E-02	2.91E-01
Streptococcus australis	208.41	1.07	0.55	1.95	5.14E-02	3.09E-01

Table E5 Top species in severe asthma

Most abundant species and species most depleted in severe asthma (n=51) vs Healthy controls and Mild asthma (n=15); Wald test used to identify species uniquely abundant or depleted in SA using DESeq2, log fold change [LFC] > 1 or <1 respectively, adjusted P value < 0.05 following adjustment for multiple comparisons using Benjamini–Hochberg procedure (FDR 0.05). LFC, log fold change; SE, standard error.

	Most abundant species					
Species	Base Mean	LFC	LFC (SE)	Wald statistic	P value	Adjusted P value
Rothia mucilaginosa	162.27	3.75	0.46	8.16	3.44E-16	8.38E-14
Rothia dentocariosa	52.98	3.10	0.60	5.11	3.22E-07	1.12E-05
Haemophilus influenzae	212.03	3.09	0.68	4.58	4.73E-06	8.21E-05
Moraxella catarrhalis	40.25	4.30	1.18	3.66	2.57E-04	2.01E-03
Streptococcus pseudopneumoniae	86.78	1.50	0.55	2.72	6.46E-03	2.45E-02
	Most depleted species					
Species	Base Mean	LFC	LFC (SE)	Wald statistic	P value	Adjusted P value
Streptococcus anginosus group	116.19	-2.29	0.53	-4.30	1.67E-05	2.54E-04
Streptococcus sp. oral taxon 061	198.59	-1.97	0.47	-4.18	2.93E-05	3.75E-04
Gemella sanguinis	216.90	-2.24	0.57	-3.90	9.69E-05	1.18E-03
Streptococcus parasanguinis	580.65	-2.13	0.56	-3.82	1.35E-04	1.42E-03
Mogibacterium diversum	100.49	-2.32	0.62	-3.74	1.86E-04	1.70E-03
Filifactor alocis	46.16	-2.48	0.66	-3.73	1.88E-04	1.70E-03
Streptococcus sp. oral taxon 431	209.08	-1.67	0.47	-3.52	4.38E-04	3.13E-03
Streptococcus sp. LPB0220	450.84	-1.89	0.55	-3.46	5.44E-04	3.70E-03
Streptococcus salivarius	268.76	-1.94	0.59	-3.28	1.04E-03	5.51E-03
Lachnoanaerobaculum umeaense	70.48	-1.64	0.59	-2.81	4.99E-03	2.15E-02
Lancefieldella parvula	103.29	-1.61	0.58	-2.80	5.14E-03	2.15E-02
Leptotrichia wadei	182.75	-1.51	0.62	-2.43	1.51E-02	5.01E-02
Streptococcus anginosus	50.74	-1.40	0.58	-2.41	1.61E-02	5.21E-02

Table E6 Single pathogen dominance in severe asthma

Dominance of a single pathogen in severe asthma

Cohort	PID†	Dominant Pathogen	%Pathogen/ bacterial reads‡	Length of reference genome (bases)	Coverage breadth of reference genome (%)§	Average coverage depth¶	Pathogen specific PCR (x10^6 copies/ml)‖	Sputum inflammatory phenotype	Clinical sputum culture result
Oxford	OAS1076	*Haemophilus influenzae*	77	1.83E+06	92.9	11.0	**179.9**	Neutrophilic	*H. influenzae*
Oxford	OAS1021	*Haemophilus influenzae*	93	1.83E+06	74.1	2.1	**175.4**	Neutrophilic	URT flora
Oxford	OAS1102	*Haemophilus influenzae*	92	1.83E+06	89.9	8.0	**135.6**	Neutrophilic	*H. influenzae*
Oxford	OAS1145	*Haemophilus influenzae*	22	1.83E+06	88.6	4.5	**83.9**	ND	ND
Oxford	OAS1041	*Moraxella catarrhalis*	59	1.86E+06	19.1	3.8	**4.3**	Neutrophilic	URT flora
Oxford	OAS1047	*Streptococcus pneumoniae*	57	2.04E+06	83.0	2.6	**28.3**	Neutrophilic	*S. pneumoniae*
Oxford	OAS1065	*Streptococcus pneumoniae*	63	2.04E+06	56.5	1.7	**15.9**	ND	*S. pneumoniae*
Oxford	OAS1017	*Pseudomonas aeruginosa*	73	6.26E+06	5.1	1.0	**4.6**	ND	URT flora
Wessex	MRCSAC0142	*Haemophilus influenzae*	78	1.83E+06	92.6	14.5	**6.2**	Neutrophilic	ND
Wessex	MRCSAC0115	*Haemophilus influenzae*	54	1.83E+06	52.8	1.5	**5.7**	Neutrophilic	ND
Wessex	MRCSAC0130	*Haemophilus influenzae*	17	1.83E+06	65.5	2.0	**4.8**	Mixed	ND
Wessex	MRCSAC0098	*Haemophilus influenzae*	93	1.83E+06	88.8	3.5	**2.1**	Neutrophilic	ND
Wessex	MRCSAC0151	*Haemophilus influenzae*	25	1.83E+06	47.3	1.5	0.8	Eosinophilic	ND
Wessex	MRCSAC0150	*Haemophilus influenzae*	72	1.83E+06	20.0	1.2	0.5	Eosinophilic	ND
Wessex	MRCSAC0101	*Moraxella catarrhalis*	79	1.86E+06	95.2	4.3	**33.8**	Eosinophilic	ND
Wessex	MRCSAC0132	*Moraxella catarrhalis*	92	1.86E+06	92.6	3.7	**18.8**	Neutrophilic	ND

Wessex	MRCSACC001	*Moraxella catarrhalis*	28	1.86E+06	23.5	1.2	**18.6**	Neutrophilic	ND
Wessex	MRCSAC0135	*Streptococcus pneumoniae*	93	2.04E+06	92.8	4.3	**18.7**	Paucigranulocytic	ND
Wessex	MRCSAC0104	*Streptococcus pneumoniae*	79	2.04E+06	79.0	2.4	0.7	Neutrophilic	ND

†Patients with severe asthma from Wessex and Oxford cohorts demonstrating dominance of single pathogenic organism using Nanopore. ‡Proportion of total bacterial reads occupied by indicated pathogenic organism (represented as bar chart). §Coverage breadth (percentage of reference genome covered, represented as bar chart). ¶Average coverage depth (at positions with ≥1 read). ||Clinically significant (≥$1x10^6$ copies/ml) PCR result shown in bold. Inflammatory phenotypes: eosinophilic >3% sputum eosinophils, neutrophilic >61% sputum neutrophils and <3% eosinophils, mixed granulocytic >61% sputum neutrophils and >3% eosinophils, paucigranulocytic <61% sputum neutrophils and <3% eosinophils. ND, no data (not performed)

Table E7 Species by inflammatory phenotype

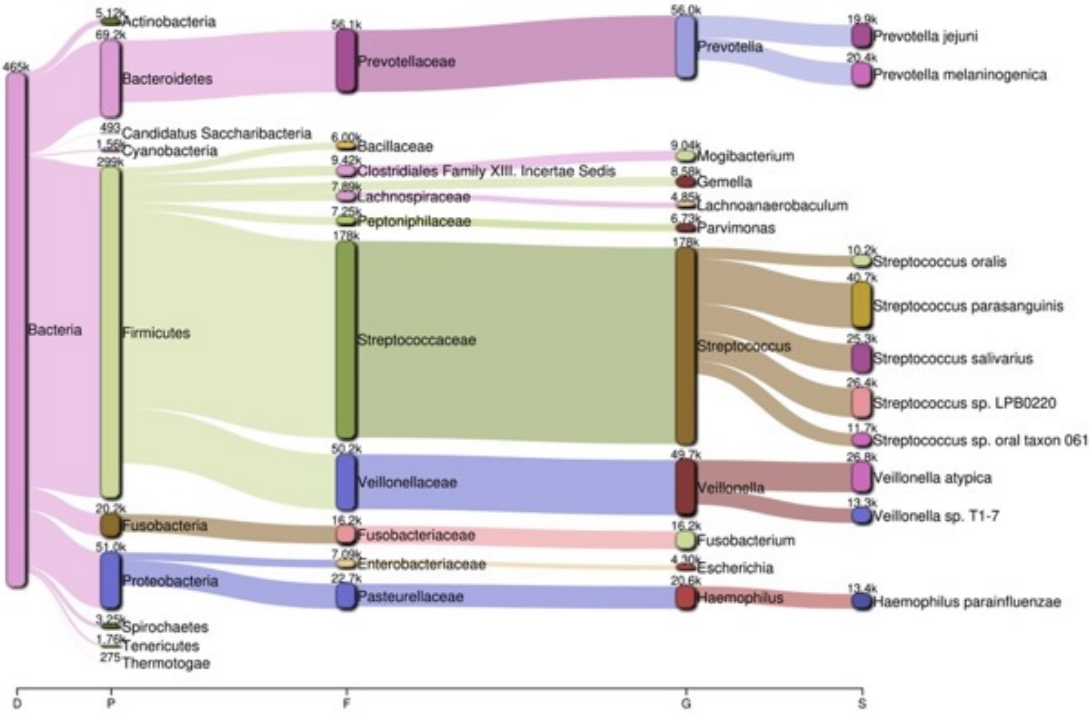
Most differentially abundant bacterial species in severe asthma by inflammatory phenotype; Neutrophilic, Eosinophilic, and Paucigranulocytic. Wald test used to identify species uniquely abundant or depleted relative to other inflammatory phenotypes (using DESeq2, adjusted P < 0.05 following adjustment for multiple comparisons using Benjamini–Hochberg procedure [FDR 0.05]).

Neutrophilic						
Species	**Base Mean**	**LFC**	**LFC (SE)**	**Wald statistic**	**P value**	**Adjusted P value**
Haemophilus influenzae	3568.22	6.70	0.70	9.58	1.01E-21	7.05E-20
Moraxella catarrhalis	601.35	8.18	0.88	9.30	1.40E-20	4.88E-19
Tropheryma whipplei	61.31	4.56	0.70	6.55	5.76E-11	1.34E-09
Streptococcus pneumoniae	779.90	3.65	0.63	5.76	8.30E-09	1.45E-07
Streptococcus salivarius	230.80	-2.26	0.49	-4.63	3.59E-06	5.03E-05
Streptococcus intermedius	29.90	-1.31	0.41	-3.17	1.52E-03	1.77E-02
Streptococcus sp. LPB0220	315.57	-1.39	0.46	-3.06	2.19E-03	1.91E-02
Streptococcus sp. oral taxon 431	110.11	-0.96	0.31	-3.06	2.18E-03	1.91E-02
Streptococcus parasanguinis	366.46	-1.23	0.43	-2.84	4.56E-03	2.90E-02
Streptococcus australis	64.02	-0.96	0.34	-2.86	4.18E-03	2.90E-02
Haemophilus haemolyticus	44.71	1.25	0.44	2.84	4.46E-03	2.90E-02
Streptococcus oralis	187.95	-0.94	0.35	-2.71	6.80E-03	3.40E-02
Streptococcus anginosus group	60.38	-0.97	0.36	-2.73	6.32E-03	3.40E-02
Prevotella enoeca	20.17	0.76	0.28	2.72	6.55E-03	3.40E-02
Eosinophilic						
Species	**Base Mean**	**LFC**	**LFC (SE)**	**Wald statistic**	**P value**	**Adjusted P value**
Streptococcus pneumoniae	779.90	-3.74	0.63	-5.89	3.76E-09	2.63E-07
Moraxella catarrhalis	601.35	4.07	0.97	4.18	2.90E-05	1.02E-03
Streptococcus intermedius	29.90	1.33	0.40	3.36	7.76E-04	1.48E-02
Actinomyces pacaensis	36.49	-1.66	0.50	-3.34	8.49E-04	1.48E-02
Haemophilus influenzae	3568.22	-2.81	0.86	-3.27	1.06E-03	1.48E-02
Veillonella parvula	189.94	1.12	0.37	3.02	2.49E-03	2.90E-02
Paucigranulocytic						
Species	**Base Mean**	**LFC**	**LFC (SE)**	**Wald statistic**	**P value**	**Adjusted P value**
Moraxella catarrhalis	601.35	-8.57	0.80	-10.76	5.55E-27	3.61E-25
Haemophilus influenzae	3568.22	-5.96	0.74	-8.01	1.12E-15	3.65E-14
Tropheryma whipplei	61.31	-5.04	0.72	-7.05	1.85E-12	4.00E-11
Mogibacterium diversum	123.71	2.00	0.47	4.27	1.95E-05	3.17E-04
Streptococcus pneumoniae	779.90	2.42	0.65	3.75	1.76E-04	1.91E-03
Treponema sp. OMZ 804	17.40	1.67	0.44	3.77	1.65E-04	1.91E-03
Streptococcus australis	64.02	1.06	0.30	3.47	5.14E-04	4.78E-03
Gemella morbillorum	42.12	1.11	0.34	3.26	1.12E-03	9.08E-03
Streptococcus gordonii	85.98	1.17	0.37	3.16	1.60E-03	1.15E-02
Schaalia odontolytica	156.13	1.76	0.56	3.11	1.84E-03	1.20E-02
Actinomyces pacaensis	36.49	1.39	0.45	3.06	2.23E-03	1.31E-02
Lachnoanaerobaculum umeaense	42.21	0.98	0.35	2.80	5.18E-03	2.59E-02
Prevotella jejuni	285.63	-1.28	0.45	-2.81	4.93E-03	2.59E-02
Streptococcus sp. oral taxon 431	110.11	0.82	0.30	2.70	6.84E-03	3.17E-02
Filifactor alocis	33.44	1.14	0.42	2.68	7.31E-03	3.17E-02
Veillonella sp. T1-7	299.93	-0.92	0.35	-2.61	9.15E-03	3.72E-02
Streptococcus anginosus	29.86	0.86	0.34	2.56	1.05E-02	4.01E-02

Figure E5 Sankey visualisations in Wessex Cohort

Sankey visualisation of taxonomic profiles in Wessex Cohort generated using Pavian.; (a) Healthy controls, (b) Mild asthma.

(a)



(b)

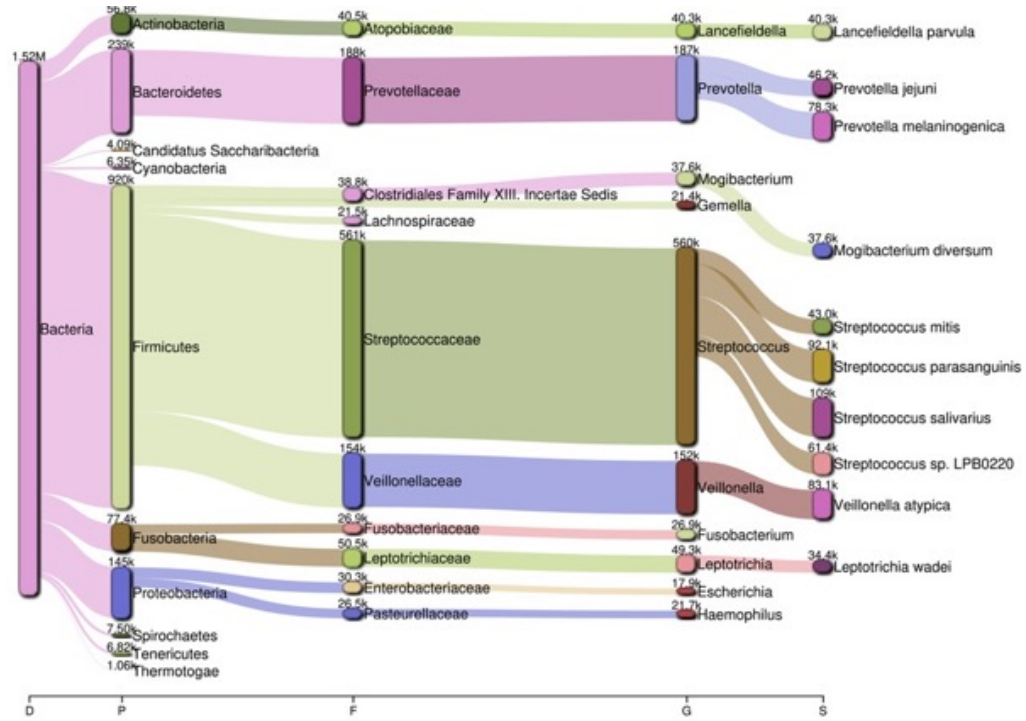
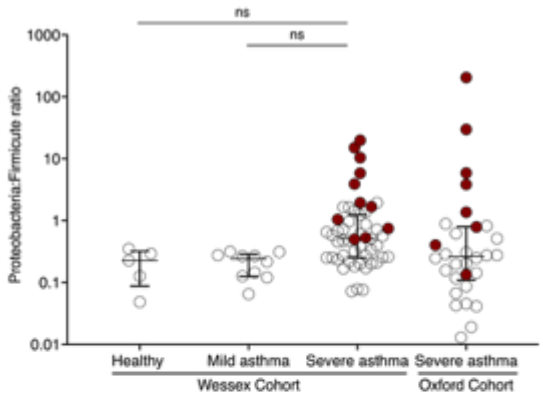


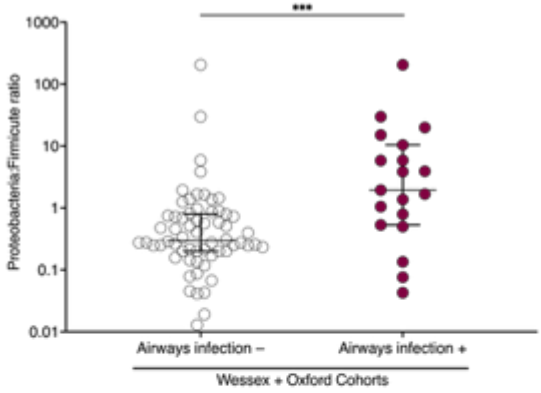
Figure E6 Proteobacteria:firmicute ratios

Ratio of Proteobacteria:Firmicute reads, grouped by: (a) Disease severity and cohort, (b) Absence or presence of airways infection, (c) Inflammatory phenotype (neutrophilic, n=22; eosinophilic, n=19; mixed, n=6; paucigranulocytic, n=24). Median/IQR shown, unpaired t-test, ns >0.05, ***P≤0.001). Data points in maroon indicate presence of airways infection.

(a) (b)

(c)





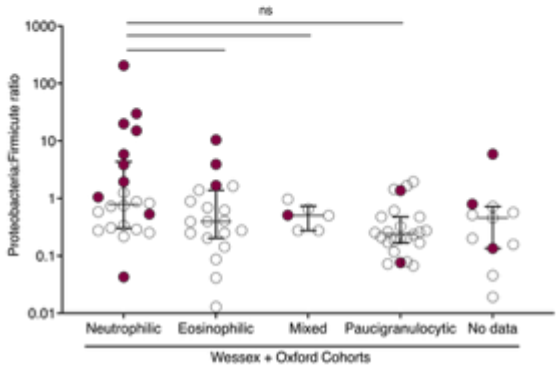


Table E8 Sputum cytokines by presence of infection

Comparison of sputum cytokines in the presence or absence of airways infection in severe asthma; Median/IQR shown −/+Airways infection alongside adjusted P value (unpaired t-test, adjusted for multiple comparisons with Benjamini–Hochberg procedure [FDR 0.05])

	Airways infection absent		Airways infection present		Adjusted P value
Cytokine (pg/ml)	Median	IQR	Median	IQR	
Elastase	2530	2892	8414	8515	0.002
TNF	0	0	25	104	0.002
IL-10	0	0	3	6	0.010
IL-1β	28	104	435	725	0.010
MIP-1β	29	239	334	521	0.010
MMP8	122066	260721	436658	143419	0.010
ECP	118	615	2333	5154	0.010
YKL40	40	74	204	225	0.010
MPO	1349	4046	7288	5774	0.014
IL-8	1611	3650	9760	6512	0.018
MIP-1α	8	183	342	279	0.019
IL-6SR	181	209	396	218	0.019
MMP9	78429	74121	215031	174057	0.020
TIMP1	324	432	464	374	0.044
IL-1RA	10689	7656	0	8500	0.045
IFNɣ	0	0	0	2	0.050
IL-17	0	1	0	1	0.053
IL-6	29	76	128	156	0.079
ENA78	231	326	400	424	0.079
GCSF	209	293	420	549	0.105
MMP3	322	1032	642	969	0.190
VEGF	588	535	970	515	0.192
MCP1	150	222	458	287	0.208
IL-5	0	1	2	16	0.216
GMCSF	0	0	0	1	0.221
MMP7	52794	111539	98919	112724	0.282
α2-macroglobulin	116	275	275	537	0.300
IL-1α	8	20	27	82	0.324
Tryptase	1	4	2	6	0.336
MMP1	172	125	181	253	0.439
Eotaxin	13	66	48	37	0.489
IL-13	0	0	0	0	0.502
IL-4	0	0	0	0	0.570
MMP2	2756	4092	2732	3886	0.570
MMP12	183	144	144	147	0.570
OPN	23231	17016	18358	23398	0.656
GROα	288	1092	770	2457	0.695
MMP13	888	607	426	727	0.785
FGF	0	0	0	0	0.799

Table E9 Bayesian Network Analysis variables

BNA variables; 60 variables selected including key clinical variables, 15 cytokines (showing statistically significant differences in absence and presence of airways infection) and 25 bacterial species (most differentially abundant in severe asthma). These variables were discretised into 2 (binary variables) or 3 to 5 (continuous variables) bins. Variables retained in the model are shown in bold.

Demographic			
Sex	Age (years)	Asthma duration (years)	BMI (kg/m^2)
Clinical parameters			
BTS step	ICS dose (BDP equivalent, mcg/d)	Macrolide use	Atopy
Nasal Polyps	Rhinosinusitis	Cough	Smoking History
ACQ7	**Infection Status**		
Pulmonary function			
FeNO (ppb)	**FEV1(%)**	**FEV1/FVC**	
Peripheral blood			
Blood eosinophils (x10^9/L)			
Sputum inflammation			
Sputum neutrophils (%)	Sputum eosinophils (%)	**Sputum IL-10**	Sputum IL-1RA
Sputum IL-1β	**Sputum TNF**	**Sputum Elastase**	**Sputum MIP1β**
Sputum MMP8	**Sputum ECP**	**Sputum YKL40**	**Sputum MPO**
Sputum IL-8	**Sputum MIP1α**	**Sputum IL-6SR**	Sputum MMP9
Sputum TIMP1			
Sputum microbiology			
Streptococcus parasanguinis	***Streptococcus viridans***	*Rothia mucilaginosa*	***Rothia dentocariosa***
Prevotella oris	***Haemophilus influenzae***	***Moraxella catarrhalis***	***Neisseria subflava***
Neisseria mucosa	***Streptococcus sp. oral taxon 061***	*Streptococcus sp. LPB0220*	***Streptococcus sp. oral taxon 431***
Streptococcus sp. A12	***Streptococcus australis***	***Streptococcus gordonii***	***Streptococcus anginosus group***
Streptococcus intermedius	*Gemella sanguinis*	*Mogibacterium diversum*	***Filifactor alocis***
Actinomyces pacaensis	***Schaalia odontolytica***	***Schaalia meyeri***	*Lancefieldella parvula*
Leptotrichia sp. oral taxon 212			

Figure E7 Correlations between inflammatory mediators

Microbial and inflammatory mediators shown to be associated through BNA. Spearman correlations shown for pairwise interactions identified in BNA. Correlations were tested with Spearman R statistic

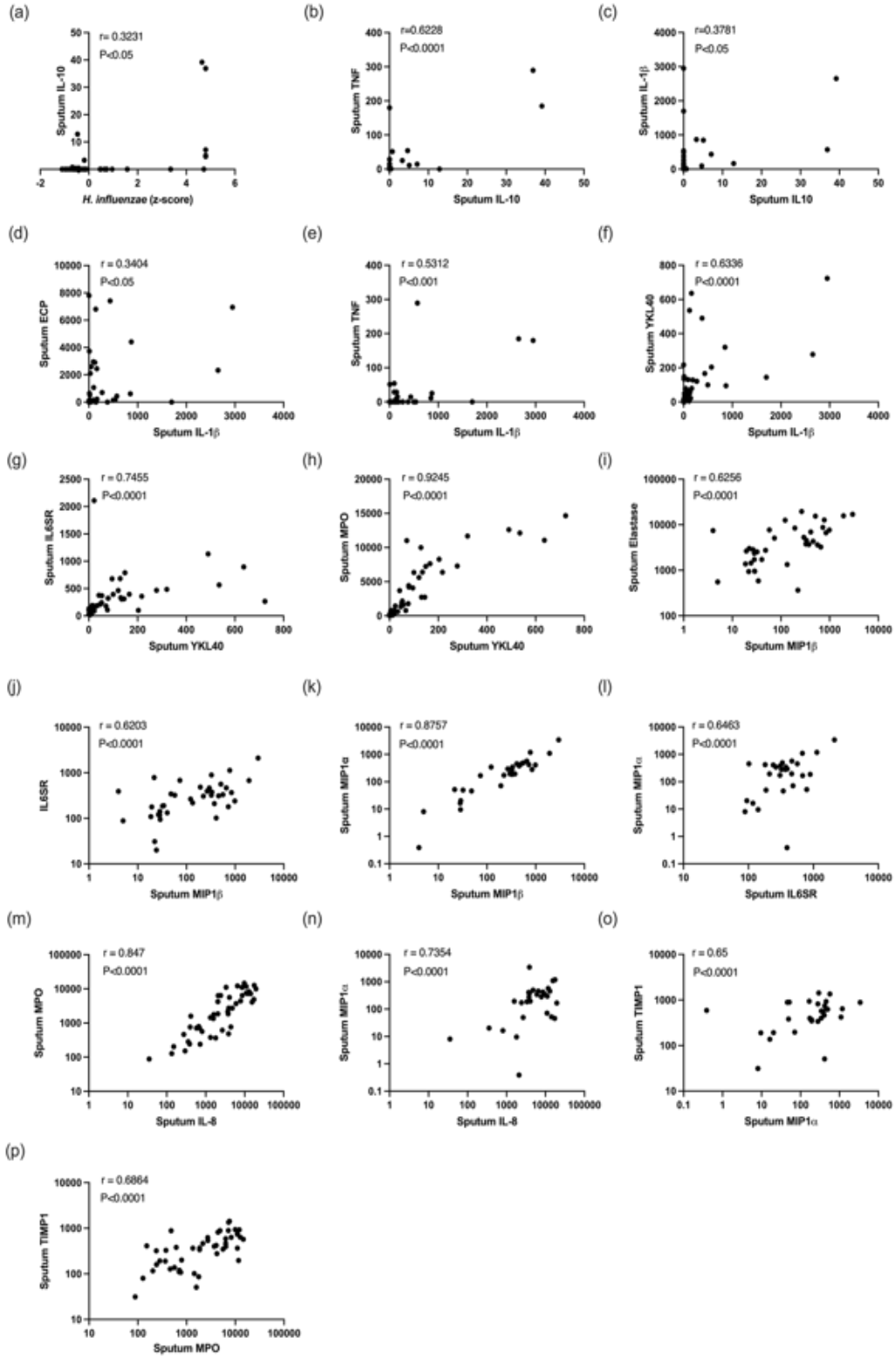


Figure E8 Relationship of FeNO to *H. influenzae* abundance

Scatter plot of relationship between *H influenzae* qPCR quantification (copies/ml) and fractional exhaled nitric oxide (FeNO) in parts per billion (ppb).

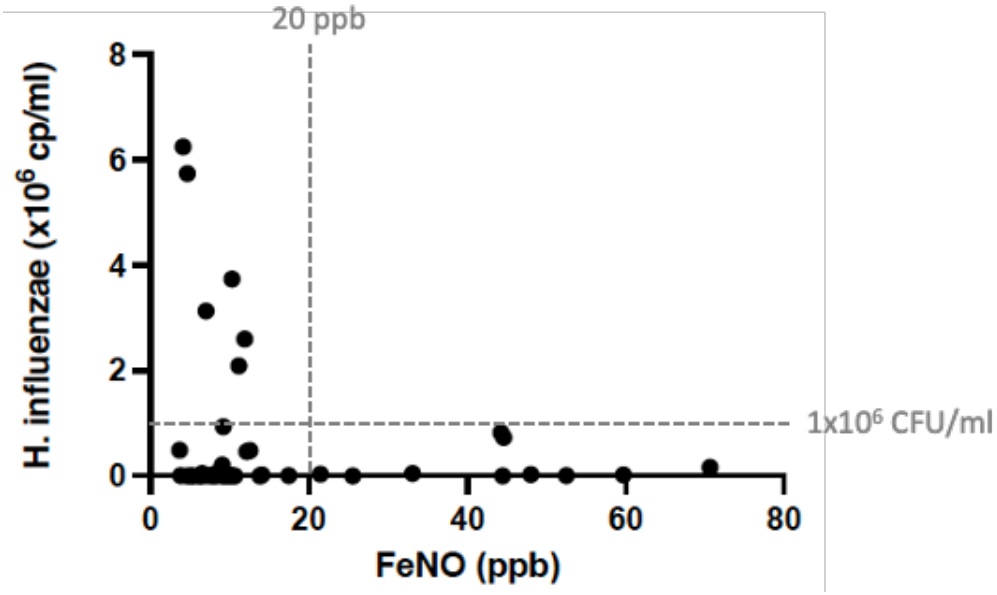


Figure E9 Pairwise associations between bacterial species

Bacteria shown to be associated through BNA. Pearson correlations shown for pairwise interactions identified in BNA. Correlations were tested with Pearson R statistic

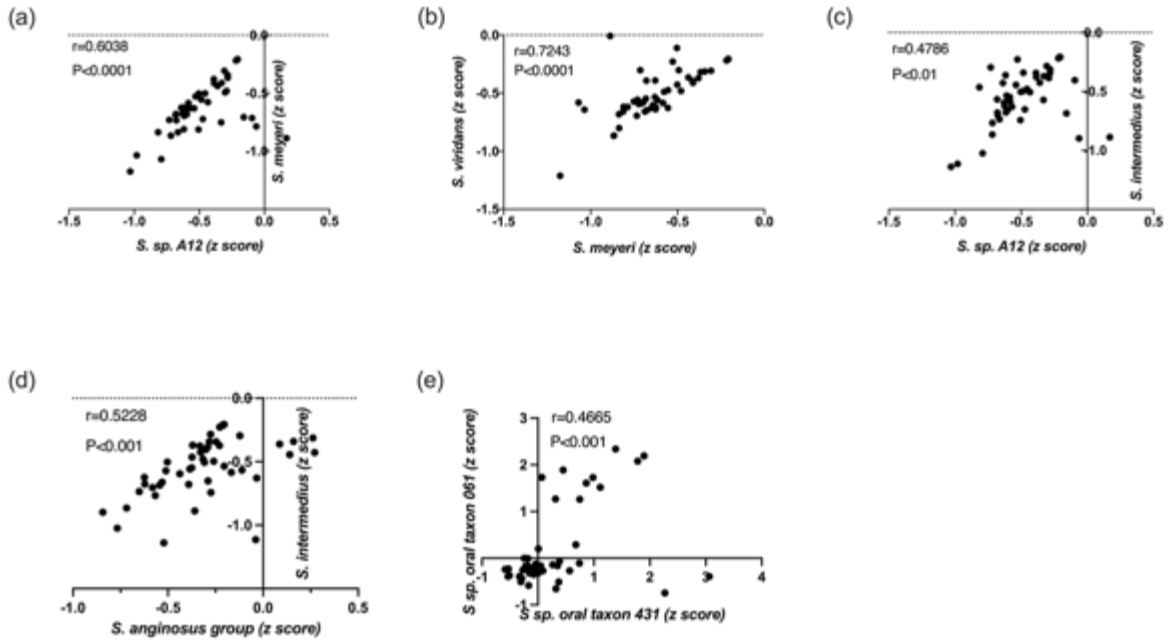
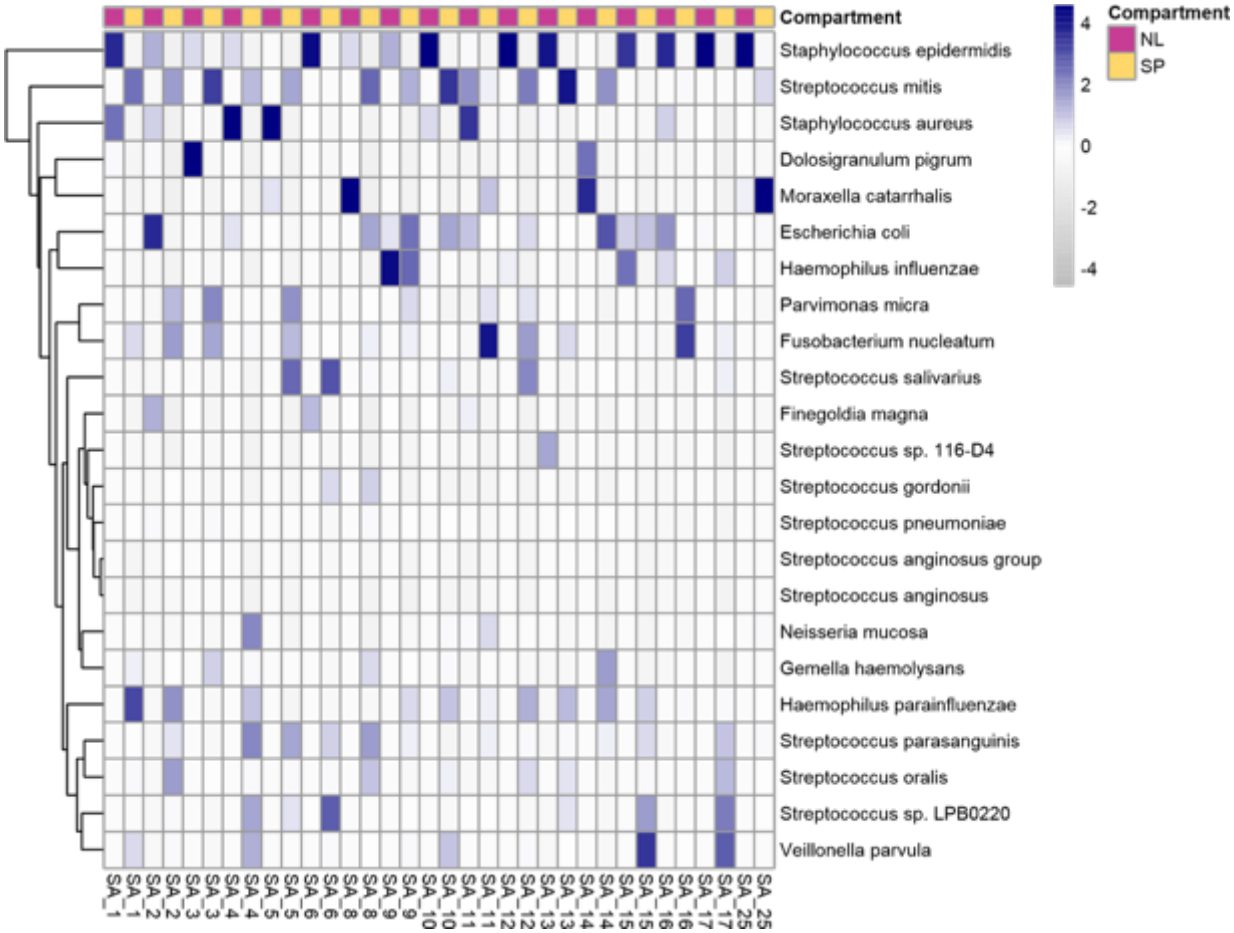


Figure E10 Upper and lower airway microbiome and cytokines

Heatmap of relative abundances of bacterial species on metagenomic sequencing of paired nasal lavage (NL) and sputum (SP) samples from severe asthmatics (n=17). Samples have been arranged to show paired upper and lower airway samples in adjacent columns for comparison. Z-score denoted by shade. Independent clustering by 23 most variable species (rows) using Euclidian distance.



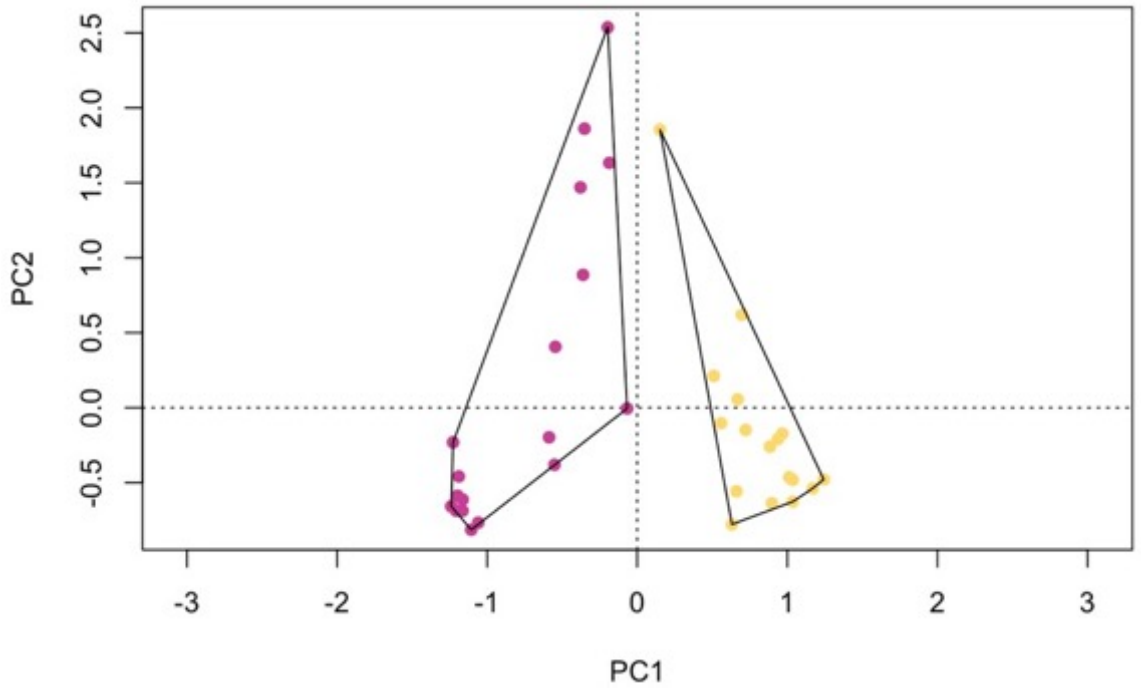
Upper and lower airway cytokine milieu is distinct in severe asthma

The cytokine milieu in the upper and lower airway was compared using paired O-link proteomic data from nasal lavage and sputum samples. The most significantly correlated (P<<0.001) proteins are displayed as a correlation matrix in Figure 5(b). There is a separation between nasal lavage and sputum compartments (that is, proteins most strongly

correlate with others from the same sample type). The exceptions to this are two clusters – the first showing strong positive correlation between sputum cytokines IL-20, FGF5 and IL-2 with nasal lavage proteins neurotrophin 3, neurturin, FGF23, IL-5, FGF5, IL-10Rα, nerve growth factor (NGF) and IL-20. The second cluster shows a negative correlation between the sputum cytokines IL-20, FGF5 and IL-2, and nasal lavage proteins urokinase, herpesvirus entry mediator ligand (HVEML), adenosine deaminase (ADA), oncostatin M, hepatocyte growth factor (HGF), S100A12, CCL44, CCL3, IL-18R1, CD318, tumour necrosis factor-like weak inducer of apoptosis (TWEAK), MMP10, VEGFA and CD40.

Figure E11 PCA of metagenomic profiles

Principal component analysis (PCA) based on metagenomic profiles with convex hulls plotted for paired nasal (pink) and sputum (yellow) samples derived from patients with severe asthma from the Wessex Severe Asthma Cohort (PERMANOVA = 0.001). First two principal components are shown.



Appendix 3: Supplemental results for Chapter 4 AMASS

Each table shown below displays the differential gene expression results (comparing effect of treatment) generated by FindMarkers in Seurat using MAST, the details of which are described in the methods. Tables display gene, average log 2 fold change, pct.1 (proportion of cells post azithromycin expressing the stated gene), pct.2 (proportion of cells pre azithromycin expressing the stated gene) and adjusted p value. Results tables are numbered the comparisons listed below

A3.1	Combined epithelial cells from bronchial biopsy
A3.2	Combined epithelial cells from nasal brush
A3.3	Multiciliated cells from bronchial biopsy
A3.4	Multiciliated cells from nasal brush
A3.5	Goblet cells from bronchial biopsy
A3.6	Goblet cells from nasal brush
A3.7	Basal cells from bronchial biopsy
A3.8	Club cells from nasal brush
A3.9	Macrophaged from bronchial biopsy
A3.10	Pooled CD8 T cells from bronchial biopsy
A3.11	All T cells from bronchial biopsy
A3.12	All T cells from nasal brush
A3.13	Neutrophils from bronchial biopsy with infection
A3.14	Neutrophils from bronchial biopsy without infection
A3.15	Macrophage from bronchial biopsy with infection
A3.16	Macrophage from bronchial biopsy without infection
A3.17	CD8 T cell from bronchial biopsy with infection
A3.18	CD8 T cell from bronchial biopsy without infection
A3.19	Multiciliated cell from bronchial biopsy with infection
A3.20	Multiciliated cell from bronchial biopsy without infection
A3.21	Goblet cell from bronchial biopsy with infection
A3.22	Goblet cell from bronchial biopsy without infection

A3.1

DGE All epitheial cells from bronchial biopsy					
	gene	avg_log2FC	pct.1	pct.2	p_val_adj
Upregulated	PRSS23	2.39	0.50	0.24	1.85E-186
	SERPINB3	3.09	0.30	0.05	4.66E-183
	S100A14	2.38	0.30	0.05	7.15E-180
	KRT5	3.19	0.25	0.03	9.61E-168
	FOXQ1	2.98	0.24	0.04	1.64E-165
	TMEM190	0.29	0.43	0.59	2.09E-165
	FGFR3	3.58	0.23	0.02	1.93E-164
	PABPC1	1.06	0.89	0.83	9.88E-159
	TCTEX1D4	0.85	0.47	0.42	4.07E-154
	KLK11	3.11	0.27	0.04	1.49E-153
	EPAS1	1.89	0.49	0.26	2.55E-153
	CD44	1.89	0.27	0.06	4.68E-152
	POU3F1	3.50	0.24	0.04	3.91E-149
	VMO1	1.22	0.23	0.05	6.07E-149
	AQP5	3.21	0.41	0.16	1.73E-142
	S100A2	2.66	0.29	0.06	2.48E-142
	GAS5	1.73	0.54	0.35	2.41E-136
	CXCL1	1.81	0.27	0.06	2.63E-135
	TNS4	3.03	0.23	0.04	9.35E-133
	GAPDH	1.22	0.92	0.85	1.28E-131
	gene	avg_log2FC	pct.1	pct.2	p_val_adj
Downregulated	MTRNR2L12	-2.83	0.33	0.67	0.00E+00
	DHFR	-2.88	0.59	0.84	0.00E+00
	AC105402.3	-3.22	0.64	0.86	0.00E+00
	PDE3A	-1.87	0.41	0.64	1.97E-234
	ATP5IF1	-0.63	0.89	0.93	5.27E-209
	RBFOX2	-0.87	0.75	0.79	5.23E-200
	DNAH12	-0.68	0.59	0.87	1.64E-196
	LRRIQ1	-0.62	0.59	0.87	3.96E-194
	AL357093.2	-1.06	0.56	0.83	9.26E-194
	CCDC170	-0.72	0.59	0.86	6.19E-192
	FAM183A	-0.47	0.58	0.84	3.63E-191
	CFAP299	-0.74	0.58	0.86	1.16E-188
	NEK10	-0.85	0.57	0.85	7.66E-188
	DNAH6	-0.66	0.57	0.85	3.13E-187
	DNAH5	-0.61	0.62	0.87	2.45E-185
	CFAP53	-0.67	0.57	0.84	1.49E-184
	RP1	-0.61	0.58	0.87	1.86E-184
	CFAP43	-0.64	0.58	0.86	3.31E-184
	CDHR3	-0.61	0.59	0.87	4.31E-184
	CFAP54	-0.78	0.57	0.85	5.85E-182

A3.2

DGE All epitheial cells from nasal brush					
	gene	avg_log2FC	pct.1	pct.2	p_val_adj
Upregulated	MT-ATP6	0.32	0.89	0.90	1.72E-100
	MT-ND1	0.32	0.91	0.92	3.02E-95
	TCTEX1D4	0.70	0.42	0.36	7.52E-77
	CFAP73	0.33	0.46	0.45	6.37E-72
	MT-ND2	0.36	0.90	0.91	3.56E-67
	TXNIP	0.33	0.88	0.84	1.61E-65
	AHNAK2	0.61	0.45	0.35	7.05E-65
	MT-ND3	0.40	0.91	0.92	1.06E-60
	HLA-E	0.62	0.87	0.84	1.14E-41
	HLA-F	0.64	0.67	0.61	3.40E-36
	LMO4	0.52	0.60	0.54	5.51E-33
	ADH7	0.35	0.76	0.74	1.10E-32
	CAPNS1	0.27	0.78	0.75	2.45E-32
	CABCOCO1	0.36	0.46	0.46	3.61E-31
	LINC01504	0.28	0.34	0.31	3.62E-30
	DPYD	0.37	0.70	0.65	4.62E-30
	AC025159.1	0.45	0.51	0.43	7.69E-28
	DANCR	0.40	0.63	0.53	3.20E-27
	UNC5B	0.42	0.33	0.24	5.58E-26
	PSCA	1.22	0.92	0.88	6.98E-26
	gene	avg_log2FC	pct.1	pct.2	p_val_adj
Downregulated	RBFOX2	-0.83	0.81	0.86	1.38E-313
	STEAP1B	-1.83	0.21	0.40	2.19E-215
	AC105402.3	-1.76	0.50	0.55	1.55E-156
	OOEP	-1.23	0.14	0.26	4.28E-93
	SAA2	-1.29	0.28	0.40	1.49E-84
	DHFR	-1.19	0.46	0.53	1.32E-82
	RPS13	-0.34	0.92	0.90	4.68E-71
	SLC35F1	-1.30	0.14	0.26	3.40E-64
	RPL28	-0.29	0.94	0.92	5.68E-64
	RPS15	-0.32	0.93	0.91	1.15E-61
	SAA1	-1.03	0.31	0.41	1.30E-61
	HIST2H2AA3	-1.24	0.06	0.12	2.08E-61
	RPLP1	-0.43	0.95	0.93	5.00E-58
	MIR924HG	-0.85	0.09	0.18	1.36E-57
	RPS12	-0.46	0.94	0.92	1.23E-56
	RPL12	-0.47	0.93	0.92	2.67E-56
	MTRNR2L12	-1.39	0.15	0.23	2.73E-54
	CLDN10	-1.75	0.09	0.22	5.11E-54
	EIF3CL	-1.19	0.07	0.13	7.18E-49
	RPS8	-0.30	0.95	0.93	2.21E-43

A3.3

DGE All multiciliated cells from bronchial biopsy					
	gene	avg_log2FC	pct.1	pct.2	p_val_adj
Upregulated	TCTEX1D4	1.42	0.78	0.48	2.12E-269
	CFAP73	0.68	0.89	0.77	3.51E-161
	STMND1	0.83	0.68	0.46	5.95E-107
	CCDC74A	1.14	0.71	0.48	4.95E-101
	PTPMT1	1.31	0.39	0.17	3.69E-71
	ACBD3-AS1	1.10	0.46	0.25	8.19E-63
	AC004832.1	0.64	0.78	0.61	3.10E-58
	HLA-DRB5	2.50	0.43	0.18	4.17E-45
	MT-ATP6	0.36	0.93	0.95	1.79E-44
	LINC00332	1.41	0.25	0.10	4.12E-44
	KDELR2	0.81	0.44	0.27	6.60E-40
	WFDC6	0.95	0.52	0.30	1.62E-36
	CABCOCO1	0.47	0.85	0.77	3.15E-35
	BTNL9	2.60	0.23	0.04	6.96E-33
	RNASE4	0.90	0.52	0.33	1.92E-31
	DANCR	0.94	0.41	0.23	8.91E-31
	DDT	1.05	0.27	0.14	5.39E-29
	LRRC61	0.76	0.59	0.44	2.90E-28
	CCDC74B	0.67	0.53	0.38	1.08E-27
	KAZN	0.33	0.85	0.80	1.58E-27
	gene	avg_log2FC	pct.1	pct.2	p_val_adj
Downregulated	MTRNR2L12	-2.59	0.37	0.69	0.00E+00
	DHFR	-2.61	0.64	0.85	0.00E+00
	AC105402.3	-3.02	0.69	0.88	0.00E+00
	RBFOX2	-1.17	0.68	0.79	6.69E-271
	STEAP1B	-2.49	0.18	0.47	1.40E-187
	MTRNR2L8	-2.78	0.06	0.28	6.35E-119
	PDE3A	-1.52	0.49	0.67	6.90E-107
	HIST2H2AA3	-1.52	0.10	0.21	1.03E-63
	SYVN1	-0.70	0.34	0.43	6.18E-60
	OOEP	-1.54	0.10	0.24	6.36E-44
	KIF21A	-0.43	0.94	0.96	6.75E-40
	EIF3CL	-1.69	0.06	0.17	3.56E-37
	MIR924HG	-2.18	0.03	0.13	2.12E-35
	ZBTB16	-0.85	0.30	0.44	4.04E-32
	SLC35F1	-1.17	0.11	0.20	8.90E-28
	MT3	-1.65	0.10	0.24	1.82E-27
	SLCO5A1	-0.86	0.22	0.32	4.00E-27
	AL357093.2	-0.48	0.93	0.93	5.68E-27
	IFITM3	-0.69	0.52	0.65	2.92E-26
	IFI6	-0.81	0.54	0.60	2.60E-24

A3.4

DGE All multiciliated cells from nasal brush					
	gene	avg_log2FC	pct.1	pct.2	p_val_adj
Upregulated	MT-ATP6	0.43	0.90	0.91	3.22E-183
	MT-ND3	0.37	0.91	0.93	1.57E-168
	MT-CO3	0.42	0.92	0.93	5.20E-132
	MT-ATP8	0.28	0.89	0.91	8.54E-112
	MT-ND1	0.52	0.91	0.92	1.29E-108
	TCTEX1D4	0.74	0.87	0.74	7.97E-107
	MT-ND4	0.30	0.90	0.92	3.90E-105
	MT-ND2	0.40	0.92	0.92	2.06E-90
	CFAP73	0.37	0.94	0.90	2.39E-82
	AHNAK2	0.82	0.72	0.52	7.05E-54
	ADH7	0.47	0.92	0.88	7.97E-39
	IDO1	0.65	0.09	0.13	3.12E-36
	LINC01765	0.26	0.69	0.62	2.67E-35
	LINC01504	0.44	0.58	0.50	3.47E-34
	AL590491.2	0.79	0.50	0.34	1.71E-33
	AC004832.1	0.43	0.75	0.65	1.62E-32
	SOX2	0.26	0.80	0.74	7.60E-31
	CABCOCO1	0.40	0.94	0.92	4.55E-30
	CETN2	0.28	0.93	0.89	7.49E-28
	AC025159.1	0.53	0.75	0.64	1.03E-27
	gene	avg_log2FC	pct.1	pct.2	p_val_adj
Downregulated	STEAP1B	-1.67	0.24	0.42	5.78E-137
	RBFOX2	-0.92	0.77	0.83	2.33E-135
	MIF	-0.33	0.91	0.88	2.76E-68
	SAA2	-1.51	0.33	0.51	7.28E-64
	AC105402.3	-2.03	0.46	0.52	7.58E-59
	HIST2H2AA3	-1.52	0.07	0.18	1.58E-52
	DUOXA2	-0.64	0.09	0.16	1.29E-51
	DUOX2	-0.27	0.26	0.31	3.10E-48
	RPL12	-0.31	0.92	0.90	5.17E-48
	SLC35F1	-1.40	0.10	0.23	2.18E-44
	OOEP	-1.20	0.12	0.23	2.80E-44
	SAA1	-1.28	0.32	0.47	1.32E-40
	LCN2	-1.21	0.32	0.39	2.12E-38
	NDUFB2	-0.31	0.88	0.87	1.07E-37
	RPS12	-0.32	0.92	0.89	9.33E-35
	CRIP1	-0.31	0.98	0.95	2.36E-34
	EIF3CL	-1.24	0.08	0.15	2.52E-33
	MIR924HG	-1.15	0.07	0.14	1.68E-32
	RPLP1	-0.34	0.94	0.92	1.23E-30
	RPS15	-0.25	0.92	0.90	4.37E-30
	IL33	-1.23	0.36	0.56	2.16E-28

A3.5

DGE All goblet cells from bronchial biopsy					
	gene	avg_log2FC	pct.1	pct.2	p_val_adj
Upregulated	TFF3	2.08	0.89	0.32	1.65E-02
	gene	avg_log2FC	pct.1	pct.2	p_val_adj
Downregulated	GALNT11	-2.35	0.16	0.04	2.59E-09
	SNED1	-1.27	0.26	0.04	4.37E-09
	CPTP	-0.84	0.28	0.04	5.37E-09
	ZNF124	-2.79	0.15	0.06	5.62E-08
	RFX3-AS1	-3.61	0.14	0.10	1.74E-07
	AL392172.1	-1.44	0.23	0.06	3.29E-07
	HAUS3	-2.01	0.13	0.04	8.46E-07
	TMEM99	-0.68	0.38	0.06	1.28E-06
	RNF8	-1.01	0.25	0.04	1.43E-06
	ERVK3-1	-0.73	0.36	0.06	1.51E-06
	DNAJB11	-1.33	0.47	0.16	1.59E-06
	ARHGAP12	-1.25	0.50	0.16	2.70E-06
	CBLL1	-2.19	0.18	0.08	4.10E-06
	DMAC2	-1.76	0.16	0.02	4.70E-06
	FZD1	-2.37	0.10	0.02	5.10E-06
	HIF1A	-2.32	0.36	0.26	6.63E-06
	ABHD5	-2.34	0.48	0.32	6.71E-06
	DLAT	-2.39	0.20	0.06	7.12E-06
	ANKRD46	-2.98	0.14	0.06	7.18E-06
	NUDT19	-2.00	0.14	0.02	8.53E-06

A3.6

DGE All goblet cells from nasal brush					
	gene	avg_log2FC	pct.1	pct.2	p_val_adj
Upregulated	HLA-B	0.63	1.00	0.99	1.02E-68
	HLA-E	0.77	0.97	0.95	4.56E-58
	PSCA	1.23	0.99	0.98	1.98E-50
	MUC1	0.69	0.98	0.95	7.06E-50
	HLA-F	0.83	0.89	0.80	2.42E-48
	LMO4	0.65	0.86	0.77	2.97E-40
	LY6E	0.68	0.98	0.98	1.54E-35
	HLA-C	0.62	1.00	0.99	2.23E-31
	SCPEP1	0.28	0.76	0.74	1.90E-30
	UNC93B1	0.61	0.76	0.65	1.06E-29
	AC104126.1	0.95	0.45	0.30	4.57E-28
	HLA-A	0.39	1.00	0.99	3.57E-27
	GRN	0.59	0.95	0.92	1.40E-24
	TXNIP	0.52	0.94	0.87	3.24E-24
	HLA-DQB1	1.94	0.60	0.24	2.01E-23
	FABP5	0.95	0.88	0.82	2.72E-23
	HLA-DRA	0.80	0.90	0.83	4.14E-23
	SGK1	0.67	0.88	0.78	9.27E-23
	CAPNS1	0.37	0.87	0.84	1.27E-22
	SORD	0.64	0.95	0.87	2.18E-22
	gene	avg_log2FC	pct.1	pct.2	p_val_adj
Downregulated	RBFOX2	-0.93	0.86	0.91	9.87E-155
	AC105402.3	-1.42	0.52	0.58	1.32E-65
	RPS12	-0.57	1.00	0.99	2.70E-55
	STEAP1B	-2.07	0.20	0.46	1.61E-54
	RPL34	-0.42	0.99	0.98	2.35E-46
	RPL39	-0.31	0.98	0.97	4.32E-43
	RPS13	-0.45	0.98	0.98	5.79E-40
	ARMC9	-1.52	0.24	0.45	3.73E-37
	RPS28	-0.25	1.00	0.99	1.42E-36
	OOEP	-1.43	0.17	0.33	2.18E-34
	RPS15	-0.37	0.99	0.98	4.02E-34
	CLDN10	-1.95	0.16	0.43	1.94E-33
	RPLP1	-0.50	1.00	0.99	2.98E-33
	DHFR	-0.98	0.48	0.56	7.99E-33
	RPL28	-0.34	0.99	0.99	1.79E-31
	RPL35A	-0.36	0.97	0.97	6.33E-30
	AGR2	-0.60	0.98	0.99	8.90E-30
	RPL36	-0.27	0.98	0.98	5.07E-28
	RPS24	-0.44	0.99	0.98	2.61E-27
	RPL12	-0.66	0.99	0.98	1.35E-26

A3.7

DGE All basal cells from bronchial biopsy					
	gene	avg_log2FC	pct.1	pct.2	p_val_adj
Upregulated	BTG1	1.10	0.97	0.97	7.28E-16
	ID2	1.30	0.86	0.63	4.84E-10
	JUN	0.67	0.99	1.00	5.48E-10
	GADD45B	1.18	0.95	0.90	2.27E-06
	IER2	0.84	0.98	0.96	2.02E-05
	TUBB4B	1.12	0.97	0.95	3.77E-05
	MAFB	1.66	0.86	0.57	4.59E-05
	BRD2	0.52	0.95	0.89	4.73E-04
	HSPA1A	0.54	0.98	0.97	7.02E-04
	TXNIP	1.06	0.93	0.77	9.76E-04
	HSPA1B	0.49	0.97	0.94	1.46E-03
	SRSF7	0.71	0.92	0.86	2.47E-03
	FUS	0.36	0.97	0.98	4.00E-03
	PABPC1	0.66	0.99	0.99	5.51E-03
	CALM1	0.37	0.99	0.99	6.12E-03
	TPI1	0.78	0.98	0.96	1.06E-02
	SRSF3	0.39	0.91	0.84	1.61E-02
	EGR1	0.91	0.97	0.88	1.70E-02
	SOCS1	1.57	0.70	0.39	2.80E-02
	HIST1H4C	1.28	0.77	0.55	2.82E-02
	gene	avg_log2FC	pct.1	pct.2	p_val_adj
Downregulated	AC105402.3	-4.14	0.59	0.91	5.77E-91
	DHFR	-3.68	0.54	0.90	1.60E-88
	MTRNR2L12	-3.73	0.26	0.77	3.99E-41
	STEAP1B	-2.03	0.40	0.74	2.79E-27
	RBFOX2	-1.57	0.89	0.99	1.03E-26
	ARMC9	-2.15	0.23	0.64	2.10E-12
	SERPINB2	-3.11	0.16	0.50	1.01E-09
	OOEP	-1.28	0.29	0.52	4.02E-06
	SYVN1	-0.58	0.64	0.65	6.72E-06
	MTRNR2L8	-3.65	0.04	0.31	3.24E-05
	MT-ATP8	-0.61	0.91	0.97	1.55E-04
	AL136454.1	-2.71	0.05	0.19	1.67E-04
	IL1R1	-0.98	0.43	0.54	1.80E-03
	PCNX2	-1.18	0.29	0.44	7.81E-03
	STX18-AS1	-0.49	0.12	0.09	1.48E-02
	MIR924HG	-1.15	0.16	0.28	1.62E-02
	MIA	-2.21	0.10	0.23	2.95E-02
	MT-ND2	-0.44	0.86	0.96	4.36E-02

A3.8

DGE All club cells from nasal brush					
	gene	avg_log2FC	pct.1	pct.2	p_val_adj
Upregulated	MUC1	0.75	0.91	0.81	2.08E-18
	PSCA	1.66	0.90	0.73	3.85E-18
	HLA-B	0.62	0.99	0.96	3.17E-14
	HLA-E	0.62	0.93	0.88	2.49E-12
	TSPAN1	0.37	0.91	0.84	2.95E-11
	HLA-A	0.37	0.98	0.96	7.64E-09
	LY6E	0.75	0.96	0.90	8.49E-09
	CLDN7	0.44	0.92	0.85	1.66E-08
	HLA-F	0.71	0.79	0.67	5.56E-08
	FABP5	0.71	0.93	0.85	1.69E-07
	HLA-C	0.69	0.98	0.95	2.62E-07
	LGALS3	0.46	0.97	0.93	6.22E-07
	NEAT1	0.54	0.88	0.82	7.89E-07
	GRN	0.58	0.88	0.81	2.28E-06
	FBP1	1.37	0.55	0.28	3.66E-06
	SCNN1A	0.35	0.79	0.69	6.31E-06
	TMSB4X	0.40	0.94	0.89	8.61E-06
	PLAAT4	0.94	0.91	0.80	9.98E-06
	S100A4	0.72	0.95	0.86	1.16E-05
	CD24	0.56	0.22	0.13	3.10E-05
	gene	avg_log2FC	pct.1	pct.2	p_val_adj
Downregulated	RBFOX2	-0.96	0.82	0.83	5.68E-84
	STEAP1B	-2.03	0.21	0.37	2.25E-24
	RPS12	-0.54	0.99	0.99	5.44E-24
	RPLP1	-0.56	1.00	0.99	3.00E-23
	AC105402.3	-1.67	0.48	0.54	5.21E-20
	RPL34	-0.41	0.97	0.97	1.14E-19
	RPS14	-0.46	0.99	0.98	8.23E-19
	RPS15	-0.45	0.97	0.98	8.69E-19
	RPS13	-0.43	0.97	0.96	1.29E-18
	RPS23	-0.43	0.97	0.95	3.40E-18
	RPL12	-0.60	0.98	0.98	3.56E-18
	DHFR	-1.34	0.42	0.51	5.12E-17
	RPL39	-0.27	0.96	0.95	1.09E-16
	RPS15A	-0.43	0.97	0.97	3.36E-15
	RPL32	-0.45	0.97	0.98	3.91E-15
	RPL30	-0.41	0.98	0.98	5.41E-15
	RPS24	-0.42	0.98	0.97	5.62E-15
	RPL28	-0.42	0.99	0.99	6.03E-15
	RPL35A	-0.36	0.96	0.94	6.82E-14
	ARMC9	-1.59	0.22	0.37	1.30E-13

A3.9

DGE All macrophages cells from bronchial biopsy					
	gene	avg_log2FC	pct.1	pct.2	p_val_adj
Upregulated	HLA-DRB5	1.39	0.60	0.39	1.10E-30
	IFI30	0.80	0.98	0.98	1.44E-27
	CTSB	1.38	0.88	0.82	2.43E-26
	CTSZ	0.85	0.88	0.79	2.28E-21
	CD63	1.33	0.74	0.62	1.22E-20
	CTSL	1.88	0.58	0.33	4.49E-20
	CD68	0.81	0.85	0.79	7.22E-20
	FABP5	1.73	0.31	0.16	2.16E-17
	LGALS3	1.43	0.86	0.79	2.77E-16
	RGCC	1.44	0.53	0.31	1.13E-15
	CSTB	1.46	0.81	0.73	2.00E-15
	HLA-DRB1	0.63	0.91	0.89	5.20E-15
	CD74	0.65	0.98	0.97	1.57E-14
	MS4A4A	1.78	0.32	0.12	2.00E-14
	NPC2	0.90	0.87	0.77	9.93E-14
	HLA-DQA1	0.52	0.51	0.37	1.62E-13
	CAPG	0.76	0.75	0.67	1.87E-13
	HLA-DPB1	0.67	0.78	0.62	2.30E-13
	S100A11	0.46	0.98	0.96	5.57E-13
	TUBA1B	0.41	0.53	0.47	1.48E-12
	gene	avg_log2FC	pct.1	pct.2	p_val_adj
Downregulated	RBFOX2	-0.79	0.56	0.67	4.08E-34
	S100A9	-1.23	0.91	0.94	5.52E-28
	CTSS	-0.82	0.94	0.96	4.48E-25
	S100A8	-0.59	0.87	0.93	4.14E-22
	RPL38	-0.30	0.90	0.91	7.80E-19
	LYZ	-0.69	0.98	0.98	3.92E-16
	MNDA	-0.74	0.68	0.89	5.76E-16
	RPS29	-0.29	0.92	0.92	1.38E-15
	LINC00309	-0.75	0.12	0.13	1.28E-14
	DHFR	-2.07	0.26	0.49	9.77E-12
	ISG15	-0.98	0.31	0.39	1.18E-11
	PMAIP1	-0.64	0.46	0.49	1.64E-11
	AC105402.3	-2.10	0.39	0.55	3.77E-11
	S100A12	-1.05	0.54	0.75	4.20E-11
	LCP1	-0.46	0.87	0.89	4.83E-11
	CSTA	-0.34	0.66	0.75	5.03E-11
	VCAN	-1.04	0.78	0.87	2.86E-10
	CCL3L1	-0.37	0.43	0.47	4.76E-10
	TET2	-0.90	0.77	0.87	1.56E-09
	ARMC9	-2.15	0.08	0.27	6.33E-09

A3.10

DGE CD8 T cells from bronchial biopsy					
	gene	avg_log2FC	pct.1	pct.2	p_val_adj
Upregulated	BTG1	0.37	1.00	0.99	1.18E-34
	DDIT4	0.56	0.86	0.82	9.57E-32
	SMAP2	0.51	0.46	0.42	1.82E-26
	HERPUD1	0.39	0.64	0.66	6.41E-23
	ISG20	0.40	0.47	0.45	6.64E-21
	TXNIP	0.47	0.41	0.38	6.88E-21
	ID2	0.45	0.65	0.61	6.77E-19
	UCP2	0.63	0.19	0.16	1.82E-16
	TBC1D10C	0.38	0.40	0.38	3.37E-15
	AREG	0.74	0.52	0.46	2.99E-14
	CCND3	0.47	0.45	0.40	3.46E-13
	ZFP36	0.38	0.96	0.96	4.52E-13
	LINC01871	0.46	0.40	0.38	4.17E-12
	RPLP0	0.32	0.92	0.94	7.65E-12
	KLF13	0.41	0.42	0.39	7.90E-12
	SAP30	0.62	0.17	0.14	1.36E-11
	ZFP36L2	0.34	0.99	0.98	3.58E-11
	RBM3	0.30	0.50	0.50	2.05E-10
	SLC25A6	0.40	0.49	0.47	2.45E-10
	RPL3	0.25	0.93	0.93	2.54E-10
	gene	avg_log2FC	pct.1	pct.2	p_val_adj
Downregulated	RBFOX2	-1.63	0.32	0.73	7.68E-237
	AC105402.3	-2.99	0.10	0.43	1.56E-155
	DHFR	-2.64	0.07	0.32	1.30E-93
	RPL39	-0.30	0.96	0.99	2.36E-89
	STEAP1B	-2.01	0.06	0.22	1.59E-72
	RPL41	-0.46	0.80	0.86	9.92E-53
	MTRNR2L12	-2.86	0.02	0.14	2.36E-50
	RSRP1	-0.62	0.59	0.78	6.38E-47
	ARMC9	-2.22	0.03	0.12	1.75E-43
	OOEP	-1.35	0.07	0.19	5.46E-34
	HSPA8	-0.26	0.98	0.99	8.21E-25
	DNAJA1	-0.52	0.84	0.92	2.89E-24
	DNAJB1	-0.42	0.74	0.87	2.74E-21
	MT-ND4	-0.49	0.52	0.75	3.26E-21
	LDHA	-0.29	0.72	0.82	1.89E-20
	JOSD1	-0.49	0.28	0.43	1.07E-17
	MT-ATP8	-0.31	0.68	0.85	3.07E-17
	SLC38A2	-0.35	0.49	0.62	1.13E-16
	BAIAP2L1	-0.92	0.06	0.11	2.43E-16
	DYNLL1	-0.34	0.74	0.85	2.43E-16

A3.11

DGE Combined cells from bronchial biopsy					
	gene	avg_log2FC	pct.1	pct.2	p_val_adj
Upregulated	BTG1	0.45	0.98	0.98	6.58E-88
	DDIT4	0.60	0.85	0.80	3.38E-73
	SMAP2	0.58	0.49	0.42	1.86E-71
	AREG	0.97	0.54	0.46	7.39E-70
	ISG20	0.49	0.48	0.43	1.01E-57
	SAP30	0.92	0.19	0.14	3.61E-53
	FKBP5	0.43	0.47	0.45	6.28E-53
	HERPUD1	0.51	0.64	0.62	1.88E-49
	ZFP36L2	0.45	0.97	0.96	8.41E-49
	TSC22D3	0.39	0.84	0.86	4.15E-45
	LINC01871	0.48	0.35	0.34	4.87E-38
	ZFP36	0.39	0.94	0.92	4.84E-36
	TMIGD2	1.18	0.11	0.06	1.74E-35
	CCR6	0.97	0.11	0.07	6.98E-33
	H1FX	0.52	0.45	0.39	2.50E-27
	PER1	0.43	0.42	0.39	4.33E-27
	CEBPD	0.78	0.29	0.23	2.40E-26
	CXCR4	0.29	0.90	0.87	2.13E-25
	SNX9	0.42	0.30	0.26	3.79E-25
	SOCS1	0.58	0.58	0.53	3.83E-25
	gene	avg_log2FC	pct.1	pct.2	p_val_adj
Downregulated	RBFOX2	-1.57	0.35	0.70	0.00E+00
	AC105402.3	-2.76	0.13	0.43	5.42E-277
	DHFR	-2.48	0.10	0.34	2.06E-201
	STEAP1B	-1.88	0.08	0.24	1.75E-143
	RPL41	-0.32	0.82	0.86	1.00E-128
	MTRNR2L12	-2.32	0.04	0.16	3.85E-109
	OOEP	-1.44	0.07	0.20	6.93E-81
	ARMC9	-1.98	0.04	0.13	8.71E-81
	RSRP1	-0.51	0.63	0.77	4.56E-77
	NKG7	-0.45	0.57	0.68	1.31E-51
	MT-ND4	-0.25	0.61	0.76	7.03E-42
	BAIAP2L1	-1.05	0.06	0.13	9.89E-36
	GAREM1	-1.40	0.04	0.11	2.43E-35
	PPP1R10	-0.48	0.37	0.52	2.57E-33
	DNAJB1	-0.32	0.72	0.83	6.84E-33
	LDHA	-0.35	0.66	0.76	3.25E-31
	P2RY8	-0.71	0.11	0.17	1.80E-29
	JOSD1	-0.53	0.26	0.38	2.82E-27
	GZMA	-0.26	0.52	0.62	3.14E-27
	DNAJA1	-0.45	0.80	0.88	3.00E-26

A3.12

DGE Combined T cells from nasal brush					
	gene	avg_log2FC	pct.1	pct.2	p_val_adj
Upregulated	MT-ND4L	0.51	0.86	0.77	2.43E-101
	JUN	0.31	0.82	0.74	3.26E-60
	UBC	0.28	0.92	0.90	1.50E-57
	FOS	0.40	0.48	0.36	1.43E-55
	MT-CO3	0.35	0.94	0.89	8.18E-50
	JUNB	0.35	0.68	0.61	5.29E-49
	IL32	0.32	0.95	0.90	1.80E-47
	CXCR3	0.36	0.62	0.52	1.93E-42
	FOSB	0.63	0.45	0.30	3.50E-42
	CISH	0.55	0.37	0.28	6.62E-38
	MT-ND1	0.47	0.84	0.75	6.98E-37
	APOBEC3G	0.38	0.52	0.41	7.00E-37
	DDX5	0.25	0.87	0.84	2.07E-36
	IER2	0.33	0.66	0.57	6.76E-35
	ANXA1	0.31	0.59	0.51	2.20E-33
	ACTG1	0.26	0.97	0.96	5.60E-32
	PCBP1	0.89	0.56	0.38	9.21E-31
	MT-ATP8	0.54	0.82	0.77	1.11E-30
	ITGB2	0.52	0.56	0.46	4.97E-28
	GZMH	0.40	0.56	0.44	8.18E-27
	gene	avg_log2FC	pct.1	pct.2	p_val_adj
Downregulated	RPS29	-0.30	0.95	0.99	8.82E-267
	RBFOX2	-1.41	0.42	0.63	4.74E-182
	RPS21	-0.33	0.97	0.99	7.10E-145
	RPL34	-0.25	0.99	0.99	4.61E-107
	RPLP2	-0.27	0.98	0.99	1.41E-102
	RPLP1	-0.34	1.00	1.00	1.51E-100
	RPS28	-0.27	0.99	0.99	1.54E-87
	AC105402.3	-1.77	0.16	0.27	5.54E-79
	STEAP1B	-1.68	0.07	0.18	1.51E-77
	RPS18	-0.27	0.99	0.99	2.62E-65
	ARMC9	-1.73	0.04	0.11	1.36E-58
	RPS12	-0.34	1.00	1.00	2.08E-58
	CTSH	-0.70	0.13	0.16	1.29E-35
	OOEP	-1.17	0.10	0.18	1.07E-34
	AL136456.1	-0.57	0.18	0.20	1.72E-32
	DHFR	-1.03	0.15	0.22	9.34E-27
	AL627171.2	-0.50	0.14	0.17	9.71E-24
	RPS14	-0.26	0.99	0.99	3.40E-22
	AC068724.3	-1.08	0.06	0.11	5.07E-21

A3.13

DGE neutrophils: Infection group					
	gene	avg_log2FC	pct.1	pct.2	p_val_adj
Upregulated	PNRC1	2.01	0.66	0.45	5.76E-60
	FCER1G	2.02	0.48	0.32	3.21E-53
	NFKBIA	2.03	0.61	0.36	1.31E-39
	IFI30	2.34	0.37	0.20	1.43E-33
	SOD2	0.69	0.85	0.91	9.95E-25
	CEBPD	1.76	0.45	0.32	2.72E-23
	TNFAIP3	1.58	0.48	0.30	5.60E-22
	H3F3B	0.97	0.88	0.84	5.90E-22
	CXCR4	2.96	0.22	0.07	8.94E-22
	CFD	3.03	0.23	0.06	1.88E-21
	IRAK3	1.21	0.36	0.25	1.77E-19
	GADD45B	2.62	0.19	0.08	7.20E-19
	TLR2	2.05	0.24	0.12	1.90E-18
	KLF6	1.65	0.27	0.19	4.86E-18
	CXCL8	1.23	0.68	0.49	2.88E-16
	ALOX5AP	1.34	0.40	0.32	4.32E-16
	ATP6V0C	1.70	0.34	0.25	1.08E-15
	FTL	0.82	0.92	0.87	1.14E-15
	CEBPB	1.63	0.35	0.23	1.18E-15
	BRI3	1.46	0.31	0.23	1.21E-14
	gene	avg_log2FC	pct.1	pct.2	p_val_adj
Downregulated	S100A9	-1.80	0.47	0.89	9.44E-51
	S100A8	-1.73	0.64	0.90	6.95E-38
	MNDA	-2.26	0.10	0.55	1.88E-20
	TBC1D8	-2.32	0.14	0.62	8.07E-16
	FCGR3B	-1.53	0.17	0.60	6.87E-15
	AC105402.3	-10.61	0.00	0.16	1.47E-12
	CNTNAP3	-2.87	0.02	0.22	8.82E-11
	S100A4	-1.77	0.12	0.49	2.41E-10
	AC099489.1	-1.68	0.15	0.53	2.19E-08
	SELL	-2.72	0.04	0.30	2.72E-08
	MX2	-1.47	0.12	0.45	4.04E-08
	SLCO3A1	-2.57	0.04	0.31	5.05E-08
	BRAF	-1.84	0.13	0.49	1.25E-07
	ATP5F1E	-1.41	0.13	0.47	2.01E-07
	CMTM2	-1.34	0.08	0.34	8.24E-07
	AGTPBP1	-2.56	0.02	0.21	1.16E-06
	STAT3	-1.35	0.20	0.58	1.28E-06
	NCF2	-1.33	0.11	0.43	1.55E-06
	COP1	-1.97	0.07	0.38	1.95E-06
	LYST	-1.40	0.05	0.29	2.89E-06

A3.14

DGE neutrophils: No infection group					
	gene	avg_log2FC	pct.1	pct.2	p_val_adj
Upregulated	IFITM3	2.17	0.51	0.14	3.18E-73
	HLA-C	1.15	0.72	0.43	1.75E-53
	PER1	2.52	0.17	0.03	2.89E-21
	HLA-B	0.61	0.78	0.58	1.05E-20
	AC084871.1	2.16	0.22	0.06	1.12E-20
	CEBPB	1.18	0.36	0.15	1.42E-18
	RNF149	0.59	0.72	0.55	1.63E-16
	ATP6V0C	1.32	0.33	0.14	1.70E-16
	CXCL16	1.74	0.20	0.05	6.98E-16
	CPD	1.36	0.30	0.11	8.50E-16
	ALOX5AP	1.22	0.38	0.19	2.59E-15
	CXCR4	1.55	0.21	0.06	7.49E-15
	LRG1	2.03	0.15	0.04	1.81E-12
	FPR1	0.67	0.55	0.33	3.18E-12
	TREM1	0.88	0.43	0.24	1.11E-11
	MGAT1	2.28	0.13	0.03	1.84E-11
	TSC22D3	1.23	0.27	0.11	5.38E-11
	BATF	2.46	0.10	0.02	8.75E-11
	DUSP1	0.58	0.69	0.55	2.13E-10
	MAP2K1	1.82	0.13	0.03	2.68E-10
	gene	avg_log2FC	pct.1	pct.2	p_val_adj
Downregulated	IL1B	-1.17	0.59	0.80	2.46E-67
	PTGS2	-1.02	0.38	0.54	6.62E-30
	NFKBIZ	-1.03	0.31	0.47	1.16E-26
	HSPA1A	-1.98	0.07	0.19	5.95E-24
	CFD	-1.93	0.05	0.16	1.13E-23
	AZIN1-AS1	-0.83	0.34	0.51	1.69E-22
	NFKBID	-1.78	0.09	0.21	6.17E-21
	BCL2A1	-0.61	0.67	0.77	5.63E-20
	PPP1R15A	-0.86	0.45	0.57	1.54E-19
	NEBL	-1.59	0.03	0.13	1.42E-18
	TAGAP	-1.31	0.20	0.32	4.07E-18
	S100A12	-1.51	0.13	0.23	1.03E-17
	DENND5A	-0.83	0.41	0.54	6.16E-17
	IL1A	-1.92	0.07	0.16	8.56E-17
	AL078604.4	-1.29	0.18	0.30	8.81E-16
	DUSP2	-1.35	0.14	0.24	7.10E-13
	GPR65	-1.17	0.18	0.28	7.68E-13
	AL049651.1	-1.11	0.22	0.34	1.35E-12
	CFLAR	-0.82	0.31	0.38	3.48E-11
	HSP90AB1	-1.54	0.07	0.15	7.19E-11

A3.15

DGE macrophage: Infection group					
	gene	avg_log2FC	pct.1	pct.2	p_val_adj
Upregulated	HLA-DRB5	3.33	0.73	0.32	1.02E-53
	IFI30	1.78	0.98	0.97	7.47E-43
	CTSB	2.71	0.91	0.81	6.48E-41
	GPNMB	6.88	0.40	0.02	2.25E-36
	LGALS3	2.65	0.86	0.75	3.24E-35
	FABP5	4.71	0.53	0.11	1.31E-34
	CSTB	2.40	0.79	0.72	3.21E-34
	CTSL	3.74	0.61	0.30	2.95E-33
	SDS	5.23	0.42	0.04	7.35E-33
	CD63	2.25	0.74	0.60	2.00E-32
	CD68	1.58	0.86	0.77	2.84E-30
	CD9	4.37	0.43	0.05	1.86E-29
	HLA-DRB1	1.67	0.93	0.87	5.08E-29
	ACP5	3.71	0.47	0.07	1.41E-28
	CAPG	1.67	0.79	0.63	4.18E-28
	C15orf48	2.06	0.67	0.40	1.03E-27
	CD81	2.72	0.54	0.23	5.75E-27
	FBP1	2.86	0.57	0.25	2.39E-26
	APOE	8.10	0.29	0.00	4.68E-26
	APOC1	6.23	0.30	0.00	5.39E-26
	gene	avg_log2FC	pct.1	pct.2	p_val_adj
Downregulated	RPL37	-1.38	0.89	0.97	3.09E-67
	RPS29	-1.44	0.77	0.91	5.16E-53
	RPL34	-1.03	0.93	0.98	2.48E-46
	RPL38	-1.36	0.76	0.91	1.73E-44
	RPS21	-1.16	0.88	0.94	3.56E-42
	RBFOX2	-2.87	0.20	0.63	2.67E-41
	LYZ	-1.18	0.97	0.98	4.59E-41
	RPL39	-0.98	0.96	0.97	1.29E-40
	S100A4	-0.99	0.95	0.98	9.42E-39
	S100A9	-1.54	0.82	0.97	1.97E-38
	CTSS	-1.18	0.91	0.95	1.25E-36
	S100A8	-1.52	0.72	0.95	1.66E-35
	RPS28	-0.80	0.97	0.98	3.29E-35
	RPL35A	-0.94	0.89	0.95	4.01E-35
	RPL37A	-1.11	0.85	0.91	2.09E-34
	RPS27	-0.81	0.97	0.96	6.24E-34
	RPS15A	-0.90	0.93	0.95	9.90E-34
	RPLP2	-0.81	0.97	0.97	2.15E-30
	RPL26	-0.79	0.94	0.96	4.21E-29
	RPL36	-0.90	0.90	0.95	3.03E-28

A3.16

DGE macrophage: No infection group					
	gene	avg_log2FC	pct.1	pct.2	p_val_adj
Upregulated	RPS28	0.56	0.99	0.98	2.45E-21
	AREG	1.66	0.76	0.57	1.76E-18
	SRGAP1	2.65	0.37	0.10	2.27E-18
	RPLP0	0.58	0.96	0.91	7.32E-18
	MIF	1.19	0.77	0.53	3.36E-17
	GRINA	0.86	0.80	0.70	7.68E-14
	FMN1	1.63	0.49	0.25	2.01E-13
	NPC2	0.71	0.86	0.81	3.37E-12
	SIGLEC10	1.82	0.36	0.14	1.76E-11
	NECTIN2	1.49	0.42	0.19	2.12E-11
	TSC22D3	1.06	0.59	0.34	2.13E-11
	SLAMF1	4.10	0.16	0.01	3.79E-11
	TNIP3	2.21	0.40	0.23	7.70E-11
	VSIG4	2.55	0.22	0.06	5.69E-10
	SPHK1	1.32	0.49	0.31	1.33E-09
	KLF6	0.57	0.88	0.84	2.69E-09
	OLR1	0.81	0.73	0.52	3.55E-09
	BATF	1.85	0.29	0.09	5.92E-09
	RPS4Y1	0.52	0.61	0.40	6.46E-09
	BTG1	0.63	0.94	0.94	6.50E-09
	gene	avg_log2FC	pct.1	pct.2	p_val_adj
Downregulated	AC105402.3	-2.28	0.41	0.65	7.48E-37
	AL078604.4	-1.48	0.61	0.84	1.16E-31
	DHFR	-2.20	0.28	0.57	3.89E-28
	ATP2B1	-0.83	0.88	0.96	2.14E-23
	NEBL	-2.63	0.04	0.28	7.53E-22
	ARHGAP26	-0.88	0.76	0.89	5.25E-21
	CXCL8	-0.96	0.92	0.99	1.33E-20
	TMEM176B	-1.05	0.30	0.65	2.45E-20
	PTGS2	-0.97	0.74	0.90	6.77E-20
	MT-ND4L	-0.74	0.80	0.95	5.99E-18
	NPHS1	-1.88	0.14	0.43	1.40E-17
	TNF	-1.24	0.50	0.76	2.65E-17
	ANTXR2	-1.19	0.50	0.65	3.88E-17
	EXT1	-1.51	0.42	0.67	3.06E-16
	MAP4K4	-0.95	0.74	0.86	4.22E-16
	MNDA	-0.81	0.71	0.89	7.65E-16
	VCAN	-0.96	0.80	0.86	1.69E-15
	QKI	-0.73	0.84	0.93	5.17E-15
	NCOA4	-0.80	0.74	0.84	6.17E-15
	MCTP1	-0.87	0.68	0.88	1.51E-14

A3.17

DGE CD8: Infection group					
	gene	avg_log2FC	pct.1	pct.2	p_val_adj
Upregulated	EEF1A1	0.57	1.00	1.00	1.44E-61
	ZFP36L2	0.59	0.99	0.98	1.20E-56
	BTG1	0.59	1.00	0.99	5.39E-47
	JUNB	0.71	0.94	0.81	3.88E-42
	HLA-B	0.81	0.98	0.96	4.05E-42
	MT-ND4L	0.70	0.94	0.81	4.83E-41
	PER1	1.03	0.69	0.43	1.15E-40
	ZFP36	0.62	0.98	0.96	4.02E-38
	AREG	1.09	0.67	0.47	2.81E-37
	CSRNP1	1.04	0.59	0.35	1.12E-31
	ARHGEF1	0.74	0.75	0.56	3.25E-28
	CEBPD	1.23	0.45	0.23	7.89E-28
	DDIT4	0.63	0.88	0.79	6.87E-27
	MKNK2	0.90	0.54	0.34	1.34E-26
	IL7R	0.73	0.77	0.71	7.53E-26
	FOS	0.81	0.73	0.53	1.34E-25
	ODC1	0.86	0.66	0.48	2.77E-24
	UBALD2	0.84	0.52	0.33	7.10E-23
	TRBC2	1.03	0.52	0.31	1.69E-22
	IFNGR1	1.32	0.38	0.19	1.95E-22
	gene	avg_log2FC	pct.1	pct.2	p_val_adj
Downregulated	RPS29	-1.56	0.80	0.99	9.50E-270
	RPL39	-1.10	0.92	0.99	1.19E-166
	RPL37	-1.06	0.90	0.99	1.40E-155
	RPS27	-0.82	1.00	1.00	1.68E-136
	AC105402.3	-3.52	0.13	0.56	9.84E-136
	RBFOX2	-2.36	0.23	0.67	8.35E-135
	RPS21	-1.08	0.86	0.97	8.93E-132
	RPL37A	-1.22	0.70	0.93	8.04E-121
	RPL34	-0.90	0.95	0.99	7.55E-116
	RPL38	-1.24	0.62	0.89	2.88E-109
	DHFR	-3.44	0.08	0.43	2.13E-100
	RPLP2	-0.84	0.95	0.98	2.88E-97
	RPL35A	-0.87	0.91	0.98	6.11E-90
	RPS28	-0.74	0.96	0.99	5.54E-74
	RPL36	-0.92	0.84	0.94	1.33E-73
	ATP5F1E	-1.07	0.63	0.84	1.64E-69
	RPS4Y1	-9.40	0.00	0.17	4.72E-66
	RPL36A	-0.97	0.70	0.89	1.82E-63
	RPS25	-0.77	0.93	0.96	3.41E-59
	RPL27A	-1.15	0.57	0.79	2.91E-57
	MT1X	-2.21	0.35	0.58	8.50E-56

A3.18

DGE CD8: No infection group					
	gene	avg_log2FC	pct.1	pct.2	p_val_adj
Upregulated	ID2	0.68	0.65	0.60	2.26E-40
	TXNIP	1.00	0.37	0.32	1.23E-38
	MT1X	1.15	0.56	0.46	1.08E-27
	MT2A	0.90	0.72	0.69	3.71E-27
	DDIT4	0.50	0.85	0.84	3.72E-27
	MT1E	1.01	0.45	0.36	3.06E-25
	LINC01871	0.67	0.41	0.39	3.44E-17
	CCND3	0.61	0.41	0.39	2.26E-16
	AREG	0.73	0.47	0.46	2.32E-16
	AL627171.2	1.64	0.15	0.09	2.97E-12
	SAP30	1.16	0.15	0.12	7.59E-11
	MT1F	1.01	0.28	0.22	1.70E-10
	HIST1H4C	0.60	0.69	0.68	2.20E-10
	SMAP2	0.58	0.39	0.37	3.14E-10
	UCP2	0.72	0.19	0.16	1.32E-08
	PEBP1	0.52	0.31	0.30	9.43E-08
	GSTP1	0.67	0.40	0.40	9.32E-07
	SNHG15	0.61	0.20	0.19	3.52E-06
	BLOC1S4	0.81	0.12	0.10	2.72E-05
	TMEM173	0.69	0.16	0.14	1.08E-04
	gene	avg_log2FC	pct.1	pct.2	p_val_adj
Downregulated	RBFOX2	-1.48	0.35	0.76	9.16E-148
	AC105402.3	-2.37	0.09	0.35	2.45E-109
	DHFR	-2.02	0.07	0.24	2.36E-60
	STEAP1B	-1.83	0.06	0.19	8.94E-54
	MT-ND4L	-0.71	0.61	0.89	8.67E-43
	RSRP1	-0.88	0.53	0.80	5.92E-41
	HSPH1	-0.98	0.57	0.78	5.27E-38
	MT-ATP8	-0.72	0.59	0.86	2.96E-36
	DNAJA1	-0.57	0.81	0.90	2.31E-32
	MTRNR2L12	-2.43	0.02	0.11	1.16E-30
	LDHA	-0.53	0.69	0.87	1.77E-27
	HSP90AB1	-0.63	0.90	0.95	3.14E-25
	MT-ND6	-1.22	0.25	0.53	4.00E-25
	MT-ND4	-0.54	0.44	0.73	6.55E-25
	RPL41	-0.60	0.80	0.88	1.90E-21
	AL157402.2	-1.49	0.08	0.28	1.29E-20
	ATP1A1	-0.74	0.29	0.53	6.88E-20
	CHORDC1	-1.00	0.27	0.54	1.06E-19
	HSPD1	-0.62	0.65	0.83	1.03E-18
	NAA50	-0.82	0.23	0.46	3.82E-16

A3.19

DGE Multiciliated: Infection group					
	gene	avg_log2FC	pct.1	pct.2	p_val_adj
Upregulated	APOD	4.87	0.75	0.06	3.96E-154
	TCTEX1D4	1.96	0.88	0.58	1.95E-138
	CCDC74A	1.53	0.84	0.54	3.68E-81
	CFAP73	0.97	0.94	0.85	6.02E-71
	SCPEP1	1.06	0.90	0.77	2.28E-59
	RYR3	3.17	0.43	0.05	3.44E-53
	GSTT2B	3.68	0.37	0.03	1.81E-51
	LRRC61	1.45	0.77	0.47	1.94E-49
	CTXN1	0.86	0.89	0.81	5.98E-43
	FAM166B	0.80	0.92	0.83	3.32E-41
	LINC00332	1.91	0.56	0.16	8.35E-41
	HLA-DQB1	2.31	0.57	0.12	5.67E-40
	JTB	0.96	0.79	0.61	3.29E-37
	CCDC74B	1.26	0.74	0.40	1.06E-36
	CABCOCO1	0.67	0.92	0.81	2.40E-33
	DYDC2	0.89	0.86	0.70	3.89E-33
	PSCA	1.26	0.87	0.78	6.07E-33
	PTPMT1	1.53	0.59	0.22	2.21E-32
	CCDC78	0.52	0.94	0.94	9.30E-29
	BDH1	0.76	0.87	0.73	2.09E-28
	gene	avg_log2FC	pct.1	pct.2	p_val_adj
Downregulated	RPL37A	-1.14	0.81	0.92	9.29E-68
	TFF3	-1.82	0.68	0.86	6.88E-63
	RPS29	-1.19	0.66	0.86	5.30E-62
	C1orf141	-1.86	0.16	0.53	1.03E-58
	RPL38	-1.14	0.77	0.90	1.49E-55
	ATP5F1E	-0.97	0.88	0.94	2.00E-53
	RPL39	-0.98	0.83	0.89	2.00E-53
	PDE3A	-2.44	0.30	0.69	7.85E-53
	NDUFA1	-1.06	0.73	0.87	1.77E-48
	RPL37	-0.91	0.87	0.91	5.39E-48
	MT-ND3	-1.19	0.92	0.96	2.98E-46
	RPL34	-0.81	0.89	0.93	1.01E-43
	COX7C	-0.88	0.84	0.91	9.37E-43
	DHFR	-2.08	0.46	0.74	3.19E-40
	RPS21	-0.91	0.79	0.87	8.47E-39
	RBFOX2	-1.35	0.53	0.70	8.38E-36
	RPS20	-1.05	0.74	0.85	1.12E-34
	AL121899.1	-1.39	0.49	0.72	1.70E-34
	ROMO1	-0.94	0.79	0.84	1.68E-32
	POLR2L	-1.04	0.74	0.83	2.14E-32
	KTN1	-0.72	0.90	0.95	2.63E-32

A3.20

DGE Multiciliated: No infection group					
	gene	avg_log2FC	pct.1	pct.2	p_val_adj
Upregulated	*RPS4Y1*	6.09	0.51	0.01	0.00E+00
	TMEM190	3.12	0.70	0.36	0.00E+00
	DDX3Y	5.21	0.39	0.01	2.23E-267
	TCTEX1D4	1.95	0.77	0.37	3.73E-265
	CFAP73	1.19	0.89	0.68	2.37E-217
	HLA-DRB5	3.88	0.40	0.10	3.91E-186
	EIF1AY	5.19	0.28	0.01	6.05E-168
	USP9Y	4.91	0.28	0.01	3.95E-166
	CCDC74A	1.41	0.69	0.40	1.81E-149
	UTY	4.30	0.28	0.02	1.87E-149
	STMND1	1.45	0.66	0.35	1.53E-134
	GSTA1	0.99	0.97	0.94	1.27E-126
	AC105446.1	2.58	0.37	0.10	4.08E-118
	PRKY	4.83	0.21	0.01	4.46E-118
	AC100781.1	3.26	0.26	0.03	2.40E-114
	RPL41	0.60	0.93	0.91	4.51E-99
	AC090371.1	3.07	0.26	0.04	2.55E-94
	GBP3	1.75	0.36	0.11	3.53E-90
	ACBD3-AS1	1.64	0.45	0.18	3.78E-90
	AC004832.1	0.87	0.78	0.57	3.18E-89
	gene	avg_log2FC	pct.1	pct.2	p_val_adj
Downregulated	STEAP1B	-3.30	0.18	0.74	0.00E+00
	MTRNR2L12	-3.33	0.38	0.93	0.00E+00
	DHFR	-3.33	0.66	0.97	0.00E+00
	AC105402.3	-3.81	0.69	0.99	0.00E+00
	RBFOX2	-1.68	0.70	0.89	0.00E+00
	MTRNR2L8	-3.56	0.06	0.48	4.43E-254
	AL357093.2	-0.95	0.93	0.97	4.84E-202
	KIF21A	-0.69	0.95	0.98	3.59E-147
	CYP4B1	-0.77	0.95	0.97	4.64E-147
	RPS4X	-0.72	0.94	0.95	3.29E-141
	EIF3CL	-2.37	0.06	0.26	3.55E-86
	HIST2H2AA3	-2.10	0.10	0.32	2.11E-85
	MIR924HG	-2.84	0.03	0.20	1.18E-83
	RSRP1	-0.62	0.81	0.90	1.97E-73
	LAYN	-1.52	0.16	0.39	1.21E-70
	IFITM10	-1.11	0.24	0.49	3.08E-70
	AP001831.1	-1.07	0.37	0.62	4.58E-68
	MT-ATP8	-0.73	0.93	0.99	1.86E-67
	KRT19	-0.54	0.91	0.93	1.27E-65
	MT3	-1.91	0.11	0.30	2.99E-62

A3.21

DGE Goblet: Infection group					
	gene	avg_log2FC	pct.1	pct.2	p_val_adj
Upregulated	TENT5C	4.98	0.95	0.05	5.37E-07
	MSLN	2.48	0.96	0.58	5.63E-05
	CFD	6.03	0.76	0.00	2.26E-04
	KLK11	4.12	0.90	0.16	1.83E-03
	SDK1	3.25	0.92	0.21	5.07E-03
	SLC4A4	2.86	0.94	0.21	3.59E-02
	gene	avg_log2FC	pct.1	pct.2	p_val_adj
Downregulated	RPS29	-2.86	0.82	0.84	9.76E-11
	RPL37A	-2.33	0.87	0.90	4.19E-09
	RPS21	-2.03	0.94	0.95	2.26E-08
	RPL37	-2.06	0.98	1.00	2.99E-07
	NDUFB4	-2.35	0.57	0.74	1.01E-06
	S100A11	-1.42	0.99	0.95	1.84E-06
	COX6C	-2.13	0.79	0.84	1.81E-05
	RPL38	-2.43	0.74	0.84	8.33E-05
	RPS16	-1.53	0.92	0.90	1.59E-04
	RNASEK	-1.15	0.82	0.74	3.98E-04
	DSTN	-1.43	0.88	0.95	5.37E-04
	RPL39	-1.66	0.94	0.90	6.46E-04
	NQO1	-2.37	0.54	0.42	7.40E-04
	COX7A2	-1.75	0.74	0.90	1.25E-03
	RPS15A	-1.34	0.96	1.00	1.29E-03
	LTF	-4.55	0.38	0.16	2.15E-03
	S100A10	-2.45	0.52	0.63	2.62E-03
	MT-ND3	-1.49	0.98	0.79	5.47E-03
	RPL31	-1.45	0.85	0.84	6.03E-03
	RPL27A	-1.54	0.79	0.79	6.55E-03
	NDUFS5	-1.73	0.62	0.63	7.25E-03
	ROMO1	-1.92	0.63	0.63	8.15E-03
	RPL34	-1.51	0.95	1.00	1.02E-02
	RPL21	-1.54	0.89	0.90	1.07E-02

A3.22

DGE Goblet: No infection group					
	gene	avg_log2FC	pct.1	pct.2	p_val_adj
Upregulated	TFF3	4.27	0.88	0.29	4.50E-03
	MAX	0.55	0.49	0.07	1.42E-02
	WFDC2	0.96	1.00	1.00	1.75E-02
	GNB2	0.62	0.89	0.19	2.13E-02
	GAPVD1	0.60	0.45	0.03	2.31E-02
	SLC39A7	1.95	0.76	0.07	2.90E-02
	gene	avg_log2FC	pct.1	pct.2	p_val_adj
Downregulated	RSU1	-2.56	0.37	0.07	4.78E-20
	WAC-AS1	-2.19	0.36	0.03	4.20E-19
	TRMT2B	-3.11	0.20	0.07	5.26E-12
	AP1M1	-3.37	0.16	0.03	8.11E-12
	PRPS1	-2.04	0.22	0.03	1.32E-11
	WWC1	-3.78	0.26	0.16	1.75E-11
	MED11	-0.86	0.44	0.03	2.50E-11
	SH3GL1	-2.01	0.39	0.10	3.00E-11
	XPO7	-1.61	0.26	0.03	3.11E-11
	DHFR	-2.57	0.64	0.48	3.73E-11
	AFTPH	-0.66	0.46	0.03	4.11E-11
	CSE1L	-3.01	0.19	0.03	4.26E-11
	AC105402.3	-3.07	0.70	0.48	5.61E-11
	MED19	-1.18	0.34	0.03	7.78E-11
	POLR3D	-2.66	0.22	0.07	9.05E-11
	SRPK1	-2.17	0.54	0.26	1.12E-10
	HDAC4	-3.12	0.19	0.07	1.42E-10
	C8orf33	-0.94	0.38	0.03	1.43E-10
	CTBP1	-1.89	0.50	0.16	1.54E-10
	KIF3B	-2.01	0.33	0.03	1.71E-10
	SNED1	-2.03	0.26	0.07	2.02E-10
	DLAT	-3.02	0.21	0.07	2.61E-10
	C9orf78	-1.30	0.53	0.10	3.30E-10
	ACOT8	-2.54	0.29	0.10	3.58E-10
	ACAT1	-1.36	0.32	0.03	4.05E-10

AMERICAN SOCIETY FOR MICROBIOLOGY | Microbiology Spectrum

RESEARCH ARTICLE

Identifying Bacterial Airways Infection in Stable Severe Asthma Using Oxford Nanopore Sequencing Technologies

Maisha F. Jabeen,[a,c] Nicholas D. Sanderson,[b,c] Dona Foster,[b] Derrick W. Crook,[b,c] Jennifer L. Cane,[a,c] Catherine Borg,[a,c] Clare Connolly,[a,c] Samantha Thulborn,[a,c] Ian D. Pavord,[a,c] Paul Klenerman,[d] Teresa L. Street,[b,c] Timothy S. C. Hinks[a,c]

[a]Respiratory Medicine Unit, Experimental Medicine Division, Nuffield Department of Medicine, University of Oxford, John Radcliffe Hospital, Oxford, United Kingdom
[b]Nuffield Department of Clinical Medicine, University of Oxford, John Radcliffe Hospital, Oxford, United Kingdom
[c]National Institute for Health Research Oxford Biomedical Research Centre, John Radcliffe Hospital, Oxford, United Kingdom
[d]Peter Medawar Building for Pathogen Research and Translational Gastroenterology Unit, Nuffield Department of Clinical Medicine, University of Oxford, Oxford, United Kingdom

ABSTRACT Previous metagenomic studies in asthma have been limited by inadequate sequencing depth for species-level bacterial identification and by heterogeneity in clinical phenotyping. We hypothesize that chronic bacterial airways infection is a key "treatable trait" whose prevalence, clinical phenotype and reliable biomarkers need definition. In this study, we have applied a method for Oxford Nanopore sequencing for the unbiased metagenomic characterization of severe asthma. We optimized methods to compare performance of Illumina MiSeq, Nanopore sequencing, and RT-qPCR on total sputum DNA extracts against culture/MALDI-TOF for analysis of induced sputum samples from highly phenotyped severe asthma during clinical stability. In participants with severe asthma (n = 23) *H. influenzae* was commonly cultured (n = 8) and identified as the dominant bacterial species by metagenomic sequencing using an optimized method for Illumina MiSeq and Oxford Nanopore. Alongside superior operational characteristics, Oxford Nanopore achieved near complete genome coverage of *H. influenzae* and demonstrated a high level of agreement with Illumina MiSeq data. Clinically significant infection was confirmed with validated *H. influenzae* plasmid-based quantitative PCR assay. *H. influenzae* positive patients were found to have sputum neutrophilia and lower FeNO. In conclusion, using an optimized method of direct sequencing of induced sputum samples, *H. influenzae* was identified as a clinically relevant pathogen in severe asthma and was identified reliably using metagenomic sequencing. Application of these protocols in ongoing analysis of large patient cohorts will allow full characterization of this clinical phenotype.

IMPORTANCE The human airways were once thought sterile in health. Now metagenomic techniques suggest bacteria may be present, but their role in asthma is not understood. Traditional culture lacks sensitivity and current sequencing techniques are limited by operational problems and limited ability to identify pathogens at species level. We optimized a new sequencing technique—Oxford Nanopore technologies (ONT)—for use on human sputum samples and compared it with existing methods. We found ONT was effective for rapidly analyzing samples and could identify bacteria at the species level. We used this to show *Haemophilus influenzae* was a dominant bacterium in the airways in people with severe asthma. The presence of *Haemophilus* was associated with a "neutrophilic" form of asthma - a subgroup for which we currently lack specific treatments. Therefore, this technique could be used to target chronic antibiotic therapy and in research to characterize the full breadth of bacteria in the airways.

KEYWORDS asthma, bacteria, *Haemophilus influenzae*, Illumina, microbiome, Oxford Nanopore, sputum

Editor Zhenjiang Zech Xu, Nanchang University

Copyright © 2022 Jabeen et al. This is an open-access article distributed under the terms of the Creative Commons Attribution 4.0 International license.

Address correspondence to Timothy S. C. Hinks, timothy.hinks@ndm.ox.ac.uk.

The authors declare no conflict of interest.

Received 19 November 2021
Accepted 2 March 2022

Downloaded from https://journals.asm.org/journal/spectrum on 24 March 2022 by 163.1.213.46.

The field of airway metagenomics has expanded with wider application of bacterial 16S rRNA sequencing, utilizing Roche/454 pyrosequencing or Illumina MiSeq platforms to profile the structure of the microbiota (1–4). Rapid developments in characterization and understanding of the lung microbiome in chronic airways disease offer growing opportunities to incorporate these findings within the "treatable trait" paradigm for disease management now considered the gold standard of care in asthma (5), which globally remains the commonest chronic lung disease. This is particularly critical for the 5–10% of individuals affected by severe, treatment-refractory asthma displaying the greatest clinical and immunopathological heterogeneity, with high exacerbation risk and mortality (6). In several reports *Haemophilus influenzae* has been identified as the commonest potentially pathogenic organism in the airway of severe asthmatics in stable disease, associated with sputum neutrophilia and altered microbial diversity, namely, reduced *Streptococcus*, *Gemella*, and *Porphyromonas* taxa (2, 7, 8). Sputum neutrophilia correlates with bacterial burden and type-1 cytokines (4, 9), with positive sputum culture present in up to 43% of patients (10). In severe asthma overall, potentially pathogenic organisms have been isolated by culture in 20–52% (11, 12). Metagenomic studies are however limited by either small sample-size (1, 7) and inadequate clinical phenotyping of a heterogenous population, or insufficient sequencing depth and inability to reliably assign taxonomic identity at species level (necessitating confirmatory PCR) (2, 4, 8). In addition, these methods generally necessitate the application of analytic approaches using descriptive measures of richness, evenness and dominance which are more appropriate for samples of very much higher bacterial abundance than those observed in the paucibacillary asthmatic airway (13).

Identifying "treatable traits" (5), including type-2 cytokine-mediated (T2-high) eosinophilic airway inflammation, has enabled highly-effective biomarker-directed approaches, targeting novel biologics according to blood and sputum eosinophilia, and fractional exhaled nitric oxide (FeNO) (5). T2-low non-eosinophilic disease is refractory to corticosteroids and existing biologics (5) and remains poorly understood. It is present in up to 30% of severe asthmatics (14), associated with airways neutrophilia, high expression of IL-17 (14) and its inducible chemokines in airway T cells, and may be driven by chronic bacterial airways infection (8, 15, 16). The macrolide antibiotic azithromycin has emerged as a potential targeted therapy for this cohort (11, 16). However, new tools are required to accurately characterize the airway microbiome direct from patient samples, both for targeting of therapies on an individual patient basis, and to provide insight into disease mechanisms.

We hypothesize that chronic bacterial airways infection is a key treatable trait, however its prevalence, clinical phenotype, and biomarkers are yet to be defined. Comprehensive coverage of airway microorganisms to a species level has not been reported independently with metagenomic sequencing in severe asthma. This approach could define the prevalence of airways infection in severe asthma and identify the most relevant pathogenic species in an unbiased manner, thereby facilitating biomarker validation and further characterization of the clinical phenotype when applied to a large cohort. In this pilot study we have optimized a method of metagenomic sequencing of total DNA extracts from induced sputum samples collected from the Oxford Severe Asthma Cohort during clinical stability using the Oxford Nanopore Technologies (ONT) platform. Oxford Nanopore sequencing has the advantages of rapid and lower cost library preparation and sequencing, real-time data acquisition and longer contiguous reads offering improved *de novo* genome reconstruction. We compared Oxford Nanopore sequencing with previously utilized short-read Illumina MiSeq sequencing alongside pathogen specific quantitative PCR assays and "gold standard" sputum culture to test the validity of this method and identified a high prevalence of *Haemophilus influenzae* associated with neutrophilic disease in stable severe asthma.

RESULTS

Overview of airway microbiome in severe asthma. Induced sputum samples were obtained during clinical stability from 23 participants with severe asthma. Clinical

Downloaded from https://journals.asm.org/journal/spectrum on 24 March 2022 by 163.1.213.46.

TABLE 1 Clinical characteristics and airway inflammatory cell parameters of participants according to presence of airway *H. influenzae*[a]

Characteristic	Severe asthma (*n* = 23)	*H. influenzae* negative (*n* = 15)	*H. influenzae* positive (*n* = 8)	*P* value
Male sex, *n* (%)	13 (57)	9 (69)	4 (31)	0.66
Age (yr), mean (SD)	67 (10)	69 (9)	62 (10)	0.07
BMI (kg/m^2), mean (SD)	28.4 (6.10)	28.2 (6.20)	28.8 (28.2)	0.83
Presence of atopy, *n* (%)	11 (48)	6 (55)	5 (46)	0.33
Presence of nasal polyps, *n* (%)	7 (30)	4 (57)	3 (43)	0.61
Ex-smoker, *n* (%)	12 (52)	7 (58)	5 (42)	0.49
Pack yr, mean (SD)	12 (10)	11 (6)	14 (15)	0.62
Baseline inhaled corticosteroid use (BDP eq., mcg/d), median (Range)	2,000 (1,700)	2,000 (1,700)	2,000 (1,200)	0.97[b]
Maintenance oral corticosteroid, *n* (%)	9 (39)	8 (89)	1 (11)	0.06
Unscheduled GP/hospital visits in 12 mo, median (range)	4 (7)	4 (5)	5 (6)	0.79[b]
Corticosteroid courses in 12 mo, median (range)	3 (10)	2 (10)	3 (9)	0.84[b]
Antibiotic courses in 12 mo, median (range)	0 (7)	0 (7)	2 (6)	0.4[b]
FEV1 (% predicted), mean (SD)	69.6 (16.8)	69.9 (15.1)	68.9 (20.8)	0.58[b]
FEV1/FVC, mean (SD)	0.58 (0.10)	0.56 (0.10)	0.62 (0.10)	0.21
FeNO (ppb), mean (SD)	62 (68)	75 (74)	40 (53)	0.26
Blood eosinophils ($\times 10^9$/L), mean (SD)	0.50 (0.44)	0.53 (0.35)	0.45 (0.58)	0.56[b]
Sputum eosinophils (%), median (range)	0.50 (23)	1 (23)	0.10 (2)	**0.01**[b]
Sputum neutrophils (%), median (range)	72 (79)	54 (65)	93 (37)	$<$**0.01**[b]
Sputum inflammatory phenotype, *n* (%)				
Total with valid data	21	13	8	
Eosinophilic	5 (24)	5 (38)	0 (0)	
Neutrophilic	13 (62)	5 (38)	8 (0)	
Mixed granulocytic	0 (0)	0 (0)	0 (0)	
Paucigranulocytic	3 (14)	3 (23)	0 (0)	

[a]BMI, body mass index; GP, general practitioner; FEV1, forced expiratory volume in 1s; FVC, forced vital capacity; FeNO, exhaled nitric oxide; 1. Percentages given are provided from subjects with valid daata; Inflammatory phenotyes: eosinophilic $>$3% sputum eosinophils, neutrophilic $>$61% sputum neutrophils and $<$3% eosinophils, mixed granulocytic $>$61% sputum neutrophils and $>$3% eosinophils, paucigranulocytic $<$61% sputum neutrophils and $<$3% eosinophils.
[b]Comparisons between groups made using unpaired *t* test or Mann-Whitney test. *P* values $<$ 0.05 are highlighted in bold.

characteristics are shown in Table 1 and further summarized by absence (HI–) or presence (HI+) of *H. influenzae*, which emerged as the dominant bacterial species most frequently detected using culture based and molecular techniques in this study. Demographic data of the healthy participant are provided in Table S1 in the supplemental material. In this small cohort, 52% of asthmatic individuals were ex-smokers with a mean history of 12 pack years, and no difference in smoking history observed between the HI– and HI+ groups. All participants with severe asthma were established on high dose inhaled corticosteroids and 39% on maintenance oral corticosteroids. Blood eosinophilia ($>0.3 \times 10^9$/L) was seen in a greater proportion of HI– (11/15, 73%) compared with HI+ (4/8, 50%) participants. Presence of *H. influenzae* in culture, or positive pathogen specific PCR assay (described below), was associated with sputum neutrophilia and a significantly lower ratio of sputum eosinophils:neutrophils (P = 0.03, Mann-Whitney test, Fig. 1) with relatively lower FeNO levels; consistent with a type 2 biomarker-low phenotype (17).

DNA extraction and performance of sequencing. DNA was extracted from induced sputum plug samples using the QIAamp DNA minikit with prior human DNA depletion using differential centrifugation. Differential centrifugation produced 2.6 to 2.7-fold increase in total unfiltered bacterial reads compared with a 2.9 to 3.1-fold increase in bacterial reads with the NEBNext Microbiome kit, this corresponded to up to 8.2% and 13.5% reduction in proportion of unfiltered human reads respectively (Fig. S1). Differential centrifugation was selected as it provided additional benefits of ease of sample processing and lower cost per sample.

A pilot method was tested to compare gold standard sputum culture with metagenomic sequencing on the Illumina MiSeq and Oxford Nanopore platforms with quantification of bacterial load using qPCR performed in parallel. Taking the approach of metagenomic sequencing of total DNA transcripts with Illumina MiSeq and Oxford Nanopore over 16S rRNA gene amplicon sequencing identified dominant airway

Downloaded from https://journals.asm.org/journal/spectrum on 24 March 2022 by 163.1.213.46.

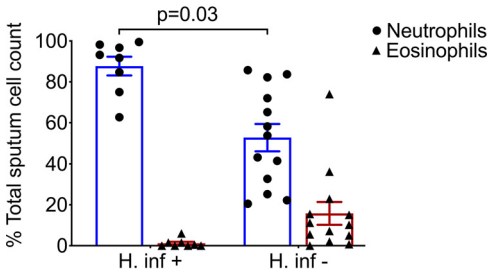


FIG 1 Presence of *H. influenzae* is associated with sputum neutrophilia; sputum differential cell counts stratified by presence or absence of *H. influenzae* by Oxford Nanopore sequencing and quantitative PCR. Statistical significance of eosinophil: neutrophil ratio assessed by Mann-Whitney test ($P = 0.03$).

organisms to a species (over genus) level. All organisms identified through standard sputum culture are shown in Table S2. *H. influenzae* was the most common pathogenic organism within the airway in severe asthma ($n = 7/23$) and positive culture was predictive of dominance within the airway metagenome defined as the majority of total bacterial reads and bacterial bases occupied by a single species (Table 2). In addition, total *H. influenzae* load was quantified by qPCR using $>1 \times 10^6$ copies/mL as a cutoff for clinically significant infection as previously validated in airways infection (18) ($n = 8/23$)—this assay yielded a positive result in one participant with severe asthma in the context of a negative sputum culture (Table 2).

A head-to-head comparison was made of Oxford Nanopore and Illumina MiSeq. Total human and bacterial reads detected by metagenomic sequencing using Oxford Nanopore and Illumina MiSeq are shown in Fig. S2 in the supplemental material, alongside the number of human reads removed bioinformatically prior to downstream analysis. Raw read statistics from fastq files have been generated using SeqKit (19) and summarized in Supplemental data file 1. Overall, this demonstrates longer reads lengths achieved with Oxford Nanopore (median of average read length/sample: Oxford Nanopore 2,013 bp versus Illumina MiSeq 172 bp) and higher quality scores using Illumina MiSeq (median [IQR] Q20: Oxford Nanopore 50% [41%] versus Illumina MiSeq 76% [20%]). Consistent taxonomic agreement was seen between these technologies. Similar microbiota compositions were observed when species level taxonomy was compared, as shown in Table 3 using paired HI+ samples, and heatmaps (Fig. 2 and 3) showing relative abundance of species detected in all samples. A difference is noted in the negative control sample when analyzed by Illumina MiSeq and Oxford Nanopore, with the classification of a small number of reads to *Escherichia coli* with Oxford Nanopore. This is likely to represent low level contamination or metagenomic misclassification, thereby also accounting for the abundance of *E. coli* in samples with relatively low total reads (participant identifier [PID]: 214, 235, 1053, 275). Metagenomic sequencing of the negative control sample using Illumina MiSeq detected 1100 bacterial reads (median bacterial reads in clinical samples was 22,563), of which *S. pneumoniae* occupied 12% of bacterial reads (135 reads). The negative control sample fell below the limit of detection of the *S. pneumoniae* PCR assay and is not considered a significant contaminating signal as it has not appeared as a dominant organism in other samples with a negative PCR result, where the proportion of reads are comparable to Oxford Nanopore (Table 3), and specifically *S. pneumoniae* occupied 88% of reads (149,030/168,844 bacterial reads) in PID 275 where a clearly positive PCR result is seen. Using Oxford Nanopore at least 88.9% of the reference *H. influenzae* genome was covered by ≥1 read in most ($n = 7/8$) HI+ samples, with only one sample achieving <25% coverage breadth (Table 4). In addition, compared with Illumina MiSeq, Oxford Nanopore provided greater *H. influenzae* genome coverage at any given depth of sequencing compared with Illumina MiSeq in all sequenced samples (Fig. 4). To study whether Oxford Nanopore can discriminate between *H. influenzae* strains, 4 strains isolated from clinical samples (PID 278,133,29 and 288) were cultured and sequenced. Consensus sequences were generated for cultured *H. influenzae* and their corresponding clinical samples (Table S3). The consensus sequences

Downloaded from https://journals.asm.org/journal/spectrum on 24 March 2022 by 163.1.213.46.

TABLE 2 Summary of sputum microbiology; pilot data ($n = 23$), sputum differential (neutrophilia >61%, eosinophilia >3%), FeNO (high: >45 ppb), culture, MALDI-TOF speciation, DNA sequencing by Oxford Nanopore; RT-qPCR for Eubacteria 16S and specific pathogens: *H. influenzae*, *S. pneumoniae*, *M. catarrhalis*, *P. aeruginosa*, *S. aureus* (positive >1 × 10^6 copies/mL)[a]

PID	Age (yrs)	Sex	Smoking status (pack yrs)	*H. inf* culture	*H. inf* reads (% total bacterial reads)	H. inf qPCR (×10^6 copies/mL)	S. pneu qPCR (×10^6 copies/mL)	M. cat qPCR (×10^6 copies/mL)	P. aeru qPCR (×10^6 copies/mL)	S. aur qPCR (×10^6 copies/mL)	Total 16S qPCR (×10^6 copies/mL)	Sputum neutrophils (%)	Sputum eosinophils (%)	FeNO (ppb)
1054	53	M	Ex (10)	+	93.5	**983.80**	**1.89**	−	−	−	8510	**93.2**	0.5	nd
278	50	M	Ex (40)	+	86.5	**435.40**	−	0.79	−	−	2832	**84.7**	0	11
133	60	F	Never	+	66.6	**91.70**	**1.99**	−	−	−	1643	**98.2**	0	29
297	76	F	Never	+	66.6	**40.00**	**1.72**	−	−	−	1042	**75**	0	21
288	67	M	Ex (9)	+	58.0	**31.00**	−	−	−	0.02	572	**96.7**	0.2	**169**
29	76	F	Ex (10)	+	47.1	**16.50**	0.17	−	−	−	633	**62.7**	0.5	9
214	54	M	Ex (<1)	+	17.1	**12.50**	−	−	−	−	338	**99.5**	0	20
1049	57	F	Never	−	51.3	**12.40**	−	−	−	−	297	**91.7**	2	20
235	57	M	Never	−	3.3	0.70	−	−	−	−	335	20.5	0.5	37
306	69	F	Never	−	0.03	0.30	−	−	−	−	1006	**82.2**	1	**85**
187	66	M	Ex (12)	−	0.05	0.03	−	−	−	−	1822	25.2	**7.5**	**300**
1052	79	M	Never	−	0.1	0.02	−	**35.63**	−	−	695	**65.2**	1.2	**125**
294	62	F	Never	−	0.05	0.02	−	−	−	−	43	nd	0.5	28
1055	70	F	Ex (15)	−	0.6	0.01	−	−	−	−	91	58.2	**15.5**	**138**
1053	59	M	Ex (10)	−	0.5	0.01	−	−	−	−	1754	**85.7**	0.7	**64**
1041	73	F	Ex (8)	−	1.0	0.01	−	−	−	−	286	43.2	0.5	8
5	67	M	Never	−	0.07	−	−	−	−	−	661	53.7	11	8
275	76	F	Never	−	2.8	−	**5.95**	−	−	−	696	**83.7**	0.7	20
315	61	M	Never	−	0.05	−	−	−	−	−	115	22.2	0.2	**78**
1060	86	M	Ex (8)	−	0.0	−	−	−	−	−	58	32.7	**22.9**	16
279	60	F	Never	−	0.05	−	−	−	−	−	216	nd	nd	48
295	81	M	Ex (20)	−	0.4	−	−	−	−	−	191	**72**	0	**78**
1058	72	M	Ex (3)	−	1.0	−	−	−	−	−	95	41.5	**15.1**	**89**

[a]Values above indicated thresholds levels shown in bold denotes pathogen not detected by PCR. Participants are ranked according to detection of *H. influenae* by quantitative PCR. +, denotes pathogen detected; −, denotes pathogen not detected by standard culture or by PCR.

Downloaded from https://journals.asm.org/journal/spectrum on 24 March 2022 by 163.1.213.46.

TABLE 3 Agreement between Oxford Nanopore and Illumina MiSeq in HI+ samples; displayed in "top 5" bacterial species occupying the majority of total bacterial reads per sample ($n = 8$)

PID	Oxford Nanopore technologies	% Bacterial reads	Ilumina MiSeq	% Bacterial reads
1054	*Haemophilus influenzae*	93.5	*Haemophilus influenzae*	90.9
	Streptococcus pneumoniae	0.8	*Streptococcus pneumoniae*	1.3
	Escherichia coli	0.3	*Neisseria meningitidis*	0.4
	Neisseria meningitidis	0.3	*Tropheryma whipplei*	0.3
	Haemophilus haemolyticus	0.2	*Haemophilus haemolyticus*	0.1
278	*Haemophilus influenzae*	86.5	*Haemophilus influenzae*	82.6
	Escherichia coli	1.3	*Moraxella catarrhalis*	0.1
	Salmonella enterica	0.3	*Haemophilus parainfluenzae*	0.1
	Shigella flexneri	0.2	*Haemophilus haemolyticus*	0.1
	Helicobacter pylori	0.2	*Streptococcus pseudopneumoniae*	0.1
133	*Haemophilus influenzae*	66.6	*Haemophilus influenzae*	72.9
	Streptococcus pneumoniae	7.3	*Streptococcus pneumoniae*	8.8
	Escherichia coli	2.7	*Haemophilus haemolyticus*	0.6
	Salmonella enterica	0.6	*Prevotella melaninogenica*	0.2
	Shigella boydii	0.5	*Haemophilus parainfluenzae*	0.2
297	*Haemophilus influenzae*	66.6	*Haemophilus influenzae*	67.6
	Streptococcus pneumoniae	12.8	*Streptococcus pneumoniae*	14.4
	Escherichia coli	3.2	*Haemophilus parainfluenzae*	0.1
	Shigella boydii	0.4	*Haemophilus haemolyticus*	0.1
	Salmonella enterica	0.3	*Streptococcus mitis*	0.1
288	*Haemophilus influenzae*	58.0	*Haemophilus influenzae*	79.8
	Escherichia coli	3.7	*Neisseria subflava*	0.9
	Shigella flexneri	1.0	*Haemophilus aegyptius*	0.5
	Salmonella enterica	0.9	*Haemophilus parainfluenzae*	0.5
	Shigella boydii	0.7	*[Haemophilus] ducreyi*	0.4
29	*Haemophilus influenzae*	47.1	*Haemophilus influenzae*	69.4
	Escherichia coli	4.6	*Streptococcus pneumoniae*	4.6
	Streptococcus pneumoniae	1.8	*Rothia dentocariosa*	1.0
	Shigella boydii	0.9	*Rothia mucilaginosa*	1.0
	Salmonella enterica	0.9	*Veillonella dispar*	0.8
214	*Haemophilus influenzae*	17.1	*Haemophilus influenzae*	80.7
	Escherichia coli	15.4	*Haemophilus haemolyticus*	0.3
	Helicobacter pylori	3.6	*Prevotella oris*	0.3
	Salmonella enterica	1.9	*Veillonella dispar*	0.2
	Shigella flexneri	1.3	*Haemophilus parainfluenzae*	0.2
1049	*Haemophilus influenzae*	51.3	*Haemophilus influenzae*	53.7
	Tropheryma whipplei	10.9	*Tropheryma whipplei*	29.9
	Escherichia coli	5.2	*Veillonella parvula*	0.6
	Shigella boydii	0.8	*Haemophilus haemolyticus*	0.3
	Shigella flexneri	0.6	*Streptococcus pseudopneumoniae*	0.2

of two clinical samples (PID 278 and 133) achieved adequate coverage (91.4% and 53.8%, respectively) for reliable comparisons to be made with cultured strains. As shown in the single nucleotide polymorphism (SNP) distance matrix in Fig. 5, there is a high degree of similarity (very low SNPs) between clinical samples and the corresponding strain of *H. influenzae* isolated.

Confirming presence of other coexistent respiratory pathogens. The PCR panel was extended to include *Streptococcus pneumoniae*, *Staphylococcus aureus*, *Moraxella catarrhalis* and *Pseudomonas aeruginosa* in addition to *H. influenzae* (Table 2). This identified presence of *S. pneumoniae* alongside *H. influenzae* above a threshold of $>1 \times 10^6$ copies/mL—previously shown to be clinically significant (18)—in a proportion of participants ($n = 3$). *S. pneumoniae* constituted the second highest proportion of bacterial reads within these samples and was identified on sputum culture. In this small cohort a positive PCR result for *M. catarrhalis* and *S. pneumoniae* alone was detected in one participant each and associated with a sputum neutrophilia. *S. pneumoniae* was the dominant organism on sequencing with Oxford Nanopore (PID: 275) in this case. *M. catarrhalis* was detected as abundant (74.5% total bacterial reads) by Illumina MiSeq, but not by Nanopore (<1% total bacterial reads) in one individual (PID:

Downloaded from https://journals.asm.org/journal/spectrum on 24 March 2022 by 163.1.213.46.

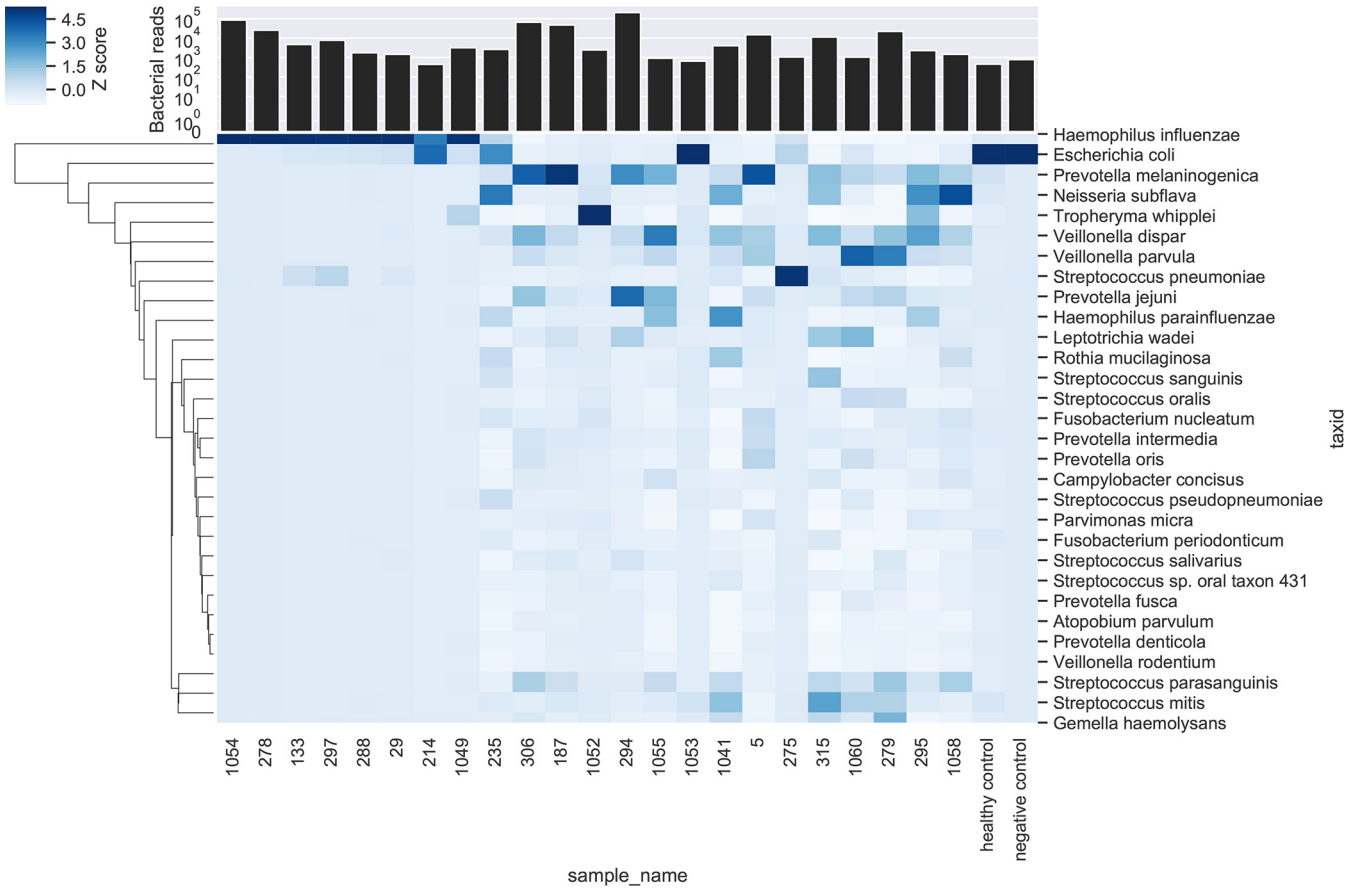


FIG 2 Heatmap of relative abundance of species sequenced by sample using ONT; Z-scores, denoted by shade, represent the number of standard deviations above the mean number of bases per taxon for each sample. Total bacterial reads detected per sample are also shown in stacked bar chart.

1052) in whom a positive PCR result was present, but sputum culture was negative (Table 2 and Fig. 3). *M. catarrhalis* was detected by Oxford Nanopore in PID 278, albeit at low levels (39/28,460 total bacterial reads, 0.1% of bacterial reads) in the context of dominance of *H. influenzae* in this sample and *M. catarrhalis* PCR result falling just below the threshold of clinical significance (0.86×10^6 copies/mL).

Limits of detection and spiking. A pooled sample was generated from individuals with no single dominant airway organism to capture the variation in lung microbiota within a cohort of severe asthmatics during stable disease. Spiking with 10^4 to 10^8 CFU/mL of *Haemophilus influenzae*, *Streptococcus pneumoniae*, *Staphylococcus aureus*, *Moraxella catarrhalis*, and *Pseudomonas aeruginosa* was performed. There was an increase in total number of bacterial reads with increasing concentration of bacterial spike which corresponded to rising bacterial load from a high background level of 4.8×10^8 copies/mL (in the unspiked pool) to 1.5×10^{10} copies/mL at the highest spiking concentration. Reads classified as *Haemophilus influenzae*, *Streptococcus pneumoniae*, *Staphylococcus aureus*, *Moraxella catarrhalis* and *Pseudomonas aeruginosa* were observed in the pooled un-spiked sample and spiked samples. *H. influenzae* and *S. pneumoniae* demonstrated the greatest rise in proportion of assigned bacterial reads with spiking as shown in Fig. 6c. Near complete genome coverage of these organisms was achieved after spiking with 10^6 CFU/mL, followed by 50% genome coverage of *P. aeruginosa* at this concentration despite only a modest increase in bacterial reads (Fig. 6a). Recovery of *S. aureus* and *M. catarrhalis* following spiking was poor by Oxford Nanopore or by qPCR (Fig. 6). As shown in Fig. 6b there was a high background level of airway *H. influenzae* ($>1 \times 10^6$ copies/mL) within the pooled sample, crossing the threshold of clinical significance. This threshold was surpassed by *S. pneumoniae* and *P.*

Downloaded from https://journals.asm.org/journal/spectrum on 24 March 2022 by 163.1.213.46.

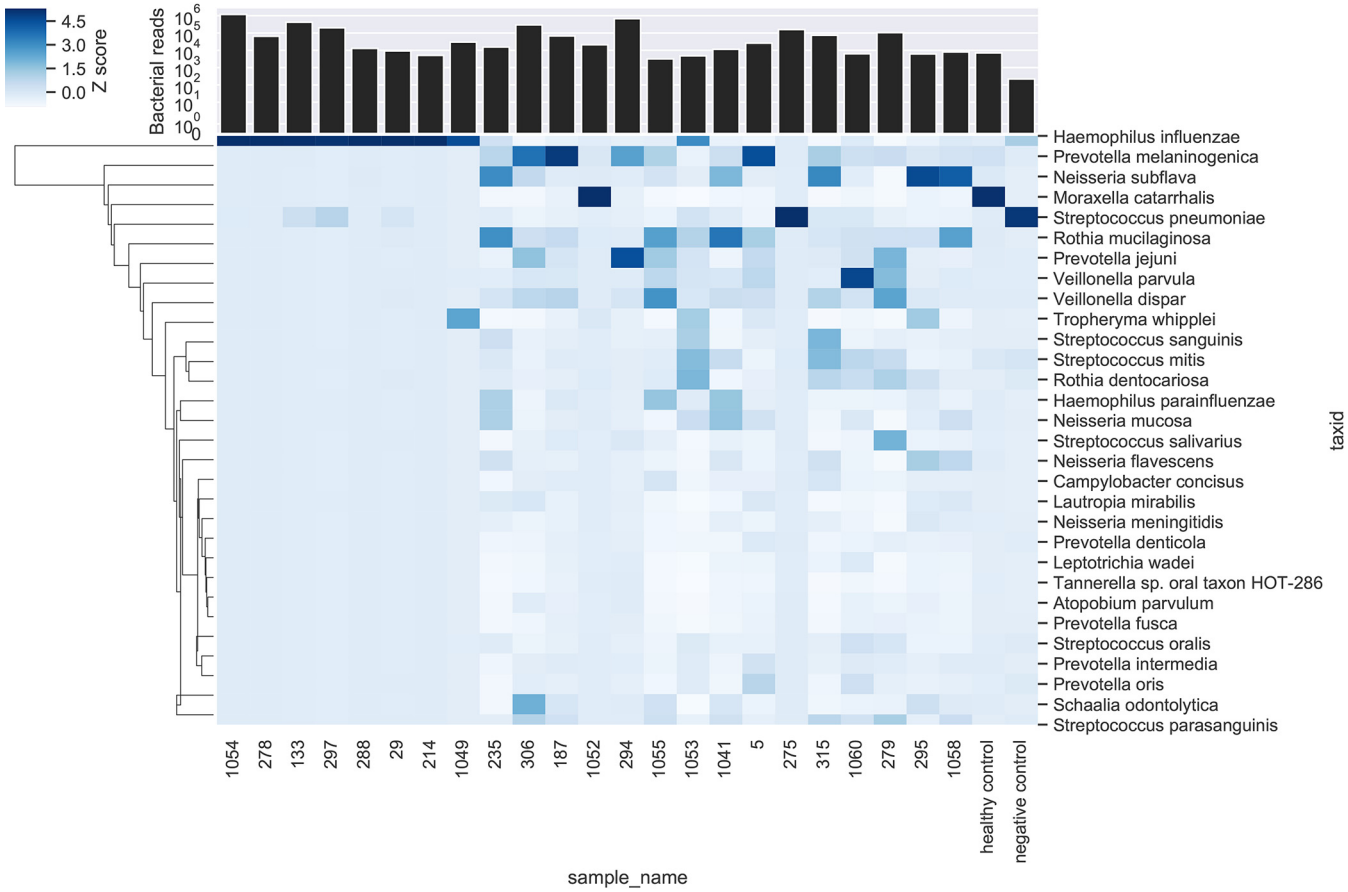


FIG 3 Heatmap of relative abundance of species sequenced by sample using Illumina MiSeq; Z-scores, denoted by shade, represent the number of standard deviations above the mean number of bases per taxon for each sample. Total bacterial reads detected per sample are also shown in stacked bar chart.

aeruginosa at spiking concentrations exceeding 10^6 CFU/mL but could not be achieved upon spiking *S. aureus* or *M. catarrhalis* up to concentrations of 10^8 CFU/mL.

DISCUSSION

In this study we report for the first time a method for DNA extraction and direct metagenomic sequencing of induced sputum samples using Oxford Nanopore in stable severe asthma. In severe asthmatics demonstrating altered microbial diversity, marked by the dominance of a single pathogenic bacterial species in the

TABLE 4 *H. influenzae* genome coverage breadth and depth with Oxford Nanopore; total and *H. inf* specific reads and bases in HI+ samples shown with coverage breadth (percentage of reference sequences covered), average coverage depth (at positions with ≥1 read) and number of positions on the *H. influenzae* genome with 1/5/10 read depth

PID	Bacterial reads	*H. inf* reads	% *H. inf*/ bacterial reads	Bacterial bases	*H. inf* bases	% *H. inf*/ *bacterial bases*	Legth of *H. inf* reference genome (bases)	Coverage breadth *H. inf* genome	Avg coverage depth	*H. inf* genome positions with:		
										1 read depth	5 reads depth	10 reads depth
1054	88101	82374	93.5	4.97E + 08	4.85E + 08	97.7	1.83E + 06	94.2	243.3	1.72E + 06	1.71E + 06	1.70E + 06
278	28460	24609	86.5	1.14E + 08	1.12E + 08	97.9	1.83E + 06	93.4	53.6	1.71E + 06	1.70E + 06	1.69E + 06
133	6054	4031	66.6	2.43E + 07	2.16E + 07	89.1	1.83E + 06	92.7	10.1	1.70E + 06	1.63E + 06	7.48E + 05
297	9228	6142	66.6	4.32E + 07	3.52E + 07	81.6	1.83E + 06	92.9	17.5	1.70E + 06	1.69E + 06	1.60E + 06
288	2775	1610	58.0	9.06E + 06	8.47E + 06	93.5	1.83E + 06	90.7	4.2	1.66E + 06	6.80E + 05	9.49E + 03
29	2604	1226	47.1	6.97E + 06	5.85E + 06	83.8	1.83E + 06	88.9	3.2	1.63E + 06	3.36E + 05	1.06E + 02
214	1344	230	17.1	8.53E + 05	6.68E + 05	78.4	1.83E + 06	24.2	1.3	4.43E + 05	0.00E + 00	0.00E + 00
1049	4632	2376	51.3	1.62E + 07	1.21E + 07	74.5	1.83E + 06	92.1	6.1	1.69E + 06	1.21E + 06	1.04E + 05

Downloaded from https://journals.asm.org/journal/spectrum on 24 March 2022 by 163.1.213.46.

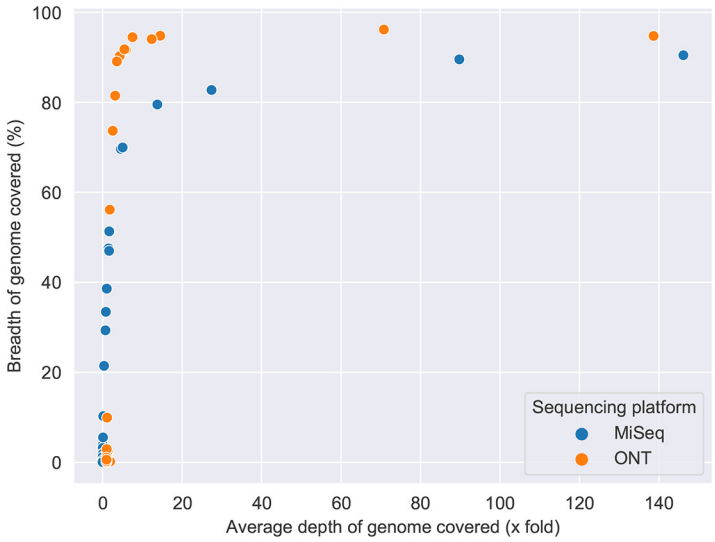


FIG 4 Comparison of read lengths and genome coverage for *H. influenzae* using Oxford Nanopore compared with Illumina MiSeq; breadth and depth of *H. influenzae* genome coverage with Oxford Nanopore and Illumina MiSeq in all samples.

airway, *H. influenzae* was the most prevalent organism. These results were validated using the established short read sequencing platform Illumina MiSeq, quantitative PCR and "gold standard" sputum culture. Oxford Nanopore has previously been used for diagnosis of bacterial lower respiratory tract infection (20) with higher biomass than respiratory samples utilized in our cohort of stable severe asthmatics. Despite this Oxford Nanopore achieved near complete bacterial genome coverage in the majority of HI+ samples.

The selected method of DNA extraction with preceding differential centrifugation provided 2.6- to 2.7-fold increase in bacterial reads. Previous studies have more extensively compared different techniques of human/extracellular DNA depletion from sputum samples; either from patients with cystic fibrosis (21) or bronchiectasis (22) using metagenomic or 16S sequencing on the Illumina MiSeq platform or from complex airways samples isolated at the time of pulmonary infection for metagenomic sequencing using Oxford Nanopore (20). These respiratory samples are distinct from sputum plug samples utilized in this study, collected during stable disease from patients with severe asthma with no concurrent antimicrobial therapy or clinical diagnosis of bronchiectasis. Use of differential centrifugation yielded a modest reduction in human DNA but allowed consistent species level discrimination with robust bacterial genome coverage in airways infection. More complete human DNA depletion may be possible to achieve,

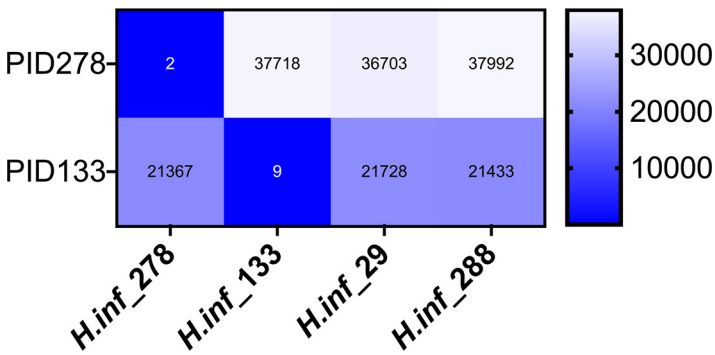


FIG 5 SNP distance matrix; pairwise comparisons between metagenomic sequences from clinical samples and sequenced clinical *H. influenzae* isolates from 4 patients following Oxford Nanopore sequencing are shown.

Downloaded from https://journals.asm.org/journal/spectrum on 24 March 2022 by 163.1.213.46.

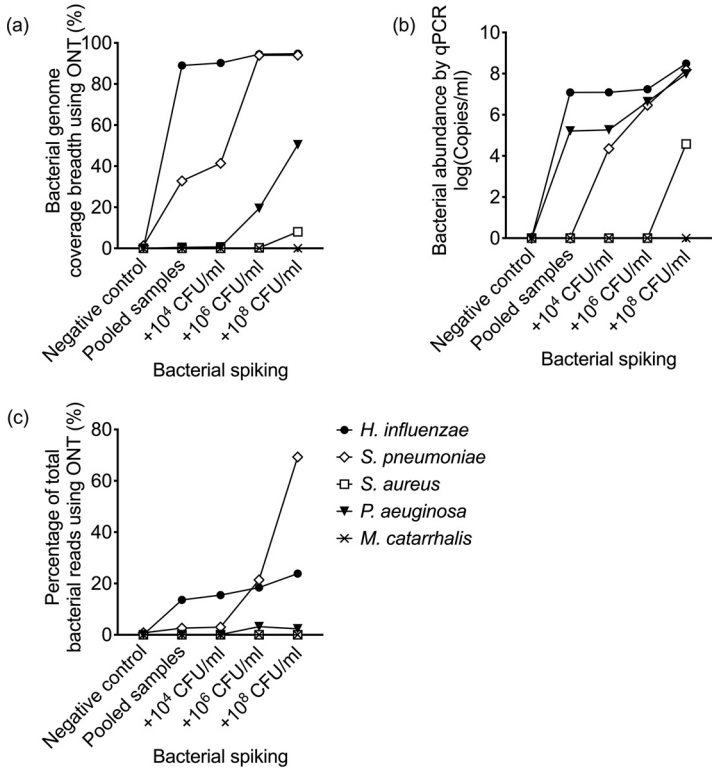


FIG 6 Spiking recovery in sputum samples by Oxford Nanopore (ONT) and by qPCR. Recovery of spiked organisms (*H. influenzae*, *S. pneumoniae*, *S. aureus*, *P. aeruginosa*, *M. Catarrhalis*) on metagenomic sequencing using Oxford Nanopore, expressed as (a) % target bacterial genome coverage breadth and (c) % bacterial reads; or (b) detected by pathogen specific PCR.

without loss of bacterial genomes, but was not within the scope of this study. When performing Oxford Nanopore sequencing, six samples were run per flow cell. This produced adequate sequencing depth and breadth for species level taxonomic identification, but potentially higher sequencing yield could be achieved, if required, by reducing the number of multiplexed samples although this would have implications on cost per sample. Such an approach may be favorable for making more detailed inferences about dominant bacterial species directly from metagenomic sequencing data as we have shown that clinical samples with high level consensus genome coverage have few SNPs when compared to direct sequencing of corresponding cultured strains of *H. influenzae*. The presence of a limited number of SNPs seen in this study between metagenomic analysis of clinical samples and paired sequences of cultured bacterial strains could be explained by the high level of genomic diversity seen in *H. influenzae* (23), particularly within non-capsulate strains most often isolated in airways disease (24–26). This method is a significant step forward from 16s rRNA sequencing by identifying dominant species clearly as those occupying the highest proportion of total bacteria reads and bases.

Oxford Nanopore was superior to Illumina MiSeq within this cohort in providing greater breadth of bacterial genome coverage within the HI+ group at any sequencing depth. Oxford Nanopore has a relatively high per base error rate of up to 6%, necessitating bioinformatic approaches to overcome this in base-called sequences and produce an acceptable consensus genome (27). Randomly generated sequencing errors can be compensated for by achieving adequate sequencing depth (28). In our data set there is a high level of agreement between Oxford Nanopore and Illumina MiSeq, reported to have an error rate $<$0.5% (29), as exemplified in Table 3. This is most notable in samples with a positive quantitative pathogen PCR result or culture. An exception to this was noted in a single sample (PID: 1052) in which only Illumina MiSeq detected the presence of *M. catarrhalis* in the

Downloaded from https://journals.asm.org/journal/spectrum on 24 March 2022 by 163.1.213.46.

presence of a positive PCR result. This is likely an artifact of Oxford Nanopore library preparation rather than a systematic sequencing technology error. In ongoing work within a larger cohort, Oxford Nanopore sequencing has identified *M. catarrhalis* as a dominant organism reliably on metagenomic sequencing with concordant positive PCR results (data not shown). Spiking experiments have shown poor recovery of *M. catarrhalis* up to spiking concentrations of 10^8 CFU/mL, however there was high background bacterial DNA levels in these samples.

Our study has several limitations. Firstly, a small sample size has been used for method development. This study lacks adequate statistical power to define cutoffs based on sequencing metrics, such as proportion of bacterial reads or bacterial bases, to support a clinically relevant diagnosis of airways infection. Further prospective validation is required in larger patient cohorts and is under way. Secondly there was additional value in performing pathogen specific PCR given the variation in limits of detection of bacterial species by sequencing within our spiking experiment. A high background bacterial level in the unspiked pooled sputum samples restricted our ability to compare limits of detection between qPCR and Oxford Nanopore, although our data suggested both were sensitive for *H. influenzae*, with superior sensitivity of qPCR for *P. aeruginosa* and of Oxford Nanopore for *S. pneumoniae*, suggesting operational characteristics may differ between technologies according to individual species. Additionally our study did not integrate metagenomic data with functional immunological readouts, an area warranting further study in an adequately powered cohort of well-phenotyped patients.

H. influenzae is emerging as the most relevant potentially pathogenic organism in severe asthma (2, 7, 8), however its overall prevalence is yet to be defined alongside a full characterization of clinical phenotype and longitudinal disease outcomes. Abundance of *H. influenzae* is predictive of response to treatment with the macrolide antibiotic azithromycin: the only established targeted therapy in T2-low asthma. This highlights the importance of identifying candidate bacterial *species* as treatable traits (5) when characterizing disease phenotype over description of compositional changes of "airway dysbiosis." The frequency of other common respiratory pathogens such as *Streptococcus pneumoniae* and *Moraxella catarrhalis* are not known in severe asthma. Colonization with these organisms alongside *H. influenzae* is predictive of wheeze and asthma in early life (30) and likely to be relevant independently or within polymicrobial communities through mechanisms including interspecies quorum sensing (31) in shaping the virulence of constituent bacteria.

In summary, we have optimized a method of direct metagenomic sequencing of induced sputum samples. Using this method, *H. influenzae* was reliably identified as a clinically-relevant pathogen in severe asthma. Future large cohort studies will be required to characterize the airway microbiome in specific asthma phenotypes, to determine the role of these other potentially pathogenic bacteria, and to explore the relationships between the presence of individual airway bacteria and the activation of specific immunological pathways which contribute to the poorly understood phenotypes of 'T2 low' asthma.

MATERIALS AND METHODS

Clinical Samples. Patients meeting the American Thoracic Society/European Respiratory Society definition of severe asthma, on Global Initiative for Asthma (GINA) step 4–5 treatment (32) (n = 23) and healthy control (n = 1) were recruited to the Oxford Severe Asthma Cohort from the Churchill Hospital, Oxford, UK between December 2017 and June 2018. This study was conducted with NHS Research Ethics approval (08/H0406/189). Induced sputum samples were collected prospectively during clinical stability. Hypertonic sputum induction and sputum differential cell counts were performed as previously described (33) and sputum plugs stored at −80°C in sterile Brain Heart Infusion (BHI, Sigma-Aldrich, Dorset, UK) broth containing 10% glycerol until required. Sputum plugs were dispersed with 0.1% dithiothreitol (DTT, Thermo Fischer, Waltham, MA, USA) and filtered before microbiological culture and DNA extraction as described below.

Sputum Culture. Routine sputum culture was performed using homogenized sputum according to the Health Protection Agency (HPA) standard operating procedures. All cultured organisms were identified by matrix-assisted laser desorption/ionization time-of-flight (MALDI-TOF) mass spectrometry on a Microflex LT using Biotyper, version 3.1 (Bruker Daltonics, Ballerica, MA, USA). In addition, prospective *Haemophilus* species were also identified using X (hemin), V (NAD) and XV disks (hemin and NAD) (BD BBL Taxo differentiation discs for *Haemophilus* spp., Wokingham, UK) on nutrient agar (Oxoid Ltd,

Downloaded from https://journals.asm.org/journal/spectrum on 24 March 2022 by 163.1.213.46.

Basingstoke, UK). *H. influenzae* strains isolated from 4 clinical samples (PID 278, 133, 29 and 288) were cultured overnight (37°C with 5% CO2, shaking at 180 rpm) in 10 mL culture broth (BHI with 10 μg/mL NAD [NAD] and hemin [Sigma-Aldrich, Dorset, UK]). Once optical density at 600 nm reached 0.5 (exponential phase) bacteria were pelleted and resuspended in BHI containing 10% glycerol and stored at −80°C until use. Clinical laboratory results from the John Radcliffe Hospital Microbiology Laboratory, Oxford, UK have been provided for three samples.

Microbial DNA extraction with human DNA depletion. Two methods for extraction of high-quality microbial DNA and depletion of human cells/DNA, were tested. The first was differential centrifugation, whereby homogenized sputum was centrifuged (400 g, 5 min) to deplete human cells. The supernatant was collected, split into smaller volume aliquots (up to 1 mL) and centrifuged again (13,000g, 5 min). This supernatant was discarded, pellets from multiple aliquots combined for DNA extraction using the QIAamp DNA minikit (Qiagen, Manchester, UK) – briefly, combined pellets were resuspended in 180 μL buffer ATL (Qiagen, Manchester, UK) before adding 20 μL proteinase K to each sample and incubating at 56°C for 1 h, vortexing the sample every 15 min. Subsequent steps were as per manufacturer's instructions. The second method for host DNA depletion utilized the NEBNext Microbiome DNA Enrichment Kit (New England Biolabs, Ipswich, MA, USA) as per manufacturer's instructions—this kit facilitates enrichment of microbial DNA by selectively binding and removing CpG-methylated human DNA.

Microbial DNA extraction from clinical *H. influenzae* isolates (*H. inf*_278, *H. inf*_133, *H. inf*_29, and *H. inf*_288) was performed from overnight culture (37°C with 5% CO2) on chocolate agar (Oxoid Ltd, Basingstoke, UK). Bacterial colonies were deposited directly into buffer ATL (Qiagen, Manchester, UK) using flat 5 μL loops and DNA extracted as described above.

Bacterial spiking. Sputum plugs collected from five donors with no significant growth of potentially pathogenic respiratory organisms on culture (PID: 1052, 5, 1055, 315, 187) were homogenized with DTT as above and pooled together to generate a baseline sample for all spiking conditions. The pooled sample was then split for spiking simultaneously with *Haemophilus influenzae*, *Streptococcus pneumoniae*, *Staphylococcus aureus*, *Moraxella catarrhalis* and *Pseudomonas aeruginosa*. Bacteria were cultured overnight (37°C with 5% CO_2, shaking at 180 rpm) in 10 mL culture broth as indicated by species (*H. influenzae* in BHI with 10 μg/mL NAD and hemin [Sigma-Aldrich, Dorset, UK], *S. pneumoniae* in BHI and *S. aureus/M. catarrhalis/P. aeruginosa* in nutrient broth [Oxoid]). Once optical density at 600 nm reached 0.5 (exponential phase) bacteria were pelleted and resuspended in BHI or nutrient broth containing 10% glycerol and stored at −80°C until use. Serial dilutions (in phosphate-buffered saline) and confirmatory CFU counts were performed to determine bacterial stock concentrations. The five cultured bacterial species were spiked simultaneously from stock solutions into the pooled homogenized sputum samples, producing three spiked samples containing 10^4, 10^6 or 10^8 CFU/mL of each bacterial species. Microbial DNA was extracted, as described previously, from the unspiked and spiked pooled samples.

Metagenomic sequencing. (i) Illumina MiSeq. After quantification with a Qubit 2.0 fluorometer (Life Technologies, Paisley, UK), DNA extracts were sequenced on a MiSeq desktop sequencer (Illumina, San Diego, CA, USA). Libraries were prepared using a variation of the Illumina Nextera XT protocol (34). Briefly, 1 ng of DNA was prepared using the Nextera XT protocol modified with 15 cycles during the index PCR. DNA quantification with a Qubit 2.0 fluorometer was followed by determination of their average sizes on an Agilent 2200 TapeStation (Agilent Technologies, Santa Clara, CA, USA) before samples were manually normalized. Paired-end sequencing was performed using a 600-cycle MiSeq reagent kit (version 3), and samples were sequenced in batches of 12 on a single flow cell.

(ii) Oxford Nanopore Technologies. Libraries were prepared for sequencing on an Oxford Nanopore GridION (Oxford Nanopore Technologies (ONT), Oxford, UK) using the Rapid Barcoding Sequencing (SQK-RBK004) (ONT) kit where 333 ng template DNA was available per sample, using the manufacturer's protocol. For low input samples (maximum 10 ng template DNA per sample) the Rapid PCR Barcoding kit (SQK-RPB004) (ONT) with modifications to the manufacturer's protocol as reported by Charalampous et al. (20) and Street et al. (28) was used. Post-PCR, DNA samples were purified with AMPure XP SPRI beads (Beckman Coulter, High Wycombe, UK) and eluted in 10 mM Tris-HCl pH 8.0 with 50 mM NaCl. DNA was quantified with a Qubit 2.0 fluorometer. Between 95 and 99.6 fmol of combined library were loaded per flowcell. Samples were sequenced on ONT FLO-MIN106D (ONT v.R9.4.1) flow cells in batches of 6 samples per flow cell for clinical samples and 4 samples per flow cell for the clinical *H. influenzae* isolates.

Pathogen specific PCR analysis. Quantitative real-time PCR (qPCR) was performed to quantify relative abundance of *H. influenzae*, *S. pneumoniae*, *S. aureus*, *M. catarrhalis* and *P. aeruginosa* DNA within the total DNA extracts. Human Pathogen Detection Genesig kits and PrecisionPLUS 2x qPCR Mastermix by Primerdesign (Eastleigh, UK) were used as per manufacturer's instructions. Primers and probes were used for the following bacterial targets: outer membrane protein P6 (*H. influenzae*), alpha fucosidase (*S. pneumoniae*), FEMB (*S. aureus*), major outer membrane protein/copB (*M. catarrhalis*) and toxin A synthesis regulating gene/RegA (*P. aeruginosa*). Reactions were performed in 20 μL with 5 μL template DNA (10 ng). Positive control templates for each bacterial species of interest (containing 2×10^5 copies/μL) were used to prepare a standard curve dilution series ranging from 2×10^5 to 20 copies/μL. Negative controls using nuclease free water (ThermoFisher, Waltham, MA, USA) in place of DNA template were used. All assays were performed in duplicate and mean values utilized in analyses. The qPCR conditions were: enzyme activation 2 min at 95°C followed by amplification for 50 cycles at 95°C for 10 s and 60°C for 60 s. qPCR assays were performed on a Bio-RadCFX96 instrument (Bio-Rad, Watford, UK).

Bioinformatic and statistical analysis. Statistical analysis was performed using GraphPad Prism (Version 9) and SPSS (Version 27.0). Parametric and nonparametric data are displayed as mean (SEM)

Downloaded from https://journals.asm.org/journal/spectrum on 24 March 2022 by 163.1.213.46.

and median (range), with comparisons between groups made using unpaired t tests or Mann-Whitney tests, respectively.

Illumina; Raw sequencing reads were adapter trimmed using BBDuk (https://sourceforge.net/projects/bbmap/) and the adapter sequence file provided within the BBMap package; the following parameters were used: minlength, 36; k,19; ktrim, r; hdist, 1; mink, 12. Taxonomic classification of trimmed reads was performed using Centrifuge (35) and a database constructed from complete genomes of bacteria, viruses, and fungi uploaded to NCBI refseq as of 2019-08-24. The human genome (GRCh38) was included for host DNA detection. *Haemophilus influenzae* classified reads were mapped to reference genome NC_000907.1 using BWA MEM (version 0.7.12-r1039) (36) and SAMtools (version 1.9) (37).

Oxford Nanopore; Sequences were basecalled using Guppy (ONT, version 3.3.0+ef22818) and analyzed using the CRuMPIT pipeline (https://gitlab.com/ModernisingMedicalMicrobiology/CRuMPIT) (38) with the same Centrifuge database used for Illumina sequence analysis. This pipeline used Minimap2 (version 2.17-r954-dirty) (39) to align *Haemophilus influenzae* classified reads to reference genome NC_000907.1. A complete description of the bioinformatics used and secondary analysis with custom scripts to summarize data and generate plots is described in this GitLab repository (https://gitlab.com/ModernisingMedicalMicrobiology/asthmas-methods-paper-analysis). For comparison of *H. influenzae* genome between clinical samples and cultured strains consensus, fasta sequences were generated using Minimap2 and CLAIR2 using the genericbugONTworflow (https://gitlab.com/ModernisingMedicalMicrobiology/genericbugontworkflow) previously optimized and described (40). A SNP analysis was performed, and a distance matrix was generated using snp-dists (41).

Data availability. Raw FASTQ data is available on the European Nucleotide Archive with the project accession PRJEB47876.

SUPPLEMENTAL MATERIAL

Supplemental material is available online only.

SUPPLEMENTAL FILE 1, XLSX file, 0.02 MB.

SUPPLEMENTAL FILE 2, PDF file, 1.4 MB.

ACKNOWLEDGMENTS

The views expressed are those of the authors and not those of the NHS, or NIHR.

M.F.J., D.F., D.W.K., I.D.P., P.K., T.L.S., T.S.C.H. contributed to conceptualization and design of the study. M.F.J., C.B., C.C., S.T., I.D.P., T.L.S., T.S.C.H., J.C. contributed to acquisition of study data. Data were analyzed by M.F.J., N.D.S., D.F., D.W.C., I.D.P., P.K., T.L.S., T.S.C.H., M.F.J., D.F., I.D.P., P.K., T.L.S., T.S.C.H. drafted the manuscript which was approved by all authors.

This work was funded by National Institute for Health Research Oxford Biomedical Research Centre Cluster Funding (MJ, TLS and TSCH), the National Institute for Health Research Academic Clinical Fellowship Award (MJ) and grants from the Wellcome Trust (104553/z/14/z, 211050/Z/18/z) (T.S.C.H.).

The study was approved by Leicestershire, Nottinghamshire and Rutland Ethics Committee, UK (08/H0406/189).

REFERENCES

1. Goleva E, Jackson LP, Harris JK, Robertson CE, Sutherland ER, Hall CF, Good JT, Jr, Gelfand EW, Martin RJ, Leung DY. 2013. The effects of airway microbiome on corticosteroid responsiveness in asthma. Am J Respir Crit Care Med 188:1193–1201. https://doi.org/10.1164/rccm.201304-0775OC.
2. Simpson JL, Daly J, Baines KJ, Yang IA, Upham JW, Reynolds PN, Hodge S, James AL, Hugenholtz P, Willner D, Gibson PG. 2016. Airway dysbiosis: Haemophilus influenzae and Tropheryma in poorly controlled asthma. Eur Respir J 47:792–800. https://doi.org/10.1183/13993003.00405-2015.
3. Durack J, Lynch SV, Nariya S, Bhakta NR, Beigelman A, Castro M, Dyer AM, Israel E, Kraft M, Martin RJ, Mauger DT, Rosenberg SR, Sharp-King T, White SR, Woodruff PG, Avila PC, Denlinger LC, Holguin F, Lazarus SC, Lugogo N, Moore WC, Peters SP, Que L, Smith LJ, Sorkness CA, Wechsler ME, Wenzel SE, Boushey HA, Huang YJ, National Heart, Lung and Blood Institute's "AsthmaNet". 2017. National Heart L, Blood Institute's A. Features of the bronchial bacterial microbiome associated with atopy, asthma, and responsiveness to inhaled corticosteroid treatment. J Allergy Clin Immunol 140:63–75. https://doi.org/10.1016/j.jaci.2016.08.055.
4. Diver S, Richardson M, Haldar K, Ghebre MA, Ramsheh MY, Bafadhel M, Desai D, Cohen ES, Newbold P, Rapley L, Rugman P, Pavord ID, May RD, Barer M, Brightling CE. 2020. Sputum microbiomic clustering in asthma and chronic obstructive pulmonary disease reveals a Haemophilus-predominant subgroup. Allergy 75:808–817. https://doi.org/10.1111/all.14058.
5. Pavord ID, Beasley R, Agusti A, Anderson GP, Bel E, Brusselle G, Cullinan P, Custovic A, Ducharme FM, Fahy JV, Frey U, Gibson P, Heaney LG, Holt PG, Humbert M, Lloyd CM, Marks G, Martinez FD, Sly PD, von Mutius E, Wenzel S, Zar HJ, Bush A. 2018. After asthma: redefining airways diseases. Lancet 391:350–400. https://doi.org/10.1016/S0140-6736(17)30879-6.
6. O'Byrne PM, Naji N, Gauvreau GM. 2012. Severe asthma: Future treatments. Clin Exp Allergy 42:706–711. https://doi.org/10.1111/j.1365-2222.2012.03965.x.
7. Green BJ, Wiriyachaiporn S, Grainge C, Rogers GB, Kehagia V, Lau L, Carroll MP, Bruce KD, Howarth PH. 2014. Potentially pathogenic airway bacteria and neutrophilic inflammation in treatment resistant severe asthma. PLoS One 9:e100645. https://doi.org/10.1371/journal.pone.0100645.
8. Taylor SL, Leong LEX, Choo JM, Wesselingh S, Yang IA, Upham JW, Reynolds PN, Hodge S, James AL, Jenkins C, Peters MJ, Baraket M, Marks GB, Gibson PG, Simpson JL, Rogers GB. 2018. Inflammatory phenotypes in patients with severe asthma are associated with distinct airway microbiology. J Allergy Clin Immunol 141:94–103. https://doi.org/10.1016/j.jaci.2017.03.044.

Downloaded from https://journals.asm.org/journal/spectrum on 24 March 2022 by 163.1.213.46.

9. Yang X, Li H, Ma Q, Zhang Q, Wang C. 2018. Neutrophilic asthma is associated with increased airway bacterial burden and disordered community composition. Biomed Res Int 2018:9230234. https://doi.org/10.1155/2018/9230234.
10. Simpson JL, Grissell TV, Douwes J, Scott RJ, Boyle MJ, Gibson PG. 2007. Innate immune activation in neutrophilic asthma and bronchiectasis. Thorax 62:211–218. https://doi.org/10.1136/thx.2006.061358.
11. Gibson PG, Yang IA, Upham JW, Reynolds PN, Hodge S, James AL, Jenkins C, Peters MJ, Marks GB, Baraket M, Powell H, Taylor SL, Leong LEX, Rogers GB, Simpson JL. 2017. Effect of azithromycin on asthma exacerbations and quality of life in adults with persistent uncontrolled asthma (AMAZES): A randomised, double-blind, placebo-controlled trial. Lancet 390:659–668. https://doi.org/10.1016/S0140-6736(17)31281-3.
12. Illing R, Hui CK, Downey K, Carr D, Stearn M, Alshafi K, Menzies-Gow A, Zhong N, Fan Chung K. 2012. Bacteria in sputum of stable severe asthma and increased airway wall thickness. Respir Res 13:35. https://doi.org/10.1186/1465-9921-13-35.
13. Dickson RP, Erb-Downward JR, Freeman CM, McCloskey L, Beck JM, Huffnagle GB, Curtis JL. 2015. Spatial variation in the healthy human lung microbiome and the adapted island model of lung biogeography. Annals ATS 12:821–830. https://doi.org/10.1513/AnnalsATS.201501-029OC.
14. Bullone M, Carriero V, Bertolini F, Folino A, Mannelli A, Di Stefano A, Gnemmi I, Torchio R, Ricciardolo FLM. 2019. Elevated serum IgE, oral corticosteroid dependence and IL-17/22 expression in highly neutrophilic asthma. Eur Respir J 54:1900068. https://doi.org/10.1183/13993003.00068-2019.
15. Singhania A, Rupani H, Jayasekera N, Lumb S, Hales P, Gozzard N, Davies DE, Woelk CH, Howarth PH. 2017. Altered epithelial gene expression in peripheral airways of severe asthma. PLoS One 12:e0168680. https://doi.org/10.1371/journal.pone.0168680.
16. Taylor SL, Ivey KL, Gibson PG, Simpson JL, Rogers GB, Group ASR, and the AMAZES Study Research Group. 2020. Airway abundance of Haemophilus influenzae predicts response to azithromycin in adults with persistent uncontrolled asthma. Eur Respir J 56:2000194. https://doi.org/10.1183/13993003.00194-2020.
17. Hinks TSC, Levine SJ, Brusselle GG. 2021. Treatment options in type-2 low asthma. Eur Respir J 57:2000528. https://doi.org/10.1183/13993003.00528-2020.
18. Bafadhel M, Haldar K, Barker B, Patel H, Mistry V, Barer MR, Pavord ID, Brightling CE. 2015. Airway bacteria measured by quantitative polymerase chain reaction and culture in patients with stable COPD: relationship with neutrophilic airway inflammation, exacerbation frequency, and lung function. COPD 10:1075–1083. https://doi.org/10.2147/COPD.S80091.
19. Shen W, Le S, Li Y, Hu F. 2016. SeqKit: A cross-platform and ultrafast toolkit for FASTA/Q file manipulation. PLoS One 11:e0163962. https://doi.org/10.1371/journal.pone.0163962.
20. Charalampous T, Kay GL, Richardson H, Aydin A, Baldan R, Jeanes C, Rae D, Grundy S, Turner DJ, Wain J, Leggett RM, Livermore DM, O'Grady J. 2019. Nanopore metagenomics enables rapid clinical diagnosis of bacterial lower respiratory infection. Nat Biotechnol 37:783–792. https://doi.org/10.1038/s41587-019-0156-5.
21. Nelson MT, Pope CE, Marsh RL, Wolter DJ, Weiss EJ, Hager KR, Vo AT, Brittnacher MJ, Radey MC, Hayden HS, Eng A, Miller SI, Borenstein E, Hoffman LR. 2019. Human and extracellular DNA depletion for metagenomic analysis of complex clinical infection samples yields optimized viable microbiome profiles. Cell Rep 26:2227–2240. https://doi.org/10.1016/j.celrep.2019.01.091.
22. Oriano M, Terranova L, Teri A, Sottotetti S, Ruggiero L, Tafuro C, Marchisio P, Gramegna A, Amati F, Nava F, Franceschi E, Cariani L, Blasi F, Aliberti S. 2019. Comparison of different conditions for DNA extraction in sputum: A pilot study. Multidiscip Respir Med 14:6. https://doi.org/10.1186/s40248-018-0166-z.
23. Power PM, Bentley SD, Parkhill J, Moxon ER, Hood DW. 2012. Investigations into genome diversity of Haemophilus influenzae using whole genome sequencing of clinical isolates and laboratory transformants. BMC Microbiol 12:273. https://doi.org/10.1186/1471-2180-12-273.
24. van Alphen L, Caugant DA, Duim B, O'Rourke M, Bowler LD. 1997. Differences in genetic diversity of nonecapsulated Haemophilus influenzae from various diseases. Microbiology 143:1423–1431. https://doi.org/10.1099/00221287-143-4-1423.
25. Connor TR, Corander J, Hanage WP. 2012. Population subdivision and the detection of recombination in non-typable Haemophilus influenzae. Microbiology (Reading) 158:2958–2964. https://doi.org/10.1099/mic.0.063073-0.
26. Pettigrew MM, Ahearn CP, Gent JF, Kong Y, Gallo MC, Munro JB, D'Mello A, Sethi S, Tettelin H, Murphy TF. 2018. Haemophilus influenzae genome evolution during persistence in the human airways in chronic obstructive pulmonary disease. Proc Natl Acad Sci U S A 115:E3256–E3265. https://doi.org/10.1073/pnas.1719654115.
27. Tyler AD, Mataseje L, Urfano CJ, Schmidt L, Antonation KS, Mulvey MR, Corbett CR. 2018. Evaluation of Oxford Nanopore's MinION Sequencing Device for Microbial Whole Genome Sequencing Applications. Sci Rep 8:10931. https://doi.org/10.1038/s41598-018-29334-5.
28. Street TL, Barker L, Sanderson ND, Kavanagh J, Hoosdally S, Cole K, Newnham R, Selvaratnam M, Andersson M, Llewelyn MJ, O'Grady J, Crook DW, Eyre DW. 2020. Optimizing DNA extraction methods for nanopore sequencing of neisseria gonorrhoeae directly from urine samples. J Clin Microbiol 58:e01822-19. https://doi.org/10.1128/JCM.01822-19.
29. Stoler N, Nekrutenko A. 2021. Sequencing error profiles of Illumina sequencing instruments. NAR Genom Bioinform 3:lqab019. https://doi.org/10.1093/nargab/lqab019.
30. Bisgaard H, Hermansen MN, Buchvald F, Loland L, Halkjaer LB, Bonnelykke K, Brasholt M, Heltberg A, Vissing NH, Thorsen SV, Stage M, Pipper CB. 2007. Childhood asthma after bacterial colonization of the airway in neonates. N Engl J Med 357:1487–1495. https://doi.org/10.1056/NEJMoa052632.
31. Swords WE. 2012. Nontypeable Haemophilus influenzae biofilms: role in chronic airway infections. Front Cell Infect Microbiol 2:97.
32. Chung KF, Wenzel SE, Brozek JL, Bush A, Castro M, Sterk PJ, Adcock IM, Bateman ED, Bel EH, Bleecker ER, Boulet LP, Brightling C, Chanez P, Dahlen SE, Djukanovic R, Frey U, Gaga M, Gibson P, Hamid Q, Jajour NN, Mauad T, Sorkness RL, Teague WG. 2014. International ERS/ATS guidelines on definition, evaluation and treatment of severe asthma. Eur Respir J 43:343–373. https://doi.org/10.1183/09031936.00202013.
33. Hinks TS, Zhou X, Staples KJ, Dimitrov BD, Manta A, Petrossian T, Lum PY, Smith CG, Ward JA, Howarth PH, Walls AF, Gadola SD, Djukanovic R. 2015. Innate and adaptive T cells in asthmatic patients: Relationship to severity and disease mechanisms. J Allergy Clin Immunol 136:323–333. https://doi.org/10.1016/j.jaci.2015.01.014.
34. Votintseva AA, Pankhurst LJ, Anson LW, Morgan MR, Gascoyne-Binzi D, Walker TM, Quan TP, Wyllie DH, Del Ojo Elias C, Wilcox M, Walker AS, Peto TE, Crook DW. 2015. Mycobacterial DNA extraction for whole-genome sequencing from early positive liquid (MGIT) cultures. J Clin Microbiol 53:1137–1143. https://doi.org/10.1128/JCM.03073-14.
35. Kim D, Song L, Breitwieser FP, Salzberg SL. 2016. Centrifuge: rapid and sensitive classification of metagenomic sequences. Genome Res 26:1721–1729. https://doi.org/10.1101/gr.210641.116.
36. Li H. 2013. Aligning sequence reads, clone sequences and assembly contigs with BWA-MEM. arXiv. http://arxiv.org/abs/1303.3997v2.
37. Li H, Handsaker B, Wysoker A, Fennell T, Ruan J, Homer N, Marth G, Abecasis G, Durbin R, 1000 Genome Project Data Processing Subgroup. 2009. The sequence alignment/map format and SAMtools. Bioinformatics 25:2078–2079. https://doi.org/10.1093/bioinformatics/btp352.
38. Sanderson ND, Street TL, Foster D, Swann J, Atkins BL, Brent AJ, McNally MA, Oakley S, Taylor A, Peto TEA, Crook DW, Eyre DW. 2018. Real-time analysis of nanopore-based metagenomic sequencing from infected orthopaedic devices. BMC Genomics 19:714. https://doi.org/10.1186/s12864-018-5094-y.
39. Li H. 2018. Minimap2: pairwise alignment for nucleotide sequences. Bioinformatics 34:3094–3100. https://doi.org/10.1093/bioinformatics/bty191.
40. Sanderson ND, Swann J, Barker L, Kavanagh J, Hoosdally S, Crook D, Street TL, Eyre DW, GonFast Investigators G. 2020. High precision Neisseria gonorrhoeae variant and antimicrobial resistance calling from metagenomic Nanopore sequencing. Genome Res 30:1354–1363. https://doi.org/10.1101/gr.262865.120.
41. Seeman T, Klötzl F, Page AJ. n.d. snp-dists. https://github.com/tseemann/snp-dists.

Downloaded from https://journals.asm.org/journal/spectrum on 24 March 2022 by 163.1.213.46.

Check for updates

Received: 13 March 2024 | Revised: 23 May 2024 | Accepted: 19 June 2024

DOI: 10.1111/all.16269

Allergy EUROPEAN JOURNAL OF ALLERGY AND CLINICAL IMMUNOLOGY EAACI WILEY

ORIGINAL ARTICLE

Asthma and Lower Airway Disease

Species-level, metagenomic and proteomic analysis of microbe-immune interactions in severe asthma

Maisha F. Jabeen[1,2,3] | Nicholas D. Sanderson[2,3] | Mariaenrica Tinè[4] | Gillian Donachie[1,2,3] | Clair Barber[5] | Adnan Azim[5] | Laurie C. K. Lau[5] | Thomas Brown[6] | Ian D. Pavord[1,2,3] | Anoop Chauhan[6] | Paul Klenerman[2,3,7] | Teresa L. Street[2,3] | Emanuele Marchi[1,2,3,7] | Peter H. Howarth[5] | Timothy S. C. Hinks[1,2,3]

[1]Nuffield Department of Medicine, Experimental Medicine Division, Respiratory Medicine Unit, John Radcliffe Hospital, University of Oxford, Oxford, UK

[2]Nuffield Department of Clinical Medicine, John Radcliffe Hospital, University of Oxford, Oxford, UK

[3]National Institute for Health Research Oxford Biomedical Research Centre, John Radcliffe Hospital, Oxford, UK

[4]Department of Cardiac, Thoracic, Vascular Sciences and Public Health, University of Padova, Padova, Italy

[5]Clinical and Experimental Sciences, University of Southampton Faculty of Medicine, Sir Henry Wellcome Laboratories and NIHR Southampton Respiratory Biomedical Research Unit, Southampton University, Southampton, UK

[6]Portsmouth Hospitals NHS Trust, Portsmouth, UK

[7]Nuffield Department of Clinical Medicine, Peter Medawar Building for Pathogen Research and Translational Gastroenterology Unit, University of Oxford, Oxford, UK

Correspondence
Timothy S. C. Hinks, Nuffield Department of Medicine, Experimental Medicine Division, Respiratory Medicine Unit, University of Oxford, Room 7400A, Level 7, John Radcliffe Hospital, Oxford OX3 9DU, UK.
Email: timothy.hinks@ndm.ox.ac.uk

Funding information
NIHR Primary Care Research Network; National Institute for Health Research Southampton Biomedical Research Centre; Wellcome Trust; NIHR Oxford Biomedical Research Centre; Medical Research Council

Abstract

Background: The airway microbiome in severe asthma has not been characterised at species-level by metagenomic sequencing, nor have the relationships between specific species and mucosal immune responses in 'type-2 low', neutrophilic asthma been defined. We performed an integrated species-level metagenomic data with inflammatory mediators to characterise prevalence of dominant potentially pathogenic organisms and host immune responses.

Methods: Sputum and nasal lavage samples were analysed using long-read metagenomic sequencing with Nanopore and qPCR in two cross-sectional adult severe asthma cohorts, Wessex ($n=66$) and Oxford ($n=30$). We integrated species-level data with clinical parameters and 39 selected airway proteins measured by immunoassay and O-link.

Results: The sputum microbiome in health and mild asthma displayed comparable microbial diversity. By contrast, 23% (19/81) of severe asthma microbiomes were dominated by a single respiratory pathogen, namely *H. influenzae* ($n=10$), *M. catarrhalis* ($n=4$), *S. pneumoniae* ($n=4$) and *P. aeruginosa* ($n=1$). Neutrophilic asthma was associated with *H. influenzae*, *M. catarrhalis*, *S. pneumoniae* and *T. whipplei* with elevated type-1

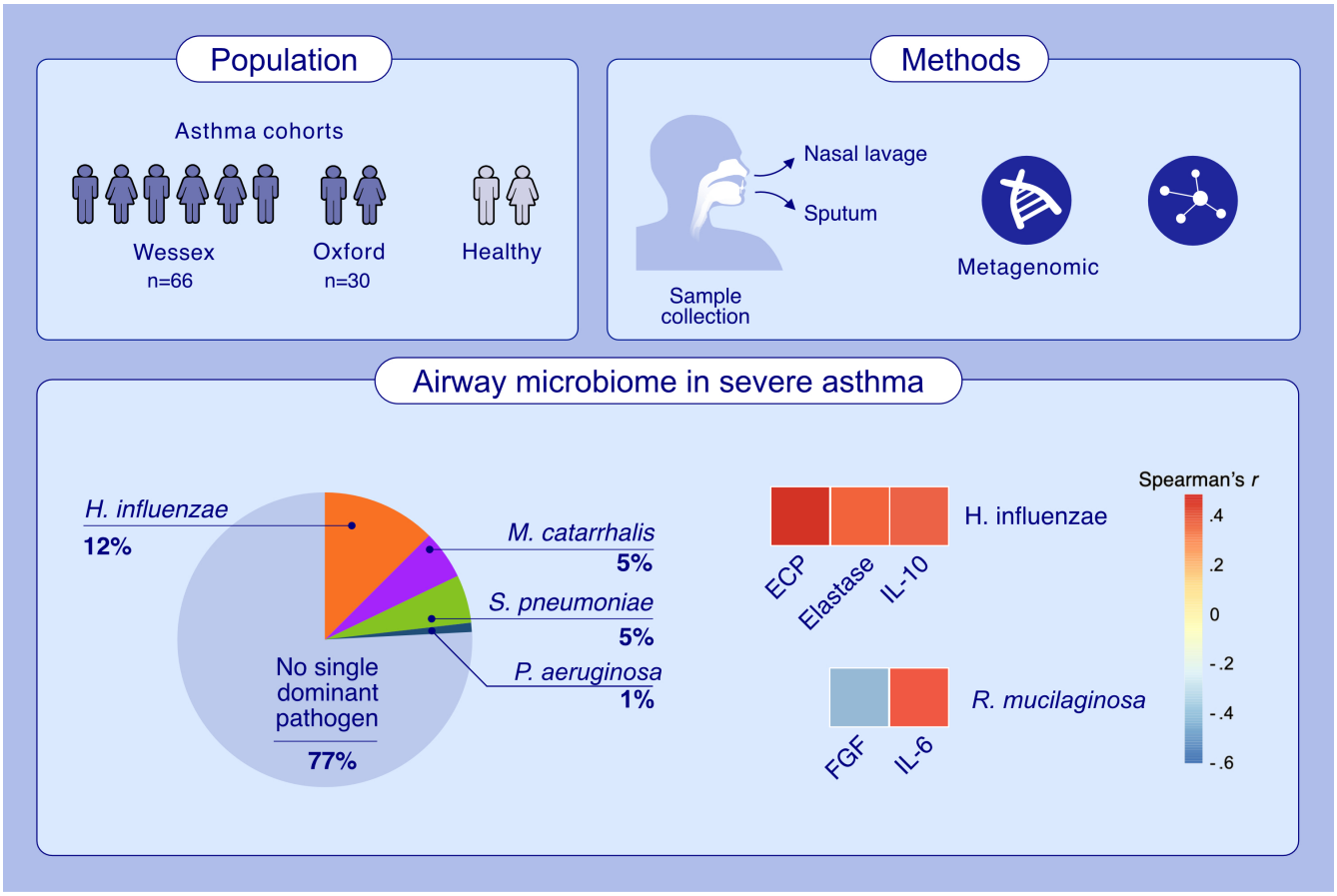
Emanuele Marchi, Peter H. Howarth and Timothy S. C. Hinks have contributed equally and are joint senior authors.

This is an open access article under the terms of the Creative Commons Attribution License, which permits use, distribution and reproduction in any medium, provided the original work is properly cited.
© 2024 The Author(s). *Allergy* published by European Academy of Allergy and Clinical Immunology and John Wiley & Sons Ltd.

cytokines and proteases; eosinophilic asthma with higher *M. catarrhalis*, but lower *H. influenzae*, and *S. pneumoniae* abundance. *H. influenzae* load correlated with Eosinophil Cationic Protein, elastase and IL-10. *R. mucilaginosa* associated positively with IL-6 and negatively with FGF. Bayesian network analysis also revealed close and distinct relationships of *H. influenzae* and *M. catarrhalis* with type-1 airway inflammation. The microbiomes and cytokine milieu were distinct between upper and lower airways.

Conclusions: This species-level integrated analysis reveals central, but distinct associations between potentially pathogenic bacteria and airways inflammation in severe asthma.

KEYWORDS
Asthma, bacteria, cytokine, microbiome, sputum



GRAPHICAL ABSTRACT

Paired long-read metagenomic sequencing and proteomics in sputum and nasal lavage identified a single dominant respiratory pathogen (*H. influenzae* more than *M. catarrhalis* and *S. pneumoniae*) in 23% of severe asthma sputum samples. Nasal and sputum microbiomes were highly discordant. *H. influenzae* load correlated with ECP, elastase and IL-10 suggesting eosinophil activation and a potential immune evasion mechanism.

Abbreviations: ECP, eosinophil cationic protein; FGF, fibroblast growth factor; *H. influenzae*, *Haemophilus influenzae*; IL, interleukin; *M. catarrhalis*, *Moraxella catarrhalis*; *P. aeruginosa*, *Pseudomonas aeruginosa*; *R. mucilaginosa*, *Rothia mucilaginosa*; *S. pneumoniae*, *Streptococcus pneumoniae*.

1 | INTRODUCTION

Asthma is a complex, heterogenous disease. Recognising 'treatable traits' ascribed to specific pathophysiological subsets of severe asthma have supported significant therapeutic advances in 'type-2 high' severe asthma[1]; a phenotype characterised by sputum (≥3% on a cytospin)[2] and blood eosinophilia, predictive of response to corticosteroid and anti-IL-5 therapy.[3] However, 30%–50% of severe

13989995, 2024, 11, Downloaded from https://onlinelibrary.wiley.com/doi/10.1111/all.16269 by Test, Wiley Online Library on [04/01/2025]. See the Terms and Conditions (https://onlinelibrary.wiley.com/terms-and-conditions) on Wiley Online Library for rules of use; OA articles are governed by the applicable Creative Commons License

asthmatics have 'type-2 low' disease refractory to currently licensed biologic therapies or systemic corticosteroids,[3] constituting an important, poorly-understood, clinical phenotype. This encompasses neutrophilic (≥61% neutrophils on cytospin) and paucigranulocytic (non-neutrophilic or eosinophilic) asthma.[3]

In type-2 low disease, emerging data implicate bacterial airways infection with neutrophilic infiltration driven by innate and adaptive immune responses, and supporting long-term macrolide therapy.[3,4] Molecular microbiological approaches have described airway microbial profiles in severe asthma, but early studies were restricted by sequencing approaches unable to assign species level taxonomic identification. These reported reduced bacterial α-diversity, Proteobacterial enrichment, particularly *Haemophilus* spp. and *Moraxella* spp.[5–7] and depletion of commensal organisms.[8] *H. influenzae* is the commonest pathogen detected in the lower airway[9–11]; it is linked to commensal depletion, neutrophilic inflammation and poor asthma outcomes.[4] However, prevalence of *H. influenzae* and other species is yet to be defined in severe asthma using a metagenomic approach resolved to species level.

Nanopore technology, in contrast to the Illumina platform, sequences DNA or RNA molecules as they pass through a protein nanopore in an electro-resistant membrane, without using PCR or chemical labelling. We recently demonstrated metagenomic sequencing using Nanopore offers rapid, species-level taxonomy from sputum samples[11] at lower-cost, offering real-time data acquisition, and longer contiguous reads for de novo genome reconstruction. In our pilot study *H. influenzae* was commonly detected in severe neutrophilic asthma.[11] We thus hypothesised that a shift towards a pathogen-dominant airway microbiome is a common treatable trait in severe asthma, confined to the lower airway, with neutrophilic airways inflammation driven by type-1 cytokine responses. We aimed to define its prevalence, by inflammatory phenotype, in a large, adult, severe asthma population at species-level, using Nanopore metagenomic sequencing of induced sputum samples in stable disease, and discern inflammatory signals driving refractory airways inflammation through integrated proteomic analysis. By comparing the upper and lower airway microbiome and proteome in severe asthma we question the 'one airway, one disease' concept.[12]

2 | METHODS

2.1 | Clinical cohorts

2.1.1 | Oxford Severe Asthma Cohort

Adult patients with American Thoracic Society/European Respiratory Society definition of severe asthma, on Global Initiative for Asthma (GINA) step 4–5 treatment ($n=30$) were recruited to the Oxford Airways Study between June 2018 and February 2020 (John Radcliffe Hospital, Oxford, UK, NHS Research Ethics approval 08/H0406/189). Participants underwent clinical phenotyping, sputum induction and phlebotomy during clinical stability. Hypertonic sputum induction and sputum differential cell counts were performed as previously described[13] and sputum plugs stored at −80°C in sterile Brain Heart Infusion (BHI, Sigma-Aldrich, Dorset, UK) broth containing 10% glycerol. Sputum plugs were dispersed, and DNA extracted and sequenced ($n=30$) using established methods.[11]

2.1.2 | Wessex Severe Asthma Cohort[13]

Adult participants with severe asthma ($n=51$), mild/moderate asthma ($n=10$) and healthy controls ($n=5$) were recruited (University Hospital Southampton and Queen Alexandra Hospital Portsmouth). The study was approved by Southampton and South-West Hampshire Research Ethics Committee A (09/H0502/37) and study protocol described elsewhere.[14] Metagenomic sequencing was performed on induced sputum ($n=66$) and nasal lavage (NL) ($n=17$), and sequencing data integrated with existing cytokine data from sputum supernatant and nasal lavage.[14]

All participants provided written informed consent.

Sputum inflammatory subtypes were defined using validated criteria.[2] These were: eosinophilic ≥3% sputum eosinophils, neutrophilic ≥61% sputum neutrophils and <3% eosinophils, mixed granulocytic ≥61% sputum neutrophils and ≥3% eosinophils, paucigranulocytic <61% sputum neutrophils and <3% eosinophils.

2.2 | Molecular microbiology

Established methods[11] were used for microbial DNA extraction from samples. Pathogen-specific qPCR and Nanopore sequencing performed and analysed as described in the online supplement.

2.3 | Measurement of inflammatory mediators

Existing data on 32 inflammatory mediators and eight metalloproteinases were available from Hinks et al.,[14] measured by enzyme-linked immunosorbent assays and cytokine bead array (Luminex®) (see online supplement). In addition, O-link Uppsala, Sweden measured 92 inflammation-related proteins on sputum and nasal lavage using in-house Proseek Multiplex Inflammation I panel.

2.4 | Statistical and bioinformatic analyses

Statistical analysis were performed using Rstudio (Version 2022.12.0+353) and GraphPad Prism (Version 9). Data were logarithmically transformed if non-normal distribution. Parametric and non-parametric data are displayed as mean (SEM) and median (range), with comparisons between groups made using unpaired *t*-test or Mann–Whitney test, respectively. For all analyses, 2-tailed $p<.05$ were considered significant. Where indicated, overall 5% significance level was adjusted for multiple comparisons with Benjamini-Hochberg procedure. Correlations were tested with Spearman's *r* statistic, as described in the text. A full description of the bioinformatic analysis is provided in the online supplement and GitLab: https://gitlab.com/Modernisin

13989995, 2024, 11, Downloaded from https://onlinelibrary.wiley.com/doi/10.1111/all.16269 by Test, Wiley Online Library on [04/01/2025]. See the Terms and Conditions (https://onlinelibrary.wiley.com/terms-and-conditions) on Wiley Online Library for rules of use; OA articles are governed by the applicable Creative Commons License

gMedicalMicrobiology/wessex_analysis. Interconnectivity between clinical and immunological parameters alongside bacterial species was explored with Bayesian Network Analysis (BNA) (Genie 2.0; Decision Systems Laboratory, University of Pittsburgh, Pittsburgh, PA), and is further described in online supplement.

3 | RESULTS

Baseline participant characteristics are summarised in Table 1 (Tables E1 and E2, online supplement). The Wessex and Oxford cohorts were temporally and geographically separated, but comparable in their demographic features, baseline ICS use and lung function in severe asthma. The Wessex severe asthma cohort encompassed health, mild and severe asthma from a pre-biologic era, and hence a greater maintenance oral corticosteroid use in severe asthma participants, with a higher proportion of neutrophilic (25.5% vs. 20%) and paucigranulocytic (39% vs. 13.3%) sputum phenotypes. In addition, there was a greater proportion of current smokers (33 vs. 3.3%), but mean pack years smoked was <10. The Oxford cohort included participants with severe asthma alone, with a higher baseline blood eosinophil count (mean 0.4×10^9/L vs. 0.2×10^9/L) and eosinophilic sputum phenotype (36.7% vs. 25.5%). Overall, patients with severe asthma had high asthma control questionnaire

TABLE 1 Clinical characteristics of the participants.

	Wessex						Oxford	
Characteristic	**Healthy (*n* = 5)**		**Mild Asthma (*n* = 10)**		**Severe Asthma (*n* = 51)**		**Severe asthma (*n* = 30)**	
Male sex, *n* (%)	3	(60)	5	(50)	22	(43)	14	(46.7)
Age (years), Mean (SD)	29	(12.3)	44.1	(15.9)	49.1	(14.7)	59.5	(15.0)
BMI (kg/m^2), Mean (SD)	25	(4.4)	27.5	(6.0)	32.2	(8.1)	29.2	(6.2)
Presence of atopy, *n* (%)	0	(0)	5	(50)	35	(69)	6	(20.0)
Presence of nasal polyps, *n* (%)	0	(0)	0	(0)	6	(12)	10	(33.3)
Smoking status, *n* (%)								
Never	4	(80)	5	(50)	27	(53)	22	(73.3)
Current	0	(0)	1	(10)	17	(33)	1	(3.3)
Ex-smoker	1	(20)	4	(40)	7	(14)	7	(23.4)
Pack years, Mean (SD)	7.5	–	1	(1.2)	8.4	(13.0)	12	(10)
Baseline inhaled corticosteroid use (BDP eq., mcg/d), Median (Q1, Q3)	na	na	300	(0, 400)	2080	(1800, 3575)	2000	(1600, 2000)
Maintenance oral corticosteroid, *n* (%)	na	na	0	(0)	19	(37)	4	(13.3)
Biologic therapy, *n* (%) (mepolizumab)	0	(0)	0	(0)	0	(0)	3	(10)
Unscheduled GP/ hospital visits in 12 months, Median (Q1, Q3)	na	na	0	(0, 0)	3	(0, 7)	2	(0,6)
FEV1 (%predicted), Mean (SD)	96	(9.8)	107	(12.8)	73.6	(24.5)	73.8	(20.6)
FEV1/FVC, Mean (SD)	1	(0.2)	0.8	(0.2)	0.6	(0.1)	0.6	(0.1)
FeNO (ppb), Median (Q1, Q3)	11	(8, 11)	31	(16, 45)	10	(7, 17)	38	(18, 64)
Blood eosinophils ($\times10^9$/L), Median (Q1, Q2)	nd	nd	0.4	(0.2, 0.4)	0.2	(0.1, 0.3)	0.4	(0.2, 0.7)
Sputum eosinophils (%), Median (Q1, Q3)	1.1	(0.9, 3.3)	2.2	(1.2, 3.1)	1	(0.3, 7.7)	4.5	(1.0, 42.2)
Sputum neutrophils (%), Median (Q1, Q3)	31	(20.2, 37.3)	23.9	(16.7, 31.7)	51.8	(28.5, 76.1)	38.1	(17.0, 86.0)
Sputum inflammatory phenotype, *n* (%)								
Eosinophilic	1	(20)	1	(10)	13	(25.5)	11	(36.7)
Neutrophilic	0	(0)	0	(0)	13	(25.5)	6	(20.0)
Mixed granulocytic	0	(0)	0	(0)	3	(6)	1	(3.3)
Paucigranulocytic	2	(40)	7	(70)	20	(39)	4	(13.3)
No data	2	(40)	2	(20)	2	(4)	8	(26.7)

Note: Inflammatory phenotypes: eosinophilic ≥3% sputum eosinophils, neutrophilic ≥61% sputum neutrophils and <3% eosinophils, mixed granulocytic ≥61% sputum neutrophils and ≥3% eosinophils, paucigranulocytic <61% sputum neutrophils and <3% eosinophils.

Abbreviations: BMI, body mass index; FeNO, exhaled nitric oxide; FEV1, Forced expiratory volume in 1s; FVC, Forced vital capacity; na, not applicable; nd, no data; Q1, quartile 1; Q3, quartile3; SD, standard deviation.

13989995, 2024, 11, Downloaded from https://onlinelibrary.wiley.com/doi/10.1111/all.16269 by Test, Wiley Online Library on [04/01/2025]. See the Terms and Conditions (https://onlinelibrary.wiley.com/terms-and-conditions) on Wiley Online Library for rules of use; OA articles are governed by the applicable Creative Commons License

(ACQ-5 in Oxford and ACQ-7 in Wessex cohort) scores indicative of uncontrolled disease (mean exceeding 1.5).[15] Nanopore sequencing was performed on 96 sputum and 17 nasal lavage samples. A summary of sequencing statistics is provided in Supplementary Data S1. In sputum samples median read length ranged from 1684 to 5490 bp (overall 2685 bp) and median bacterial reads per sample was 8099, and in nasal lavage samples median read length ranged from 2051 to 3904 bp (overall 2935 bp) and median bacterial reads per sample was 4010. A further integrated analysis, incorporating clinical and cytokine data, was performed in 66 participants from the Wessex cohort (Figure E1, online supplement).

3.1 | Nanopore sequencing defines distinct species-level metagenomes in severe asthma and identifies patients with a pathogen-dominant microbiome

Z-scores of bacterial species with greatest variability in abundance across health (HC), mild (MA) and severe asthma (SA) are displayed in Figure 1 combining the Oxford and Wessex cohorts, and shown separately by cohort in Figure E2 (online supplement).

Hierarchical clustering revealed a cluster of 19/96 participants, each with severe asthma and skewed airway microbiome dominated by a single respiratory pathogen, namely *H. influenzae*, *M. catarrhalis* or *S. pneumoniae*. Remaining participants displayed greater microbial diversity with variable abundance of commensal organisms, predominantly phyla Actinobacteria, Bacteroidetes and Firmicutes. A principal component analysis (PCA) plot on normalised read counts filtered by abundance and variability (online supplement) for patients with severe asthma from the Wessex and Oxford cohorts is shown in Figure E3B (online supplement). There was no significant difference in the microbial composition between these groups (PERMANOVA = 0.19).

Differential abundance of species was tested across health ($n = 5$), mild ($n = 10$) and severe asthma ($n = 51$) in the Wessex cohort only, which alone included these distinct groups. The most conserved species in HC sputum (HC vs MA/SA, log fold change [LFC] >1, adjusted $p < .05$) include *Streptococcus viridans*, *Streptococcus sp A12*, *Streptococcus australis* and *Schaalia odontolytica* (Table E3,

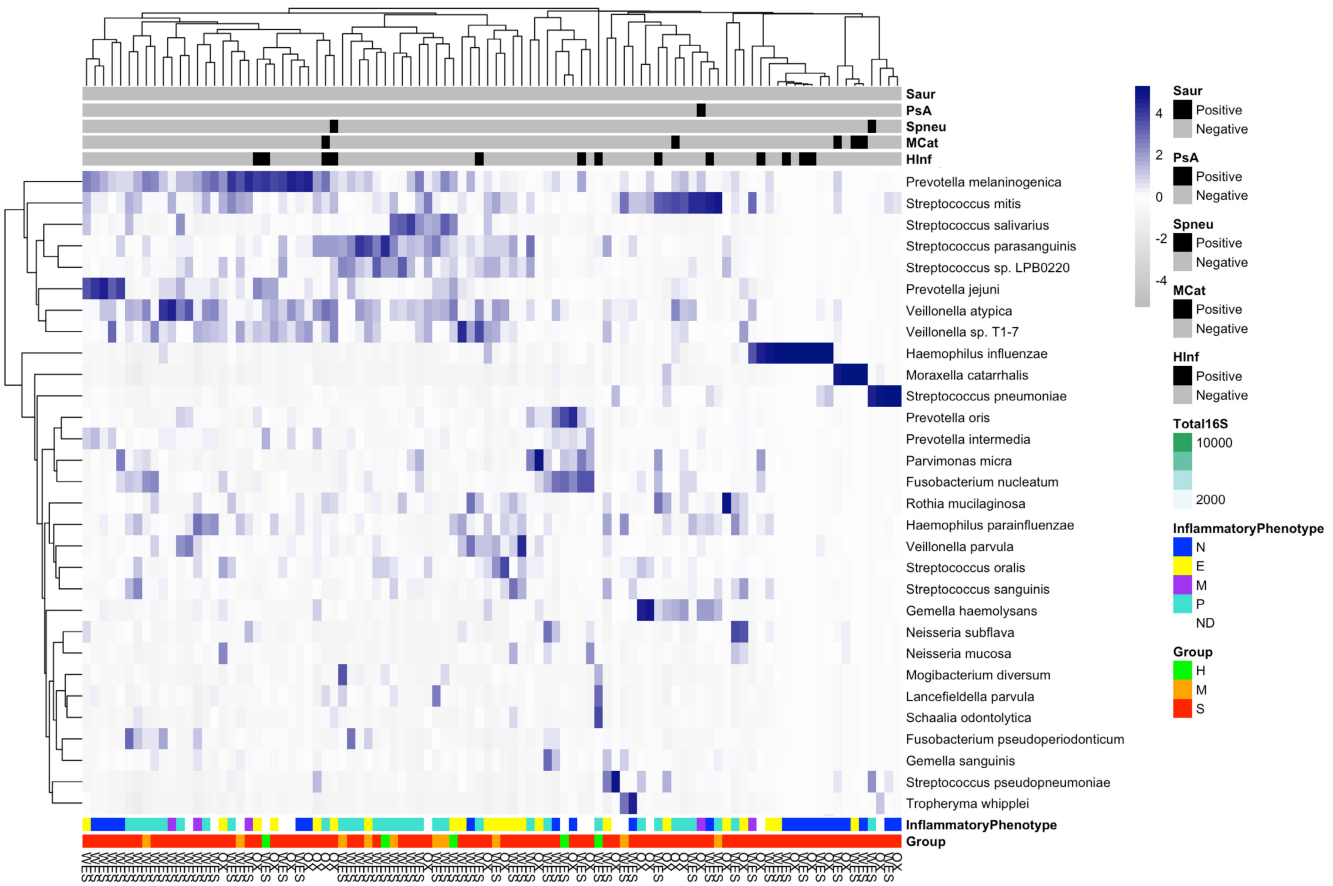


FIGURE 1 Relative abundance of species in sputum. Heatmap of relative abundance of species from induced sputum sequenced samples using ONT; Z-scores, denoted by shade, represent the relative abundance of each taxon within each individual patient (columns). Cohorts include Wessex (WES; Healthy [H]: $n = 5$, Mild [M]: $n = 10$ and Severe asthma [S]: $n = 51$) and Oxford (OX; Severe asthma [S]: $n = 30$). Clustering by species (rows) and individuals (columns) using Euclidian distance performed independently on samples and most differentially abundant bacterial species. Sputum inflammatory phenotypes are eosinophilic (E), neutrophilic (N), mixed granulocytic (M) and paucigranulocytic (P). Positive pathogen specific PCR results (>1 × 106 copies/mL) are indicated in black: *S. aureus* (Saur), *P. aeruginosa* (PsA), *S. pneumoniae* (Spneu), *M. catarrhalis* (Mcat) and *H. influenzae* (Hinf). Total eubacteria (16S) PCR load is denoted by shade (×106 copies/mL).

13989995, 2024, 11, Downloaded from https://onlinelibrary.wiley.com/doi/10.1111/all.16269 by Test, Wiley Online Library on [04/01/2025]. See the Terms and Conditions (https://onlinelibrary.wiley.com/terms-and-conditions) on Wiley Online Library for rules of use; OA articles are governed by the applicable Creative Commons License

online supplement). In MA (MA vs. HC/SA) 29 species, predominantly Firmicutes, were similarly identified, of which *Filifactor alocis*, *Mogibacterium diversum* and *Streptococcus* sp. *A12* were significantly enriched (Table E4, online supplement). SA (SA vs. HC/MA) is associated with a marked compositional shift and greater abundance of species including *Rothia mucilaginosa*, *Rothia dentocariosa*, *H. influenzae* and *M. catarrhalis* (Table E5, online supplement), and relative depletion of oropharyngeal commensals (Table E5, online supplement).

We defined pathogen dominance—metagenomic dominance by a single airway pathogen—in an individual if a known respiratory pathogen (*H. influenzae*, *M. catarrhalis*, *S. pneumoniae* or *P. aeruginosa*, in this dataset) was the most abundant (%reads/total bacterial reads) species and the proportion of detected reads (Table E6) was ≥2-fold of the second ranked abundant species in the sample. Across two cohorts, pathogen-dominant microbiome was present during clinical stability in 23% of severe asthmatics ($n = 19/81$). *H. influenzae* ($n = 10$) was most prevalent, followed by *M. catarrhalis* ($n = 4$) and *S. pneumoniae* ($n = 4$). In most ($n = 18/19$) samples, sequences covered ≥1/5th of the reference genome, providing high confidence species-level classification. *P. aeruginosa* was detected in one individual with high proportion of total reads (73%) but lower genome coverage (5.1%). The relative abundance of these respiratory pathogens in individuals with a pathogen-dominant microbiome is shown in Sankey visualisations (Figure E4) and was significantly greater than other detected species (Wilcoxon rank-sum test, Benjamini-Hochberg [BH] correction FDR 0.05; Figure E4B Wessex, *H. influenzae* $p = 6.3 \times 10^{-5}$; Figure E4C Wessex, *M. catarrhalis* $p = 8.7 \times 10^{-4}$; Figure E4C Wessex, *S. pneumoniae* $p = .01$; Figure E4F Oxford, *H. influenzae* $p = 3.8 \times 10^{-3}$; Figure E5A Oxford, *S. pneumoniae* $p = .01$). Semiquantitative pathogen-specific qPCR results are shown in Figure 1 and Table E6. A clinically significant positive result was identified as ≥1×10^6 copies/mL, previously demonstrated to be longitudinally reproducible in COPD for identifying bacteria-associated neutrophilic inflammation[16] and correlating with positive sputum culture in asthma.[11] By this definition a positive qPCR result was identified in all Oxford samples shown in Table E6 and 8/11 Wessex samples. Bacterial load was quantified with 16S qPCR (Figure 1) and was higher in Oxford (median 364×10^6, IQR 823×10^6 copies/mL) versus Wessex sputum samples (median 23×10^6, IQR 83×10^6 copies/mL).

3.2 | Sputum inflammatory phenotype is predictive of the presence of airway pathogens

A pathogen-dominant microbiome in severe asthma (Figures E4 and E5, online supplement) was associated with a higher Proteobacteria:Firmicutes ratio ($p < .001$, Figure E6, online supplement), consistent with previous reports,[10,17] but no significant differences were observed between SA ($n = 51$) and HC ($n = 5$) or MA ($n = 10$), or across inflammatory phenotypes. This was consistent with Proteobacterial species *H. influenzae* and *M. catarrhalis* being the most prevalent airway pathogens in severe disease. A pattern of pathogen dominance of the microbiome was not observed in health or mild asthma. Airways neutrophilia was associated with *H. influenzae*, *M. catarrhalis*, *S. pneumoniae* and *P. aeruginosa* dominance in severe asthma sputum, with higher overall sputum neutrophil count (Figure 2B, $p < .05$) and higher prevalence of neutrophilic asthma (Table E2 online supplement, $p < .05$).

Defining bacterial species associated with severe asthma inflammatory phenotypes were sought (LFC >1, adjusted $p < .05$). Consistent with the above findings, *H. influenzae*, *M. catarrhalis*, *T. whipplei* and *S. pneumoniae* were strongly associated with neutrophilic asthma, whilst commensal *Streptococcus* spp. (Table E7, online supplementary) including *S. salivarius*, *S. intermedius*, *S. oralis* were relatively depleted (LFC < −1, adjusted $p < .05$). In paucigranulocytic disease, there was lower *M. catarrhalis*, *H. influenzae* and *T. whipplei* abundance (Table E7, online supplement). Eosinophilic asthma was characterised by high relative abundance of *M. catarrhalis*, *S. intermedius* and *V. parvula* and less *H. influenzae*, *S. pneumoniae* and *Actinomyces pacaensis*, a relatively newly-isolated Gram-positive human respiratory microbiome[18] organism (Table E7, online supplementary). No organisms uniquely defined the mixed inflammatory phenotype.

3.3 | Integrated cytokine and metagenomic analyses

We integrated sputum metagenomes in the Wessex cohort ($n = 66$) with existing cytokine data measured by immunoassay ($n = 40$) (Figure 2A).[14] Unsupervised clustering identified HC and MA with higher expression of FGF, IL-1RA, IL-2 and IL-4 relative to SA clusters. Amongst SA two clusters were seen. One was associated with predominantly proinflammatory and type 1 cytokines (left) including IL-1α, IL-1β, TNF, IFN-γ, MMP8, MMP9, MPO, YKL40, IL-17, IL-6, elastase, ECP, IL-8, GROα, G-CSF, eotaxin and TIMP-1, typically in presence of a pathogen-dominant microbiome. The second cluster (right) represents a mixture of sputum inflammatory phenotypes, without infection, with high expression of MMPs.

To further dissect the mucosal immune response to individual species we integrated these data, clustering (hierarchical) by species and by cytokine (Figure 3 and Supplementary Data), selecting the 50 species with greatest variance in abundance across subjects. The strongest positive correlations were between *H. influenzae* and Eosinophil Cationic Protein (ECP) ($r = .5$, $p \leq .007$), IL-10 ($r = .4$, $p = .05$) and elastase ($r = .4$, $p = .05$); between *Rothia mucilaginosa* and IL-6 ($r = .4$, $p < .05$); between *Streptococcus pseudopneumoniae* and MMP1 ($r = .4$, $p < .05$); and between *Streptococcus parasanguinis* and IL-1RA ($r = .4$, $p < .05$) implying species-specific immune modulation. Negative correlations between predominantly Gram-positive oropharyngeal/respiratory commensals (top middle species cluster Figure 3) and pro-inflammatory cytokines were identified, exemplified using markers of neutrophilic

13989995, 2024, 11, Downloaded from https://onlinelibrary.wiley.com/doi/10.1111/all.16269 by Test, Wiley Online Library on [04/01/2025]. See the Terms and Conditions (https://onlinelibrary.wiley.com/terms-and-conditions) on Wiley Online Library for rules of use; OA articles are governed by the applicable Creative Commons License

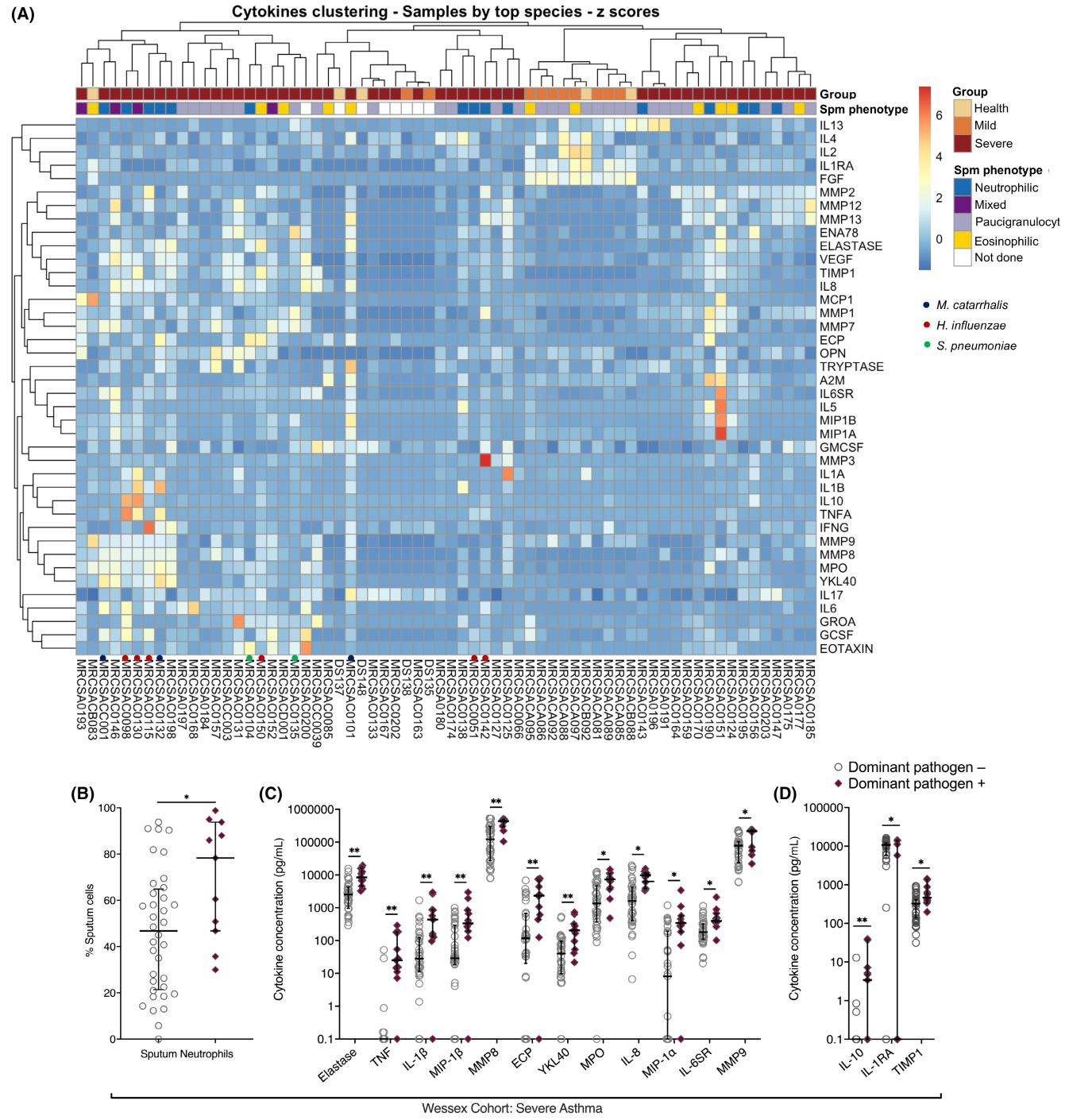


FIGURE 2 Integrated analyses of microbiome and inflammatory mediators in sputum. Integrated cytokine analysis (A) Heatmap of scaled and centralised sputum cytokines in health, mild and severe asthma. Z-score centralised cytokine measurements denoted by shade. Independent clustering performed by subject (columns) and cytokine (rows). Clustering distances shown are representative of correlation distances. In severe asthma, presence of a dominant pathogenic organism on metagenomic sequencing is indicated as HI (*H. inf*), MC (*M. cat*) and SP (*S. pneu*); the pathogen-dominant microbiome in severe asthma (data only shown for participants with severe asthma) is associated with (B) sputum neutrophilia, (C) elevated type-1 cytokines and (D) anti-inflammatory mediators in sputum supernatant. Median/IQR shown −/+ pathogen dominance ([C] Mann–Whitney test, [D]/[E] unpaired *t*-test, adjusted for multiple comparisons with BH procedure [FDR 0.05]. $^{*}p \le .05$, $^{**}p \le .01$).

inflammation –YKL40, MPO, IL-6 and IL-8 which correlated negatively ($r < -.4$, $p < .05$) with anaerobic Gram-positives *Mogibacterium diversum*, *Lachnoanaerobaculum umeaense* and the uncultured bacteria *Candidatus Saccharimonas aalborgensis*. TIMP-1 and MMP8 correlated negatively Gram-positive and negative commensals. Conversely *R. mucilaginosa*, a species with greatest overall detected reads in severe asthma (Table E5, online supplement), was linked to low FGF levels ($r = -.4$, $p < .05$).

13989995, 2024, 11, Downloaded from https://onlinelibrary.wiley.com/doi/10.1111/all.16269 by Test, Wiley Online Library on [04/01/2025]. See the Terms and Conditions (https://onlinelibrary.wiley.com/terms-and-conditions) on Wiley Online Library for rules of use; OA articles are governed by the applicable Creative Commons License

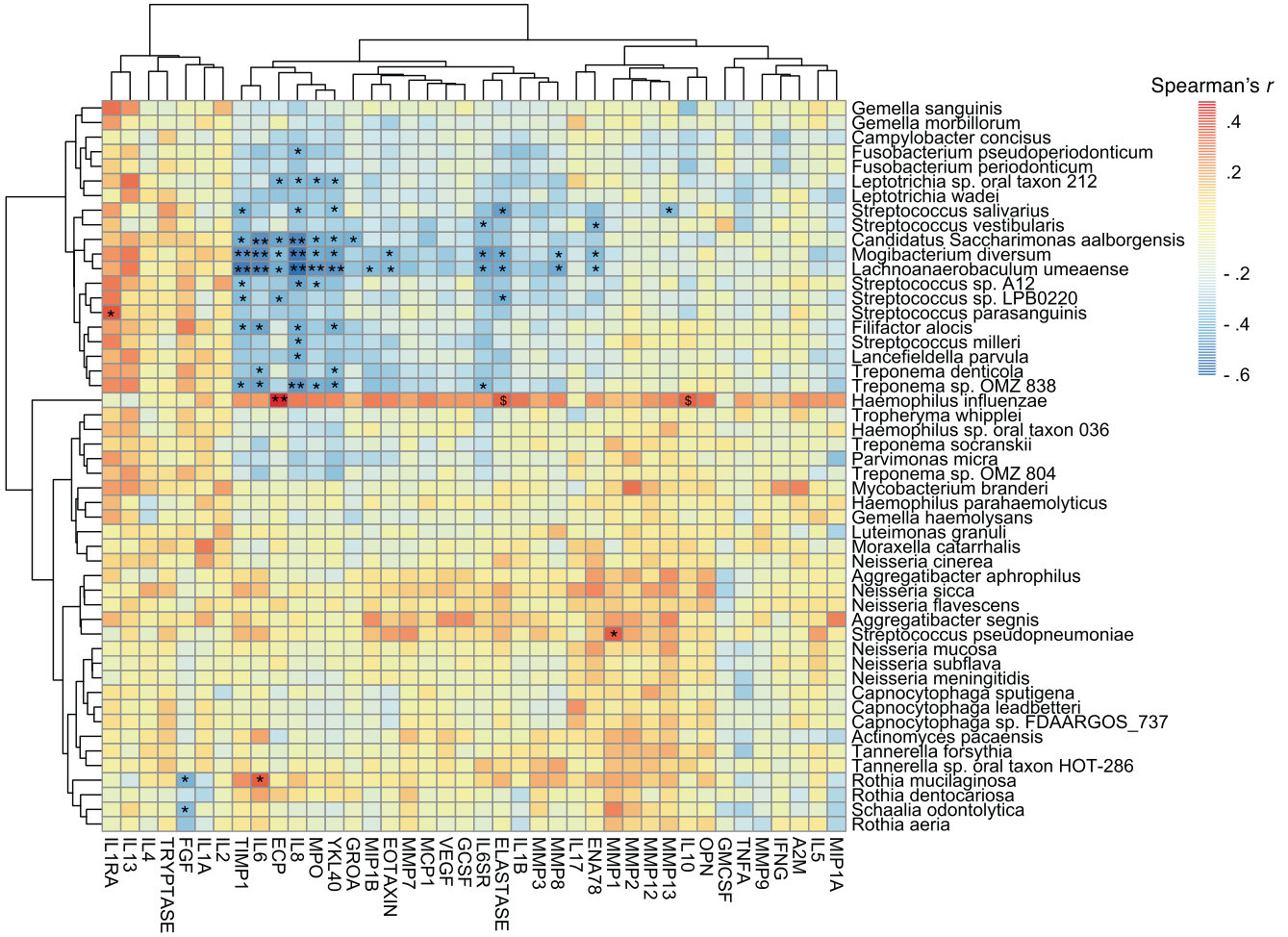


FIGURE 3 Heatmap displaying correlations between integrated sputum microbiome and cytokine data. The 50 most variable bacterial species across all subjects were selected. Spearman correlation coefficients between species and cytokines denoted by shade. Independent clustering performed by cytokine (columns) and species (rows). Statistically significant correlations have been annotated as $^{\$}p = .05$, $^{*}p < .05$ and $^{**}p < .01$. Adjustment for multiple comparisons was made using BH- procedure (FDR 0.05).

3.4 | Neutrophilic inflammation with pathogen dominance is accompanied by elevated type-1 cytokine and protease activity, elevated IL-10 and deficiency of IL-1RA in severe asthma

Using the above pragmatic sequencing definition of pathogen-dominance, we dichotomised severe asthma by presence or absence of this trait. A pathogen-dominant microbiome was associated with sputum neutrophilia (Figure 2B, $p < .05$), significantly elevated type-1 cytokines and airway proteases, namely: elastase, TNF, IL-1βα, MIP-1β, MMP8, ECP, YKL40, MPO, MIP-1α, IL-6SR and MMP9 (Figure 2C, $p < .05$ and Table E8, online supplementary). Of the immunomodulatory mediators IL-1RA was deficient, whereas TIMP-1 and IL-10 levels were higher in the presence of pathogen dominance (Figure 2D, $p < .05$ and Table E8, online supplement).

3.5 | BNA in severe asthma

A Bayesian network is an acyclic directed graph in which variables are represented in nodes, and arcs represent the direct probabilistic dependencies between these.[19] In essence it an unbiased probabilistic method to explore how different parameters relate to each other, as the network structure models the interactions among the variable in the model. BNA was applied to cytokines significantly elevated in a pathogen-dominant microbiome ($n = 15$), clinical parameters ($n = 20$), and bacterial species with significant differential abundance (either increased or decreased) in severe asthma ($n = 25$), in 51 severe asthmatics (Figure 4). The 'clustering algorithm' was applied.[20,21] The analysis retained 34/60 parameters in the model (Table E9). To further explore pair-wise interactions retained in this network, in a sperate secondary analysis, Pearson (between bacterial species) or Spearman (between cytokine) correlations were performed. Positive

13989995, 2024, 11, Downloaded from https://onlinelibrary.wiley.com/doi/10.1111/all.16269 by Test, Wiley Online Library on [04/01/2025]. See the Terms and Conditions (https://onlinelibrary.wiley.com/terms-and-conditions) on Wiley Online Library for rules of use; OA articles are governed by the applicable Creative Commons License

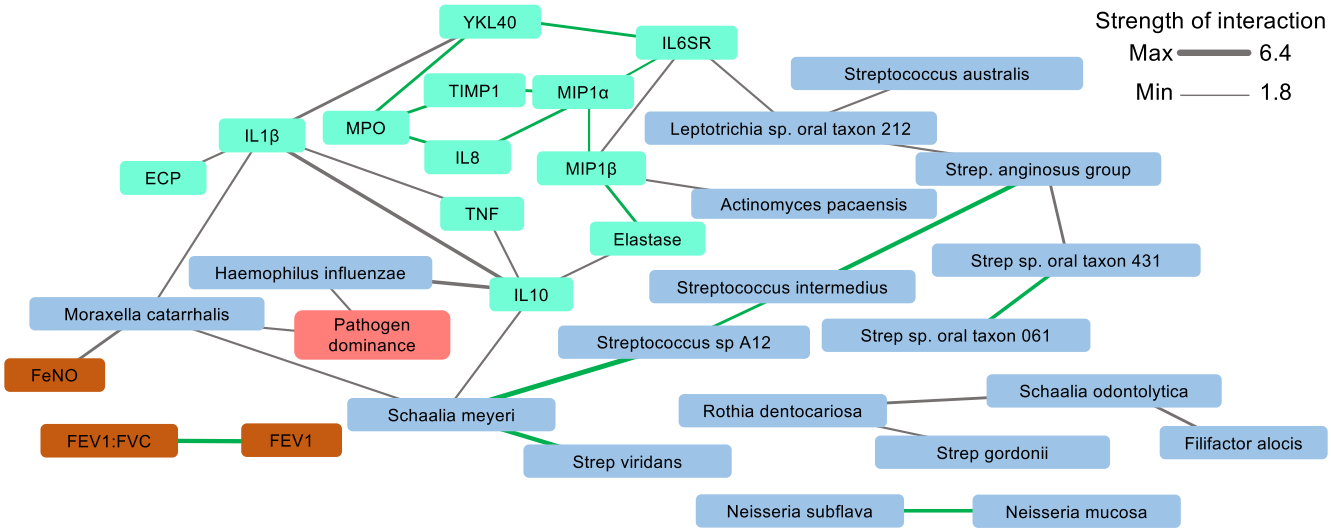


FIGURE 4 Integrated Bayesian Network Analysis. Bayesian network showing strongest interactions between most differentially abundant bacterial species, inflammatory mediators, and clinical features in severe asthma (WES, $n = 51$). Nodes are coloured by class: bacterial species (blue), infection status (red), inflammatory mediators (green) and clinical features (brown). Nodes without strong interactions have been excluded. Line thickness represents strength of interaction (Euclidean distance) as shown in the scale. Interactions with a positive linear correlation are shown with a green edge.

linear correlations are highlighted with a green edge. No negative correlations were found. This analysis provided an exploration of the inter-relationships between these key microbial and immune variables specifically in severe asthma, thereby supplementing the earlier integrated analyses performed in the full Wessex cohort.

Connectivity was observed between *H. influenzae*/*M. catarrhalis* abundance nodes and 'pathogen dominance', and between cytokines linked to pathogen dominance in earlier analyses. There was a non-linear relationship between *M. catarrhalis* and FeNO or IL-1β (Figure E7), and a mutually exclusive relationship between elevated FeNO and abundant *H. influenzae* (shown in Figure E8). In addition, connectivity appeared with positive correlations between related bacterial species, most notably species belonging to phylum Firmicutes, and *Neisseria* spp (Figure E9).

This approach highlighted associations between sputum IL-10 and *H. influenzae* abundance (Figure E7A, $r = .32$, $p < .05$), and IL-10 and TNF (Figure E7b, $r = .62$, $p < .0001$). The macrophage chemoattractant MIP1α node was highly connected within the network (Figure 4 and Figure E7, online supplement) specifically to complementary chemokine MIP1β ($r = .88$, $p < .0001$), alongside IL-6SR ($r = .65$, $p < .0001$), TIMP-1 ($r = .65$, $p < .0001$) and IL-8 ($r = .73$, $p < .0001$). Sputum YKL40 was strongly connected to MPO ($r = .92$, $p < .0001$), IL-6SR ($r = .75$, $p < .0001$) and IL-1β ($r = .63$, $p < .0001$). Neutrophilic mediators MPO and IL-8 strongly correlated ($r = .85$, $p < .0001$).

3.6 | Distinct microbiomes and cytokine milieus between upper and lower airways in severe asthma

Paired nasal lavage and sputum samples were collected in severe asthma ($n = 17$). We consider nasal lavage as typical of part of the upper airway compartment, whereas, despite an inevitable component of oral contamination, sputum samples are more representative of the lower airways. Relative abundances of shared bacterial species between the upper and lower airways are shown in Figure 5A and Figure E10. Samples and species clustered distinctly by anatomical location (PCA plot shown in Supplementary Figure E11, PERMANOVA = 0.001). In severe asthma, nasal lavage was enriched in *S. epidermidis* and *S. aureus*, with higher abundance of *D. pigrum*, *M. catarrhalis* and *E. coli* compared to sputum. Sputum was enriched for Firmicutes (predominantly *Streptococcal* spp.) with greater relative abundance of *H. influenzae* and *H. parainfluenzae*.

The cytokine milieu in the upper and lower airway was compared using paired O-link proteomics from nasal lavage and sputum samples (Figure 5B), proteins with statistically significant correlations are shown. Proteins were discordant between nasal lavage and sputum compartments (that is, proteins most strongly correlate with others from the same compartment), with the exception of significant associations between sputum cytokines IL-20, FGF5 and IL-2 and specific nasal lavage proteins (described further in Supplementary Results).

4 | DISCUSSION

Using long-read Nanopore sequencing we provide the first large-scale, species-level definition of the airway microbiome in severe asthma. We identified presence of a pathogen-dominant microbiome, with dominance of a single pathogenic bacterial species, and associated mucosal inflammation, in 20%–30% of individuals during stable disease. Such dominance with a limited repertoire of species: *H. influenzae* being the most prevalent, followed by *M. catarrhalis* and

13989995, 2024, 11, Downloaded from https://onlinelibrary.wiley.com/doi/10.1111/all.16269 by Test, Wiley Online Library on [04/01/2025]. See the Terms and Conditions (https://onlinelibrary.wiley.com/terms-and-conditions) on Wiley Online Library for rules of use; OA articles are governed by the applicable Creative Commons License

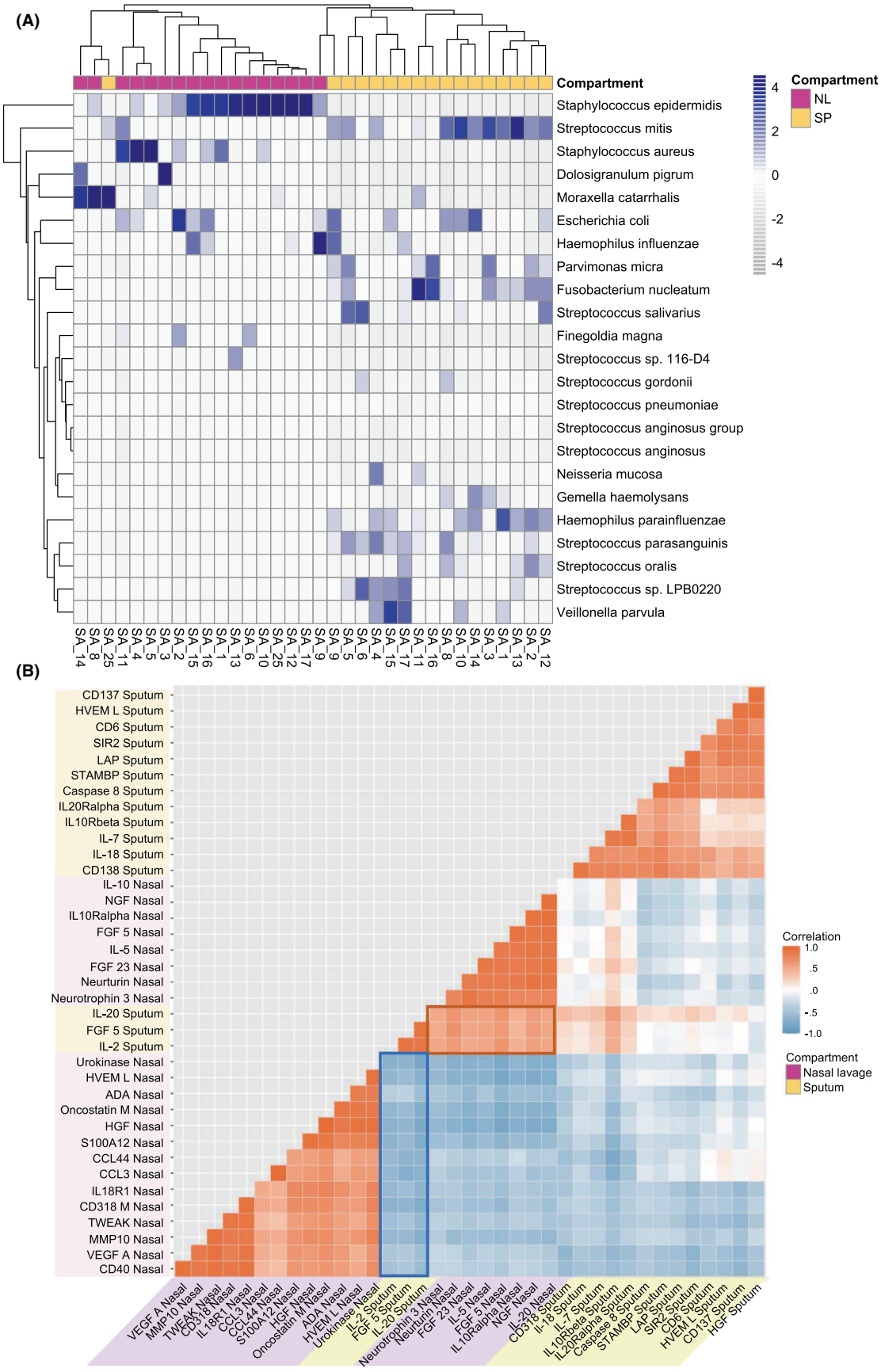


FIGURE 5 Upper and lower airway microbiome and cytokines. (A) Heatmap of relative abundances of bacterial species on metagenomic sequencing of paired nasal lavage (NL) and sputum (SP) samples from severe asthmatics ($n = 17$). Z-score denoted by shade. Independent clustering by samples (columns) and 23 most variable species (rows) using Euclidian distance. (B) Correlation matrix of the most significantly correlated ($p < .001$) proteins in paired nasal lavage (NAS) and sputum (SPU) cytokines (O-link). Significantly correlated pairs displayed ($p < .001$, adjusted for multiple comparisons with Benjamini–Hochberg procedure [FDR 0.05]).

13989995, 2024, 11, Downloaded from https://onlinelibrary.wiley.com/doi/10.1111/all.16269 by Test, Wiley Online Library on [04/01/2025]. See the Terms and Conditions (https://onlinelibrary.wiley.com/terms-and-conditions) on Wiley Online Library for rules of use; OA articles are governed by the applicable Creative Commons License

S. pneumoniae. Whilst metagenomic measures do not imply bacterial tissue invasion, we identified strong correlation between dominance of potentially pathogenic bacteria and evidence of airway neutrophilia and mucosal inflammation beyond that expected by simple commensal colonisation. Using novel supervised and unsupervised approaches our integration of species-level metagenomics with cytokine and protein datasets shows consistent evidence of type-1 inflammatory responses accompanied by neutrophilia in presence of a pathogen-dominant microbiome. This coincides with commensal depletion (largely Firmicutes), previously linked to worse asthma outcomes.[4] Commensal organisms detected in induced sputum showed an expected overlap with oropharyngeal flora.[22] Our results are consistent with and build upon findings of previous studies.[4,8,10] Finally, we demonstrate that lower (sputum) airway microbiome remains distinct from the upper (nasal) airways in severe asthma, with anatomical compartmentalisation of the cytokine milieu.

Just three species dominate the airway microbiome in severe asthma, and their presence observed in both neutrophilic and non-neutrophilic phenotypes might explain the striking clinical efficacy of long-term, low dose azithromycin therapy in both phenotypes,[23] but most notably in those with greatest *H. influenzae* abundance, measured by qPCR.[24] In the BNA, symptom score (ACQ-7) was not linked to presence of a dominant pathogen, likely due to insensitivity of ACQ-7 to sputum volume or purulence. Indeed, azithromycin therapy produced a very small change in symptom score (0.1 points on ACQ-6) amongst severe asthmatics in the AMAZES trial.[23] Mechanistically, whilst azithromycin is primarily antibacterial, additional anti-viral[25] and anti-inflammatory[26] effects are reported. However, antimicrobial resistance with widespread azithromycin therapy is a significant concern,[27] and if the antibacterial effect is dominant, this could be addressed through targeting therapy to those with pathogen dominance identified through molecular techniques. We have previously reported that Nanopore sequencing identifies clinically-relevant airway pathogens and shows agreement with sputum culture and semi-quantitative pathogen specific qPCR.[11]

In this present study similar consistency is seen between a pathogen-dominant airway microbiome identified by Nanopore sequencing and positive pathogen specific qPCR results for *H. influenzae*, *S. pneumoniae*, *M. catarrhalis* and *P. aeruginosa* in samples from the Oxford cohort. The lower, 73% concordance between sequencing and qPCR results in Wessex samples ($n = 8/11$) may be attributable to age-related sample degradation in this historical cohort, as total 16S load was >15-fold lower in Wessex than Oxford samples. A stringent qPCR cut-off of 1×10^6 copies/mL was set for a positive result based on its ability to identify bacteria associated neutrophilic inflammation in COPD following longitudinal sampling and our previous report on agreement sputum culture results in asthma. It is worth noting that prevalence of potentially pathogenic microorganisms in COPD is relatively high[28] and sputum culture lacks sensitivity.[16] If a lower threshold of 0.5×10^6 copies/mL was set, concordance would have been 100%. Overall, Nanopore sequencing provided a detailed species level description of the overall microbiome. Currently, for operational reasons, qPCR on selected pathogens may offer the most accessible and accurate means of identifying pathogen-dominance for targeted therapy in routine clinical practice. However, rapid progress is being made with the operationalisation of Nanopore sequencing for direct clinical application, and a pilot study has shown successful implementation of Nanopore in a routine clinical setting with a turnaround from sample receipt to metagenomic report of <7 h, allowing same day reporting in >90% of cases.[29] This has important clinical implications as, with standardised workflows, more cost-effective sample multiplexing, and pipelines able to identify antimicrobial resistance genes, there is the potential to accurately guide antimicrobial therapies on a per-patient basis in severe asthma and other airways diseases.

Nanopore sequencing provides further insight into microbiome of distinct sputum inflammatory phenotypes. In addition to *H. influenzae*, *M. catarrhalis* and *S. pneumoniae*, *T. whipplei* was strongly associated with neutrophilic asthma. This predominantly intracellular bacterium causes chronic multi-system inflammation in Whipple's disease and may be involved in airways disease. *T. whipplei* has been detected in up to 40% of severe asthmatics, linked to both eosinophilic[9] and corticosteroid resistant inflammation[30] albeit in smaller cohorts. Its ability to grow within acidic vacuoles, induce M2 macrophage polarisation and apoptosis are virulence traits capable of promoting chronic infection.[31] The asthmatic airway is susceptible to persistent infection with intracellular bacteria, most commonly non-typeable strains of *H. influenzae*[3] (NTHi) which facultatively enter macrophages and airway epithelial cells, and is associated with airway neutrophilia and type 17 inflammatory mediators.[32] High dose ICS exposure may also render mucosa susceptible to *T. whipplei*. Further research is needed to determine if specific innate immune deficiencies promote this intracellular infection. The microbiome in eosinophilic asthma varies with disease severity and in severe disease displays high relative abundance of Firmicutes.[17] The Proteobacteria *M. catarrhalis* was associated with eosinophilic asthma in this study, alongside Firmicutes *S. intermedius* and *V. parvula*, though this comparison is underpowered and requires replication. BNA linked *M. catarrhalis* abundance to FeNO level, previously shown to correlate negatively with Proteobacteria abundance.[17] We observed a mutually exclusive relationship between high FeNO and abundance of *H. influenzae* suggesting that this bacterium may inhibit FeNO production by the airway mucosa.

In SA, notably in absence of a dominant pathogen, there is greater abundance of *Rothia* spp., previously detected in mild non-eosinophilic asthma[33] and bronchiectasis, where abundance negatively correlated with IL-8, IL-1β, MMP-1, MMP-8 and MMP-9 in sputum.[34] Of these species, *R. mucilaginosa* is most often detected in chronic lung diseases and inhibits NF-κB activation in lung epithelium *in vitro*.[34] *R. mucilaginosa* is believed to produce anti-inflammatory mediators which directly inhibit NF-κB signalling, probably at the level of IKK activation and can reduce lung pathology *in vivo*.[34] It is not known why *Rothia* are more abundant in SA, but potentially as facultative anaerobes they may be better able to colonise airways

13989995, 2024, 11, Downloaded from https://onlinelibrary.wiley.com/doi/10.1111/all.16269 by Test, Wiley Online Library on [04/01/2025]. See the Terms and Conditions (https://onlinelibrary.wiley.com/terms-and-conditions) on Wiley Online Library for rules of use; OA articles are governed by the applicable Creative Commons License

with reduced oxygen tension secondary to mucus plugging. We saw association between IL-6 and *R. mucilaginosa*, but a strong negative correlation with FGF which itself positively correlated with oropharyngeal commensals. FGFs are a diverse group of growth factors exerting pleiotropic effects via tyrosine kinase receptors. FGF-2 promotes bronchial smooth muscle hyperplasia, shows higher expression in asthma, and with FGF-1 stimulates MAPK-dependent VEGF production, inhibited by azithromycin and dexamethasone.[35] Thus, microbial composition could influence airway remodelling processes further manipulated by corticosteroids and macrolides.

Integration of metagenome and inflammatory mediators, together with BNA offer additional novel insights. Overall, a pattern emerges linking a pathogen-dominant microbiome and type-1 inflammation (IL-1β, TNF) with neutrophilic infiltration (IL-8, YKL40), release of neutrophil granule proteins and proteases (MMP8, MMP9, MPO and elastase), counter regulatory mechanisms (TIMP-1, IL-10), and macrophage recruitment (MIP1α and MIP1β) which could be facilitated through IL-6 signalling (IL-6SR). *H. influenzae* correlated with the anti-inflammatory cytokine IL-10, consistent with data in *in vitro*[36] and in COPD.[37] Co-production of IL-10/TNF, induced via MyD88-dependent TLR activation following NTHi infection, may offer a regulatory response, and *H. influenzae* could harness excess IL-10 secretion as a virulence strategy. This could be explored further in murine studies.

H. influenzae also correlated strongly with sputum ECP (RNase 3), a cytotoxic eosinophil granule basic protein released on eosinophil activation. ECP has antibacterial properties but is also associated with airways remodelling, and inflammation and can induce mucus hypersecretion, potentially explaining its association with chronic bronchitis.[38] The strong association we observe could result either from eosinophilic inflammation predisposing to acquisition of *Haemophilus*, or, perhaps more likely, is a harmful consequence of *Haemophilus* infection. To this end data from recent on-biologic studies are suggestive. In the MEX study respiratory bacteria were detectable at high copy number at stable state in 36% of patients established on mepolizumab, a higher proportion than our cohort.[39] Furthermore therapy with benralizumab—which causes more profound eosinophil depletion, besides effects on other IL-5R-expressing cell types—is associated with a significant threefold increased incidence of respiratory infections, consistent with an antibacterial role of eosinophils, though the situation is likely complex due to the opposing effects of eosinophil and bacteria-induced mucus plugging.[40]

IL-1RA and TIMP-1 were differentially regulated in presence of a dominant pathogen. IL-1RA, an antagonist to IL-1β and its receptor, was reduced, consistent with reduced IL-1RA:IL-1β ratio in neutrophilic asthma,[41] potentially representing IL-1β quenching during infection. IL-1RA is upregulated in steroid-naïve atopic asthma,[42] with IL-1RA polymorphisms increasing asthma risk. ICS dampens IL-1RA production, as supported by relatively higher concentrations in healthy/mild asthmatic sputum (Figure 2A). TIMP-1, also elevated in presence of a dominant pathogen, possesses antiprotease activity, and MMP-9:TIMP-1 ratio is reduced in asthma and chronic bronchitis,[43] correlating inversely with airflow obstruction, with TIMP-1 polymorphisms associated with female asthma.[44] Thus, whilst TIMP-1 blocks proteolytic activity, in excess it might reduce extracellular matrix turnover resulting in remodelling. IL-10, IL-1RA and TIMP-1 are thereby integral to complex regulatory networks with likely differing roles dependant on the wider inflammatory landscape. This could be better characterised through dedicated transcriptomic and proteomic studies in well phenotyped severe asthmatics.

We have shown that the 'one airway, one disease' concept does not apply to the airway microbiome in severe asthma where distinct microbial niches are maintained in the nasopharynx and lower airway. This is consistent with mild atopic asthma and health.[7,22] The nasal microbiome can be informative and has been shown to predict exacerbation risk in paediatric asthma when dominated by *Moraxella* species, but our data and previous studies in mild asthma suggests nasopharyngeal samples should not replace lower airway sampling in stable state or exacerbation in adult asthma.[45] This distinction between paediatric and adult asthma remains unexplained. We found the cytokines IL-20[46] and IL-2[47] in sputum, which have been linked to airway remodelling and allergic inflammation in asthma respectively, to correlate with nasal proteins involved in diverse cellular responses. The importance of cross-signalling between these compartments is not known but of interest given the burden of comorbid sinonasal disease in severe asthma.

This study had some limitations. Samples from the Wessex cohort, collected between 2009 and 2014, are from a pre-biologic era with widespread maintenance oral corticosteroid use which may confound detection of sputum inflammatory mediators. Sample collection and storage protocols can affect quality of metagenomic data, particularly in low biomass samples, and we suspect some storage-related DNA degradation in Wessex samples as DNA was extracted after <11½years of storage. This study has limited power given the moderate sample size, particularly the low number of healthy controls and those with mild asthma, which will limit detection of significant but smaller differences in microbial composition within the cohort. Future studies could be strengthened by including a larger cohort with mild and moderate asthma, and longitudinal data spanning exacerbations. Due to the nature of human respiratory samples with high host DNA content,[11,48] sequencing depth in direct from clinical sample extracts can be inherently limited and variable, despite efforts to deplete host DNA. Previous work by Sanderson et al. has shown that ~20× coverage is required for consensus whole genome sequences allowing confident identification of antibiotic resistant determinants, and SNPs, or similarly strain inferences. Consistent high depth sequences of this order are typically derived following sequencing of bacterial isolates; clinical samples show far greater variation. The sequencing depth in this study was therefore inadequate for such functional analyses in the full dataset. Approached to overcome these limitations could include achieving greater depth by sequencing fewer samples per flow cell or using probe-based enrichment of pathogen specific DNA enabling deeper sequencing.

13989995, 2024, 11, Downloaded from https://onlinelibrary.wiley.com/doi/10.1111/all.16269 by Test, Wiley Online Library on [04/01/2025]. See the Terms and Conditions (https://onlinelibrary.wiley.com/terms-and-conditions) on Wiley Online Library for rules of use; OA articles are governed by the applicable Creative Commons License

In conclusion, we show that a pathogen-dominant microbiome is a common treatable trait in severe asthma, present in 20%–30% of patients, most often with *H. influenzae*. It is accompanied by neutrophilic inflammation, elevated airway proteases and disruption of counterregulatory immune responses which could facilitate pathogen persistence and airway remodelling.

AUTHOR CONTRIBUTIONS

M.F.J., T.S.C.H., P.H.H., A.C., P.K. and I.D.P. contributed to conceptualisation and design of the protocol. M.F.J., M.T., G.D., C.B., L.C.K.L., A.C., T.B., T.S., P.H.H., T.S.C.H. contributed to acquisition of study data. Data were analysed by E.M., M.F.J., N.S., T.S., C.B., A.A., T.S.C.H.. E.M., M.F.J., N.S. have accessed and verified the data. MFJ and TSCH drafted this submission which was approved by all authors.

ACKNOWLEDGEMENTS

The authors are grateful to all the participants who volunteered and to the clinical and research teams at all the participating centres. For the purpose of Open Access, the author has applied a CC BY public copyright licence to any Author Accepted Manuscript version arising from this submission. The views expressed are those of the authors and not necessarily those of the NHS, the NIHR or the Department of Health and Social Care. The authors vouch for the integrity and completeness of the data and the fidelity of the trial to the protocol. This study has been conducted in accordance with the Declaration of Helsinki and any applicable regulatory requirements.

FUNDING INFORMATION

Supported by the Medical Research Council (G0800649) and by the National Institute for Health Research (NIHR) Oxford Biomedical Research Centre (BRC). TSCH is supported by a Wellcome Trust Fellowship (211050/Z/18/z). MFJ was supported by a National Institute for Health Research Academic Clinical Fellowship Award and by the Nuffield Department of Medicine. PK was suInfrastructure support was funded by the National Institute for Health Research (NIHR) Southampton Respiratory Biomedical Research Unit and the NIHR through the Primary Care Research Network. All authors had full access to the full data in the study and accept responsibility to submit for publication.

CONFLICT OF INTEREST STATEMENT

Maisha Farzana Jabeen received funding from UKRI and the National Institute for Health Research (NIHR) Oxford Biomedical Research Centre. Clair Barber, and Adnan Azim are employees of AstraZeneca, Ian D Pavord has received funding from Merck, from Chiesi and consultancy fees from AstraZeneca, Boehringer Ingelheim, Aerocrine, Almirall, Novartis, Teva, Chiesi, Sanofi/Regeneron, Menarini, GSK, Circassia, Knopp outside the submitted work. Anoop Chauhan has received funding from Airsonett and consultancy fees from Sanofi Genzyme, Novartis, XIM, Glyconics and Exhalation Technology. Mariaenrica Tinè, Gillian Donachie, Laurie CK Lau, Thomas Brown and Paul Klenerman has received funding from the National Institute for Health Research (NIHR) Oxford Biomedical Research Centre, the Wellcome Trust (222426/Z/21/Z), and GSK. Nicholas D Sanderson and Teresa L Street received funding from the National Institute for Health Research (NIHR) Oxford Biomedical Research Centre. Emanuele Marchi has received funding from Asthma+Lung UK. Peter H Howarth is an employee of GSK. Timothy SC Hinks reports grants from The Wellcome Trust, grants from The Guardians of the Beit Fellowship, grants from Pfizer, grants from NIHR Oxford BRC, grants from University of Oxford, grants from Kymab, grants from Arcturis, grants from Asthma+Lung UK, during the conduct of the study; personal fees from Astra Zeneca, personal fees from TEVA, personal fees from Peer Voice, personal fees from AZ Pieris, outside the submitted work.

DATA AVAILABILITY STATEMENT

The data that support the findings of this study are openly available in European Nucleotide Archive at https://www.ebi.ac.uk/ena/browser/home, reference number PRJEB62780.

ORCID

Maisha F. Jabeen https://orcid.org/0000-0002-1887-596X
Nicholas D. Sanderson https://orcid.org/0000-0001-6370-1961
Mariaenrica Tinè https://orcid.org/0000-0002-3094-5721
Gillian Donachie https://orcid.org/0000-0002-8873-6455
Clair Barber https://orcid.org/0000-0001-5335-5129
Adnan Azim https://orcid.org/0000-0001-5960-1159
Laurie C. K. Lau https://orcid.org/0000-0002-5851-3867
Thomas Brown https://orcid.org/0000-0001-7336-4719
Ian D. Pavord https://orcid.org/0000-0002-4288-5973
Anoop Chauhan https://orcid.org/0000-0003-4044-6114
Paul Klenerman https://orcid.org/0000-0003-4307-9161
Teresa L. Street https://orcid.org/0000-0001-8491-240X
Emanuele Marchi https://orcid.org/0000-0003-1741-9353
Peter H. Howarth https://orcid.org/0000-0003-0619-7927
Timothy S. C. Hinks https://orcid.org/0000-0003-0699-2373

REFERENCES

1. Pavord ID, Beasley R, Agusti A, et al. After asthma: redefining airways diseases. *Lancet*. 2018;391:350-400.
2. Simpson JL, Scott R, Boyle MJ, Gibson PG. Inflammatory subtypes in asthma: assessment and identification using induced sputum. *Respirology*. 2006;11:54-61.
3. Hinks TSC, Levine SJ, Brusselle GG. Treatment options in type-2 low asthma. *Eur Respir J*. 2021;57:2000528.
4. Abdel-Aziz MI, Brinkman P, Vijverberg SJH, et al. Sputum microbiome profiles identify severe asthma phenotypes of relative stability at 12 to 18 months. *J Allergy Clin Immunol*. 2021;147:123-134.
5. Green BJ, Wiriyachaiporn S, Grainge C, et al. Potentially pathogenic airway bacteria and neutrophilic inflammation in treatment resistant severe asthma. *PLoS One*. 2014;9:e100645.
6. Huang YJ, Nariya S, Harris JM, et al. The airway microbiome in patients with severe asthma: associations with disease features and severity. *J Allergy Clin Immunol*. 2015;136:874-884.
7. Hilty M, Burke C, Pedro H, et al. Disordered microbial communities in asthmatic airways. *PLoS One*. 2010;5:e8578.

13989995, 2024, 11, Downloaded from https://onlinelibrary.wiley.com/doi/10.1111/all.16269 by Test, Wiley Online Library on [04/01/2025]. See the Terms and Conditions (https://onlinelibrary.wiley.com/terms-and-conditions) on Wiley Online Library for rules of use; OA articles are governed by the applicable Creative Commons License

8. Taylor SL, Leong LEX, Choo JM, et al. Inflammatory phenotypes in patients with severe asthma are associated with distinct airway microbiology. *J Allergy Clin Immunol*. 2018;141:94-103 e115.
9. Simpson JL, Daly J, Baines KJ, et al. Airway dysbiosis: *Haemophilus influenzae* and *Tropheryma* in poorly controlled asthma. *Eur Respir J*. 2016;47:792-800.
10. Diver S, Richardson M, Haldar K, et al. Sputum microbiomic clustering in asthma and chronic obstructive pulmonary disease reveals a *Haemophilus*-predominant subgroup. *Allergy*. 2020;75:808-817.
11. Jabeen MF, Sanderson ND, Foster D, et al. Identifying bacterial airways infection in stable severe asthma using Oxford Nanopore sequencing technologies. *Microbiol Spectr*. 2022;10:e0227921.
12. Samitas K, Carter A, Kariyawasam HH, Xanthou G. Upper and lower airway remodelling mechanisms in asthma, allergic rhinitis and chronic rhinosinusitis: the one airway concept revisited. *Allergy*. 2018;73:993-1002.
13. Hinks TS, Zhou X, Staples KJ, et al. Innate and adaptive T cells in asthmatic patients: relationship to severity and disease mechanisms. *J Allergy Clin Immunol*. 2015;136:323-333.
14. Hinks TSC, Brown T, Lau LCK, et al. Multidimensional endotyping in patients with severe asthma reveals inflammatory heterogeneity in matrix metalloproteinases and chitinase 3-like protein 1. *J Allergy Clin Immunol*. 2016;138:61-75.
15. Juniper EF, Svensson K, Mork AC, Stahl E. Measurement properties and interpretation of three shortened versions of the asthma control questionnaire. *Respir Med*. 2005;99:553-558.
16. Bafadhel M, Haldar K, Barker B, et al. Airway bacteria measured by quantitative polymerase chain reaction and culture in patients with stable COPD: relationship with neutrophilic airway inflammation, exacerbation frequency, and lung function. *Int J Chron Obstruct Pulmon Dis*. 2015;10:1075-1083.
17. Diver S, Haldar K, McDowell PJ, et al. Relationship between inflammatory status and microbial composition in severe asthma and during exacerbation. *Allergy*. 2022;77:3362-3376.
18. Fonkou MDM, Bilen M, Cadoret F, Fournier PE, Dubourg G, Raoult D. '*Enterococcus timonensis*' sp. nov., '*Actinomyces marseillensis*' sp. nov., '*Leptotrichia massiliensis*' sp. nov., '*Actinomyces pacaensis*' sp. nov., '*Actinomyces oralis*' sp. nov., '*Actinomyces culturomici*' sp. nov. and '*Gemella massiliensis*' sp. nov., new bacterial species isolated from the human respiratory microbiome. *New Microbes New Infect*. 2018;22:37-43.
19. Puga JL, Krzywinski M, Altman N. Bayesian networks. *Nat Methods*. 2015;12:799-800.
20. BayesFusion. GeNIe Clustering Algorithm.
21. Lauritzen SL, Spiegelhalter DJ. Local computations with probabilities on graphical structures and their application to expert systems. *J R Stat Soc B Methodol*. 1988;50:157-194.
22. Durack J, Huang YJ, Nariya S, et al. Bacterial biogeography of adult airways in atopic asthma. *Microbiome*. 2018;6:104.
23. Gibson PG, Yang IA, Upham JW, et al. Effect of azithromycin on asthma exacerbations and quality of life in adults with persistent uncontrolled asthma (AMAZES): a randomised, double-blind, placebo-controlled trial. *Lancet*. 2017;390:659-668.
24. Taylor SL, Ivey KL, Gibson PG, Simpson JL, Rogers GB, and the AMAZES Study Research Group. Airway abundance of *Haemophilus influenzae* predicts response to azithromycin in adults with persistent uncontrolled asthma. *Eur Respir J*. 2020;56:2000194.
25. Oliver ME, Hinks TSC. Azithromycin in viral infections. *Rev Med Virol*. 2021;31:e2163.
26. Niessen NM, Gibson PG, Baines KJ, et al. Sputum TNF markers are increased in neutrophilic and severe asthma and are reduced by azithromycin treatment. *Allergy*. 2021;76:2090-2101.
27. Serisier DJ. Risks of population antimicrobial resistance associated with chronic macrolide use for inflammatory airway diseases. *Lancet Respir Med*. 2013;1:262-274.
28. Wang Z, Locantore N, Haldar K, et al. Inflammatory endotype-associated airway microbiome in chronic obstructive pulmonary disease clinical stability and exacerbations: a multicohort longitudinal analysis. *Am J Respir Crit Care Med*. 2021;203:1488-1502.
29. Charalampous T, Alcolea-Medina A, Snell LB, et al. Routine metagenomics service for ICU patients with respiratory infection. *Am J Respir Crit Care Med*. 2024;209:164-174.
30. Goleva E, Jackson LP, Harris JK, et al. The effects of airway microbiome on corticosteroid responsiveness in asthma. *Am J Respir Crit Care Med*. 2013;188:1193-1201.
31. Gorvel L, Al Moussawi K, Ghigo E, Capo C, Mege JL, Desnues B. Tropheryma whipplei, the Whipple's disease bacillus, induces macrophage apoptosis through the extrinsic pathway. *Cell Death Dis*. 2010;1:e34.
32. Ackland J, Barber C, Heinson A, et al. Nontypeable *Haemophilus influenzae* infection of pulmonary macrophages drives neutrophilic inflammation in severe asthma. *Allergy*. 2022;77:2961-2973.
33. Sverrild A, Kiilerich P, Brejnrod A, et al. Eosinophilic airway inflammation in asthmatic patients is associated with an altered airway microbiome. *J Allergy Clin Immunol*. 2017;140:407-417.
34. Rigauts C, Aizawa J, Taylor SL, et al. R othia mucilaginosa is an anti-inflammatory bacterium in the respiratory tract of patients with chronic lung disease. *Eur Respir J*. 2022;59:2101293.
35. Willems-Widyastuti A, Vanaudenaerde BM, Vos R, et al. Azithromycin attenuates fibroblast growth factors induced vascular endothelial growth factor via p38(MAPK) signaling in human airway smooth muscle cells. *Cell Biochem Biophys*. 2013;67:331-339.
36. Hosoki K, Nakamura A, Kainuma K, et al. Differential activation of eosinophils by bacteria associated with asthma. *Int Arch Allergy Immunol*. 2013;161(Suppl 2):16-22.
37. Barker BL, Haldar K, Patel H, et al. Association between pathogens detected using quantitative polymerase chain reaction with airway inflammation in COPD at stable state and exacerbations. *Chest*. 2015;147:46-55.
38. Granger V, Zerimech F, Arab J, et al. Blood eosinophil cationic protein and eosinophil-derived neurotoxin are associated with different asthma expression and evolution in adults. *Thorax*. 2022;77:552-562.
39. McDowell PJ, Diver S, Yang F, Borg C, et al. The inflammatory profile of exacerbations in patients with severe refractory eosinophilic asthma receiving mepolizumab (the MEX study): a prospective observational study. *Lancet Respir Med*. 2021;9:1174-1184.
40. Poznanski SM, Mukherjee M, Zhao N, et al. Asthma exacerbations on benralizumab are largely non-eosinophilic. *Allergy*. 2021;76:375-379.
41. Gao P, Gibson PG, Baines KJ, et al. Anti-inflammatory deficiencies in neutrophilic asthma: reduced galectin-3 and IL-1RA/IL-1beta. *Respir Res*. 2015;16:5.
42. Sousa AR, Lane SJ, Nakhosteen JA, Lee TH, Poston RN. Expression of interleukin-1 beta (IL-1beta) and interleukin-1 receptor antagonist (IL-1ra) on asthmatic bronchial epithelium. *Am J Respir Crit Care Med*. 1996;154:1061-1066.
43. Vignola AM, Riccobono L, Mirabella A, et al. Sputum metalloproteinase-9/tissue inhibitor of metalloproteinase-1 ratio correlates with airflow obstruction in asthma and chronic bronchitis. *Am J Respir Crit Care Med*. 1998;158:1945-1950.
44. Johnson SR. TIMP-1 in asthma: guilty by association. *Thorax*. 2005;60:617-618.
45. Zhou Y, Jackson D, Bacharier LB, et al. The upper-airway microbiota and loss of asthma control among asthmatic children. *Nat Commun*. 2019;10:5714.
46. Gong W, Wang X, Zhang Y, et al. Interleukin-20 promotes airway remodeling in asthma. *Inflammation*. 2014;37:2099-2105.
47. Hondowicz BD, An D, Schenkel JM, et al. Interleukin-2-dependent allergen-specific tissue-resident memory cells drive asthma. *Immunity*. 2016;44:155-166.

13989995, 2024, 11, Downloaded from https://onlinelibrary.wiley.com/doi/10.1111/all.16269 by Test, Wiley Online Library on [04/01/2025]. See the Terms and Conditions (https://onlinelibrary.wiley.com/terms-and-conditions) on Wiley Online Library for rules of use; OA articles are governed by the applicable Creative Commons License

48. Charalampous T, Kay GL, Richardson H, et al. Nanopore metagenomics enables rapid clinical diagnosis of bacterial lower respiratory infection. *Nat Biotechnol*. 2019;37:783-792.

SUPPORTING INFORMATION

Additional supporting information can be found online in the Supporting Information section at the end of this article.

How to cite this article: Jabeen MF, Sanderson ND, Tinè M, et al. Species-level, metagenomic and proteomic analysis of microbe-immune interactions in severe asthma. *Allergy*. 2024;79:2966-2980. doi:10.1111/all.16269

13989995, 2024, 11, Downloaded from https://onlinelibrary.wiley.com/doi/10.1111/all.16269 by Test, Wiley Online Library on [04/01/2025]. See the Terms and Conditions (https://onlinelibrary.wiley.com/terms-and-conditions) on Wiley Online Library for rules of use; OA articles are governed by the applicable Creative Commons License